

QATAR UNIVERSITY

COLLEGE OF PHARMACY

DESIGN, SYNTHESIS AND BIOLOGICAL EVALUATION OF NOVEL CHALCONE

ANALOGS AS POTENTIAL THERAPEUTIC AGENTS FOR CASTRATION

RESISTANT PROSTATE CANCER

BY

OLA HUSSEIN

A Thesis Submitted to
the College of Pharmacy
in Partial Fulfillment of the Requirements for the Degree of
Masters of Science in Pharmacy

June 2021

© 2021 Ola Hussein. All Rights Reserved.

COMMITTEE PAGE

The members of the Committee approve the Thesis of
Ola Hussein defended on 27/04/2021.

Dr. Ashraf Khalil
Thesis Supervisor

Dr. Ala-Eddin Al Moustafa
Thesis Co-Supervisor

Dr. Feras Alali
Thesis Co-Supervisor

Approved:

Mohammad Diab, Dean, College of Pharmacy

ABSTRACT

HUSSEIN, OLA, J., Masters : June : 2021, Pharmaceutical Sciences

Title: Design, Synthesis and Biological Evaluation of Novel Chalcone Analogs as Potential Therapeutic Agents for Castration-Resistant Prostate Cancer

Supervisor of Thesis: Ashraf, A. Khalil.

Prostate cancer (PCa) is the second most frequently diagnosed malignancy, as well as a leading cause of cancer-related mortality in men globally. Despite the initial response to hormonal targeted therapy, the majority of patients ultimately progress to a lethal form of the disease, castration-resistant prostate cancer (CRPC), which currently lacks curative therapeutic options and is associated with poor prognosis. Therefore, the objective of this study was to discover and develop novel treatment modalities for CRPC. Chalcones, also known as 1,3-diphenyl-2-propen-1-ones, are among the highly attractive scaffolds being investigated for their antitumor activities. A library of 26 cyclic (tetralone-based) and acyclic chalcone analogs, in which ring B was either substituted with nitrogen mustard or replaced by pyrrole or pyridine heterocyclic rings, were designed, synthesized and evaluated as potential therapies for CRPC. The design was guided by in-silico ADMET prediction in which analogs with favorable drug-likeness properties were prioritized. The new compounds were synthesized by Claisen-Schmidt condensation reaction, purified and characterized by extensive structural elucidation studies. The compounds in vitro cytotoxicity was evaluated against two androgen receptor (AR)-negative prostate cancer cell lines (PC3 and DU145). Among the tested compounds, thienyl pyridine containing analogs (**13**, **15** and **16**) showed potent antiproliferative activities at low micromolar levels with IC₅₀ values ranging between 4.32-6.47 μ M against PC3 and DU145 cell lines. Detailed biological studies

of the lead molecule **16** revealed that it can significantly induce apoptosis through upregulation of Bax and downregulation of Bcl-2. In addition, compound **16** potently inhibited colony formation and reduced cell migration of AR-negative PCa cell lines (PC3 and DU145). The molecular pathway analysis showed that the anticancer activity of compound **16** is associated with blocking of ERK1/2 and Akt activities. Furthermore, compound **16** inhibited angiogenesis in the chick chorioallantoic membrane (CAM) model as compared to control. Structure-activity relationship study on thienyl pyridine-based chalcones revealed that the cytotoxicity could dramatically improve via changing the methoxylation pattern by more than 2-folds ($IC_{50} \ll 2.5 \mu M$). These results indicate that thienyl pyridine-based chalcones could serve as promising lead molecules for the treatment of CRPC; thus, further *in vitro* and *in vivo* studies are warranted.

DEDICATION

To my parents,

*The reason, after God, for what I've become today. Thank you for your endless
support and care*

To the soul of my sister and best friend Haneen Maher,

You left the day I started my degree, but your memory continues to inspire me

ACKNOWLEDGMENTS

Many people helped me complete this thesis, and I would like to take this opportunity to express my appreciation to all individuals who contributed to the work presented in this thesis.

Foremost, I would like to express my sincere gratitude to my devoted supervisor, who believed in my abilities and ambitions, Dr. Ashraf Khalil, for his unwavering support, extensive personal and professional guidance, and encouragement. Special words of thanks should go to my co-supervisor, Dr. Ala-Eddin Al Mustafa, for his assistance at every stage of the research project. He always was keen to offer his help and support before I ask for them. Further, I am deeply grateful to my co-supervisor, Dr. Feras Alali, for his insightful comments, remarks, and engagement. I am extremely thankful to the whole research team as their enormous knowledge and considerable experience have motivated me in all the time of my academic research.

I should thank Dr. Farhan Cypryan, for his help with the cell cycle and apoptosis assays. Additionally, I would like to express my gratitude to Dr. Haw-Lih Su, for his assistance in running the NMR analysis and providing me with the required training on the NMR spectrometer. I am also thankful to Dr. Lotfi Chouchane, for providing the prostate cancer cell lines (DU145, C4-2 and LNCaP). Likewise, I would like to thank Dr. Ousama Rachid, for providing access to ADMET Predictor® software. Moreover, words of thank should go to Ms. Taqdees Mahroof, for her technical support in the laboratory, as well as the laboratory team members: Hadeel Kheraldine, Mohammed Akkbik, Ayesha Jabeen, Arij Hassan, and Ishita Gupta. Thanks to the Central Laboratories Unit team at Qatar University for their assistance in running the Spectroscopic analysis. I wish to extend my special thanks to the College of Pharmacy

at Qatar University, under the leadership of Dr. Mohammed Diab. Many thanks to the faculty members and the administrative staff who accompanied me during my journey, starting with a BSc degree and finishing with an MSc.

Unique mention goes to my family, where I had their love and full support throughout the program. Besides, I would like to thank my colleague, Dana Elkhalifa for her invaluable support and honest advice during my master's studies.

TABLE OF CONTENTS

DEDICATION	v
ACKNOWLEDGMENTS	vi
LIST OF TABLES	xii
LIST OF FIGURES	xiii
LIST OF ABBREVIATIONS	xvi
CHAPTER 1: INTRODUCTION	1
1.1 Prostate Cancer	1
1.1.1 Epidemiology and Etiology	1
1.1.2 Cellular and Molecular Origin.....	2
1.1.3 Role of Androgens and Androgen Receptor (AR)	5
1.1.4 Castration-Sensitive Prostate Cancer	7
1.1.5 Castration-Resistant Prostate Cancer	8
1.1.5.1 Current CRPC Therapeutic Options	9
1.1.6 Mechanisms Driving Castration Resistance.....	12
1.1.7 Targeting Prostate Cancer Beyond AR.....	17
1.1.8 Need for New Effective Therapeutic Options	18
1.2 Chalcones.....	18
1.2.1 Plant Derived Chalcones	20
1.2.2. Synthetic Chalcones.....	21
1.2.3 Chalcone Derivatives as Potential Candidates for PCa Treatment.....	23

1.2.4 Promising Chalcone Targets in PCa	24
1.2.4.1 Apoptosis Signaling Pathways.....	24
1.2.4.2 Cell Cycle Signaling.....	26
1.2.4.3 Cell Migration, Invasion and Metastasis	29
1.2.4.4 Inhibition of Angiogenesis.....	30
1.2.4.5 Androgen Receptor Signaling	32
1.2.4.6 PI3k/Akt/mTOR Pathway	33
1.3 Study Objectives and Rationale	34
CHAPTER 2: MATERIALS AND METHODS.....	35
2.1 Chemistry.....	36
2.1.1 Materials.....	36
2.1.2 Design of Novel Chalcones	38
2.1.3 Chemical Synthesis.....	38
2.1.4 Characterization and Structure Elucidation.....	40
2.1.4.1 Fourier Transform-Infrared analysis (FT-IR)	40
2.1.4.2 Mass Spectroscopy	40
2.1.4.3 Nuclear Magnetic Resonance (NMR)	41
2.1.4.4 Elemental Analysis.....	41
2.2 Pharmacological Screening	42
2.2.1 Cell Culture	42
2.2.2 Cell Viability	42

2.2.3 Morphological Examination.....	44
2.2.4 Annexin V Apoptosis Assay	44
2.2.5 Cell Cycle Analysis	45
2.2.6 Colony Formation Assay.....	46
2.2.7 Wound Healing Assay	46
2.2.8 Trans-well Migration Assay.....	47
2.2.9 Western Blot Analysis	47
2.2.10 Chorioallantoic Membrane (CAM) Angiogenesis Assay	49
2.2.11 Statistical Analysis.....	51
CHAPTER 3: RESULTS.....	52
3.1 Chemistry.....	52
3.1.1 Design of novel chalcone derivatives	52
3.1.2 Chemical Synthesis.....	55
3.1.3 Structure Elucidation	58
3.2 <i>In Silico</i> ADMET Screening.....	74
3.3 Pharmacological Anticancer Screening.....	77
3.3.1 General Screening (Compounds 1-16).....	77
3.2.1.1 Cell Viability.....	77
3.2.1.2 Morphological Examination	80
3.3.2 Molecular Pathway study of compounds 13, 15, and 16	84
3.3.2.1 IC ₅₀ and Selectivity Evaluation.....	84

3.3.2.2 Effect on Cell Morphology	87
3.3.2.3 Effect on Apoptosis Pathway	90
3.3.2.4 Effect on Cell Cycle	95
3.3.2.5 Effect on Colony Formation	98
3.3.2.6 Effect on Cells Migration	102
3.3.2.7 Effect on other Molecular Pathways	110
3.3.2.8 Effect on Angiogenesis	113
3.3.3 Expanded SAR Study (Compounds 13-26)	115
CHAPTER 4: DISCUSSION.....	119
CHAPTER 6: CONCLUSION AND FUTURE DIRECTIONS.....	128
REFERENCES.....	130
APPENDIX A. REPORTED CHALCONES' ACTIVITY AGAINST PCA.....	173
APPENDIX B. SPECTROSCOPIC ANALYSIS	186

LIST OF TABLES

Table 1.1 List of fine chemicals and solvents used in this study	37
Table 2 List of used primary and secondary antibodies	49
<i>Table 3.</i> General structures and numbering of the synthesized chalcones	56
Table 4. IC ₅₀ and LD ₅₀ of compounds 13 , 15 and 16 on AR-negative PCa and normal cells	87

LIST OF FIGURES

Figure 1. Chemical Structure of chalcone Scaffold.....	19
Figure 2. Structures of clinically approved chalcone based drugs.	21
Figure 3. Molecular hybridization of chalcones.....	23
Figure 4. Synthetic scheme of (A) tetralone-based chalcones and (B) non-cyclic chalcone analogs.....	39
Figure 5. Illustration of the used purification techniques	40
Figure 6. Illustration of Alamar Blue Assay.	44
Figure 7. Timeline of Chorioallantoic Membrane (CAM) Angiogenesis Assay	51
Figure 8. Design of nitrogen mustard tetralone-based chalcones (A) and cyclopropyl pyrrole-based chalcones (B).....	53
Figure 9. The rationale for the design of pyridine-chalcone Hybrids.	54
Figure 10. Chemical structures of the synthesized chalcone analogs.....	57
Figure 11. Characteristic coupling constants of (A) pyrrole ring (compounds 6-9) and (B) thienyl pyridine rings (compounds 13-26).....	59
Figure 12. Key ^1H - ^1H COSY , ^1H - ^{13}C HMBC and ^1H - ^{15}N HMBC correlations of compounds 13 and 16	60
Figure 13. Predicted drug-likeness properties of compound 17 by SwissADME web tool.....	75
Figure 14. ADMET Risk scores of the synthesized chalcone analogs (1-26), presented as heat map predicted by ADMET Predictor®.	76
Figure 15. Effect of compounds 1-16 on the cell viability of (A) PC3 and (B) DU145 cell lines.	78
Figure 16. Effect of compounds 1-16 on the cell morphology of PC3 cell line..	82
Figure 17. Effect of compounds 1-16 on the cell morphology of DU145 cell line.....	83

Figure 18. The effect of compounds 13 , 15 and 16 on cell viability of AR-negative prostate cancer cell lines	86
Figure 19. Effect of compound 13 on the cell morphology of AR-positive (C4-2 and LNCaP) and AR-negative (PC3 and DU145) prostate cancer cell lines..	88
Figure 20. Effect of compound 16 on the cell morphology of AR-negative (PC3 and DU145) prostate cancer cell lines.	89
Figure 21. Induction of apoptosis by compounds 13 , 15 and 16 in PC3 cells, as determined by Annexin V-FITC/7-AAD apoptosis assay.	91
Figure 22. Induction of apoptosis by compounds 13, 15 and 16 in DU145 cells, as determined by Annexin V-FITC and 7-AAD apoptosis assay	92
Figure 23. Effect of compounds 13 , 15 and 16 on the expression of apoptosis-related proteins in PC3 cells.	93
Figure 24. Effect of compounds 13 , 15 and 16 on the expression of apoptosis-related proteins in DU145 cells..	94
Figure 25. Effect of compounds 13 , 15 and 16 on cell cycle progression of PC3 cells.	96
Figure 26. Effect of compounds 13 , 15 and 16 on cell cycle progression of DU145 cells	97
Figure 27. Effect of compounds 13 and 16 on colony formation of PC3 cell line.	99
Figure 28. Effect of compounds 13 and 16 on colony formation of DU145 cell line.	101
Figure 29. Effect of compounds 13 , 15 and 16 on Transwell migration of PC3 cells..	103
Figure 30. Effect of compounds 13 , 15 and 16 on Transwell migration of DU145 cells.	104

Figure 31. Effect of compounds 13 , 15 and 16 on the migration of PC3 cells in wound healing assay..	105
Figure 32. Effect of compounds 15 and 16 on the migration of DU145 cells in wound healing assay..	106
Figure 33. Protein expression of EMT-related biomarkers on PC3 cell line.....	108
Figure 34. Protein expression of EMT-related biomarkers on DU145cell line.	109
Figure 35. Protein expression of JNK, ERK, and AKT-related biomarkers on PC3 cell line..	111
Figure 36. Protein expression of JNK, ERK, and AKT-related biomarkers on DU145 cell line.....	112
Figure 37. Effect of Compound 16 on Angiogenesis of the CAM	114
Figure 38. Effect of thienyl pyridine chalcone hybrids (13-26) on the cell viability of (A) PC3 and (B) DU145 cell lines.	116
Figure 39. Key structure-activity relationship (SAR) findings.....	118
Figure 40. Summary of the known heteroaromatic-based chalcone derivatives with reported activity against PCa and our novel lead molecule (compound 17)..	127
Figure 1. Summary of the main study findings.....	129

LIST OF ABBREVIATIONS

7-AAD: 7-Amino-Actinomycin

ADT: Androgen deprivation therapy

Anal. calcd.: Analytical calculated

AR: Androgen receptor

ARAT: Androgen receptor axis targeted agents

ATCC: American type culture collection

Bax: BCL-2-associated X protein

Bcl-2: B-Cell lymphoma-2

BPH: Benign prostatic hyperplasia

BRCA2: Breast cancer gene 2

BSA: Bovine serum albumin

¹³C: Carbon-13 isotope

CAM: Chorioallantoic membrane

CDCl₃: Deuterated chloroform

CDKs: Cyclin-dependent kinases

COSY: Homonuclear correlation spectroscopy

CRPC: Castration-resistant prostate cancer

CSC: Cancer stem cells

CZ: Central zone

d (NMR): Doublet splitting

DBD: DNA-binding domain

dd (NMR): Doublet of doublet splitting

ddd (NMR): Doublet of doublet of doublet splitting

DHT: Dihydrotestosterone

DMSO: Dimethyl Sulfoxide

DNA: Deoxyribonucleic acid

DTX: Docetaxel

EDTA: Ethylenediaminetetraacetic acid

EGFR: Epidermal growth factor receptor

EMT: Epithelial–mesenchymal transition

ER: Estrogen receptor

ErbB: Erythroblastic oncogene B

ERK1/2: Extracellular signal-regulated protein kinase

EtOH: Ethanol

FBS: Fetal bovine serum

FDA: US Food and Drug Administration

FSC: Forward scatter

FT-IR: Fourier-transform infrared spectroscopy

G0: Quiescence, cell cycle phase

G1: Gap 1, cell cycle phase

G2: Gap 2, cell cycle phase

GAPDH: Glyceraldehyde 3 phosphate dehydrogenase

GR: Glucocorticoid receptor

¹H: Proton/Hydrogen-1 isotope

HER2: Human epidermal growth factor receptor 2

HMBC: Heteronuclear multiple bond correlation

HMQC: Heteronuclear multiple quantum coherence

HPLC: High-performance liquid chromatography

HSP-90: Heat shock protein-90

HSQC: Heteronuclear Single quantum coherence

IC₅₀: Half maximal inhibitory concentration

IL-6: Interleukin 6

IUPAC: International Union of Pure and Applied Chemistry

J: Coupling constant

JNK: c-Jun N-terminal kinases

Ki-67: proliferation associated protein ki67

LBD: Ligand-binding domain

LC/MS: Liquid chromatography–mass spectrometry

LD₅₀: The concentration required to kill 50% of the cells

LHRH: Luteinizing hormone-releasing hormone

m (NMR): Multiplet splitting

m/z: Mass-to-charge ratio

M: Mitosis, cell cycle phase

mCRPC: Metastatic castration-resistant prostate cancer

MET: Mesenchymal–epithelial transition

MMP-1: Matrix metalloproteinase 1

MMP-9: Matrix metalloproteinase 9

MR: Mineralocorticoid receptor

mTOR: Mammalian target of rapamycin

MTT: (3-(4, 5-dimethylthiazolyl-2)-2, 5-diphenyltetrazolium bromide)

MW: Molecular weight

NaOH: Sodium hydroxide

NE: Neuroendocrine

NEPC: Neuroendocrine prostate cancer

ND: Normal primary dental cells

NF- κ B: Nuclear factor-kappa B

NMR: Nuclear magnetic resonance

P38 MAPK: P38 mitogen-activated protein kinases

P53: Tumor suppressor protein 53

PAGE: Polyacrylamide gel electrophoresis

PARP: Poly (adenosine diphosphate-ribose) polymerase

PBS: Phosphate buffered saline

PCa: Prostate cancer

PE: Phycoerythrin

PI: Propidium iodide

PI3K: Phosphatidylinositide 3 kinase

PIN: Prostatic intraepithelial neoplasia

PR: Progesterone receptor

PR: Progesterone receptor

Prep-HPLC: Preparative high-performance liquid chromatography

Prep-TLC: Preparative thin layer chromatography

PI: Propidium iodide

PSA: Prostate-specific antigen

PVDF: Polyvinylidene fluoride

PZ: Peripheral zone

ROS: Reactive oxygen species

s (NMR): Singlet splitting

S: Synthesis, cell cycle phase

SDS: Sodium dodecyl sulfate

SEM: Standard error of the mean

SD: Standard deviation

SI: Selective index

SSC: Side scatter

TAD: Transactivation domain

TBS: Tris-buffered saline

TBS-T: Tris-buffered saline-Tween

TLC: Thin layer chromatography

TNBC: Triple negative breast cancer

t-NEPC: treatment-related neuroendocrine prostate cancer

TNF- α : Tumor necrosis factor alpha

TRAIL: TNF-related apoptosis-inducing ligand

TZ: Transition zone

VEGF: Vascular endothelial growth factor

$\Delta\psi_m$: Mitochondrial membrane potential

CHAPTER 1: INTRODUCTION

1.1 Prostate Cancer

1.1.1 Epidemiology and Etiology

Prostate cancer (PCa) is the second most frequently diagnosed malignancy, as well as a leading cause of cancer-related mortality in men globally (1, 2). PCa is especially prevalent in the western world, with more than 25-fold higher incidence in some developed countries as compared to their developing counterparts (3). In the United States, PCa is the most commonly diagnosed non-cutaneous cancer accounting for 24.4% of all new cancer cases and the second-highest cause of cancer-related deaths in men (1). American Cancer Society estimated that around 191,930 men would be diagnosed with PCa and about 33,330 will die from it in 2020 in the United States alone (4). Similarly, the incidence of PCa is relatively elevated in Qatar, where it stands as the second most prevalent type of cancer among men (1, 5).

Over the past few decades, advances in early detection and diagnosis, in addition to the development of new therapeutic options, have led to significant improvement in the overall survival of PCa patients. The 5-year survival rate for PCa increased from 66.5% in 1975 to 98.2% in 2012 in the USA (6). Despite the initial good prognosis, PCa remains a major health burden and the second leading cause of cancer-related deaths in men (7). Unlike localized PCa, patients presenting with metastatic disease have a poor prognosis with a dramatically reduced survival rate (30.2% 5-year survival) (6). Besides, around 20-30% of patients with localized prostate cancer will develop recurrence and ultimately progress to metastatic PCa, which currently lacks curative therapeutic options (8).

Several genetic and environmental factors were studied as contributors to the

development of PCa, among which age, race and family history were identified as the most established risk factors (9). The risk of PCa increases dramatically with aging, where around 60% of the cases are diagnosed in men older than 65 (6). On the other hand, the incidence of PCa in men younger than 45 is extremely rare, accounting for less than 0.5% of the cases (6). In addition, African Americans are disproportionately affected by PCa, with around 60% higher incidence and at least two times the mortality rate as compared to men from other ethnic groups, whereas native Asians have the lowest risk of developing PCa (6, 10). Family history is another major risk factor; having a family member with a PCa doubles the risk of developing this disease. The risk is magnified if more than one relative were affected with PCa or if they were diagnosed at an age younger than 65 (11, 12). Two categories of hereditary mutations were associated with increased risk of PCa; common high-risk mutations and rare low-risk variants (13). Breast cancer susceptibility gene 2 (BRCA2) is an example of the rare but deleterious mutations that are prevalent in only 1.2% of early-onset PCa patients (14). However, carriers of this mutation are predisposed to a 5-7 times higher risk of PCa as compared to non-carriers (13, 15). Genome-wide association studies resulted in the identification of 77 single-nucleotide polymorphisms (SNPs) that are associated with a modest risk of PCa (13, 16).

Moreover, studies pointed towards other potential less established risk factors, including high consumption of red meat or dairy products and exposure to environmental toxins such as Agent Orange or cadmium (17-19). On the contrary, high vegetable and fruit intake and increased physical activity are potentially associated with a lower incidence of PCa (20).

1.1.2 Cellular and Molecular Origin

The prostate is a walnut-sized gland that is located below the urinary bladder,

surrounding the upper portion of the urethra. The primary function of the prostate is to produce an alkaline fluid that aids in nurturing and transporting sperms (21). The prostate consists of four zones: peripheral zone (PZ), central zone (CZ), transition zone (TZ) and anterior fibromuscular stroma (22, 23). Most prostate carcinomas (~75%) develop in the PZ, whereas benign prostatic hyperplasia (BPH) originates mainly in the TZ, which grows larger over time (24, 25). The rest of prostate cancers arise from TZ (~20%), while only 2.5% develop from CZ; however, it is thought that cancers developing in this zone are more aggressive than cancers in other zones (26, 27).

Histologically, the human prostate is comprised of pseudostratified epithelium and stroma separated by a basement membrane. The mature prostate epithelium is composed of two major cell types, luminal and basal cells, in addition to a minor scattered population known as neuroendocrine cells (23, 28). Luminal cells are terminally differentiated columnar epithelium secretory cells that express cytokeratin (CK, 8, and 18) and secrete proteins such as prostate-specific antigen (PSA) (29, 30). Whereas basal cells are proliferating non-secretory cells located beneath the luminal layer, separating it from the basement membrane and express cytokeratin (5 and 14) and p63 (29, 30). Neuroendocrine cells are intraepithelial regulatory cells that display hybrid epithelial/neural/endocrine characteristics and secrete neuropeptides and various hormones (28, 31). Unlike luminal cells that express high levels of androgen receptor (AR), basal and neuroendocrine cells either lack AR expression or have low levels of AR (23, 32).

More than 95% of prostate cancers are classified as adenocarcinoma, a type of cancer that arises from epithelial cells of the secretory glands (21). Cellular origins of prostate cancer have been debated for a long time and remain not entirely understood. Pathological examination of biopsy specimens shows that tumor tissues consist of

luminal, not basal, cells. Besides, prostate adenocarcinoma diagnosis is confirmed by the absence of basal cell markers (p63, CK5, CK14) and overexpression of luminal markers (33, 34). Thus, pathologists argued that PCa originates from luminal cells. On the other hand, biologists reported that PCa arises from basal cells due to their higher regenerative potential (35). Recent data suggest that prostate cancer could originate from both luminal or basal cells; however, it is not clear which of them is more aggressive than the other (36-38). Unlike breast cancer, gene-expression profiling data of PCa do not suggest molecular sub-classification based on luminal versus basal differentiation (13, 39).

Malignant progression of prostate cancer is a long, multi-step process that extends over decades (40). Studying the transformation of precancerous lesions is crucial for the understanding of carcinogenesis and the development of chemopreventive measures for PCa. It is widely accepted that most prostate adenocarcinomas develop from a precursor lesion known as prostatic intraepithelial neoplasia (PIN) (41). This lesion subsequently transforms into localized invasive adenocarcinoma and ultimately progresses to advanced metastatic PCa (38).

PIN is a neoplastic proliferation of prostatic epithelial cells within acini (glands) or ducts that results in a layer of crowded, pseudostratified, and irregularly spaced epithelial cells (42). PIN is classified into low-grade (LG) and high grade (HG) lesions. HG-PIN differs from LG-PIN by the presence of more prominent cytologic atypia (abnormality), especially the appearance of nucleoli (41). In contrast to adenocarcinoma, HG-PIN is a non-invasive pre-malignant lesion, similar to in situ carcinoma, which does not result in a growth of tumor mass or clinical symptoms (41, 43). Histologically, HG-PIN is distinguished from adenocarcinoma by the presence of basal cells, which are absent in PCa (44).

More than 50 genetic and molecular alterations have been identified in HG-PIN, which are either shared with PCa or intermediate between normal prostate and PCa (45). One of the most frequently reported mutations in HG-PIN is the loss of regions from chromosome 8p and gains at chromosome 8q (46, 47). Besides, HG-PIN is usually associated with dysregulation of cellular proliferation and survival balance, which could be partially explained by the overexpression of several oncogenic proteins and downregulation of tumor suppressor genes. For instance, elevated expression of the anti-apoptotic protein Bcl-2 is reported in a subset of HG-PIN lesions, which confers resistance to apoptosis during malignant transformation (48, 49). In addition, increased expression of Ki-67, a proliferation marker, and reduced expression of p27 (Kip1), a cyclin-dependent kinase inhibitor, were also detected in HG-PIN (43, 50). Other reported abnormalities include a reduction in expression of NKX3, a gene that is required for the development and differentiation of normal prostate, glutathione S-transferase P1 (GSTP1) hypermethylation, and overexpression of alpha-methyl acyl-CoA racemase (AMACR) (51-54).

Upon accumulation of mutations and molecular alterations, HG-PIN starts to progress to adenocarcinoma (47, 55). Many of the molecular and genetic abnormalities of HG-PIN are detected in carcinomas at a higher grade and frequency (38, 56). For example, ERG rearrangement, one of the PCa markers, is detected in 7-20% of HG-PIN while it is positive in 40-50% of PCa cases (57, 58). Besides, several alterations appear during progression, such as a reduction in PTEN, loss of Rb1 and increased telomerase activity (54, 59, 60).

1.1.3 Role of Androgens and Androgen Receptor (AR)

Androgens and androgen receptor (AR) signaling are pivotal for the development, differentiation and function of the normal prostate during fetal and adult

life (61). Similarly, AR signaling plays a central role in the initiation and progression of PCa (8). The role of androgen in PCa was demonstrated by Charles Huggins earlier in the 1940s. Huggins showed that surgical removal of testes (the source of >90% of circulating androgens) induces PCa regression and impressive improvement in symptoms (62). Since that time, androgen deprivation therapy (ADT) has become the cornerstone for the management of advanced PCa (63). Therefore, it is necessary to recognize the role of the AR signaling to have a good understanding of PCa biology.

Androgen receptor (AR) belongs to the steroid hormone group of the nuclear receptor family, which includes progesterone receptor (PR), estrogen receptor (ER), glucocorticoid receptor (GR) and mineralocorticoid receptor (MR). As a member of the steroid nuclear receptors family, AR is composed of three major functional domains: 1) ligand-binding domain (LBD), 2) DNA-binding domain (DBD) and 3) transactivation domain (TAD) (64, 65). AR works as a ligand-activated transcription factor that facilitates the expression of genes involved in growth, differentiation and survival (63, 65). The androgen hormones, testosterone and dihydrotestosterone (DHT), are the main endogenous ligands for AR. Around 95% of the testosterone is produced in the testis, while the remaining 3-5% are derived from adrenal glands (66). Testosterone could be converted to a more potent analog, DHT, by the 5-alpha-reductase enzyme in prostate tissues (67). Both testosterone and DHT can activate AR through binding to LBD (63).

In the absence of androgens, AR remains located in the cytoplasm in an inactive conformation where it is bound to molecular chaperones, particularly heat shock protein 90 (HSP-90) (8). Upon binding of hormones, AR dissociates from HSP-90, forms heterodimers, and translocates to the nucleus. AR-dimers then bind the promoter regions of target genes and facilitates their expression (8, 63). Prostate-specific antigen

(PSA) is among the primary transcribed genes and its serum level is used in the diagnosis and monitoring of PCa progression (67). In addition to the conventional (genomic) action, studies suggest that AR can also enhance cellular proliferation and survival directly by interacting with substrates in the cytoplasm and subsequently activating intracellular kinases (61, 68). This action is known as non-genomic signaling and unlike the genomic pathway, it induces immediate effect without transcription of AR target genes or synthesizing new proteins (61, 68). This crosstalk between AR and other signaling pathways could partially explain the development of resistance to hormone ablation and progression to metastatic PCa.

1.1.4 Castration-Sensitive Prostate Cancer

At the time of diagnosis, most PCa patients present with clinically localized disease that generally has a good prognosis (6). Therefore, treatment at this stage is generally confined to patients with a high risk of progression to advanced or metastatic PCa. Patients are stratified into different risk groups according to their clinical stage, pretreatment PSA level and Gleason score (69). Management options for localized PCa range from watchful waiting and active surveillance to radical prostatectomy, radiation and, less commonly, androgen deprivation therapy (ADT) (70, 71). Regardless of the selected management plan, around 30% of patients will still develop recurrence and progress to advanced and metastatic disease (72). In addition, 20% of the newly diagnosed PCa cases present with regional lymph node involvement or metastasis to distant organs (6).

Most of the previously untreated PCa cases are androgen-sensitive and rely on androgen signaling for their continued growth and progression (67). Therefore, androgen deprivation therapy (ADT) is considered the standard initial treatment for metastatic PCa (73, 74). The objective of ADT is to reduce serum testosterone levels

and thus the androgen available for binding with AR, which results in suppression of the transcriptional activity of AR. Androgen deprivation could be achieved either by surgical castration through orchiectomy (removal of testes) or reversible medical castration (73, 74).

Medical castration works on suppressing testosterone production in the testes by targeting the hypothalamic-pituitary axis. This approach involves the use of pharmacological treatments such as luteinizing hormone-releasing hormone (LHRH) agonists (e.g., leuprolide or goserelin) or LHRH antagonist (e.g., degarelix) (8, 74). In addition to ADT, anti-androgens (e.g., bicalutamide), which can directly bind to AR and block its signals, are sometimes added to neutralize the action of remaining androgens produced by adrenal glands (67, 75). Collectively, these therapies can induce PCa regression, normalize PSA level, and improve quality of life. However, the effect of ADT is transient, with a median response duration of 18-24 months (76, 77). Despite the initial effectiveness of ADT, eventually, all patients will develop resistance and progress to a lethal advanced form of the disease, termed as castration-resistant prostate cancer (CRPC) (78).

1.1.5 Castration-Resistant Prostate Cancer

PCa is classified as castrate-resistant if the patient presents with disease progression despite being managed with ADT and achieving chemical castration (testosterone serum level ≤ 50 ng/dL) (79). Evidence of disease progression could appear as either an asymptomatic increase in PSA serum levels (biochemical progression), growth of new metastatic lesion (radiographic progression), or development of cancer-related symptoms (clinical progression) (75, 80). Previously, CRPC was termed as androgen-independent or hormone-resistant PCa (81); however, recent data showed that in many cases, CRPC continues to rely on AR signaling despite

the depletion of systemic androgens (75, 82). Based on these findings, several therapeutic options were developed, but primary and secondary resistance have already been reported for most of these drugs.

1.1.5.1 Current CRPC Therapeutic Options

Today, metastatic CRPC (mCRPC) remains a major clinical challenge despite the emergence of several new therapeutic options in the past few years. The role of chemotherapy in mCRPC was not established until 2004, when the US Food and Drug Administration (FDA) approved docetaxel, a cytotoxic anti-microtubule agent, for the treatment of mCRPC (78, 83). Although several other cytotoxic chemotherapies (i.e., Cisplatin, 5-fluorouracil, Doxorubicin and Capecitabine) were studied in earlier trials, none was able to produce survival benefits and the objective response was observed in only 10-20% of the patients (84). Docetaxel approval was based on the results of phase III clinical trials, which showed a modest survival benefit of 2-3 months in mCRPC patients (85, 86). Since that time, docetaxel became the first-line treatment for mCRPC and remained the only available drug with a life-prolonging effect until 2010 (83). However, the survival benefit of docetaxel is limited, and the treatment resistance is inevitable. Moreover, docetaxel is highly toxic chemotherapy with a narrow therapeutic window that is associated with severe adverse drug reactions, including neutropenia, anemia, and hypersensitivity reactions (87, 88).

Over the past decade, five new drugs were approved by the FDA for the treatment of mCRPC. However, the approved drugs could not prolong the overall survival for more than five months (63, 89). Besides, many patients had intrinsic resistance and did not respond to the tested therapies. The approved drugs include three non-endocrine-based agents (cabazitaxel, sipuleucel-T and Alpharadin) and two AR axis targeted agents (abiraterone and enzalutamide).

First, cabazitaxel, a new semisynthetic taxane, was approved in 2010 for the treatment of patients who develop resistance to docetaxel (90, 91). Later in 2017, the FIRSTANA trial showed that cabazitaxel was non-inferior to docetaxel; thus, it is now considered as an option for some chemotherapy naïve mCRPC (69, 92).

In the same year, the first immunotherapy for mCRPC, sipuleucel-T, was approved for the treatment of mCRPC patients who are asymptomatic or have minor symptoms (69). Sipuleucel-T, also known as cancer vaccine, is autologous immunotherapy that works by programming patients' dendritic cells to target prostatic acid phosphatase (PAP), an antigen that is expressed in 95% of PCa tissues (93, 94). Although it resulted in overall survival improvement, sipuleucel-T was not associated with an increase in progression-free survival and did not induce short-term changes (95). Therefore, its use is confined to patients with slowly progressing disease, where rapid response is not needed (89).

Xofigo (radium-223) is another newly approved drug that could benefit a subset of mCRPC. Radium-223 is a calcium mimetic radioisotope that preferentially targets bone metastasis, the primary site of metastasis in PCa (96). Therefore, Radium-223 use is limited to patients with symptomatic bone metastasis with no evidence of visceral metastasis (69). While each of the previous therapies can prolong the overall survival by 2-4 months, none is curative and ultimately, most patients will develop resistance (63, 92, 95, 97).

In recent years, it becomes increasingly accepted that AR signaling continues to play a central role in the progression of a significant proportion of mCRPC cases. Although ADT could effectively deplete systemic androgen by 90-95%, it was shown that intratumor androgen levels decrease by only 50% (98, 99). Based on these findings and the improved understanding of AR signaling, second-generation AR axis targeted

(ARAT) agents that allow more potent inhibition of the AR axis were developed (100). Among this class, two drugs, abiraterone and enzalutamide, showed improvement in overall survival and were approved by the FDA for use in mCRPC.

Abiraterone works on depleting intratumor androgens by blocking cytochrome P450 17A1 (CYP17A1), an enzyme involved in adrenal and intra-tumoral de-novo biosynthesis of testosterone (8, 101). On the other hand, Enzalutamide is a nonsteroidal antiandrogen that target AR signaling through multiple sites. Similar to 1st generation antiandrogens, enzalutamide act as a competitive AR antagonist through directly interacting with LBD and blocking androgen binding, but it has a 5-8-fold higher binding affinity (67, 102). Besides, enzalutamide further blocks the AR axis by inhibiting AR translocation to the nucleus and binding to DNA, thus inhibiting tumor genes transcription (102, 103). Although enzalutamide and abiraterone resulted in a significant increase in overall survival (up to 4.8 months), around 20-40% had primary resistance and did not respond to them (82, 104, 105). In addition, the efficacy in responsive patients lasts for only a few months, upon which all would eventually develop secondary resistance. Refractory patients will not only have limited therapeutic options with unproven survival benefits; ARAT agents can induce significant changes in the biological characteristics of cancer cells, making future management of PCa challenging (106).

Recently, targeted treatments for minor mCRPC populations carrying certain mutations were approved by the FDA. In May 2020, rucaparib, a poly(ADP-ribose) polymerase (PARP) inhibitor, gained accelerated approval for use in patients with BRCA mutation-associated mCRPC who have been previously managed with ADT or chemotherapy (107). BRCA mutation carriers account for 5.3% of mCRPC patients and are known to have a poor prognosis and shorter overall survival than non-carriers (108).

Similarly, olaparib, another PARP inhibitor, was also approved in May 2020 for mCRPC with homologous recombination repair (HRR) alterations, including BRCA mutation (109). Besides, Pembrolizumab, a programmed cell death receptor 1 (PD-1) inhibitor, was approved in 2017 for advanced solid tumors, including PCa, with mismatch repair deficiency or microsatellite instability (89, 110). Mismatch repair mutations could be detected in 2-5% of mCRPC patients (69).

Despite the widening in the therapeutic landscape of mCRPC over the last decade, the disease remains largely incurable with limited survival benefit. Besides, a significant proportion of mCRPC patients fails to respond to current treatments and the remaining will ultimately develop resistance, mostly within a few months. Patients with mCRPC still have a poor prognosis with a median overall survival of 1-2 years (89). Therefore, there is an urgent unmet need for new effective therapeutic strategies.

1.1.6 Mechanisms Driving Castration Resistance

Whereas most of the initially diagnosed, hormone-sensitive PCa cases, have a good prognosis, mCRPC remains incurable and is associated with a poor prognosis. Therefore, understanding the molecular mechanisms behind progression to CRPC and resistance to treatment is crucial for developing new therapeutic strategies to overcome resistance and improve patients' survival. Extensive efforts were made attempting to understand the mechanisms behind castration resistance, yet it remains not entirely understood and a matter of ongoing research (8, 75, 78). These attempts resulted in identifying several genetic mutations and signaling alterations that could partially contribute to the development of resistance.

The identified mechanisms could be categorized according to their dependence on AR to three categories: 1) Persistent AR transactivation, 2) AR bypassing, and 3) AR indifference (106). While cancer cells continue to be dependent on the AR axis in

the first two mechanisms, either by direct activation of AR or indirect activation of downstream signaling through alternative pathways, AR signaling is completely lost in the third category.

1.1.7.1 Persistent AR Transactivation

Although ADT and second-generation ARAT agents have advanced the management of PCa, most patients eventually develop resistance. Several studies have shown that a considerable proportion of mCRPC cells remains dependent on AR-signaling despite the depletion of systemic androgens. These studies have pointed towards several possible escape mechanisms that can drive persistent AR activation in CRPC. AR-mediated resistance mechanisms include AR overexpression, increased sensitivity of AR, intertumoral synthesis of DHT, and AR somatic mutations (8, 106). In these mechanisms, cancer cells continue to rely on ligand-dependent activation of AR. Therefore, strategies involving more potent inhibition of AR, such as dose-escalation, combined AR targeted therapies and the development of new AR antagonists, are currently being investigated in clinical trials for the treatment of resistant cases (106).

On the other hand, ligand-independent activation of AR has also been reported as a potential resistant mechanism. One of the most investigated ligand-independent mechanisms is the presence of AR splice variants (e.g., AR-v7), which results in encoding truncated androgen receptor proteins that lack ligand-binding domain (LBD) but retain the N-terminal domain (NTD) and DNA-binding domain (DBD) (111). As a result, these proteins are constitutively active and are able to induce the transcription of AR target genes in an androgen-independent manner (111, 112). AR splice variants' role was clinically validated through the detection of AR-V7 in circulating tumor cells from mCRPC patients treated with abiraterone or enzalutamide (82, 111). Patients with

detectable AR-v7 had lower PSA response rates and poorer clinical outcomes. Since all the currently FDA approved ARAT agents inhibit AR through directly or indirectly targeting LBD, constitutively active AR splice variants confer resistance to all available ARAT medications. Novel drugs that could target AR through other domains, facilitate AR degradation, or inhibit AR dimer formation are being investigated as a means to overcome this debilitating resistance (106). However, they did not succeed in passing clinical trials until now. For instance, niclosamide, an FDA approved anti-helminthic drug, has shown potent anticancer activity in preclinical models of CRPC and effectively inhibited AR-v7, mainly through enhancing its degradation (113). A combination of niclosamide and enzalutamide was tested in phase I clinical trial, but the results were disappointing since the minimum plasma concentration required for achieving the antitumor activity could not be reached and the dose could not be further escalated due to toxicity limits (114). Similarly, EPI-506, an NTD inhibitor, was also tested in phase I/II study for the treatment of mCRPC, but the trial was discontinued due to adverse events. Other AR targeting agents (e.g., galeterone, seviteronel) were also tested but failed to show a significant improvement (115, 116).

1.1.7.2 AR Bypassing

As mentioned earlier, in section (1.1.4), AR belongs to the nuclear receptor family. Members of this family share similar basic structural components and mechanism of action. For instance, GR shares a highly similar DBD with AR and, as a result, can induce transcription of several AR target genes (117). Preclinical studies suggested that overexpression of GR induced by AR antagonism can mediate resistance against ARAT agents and docetaxel through bypassing AR (118). Besides, the upregulation of PR, another nuclear receptor family member, was correlated with PCa progression and recurrence, suggesting a possible role in resistance (119, 120).

1.1.7.3 AR indifference

1.1.7.3.1 Neuroendocrine Prostate Cancer

Whereas the majority of CRPC continues to rely on the androgen axis, a subset of recurrent cases loses AR expression and become completely androgen-independent (67). Accumulating evidence suggests that prolonged exposure to androgen ablation therapy promotes trans differentiation of prostate adenocarcinoma to neuroendocrine prostate cancer (NEPC), an extremely aggressive and lethal malignancy (121-123). Since epithelial cells in the prostate require AR signaling for their differentiation, blocking the AR pathway can trigger developmental reprogramming of prostate adenocarcinoma to NEPC (124, 125). Genomic profiling studies revealed significant overlaps between CRPC and NEPC in mutational and gene copy numbers, suggesting that NEPC is derived from adenocarcinoma precursors and were previously AR-dependent (106, 126, 127). In addition to androgen depletion, several cell growth and microenvironmental conditions such as long-term use of chemotherapy, ionizing radiation and adrenergic agents are thought to play a role in driving prostate cancer cells trans-differentiation (128, 129).

NE cells are characterized by the expression of neuroendocrine markers (synaptophysin, chromogranin, or CD56) and, in most cases, the absence of AR or PSA expression (55, 130). Besides, NE cells have the ability to secrete neuropeptides, such as serotonin and bombesin, which can act as an autocrine or paracrine growth factor and thus stimulate cancer cell proliferation (75, 131). However, NE cells typically remain quiescent and are rarely identified in primary prostate cancer cases (131). While neuroendocrine phenotypes are only detected in around 1% of primary PCa cases, they are detected in up to 25-30% of recurrent mCRPC who have been previously treated with ADT (128, 132). This dramatic increase in the prevalence of NE in CRPC suggests

possible transdifferentiation of adenocarcinoma cells to NE cells upon exposure to treatment (122). Therefore, these cancers are called treatment-related neuroendocrine prostate cancer (t-NEPC) and their incidence is expected to rise more sharply with the increased use of more potent AR targeted treatments (133). NEPC encompasses a heterogeneous group of tumors, including adenocarcinoma with NE differentiation, well-differentiated NE tumors, small-cell NE carcinoma and large cell NE carcinoma (134, 135).

Unlike prostate adenocarcinoma, NE tumors are highly aggressive, lack responsiveness to hormonal therapies and are associated with poor prognosis (136). While the incidence of t-NEPC is rising, survival rates of these patients have unfortunately remained constant over the last decade due to the lack of optimal therapies (137, 138). Similar to small cell lung carcinoma, first-line treatment for t-NEPC usually consist of platinum-based chemotherapy (133, 136). However, these agents do not induce long-term remission and cause significant toxicities(139). Several drugs are currently being developed to treat t-NEPC, but only a few reached clinical trials, including Alisertib, which did not succeed in meeting the primary endpoint. Thus, there is an urgent need to develop effective treatments for this subtype of PCa.

1.1.7.3.1 Prostate Cancer Stem-Like Cells

Cancer stem cells (CSCs) are a rare subpopulation of tumor cells featured by their stem cell-like characteristics, mainly self-renewal capacity, multilineage differentiation and ability to initiate tumor formation (75, 141). Thus, it is thought that CSC might be responsible for tumor recurrence, metastasis and therapeutic relapse (142, 143). The standard gold method for identifying the CSC population is by their capability to generate serially transplantable xenograft tumors that histopathologically resemble the parental tumor (144, 145). However, CSCs are more commonly identified

using surrogate markers of cancer stem-like properties, including unique cell surface biomarkers (e.g., CD44, CD133, integrin $\alpha 2\beta 1$) and tumor sphere-forming ability (146-148). Multiple studies demonstrated that prostate CSCs are AR-negative or express very low levels of AR, suggesting a possible role in progression to CRPC and lack of responsiveness to AR targeting agents (75, 147). Besides, several studies showed that CSCs possess resistance to most chemotherapies and radiation and, as a result, may survive and evolve following initial treatment (149-151). Therefore, targeting CSCs might help to overcome resistance, eradicate PCa and prevent tumor relapse.

1.1.7 Targeting Prostate Cancer Beyond AR

Several potent AR targeting agents were developed over the past decade, yet treatment resistance in PCa remains inevitable. Although the AR axis is an essential mediator in CRPC, it is not the only player (152). Alterations in alternative pathways as well were correlated with progression, metastasis and development of resistance in prostate cancer (75). Therefore, it becomes increasingly accepted that relying on AR as a single target for the treatment of PCa might not be sufficient for achieving the targeted outcomes (152-154). Moreover, the use of AR targeted treatments induces significant changes in cancer cell biology and leads to the accumulation of AR negative populations (106, 155). These cells are not only refractory to AR targeted treatments; they are also associated with more aggressive behavior and worse clinical outcomes (106). Upon continued blockage of AR, cancer cells try to adapt by upregulating alternative pathways that are known to play a role in carcinogenesis (75, 106).

Targeting other pathways early in the course of PCa treatment in combination with AR inhibitors is suggested as a potential strategy to prevent the accumulation of aggressive subpopulations (153, 156, 157). Besides, accumulating evidence showed that the current therapeutic strategy of using sequential AR targeting agents might

promote cross-resistance not only to AR targeting agents but possibly to all approved treatments, including taxane chemotherapy (157-159). Therefore, there is an urgent need for new therapies that could target alternative pathways to be used as a potential treatment for refractory PCa cases or as an adjuvant therapy to improve the efficacy of AR targeting agents.

1.1.8 Need for New Effective Therapeutic Options

Despite the impressive progress in the therapeutic landscape of mCRPC, the disease remains largely incurable and the survival benefits are unsatisfactory. Patients with mCRPC still have a poor prognosis, with most patients succumbing to cancer within 1-2 years (89). Being the second most frequently diagnosed malignancy among men, in addition to the poor survival in mCRPC, makes the lack of curative therapies a grand challenge. Therefore, there is an urgent need for new effective and safe therapeutic agents that could improve PCa patients' survival and quality of life.

One of the highly attractive scaffolds that are currently being investigated as potential multitargeted anticancer agents is chalcone. Due to their fascinating biological properties, chalcones rich plants were historically used in traditional medicine. Besides, population-based studies in countries with a high dietary intake of chalcones were correlated with a lower incidence of cancer (160). Therefore, chalcones could serve as excellent potential candidates for the development of new lead molecules or anticancer drugs.

1.2 Chalcones

Chalcones, also known as benzylideneacetophenone or 1,3-diphenyl-2-propen-1-ones, are open-chain flavonoids that are widely distributed in various plant species (Figure 1). The term “Chalcone” is derived from the Greek word “chalcos,” meaning

“bronze,” which represents the colors of the majority of natural chalcones (161). Chemically, the chalcone scaffold consists of two phenyl rings linked through a three-carbon α,β -unsaturated carbonyl bridge (C6-C3-C6) (162). Chalcones may exist as cis or trans isomers, of which trans isomer form is more thermodynamically stable, making it the predominant configuration of the chalcones (163, 164).

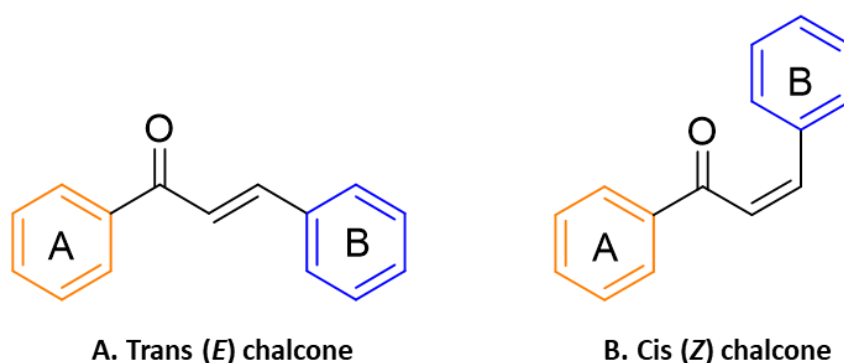


Figure 2. Chemical Structure of chalcone Scaffold.

Chalcone is an exceptional chemical scaffold with multifarious biological activities, including antidiabetic (165), anti-inflammatory (166), antimicrobial (167), antioxidant (168), antihypertensive (169) and anticancer (170). The variety in biological activity stems from the unique features of the chalcone skeleton. Chalcones are composed of numerous replaceable hydrogens that allow a large number of derivatives to be generated that differ in their specificity and reactivity with biological targets (162). Besides, the α,β -unsaturated ketone functional group in chalcone scaffold can act as a potential Michael acceptor, which may form covalent bonds with the sulfhydryl of cysteine or other thiols in different proteins modulating their functions (161). The extent to which different chalcones can act as Michael acceptors is affected by the presence/ absence of electron-withdrawing or donating functional groups. These groups affect the electron density on the two aromatic rings and, as a result, the enone's

electrophilicity for the reaction (161, 171). In addition to their interesting biological activities, chalcones have long fascinated medicinal chemists due to their ease of synthesis, numerous modification possibilities, poor interaction with DNA and low risk of mutagenicity (172, 173). Therefore, natural chalcones and their synthetic derivatives are widely exploited as targets in drug design and discovery projects.

1.2.1 Plant Derived Chalcones

Chalcones belong to the flavonoids family and are widely distributed in the plant kingdom. Natural chalcones act mainly as a floral pigment but were also found in the heartwood, bark, leaves, fruits and roots of various plant species (174). Chalcones are biosynthesized through shikimate and acetate pathways, where they serve as crucial intermediates in the biosynthesis of flavonoids and isoflavonoids (175). Besides, as end products, chalcones are considered major secondary metabolites that serve essential roles in protecting and regulating plants physiology, including pollination, pathogen protection, UV protection and insect repellent (176, 177). In addition, chalcones offer valuable health benefits to humans as nutraceuticals and display various attractive biological activities (175). Therefore, chalcone abundant plants, such as *Camellia sinensis* (Green tea), *Angelica*, *Glycyrrhiza*, *Piper* and *Ruscus* species, have long been used in traditional folk medicine across the world (172, 178).

Several pure chalcones were isolated from plants and were approved for use in humans (Figure 2). For instance, Metochalcone, a natural chalcone isolated from the heartwood of *Pterocarpus marsupium*, was approved for use as a choleric and diuretic agent (179). Similarly, sofalcone, a natural chalcone found in *Sophora tonkinensis*, was marketed as an anti-ulcer agent that increases secretion of mucosal prostaglandin, conferring a neuroprotective effect against *Helicobacter pylori* (180, 181). In addition, hesperidin methyl chalcone was tested in clinical trials as a treatment for venous

lymphatic insufficiency and is marketed in combination with two other active substances under the brand name “Cyclo 3 Fort” (182, 183).

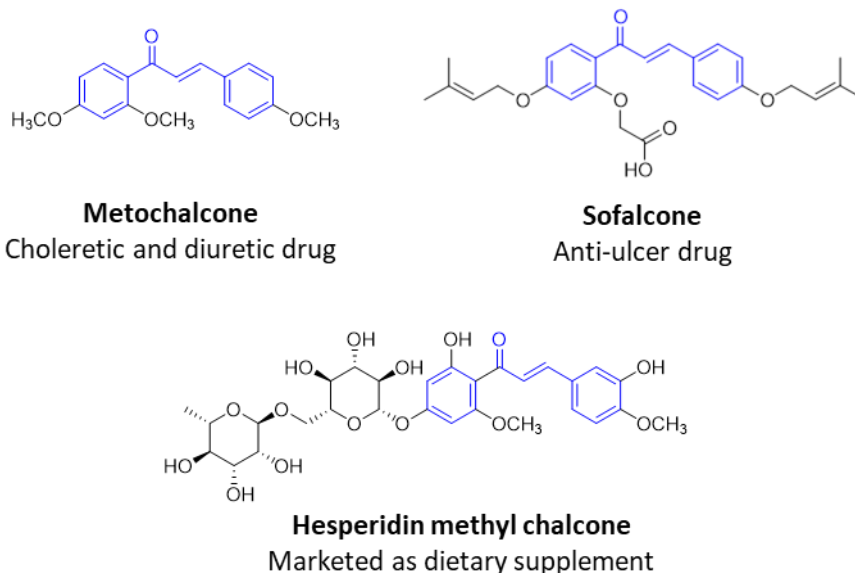


Figure 3. Structures of clinically approved chalcone based drugs.

1.2.2. Synthetic Chalcones

Although plants are considered a rich source of chalcones, isolation and purification of chemicals from nature are very complicated, requiring lengthy procedures and results in low yields. Therefore, chalcones' chemical synthesis is considered a valuable alternative to the tedious extraction procedures of natural products. In addition to simplifying the procedure, reducing time and cost, and improving the yield, chemical synthesis allows for generating a wider variety of chalcone derivatives that are not limited to naturally occurring chalcones.

Chalcones are typically synthesized by Claisene Schmidt condensation reactions in which an equimolar quantity substituted benzaldehyde react with substituted acetophenone under basic or acidic conditions (175, 184). In base-catalyzed reactions, acetophenones react with a base to give a highly reactive enolate anion. The

enolate will then attack the benzaldehyde forming an intermediate (aldol addition), followed by loss of water molecule (dehydration) to give a chalcone. In efforts to improve the yields and to achieve greener chemistry in chalcone synthesis, numerous researchers reported alternative reactions and methods to the traditional Claisen Schmidt condensation. These methods include Ultrasound and microwave-assisted synthesis, Suzuki-Miyaura reaction, Friedel-Crafts reaction, Julia-Kocienski reaction in addition to the green synthetic procedures like solvent-free synthesis, one-pot synthesis solid acid catalyst mediated synthesis (175, 184).

The successful application of natural chalcones as a potential treatment for various diseases has inspired synthetic chemists to develop novel synthetic chalcones with improved biological activities. Structural manipulation of chalcones traditionally focused on phenyl ring substitutions. A variety of chalcones were derived by substituting one or more aromatic protons with other functional groups such as aryls, alkyl, halogens amino-, nitro-, and carboxylic groups. Similar to naturally occurring chalcones, position and type of functional groups significantly altered the biological activities against different targets (185).

Recently, new strategies were applied for the design and development of chalcones in which the phenyl rings are completely replaced with heterocyclic rings or other scaffolds, resulting in chalcone hybrids (Figure 3) (186). Molecular hybridization is a relatively new concept in drug design (187). It involves combining pharmacophoric moieties of various bioactive molecules to produce new hybrid compounds with improved biological activity, selectivity, pharmacokinetic properties, safety profile and/or reduced drug resistance (188, 189). Several hybrid chalcones formulated by linking chalcones to other scaffolds with prominent anticancer activities such as pyrrole, coumarin, pyrimidine, and tetralone have demonstrated synergistic or additive

pharmacological activities (186). The successful application of molecular hybridization in discovering novel derivatives with improved anticancer activity makes hybrid molecule a rationally attractive target for current drug discovery projects.

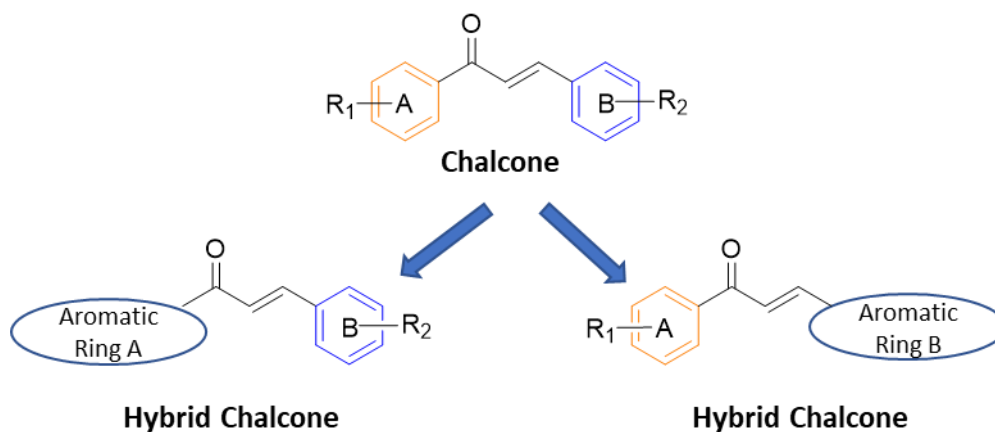


Figure 4. Molecular hybridization of chalcones.

1.2.3 Chalcone Derivatives as Potential Candidates for PCa Treatment

Various natural and synthetic-derived chalcones have shown promising anticancer activities against cell processes and signaling pathways involved in different stages of prostate carcinogenesis and other types of cancer. Cellular processes affected by chalcones include proliferation, apoptosis, cell cycle, angiogenesis, and metastasis. In addition, chalcones' antiproliferative activity was frequently associated with the modulation of cancer-related signaling pathways, including PI3k/Akt/mTOR, nuclear factor-kappa B (NF- κ B), and β -catenin/Wnt. Moreover, chalcones possessed cytotoxic activity against aggressive populations that are resistant to conventional cancer therapies, such as cancer stem cells. The wide distribution of chalcones in edible plants and their multitargeted nature suggests that chalcones might have a relatively wide therapeutic window and non-overlapping toxicities (185). Therefore, chalcone analogs could potentially serve as promising future anticancer drugs with improved efficacy

and safety profile for the treatment of PCa. This hypothesis is further supported by population-based studies, which showed a close inverse correlation between cancer incidence and the consumption of kava extract, a chalcone rich plant (190). Table 1. In appendix A. comprehensively lists all studies on chalcone derivatives that were tested against different prostate cancer *in vitro* and *in vivo* models. Below is a review of the main cellular processes and signaling pathways identified as potential targets for chalcones in PCa.

1.2.4 Promising Chalcone Targets in PCa

1.2.4.1 Apoptosis Signaling Pathways

Apoptosis, or programmed cell death, is a tightly regulated cellular process that plays a fundamental role in maintaining tissue homeostasis by eliminating aged or defective cells (191). Defects in this natural defense mechanism induce a loss of balance between cell survival and cell death, promoting malignant transformation and tumor growth (192, 193). Hence, evasion of apoptosis is a well-recognized hallmark of cancer and a vital component in treatment resistance. Apoptosis execution often results from the activation of a group of cysteine proteases called caspases, which can be triggered either by the intrinsic mitochondrial pathway or the extrinsic death receptor pathway (194). The extrinsic pathway is initiated by the attachment of cell-surface death receptors to apoptosis-inducing ligands, such as tumor necrosis factor (TNF), TNF-related apoptosis-inducing ligand (TRAIL), and Fas (CD95) (195). On the other hand, the intrinsic pathway is triggered by the mitochondrial release of cytochrome-c, which is regulated by members of the Bcl-2 protein family (196). Members of this family are classified based on their role to pro-apoptotic proteins (Bax, Bad, Bcl-Xs Bid, and Bim) and anti-apoptotic proteins (Bcl-2, Bcl-XL, and Mcl-1) (194). Although each pathway

utilizes a distinct signaling cascade for apoptosis initiation, both eventually converge at the point of caspase-3 activation, resulting in cleavage of essential cell survival substrates such as DNA and cytoskeletal proteins, and subsequently, cell death (197).

Alterations in apoptosis executors or regulating proteins are commonly reported in cancer, leading to apoptosis evasion. In PCa, dysregulation of apoptosis machinery was correlated with resistance to androgen-ablation and disease progression to a more aggressive cancer phenotype (198, 199). For instance, Bcl-2, an anti-apoptotic protein, was found to be overexpressed in androgen-independent PCa cases, allowing cells to survive in an androgen deficient environment (200). On the contrary, the expression of caspase-1 and -3 was significantly downregulated in PCa specimens as compared to normal prostate tissue (201). Moreover, PCa often confers intrinsic resistance to TRAIL-induced apoptosis due to alteration in chromosomal region 8p21-22 that code TRAIL receptor (DR5) or increase in anti-apoptotic proteins (202, 203). Since the majority of anticancer therapies involve the induction of apoptosis to eliminate malignant cells, dysregulation of apoptosis signaling pathways allows cancer cells to escape programmed cell death leading to uncontrolled proliferation and therapeutic resistance (195). Nevertheless, being a doubled-edge sword, defects in apoptosis pathways may also be potential targets for developing new cancer therapies (204). Treatments that can restore apoptotic signaling are expected to eradicate cancer cells directly by promoting apoptosis and indirectly by sensitizing cancer cells to other therapeutic agents.

A large spectrum of chalcone derivatives has demonstrated the ability to selectively induce apoptosis in PCa through modulating various apoptotic pathways. For example, several chalcones were found to reduce mitochondrial membrane potential in different PCa cell lines, leading to apoptosis induction (205-207). Effect on

the mitochondrial membrane was frequently accompanied by activation of caspase-3 and -9 (208), upregulation of pro-apoptotic proteins Bax and Bid (209, 210), and downregulation of anti-apoptotic protein Bcl-2 and Bcl-X (206, 209). Besides, studies have shown that some chalcones can also promote cancer cell apoptosis by targeting the extrinsic apoptosis pathway, particularly TRAIL-induced apoptosis (211-214). TRAIL is a natural endogenous anticancer agent that selectively induces apoptosis in cancer cells without affecting normal cells (215). However, some PCa cell lines are resistant to TRAIL-induced apoptosis (211). Ismail et al. demonstrated that 2'-Hydroxy-4-methylsulfonyl chalcone could restore sensitivity to TRAIL-induced apoptosis in TRAIL-resistant PCa cells (PC3 and LNCaP) (213). The effect of this compound was mediated through upregulation of TRAIL death receptor (DR5) and downregulation of Bcl-2. Similarly, Kłósek et al. showed a synergistic effect between xanthohumol, a prenylated chalcone, and TRAIL on the apoptosis of LNCaP cells (209). While treating the cells with 50 μ M xanthohumol or 50 ng/ml TRAIL resulted in only 11.1% and 12.57%, respectively, their combination significantly increased the percentage of apoptosis to 76.58%. These studies collectively show that chalcones could serve as promising primary or adjuvant potential therapeutic agents for PCa through induction of apoptosis or sensitizing resistant cells to other treatments.

1.2.4.2 Cell Cycle Signaling

The cell cycle is a highly organized and precisely controlled process that governs cell growth and division. The proliferation of cells involves four sequential phases of the cell cycle Gap 1 (G0/G1), DNA synthesis (S), Gap2 (G2) and mitosis (M), and multiple checkpoints that prevent uncontrolled proliferation and ensure the integrity of genetic material during cell division (216). The cell cycle is mainly regulated by a group of cyclin-dependent kinases (CDKs) and their heterodimeric

cyclin partners. CDKs are small serine/threonine kinases that, upon binding to cyclins, can phosphorylate and activate other proteins that trigger cells to advance to the next cell cycle phase (217). The Cyclin-CDKs complexes are negatively regulated by interaction with cyclin-dependent kinase inhibitors (CDKIs) such as P21 CIP1, P27KIP1, and P57Kip2 (218). The activity of CDKs is induced by mitogenic signals and inhibited by the activation of cell cycle checkpoints (216). When cell cycle checkpoints detect DNA damage or replication error, inhibitory signals are initiated, leading to cell cycle arrest until the problem is solved. If the damage was unreparable, the cells would be driven to senescence or apoptosis (219). Therefore, defects in cell cycle regulatory machinery lead to uncontrolled cell proliferation and promote neoplastic transformation.

Most if not all cancers show direct or indirect alterations in the cell cycle, making it one of the cancer hallmarks (220). Links between defects in the cell cycle and tumorigenesis have been reported for almost all regulatory proteins involved cell cycle (219). In prostate cancer, cyclin D1 was found to be highly expressed in androgen-independent PCa and was associated with tumor metastasis (221-223). Besides, loss of the CDK inhibitor p27 was detected in 16-68% of PCa cases and was significantly associated with aggressive tumor behavior (224). Given the high prevalence of cell cycle defects in PCa and their significant impact on tumorigenesis, designing new cancer therapies that target the cell cycle and its regulatory protein is proposed as a potential strategy for the treatment of PCa.

The antiproliferative activity of chalcones against PCa has been repeatedly linked with their effects on cell cycle progression in several studies. For instance, licochalcone-A was shown to reduce cyclin B1 and its catalytic partner cdc2 in PC3 prostate cancer cell line leading to cell cycle arrest at the G2/M phase (225). Similarly,

a dithiocarbamates-based chalcone led to G2/M arrest through upregulation of CDK inhibitor (p21) and downregulation of cyclin B1 and CDK1 (226). While the majority of chalcone derivatives result in G2/M cell cycle arrest, some studies reported G1 arrest as well. Sun et al. evaluated the antiproliferative activity of a methoxy-chalcone derivative against PC3 cell line (227). This compound induced time and concentration-dependent cell cycle arrest at the G1 phase, which was accompanied by a reduction in G1 regulators including cyclin D1, cyclin E, CDK-4, CDK-2, phosphor-retinoblastoma (Rb) tumor suppressor protein, E2F-1, and Cdc25A. Moreover, studies have shown that even the same chalcone derivative may have differential effects on the cell cycle when tested against various cell lines or time points. Isoliquiritigenin was shown to induce G1 or G2/M phase arrest in DU145 prostate cancer cell line when treated for 2 or 4 hours, respectively (228). Another study reported cell cycle arrest at G2/M phase in P53 mutant cells (22Rv1) and at G0/G1 in wild-type P53 cells (LNCaP and C4-2) upon treatment with a methoxy chalcone derivative (229). Regardless of the cell cycle targeting mechanism, chalcone induced cell cycle arrest eventually triggers apoptosis.

The ability of chalcones to bind with tubulin and subsequently disturb the microtubule network is another plausible mechanism that leads to the blocking of cell cycle progression. The anticancer activity of chalcones has been correlated with their affinity towards binding with tubulin, thereby disturbing mitotic spindles and halt mitosis (162). Similar to other antimitotic drugs, chalcones can target microtubule by blocking tubulin polymerization (like combretastatin and colchicine) or stabilizing microtubule and enhancing their polymerization (like taxanes). The use of chalcones as an inhibitor of microtubule assembly represents one of the earliest studied applications of chalcones (230). Several studies reported tubulin polymerization inhibition through binding to colchicine binding site, as evident through docking studies

(231-233). Hussain et al. synthesized a series of 1,2,3-triazole based chalcone analogs and evaluated their cytotoxicity against DU-145 prostate cancer cell line (233). These compounds showed potent inhibition of tubulin polymerization and induced cell cycle arrest at the G2/M phase. On the contrary, some studies reported an increase in tubulin polymerization (234). For instance, Shaffer et al. isolated a new iso-prenylated chalcone, named sanjuanolide, from *Dalea frutescens* with anticancer activity against AR-Prostate cancer cells with IC₅₀ 7-11 μM. Mechanistic studies on this compound revealed an increase in tubulin polymerization rate, which was accompanied by G2/M arrest (234). Regardless of the microtubule targeting mechanism, chalcones' interaction with tubulin was associated with G2/M arrest and antiproliferative activity. Thus, they can act as potential antimitotic agents.

1.2.4.3 Cell Migration, Invasion and Metastasis

While localized prostate cancer has a good prognosis, progression to metastatic PCa dramatically reduces the 5-year survival rate to 30.2% (6). Metastatic spread of cancer involves loss of cell-cell tight junctions, detachment of cells from the primary site, cell migration to nearby tissues, invasion into blood/lymphatic vessels, extravasation, and colonization at secondary tumor sites (235). At the molecular level, epithelial to mesenchymal transition (EMT) is thought to be an important mechanism responsible for metastasis (236). In this process, epithelial cells undergo morphological changes towards mesenchymal phenotype, where they transfer from cuboidal to spindle-shaped (237). Besides, they undergo gene's expression changes in which the mesenchymal markers (N-cadherin, fibronectin, and vimentin) get upregulated, and the epithelial markers (E-cadherin and occludins) get down-regulated (238). These changes lead to loss of cell-cell adhesion and gain of stemness and invasive properties, which are needed for metastasis (239). The EMT can be regulated directly or indirectly by

various signaling cascades and molecules, including transforming growth factor-beta (TGF- β), epidermal growth factor (EGF), Wnt/ β -catenin, NF- κ B, MAPK, and PI3K (237, 239).

Several chalcone derivatives were found to inhibit EMT and, subsequently, invasion of different types of cancer (170, 240, 241). In Prostate cancer, the role of chalcones in modulating EMT is less explored. Only one study reported EMT inhibition mediated anticancer activity in PCa. In this study, a novel series of dithiocarbamate based chalcones was found to reduce cell migration and inhibit EMT by upregulation of E-cadherin and downregulation of N-cadherin, activated-MMP9, activated-MMP2, and Vimentin in PC3 prostate cancer cell line (226). Although not directly studied, EMT inhibition could be an important mechanism in chalcones antiproliferative activity against prostate cancer. Different chalcone derivatives inhibited PCa cells' invasion and migration through targeting EMT regulating pathways or effectors such as VEGF, TGF- β , NF- κ B and MMP (242-245). Taken together, these findings indicate that chalcones can inhibit PCa cells migration, invasion and metastasis, potentially through inhibition of EMT.

1.2.4.4 Inhibition of Angiogenesis

Angiogenesis is the physiological process by which new blood vessels develop from pre-existing vessels. Uncontrolled angiogenesis is a key factor in cancer progression, invasion and metastasis (246). Although angiogenesis is not essential for cancer initiation, once the tumor grows beyond a few millimeters, blood vessel formation becomes crucial to supply cancer cells with the required nutrients and oxygen to support their viability and proliferation (247, 248). Tumors can initiate angiogenesis by altering the balance between pro-and anti-angiogenic signals (249). Vascular endothelial growth factor (VEGF) is among the main angiogenesis activator which

promotes endothelial cells proliferation and vascular permeability (250). In prostate cancer, overexpression of VEGF was associated with increased metastasis and resistance to radiotherapy (251-253). Therefore, angiogenesis is recognized as one of the cancer hallmarks and its inhibition is perceived as an attractive target strategy for cancer therapy.

Several antiangiogenic therapies were evaluated in clinical trials for the treatment of PCa; however, the results were inconsistent and mostly disappointing (248). Supplementation of hormone therapy with bevacizumab in hormone-sensitive PCa was associated with improvement in relapse-free survival, supporting the hypothesis that angiogenesis plays a role in PCa (254). However, when bevacizumab was used in combination with docetaxel and prednisone in CRPC, it did not improve overall survival and increased treatment-related deaths (255). Similar to bevacizumab, the use of other antiangiogenic (aflibercept, sunitinib, lenalidomide) in CRPC did not improve overall survival (256-258). Moreover, antiangiogenic therapies are typically used in combination with other therapies since they work by restricting tumor growth through inhibition of blood vessels and are not frequently associated with tumor eradication. (248) Therefore, efforts must be directed towards the development of safer and more effective antiangiogenic therapies that might target cancer through multiple modalities.

As a multitargeted agent with excellent antiangiogenic effect, chalcones might serve as a potential alternative for the current antiangiogenic therapies. For instance, Moon et al. have shown that 3,4,2',4'-Tetrahydroxychalcone (butein) dramatically inhibited tumor cell-induced angiogenesis through attenuation of VEGF and MMP-9 expressions (243). In this study, PC3 prostate cancer cells were mixed with Matrigel and implanted in mice. As compared to controls, butein -treated PC3 significantly

lowered blood vessel formation in the Matrigel Plugs (243). Although not directly linked to activity against prostate cancer, other studies reported chalcones with strong angiogenic inhibition on the chicken embryos' chorioallantoic membrane, which was associated with *in vitro* antiproliferative activity against other types of tumors (170, 259). Besides, Ma et al. developed a novel 3',5'-diprenylated chalcone that significantly downregulates VEGF, an important activator of angiogenesis, in PC3 prostate cancer cells (244). The same compound was found to reduce *in vivo* tumor growth of PC3 xenograft, suggesting that the antiangiogenic effect might be one of the mechanisms mediating the anticancer activity (260). Taken together, these findings suggest that chalcones might be potential antiangiogenic therapy for prostate cancer.

1.2.4.5 Androgen Receptor Signaling

Chalcones were investigated for their role in targeting AR in some studies (261-263). For instance, Jackson K. et al. tested the anticancer effects of Dibenzoylmethane, a chalcone, in PCa and reported a significant downregulation of AR protein and gene expression in a dose-dependent manner (261). Additionally, this chalcone derivative was also able to inhibit the secretion of prostate-specific antigen (PSA), which is an AR-regulated tumor marker (261). Another study reported the same effects on AR protein expression and downregulation of PSA expression with a different chalcone derivative, Isoliquiritigenin, which confirms that chalcones can target AR (262). Furthermore, an ionone-based synthetic chalcone was reported to exert a potent inhibitory effect in LNCaP PCa cell line (263). The molecule had also potently antagonized Dihydrotestosterone (DHT)-induced transactivation of the AR wild type (263). The same effect was also noted on clinically relevant W741C, H874Y and T877A mutated ARs (263). Taken together, these reported activities prove chalcone derivatives as potential candidates for treating AR naive PCa, as well as mutant and

advanced forms of the disease.

1.2.4.6 PI3k/Akt/mTOR Pathway

The PI3K/AKT/mTOR signaling pathway has an important role in several physiological and pathological conditions since it is responsible for the regulation of cell metabolism, survival and proliferation (264). The crucial components of this cascade are Phosphatidylinositide 3 kinases (PI3Ks) and their downstream mediators AKT and mammalian target of rapamycin (mTOR), which are closely interconnected and thus were regarded as a single pathway (264). Oncogenic activation of this cascade was reported to occur in PCa, which correlates with tumor growth, disease progression and resistance to therapy (264, 265). Several studies reported an elevated activity of PI3K-AKT-mTOR signaling in prostate cancer, which was reported to be more significant in CRPC (155, 266). Besides, genomic profiling has disclosed that genetic alterations of PI3K pathway components are very common in PCa patients, with a report of around 42% occurrence in primary and 100% occurrence in metastatic prostate cancer samples (155, 265, 267, 268). Chalcones were reported in the literature as potential therapeutic options against PCa targeting the PI3K/AKT/mTOR signaling pathway (207, 213, 227, 269-271). For instance, a chalcone derivative with methylsulfonyl and hydroxy substitutions was shown effective at overcoming tumor necrosis factor-related apoptosis-inducing ligand (TRAIL) resistance in PC-3 and LNCaP PCa cell lines (213). This molecule enhanced TRAIL-induced apoptosis through downregulating of PI3K/Akt, Bcl-2, NF- κ B, and cyclooxygenase-2 (COX-2) pathways (213). Isoliquiritigenin, which has been shown by numerous studies to act through different mechanisms of actions on PCa, was also reported to act on the PI3K/AKT/mTOR signaling pathway (269). Jung J. et al. reported that this molecule inhibited ErbB3 signaling and the PI3K/Akt pathway by reducing ErbB3 gene

expression and its phosphorylation inhibited the recruitment of the p85 regulatory subunit of PI3K to ErbB3 and reduced Akt phosphorylation (269). Since limited reports of these significant *in vitro* activities were performed *in vivo* (269), further investigations should be carried *in vivo* on these lead molecules to confirm their mechanisms of action on this signaling pathway and their role in PCa treatment.

In conclusion, discoveries on the anticancer properties of natural and synthetic molecules are continuously expanding. Chalcones are a class of organic molecules that can be extracted from natural or synthetic sources. Their underlying molecular anticancer bioactivities have been investigated in different types of PCa, including CRPC. A large body of evidence indicates that chalcone derivatives and analogs can simultaneously modulate multiple signaling pathways and cancer processes in different types of PCa and exert chemo-preventive potential. When combined with conventional chemotherapy, they were also shown to eliminate drug resistance and increase the efficacy of these medications. Taken together, the reported pharmacological actions of chalcones in PCa are impressive and hold promise to overcome the various drawbacks in current treatment options.

1.3 Study Objectives and Rationale

Today, mCRPC remains a major clinical challenge despite the emergence of several new therapeutic options in the past few years. Patients with mCRPC still have a poor prognosis with a median overall survival of 1-2 years. Therefore, there is an urgent unmet need for new effective therapeutic strategies.

Chalcones are among the highly attractive scaffolds being investigated for their antitumor activities in mCRPC. Particularly, molecular hybridization of chalcones with active pharmacophoric moieties attracted a great deal of interest due to their potential synergistic activities. Despite their ability to modulate multiple signaling pathways and

cancer processes, no chalcone had been moved into subsequent developmental steps for the treatment of PCa. This could be partially attributed to their poor pharmacokinetic profile, lack of selectivity and/ or modest potency.

Optimization of chalcones' activity through hybridization with heteroaromatic rings that are known to possess anticancer activity such as pyridine, pyrrole and thiophene may improve chalcones' efficacy and selectivity. Moreover, incorporating *in-silico* ADMET prediction early in the design process could increase the probability of identifying molecules with favorable physiochemical properties that are more likely to move along the drug development process. Combining both strategies simultaneously may lead to overcoming current chalcones' limitations. Therefore, we speculate that *In silico* guided development of new heteroaromatic-based chalcones could result in promising lead molecules with improved efficacy, safety and pharmacokinetic profiles for the treatment of mCRPC.

Objective 1: To design novel chalcone hybrids with potentially promising anticancer activities.

Objective 2: To conduct *in-silico* ADMET screening to eliminate analogs with low drug-likeness properties

Objective 3: To synthesize and elucidate the structures of the proposed chalcone analogs

Objective 4: To evaluate the anticancer activity of the synthesized chalcones in AR-negative prostate cancer cells

Objective 5: To investigate the antiangiogenic activity of chalcone analogs *in ovo* using the chorioallantoic membrane (CAM) of the chicken embryo model

CHAPTER 2: MATERIALS AND METHODS

2.1 Chemistry

2.1.1 Materials

All chemicals and reagents were obtained from Sigma-Aldrich (USA) unless stated otherwise and used without further purification. Solvents used in the synthesis and purification were of analytical or HPLC grade with purity >98% and were purchased from Sigma-Aldrich (USA) or Merck (Germany). The main used fine chemicals and solvents are listed in Table 2.1. Doubled distilled H₂O was prepared with a Milli-Q (Bedford, MA, USA) H₂O purification system. Thin-layer chromatography (TLC) was done on pre-coated silica gel aluminum plates from Sigma-Aldrich (USA). Prepacked Biotage® SNAP KP-SIL cartridges (Biotage AB, Sweden) were used for column chromatography.

Table 1.1 List of fine chemicals and solvents used in this study

Chemicals/ Solvents		
	Chemical Name	Molecular Weight (density g/ml)
Tetralones	5,8-Dimethoxy-1-tetralone	206.24
	5-Methoxy-1-tetralone	176.21
	6,7-Dimethoxy-1-tetralone	206.24
	6-Methoxy-1-tetralone	176.21
	7-Methoxy-1-tetralone	176.21
Acetophenones	2-Methoxyacetophenone	150.17
	3-Methoxyacetophenone	150.17 (1.094)
	4-Methoxyacetophenone	150.17
	3,4-Dimethoxyacetophenone	180.20
	2,3,4-Trimethoxyacetophenone	210.23 (1.155)
	2,4,6-Trimethoxyacetophenone	210.23
	3,4,5-Trimethoxyacetophenone	210.23
	4'-(Methylsulfonyl)acetophenone	198.24
	2-Hydroxyacetophenone	136.15 (1.131)
	2-(Trifluoromethyl)acetophenone	188.15 (1.255)
4-Fluoroacetophenone	138.14 (1.138)	
Carboxy-aldehydes	4-[Bis-(2-chloroethyl)amino]benzaldehyde	246.13
	Pyrrole-2-carboxaldehyde	95.10
	1-Cyclopropyl-1H-pyrrole-2-carbaldehyde	135.16
	6-Methoxy-2-pyridinecarboxaldehyde	137.14
	6-(Trifluoromethyl)pyridine-2-carboxaldehyde	175.11
	6-(3-Thienyl)pyridine-2-carboxaldehyde	189.23
	Thieno[3,2-b]thiophene-2-carboxaldehyde	168.24
Reagents	Sodium hydroxide (NaOH)	40.00
Solvents	Acetonitrile, chloroform, chloroform-d, dichloromethane, ethanol, ethyl acetate, hexane, isopropanol, methanol, toluene and diethyl ether	

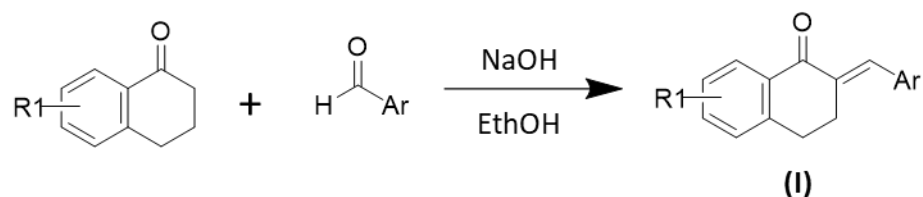
2.1.2 Design of Novel Chalcones

New series of hybridized chalcones were designed based on findings generated from previous work conducted in our lab and data from published literature on promising biologically active scaffolds. The novelty of the proposed compounds was checked through structure based-search (i.e., SciFinder) and chemical name-based search using relevant scholarly databases (e.g., ScienceDirect and PubMed). Inclusion in the study was limited to new analogs that were not investigated in any sort of application.

2.1.3 Chemical Synthesis

Chalcones were synthesized by Claisen–Schmidt condensation reaction (Figure 4). For each analog, appropriate aromatic carboxaldehyde (1mmol, 1 eq.) was added to a solution of methoxy substituted -tetralone or -acetophenone (1mmol, 1 eq.) and stirred until completely dissolved. The mixture was then cooled on Ice to 0°C and 0.5 ml of aqueous sodium hydroxide (3mmol, 3 eq.) was added drop wisely. Reaction mixtures were stirred at room temperature, for 1-72 hours, until completion of the reaction or an increase in the ratio of byproducts. Reactions progress was monitored by TLC using appropriate solvent mixture and visualized under UV light (254nm and 365nm).

A. Tetralone Based Chalcones



B. Non-cyclic chalcones

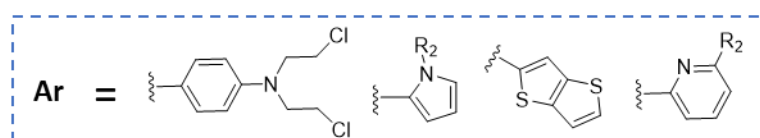
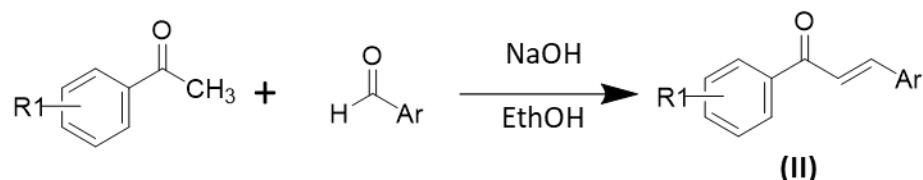


Figure 5. Synthetic scheme of (A) tetralone-based chalcones and (B) non-cyclic chalcone analogs; R1= OCH₃, OH, CF₃, SO₂CH₃; R2= OCH₃, CF₃, thienyl.

After completion, the formed precipitate was filtered, washed with cold water and ethanol and dried under vacuum. For compounds that do not form a precipitate, the solvent was evaporated under reduced pressure using the rotary evaporator, and the residue was neutralized with dilute HCl. Then, the product was extracted from the aqueous layer using ethyl acetate, followed by evaporation of the organic layer to isolate the product. Crude products were purified by recrystallization, column chromatography, Preparative-HPLC, flash chromatography, preparative-TLC or Sephadex L-H20 using different solvent systems (Figure 5).

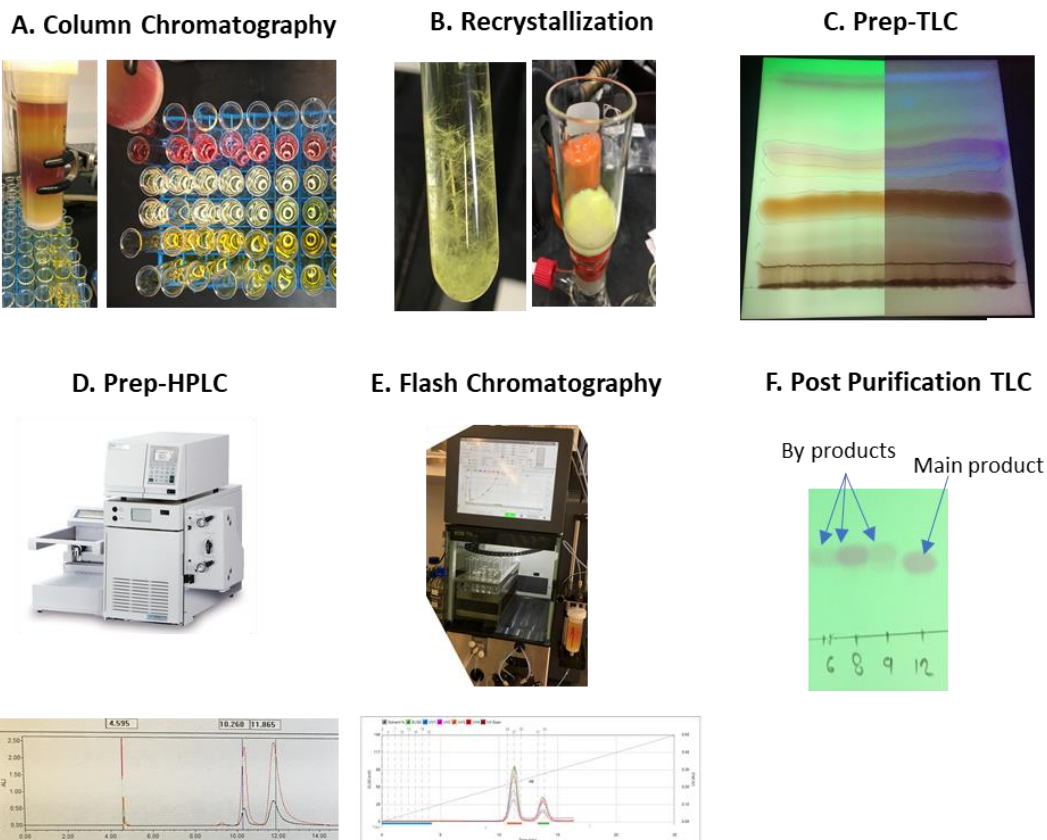


Figure 6. Illustration of the used purification techniques

2.1.4 Characterization and Structure Elucidation

2.1.4.1 Fourier Transform-Infrared analysis (FT-IR)

Infrared (IR) spectra were recorded using Perkin Elmer Spotlight 400 FTIR. All spectra were recorded at room temperature over the mid-infrared range ($4000\text{--}400\text{ cm}^{-1}$). FT-IR spectra were used to confirm the presence of the main functional groups in the synthesized analogs.

2.1.4.2 Mass Spectroscopy

Mass spectra were recorded on Agilent 6460 Triple Quadrupole Liquid chromatography-mass spectrometry (LC/MS) system combined with electrospray ionization (ESI) source. The analyses were performed using positive ionization mode (ESI+) with the capillary voltage set at 80 v and mass/charge (m/z) ratio acquisition in

the range 40–610 m/z. Samples were dissolved in acetonitrile and analyzed by direct infusion using 50% ACN: 50% of 0.1% Formic acid mobile phase at a flow of 0.5ml/min. The molecular weight of the synthesized compounds was confirmed by the presence of the molecular ion peaks at [M+1] +.

2.1.4.3 Nuclear Magnetic Resonance (NMR)

^1H NMR and ^{13}C NMR spectra were recorded on JEOL 600 MHz spectrometer at a frequency of 600 and 150 MHz, respectively, using chloroform-*d* or chloroform-*d* with/without 0.05% v/v of tetramethylsilane (TMS) as a solvent. Chemical shifts (δ) are expressed as parts per million (ppm) relative to the solvent peak (7.24 ppm for ^1H NMR and 77 ppm for ^{13}C NMR). ^1H - ^1H coupling constant (J) values are reported in Hz. Additional 2-dimensional (2D) ^1H - ^1H correlation spectroscopy (COSY) and ^1H - ^{13}C heteronuclear single quantum coherence (HSQC), ^1H - ^{13}C -Heteronuclear Multiple Bond Correlation (HMBC), ^1H - ^{15}N HMBC, ^1H - ^1H -nuclear overhauser effect spectroscopy (NOESY) NMR and 1D-NMR for ^{15}N and ^{19}F nucleus were conducted for selected samples to confirm the assignment of protons and carbons chemical shifts. NMR data were processed using Delta NMR Software, Version 5.1.3. (JEOL, USA). Multiplicities were described using the following abbreviations: s = singlet, d = doublet, t = triplet, q= quartet, dd = doublet of doublets, dt= doublet of triplets, td= triplet of doublets, m = multiplet, and b=broad. The full NMR spectra are available in Appendix B.

2.1.4.4 Elemental Analysis

Elemental analyses were carried out using Thermo Scientific FLASH 2000 CHN analyzer to aid in confirming molecular structures by calculating the percentage of C, H and N in each of the synthesized compounds.

2.2 Pharmacological Screening

2.2.1 Cell Culture

The synthesized compounds were screened against androgen-positive (LNCaP and C4-2) and androgen-negative (PC3 and DU-145) human prostate cancer cell lines. PC3 cell line was obtained from the American Type Tissue Culture (ATCC, Manassas, VA, USA). DU-145, LNCaP and C4-2 cell lines were a kind gift from Dr. Lotfi Chouchane (Weill Cornell Medical College in Qatar), which were originally purchased from ATCC. All cell lines were cultured in Gibco® RPMI 1640 with L-glutamine (Thermo Fisher Scientific, USA) supplemented with 10% Fetal bovine serum (FBS), 100 IU/mL Penicillin, and 100 µg/mL streptomycin (Thermo Fisher Scientific, USA), and maintained at 37°C in a humidified incubator with 5% CO₂. Cells were grown in T-75 tissue culture flasks and were routinely passaged when reaching confluency of 80-90% with a sub-culture ratio of 1:3 to 1:6. Cells were harvested using 0.25% trypsin EDTA and cryopreserved in growth media containing 5% dimethyl sulfoxide (DMSO) and supplemented with 35% FBS. The selectivity of the most potent compounds was tested against primary human dental bulb cells (ND), which is available in the lab, due to difficulty in ordering more relevant cells (i.e., human primary prostate epithelial cells) during the current pandemic.

2.2.2 Cell Viability

The *in vitro* cytotoxicity of the compounds was assessed by Alamar Blue assay (Invitrogen™, ThermoFisher Scientific, USA). Alamar Blue (resazurin) is a cell-permeable, weakly fluorescent blue dye that is reduced by mitochondrial enzymes in viable cells to resorufin, a highly fluorescent red molecule (Figure 6). Thus, it was used as a cell health indicator by measuring the reducing power of living cells, which

quantitatively reflects cell viability.

Briefly, cells were seeded into 96-well plates at a density of 5000 and 7500 cells per well for PC3 and DU145, respectively, in RPMI media supplemented with 10% FBS and incubated overnight. Once cells are attached, the culture media was aspirated and fresh media containing increasing concentrations of the synthesized compounds (1-40 μM), docetaxel (0.001 μM -100 μM), or vehicle (DMSO) was added and incubated for 48 hours. The final concentration of DMSO was $\leq 0.1\%$. After 48 hours, treatment was removed and 100 μL of 1:10 Alamar blue reagent in media was added to each well and incubated for 2-4 hours (optimized according to the metabolic activity of each cell line). Then, fluorescence intensity was measured using Infinite 200 PRO Microplate Reader (Tecan, Switzerland) at 560 nm excitation wavelength and 590 emission wavelength. Relative cell viability was calculated according to the following formula:

$$\% \text{ Viability} = \frac{\text{Fluorescence of treated wells} - \text{Blank}}{\text{Fluorescence of control wells} - \text{Blank}} \times 100\%$$

For most potent compounds, a dose-response curve was created and IC_{50} , the concentration the induced 50% reduction in viability compared to control, was computed by non-linear regression (curve fit) analysis using GraphPad Prism Software and were expressed as mean \pm SEM. Treatments were tested in 6 technical replicates, and each experiment was repeated independently three times.

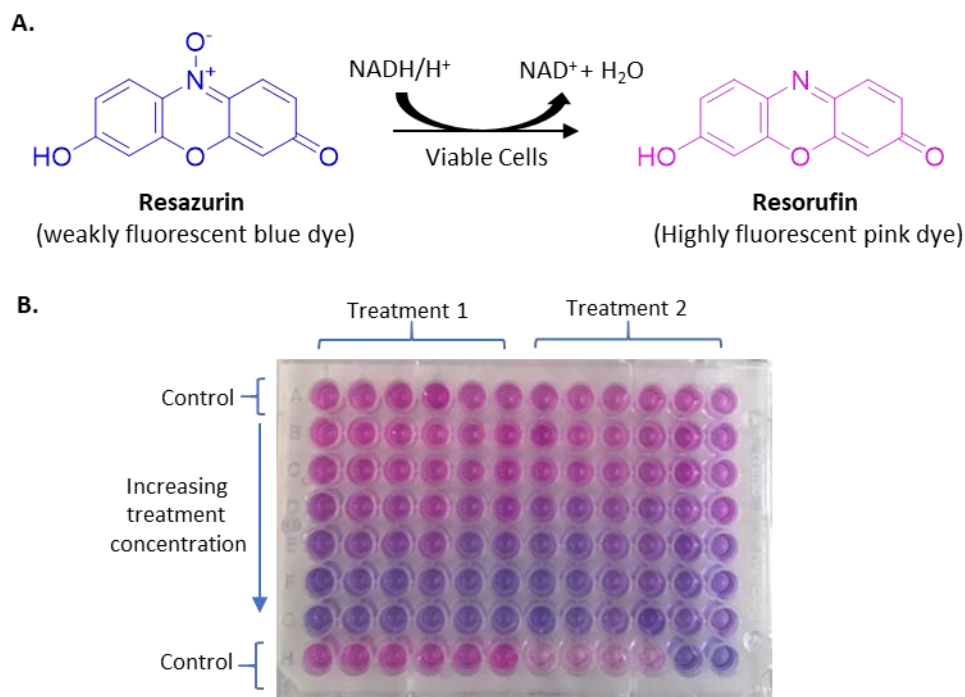


Figure 7. Illustration of Alamar Blue Assay. (A) Resazurin dye reduction by viable cells to resorufin. (B) Typical plate layout for dose-response evaluation.

2.2.3 Morphological Examination

Cells were seeded in 6 wells plate at a density of 150,000-200,000 cells/ well and were incubated overnight. Then, cells were treated with the synthesized compounds at 5-10 μM concentration for 48 hours. Morphological changes were monitored using a DMI8 inverted microscope (Leica, Germany) and images were captured with a Leica MC170 HD camera.

2.2.4 Annexin V Apoptosis Assay

Cellular apoptosis was assessed by PE Annexin V apoptosis Detection Kit (BD Pharmingen, USA) as per the manufacturer's protocol. Briefly, cells were seeded in 100mm Petri dishes at a density of 1.5 million cells/ dish and incubated overnight. On the next day, cells were treated with one of the three most potent compounds (**13**, **15**, and **16**), docetaxel or vehicle alone (DMSO) for 48 hours. Adherent and floating cells

were then harvested by trypsin, washed twice by PBS, resuspended in binding buffer and stained with Phycoerythrin (PE) conjugated Annexin-V, 7-AAD or both stains for 15 minutes. After staining, samples were analyzed by BD FACSAria™ II Flow Cytometer and FlowJo software. First, the cell population, excluding debris, was gated with forward scatter (FSC-A) and side scatter (SSC-A). Then, doublets were excluded using FSC-height and FSC-width plots. Singlet cells were then presented as dot plots of FITC-A (annexinV) against PerCP-Cy5.5-A (7-AAD) channels. Quad Gates were used to calculate the percentage of viable cells (annexin V low, 7-AAD low), early proapoptotic cells (annexin V high, 7-AAD low) and late apoptosis/dead cells (annexin V high, 7-AAD high).

2.2.5 Cell Cycle Analysis

The compounds' effect on cell cycle distribution of PC3 and DU145 was assessed by flow cytometry using propidium iodide (PI). Cells were seeded in 100mm Petri dishes at a density of 1.5 million cells/dish and incubated in RPMI supplemented with 10% FBS overnight at 37°C. Complete culture media was then removed, and cells were starved in serum serum-free for 16 hours to synchronize cells at the G0/G1 phase of the cell cycle. Subsequently, cells were treated with the compounds **13**, **15**, and **16** or docetaxel for 48 hours. After treatment, floating and adherent cells were collected, washed with ice-cold PBS and centrifuged at 500g for 10 minutes at 4°C. Next, cells were fixed with ice-cold 70% ethanol added drop wisely while vortexing and stored at -20°C for at least 24 hours. On the day of analysis, cells were pelleted (centrifuged at 800g for 10 minutes at 4°C), washed twice with ice-cold PBS and counted. Around one million cells of each sample were resuspended in 500µl of FxCycle PI/RNase staining solution® (Thermo Fisher Scientific, USA) supplemented with 200µg/ml RNase and

incubated for 50 minutes at 37°C in a shaking water bath, protected from light. Following incubation, cells were immediately analyzed by BD FACSAria™ II Flow Cytometer, at least 50,000 events were acquired for each sample. The proportion of cells in each cell cycle phase: G1, S and G2-M was determined using FlowJo software based on cells' DNA content as represented by histograms of PI signal intensity.

2.2.6 Colony Formation Assay

Anchorage-independent growth, a characteristic of transformed cells that correlate with *in vivo* tumorigenic potential, was assessed by soft agar assay. First, a 2% noble agar (Sigma-Aldrich) stock solution was prepared in deionized and autoclaved water. Next, 10,000 cells of PC3 or DU145 were seeded in duplicate in 1ml of 0.2% (w/v) agar in a complete RPMI medium containing 5-10µM of the compounds on top of a pre-solidified 0.4% agar layer in 6-well plates. Colony formation was monitored for 14-21 days, and images were captured from different fields every seven days using a DMI8 inverted microscope equipped with a Leica MC170 HD camera. After 14 days, the average number of colonies in each well was counted manually under the microscope and confirmed by ImageJ; only colonies with an area larger than 100µm² were counted to avoid the inclusion of non-proliferating dead cells. Besides, the size of colonies in each treatment condition was measured by ImageJ from at least six random fields per well. Colonies were then categorized according to their size into small (100-500 µm²), medium (500-1000 µm²) and large (>1000 µm²).

2.2.7 Wound Healing Assay

PC3 and DU145 cells were seeded in 6-well plates at a concentration of 400,000 cells/well and were grown to 80-90% confluence in a complete RPMI culture medium. Following, Cells were washed with PBS and incubated in serum-free RPMI for 4 hours. Then, the cell layer was scratched with a 20µl pipette tip and washed with PBS to

remove floating cells. Next, cells were treated with an increasing concentration of the compounds prepared in 0.5% FBS containing medium for 48 hours. Wound areas were imaged in six different locations for each well at 0, 24, 48 hours by DMI8 inverted microscope equipped with a Leica MC170 HD camera and quantified using ImageJ software. The average extent of wound closure was calculated by the following equation:

$$\% \text{ Wound closure} = \frac{\text{Wound area at 0h} - \text{Wound area at 48h}}{\text{Wound area at 0h}} \times 100\%$$

2.2.8 Trans-well Migration Assay

Trans-well migration assay was carried out in a multi-well permeable support system with 8.0µm-pore Polyethylene terephthalate (PET) membrane (BD Falcon™, USA). Briefly, 50,000 PC3 or DU-145 cells were suspended in 500 µL of serum-free RPMI medium, containing 5-10 µM of the compounds or vehicle, and loaded in the upper chamber. Lower chambers were filled with 600µL of complete growth medium (RPMI with 10% FBS) as a chemoattractant. Cells were allowed to migrate for 48 hours, after which non-migrating cells on the upper side of the chamber were removed with a cotton swab. Migrating cells were then fixed in 3.7% formaldehyde for 10 minutes, permeabilized with methanol for 5 minutes and stained with 0.5% crystal violet prepared in 2% ethanol for 15 minutes. Images were taken with an inverted microscope (10x objective) equipped with a digital camera. The average number of migrated cells from at least four random fields/well was quantified by ImageJ software.

2.2.9 Western Blot Analysis

PC3 and DU145 cells were seeded in 100mm Petri dishes at a concentration of 2.5 million cells/dish and incubated overnight. On the next day, cells were treated with

the synthesized compounds, vehicle (DMSO) or positive control (docetaxel), at concentrations of 5-10 μ M for 48 hours. Floating and adherent cells were then washed, harvested, lysed with sodium dodecyl sulphate (SDS) lysis buffer (0.5M Tris pH 6.8, 0.2% SDS) supplemented with Halt™ Protease and Phosphatase Inhibitor Cocktail (Thermo Fisher Scientific, USA), and stored at -20°C. Next, Cell lysates were sonicated and centrifuged at 16,000 g x 15 minutes at 4°C. Protein concentration was determined using the Pierce BCA Protein Assay Kit (Thermo Scientific, USA) according to the manufacturer protocol.

Proteins were separated on SDS–polyacrylamide gel electrophoresis (SDS-PAGE). First, cell lysates were mixed with Pierce™ Lane Marker Reducing Sample Buffer (Thermo Fisher Scientific, USA), boiled at 95°C for 10 minutes and 30mg of protein from each sample was loaded on 10% polyacrylamide gels. PageRuler™ Prestained Protein Ladder, 10-180kDa, (Thermo Scientific, USA) was used as a standard to estimate the size of the resolved proteins. After that, electrophoretic separation was performed using the Mini-PROTEAN Electrophoresis System (BioRad) in two steps, starting with 60 volts for 15 minutes, followed by 120 volts for 90-120 minutes. Afterward, proteins were transferred into 0.45 μ m PVDF membrane at 100 Voltage for 120 minutes and blocked with 5% BSA in TBS for one hour at room temperature. Next, membranes were incubated with different primary antibodies diluted 1:1000 in 1% BSA in TBS-T overnight at 4°C (Table), followed by three washes with TBS-T. The blots were then incubated with relevant secondary antibody diluted 1:1000 in 1% BSA in TBS, for 2 hours at room temperature, followed by three additional washes in TBS-T. Protein bands were developed by chemiluminescence using Pierce™ ECL Western Blotting Substrate and blots were imaged using ibrightCL1000 imaging system. Relative band intensities were quantified using ImageJ

software.

Table 2 List of used primary and secondary antibodies

No.	Antibody	Type	Source	MW of target protein	Manufacturer
1	Anti-Mouse	Polyclonal and monoclonal	Goat	NA	Cell Signaling Technology, Inc., USA
2	Anti-Rabbit	Polyclonal and monoclonal	Goat	NA	Cell Signaling Technology, Inc., USA
3	GAPDH		Rabbit	37 kDa	Abcam, USA
4	E-cadherin	Monoclonal	Mouse	135 kDa	Abcam, USA
5	β -Catenin	Polyclonal		92 kDa	Cell Signaling Technology, Inc., USA
6	Phospho- β -Catenin	Monoclonal		92 kDa	Cell Signaling Technology, Inc., USA
7	Fascin	polyclonal		54 kDa	Abcam, USA
8	Cleaved Caspase-3	Polyclonal	Rabbit	17 kDa	Abcam, USA
9	Bcl-2	Monoclonal	Mouse	26	Abcam, USA
10	Bax	Monoclonal	Mouse	23	Invitrogen, USA
11	ERK 1/2	Polyclonal	Rabbit	44, 42	Abcam, USA
12	P-ERK1/2 (Thr202,Tyr204)	Polyclonal	Rabbit	44, 42	Invitrogen, USA
13	Total Akt	Polyclonal	Rabbit	60	Cell Signaling Technology, Inc., USA
14	Phospho-Akt	Polyclonal	Rabbit	60	Cell Signaling Technology, Inc., USA
15	JNK1/2/3	Polyclonal	Rabbit	54	Abcam, USA

NA: Not Applicable

2.2.10 Chorioallantoic Membrane (CAM) Angiogenesis Assay

Fertilized white leghorn chicken eggs were obtained from Arab Qatari for Poultry Production, Doha, Qatar. Eggs were incubated in a rotary humidified MultiQuip Incubator at 37 °C with 60% humidity. Ethics approval was obtained from

Institutional Animal Care & Use Committee and Institutional Bio-safety committee at Qatar University. After 5 days of incubation, chicken embryos were treated with compound **16** or vehicle (DMSO). Briefly, eggshells were disinfected with ethanol and a small opening was made in the shell over the air sac. Next, 200 μ l of 1x PBS was added and the shell membrane was carefully removed. Then, 2 μ l of 10mM (3.21 μ g/ml) compound **16** stock solution or 2 μ L of DMSO were loaded on a round coverslip (0.5 cm²) and directly placed over the CAM. Subsequently, opened windows were sealed and the eggs were returned to a stationary incubator (Figure 7).

The effect of compounds on angiogenesis was monitored for 48 hours post-treatment and microscopic images of exposed (under coverslip) and unexposed area in each embryo were captured at equivalent magnification. Images were then analyzed using AngioTool software using the following parameters: vessel diameter thresholds at [10,255], vessel thickness at 7 and 10, removed small particles at 60, and filled holes at 183. The difference in blood vessel formation between treated and untreated embryos was assessed based on average vessel length, vessel percentage area and the total number of blood vessel junctions. To reduce the negative impact of variabilities between embryos, the exposed area in each embryo was first corrected to the unexposed area within the same embryo before being compared to untreated embryos. Besides, at least 15 embryos were treated in each group.

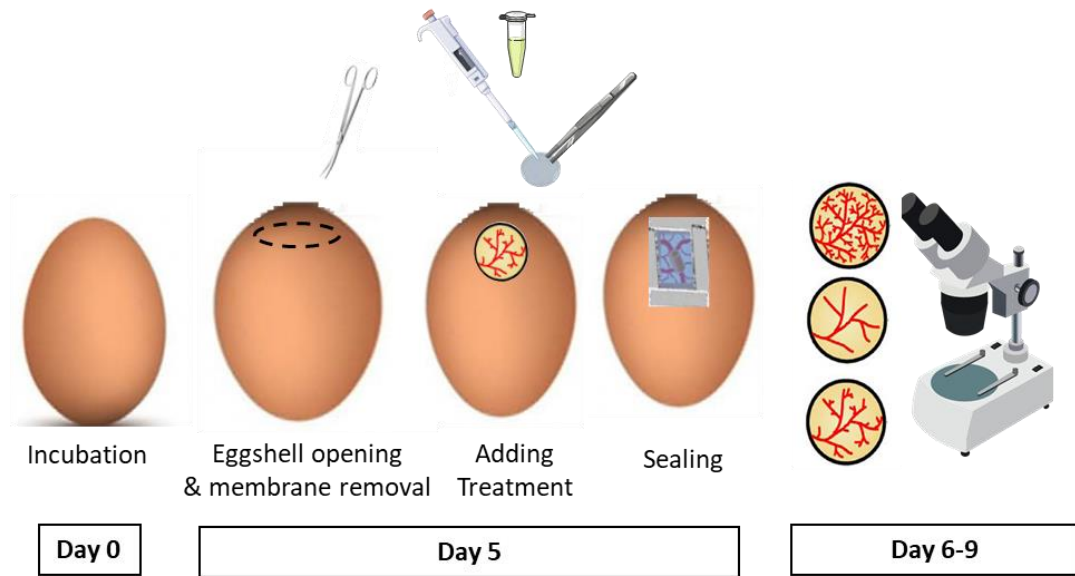


Figure 8. Timeline of CAM Angiogenesis Assay

2.2.11 Statistical Analysis

All data were analyzed by GraphPad Prism9 software. Data are presented as the mean \pm standard error of the mean (SEM) of three biologically independent experiments unless otherwise stated in figure legends. Two-group datasets were analyzed by Student's unpaired t-test. One-way analysis of variance (ANOVA) followed by Tukey's or Dunnett's posthoc tests were used to compare three or more groups. Tukey's posthoc test was used to compare treatment groups to each other, while Dunnett's test was used to compare treatment groups with the control only. Differences were considered statistically significant when P-values were <0.05 . For all the statistical analysis, * = $p < 0.05$, ** = $p < 0.01$, and *** = $p < 0.001$ unless otherwise stated in the figure caption.

CHAPTER 3: RESULTS

3.1 Chemistry

3.1.1 Design of novel chalcone derivatives

In an attempt to identify potential effective anticancer compounds, a novel (Bis-(2-chloroethyl) amine), nitrogen mustard, based chalcone (**DK14**) have been recently developed by our research group. The compound showed promising anti-proliferative activities *in vitro* against triple negative-breast cancer cell lines (IC₅₀ 6.3-9.22 μM) and *in vivo* in a nude mice xenograft model (170). Based on these findings, a US patent was recently filled (272).

In continuation of this effort, in this study, a new library of chalcone analogs was designed, aiming to improve the potency and the pharmacokinetic profile of the reported analogs. In the first series, we explored the effect of substituting the non-cyclic ketone in (Bis-(2-chloroethyl) amine) based chalcone (**DK14**) with a closed ring (tetralone), resulting in α -conformationally restricted (cyclic) chalcone analogs (Figure 8-A). Tetralone, also known as 3,4-dihydro-2H-naphthalen-1-one, is a promising scaffold that showed a wide range of biological activities such as antitumor, antibacterial, and antimalarial activity (273-275). Next, a second series was designed to investigate the effect of replacing the nitrogen mustard group in **DK14** with cyclopropyl pyrrole. This functional group might potentially act as a bio-isostere that retains similar or enhanced potency while improving the pharmacokinetic profile (Figure 8-B).

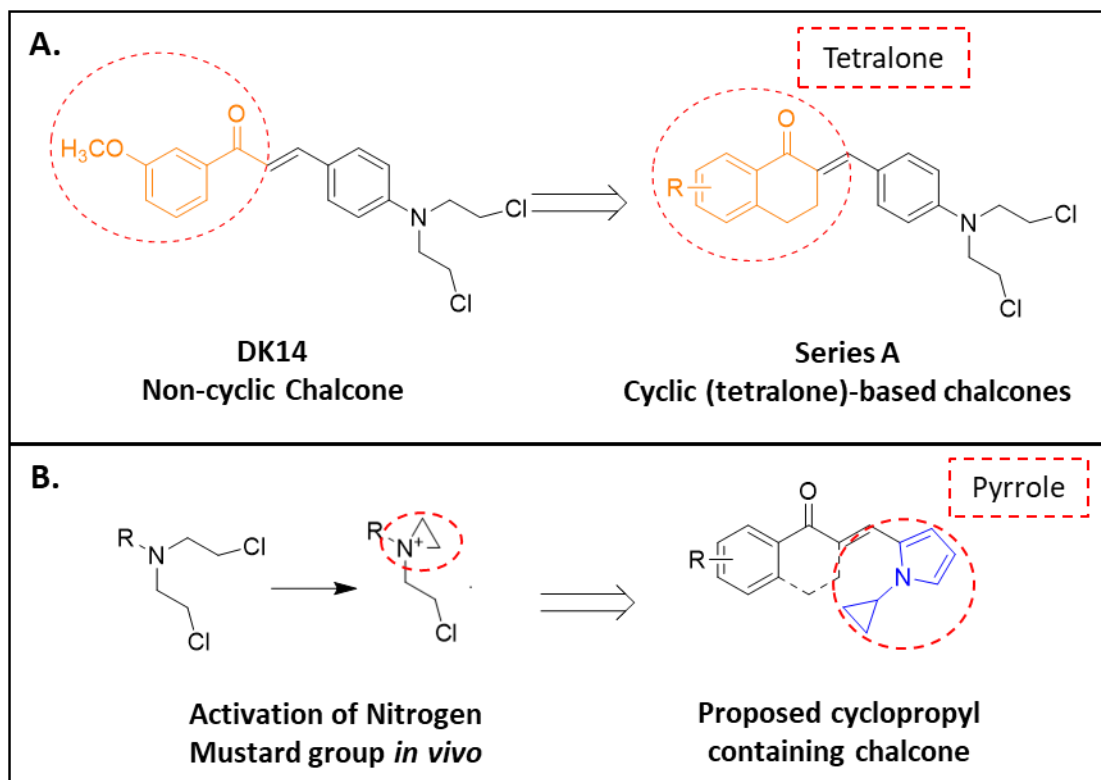


Figure 9. Design of nitrogen mustard tetralone-based chalcones (A) and cyclopropyl pyrrole-based chalcones (B).

Additionally, a new line of chalcone derivatives was designed through molecular hybridization of chalcones with pharmacologically active heterocycle rings, including pyrrole, pyridine, and thiophene (Figure 9). Similar to the first series, non-cyclic chalcones were compared to their corresponding cyclic chalcones by incorporating either aryl or tetralone rings, respectively.

The design process was guided by both *in silico* ADMET study findings and biological screening data. Hits showing promising ADMET profiles or biological activity were selected for expanded investigation in the subsequent phases of the project. The novelty of the proposed analogs was checked by both structure based-search as well as chemical name-based search. Analogs that were previously reported or synthesized were excluded from the study.

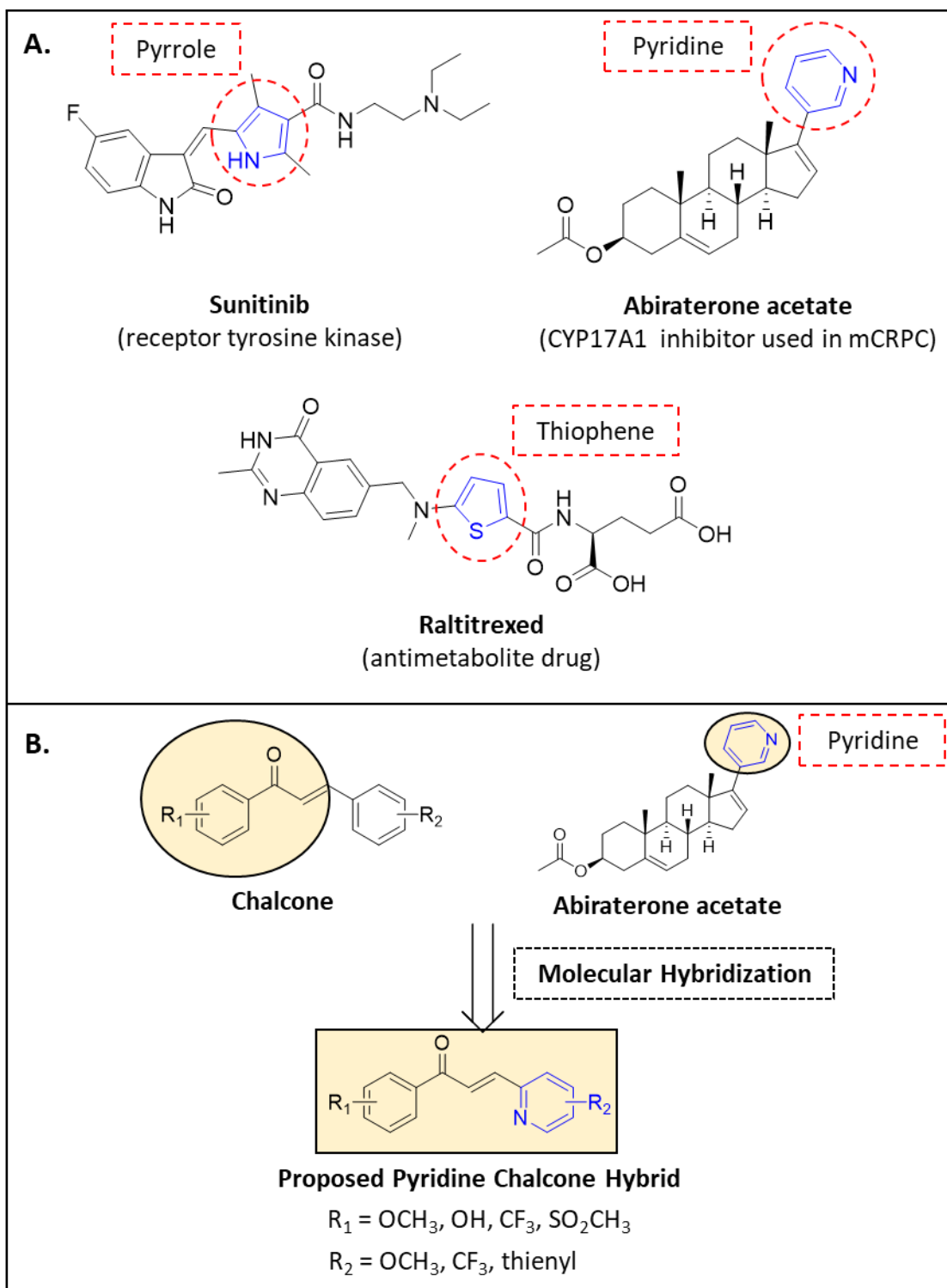


Figure 10. Examples of clinically approved drugs containing the heteroaromatic rings (pyrrole, pyridine, and thiophene) investigated in this study (A). The rationale for the design of pyridine-chalcone Hybrids (B).

3.1.2 Chemical Synthesis

The designed chalcone analogs were synthesized through base-catalyzed Claisen–Schmidt condensation reaction of substituted tetralone or acetophenone with substituted carboxaldehyde (Figure 4). The products were primarily collected by filtration and purified by appropriate chromatographic method (i.e., column chromatography, flash-chromatography, Prep-TLC, Prep-HPLC).

Twenty-six (**1-26**) novel chalcone analogs containing nitrogen mustard, pyridine, pyrrole, or thieno-thiophene in ring B and various electron-donating or withdrawing groups on ring A were successfully synthesized (Table 3 and Figure 10).

The time required for reactions to complete and the yield varied significantly between analogs. Tetralone-based chalcones took a significantly longer time to complete (>72 hours) and resulted in relatively low yields, mostly between 31-43%. On the other hand, the synthesis of non-cyclic chalcones took less time to complete and resulted in higher yields. Specifically, the synthesis of thienyl pyridine bearing chalcones completed in few hours and generated a yield of 65-87%.

Table 3. General structures and numbering of the synthesized chalcones

#	Scheme	Ar	R ₁	R ₂
1	I	A	5-OCH ₃	-
2	I	A	6-OCH ₃	-
3	I	A	7-OCH ₃	-
4	I	A	6,7-OCH ₃	-
5	I	A	5,8-OCH ₃	-
DK14	II	A	3-OCH ₃	-
6	I	B	6-OCH ₃	H
7	I	B	6-OCH ₃	cyclopropyl
8	I	B	6,7-OCH ₃	cyclopropyl
9	II	B	3-OCH ₃	cyclopropyl
10	I	D	6,7-OCH ₃	-
11	I	C	6,7-OCH ₃	OCH ₃
12	I	C	6,7-OCH ₃	CF ₃
13	I	C	6,7-OCH ₃	thiophen-3yl
14	I	C	6-OCH ₃	thiophen-3yl
15	I	C	7-OCH ₃	thiophen-3yl
16	II	C	3-OCH ₃	thiophen-3yl
17	II	C	2-OCH ₃	thiophen-3yl
18	II	C	4-OCH ₃	thiophen-3yl
19	II	C	3,4-OCH ₃	thiophen-3yl
20	II	C	2,3,4-OCH ₃	thiophen-3yl
21	II	C	2,4,6-OCH ₃	thiophen-3yl
22	II	C	3,4,5-OCH ₃	thiophen-3yl
23	II	C	2-CH ₃ SO ₂	thiophen-3yl
24	II	C	2-OH	thiophen-3yl
25	II	C	2-CF ₃	thiophen-3yl
26	II	C	4-F	thiophen-3yl

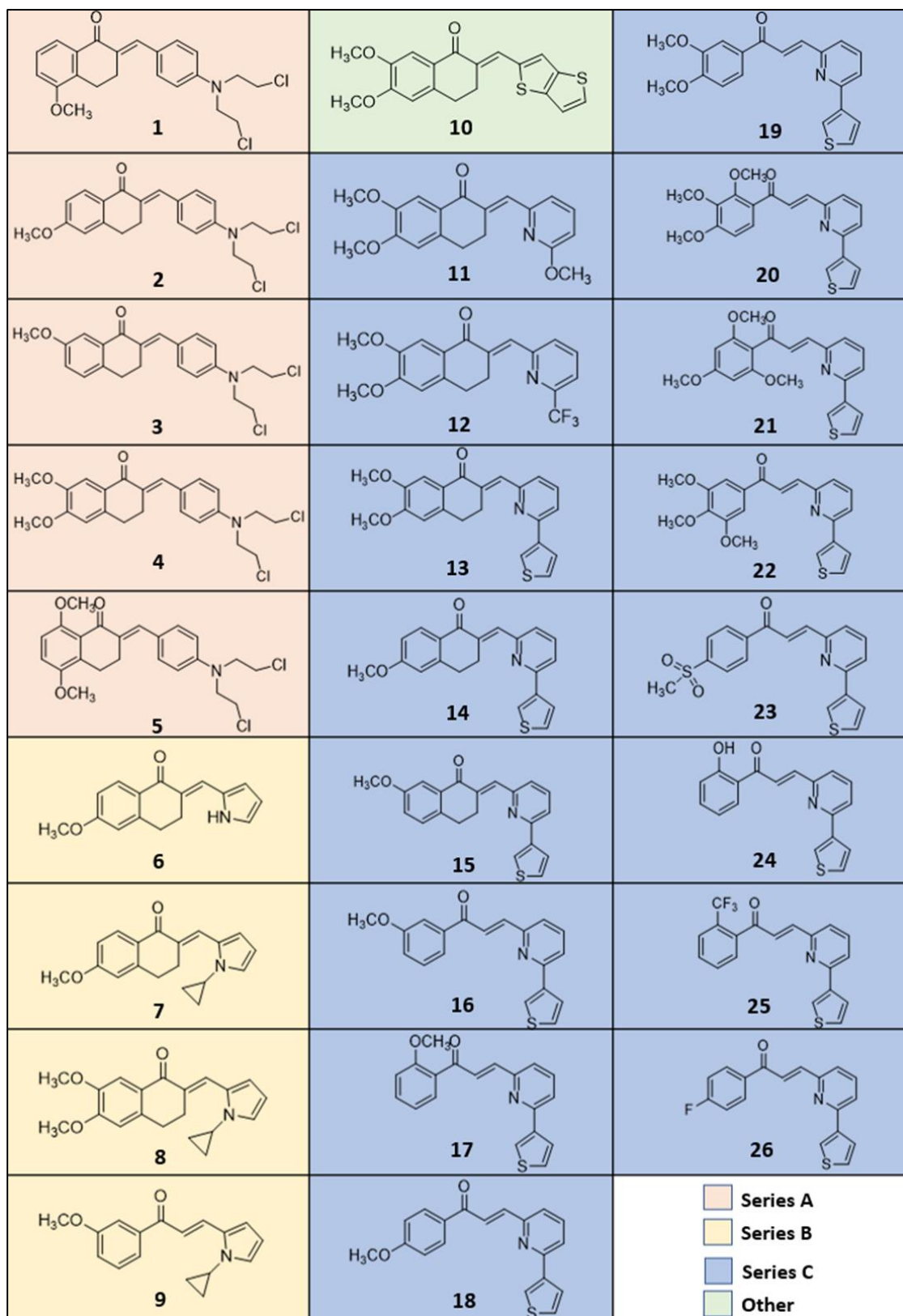


Figure 11. Chemical structures of the synthesized chalcone analogs. Structures are color-coded according to ring B substitution, nitrogen mustard (pink), pyrrole (yellow), thieno-thiophene (green), and pyridine (blue).

3.1.3 Structure Elucidation

The structures of the synthesized compounds (**1-26**) were elucidated by FT-IR, ¹H-NMR, ¹³C-NMR, ESI-MS and elemental analysis. The FT-IR spectra confirmed the presence of the major functional groups in the synthesized analogs. All chalcones exhibited a characteristic C=O stretching band at 1644-1662 cm⁻¹. The appearance of the C=O band at a lower wavelength than what is typically observed with ketones (>1700 cm⁻¹), confirms the conjugation of the carbonyl with C=C in chalcone structure. Another characteristic band shown by different chalcone analogs is the C=C stretching vibration between 1514-1610 cm⁻¹. We also noted C-N stretching bands at 1176-1178 in nitrogen mustard-containing analogs (**1-5**). The mass spectra (+ESI) of all compounds showed an [M+1]⁺ peak equivalent to their calculated molecular weights, suggesting a correct chemical composition. In addition, elemental analysis results (C, H, N) were relatively similar to the calculated values.

The configuration of the synthesized analogs was confirmed through ¹H-NMR. Typically coupling constant between α and β olefinic protons in α, β unsaturated ketones are used to differentiate between *E* and *Z* configuration where *E* isomer present with a larger coupling (*J*=15 Hz) than *Z* isomer (*J*=12 Hz). Proton NMR spectra of the synthesized α-unsubstituted (non-cyclic) chalcones (**9** and **17-26**) exhibited two doublets with a large coupling constant (*J*= 15.1-15.8 Hz), confirming (*E*) configuration. However, our tetralone-based chalcones (**1-8**, **10** and **13-16**) lack the α-olefinic proton, thus assignment based on the coupling is not possible. Therefore, alternative methods were needed to confirm the configuration. Inspection of the compound's (**8**) NOESY spectrum revealed correlations between β-olefinic proton and H-3 of the tetralone, which suggests (*E*) configuration. Besides, x-ray crystallography analysis of previously reported related tetralone-based chalcones confirmed *E*-configuration (276, 277). Due to steric interactions between the carbonyl and ring B in

chalcones, the formation of *E*-isomer was favored over *Z*-isomer in the majority of the reported chalcones.

Due to the presence of 2-3 distinct aromatic rings in the synthesized analogs and thus several overlapping aromatic proton peaks in the region of 7.0-8.0 ppm, 2D ^1H - ^1H COSY NMR in addition to 1D ^1H and ^{13}C NMR were run for all analogs to aid in peak assignment. Synthesis of multiple related analogs within each series enabled assignment with high confidence by comparing spectra of different analogs. Aromatic rings were distinguished by their characteristic J-coupling values and expected splitting pattern (Figure 11).

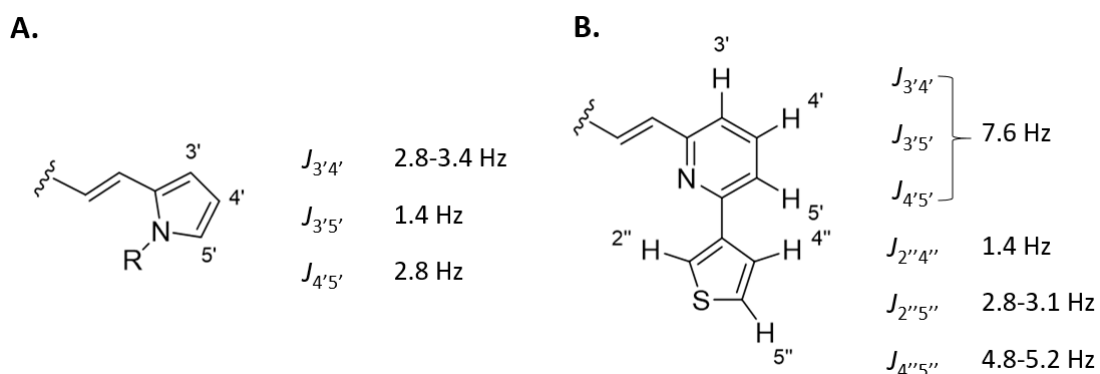


Figure 12. Characteristic coupling constants of (A) pyrrole ring (compounds **6-9**) and (B) thienyl pyridine rings (compounds **13-26**).

Additionally, 2D NMR experiments (COSY, HSQC, ^1H - ^{13}C -HMBC, ^1H - ^{15}N -HMBC and NOESY) were conducted for two representative analogs (**13** and **16**) for full assignment of carbons, protons and their connectivity (Figure 12). Notably, ^1H - ^{15}N -HMBC NMR of compound **13** showed a correlation between the nitrogen in the pyridine ring and β -olefinic proton, confirming its location within 2-3 bonds. Another NMR characteristic observation was noted in ^{13}C -NMR of compound (**25**). The presence of the CF_3 functional group was confirmed by the ^{13}C -NMR splitting of CF_3

and adjacent aryl carbons to quartets with large J -couplings of 274.5, 32.3 and 4.8, respectively. This observation was further confirmed by ^{19}F NMR, where a fluorine peak appear at -57.7 ppm consistent with the expected region for CF_3 (-50 to -70 ppm).

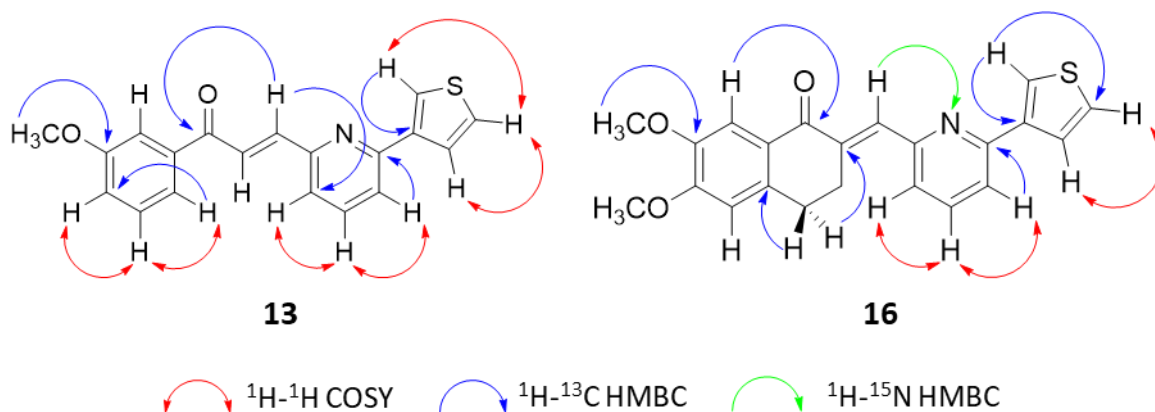


Figure 13. Key ^1H - ^1H COSY (red arrows), ^1H - ^{13}C HMBC (blue arrows) and ^1H - ^{15}N HMBC (green arrow) correlations of compounds **13** and **16**.

All spectra (FT-IR, ^1H -NMR, ^{13}C -NMR, ^{19}F -NMR, COSY, HMBC, HSQC, HMQC, NOESY, and ESI-MS) are included in Appendix B. The results of the characterization experiments for compounds **1-26** are summarized below.

1. (E)-2-(4-(bis(2-chloroethyl)amino)benzylidene)-5-methoxy-3,4-dihydronaphthalen-1(2H)-one (**1**)

Orange-brown semi-solid oil; yield: 31.0%; ^1H -NMR (CDCl_3 with 0.05% v/v of TMS, 600 MHz) δ 7.79 (s, 1H, β -olefinic), 7.74 (d, $J = 6.9$ Hz, 1H, H-8), 7.44 (d, $J = 9.0$ Hz, 2H, H-2' and H-6'), 7.31 (t, $J = 7.9$ Hz, 1H, H-7), 7.03 (d, $J = 7.6$ Hz, 1H, H-7), 6.72 (d, $J = 9.0$ Hz, 2H, H-3' and H-5'), 3.87 (s, 3H, OCH_3 -5), 3.79 (t, $J = 6.9$ Hz, 4H, N- CH_2), 3.67 (t, $J = 7.2$ Hz, 4H, Cl- CH_2), 3.12 (td, $J = 6.5, 1.4$ Hz, 2H, H-3), 2.92 (t, $J = 6.5$ Hz, 2H, H-4); ^{13}C -NMR (CDCl_3 , 150 MHz) δ 187.9, 156.1, 146.3, 136.6,

134.7, 132.3, 132.2, 131.9, 127.0, 125.2, 119.8, 114.0, 111.5, 55.7, 53.3, 40.2, 26.6, 21.2; FT-IR (KBr, cm^{-1}): 3072 (C=C-H), 2956, 2837 (C-C-H), 1659 (C=O), 1596, 575, 1514 (C=C), 1176 (C-N); Anal. calcd. for $\text{C}_{22}\text{H}_{23}\text{Cl}_2\text{NO}_2$: C, 65.35; H, 5.73; N, 3.46; Found: C, 64.53; H, 5.85; N, 3.44; LC-MS (+)-ESI (m/z): calculated 403.11, observed 404.0 $[\text{M}+1]^+$.

2. (E)-2-(4-(bis(2-chloroethyl)amino)benzylidene)-6-methoxy-3,4-dihydronaphthalen-1(2H)-one (2)

Dark yellow solid; yield: 40.1%; $^1\text{H-NMR}$ (CDCl_3 with 0.05% v/v of TMS, 600 MHz) δ 8.09 (d, $J = 9.0$ Hz, 1H, H-8), 7.79 (s, 1H, β -olefinic), 7.42 (d, $J = 9.0$ Hz, 2H, H-2' and H-6'), 6.87 (dd, $J = 9.0, 2.8$ Hz, 1H, H-7), 6.71 (d, $J = 9.0$ Hz, 2H, H-3' and H-5'), 6.70 (d, $J = 2.1$ Hz, 1H, H-5), 3.87 (s, 3H, OCH_3 -6), 3.79 (t, $J = 7.2$ Hz, 4H, N- CH_2), 3.66 (t, $J = 7.2$ Hz, 4H, Cl- CH_2), 3.14 (td, $J = 6.5, 2.1$ Hz, 2H, H-3), 2.91 (t, $J = 6.5$ Hz, 2H, H-4); $^{13}\text{C-NMR}$ (CDCl_3 , 150 MHz) δ 186.7, 163.3, 146.2, 145.4, 136.2, 132.4, 132.2, 130.6, 127.3, 125.3, 113.1, 112.2, 111.5, 55.4, 53.3, 40.3, 29.2, 27.3; FT-IR (KBr, cm^{-1}): 3013 (C=C-H), 2938, 2838 (C-C-H), 1658 (C=O), 1600, 1580, 1515 (C=C), 1185 (C-N); Anal. calcd. for $\text{C}_{22}\text{H}_{23}\text{Cl}_2\text{NO}_2$: C, 65.35; H, 5.73; N, 3.46; Found: C, 64.82; H, 6.07; N, 3.41; LC-MS (+)-ESI (m/z): calculated 403.11, observed 404.0 $[\text{M}+1]^+$.

3. (E)-2-(4-(bis(2-chloroethyl)amino)benzylidene)-7-methoxy-3,4-dihydronaphthalen-1(2H)-one (3)

Yellow-orange solid; yield: 43.2%; $^1\text{H-NMR}$ (CDCl_3 with 0.05% v/v of TMS, 600 MHz) δ 7.81 (s, 1H, β -olefinic), 7.61 (d, $J = 2.8$ Hz, 1H, H-8), 7.44 (d, $J = 9.0$ Hz, 2H, H-2' and H-6'), 7.15 (d, $J = 8.3$ Hz, 1H, H-5), 7.05 (dd, $J = 8.3, 2.8$ Hz, 1H, H-6),

6.72 (d, $J = 9.0$ Hz, 2H, H-3' and H-5'), 3.87 (s, 3H, OCH₃-7), 3.79 (t, $J = 6.9$ Hz, 4H, N-CH₂), 3.67 (t, $J = 7.2$ Hz, 4H, Cl-CH₂), 3.13 (td, $J = 6.5, 1.4$ Hz, 2H, H-3), 2.88 (t, $J = 6.5$ Hz, 2H, H-4); ¹³C-NMR (CDCl₃, 150 MHz) δ 187.6, 158.6, 146.4, 137.0, 135.6, 134.6, 132.3, 132.2, 129.2, 125.1, 121.0, 111.5, 110.3, 55.5, 53.3, 40.2, 27.9, 27.5; FT-IR (KBr, cm⁻¹): 3071(C=C-H), 2959, 2835 (C-C-H), 1652 (C=O), 1603, 1571, 1516 (C=C), 1177 (C-N); Anal. calcd. for C₂₂H₂₃Cl₂NO₂: C, 65.35; H, 5.73; N, 3.46; Found: C, 64.96; H, 5.77; N, 3.59; LC-MS (+)-ESI (m/z): calculated 403.11, observed 404.1 [M+1]⁺.

4. (E)-2-(4-(bis(2-chloroethyl)amino)benzylidene)-6,7-dimethoxy-3,4-dihydronaphthalen-1(2H)-one (**4**)

Yellow crystalline solid; yield: 36.2%; ¹H-NMR (CDCl₃ with 0.05% v/v of TMS, 600 MHz) δ 7.77 (s, 1H, β -olefinic), 7.62 (s, 1H, H-8), 7.42 (d, $J = 9.0$ Hz, 2H H-2' and H-6'), 6.71 (d, $J = 9.0$ Hz, 2H, H-3' and H-5'), 6.67 (s, 1H, H-5), 3.95 (2s, 6H, OCH₃-6 and OCH₃-7), 3.79 (t, $J = 6.9$ Hz, 4H, N-CH₂), 3.66 (t, $J = 7.2$ Hz, 4H, Cl-CH₂), 3.15 (td, $J = 6.5, 1.4$ Hz, 2H, H-3), 2.89 (t, $J = 6.5$ Hz, 2H, H-4); ¹³C-NMR (CDCl₃, 150 MHz) δ 186.7, 153.2, 148.1, 146.2, 137.8, 136.2, 132.2, 126.9, 125.3, 111.5, 109.7, 109.6, 56.1, 56.0, 53.3, 40.3, 28.5, 27.6; FT-IR (KBr, cm⁻¹): 3071 (C=C-H), 2934, 2835 (C-C-H), 1647 (C=O), 1599, 1567, 1507 (C=C), 1179 (C-N); Anal. calcd. for C₂₃H₂₅Cl₂NO₃: C, 63.60; H, 5.80; N, 3.22; Found: C, 63.50; H, 6.09; N, 3.20; LC-MS (+)-ESI (m/z): calculated 433.12, observed 434.0 [M+1]⁺.

5. (E)-2-(4-(bis(2-chloroethyl)amino)benzylidene)-5,8-dimethoxy-3,4-dihydronaphthalen-1(2H)-one (**5**)

Orange-brown solid; yield: 80.8%; ¹H-NMR (CDCl₃ with 0.05% v/v of TMS,

600 MHz) δ 7.78 (s, 1H, β -olefinic), 7.43 (d, $J = 9.0$ Hz, 2H, H-2' and H-6'), 6.98 (d, $J = 9.0$ Hz, 1H, H-7), 6.83 (d, $J = 9.0$ Hz, 1H, H-6), 6.70 (d, $J = 9.0$ Hz, 2H, H-3' and H-5'), 3.88 (s, 3H, OCH₃-5), 3.82 (s, 3H, OCH₃-8), 3.78 (t, $J = 6.9$ Hz, 4H, N-CH₂), 3.66 (t, $J = 6.9$ Hz, 4H, Cl-CH₂), 2.99 (td, $J = 6.7, 2.3$ Hz, 2H, H-3), 2.85 (t, $J = 6.5$ Hz, 2H, H-4); ¹³C-NMR (CDCl₃, 150 MHz) δ 187.0, 153.9, 149.4, 146.2, 135.8, 133.6, 133.4, 132.2, 125.4, 124.5, 115.3, 111.5, 110.4, 56.4, 56.2, 53.3, 40.2, 26.5, 21.3; FT-IR (KBr, cm⁻¹): 2994 (C=C-H), 2901, 2837 (C-C-H), 1661 (C=O), 1584, 1575, 1515 (C=C), 1178 (C-N); Anal. calcd. for C₂₃H₂₅Cl₂NO₃: C, 63.60; H, 5.80; N, 3.22; Found: C, 62.91; H, 6.04; N, 3.31; LC-MS (+)-ESI (m/z): calculated 433.12, observed 434.1 [M+1]⁺.

6. (E)-2-((1H-pyrrol-2-yl)methylene)-6-methoxy-3,4-dihydronaphthalen-1(2H)-one
(**6**)

Dark green crystalline solid; yield: 39.2%; ¹H-NMR (CDCl₃, 600 MHz) δ 9.23 (s, 1H, NH), 8.08 (d, $J = 9.0$ Hz, 1H, H-8), 7.86 (s, 1H, β -olefinic), 7.01 (td, $J = 2.8, 1.4$ Hz, 1H, H-5'), 6.88 (dd, $J = 8.6, 2.4$ Hz, 1H, H-7), 6.73 (d, $J = 2.1$ Hz, 1H, H-5), 6.67 (br, 1H H-3'), 6.38 (m, 1H, H-4'), 3.88 (s, 3H, OCH₃-6), 3.14 (td, $J = 6.7, 1.8$ Hz, 2H, H-3), 2.97 (t, $J = 6.5$ Hz, 2H, H-4); ¹³C-NMR (CDCl₃, 150 MHz) δ 186.3, 163.3, 145.5, 130.3, 129.3, 129.0, 127.4, 126.5, 121.5, 113.3, 113.1, 112.3, 111.2, 55.4, 28.5, 27.0; FT-IR (KBr, cm⁻¹): 3247 (N-H), 3100 (C=C-H), 2919, 2849 (C-C-H), 1644 (C=O), 1598, 1580, 1547 (C=C); Anal. calcd. for C₁₆H₁₅NO₂: C, 75.87; H, 5.97; N, 5.53; Found: C, 75.71; H, 6.17; N, 5.65; LC-MS (+)-ESI (m/z): calculated 253.11, observed 254.2 [M+1]⁺.

7. (E)-2-((1-cyclopropyl-1H-pyrrol-2-yl)methylene)-6-methoxy-3,4-

dihydronaphthalen-1(2H)-one (**7**)

Pale yellow solid; yield: 70.3%; ¹H-NMR (CDCl₃ with 0.05% v/v of TMS, 600 MHz) δ 8.17 (s, 1H, β-olefinic), 8.09 (d, *J* = 9.0 Hz, 1H, H-8), 6.88-6.87 (overlapped, 1H, H-5'), 6.87 (dd, *J* = 9.0, 2.8 Hz, 2H, H-7), 6.72 (d, *J* = 2.8 Hz, 1H, H-5), 6.56 (d, *J* = 2.8 Hz, 1H, H-3'), 6.21 (t, *J* = 3.4 Hz, 1H, H-4'), 3.87 (s, 3H, OCH₃-6), 3.39-3.29 (m, 1H, H-1''), 3.12 (td, *J* = 6.7, 1.8 Hz, 2H, H-3), 2.95 (t, *J* = 6.5 Hz, 2H, H-4), 1.12 (td, *J* = 7.1, 5.3 Hz, 2H, H-2a'' and H-3a''), 1.04-0.95 (m, 2H, H-2b'' and H-3b''); ¹³C-NMR (CDCl₃, 150 MHz) δ 186.1, 163.2, 145.3, 131.1, 130.4, 129.8, 127.5, 125.1, 124.7, 113.9, 113.0, 112.2, 108.8, 55.4, 28.5, 28.3, 27.3, 7.1; FT-IR (KBr, cm⁻¹): 3133, 3009 (C=C-H), 2939, 2835 (C-C-H), 1649 (C=O), 1599, 1582, 1570, 1494 (C=C); Anal. calcd. for C₁₉H₁₉NO₂: C, 77.79; H, 6.53; N, 4.77; Found: C, 76.33; H, 6.63; N, 4.8; LC-MS (+)-ESI (*m/z*): calculated 293.14, observed 294.2 [M+1]⁺.

8. (E)-2-((1-cyclopropyl-1H-pyrrol-2-yl)methylene)-6,7-dimethoxy-3,4-dihydronaphthalen-1(2H)-on (**8**)

Green crystalline solid; yield: 76.13%; ¹H-NMR (CDCl₃ with 0.05% v/v of TMS, 600 MHz) δ 8.17 (s, 1H, β-olefinic), 7.63 (s, 1H, H-8), 6.88 (dd, *J* = 2.8, 1.4 Hz, 1H, H-5'), 6.69 (s, 1H, H-5), 6.56 (d, *J* = 2.8 Hz, 1H, H-3'), 6.21 (t, *J* = 3.1 Hz, 1H, H-4'), 3.95 (2s, 6H, 2 OCH₃), 3.33 (m, 1H, H-1''), 3.13 (td, *J* = 6.7, 1.8 Hz, 2H, H-3), 2.94 (t, *J* = 6.5 Hz, 2H, H-4), 1.12 (td, *J* = 7.2, 5.2 Hz, 2H, H-2a'' and H-3a''), 1.05-0.96 (m, 2H, H-2b'' and H-3b''); ¹³C-NMR (CDCl₃, 150 MHz) δ 186.0, 153.1, 148.1, 137.7, 131.1, 129.5, 127.0, 125.0, 124.9, 113.8, 109.8, 109.5, 108.8, 56.00, 55.96, 28.3, 27.8, 27.4, 7.1; FT-IR (KBr, cm⁻¹): 3132, 3087, 3014 (C=C-H), 2936, 2836 (C-C-H), 1649 (C=O), 1602, 1572, 1506 (C=C); Anal. calcd. for C₂₀H₂₁NO₃: C, 74.28; H, 6.55; N, 4.33; Found: C, 74.05; H, 6.64; N, 4.45; LC-MS (+)-ESI (*m/z*): calculated 323.15,

observed 324.2 [M+1]⁺.

9. (E)-3-(1-cyclopropyl-1H-pyrrol-2-yl)-1-(3-methoxyphenyl)prop-2-en-1-one (9)

Yellow-brown oil; yield: 37.4%; ¹H-NMR (CDCl₃ with 0.05% v/v of TMS, 600 MHz) δ 8.07 (d, *J* = 15.1 Hz, 1H, β-olefinic), 7.57 (dt, *J* = 7.7, 1.3 Hz, 1H, H-6), 7.53 (t, *J* = 2.1 Hz, 1H, H-2), 7.38 (t, *J* = 7.9 Hz, 1H, H-5), 7.31 (d, *J* = 15.8 Hz, 1H, α-olefinic), 7.09 (ddd, *J* = 8.3, 2.8, 1.4 Hz, 1H, H-4), 6.88 (dd, *J* = 2.8, 1.4 Hz, 1H, H-5'), 6.78 (dd, *J* = 3.4, 1.4 Hz, 1H, H-3'), 6.17 (t, *J* = 3.4 Hz, 1H, H-4'), 3.87 (s, 3H, OCH₃-3), 3.39-3.30 (m, 1H, H-1''), 1.10 (td, *J* = 7.2, 5.3 Hz, 2H, H-2a'' and H-3a''), 1.03-0.98 (m, 2H, H-2b'' and H-3b''); ¹³C-NMR (CDCl₃, 150 MHz) δ 189.9, 159.8, 140.3, 133.1, 131.6, 129.4, 126.9, 120.7, 118.7, 116.8, 112.8, 109.4, 55.4, 28.3, 7.2; FT-IR (KBr, cm⁻¹): 3096, 3008 (C=C-H), 2934, 2835 (C-C-H), 1652 (C=O), 1567 (C=C); Anal. calcd. for C₁₇H₁₇NO₂: C, 76.38; H, 6.41; N, 5.24; Found: C, 75.45; H, 6.767; N, 5.34; LC-MS (+)-ESI (*m/z*): calculated 267.13, observed 268.1 [M+1]⁺.

10. (E)-6,7-dimethoxy-2-(thieno[3,2-b]thiophen-2-ylmethylene)-3,4-dihydronaphthalen-1(2H)-one (10)

Yellow solid; yield: 71.7%; ¹H-NMR (CDCl₃, 600 MHz) δ 8.01 (s, 1H, H-3'), 7.62 (s, 1H, H-8), 7.54 (s, 1H, β-olefinic), 7.48 (d, *J* = 4.8 Hz, 1H, H-5'), 7.28 (d, *J* = 4.8 Hz, 1H, H-6'), 6.71 (s, 1H, H-5), 3.97 (s, 3H, OCH₃), 3.96 (s, 3H, OCH₃), 3.24 (td, *J* = 6.5, 1.3 Hz, 2H, H-3), 3.00 (t, *J* = 6.5 Hz, 2H, H-4); ¹³C-NMR (CDCl₃, 150 MHz) δ 185.8, 153.4, 148.3, 142.2, 141.4, 139.4, 137.9, 132.0, 129.6, 126.7, 124.7, 119.5, 109.8, 109.6, 56.3, 28.1, 27.4; FT-IR (KBr, cm⁻¹): 3113, 3081, 3008 (C=C-H), 2930, 2835 (C-C-H), 1646 (C=O), 1597, 1568, 1508 (C=C); Anal. calcd. for C₁₉H₁₆O₃S₂: C, 64.02; H, 4.52; Found: C, 64.16; H, 4.48; N, 0.02; LC-MS (+)-ESI (*m/z*): calculated

356.05, observed 357.0 [M+1]⁺.

11. (E)-6,7-dimethoxy-2-((6-methoxypyridin-2-yl)methylene)-3,4-dihydronaphthalen-1(2H)-one (**11**)

Off-white solid; yield: 66.13%; ¹H-NMR (CDCl₃, 600 MHz) δ 7.63 (s, 1H, H-8), 7.62-7.57 (m, 2H, β-olefinic and H-4'), 7.06 (d, *J* = 7.6 Hz, 1H, H-3' or H-5'), 7.10 (s, 1H, overlapped, H-5), 6.69 (d, *J* = 7.6 Hz, 1H, H-3' or H-5'), 3.98 (s, 3H, OCH₃), 3.96 (2s, 6H, 2 OCH₃), 3.77-3.67 (m, 2H, H-3), 2.97 (t, *J* = 6.2 Hz, 2H, H-4); ¹³C-NMR (CDCl₃, 150 MHz) δ 187.1, 163.2, 153.5, 152.9, 148.1, 139.1, 138.8, 138.5, 132.8, 126.5, 120.8, 110.6, 109.9, 109.6, 56.1, 53.5, 28.6, 27.1; FT-IR (KBr, cm⁻¹): 3084 (C=C-H), 2920, 2850 (C-C-H), 1636 (C=O), 1609, 1582, 1509 (C=C); LC-MS (+)-ESI (*m/z*): calculated 325.13, observed 362.2 [M+1]⁺.

12. (E)-6,7-dimethoxy-2-((6-(trifluoromethyl)pyridin-2-yl)methylene)-3,4-dihydronaphthalen-1(2H)-one (**12**)

White solid ; yield: 67.0%; ¹H-NMR (CDCl₃, 600 MHz) δ 7.90 (t, *J* = 7.9 Hz, 1H, H-4'), 7.69 (t, *J* = 1.7 Hz, 1H, β-olefinic), 7.62 (s, 1H, H-8), 7.59 (dd, *J* = 7.9, 4.5 Hz, 2H, H-3' and H-5'), 6.71 (s, 1H, H-5), 3.97 (s, 3H, OCH₃), 3.96 (s, 3H, OCH₃), 3.63 (td, *J* = 6.5, 1.4 Hz, 2H, H-3), 2.97 (t, *J* = 6.5 Hz, 2H, H-4); ¹³C-NMR (CDCl₃, 150 MHz) δ 186.8, 155.9, 153.8, 148.3, 141.5, 139.4, 137.8, 130.7, 129.1, 126.2, 118.9, 109.9, 109.6, 56.13, 56.08, 28.4, 27.0; FT-IR (KBr, cm⁻¹): 3070 (C=C-H), 2928, 2839 (C-C-H), 1657 (C=O), 1588, 1511 (C=C); Anal. calcd. for C₁₉H₁₆F₃NO₃: C, 62.81; H, 4.44; N, 3.86; Found: C, 62.99; H, 4.60; N, 4.01; LC-MS (+)-ESI (*m/z*): calculated 363.11, observed 364.1 [M+1]⁺.

13. (E)-6,7-dimethoxy-2-((6-(thiophen-3-yl)pyridin-3-yl)methylene)-3,4-dihydronaphthalen-1(2H)-one (**13**)

Pale yellow solid; yield: 80.3%; ¹H-NMR (CDCl₃ with 0.05% v/v of TMS, 600 MHz) δ 7.94 (dd, *J* = 2.8, 1.4 Hz, 1H, H-2''), 7.81-7.70 (m, 3H, H-4', β-olefinic and H-4''), 7.65 (s, 1H, H-8), 7.55 (d, *J* = 8.3 Hz, 1H, H-5'), 7.42 (dd, *J* = 4.8, 2.8 Hz, 1H, H-5''), 7.32 (d, *J* = 7.6 Hz, 1H, H-3'), 6.71 (s, 1H, H-5), 3.96 (s, 6H, OCH₃-7 and OCH₃-8), 3.80-3.72 (m, 2H, H-3), 2.99 (t, *J* = 6.2 Hz, 2H, H-4); ¹³C-NMR (CDCl₃, 150 MHz) δ 187.1 (C=O), 155.2 (C-2'), 153.6 (C-7), 152.8 (C-6'), 148.2 (C-6), 142.3 (C-3''), 139.2, 139.1 (C-4a and C-2), 137.1 (C-4'), 132.9 (Cβ), 126.5 (C-5''), 126.29 (C-4''), 126.26 (C-8a), 125.2 (C-3'), 123.7 (C-2''), 119.0 (C-5'), 109.9 (C-5), 109.6 (C-8), 56.1 (O-CH₃), 56.0 (O-CH₃), 28.6 (C-4), 27.2 (C3); FT-IR (KBr, cm⁻¹): 3092 (C=C-H), 2918, 2851 (C-C-H), 1656 (C=O), 1586, 1508 (C=C), 1262 (C=S); Anal. calcd. for C₂₂H₁₉NO₃S: C, 70.01; H, 5.07; N, 3.71; Found: C, 68.54; H, 5.06; N, 3.74; LC-MS (+)-ESI (*m/z*): calculated 377.11, observed 378.9 [M+1]⁺.

14. (E)-6-methoxy-2-((6-(thiophen-3-yl)pyridin-2-yl)methylene)-3,4-dihydronaphthalen-1(2H)-one (**14**)

Beige solid; yield: 70.9%; ¹H-NMR (CDCl₃ with 0.05% v/v of TMS, 600 MHz) δ 8.14 (d, *J* = 8.3 Hz, 1H, H-8), 7.94 (dd, *J* = 2.8, 1.4 Hz, 1H, H-2''), 7.74 (t, *J*=7.6, 1H, H-4'), 7.73 (overlapped, 1H, β-olefinic), 7.71 (dd, *J* = 5.5, 1.4 Hz, 1H, H-4''), 7.55 (d, *J* = 7.6 Hz, 1H, H-5'), 7.42 (dd, *J* = 5.2, 3.1 Hz, 1H, H-5''), 7.32 (d, *J* = 7.6 Hz, 1H, H-3'), 6.89 (dd, *J* = 8.6, 2.4 Hz, 1H, H-7), 6.74 (d, *J* = 2.1 Hz, 1H, H-5), 3.88 (s, 3H, OCH₃-6), 3.75 (td, *J* = 6.5, 1.8 Hz, 2H, H-3), 3.02 (t, *J* = 6.2 Hz, 2H, H-4); ¹³C-NMR (CDCl₃, 150 MHz) δ 187.2, 163.6, 155.2, 152.9, 146.5, 142.3, 139.4, 137.1, 132.9, 130.8, 127.0, 126.3, 125.3, 123.7, 119.0, 113.3, 112.3, 55.4, 29.2, 27.0; Anal. calcd. for C₂₁H₁₇NO₂S: C, 72.60; H, 4.93; N, 4.03; Found: C, 71.33; H, 4.84; N, 4.13; LC-MS

(+)-ESI (m/z): calculated 347.10, observed 348.0 $[M+1]^+$.

15. (E)-7-methoxy-2-((6-(thiophen-3-yl)pyridin-2-yl)methylene)-3,4-dihydronaphthalen-1(2H)-one (**15**)

Fluffy off-white crystalline solid; yield: 73.9%; $^1\text{H-NMR}$ (CDCl_3 with 0.05% v/v of TMS, 600 MHz) δ 7.94 (dd, $J = 3.4, 1.4$ Hz, 1H, H-2''), 7.75 (t, $J = 7.6$ Hz, 1H, H-4'), 7.75 (overlapped, 1H, β -olefinic), 7.72 (dd, $J = 5.5, 1.4$ Hz, 1H, H-4''), 7.64 (d, $J = 2.8$ Hz, 1H, H-8), 7.56 (d, $J = 8.3$ Hz, 1H, H-5'), 7.42 (dd, $J = 5.2, 3.1$ Hz, 1H, H-5''), 7.33 (d, $J = 8.3$ Hz, 1H, H-3'), 7.20 (d, $J = 8.3$ Hz, 1H, H-5), 7.10 (dd, $J = 8.6, 3.1$ Hz, 1H, H-6), 3.88 (s, 3H, OCH_3 -7), 3.74 (td, $J = 6.5, 1.8$ Hz, 2H, H-3), 2.99 (t, $J = 6.5$ Hz, 2H, H-4); $^{13}\text{C-NMR}$ (CDCl_3 , 150 MHz) δ 187.2, 163.6, 155.2, 152.9, 146.5, 142.3, 139.4, 137.1, 132.9, 130.8, 127.0, 126.3, 125.3, 123.7, 119.0, 113.3, 112.3, 55.4, 29.2, 27.0; FT-IR (KBr, cm^{-1}): 3107 (C=C-H), 2927, 2833 (C-C-H), 1662 (C=O), 1597, 1579, 1494 (C=C), 1240 (C=S); Anal. calcd. for $\text{C}_{21}\text{H}_{17}\text{NO}_2\text{S}$: C, 72.60; H, 4.93; N, 4.03; Found: C, 66.35; H, 4.58; N, 3.91; LC-MS (+)-ESI (m/z): calculated 347.10, observed 348.0 $[M+1]^+$.

16. (E)-1-(3-methoxyphenyl)-3-(6-(thiophen-3-yl)pyridin-2-yl)prop-2-en-1-one (**16**)

White solid; yield: 72.7%; $^1\text{H-NMR}$ (CDCl_3 with 0.05% v/v of TMS, 600 MHz) δ 8.16 (d, $J = 15.8$ Hz, 1H, β -olefinic), 8.01 (dd, $J = 2.4, 1.0$ Hz, 1H, H-2''), 7.79 (d, $J = 15.1$ Hz, 1H, α -olefinic), 7.77-7.73 (m, 2H, H-4'' and H-4'), 7.70 (d, $J = 7.6$ Hz, 1H, H-6), 7.63 (d, $J = 8.3$ Hz, 1H, H-5'), 7.61 (dd, $J = 2.8, 1.4$ Hz, 1H, H-2), 7.49-7.41 (m, 2H, H-5 and H-5''), 7.36 (d, $J = 7.6$ Hz, 1H, H-3'), 7.16 (dd, $J = 8.3, 2.8$ Hz, 1H, H-4), 3.90 (s, 3H, OCH_3 -3); $^{13}\text{C-NMR}$ (CDCl_3 , 150 MHz) δ 190.6 (C=O), 159.9 (C-3), 153.6 (C-6'), 152.8 (C-2'), 143.1 (C- β), 141.9 (C3''), 139.4 (C-1), 137.5 (C-4'), 129.6 (C-5),

126.4, 126.3 (C-4'' and C-5''), 125.8 (C- α), 124.2 (C-2''), 123.4 (C-3'), 121.4 (C-6), 121.1 (C-5'), 119.6 (C-4), 112.8 (C-2), 55.5 (OCH₃); FT-IR (KBr, cm⁻¹): 3105 (C=C-H), 2999, 2933, 2833 (C-C-H), 1663 (C=O), 1615, 1600, 1575, 1524 (C=C), 1261 (C=S); Anal. calcd. for C₁₉H₁₅NO₂S: C, 71.01; H, 4.70; N, 4.36; Found: C, 71.19; H, 4.65; N, 4.43; LC-MS (+)-ESI (*m/z*): calculated 321.08, observed 322.8 [M+1]⁺.

17. (E)-1-(2-methoxyphenyl)-3-(6-(thiophen-3-yl)pyridin-2-yl)prop-2-en-1-one (17)

Pale yellow gummy mass; ¹H-NMR (CDCl₃ with 0.05% v/v of TMS, 600 MHz) δ 8.00-7.92 (m, 2H, H2'' and β -olefinic), 7.76-7.70 (m, 2H, H-4'' and H-4'), 7.65 (dd, *J* = 7.6, 2.1 Hz, 1H, H-6), 7.63-7.57 (m, 2H, α -olefinic and H-5'), 7.49 (td, *J* = 7.7, 1.8 Hz, 1H, H-4), 7.40 (dd, *J* = 5.2, 3.1 Hz, 1H, H-5''), 7.33 (d, *J* = 7.6 Hz, 1H, H-3'), 7.05 (t, *J* = 7.9 Hz, 1H, H-5), 7.01 (d, *J* = 8.3 Hz, 1H, H-3), 3.93 (s, 3H, OCH₃-2); ¹³C-NMR (CDCl₃, 150 MHz) δ 193.3, 158.3, 153.5, 153.2, 142.0, 141.9, 137.3, 133.0, 130.6, 130.3, 129.1, 126.3, 123.9, 122.7, 120.7, 120.6, 111.7, 55.7; LC-MS (+)-ESI (*m/z*): calculated 321.08, observed 322.2 [M+1]⁺.

18. (E)-1-(4-methoxyphenyl)-3-(6-(thiophen-3-yl)pyridin-2-yl)prop-2-en-1-one (18)

Fluffy white solid; yield: 78.7%; ¹H-NMR (CDCl₃ with 0.05% v/v of TMS, 600 MHz) δ 8.21 (d, *J* = 15.1 Hz, 1H, β -olefinic), 8.12 (dt, *J* = 9.4, 2.6 Hz, 2H, H-2 and H-6), 8.01 (dd, *J* = 2.9, 1.2 Hz, 1H, H-2''), 7.80-7.76 (m, 2H, α -olefinic and H-4''), 7.74 (t, *J* = 7.6 Hz, 1H, H-4'), 7.62 (d, *J* = 7.6 Hz, 1H, H-5'), 7.43 (dd, *J* = 4.8, 3.4 Hz, 1H, H-5''), 7.34 (d, *J* = 7.6 Hz, 1H, H-3'), 7.01 (dt, *J* = 9.4, 2.4 Hz, 2H, H-3 and H-5), 3.90 (s, 3H, OCH₃-4); ¹³C-NMR (CDCl₃, 150 MHz) δ 189.0, 163.56, 153.5, 153.0, 142.2, 142.0, 137.5, 131.0, 126.4, 126.3, 125.6, 124.1, 123.4, 120.9, 113.9, 55.5; FT-IR (KBr, cm⁻¹): 3109, 3091 (C=C-H), 2961 (C-C-H), 1660 (C=O), 1600, 1575, 1527, 1509

(C=C), 1248 (C=S); Anal. calcd. for C₁₉H₁₅NO₂S: C, 71.01; H, 4.70; N, 4.36; Found: C, 70.04; H, 4.77; N, 4.44; LC-MS (+)-ESI (*m/z*): calculated 321.08, observed 322.1 [M+1]⁺.

19. (E)-1-(3,4-dimethoxyphenyl)-3-(6-(thiophen-3-yl)pyridin-2-yl)prop-2-en-1-one
(19)

Fluffy white solid; yield: 87.3%; ¹H-NMR (CDCl₃ with 0.05% v/v of TMS, 600 MHz) δ 8.22 (d, *J* = 15.1 Hz, 1H, β-olefinic), 8.01 (dd, *J* = 3.4, 1.4 Hz, 1H, H-2''), 7.86-7.70 (m, 4H, H-6, α-olefinic, H-4'', H-4'), 7.68 (d, *J* = 2.1 Hz, 1H, H-2), 7.62 (d, *J* = 6.9 Hz, 1H, H-5'), 7.43 (dd, *J* = 5.2, 3.1 Hz, 1H, H-5''), 7.35 (d, *J* = 7.6 Hz, 1H, H-3'), 6.97 (d, *J* = 8.3 Hz, 1H, H-5), 4.00, 3.97 (2s, 6H, OCH₃-3 and OCH₃-4); ¹³C-NMR (CDCl₃, 150 MHz) δ 188.9, 153.5, 153.4, 153.0, 149.3, 142.2, 142.0, 137.5, 131.2, 126.4, 126.3, 125.4, 124.1, 123.5, 123.4, 120.9, 110.7, 110.0, 56.1, 56.0; FT-IR (KBr, cm⁻¹): 3103 (C=C-H), 2961, 2839 (C-C-H), 1660 (C=O), 1610, 1578, 1512 (C=C), 1270 (C=S); Anal. calcd. for C₂₀H₁₇NO₃S: C, 68.36; H, 4.88; N, 3.99; Found: C, 67.04; H, 4.84; N, 4.13; LC-MS (+)-ESI (*m/z*): calculated 351.09, observed 352.1 [M+1]⁺.

20. (E)-3-(6-(thiophen-3-yl)pyridin-2-yl)-1-(2,4,6-trimethoxyphenyl)prop-2-en-1-one
(20)

Off-white solid; yield: 49.8%; ¹H-NMR (CDCl₃, 600 MHz) δ 8.04 (d, *J* = 15.8 Hz, 1H, β-olefinic), 7.97 (dd, *J* = 3.4, 1.4 Hz, 1H, H-2''), 7.80-7.69 (m, 2H, H-4'' and H-4'), 7.66 (d, *J* = 15.8 Hz, 1H, α-olefinic), 7.60 (d, *J* = 7.6 Hz, 1H, H-5'), 7.53 (d, *J* = 9.0 Hz, 1H, H-6), 7.40 (dd, *J* = 4.8, 3.4 Hz, 1H, H-5''), 7.35 (d, *J* = 6.9 Hz, 1H, H-3'), 6.77 (d, *J* = 8.3 Hz, 1H, H-5), 3.99 (s, 3H, OCH₃-2), 3.93 (s, 3H, OCH₃), 3.92 (s, 3H, OCH₃); ¹³C-NMR (CDCl₃, 150 MHz) δ 191.1, 157.2, 154.0, 153.5, 153.3, 142.1, 142.0, 141.6,

137.3, 130.3, 126.5, 126.28, 126.25, 125.9 123.9, 122.7, 120.6, 107.2, 62.0, 61.0, 56.1; FT-IR (KBr, cm^{-1}): 3123 (C=C-H), 2964 (C-C-H), 1652 (C=O), 1601, 1582, 1526 (C=C); Anal. calcd. for $\text{C}_{21}\text{H}_{19}\text{NO}_4\text{S}$: C, 66.12; H, 5.02; N, 3.67; Found: C, 65.61; H, 5.11; N, 3.66; LC-MS (+)-ESI (m/z): calculated 381.10, observed 382.0 $[\text{M}+1]^+$.

21. (E)-3-(6-(thiophen-3-yl)pyridin-2-yl)-1-(2,4,6-trimethoxyphenyl)prop-2-en-1-one
(**21**)

White solid; $^1\text{H-NMR}$ (CDCl_3 , 600 MHz) δ 7.94 (dd, $J = 3.4, 1.4$ Hz, 1H, H-2''), 7.73-7.67 (m, 2H, H-4' and H-4''), 7.56 (d, $J = 7.6$ Hz, 1H, H-5'), 7.47 (d, $J = 15.8$ Hz, 1H, β -olefinic), 7.42-7.34 (m, 2H, α -olefinic and H-5''), 7.31 (d, $J = 7.6$ Hz, 1H, H-3'), 6.17 (s, 2H, H-3 and H-5), 3.86 (s, 3H, OCH_3 -4), 3.77 (s, 6H, OCH_3 -2 and OCH_3 -6); $^{13}\text{C-NMR}$ (CDCl_3 , 150 MHz) δ 194.6, 162.5, 158.9, 153.5, 153.4, 142.9, 141.9, 137.2, 132.4, 126.3, 124.0, 122.3, 120.5, 111.7, 90.7, 55.9, 55.4; FT-IR (KBr, cm^{-1}): 3104, 3052 (C=C-H), 2939, 2839 (C-C-H), 1635 (C=O), 1607, 1584 (C=C); Anal. calcd. for $\text{C}_{21}\text{H}_{19}\text{NO}_4\text{S}$: C, 66.12; H, 5.02; N, 3.67; Found: C, 65.64; H, 5.15; N, 3.68; LC-MS (+)-ESI (m/z): calculated 381.10, observed 382.0 $[\text{M}+1]^+$.

22. (E)-3-(6-(thiophen-3-yl)pyridin-2-yl)-1-(3,4,5-trimethoxyphenyl)prop-2-en-1-one
(**22**)

Pale yellow solid; yield: 58.0%; $^1\text{H-NMR}$ (CDCl_3 with 0.05% v/v of TMS, 600 MHz) δ 8.13 (d, $J = 15.1$ Hz, 1H, β -olefinic), 7.99 (dd, $J = 2.6, 1.2$ Hz, 1H, H-2''), 7.85-7.72 (m, 3H, α -olefinic, H-4 and H-4''), 7.64 (d, $J = 7.6$ Hz, 1H, H-5'), 7.43 (dd, $J = 4.8, 3.4$ Hz, 1H, H-5''), 7.37 (d, $J = 7.6$ Hz, 1H, H-3'), 7.34 (s, 2H, H-2 and H-6), 3.97 (s, 6H, OCH_3 -3 and OCH_3 -5), 3.95 (s, 3H, OCH_3 -4); $^{13}\text{C-NMR}$ (CDCl_3 , 150 MHz) δ 189.6, 153.6, 153.1, 152.8, 143.0, 142.7, 141.9, 137.6, 133.3, 126.4, 126.2, 125.5,

124.1, 123.4, 121.1, 106.3, 61.0, 56.4; LC-MS (+)-ESI (m/z): calculated 381.10, observed 382.1 $[M+1]^+$.

23. (E)-1-(4-(methylsulfonyl)phenyl)-3-(6-(thiophen-3-yl)pyridin-2-yl)prop-2-en-1-one (**23**)

Fluffy pale yellow solid; yield: 79.1%; $^1\text{H-NMR}$ (CDCl_3 with 0.05% v/v of TMS, 600 MHz) δ 8.24 (d, $J = 8.3$ Hz, 2H, H-2 and H-6), 8.15 (d, $J = 15.1$ Hz, 1H, β -olefinic), 8.12 (d, $J = 8.3$ Hz, 2H, H-3 and H-5), 8.01 (dd, $J = 3.4, 1.4$ Hz, 1H, H-2''), 7.86-7.75 (m, 3H, α -olefinic, H-4' and H-4''), 7.67 (d, $J = 8.3$ Hz, 1H, H-5'), 7.45 (dd, $J = 5.2, 3.1$ Hz, 1H, H-5''), 7.38 (d, $J = 7.6$ Hz, 1H, H-3'), 3.12 (s, 3H, CH_3); $^{13}\text{C-NMR}$ (CDCl_3 , 150 MHz) δ 189.8, 153.8, 152.2, 144.7, 143.8, 142.2, 141.7, 137.7, 129.4, 127.8, 126.6, 126.3, 125.0, 124.3, 123.9, 121.6, 44.4; FT-IR (KBr, cm^{-1}): 3075, 3010 (C=C-H), 2925, 2852 (C-C-H), 1660 (C=O), 1603, 1563, , 1524 (C=C), 1304, 1287 (S=O), 1260 (C=S); Anal. calcd. for $\text{C}_{19}\text{H}_{15}\text{NO}_3\text{S}_2$: C, 61.77; H, 4.09; N, 3.79; Found: C, 62.42; H, 5.00; N, 3.25; LC-MS (+)-ESI (m/z): calculated 369.05, observed 370.0 $[M+1]^+$.

24. (E)-1-(2-hydroxyphenyl)-3-(6-(thiophen-3-yl)pyridin-2-yl)prop-2-en-1-one (**24**)

Fluffy yellow solid; yield: 80.7%; $^1\text{H-NMR}$ (CDCl_3 with 0.05% v/v of TMS, 600 MHz) δ 12.80 (s, 1H, OH), 8.34 (d, $J = 14.5$ Hz, 1H, β -olefinic), 8.04 (dd, $J = 8.3, 1.4$ Hz, 1H, H-6), 8.02 (dd, $J = 3.4, 1.4$ Hz, 1H, H-2''), 7.88 (d, $J = 15.1$ Hz, 1H, α -olefinic), 7.81-7.74 (m, 2H, H-4' and H-4''), 7.65 (d, $J = 6.9$ Hz, 1H, H-5'), 7.59-7.50 (m, 1H, H-4), 7.45 (dd, $J = 5.2, 3.1$ Hz, 1H, H-5''), 7.37 (d, $J = 7.6$ Hz, 1H, H-3'), 7.05 (dd, $J = 8.3, 1.4$ Hz, 1H, H-3), 6.97 (td, $J = 7.6, 1.4$ Hz, 1H, H-5); $^{13}\text{C-NMR}$ (CDCl_3 , 150 MHz) δ 194.2, 163.6, 153.7, 152.4, 143.5, 141.8, 137.6, 136.6, 130.2, 126.5, 126.3,

124.3, 124.1, 123.9, 121.4, 120.1, 119.0, 118.5; FT-IR (KBr, cm^{-1}): 3104 (O-H), 3061 (C=C-H), 1660 (C=O), 1603, 1563, 1524 (C=C), 1304, 1287 (S=O), 1260 (C=S); Anal. calcd. for $\text{C}_{18}\text{H}_{13}\text{NO}_2\text{S}$: C, 70.34; H, 4.26; N, 4.56; Found: C, 69.12; H, 4.14; N, 4.81; LC-MS (+)-ESI (m/z): calculated 307.07, observed 308.0 $[\text{M}+1]^+$.

25. (E)-3-(6-(thiophen-3-yl)pyridin-2-yl)-1-(2-(trifluoromethyl)phenyl)prop-2-en-1-one (**25**)

Pale yellow solid; yield: 61.2%; $^1\text{H-NMR}$ (CDCl_3 , 600 MHz) δ 7.96 (dd, $J = 2.8, 1.4$ Hz, 1H, H-2''), 7.79 (d, $J = 8.3$ Hz, 1H, H-3), 7.73 (t, $J = 7.9$ Hz, 1H, H-4'), 7.71 (dd, $J = 5.5, 1.4$ Hz, 1H, H-4''), 7.68-7.60 (m, 4H, H-4, β -olefinic, H-5' and H-5), 7.52 (d, $J = 7.6$ Hz, 1H, H-6), 7.40 (dd, $J = 4.8, 2.8$ Hz, 1H, H-5''), 7.37-7.28 (m, 2H, α -olefinic, H-3'); $^{13}\text{C-NMR}$ (CDCl_3 , 150 MHz) δ 195.3, 153.8, 152.2, 146.2, 141.6, 138.7, 137.5, 131.6, 130.1, 130.0, 128.1, 127.9 (q, $J = 32.3$ Hz, C-2), 126.8 (q, $J = 4.8$ Hz, C-3 or C-1), 126.5, 126.2, 124.3, 123.6 (q, $J = 274.5$, CF_3) 123.0, 121.3; FT-IR (KBr, cm^{-1}): 3040 (C=C-H), 2984 (C-C-H), 1677 (C=O), 1614, 1578, 1522 (C=C), 1308 (C-F), 1270 (C=S); Anal. calcd. for $\text{C}_{19}\text{H}_{12}\text{F}_3\text{NOS}$: C, 63.50; H, 3.37; N, 3.90; Found: C, 62.97; H, 3.53; N, 4.09; LC-MS (+)-ESI (m/z): calculated 359.06, observed 359.9 $[\text{M}+1]^+$.

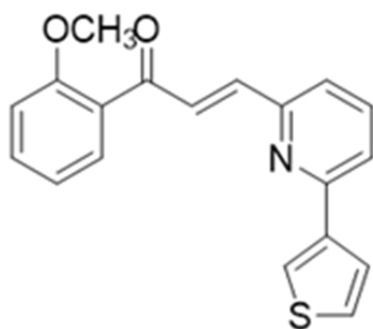
26. (E)-1-(4-fluorophenyl)-3-(6-(thiophen-3-yl)pyridin-2-yl)prop-2-en-1-one (**27**)

Off-white Solid; yield: 64.7%; $^1\text{H-NMR}$ (CDCl_3 , 600 MHz) δ 8.17 (d, $J = 15.1$ Hz, 1H, β -olefinic), 8.14 (m, 2H, H-2 and H-6), 8.01 (dd, $J = 2.8, 1.4$ Hz, 1H, H-2''), 7.86-7.73 (m, 3H, α -olefinic, H-4' and H-4''), 7.64 (d, $J = 7.6$ Hz, 1H, H-5'), 7.44 (dd, $J = 5.2, 3.1$ Hz, 1H, H-5''), 7.36 (d, $J = 7.6$ Hz, 1H, H-3'), 7.20 (tt, $J = 9.0, 2.4$ Hz, 2H, H-3 and H-5).

3.2 *In Silico* ADMET Screening

Drug discovery and development are very costly, with an estimated cost of two billion dollars for each successful drug (278). Twenty years ago, the major reason for drugs to fail in late drug development stages was attributed to poor pharmacokinetic profiles. However, with the advancement of technology and the development of software that can predict pharmacokinetic profiles at earlier stages, this percentage dropped significantly by 10% (278). In our study, we incorporated absorption, distribution, metabolism, excretion and toxicity (ADMET) *in silico* prediction in the design process to screen all the proposed analogs and prioritize hits with favorable profiles. Two ADMET predicting software were used, ADMET Predictor and SwissADME. Figure 13 shows the predicted drug-likeness properties for compound **17** (generated by the SwissADME web tool). Our lead compound showed favorable properties in all tested aspects except for insaturation. Nevertheless, this is not a major limitation as this property is related to the feasibility of synthesis rather than the pharmacokinetic profile. The expected ADMET risk scores for all analogs as predicted by ADMET Predictor are summarized in Figure 14. Generally, all thienyl-based chalcones (**13-26**), the most active series in our study, had favorable ADMET profiles with overall risk below the ADMET threshold of 6.5, except for compound **15**.

A.



Lead Molecule
(Compound **17**)

B.

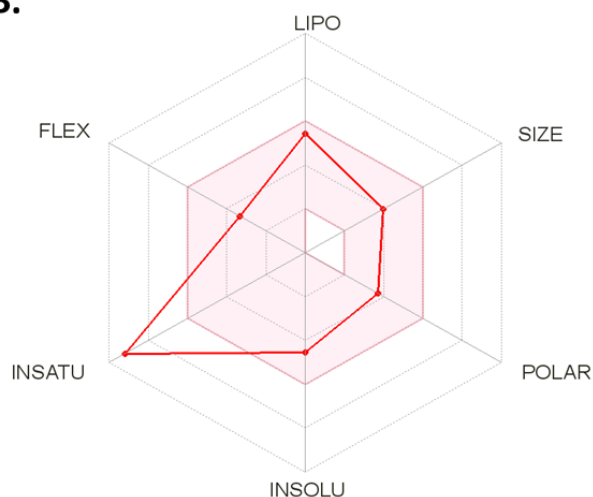


Figure 14. Predicted drug-likeness properties of compound **17** by SwissADME web tool (<http://www.swissadme.ch/>). (A) shows the chemical structure of compound **17**. (B) The predicted drug-likeness properties where the colored zone highlights the suitable physiochemical space for oral bioavailability. Compound **17** fulfills the criteria except for INSATU, which predicts synthetic feasibility. Lipo: lipophilicity; Polar: polarity; INSOL: insolubility; INSATU: insaturation; FLEX: flexibility.

n.	Overall ADMETRisk	Absn_Risk	TOX_Risk	MUT_Risk	CYP_Risk	Lipinski RuleOf5 Violation
1	6.969 Kow; Sw; fu; hERG; 1A2; 3A4; CL; ti	2 Kow; Sw	0.348 hERG	0.5 m100	3.633 1A2; 3A4; CL; ti	1 LP
2	7.283 Kow; Sw; fu; hERG; 1A2; 3A4; CL; ti	2 Kow; Sw	0.294 hERG	0.5 m100	4 1A2; 3A4; CL; ti	1 LP
3	7.094 Kow; Sw; fu; hERG; 1A2; 3A4; CL; ti	2 Kow; Sw	0.323 hERG	0.5 m100	3.782 1A2; 3A4; CL; ti	1 LP
5	6.692 Kow; Sw; fu; hERG; 1A2; 3A4; CL; ti	2 Kow; Sw	0.444 hERG	0.5 m100	3.429 1A2; 3A4; CL; ti	0
6	0.799 Sw	0.799 Sw	0	0.5 m100	0	0
7	1.609 1A2; 3A4; CL	0.236 Kow	0	0.5 m100	1.373 1A2; 3A4; CL	0
8	2.148 1A2; CL	0.665 Kow; Sw	0	0.5 m100	1.483 1A2; CL	0
9	2.534 1A2; CL; ti	0	0	0.5 m100	2.534 1A2; CL; ti	0
10	6.089 Kow; Sw; fu; Xm; MUT; 1A2; CL	2 Kow; Sw	2 Xm; MUT	2 S_97; S_98; m100	1.879 1A2; CL	0
11	1.489 1A2	0.489 Sw	0	0.5 m100	1 1A2	0
12	3.167 1A2; CL	1.486 Kow; Sw	0	0	1.68 1A2; CL	0
13	4.016 Sw; Xm; 1A2; CL	2 Kow; Sw	0.016 Xm	0.5 m100	2 1A2; CL	0
14	4.694 Kow; Sw; Xr; 1A2; 3A4; CL	1.815 Kow; Sw	0.429 Xr	0.5 m100	2.45 1A2; 3A4; CL	0
15	6.733 Kow; Sw; Xr; Xm; 1A2; 2D6; 3A4; CL	2 Kow; Sw	0.956 Xr; Xm	0.5 m100	3.777 1A2; 2D6; 3A4; CL	0
16	4.509 Kow; Sw; Xm; 1A2; 2D6; 3A4; CL	1.685 Kow; Sw	0.144 Xm	0.5 m100	2.68 1A2; 2D6; 3A4; CL	0
17	3.742 Sw; 1A2; 3A4; CL	1.187 Kow; Sw	0	0.5 m100	2.555 1A2; 3A4; CL; mi	0
18	3.437 Sw; 1A2; 3A4; CL	1.341 Kow; Sw	0	0.5 m100	2.096 1A2; 3A4; CL	0
19	4.289 Sw; 1A2; 2D6; CL	1.705 Kow; Sw	0	0.5 m100	2.584 1A2; 3A4; CL	0
20	3.67 1A2; CL	1.67 Kow; Sw	0	0.5 m100	2 3A4; CL; mi	0
21	4.064 Sw; MUT; 1A2; CL	1.691 Kow; Sw	1 MUT	2 m_97; S_98; m100	1.373 1A2; CL	0
22	3.601 1A2; CL	1.601 Kow; Sw	0	0	2 CL	0
23	2.76 Sw; MUT; CL	1 Sw	1 MUT	1.5 S_97; m_98	0.176 3A4; CL; ti	0
24	4.062 Kow; Sw; MUT; 1A2; 2C9; CL	1.455 Kow; Sw	1 MUT	1.5 S_97; S_98	1.607 1A2; CL	0
25	5.604 Kow; Sw; fu; Xr; 3A4; CL; mi; ti	2 Kow; Sw	1 Xr	1 S_97	2.088 1A2; CL; ti	0
26	4.932 Kow; Sw; MUT; 1A2; 3A4; CL; mi	1.761 Kow; Sw	1 MUT	2 S_97; S_98; m100	2.171 1A2; 3A4; CL; ti	0
DK14	5.774 Kow; Sw; fu; hERG; 1A2; 3A4; CL; ti	2 Kow; Sw	0.072 hERG	0.5 m100	3.11 1A2; 3A4; CL; ti	1 LP

Figure 15. ADMET Risk scores of the synthesized chalcone analogs (1-26), presented as heat map predicted by ADMET Predictor®.

Abbreviations Absn: Absorption; Tox: Toxicity; MUT: Mutagenicity; Sw: Water Solubility; CL: Clearance; Kow n-Octanol/Water Partition Coefficient.

Recommended Parameters Range by AMDET Predictor: overall ADMET risk (<6.5), Absn_Risk (<3.5), Tox_Risk (<2), MUT (<1), CYP_Risk (<2.5)

3.3 Pharmacological Anticancer Screening

3.3.1 General Screening (Compounds 1-16)

Initially, sixteen novel chalcone analogs were synthesized and screened for their antiproliferative activity and effect on cell morphology against two of the most aggressive AR negative human prostate cancer cell lines (PC3 and DU145), which represent castration-resistant prostate cancer (CRPC). Compounds were screened at 10 μ M concentrations in comparison to the vehicle (0.1% DMSO) as the negative control, docetaxel as positive control, and the parent compound (**DK14**) as reference. Compounds showing >50% reduction in cell viability at 10 μ M were selected for dose-response evaluation and further anticancer mechanistic study.

3.2.1.1 Cell Viability

The *in vitro* cytotoxicity of synthesized chalcones against PCa cell lines was evaluated using AlamarBlue viability assay. AlamarBlue is a reliable and highly sensitive method that can quantitatively reflect cell viability. AlamarBlue (resazurin) is a cell-permeable, weakly fluorescent blue dye that is reduced by mitochondrial enzymes in viable cells to resorufin, a highly fluorescent pink molecule. Unlike the widely used MTT (3-(4, 5-dimethyl thiazolyl-2)-2, 5-diphenyltetrazolium bromide) colorimetric assay, AlamarBlue has the advantage of being water-soluble; thus, it does not need crystal solubilization and can be directly quantified after reduction by fluorescence or UV reader.

The cytotoxic activities of compounds (**1-16**) were primarily screened at 10 μ M concentration against AR negative PCa cell lines (PC3 and DU145) using docetaxel as

a positive control. After 48 hours of treatment, the cell viability of treated cells was calculated relative to DMSO-treated controls (Figure 15). Overall, out of the sixteen tested compounds, thienyl pyridine containing chalcones (**13** and **16**) induced the most significant reduction in cell viability in both cell lines, which was more prominent than the reduction with the reference drug (docetaxel). Interestingly, thienyl pyridine was not previously linked to in any chalcone, and we are the first group to report this molecular hybrid.

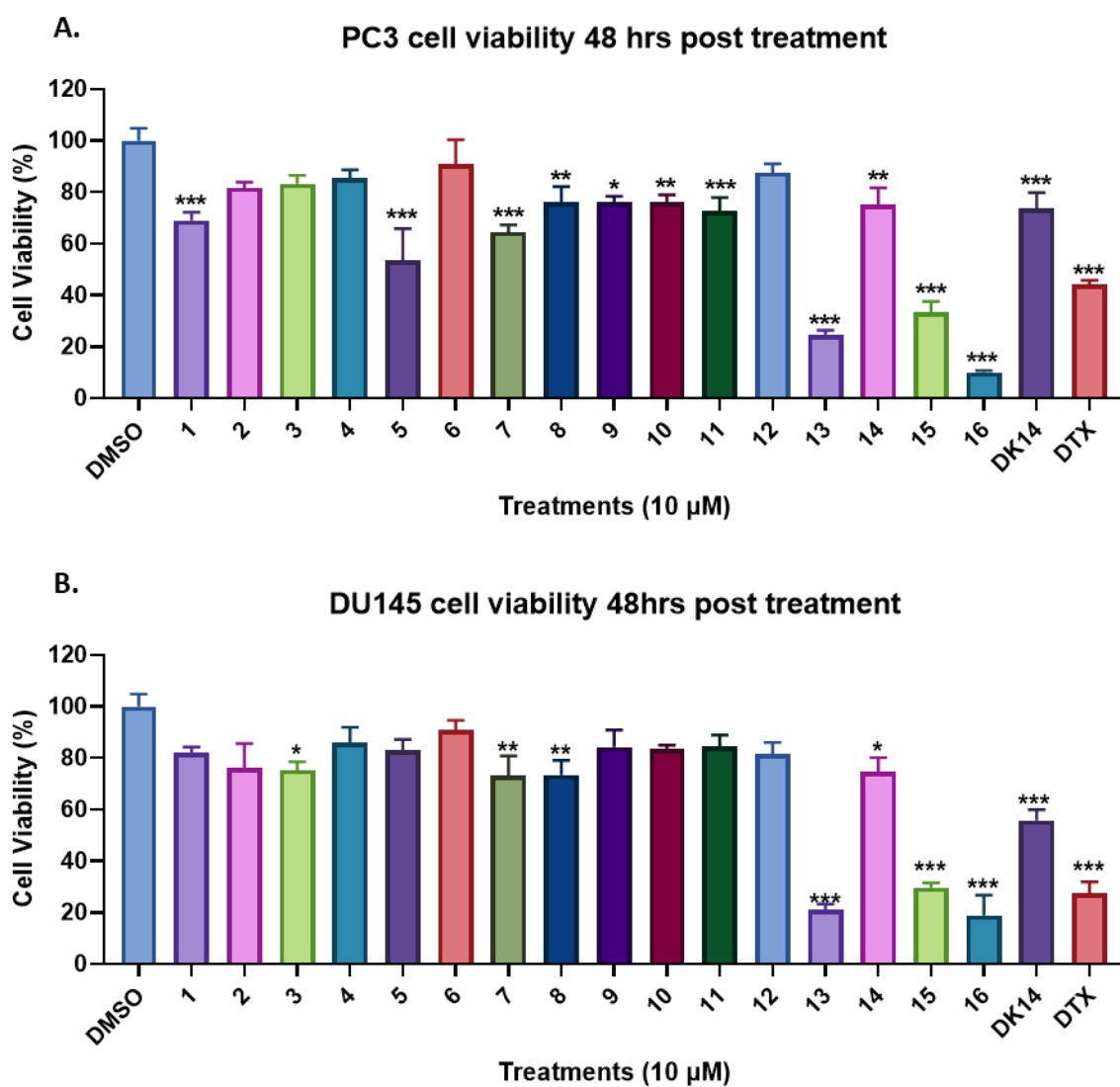


Figure 16. Effect of compounds **1-16** on the cell viability of (A) PC3 and (B) DU145 cell lines. The cells were treated with a 10 μ M concentration of compounds **1-16**, docetaxel (DTX) or

DK14. Cell viability relative to control (0.1% DMSO) was measured by AlamarBlue after 48 hours of treatment. Data are presented as Mean \pm SEM of three independent experiments. One-way ANOVA followed by Tukey's posthoc test was used to compare the treatment groups. Results were considered statistically significant when $p < 0.05$. * $p < 0.05$, ** $p < 0.01$, and *** $p < 0.001$.

3.2.1.1.1 Effect of Series A (compounds 1-5)

Based on the excellent activity of **DK14** chalcone on TNBC (170), closed ring (tetralone-based) chalcone analogs bearing the same substituents (OCH₃ and nitrogen mustard) were synthesized and evaluated against prostate cancer cell lines. The cell viability results indicated that both **DK14** and its related tetralone based chalcone analogs (compounds **1-5**) displayed moderate to no cytotoxic effect at 10 μ M (<50% reduction in viability) against PCa cell lines (PC3 and DU145) as compared to TNBC cell lines (IC₅₀ 6.3-9.22 μ M). Compounds with a methoxy substituent at position-5 (compound **1** and **5**) displayed preferential cytotoxicity to PC3 cell line, whereas analogs bearing methoxy at position 7 (compound **3**) or its equivalent in open-chain chalcone (**DK14**) induced higher cytotoxicity in DU145. Although **DK14** was slightly more cytotoxic than its corresponding tetralone analog in both tested cell lines, the difference between them was not statistically significant (P-value 0.44 and 0.99).

3.2.1.1.2 Effect of Series B (compounds 6-9)

Next, a second attempt was made to improve the activity and pharmacokinetic profile of **DK14**. In this series, the nitrogen mustard group in **DK14** was replaced with cyclopropyl pyrrole, a potential bio-isostere with a highly improved pharmacokinetic profile compared to the parent compound. Similar to series A, pyrrole-based chalcones showed marginal cytotoxicity. Comparing the cytotoxicity of **DK14** with its matched cyclopropyl pyrrole-based non-cyclic chalcone (**9**) revealed a statistically significant difference in DU145 cell line in-favor **DK14** (P-value 0.02). On the other hand,

cyclopropyl pyrrole cyclic (tetralone-based) chalcones (**7** and **8**) bearing a different methoxy substituents pattern showed comparable cytotoxicity to **DK14**. Notably, H-pyrrole tetralone-based chalcone (**6**) did not significantly reduce cell proliferation in any of the cell lines, suggesting that cyclopropyl moiety is essential for anticancer activity.

3.2.1.1.3 Effect of Series C (compounds 10-16)

Due to unsatisfactory results with **DK14** related analogs, a new line of chalcone derivatives was synthesized and evaluated. Among different heteroaromatic rings, a focus was given to the pyridine ring due to its promising anticancer activity and repeated success in the clinically approved drugs. Different 3'-pyridine substituted chalcones were developed, among which thienyl pyridine-containing analogs (**13**, **15**, and **16**) showed excellent cytotoxicity. Compound **16** induced the most significant reduction in cell viability of PC3 and DU145 (89.94% and 81.05%, respectively). Interestingly, compound **16** performed better than the first-line drug (docetaxel), especially in PC3 cell line (89.94% vs. 55.89%, P-value <0.01). Although docetaxel started killing cancer cells at a much lower concentration and displayed a lower IC₅₀, its cytotoxicity reached a plateau and was less effective than the synthesized analogs at 10 μM concentration, suggesting the presence of a docetaxel resistant subpopulation. Based on the highly promising activity, compounds **13**, **15** and **16**, were selected for further evaluation to assess their antitumor potential and explore their mechanism of action against prostate cancer.

3.2.1.2 Morphological Examination

The induction of apoptosis in cancer cells has been widely considered an important criterion in developing anticancer drugs. To confirm whether the synthesized compounds could reduce cell viability and induce apoptosis in PC3 and DU145,

prostate cancer cells were treated with compounds **1-16** at 10 μ M concentrations for 48 hours. Cells were examined for the formation of apoptotic bodies or death by phase-contrast microscopy (Figure 16 and 17). More importantly, cells were monitored for characteristic changes in cell morphology as they can provide insight into cell differentiation, invasiveness, survival, and genetic alterations.

Consistent with the cell viability results, compounds **13,15** and **16** induced the most significant morphological changes. Treatment with these compounds for 48 hours caused cell detachment, shrinkage, and wall deformation, indicating cell death in PC3 and DU145. Notably, nitrogen mustard-containing compounds (**1** and **3**) caused the elongated spindle-like PC3 cells to become more round and larger in size. Since small cell size and elongated shape are correlated with the metastatic potential in human cancer cells, these compounds might have a role in blocking metastasis (279). These findings are consistent with observation reported in Khalifa et al. study on related non-cyclic nitrogen mustard containing chalcone (**DK14**), which shows a similar pattern of morphological changes in addition to a reduction in cell migration and invasion (170). Likewise, the cyclopropyl-containing compound (**7**) caused PC3 cells to be rounder, but to a lower extent due to the formation of apoptotic bodies, suggesting that this moiety can act as a potential bio isostere for nitrogen mustard. However, these observations need to be confirmed with additional docking and *in vitro* experiments. For the scope of this study, we focused on thienyl pyridine-based chalcones (**13-16**), as they showed the most promising anticancer potential. The magnitude of morphological changes with remaining compounds was not very promising, with a minor reduction in cell density or absence of detectable difference.

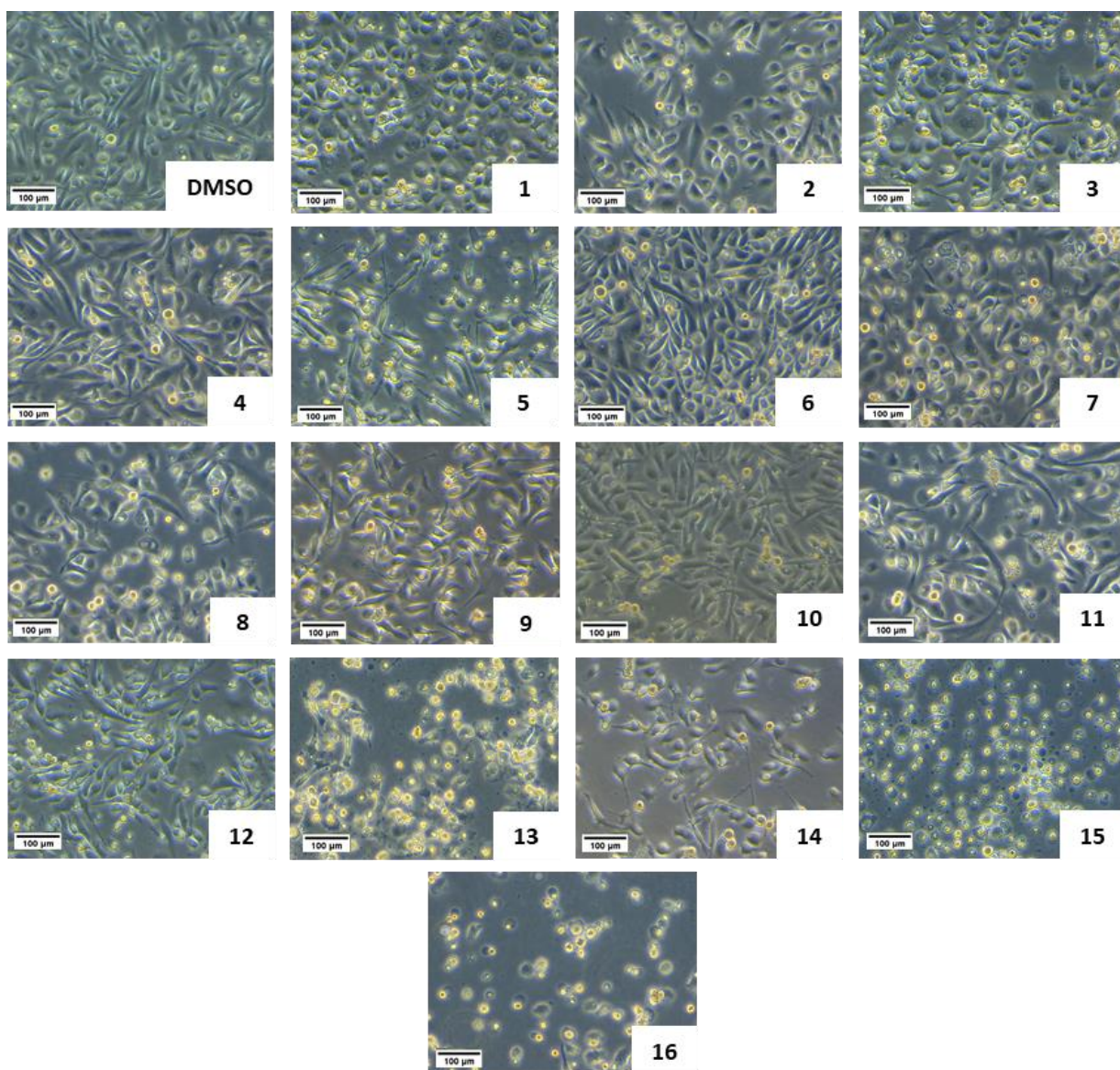


Figure 17. Effect of compounds **1-16** on the cell morphology of PC3 cell line. Morphological changes were observed by phase-contrast microscopy following treatment with 10 μM concentration for 48 hours. Images were taken using a 10x objective (N=3). Scale bar represents 100 μm .

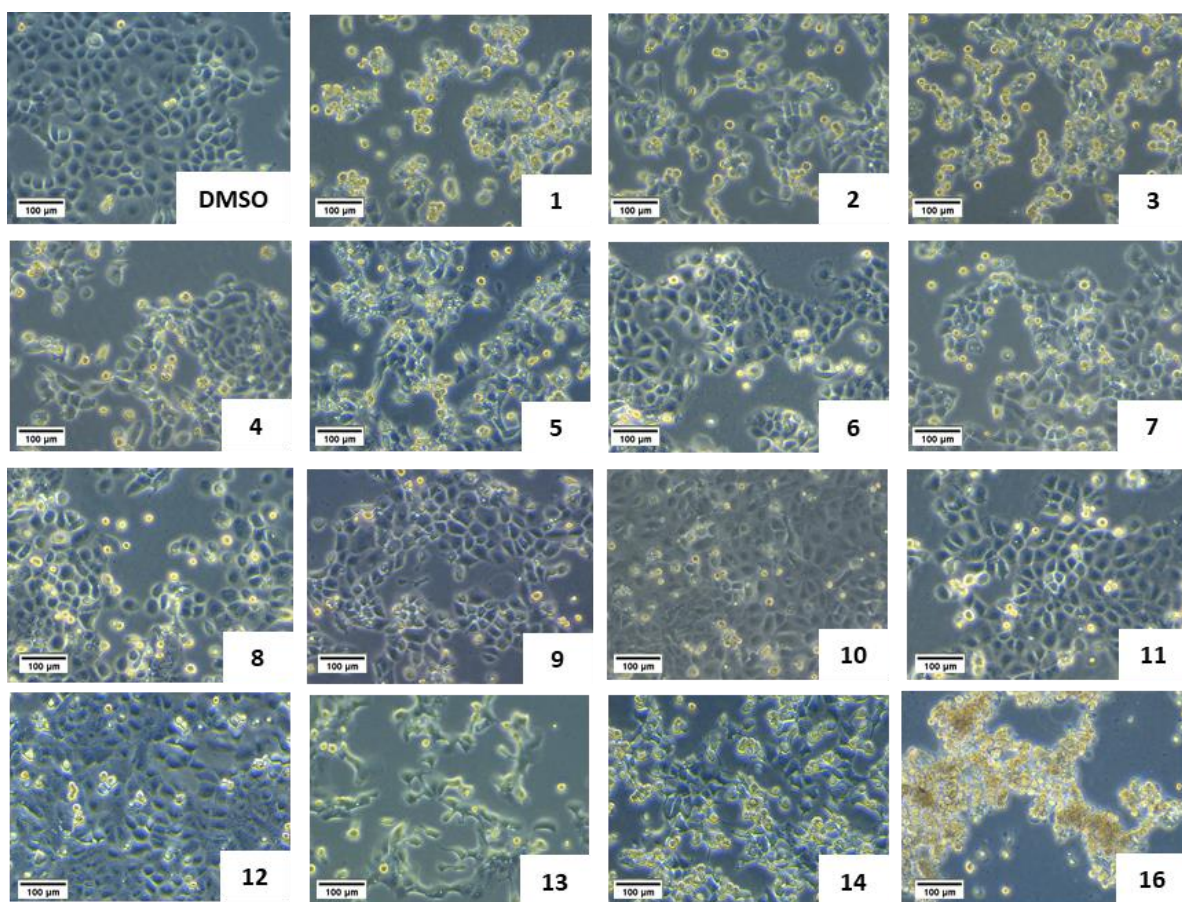


Figure 18. Effect of compounds **1-16** on the cell morphology of DU145 cell line. Morphological changes were observed by phase-contrast microscopy following treatment with 10 μM concentration for 48 hours. Images were taken using a 10x objective (N=3). Scale bar represents 100 μm .

3.3.2 Molecular Pathway study of compounds **13**, **15**, and **16**

Based on the cell viability and morphological examination screening of the first sixteen synthesized analogs, thienyl pyridine-based chalcones (**13**, **15** and **16**) showed the most promising activity against both cell lines (PC3 and DU145). Therefore, these compounds were selected for further mechanistic studies to evaluate their antitumor potential on castration-resistant prostate cancer (CRPC).

Since the ultimate goal of designing a new drug is to improve the efficacy and reduce non-specific toxicities, the IC_{50} against PCa cell lines and LD_{50} against normal cells for the selected analogs were evaluated to assess the potency and selectivity. Next, additional assays were conducted to explore the mechanism behind the observed anticancer activity. The effect of the compounds on the main carcinogenesis-related cellular processes, namely colony formation, cell cycle, apoptosis, migration, EMT, and angiogenesis, was explored. Besides, their effect on major cancer-related molecular pathways was studied by western blot. The compounds were studied *in vitro* against AR-negative PCa cell lines (PC3 and DU145) and *in ovo* using the CAM of the chicken embryos. Docetaxel, first-line chemotherapy for CRPC, was used as a reference drug and positive control.

3.3.2.1 IC_{50} and Selectivity Evaluation

To assess whether the new analogs can serve as potential lead anticancer agents with improved efficacy and safety profile, the IC_{50} and LD_{50} were calculated for compounds showing >50% reduction in the initial cell viability screening. Prostate cancer (PC3 and DU145) and normal primary dental bulb cells were treated with increasing concentrations of compounds (**13**, **15** and **16**) for 48 hours, and their viability was assessed by AlamarBlue.

As seen in Figure 18, the three compounds showed a dose-dependent reduction in cell viability against both PC3 and DU145 cell lines. Compound **16** showed the most potent cytotoxicity with an IC_{50} of 4.3 and 5.2 μ M against PC3 and DU145, respectively (Table 4). All analogs were slightly more potent in PC3 than in DU145. Interestingly, the compounds exhibited preferential cytotoxicity towards prostate cancer cell line as compared to normal cells. Compounds were at least 4.7-8.8 times more toxic to cancer cells than normal cells. However, the selectivity data need to be interpreted with caution since normal dental cells were used for safety assessment due to the lack of more relevant models (i.e., primary prostate epithelial cells).

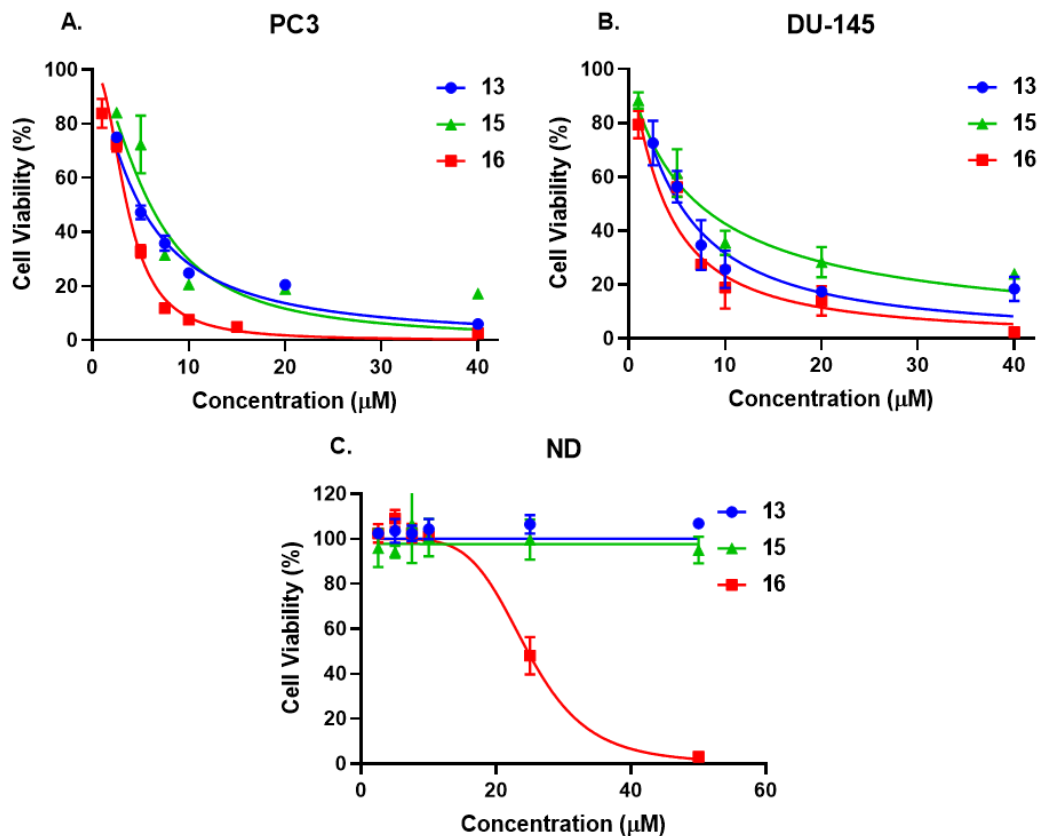


Figure 19. The effect of compounds 13, 15 and 16 on cell viability of AR-negative prostate cancer cell lines PC3 (A) and DU145 (B), and normal dental cells (C) as determined by AlamarBlue assay, 48 hours post-treatment. Results are presented as representative dose-response curves of three independent experiments. Data are expressed as mean values of four technical replicates \pm SEM.

Table 4. IC₅₀ and LD₅₀ of compounds **13**, **15** and **16** on AR-negative PCa and normal dental cells.

	13	15	16
PC3 IC ₅₀ (μM)	5.60 ± 0.38	6.60 ± 0.49	4.32 ± 0.37
DU145 IC ₅₀ (μM)	5.63 ± 1.07	6.47 ± 0.57	5.20 ± 0.46
ND LD ₅₀ (μM)	> 50.0	>50.0	24.67 ± 1.03

ND= Normal primary dental cells; Values are expressed as Mean ± SEM of three independent experiments. IC₅₀ and LD₅₀ for each experiment were computed by non-linear regression using GraphPad Prism.

3.3.2.2 Effect on Cell Morphology

Based on the promising findings and the potent cytotoxic activity observed in the general screening with compounds (**14-16**) against AR-negative prostate cancer cell lines, we decided to investigate further their effect on the morphology of two AR-positive cell lines (C4-2 and LNCaP) in addition to the AR-negative PCa (PC3 and DU145) cell lines. As shown in Figure 19, compound **13** caused C4-2 and LNCaP to lose their shape, shrink in size, and increased cell death. Notably, the compound was profoundly more cytotoxic to the more aggressive and highly invasive prostate cancer cell lines (PC3) as compared to the less aggressive AR-positive cells. Moreover, we examined the effect of compound **16** at a lower concentration (5 μM) since the cells were almost completely dead at 10 μM. Treatment of PC3 and DU145 cells with 5 μM of compound **16** showed increased cell detachment, the formation of apoptotic bodies, and cell shrinkage, without other characteristic changes on cell adhesion (Figure 20).

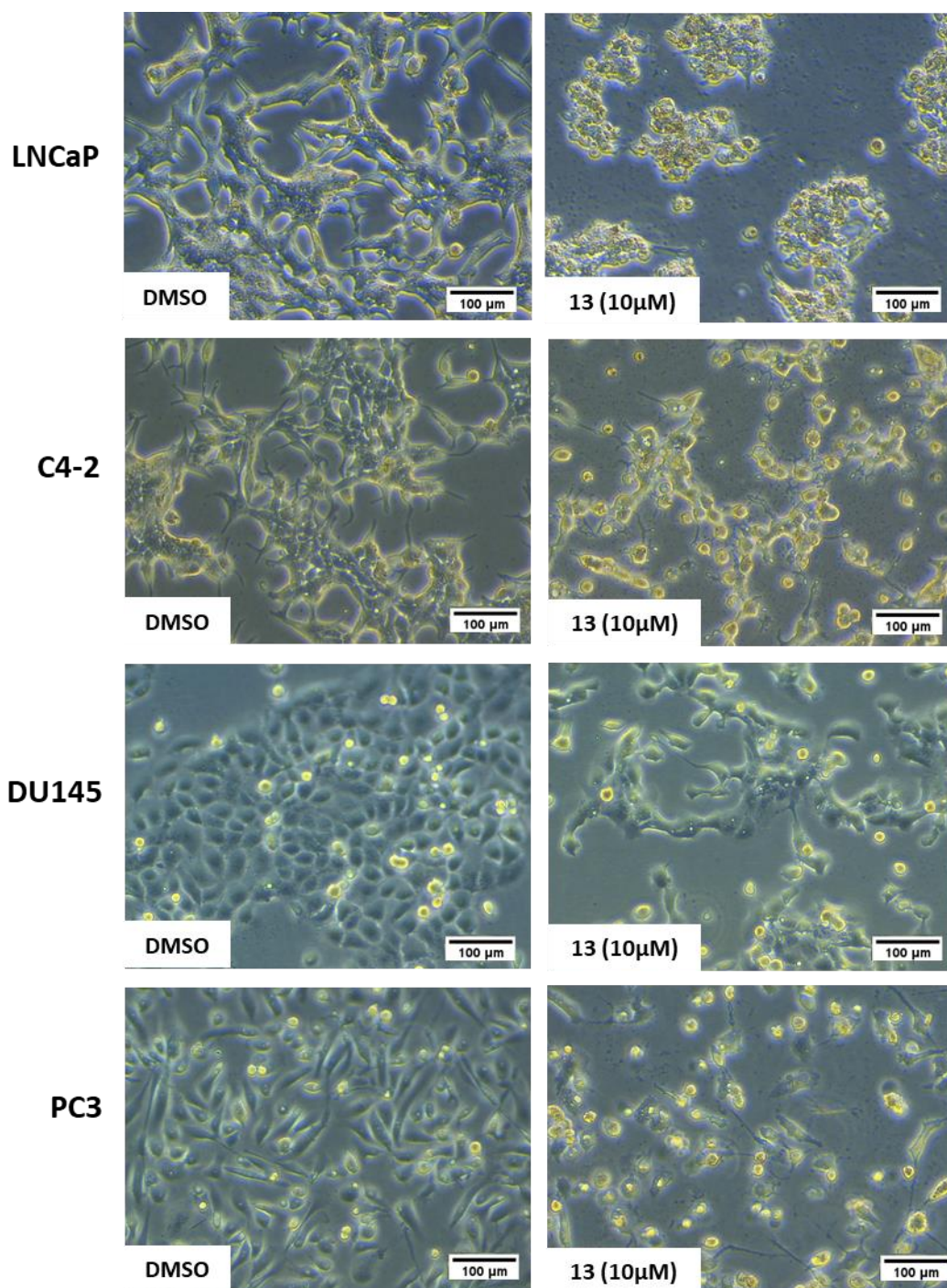


Figure 20. Effect of compound **13** on the cell morphology of AR-positive (C4-2 and LNCaP) and AR-negative (PC3 and DU145) prostate cancer cell lines. Morphological changes were observed by phase-contrast microscopy following treatment with 10 μM concentration for 48 hours. Images were taken using a 10x objective (N=3). Scale bar represents 100 μm.

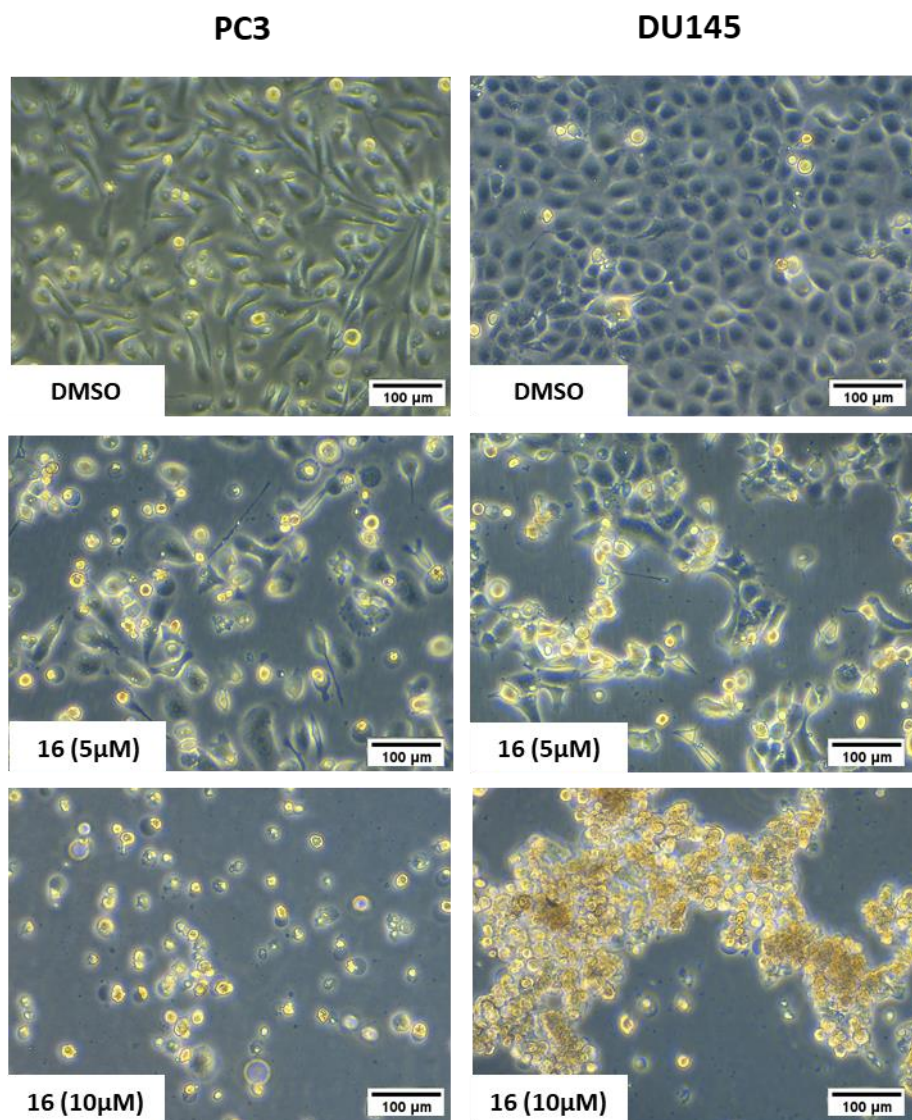


Figure 21. Effect of compound **16** on the cell morphology of AR-negative (PC3 and DU145) prostate cancer cell lines. Morphological changes were observed by phase-contrast microscopy following treatment with 5 and 10 μM concentrations for 48 hours. Images were taken using a 10x objective (N=3). Scale bar represents 100 μm .

3.3.2.3 *Effect on Apoptosis Pathway*

Based on our morphological observations, we hypothesized that the cytotoxic activity of our molecules (**13**, **15** and **16**) might be at least partially mediated by apoptosis induction. To confirm these findings, we decided to directly measure the percentage of apoptotic cells by Annexin V-FITC/ 7-AAD assay using flow cytometry. As shown in Figures 21 and 22, compound **16** resulted in profound induction of apoptosis in both PC3 and DU145 by 34.7% and 47.8%, respectively. Interestingly, the apoptosis induced by compound **16** was higher than apoptosis with docetaxel, first-line chemotherapy in mCRPC. Further, we examined the effect of our compounds on the expression of three apoptosis-related biomarkers (pro-apoptotic proteins: Bax and caspase-3, and anti-apoptotic protein: Bcl-2) in PC3 and DU145 cell lines (Figure 23 and 24). Our findings showed that following 48 hours of treatment, the three compounds can enhance the expression of Bax and downregulate Bcl-2, which led to a significant increase in Bax/Bcl-2 ratio in both investigated cell lines as compared to the control. Of note, compound **16** was the most effective among the tested compounds.

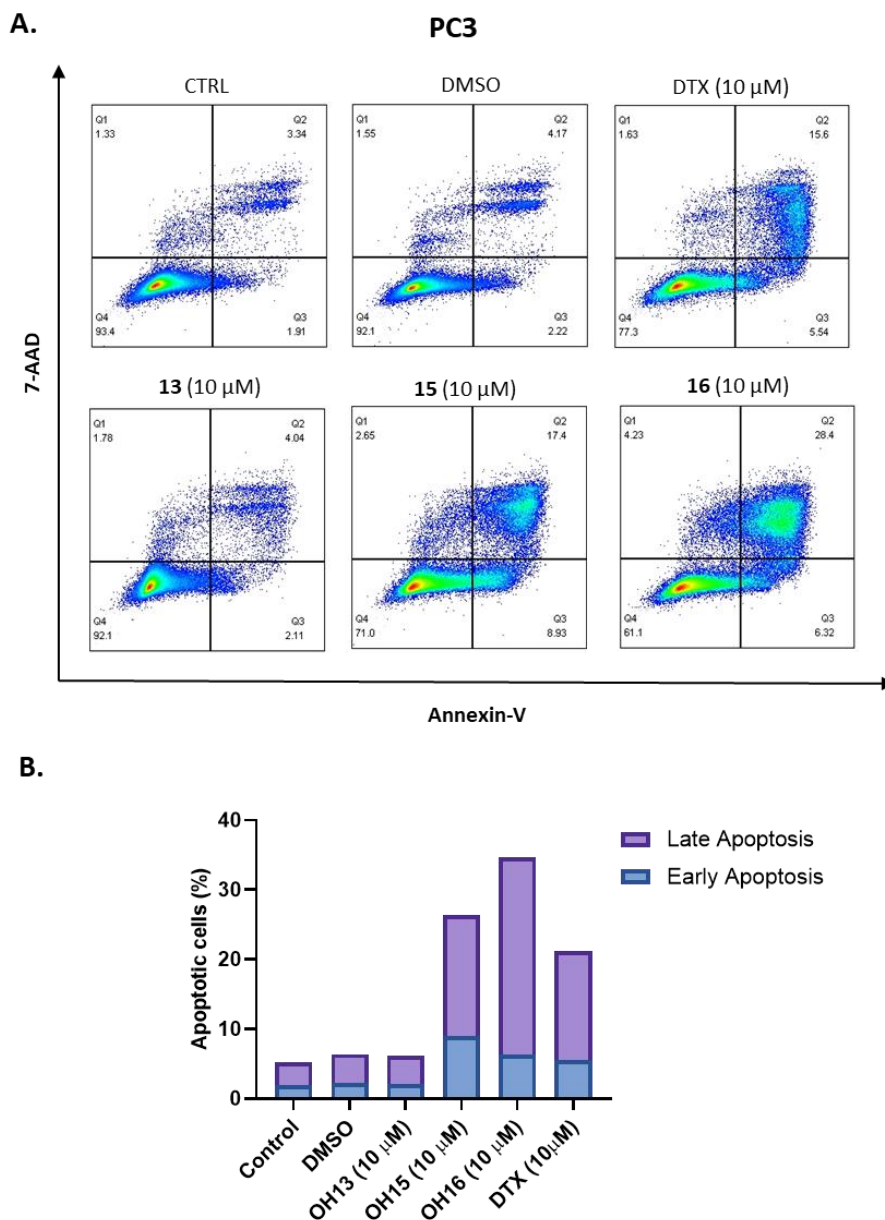


Figure 22. Induction of apoptosis by compounds **13**, **15** and **16** in PC3 cells, as determined by Annexin V-FITC/7-AAD apoptosis assay. (A) Annexin V-FITC and 7-AAD staining of PC3 cells following 48 hours of treatment with molecules **13**, **15** and **16** at 10 μ M concentration. Media only (CTRL) and DMSO were used as a negative and vehicle control; and docetaxel (DTX) at 10 μ M was used as a positive control. The top right quadrant denotes dead/late apoptotic cells, the bottom right quadrant represents cells in early apoptosis, and the bottom left quadrant indicates viable cells (N=2). (B) Quantification of apoptosis induction in cells treated with 10 μ M of the compounds.

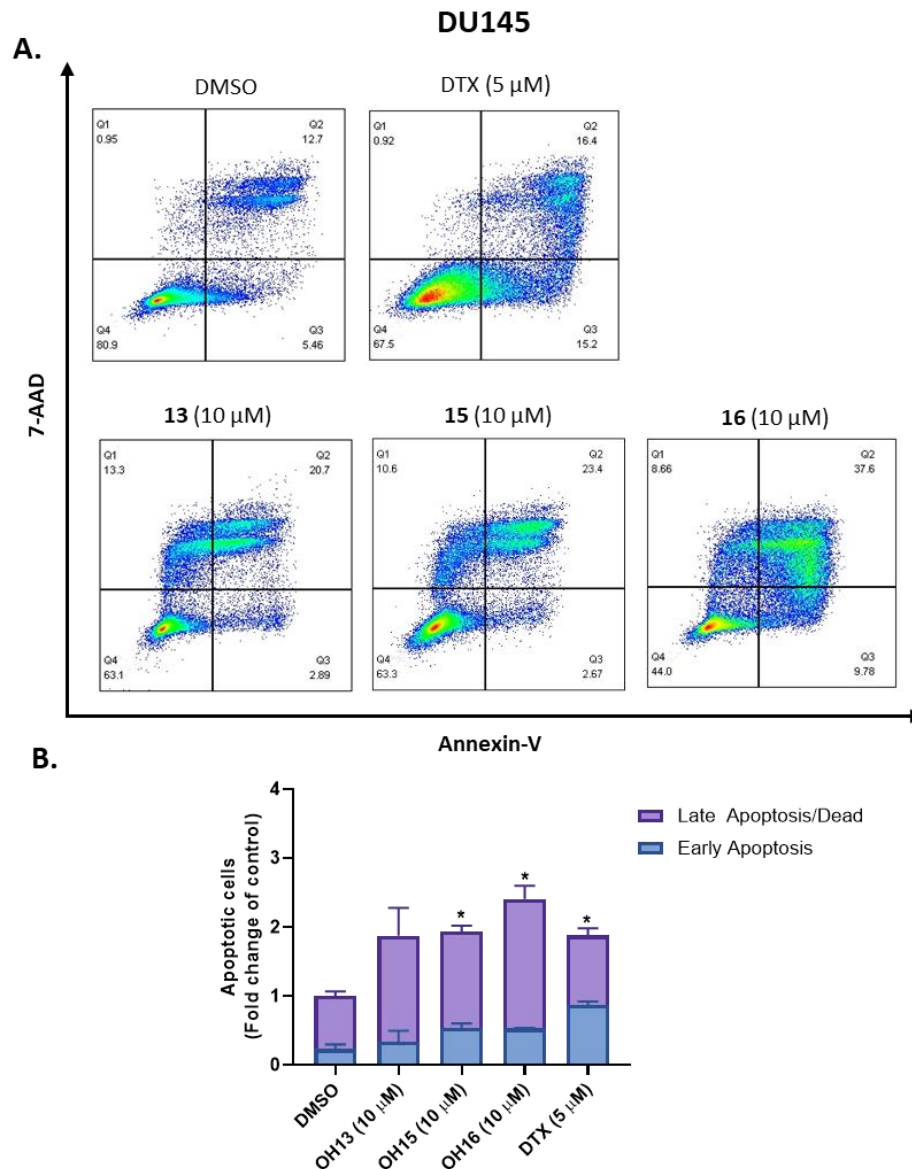


Figure 23. Induction of apoptosis by compounds 13, 15 and 16 in DU145 cells, as determined by Annexin V-FITC and 7-AAD apoptosis assay. (A) Annexin V-FITC and 7-AAD staining of PC3 cells following 48 hours of treatment with molecules 13, 15, and 16 at 10 μ M concentration. Media only (CTRL) and DMSO were used as a negative and vehicle control; and docetaxel (DTX) at 10 μ M was used as a positive control. The top right quadrant denotes dead/late apoptotic cells, the top left quadrant indicates necrotic cells, the bottom right quadrant represents cells in early apoptosis, and the bottom left quadrant indicates viable cells. (B) Quantification of apoptosis induction in cells treated with 10 μ M of the compounds. Data are presented as Mean \pm SEM (N=2). Results were considered statistically significant when $p < 0.05$.

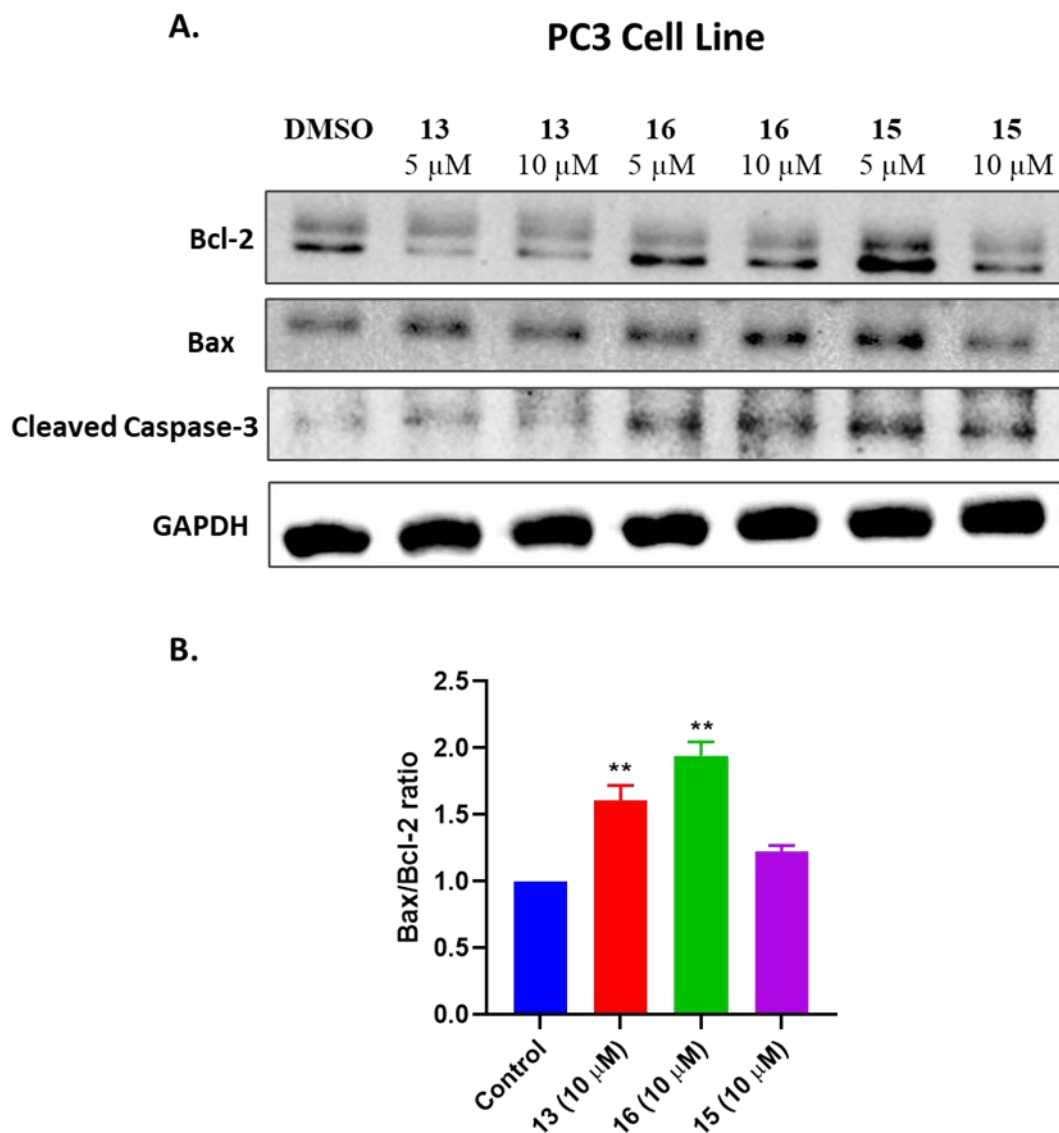


Figure 24. Effect of compounds **13**, **15** and **16** on the expression of apoptosis-related proteins in PC3 cells. A) The expression levels of Bcl-2, Bax and cleaved caspase-3 as assessed by western blot analysis. Cells were treated for 48 hours with compounds **13**, **15** and **16** at a concentration of (5 and 10 μM). DMSO was used as a negative control. (B) The Bax/Bcl-2 ratio was calculated based on densitometric quantification of Bcl-2 and Bax bands. Values were corrected for the expression of housekeeping protein GAPDH to ensure equal loading and expressed as fold change of control. Data are presented as Mean ± SEM (N=2-3). Results were analyzed using One-way ANOVA followed by Dunnett's post-hoc test. *P-value<0.05 was considered for statistical significance. *P-value<0.05; **P-value<0.01.

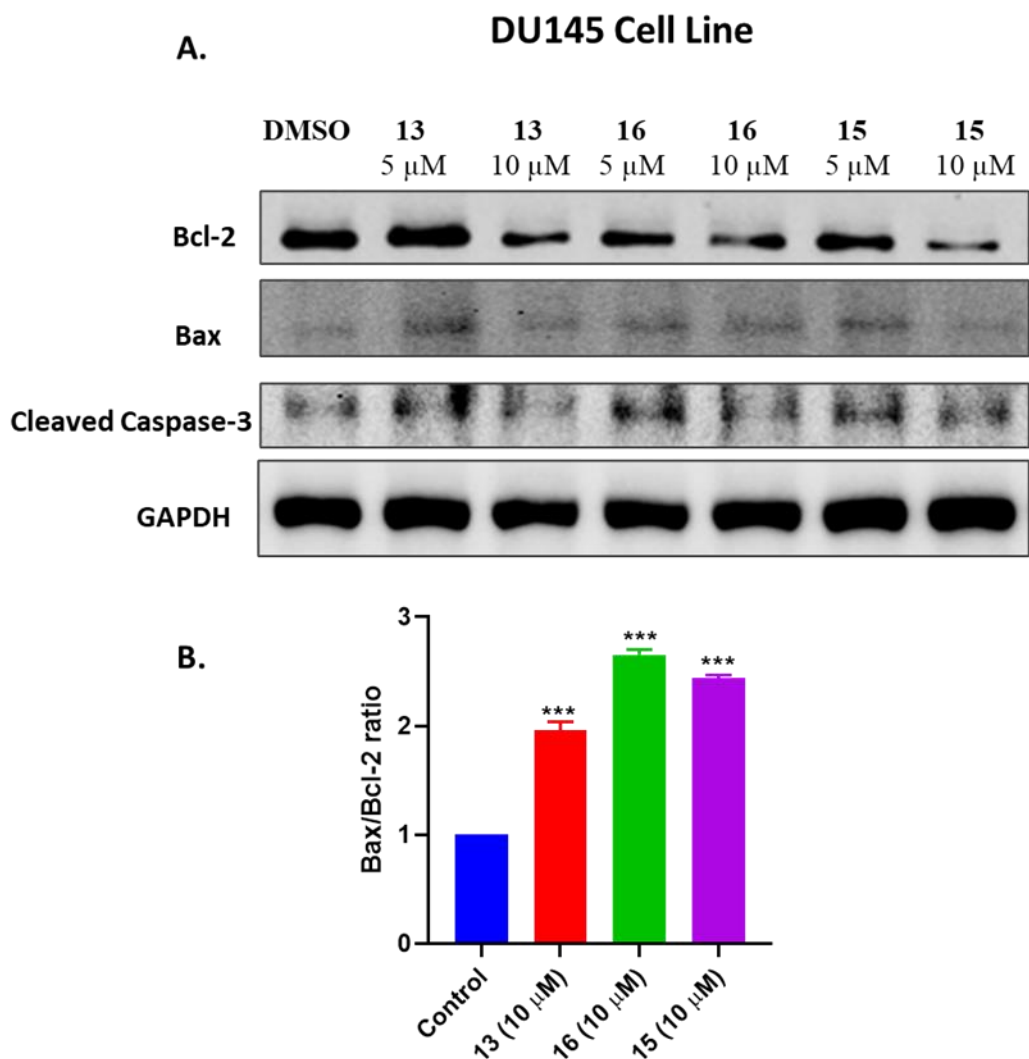


Figure 25. Effect of compounds **13**, **15** and **16** on the expression of apoptosis-related proteins in DU145 cells. A) The expression levels of Bcl-2, Bax and cleaved caspase-3 as assessed by western blot analysis. Cells were treated for 48 hours with compounds **13**, **15** and **16** at a concentration of (5 and 10 μM). DMSO was used as a negative control. (B) The Bax/Bcl-2 ratio was calculated based on densitometric quantification of Bcl-2 and Bax bands. Values were corrected for the expression of housekeeping protein GAPDH to ensure equal loading and expressed as fold change of control. Data are presented as Mean ± SEM (N=2-3). Results were analyzed using One-way ANOVA followed by Dunnett's post-hoc test. *P-value<0.05 was considered for statistical significance. *P-value<0.05; **P-value<0.01.

3.3.2.4 Effect on Cell Cycle

To examine whether the antiproliferative effect induced by compounds (**13**, **15** and **16**) on PC3 and DU45 cell lines is associated with cell cycle arrest, treated cells were stained with propidium iodide (PI) and subjected to flow cytometric analysis. The distribution of cells across different cell cycle phases was assigned based on the intensity of PI stain, which correlates with the quantity of DNA content in each phase. A representation of different cell cycle phases can be seen in Figures 25-A and 26-A, which represent in order cells in G0/G1, S, and G2/M phases. Our results showed that compounds **13**, **15** and **16** induced a slight accumulation in G2/M and sub G1 phases, which was accompanied by a reduction in G1/G0 and S phases in DU145 cell line; however, the effect was not statistically significant ($P > 0.05$). On the other hand, the G2/M phase was markedly increased with docetaxel by 1.9-2.6 folds as compared to control. These findings suggest that our compounds act through a distinct mechanism of action.

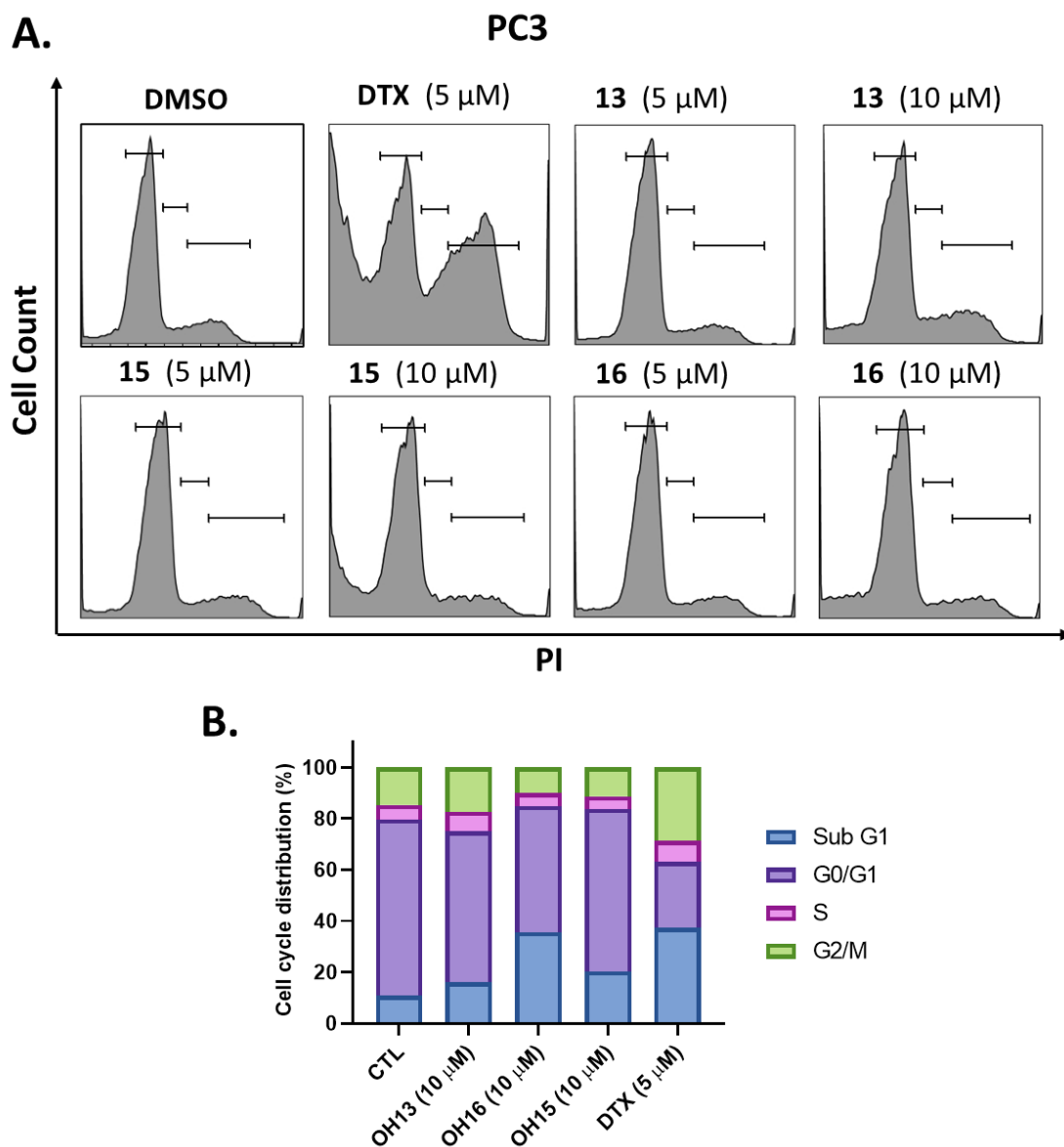


Figure 26. Effect of compounds **13**, **15** and **16** on cell cycle progression of PC3 cells. Cells were treated with DMSO, compounds **13**, **15** and **16** (5-10 μM), or docetaxel (5 μM) for 48 hours. (A) Cell cycle analysis by propidium iodide (PI) staining followed by flow cytometry of PC3 treated cells. (B) Quantitative measurement of cell distribution across different cell cycle phases (Sub G1, G0/G1, S, and G2/M, respectively) (N= 1).

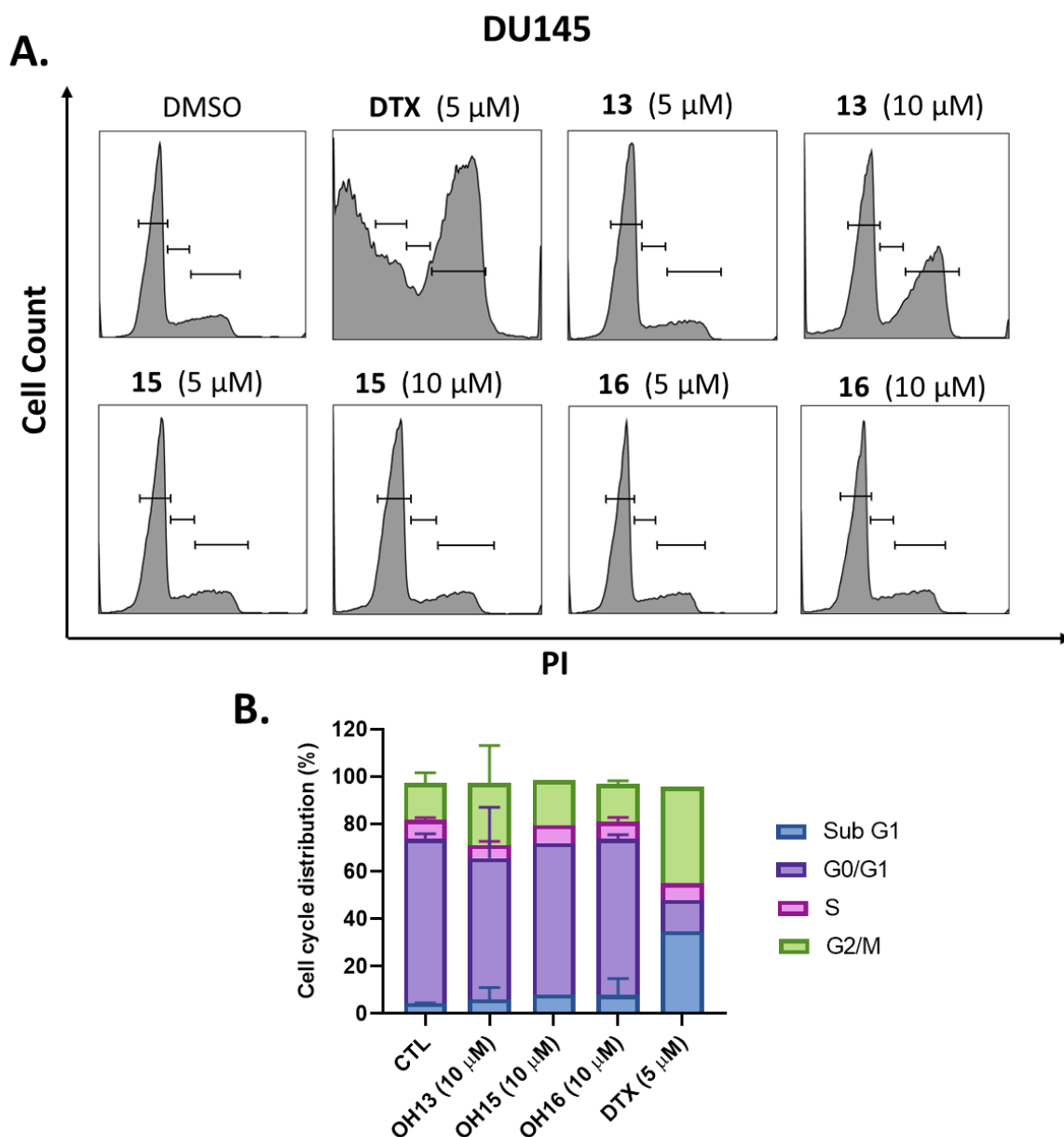


Figure 27. Effect of compounds **13**, **15** and **16** on cell cycle progression of DU145 cells. Cells were treated with DMSO, compounds **13**, **15** and **16** (5-10 μM), or docetaxel (5 μM) for 48 hours. (A) Cell cycle analysis by propidium iodide (PI) staining and following flow cytometry of DU145 treated cells. (B) Quantitative measurement of cell distribution across different cell cycle phases (Sub G1, G0/G1, S, and G2/M, respectively) expressed as Mean \pm SEM (N= 2). One-way ANOVA followed by Dunnett's posthoc test were used to compare the treatment groups with control. Results were considered statistically significant when $p < 0.05$.

3.3.2.5 Effect on Colony Formation

Anchorage-independent growth is a well-known characteristic of transformed cells that correlate with *in vivo* tumorigenic potential. Soft agar colony formation assay is a robust *in vitro* method used to estimate the ability of cells to grow and form tumors in-vivo. Therefore, we investigated colony formation of PC3 and DU145, in soft agar, under the effect of compounds **13** and **16** at 5 and 10 μM , for 14 days. Figures 27 and 28 show that compounds **13** and **16** resulted in a significant reduction in both the total number of colonies and average colony size in both cell lines. Specifically, compound **16** at 10 μM significantly reduced the number of colonies by 82.8% and 84.9% in PC3 and DU145 cell lines, in comparison to control, respectively. Similarly, the average size of detected colonies dramatically reduced from 583.2 to 20.0 mm^2 and from 196.0 to 18.7 mm^2 in PC3 and DU14, respectively, when exposed to 10 μM of compound **16** as compared to control. Interestingly, the reduction in average colony size induced by compound **16** on PC3 cells was stronger than the positive control, docetaxel, when compared at the same concentration ($P < 0.001$).

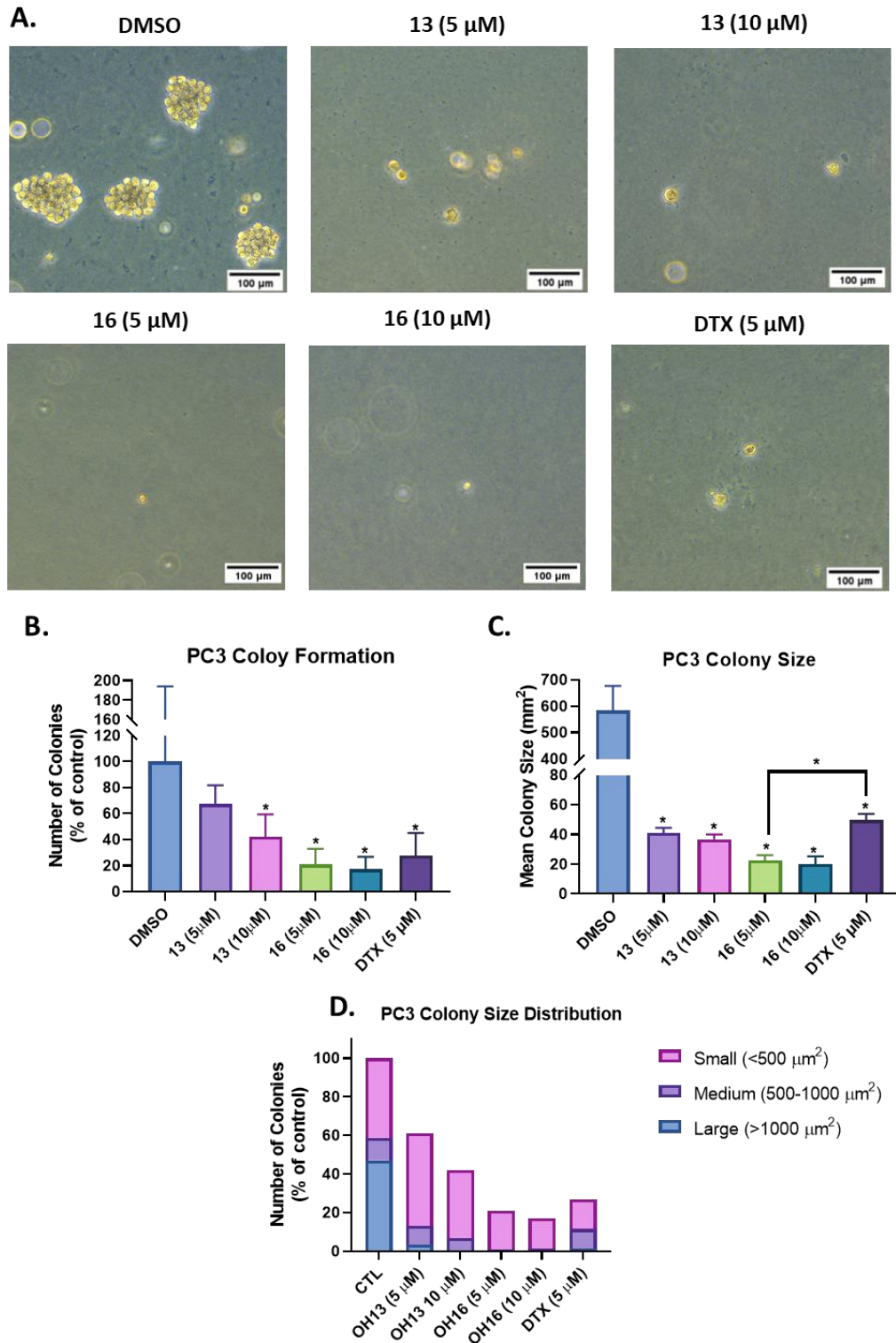


Figure 28. Effect of compounds **13** and **16** on colony formation of PC3 cell line. Cells were allowed to grow in soft agar for 14 days in the presence of the tested compounds. DMSO was used a negative control and docetaxel (DTX) at 5 μM as a positive control. A) Representative images of the soft agar colony formation on day 14. (B) Quantification of the number of colonies (>100 μm²) expressed as a percentage of

treatment relative to the control (Mean \pm SEM). (C) Average size (μm^2) of the formed colonies upon exposure to different treatments expressed as Mean \pm SEM. (D) Distribution of colonies into different size categories: Small (100-500 μm^2), Medium (500-1000 μm^2), and Large (>1000 μm^2). Colonies' size and number were quantified by ImageJ software in at least six random fields per treatment. Results were analyzed using One-way ANOVA followed by Dunnett's posthoc test. Results were considered statistically significant when $p < 0.05$. Scale bar represents 100 μm . * $p < 0.05$.

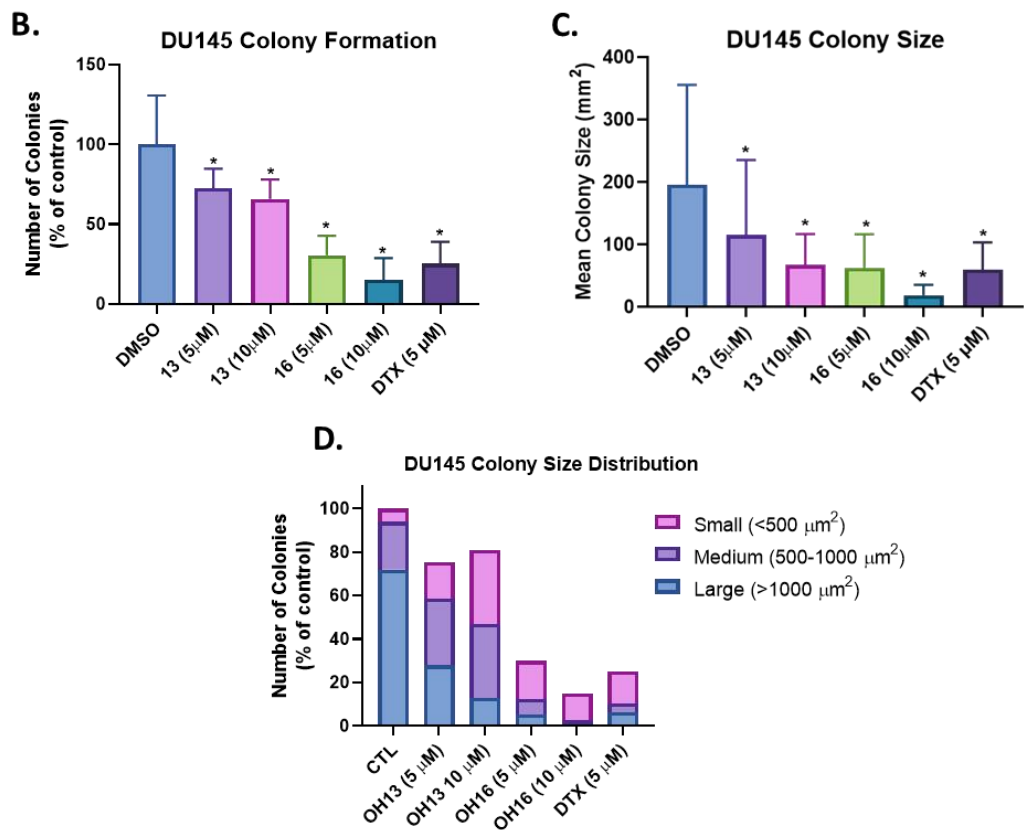
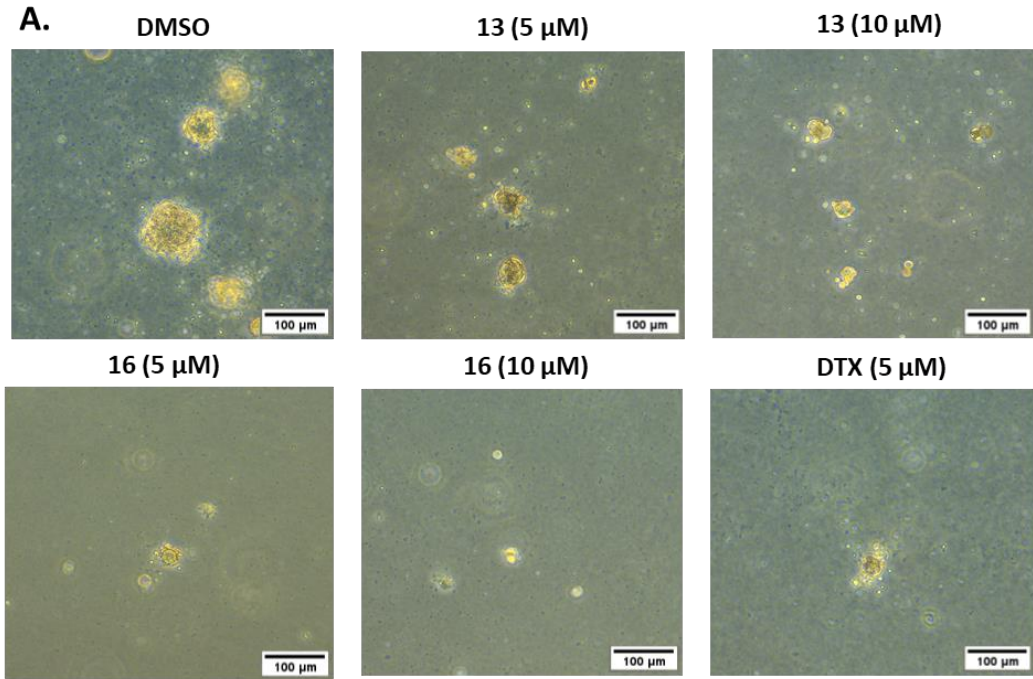


Figure 29. Effect of compounds **13** and **16** on colony formation of DU145 cell line. Cells were allowed to grow in soft agar for 14 days in the presence of the tested compounds. DMSO was used as a negative control and docetaxel (DTX) at 5 μM as a positive control. A) Representative images of the soft agar colony formation on day 14. (B) Quantification of the number of

colonies ($>100 \mu\text{m}^2$) expressed as a percentage of treatment relative to the control (Mean \pm SEM). (C) Average size (mm^2) of the formed colonies upon exposure to different treatments expressed as Mean \pm SEM. (D) Distribution of colonies into different size categories: Small ($100\text{-}500 \mu\text{m}^2$), Medium ($500\text{-}1000 \mu\text{m}^2$), and Large ($>1000 \mu\text{m}^2$). Colonies' size and number were quantified by ImageJ software in at least six random fields per treatment. Results were analyzed using One-way ANOVA followed by Dunnett's posthoc test. Results were considered statistically significant when $p < 0.05$. Scale bar represents $100 \mu\text{m}$. * $p < 0.05$.

3.3.2.6 *Effect on Cells Migration*

While localized prostate cancer has a good prognosis, progression to metastatic PCa dramatically reduces the 5-year survival rate to 30.2%. Therefore, we investigated the effect of compounds **13**, **15** and **16** on inhibiting the migratory potential of the invasive prostate cancer cell lines (PC3 and DU145). Two assays were used for this purpose; the first evaluated the effect on trans-well migration across pores and the other investigated migration over the plate surface. Our data revealed that compounds **13**, **15** and **16** significantly reduced trans-well migration of PC3 cells by 72.4%, 78.8%, and 96.2% ($P < 0.0001$), respectively, as compared to control when tested at $10 \mu\text{M}$ concentration (Figure 29). Moreover, the same compounds showed a dose-dependent reduction in wound closure against both cell lines, which was significant starting from $5 \mu\text{M}$ concentration in PC3 cells (Figures 31 and 32).

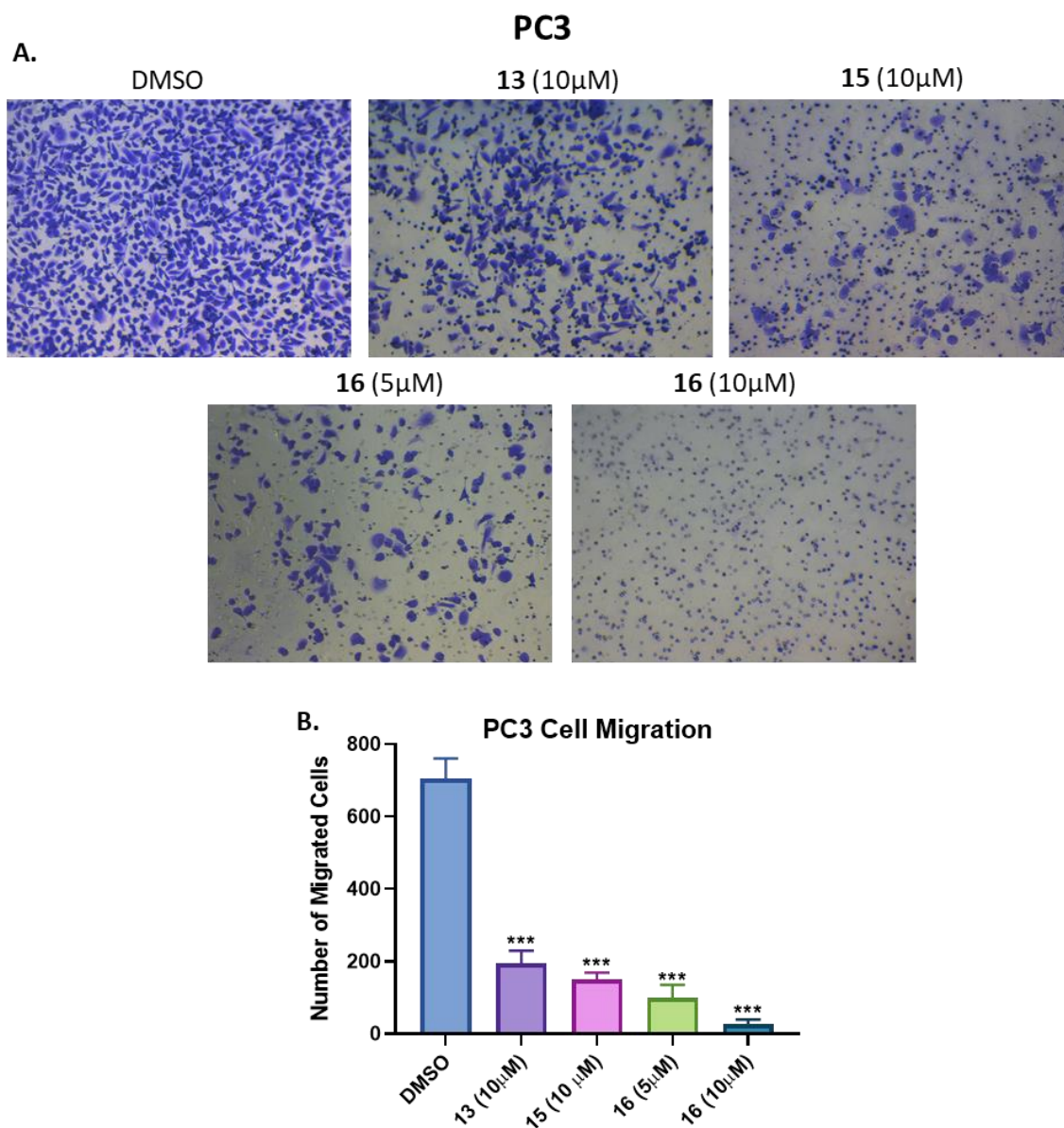


Figure 30. Effect of compounds **13**, **15** and **16** on Transwell migration of PC3 cells. (A) Representative microscopic images of migrated cells following 48 hours incubation with the indicated treatment. (B) The average number of migrated cells counted using ImageJ from 4-6 random fields (N=2). Results were analyzed using one-way ANOVA followed by Dunnett's posthoc test. Results were considered statistically significant when $p < 0.05$. *P-value < 0.05 ; **P-value < 0.01 ; ***P-value < 0.001 .

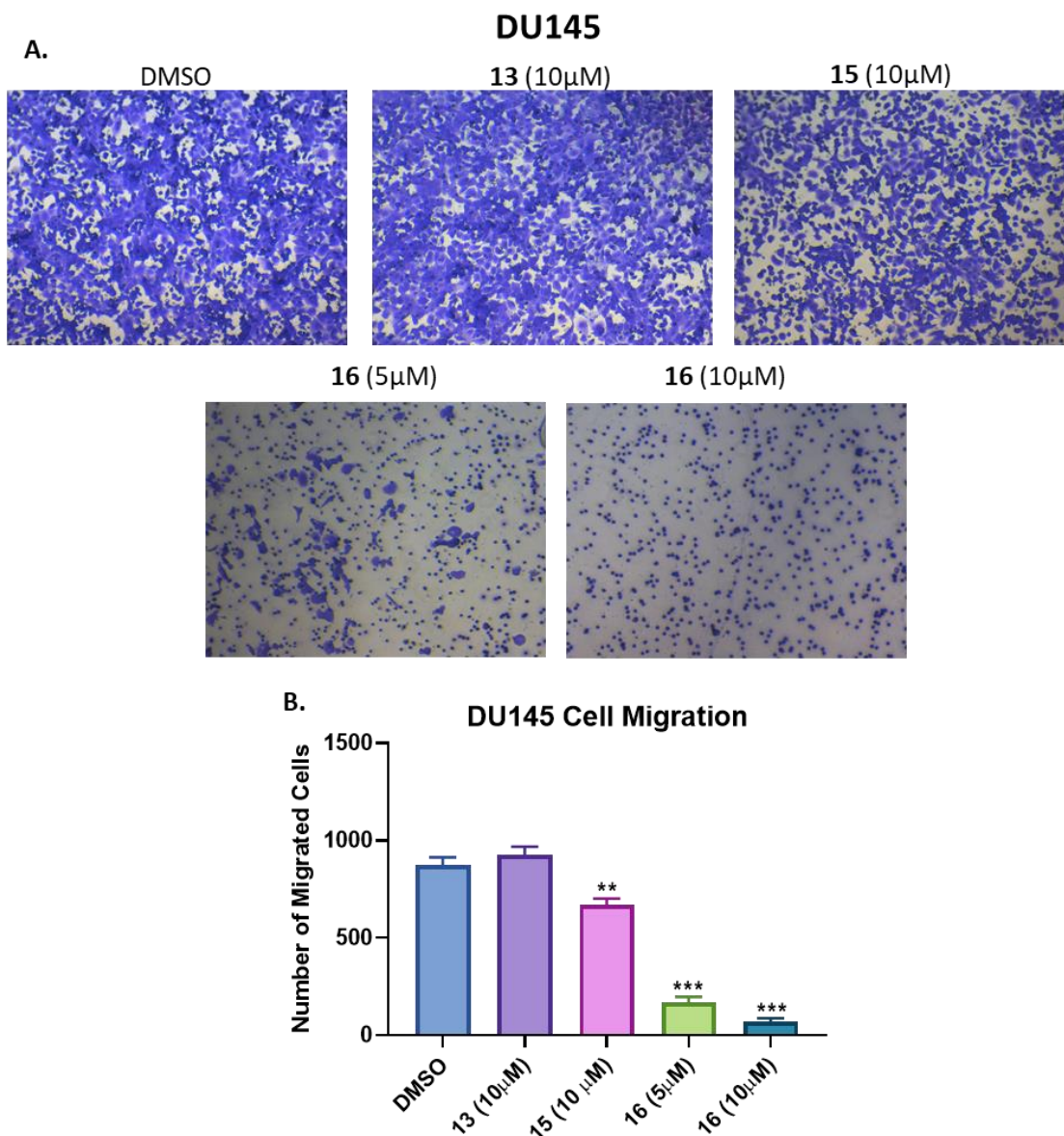


Figure 31. Effect of compounds **13**, **15** and **16** on Transwell migration of DU145 cells. (A) Representative microscopic images of migrated cells following 48 hours incubation with the indicated treatment. (B) The average number of migrated cells counted using ImageJ from 4-6 random fields (N=2). Results were analyzed using one-way ANOVA followed by Dunnett's posthoc test. Results were considered statistically significant when $p < 0.05$. *P-value < 0.05 ; **P-value < 0.01 ; ***P-value < 0.001 .

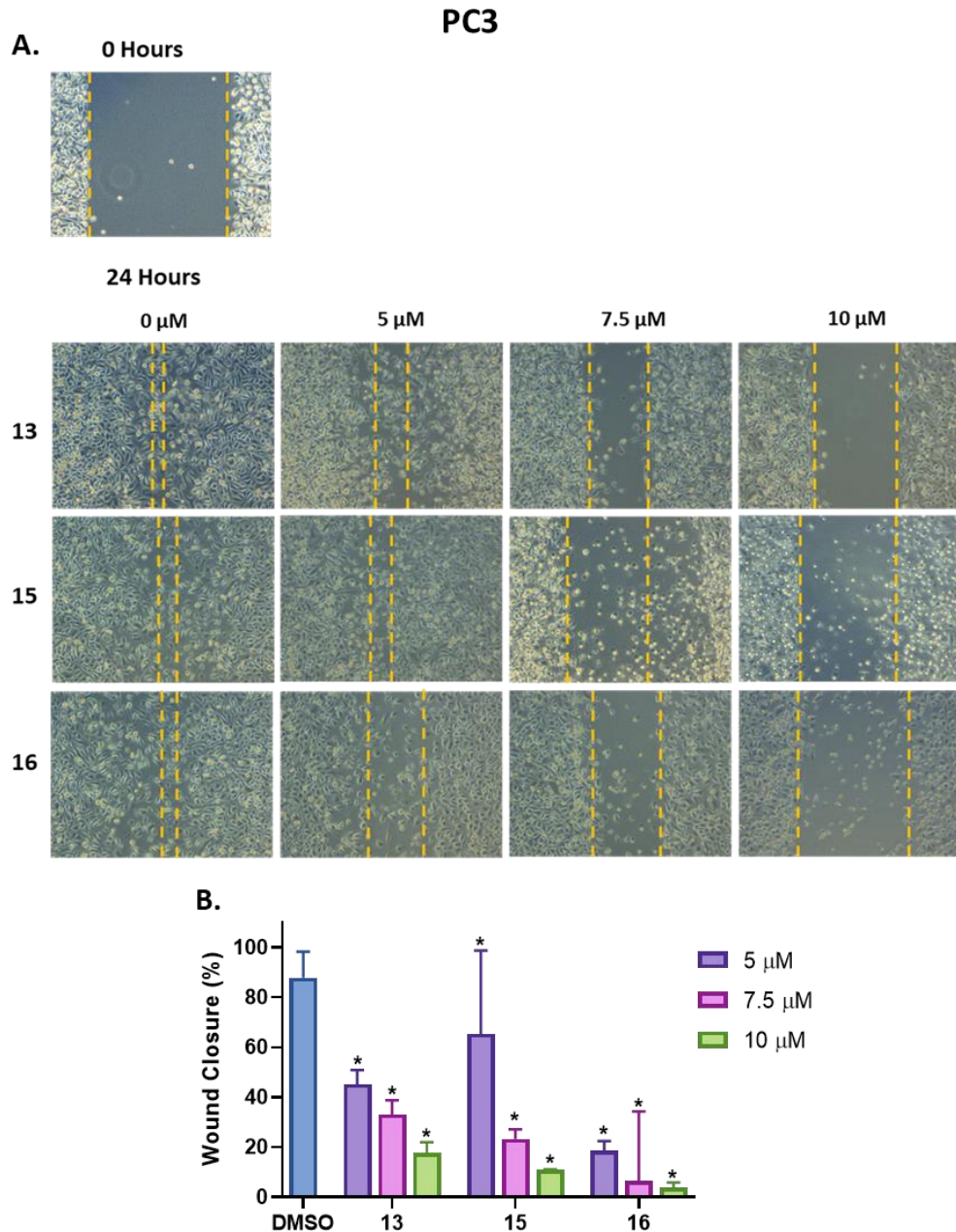


Figure 32. Effect of compounds **13**, **15** and **16** on the migration of PC3 cells in wound healing assay. A) Shows representative images of the scratch at $t=0$ and 48hours post-treatment ($N=2 \times 2$). B) Quantitative analysis of cell migration based on wound area at 24 hours over the initial area measured at three different points per scratch. Values are expressed as a percentage of wound closure at the end of the experiment relative to $t=0$ hours (Mean \pm SEM). One-way ANOVA followed by Dunnett's posthoc test were used to compare the treatment groups with Control. Results were considered statistically significant when $p<0.05$.

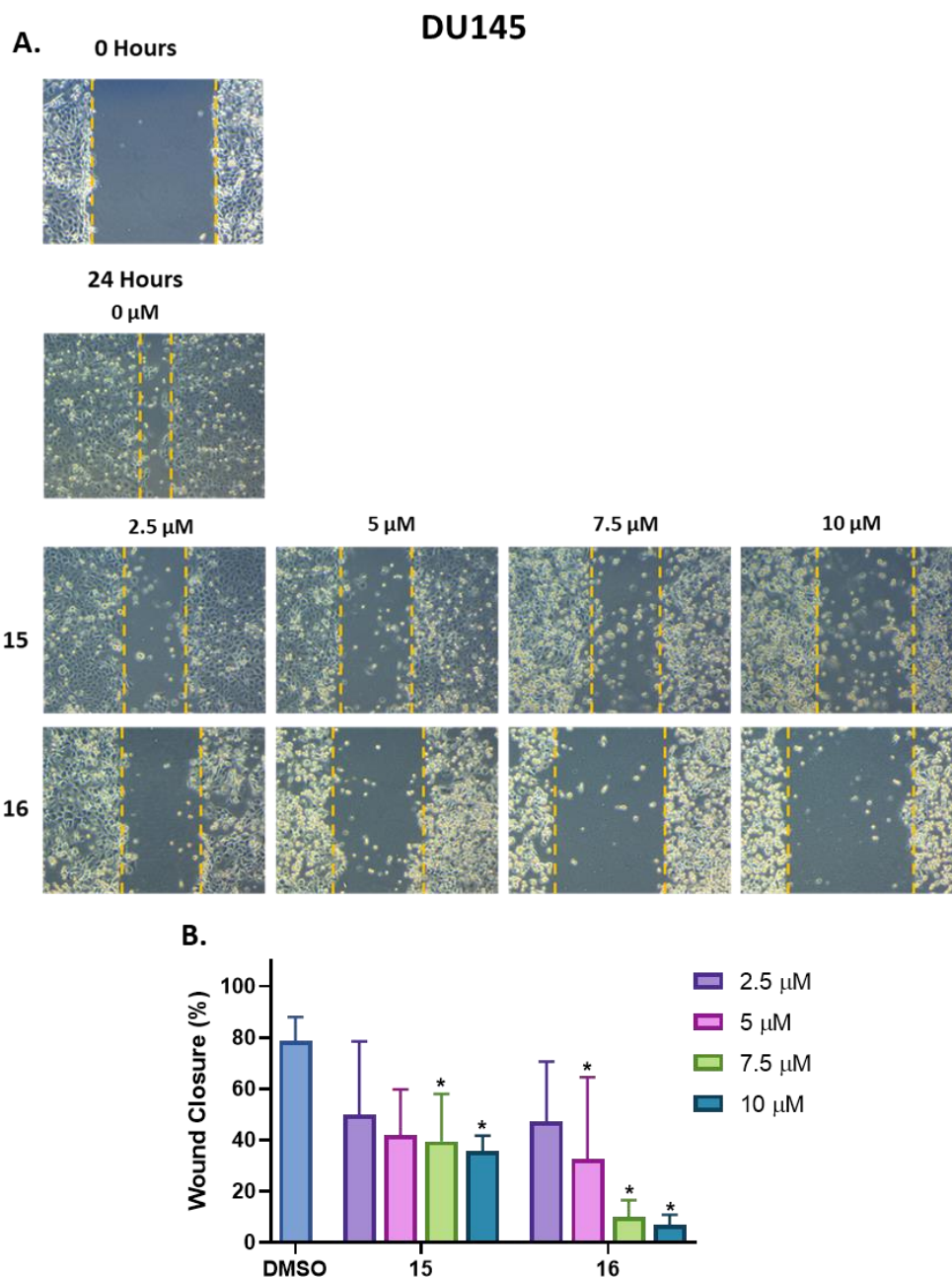


Figure 33. Effect of compounds **15** and **16** on the migration of DU145 cells in wound healing assay. A) Shows representative images of the scratch at $t=0$ and 48 hours post-treatment ($N=2 \times 2$). B) Quantitative analysis of cell migration based on wound area at 48 hours over the initial area measured at three different points per scratch. Values are expressed as a percentage of wound closure at the end of the experiment relative to $t=0$ hours (Mean \pm SEM). One-way ANOVA followed by Dunnett's posthoc test were used to compare the treatment groups with Control. Results were considered statistically significant when $p < 0.05$.

Based on findings from cell migration assays, we hypothesized that compounds **13**, **15**, and **16** might play a role in modulating the EMT process, which is linked to cancer invasion and metastasis. Therefore, we explored the effect of our compounds on key proteins involved in EMT using two cell lines (PC3 and DU145). The explored proteins included E-cadherin, total and phosphorylated β -catenin, and fascin. As shown in Figures 33 and 34, there was a trend towards modest reduction in total and phospho- β -catenin in both cell lines, significant only for total β -catenin in DU145. Additionally, compound **16** was able to significantly upregulate the expression of E-cadherin in DU145 cells (P-value 0.05). However, no significant changes were noted for the compounds on the expression of fascin in both cell lines. These findings indicate that compounds **13**, **15** and **16** might potentially target EMT in PCa; however, the observed effect was not strong enough to explain the anticancer potential of the compounds.

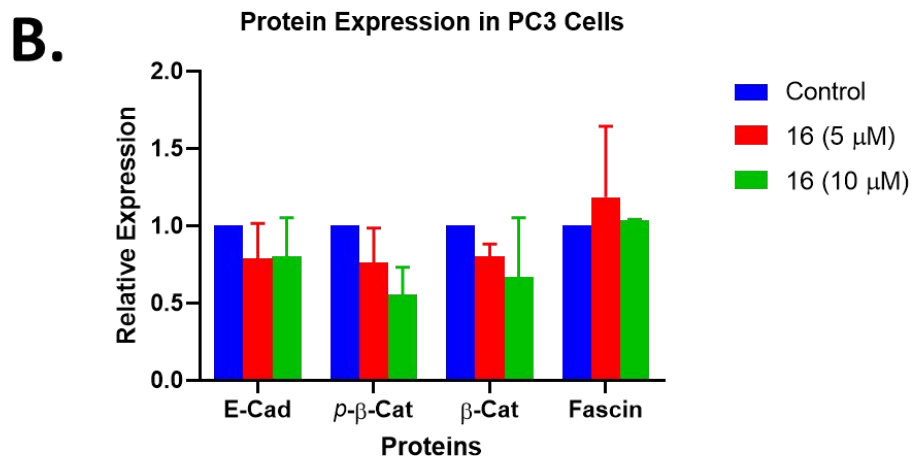
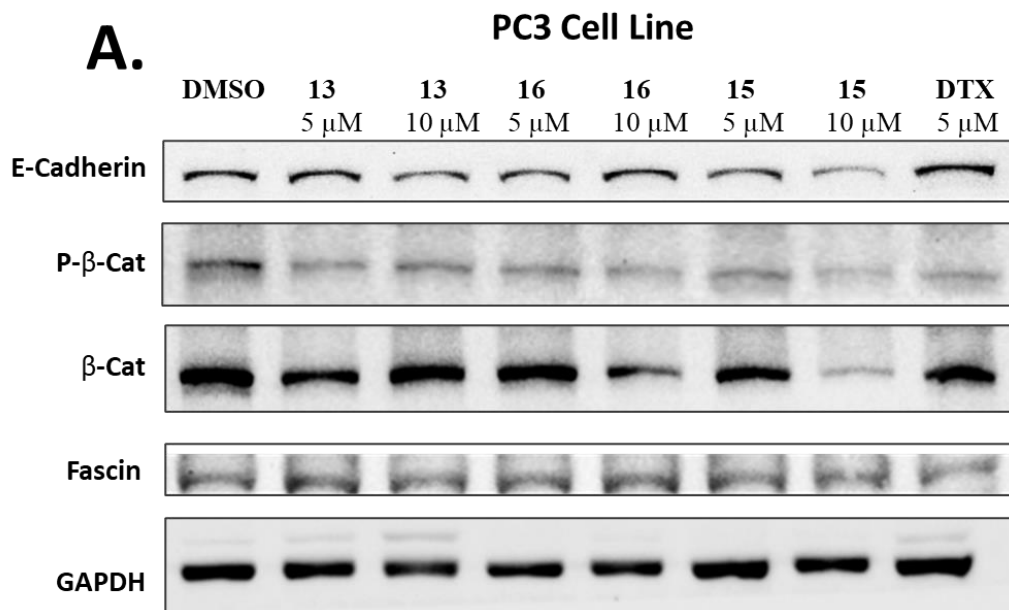


Figure 34. Protein expression of EMT-related biomarkers on PC3 cell line. A) Representative outcomes of molecules **13**, **15** and **16** (5 and 10 μ M) on the expression of E-cadherin, p- β -catenin, β -catenin, and fascin proteins at 48 hours posttreatment. DMSO and 5 μ M docetaxel (DTX) were used negative and positive controls, respectively. B) Protein expression of compound **16** bands quantified as a percentage relative to DMSO. GAPDH was used as a house-keeping protein for the normalization of values. The values were expressed as Mean \pm SEM (N=2-3). Results were analyzed using One-way ANOVA followed by Dunnett's posthoc test. *P-value<0.05 was considered for statistical significance.

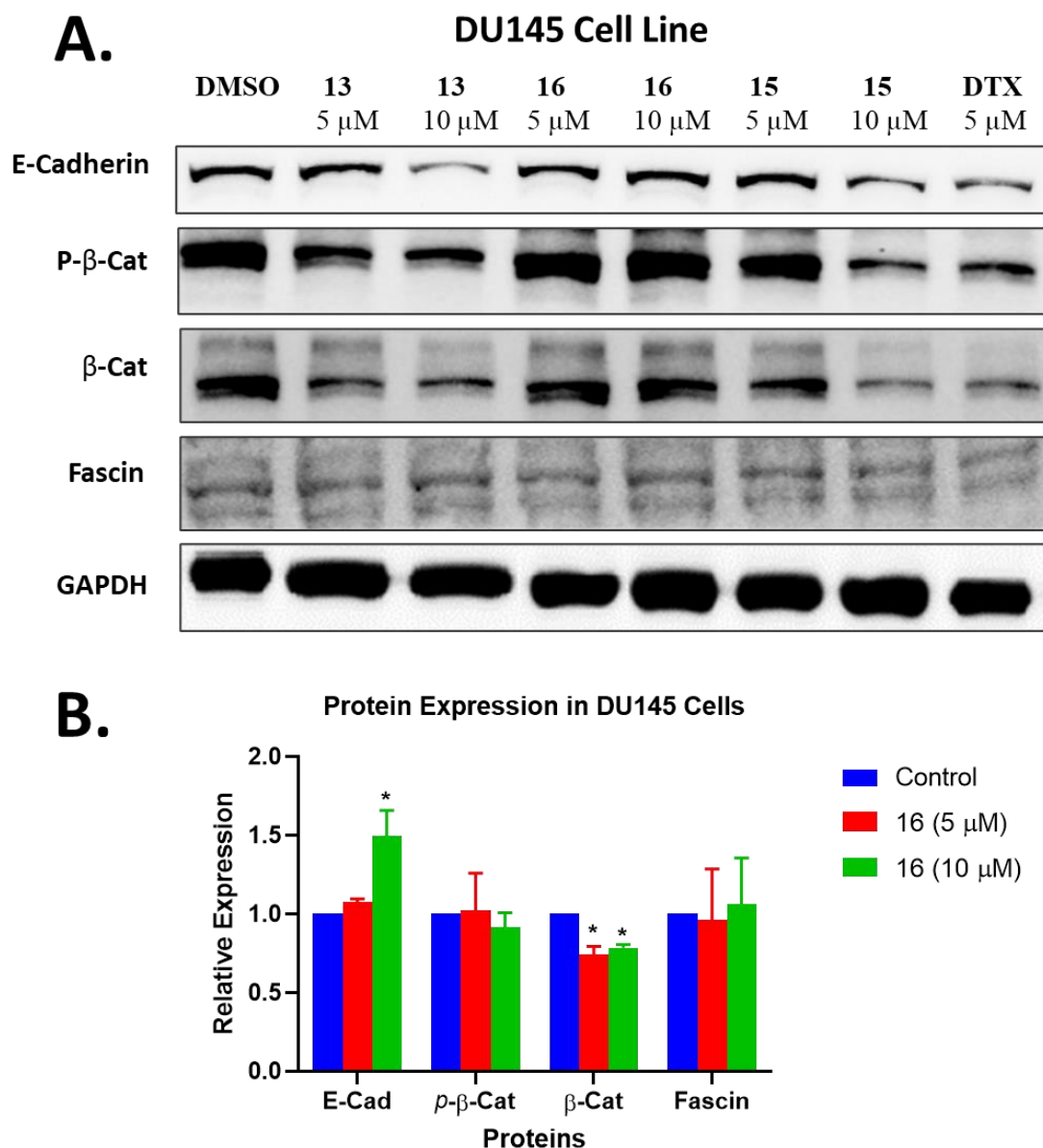


Figure 35. Protein expression of EMT-related biomarkers on DU145 cell line. A) Representative outcomes of molecules **13**, **15** and **16** (5 and 10 μ M) on the expression of E-cadherin, p- β -catenin, β -catenin, and fascin proteins at 48 hours posttreatment. DMSO and 5 μ M docetaxel (DTX) were used as negative and positive controls, respectively. B) Protein expression of compound **16** bands quantified as a percentage relative to DMSO. GAPDH was used as a house-keeping protein for the normalization of values. The values were expressed as Mean \pm SEM (N=2-3). Results were analyzed using One-way ANOVA followed by Dunnett's posthoc test. *P-value < 0.05 was considered for statistical significance.

3.3.2.7 *Effect on other Molecular Pathways*

JNK/JUN, PI3K/AKT and MEK/ERK signaling pathways were reported to be activated in various cancers, including PCa. Therefore, we attempted to explore the direct effect of the most active compounds on JNK1/2/3, total and phosphorylated ERK, and total and phosphorylated AKT. Our results revealed that in PC3 cell line, molecule **16** had significantly reduced the expression of JNK1/2/3 and phosphorylated ERK1/2, without significantly altering ERK1/2, p-Akt, and Akt (Figure 35). In effect comparable to that of compound **16**, compound **15** had reduced the expression of JNK1/2/3, p-ERK1/2, Akt and p-Akt. Both compounds maintained the same effect on JNK1/2/3 in DU145 cell line (Figure 36). All compounds were also able to maintain the downregulation of AKT in DU145 cell line without altering the expression of p-Akt.

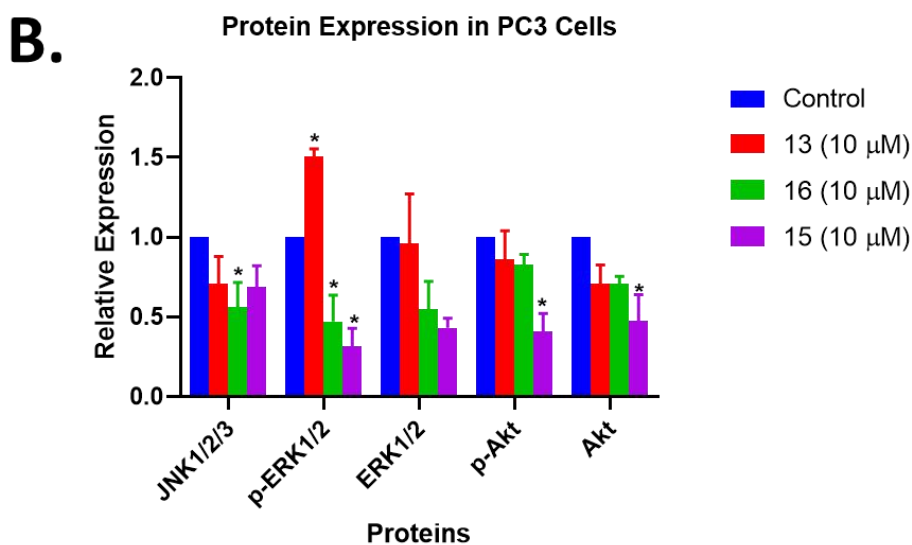
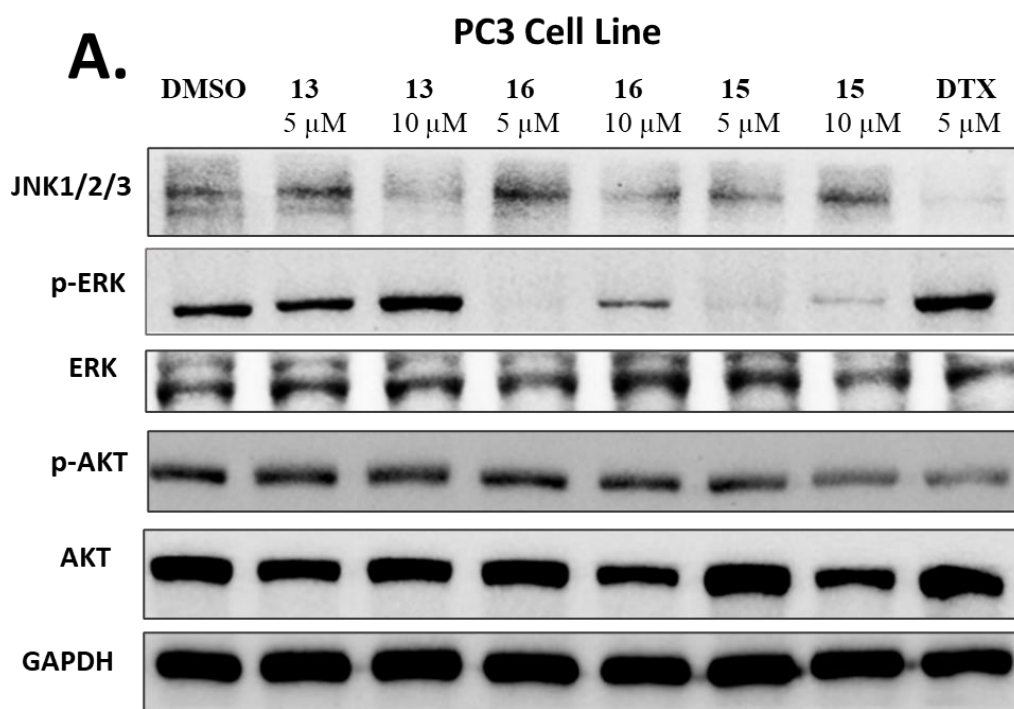


Figure 36. Protein expression of JNK, ERK, and AKT-related biomarkers on PC3 cell line. A) Representative outcomes of molecules **13**, **15** and **16** (5 and 10 μ M) on the expression of JNK1/2/3, p-ERK, ERK, P- AKT and AKT proteins at 48 hours posttreatment. DMSO and 5 μ M docetaxel (DTX) were used negative and positive controls, respectively. B) Protein expression of the bands quantified as a percentage relative to DMSO. GAPDH was used as a house-keeping protein for the normalization of values. The values were expressed as Mean \pm SEM (N=2-3). Results were analyzed using One-way ANOVA test. *P-value<0.05 was considered for statistical significance.

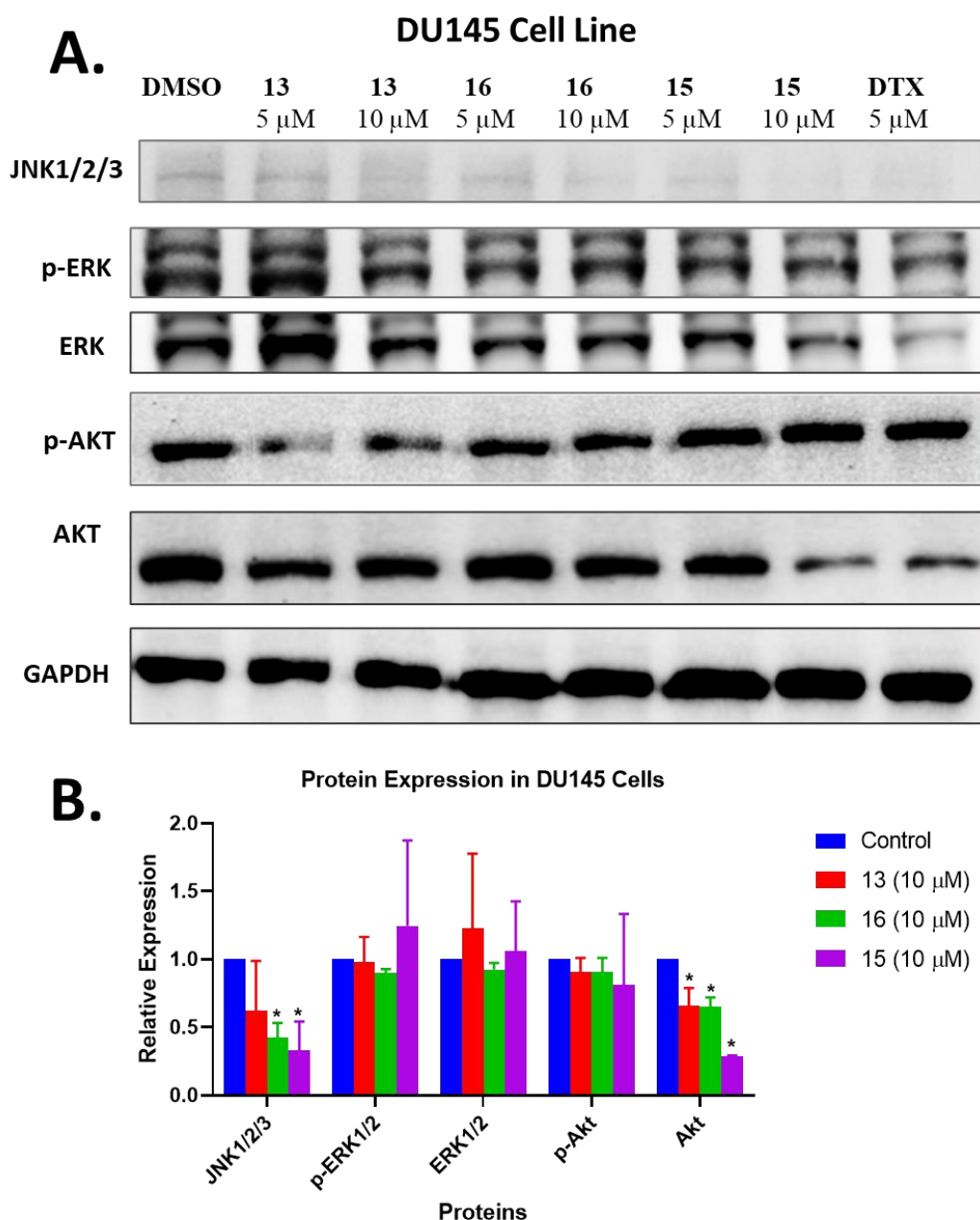


Figure 37. Protein expression of JNK, ERK, and AKT-related biomarkers on DU145 cell line. A) Representative outcomes of molecules **13**, **15** and **16** (5 and 10 μ M) on the expression of JNK1/2/3, p-ERK, ERK, P- AKT and AKT proteins at 48 hours posttreatment. DMSO and 5 μ M docetaxel (DTX) were used negative and positive controls, respectively. B) Protein expression of the bands quantified as a percentage relative to DMSO. GAPDH was used as a house-keeping protein for the normalization of values. The values were expressed as Mean \pm SEM (N=2-3). Results were analyzed using One-way ANOVA test. *P-value<0.05 was considered for statistical significance.

3.3.2.8 *Effect on Angiogenesis*

Uncontrolled angiogenesis is a key factor in cancer progression, invasion, and metastasis. Therefore, we sought to investigate the effect of our compounds on angiogenesis using the CAM of chicken embryos. Treating embryos with compound **16** leads to a significant reduction in average vessel length, a total number of junctions, and vessel area, suggesting that it might act as an angiogenesis inhibitor (Figure 37). The impact of the antiangiogenic effect might be more evident when the antitumor activity is evaluated *in vivo*. Inhibition of blood vessel formation blocks blood supply for tumor and thus inhibit its growth.

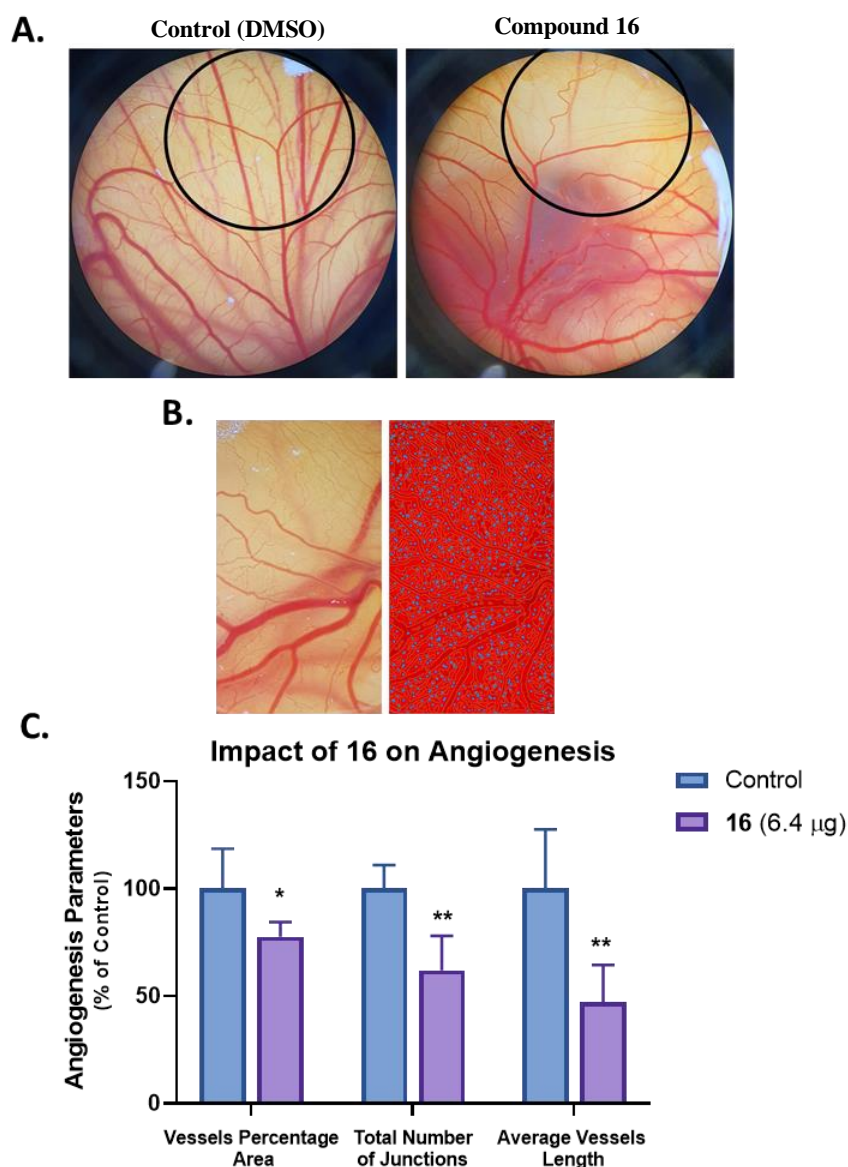


Figure 38. Effect of Compound **16** on Angiogenesis of the CAM of chicken embryos. (A) Embryos were treated with DMSO (2 μ L) or compound **16** (6.42 μ g in 2 μ L DMSO), and images were taken using stereomicroscope 48 hours post-treatment (N = 15). We note that compound **16** treatment inhibits the CAM's angiogenesis in comparison with the internal control (untreated area of CAM) and external control (untreated embryos). (B) Illustration of angiogenesis quantification by AngioTool software. (C) Percentage of reduction in angiogenesis parameters (vessel percentage area, total number of junctions, and average vessel length) relative to DMSO treated embryos (Mean \pm SEM; N=15). Unpaired t-test was used to compare treatment groups and results were stated as statistically significant when $p < 0.05$ compared to the control. * $p < 0.05$, ** $p < 0.01$.

3.3.3 Expanded SAR Study (Compounds 13-26)

Out of the sixteen synthesized and evaluated compounds in the first phase of the study, thienyl pyridine chalcone hybrids (**13**, **15** and **16**) exhibited the most promising anticancer potential against two of the most aggressive prostate cancer cell lines (PC3 and DU145). This was clearly evident from their highly potent cytotoxicity and attractive effect on modulating cancer-related pathways. Based on these findings and since our study is the first to report the incorporation of thienyl pyridine within the chalcone scaffold, we decided to expand further in this series. Therefore, ten additional thienyl pyridine chalcone hybrids were synthesized to explore structural attributes that may enhance or diminish the activity. The structural diversity in the new analogs was introduced by varying substitutions at ring A of the chalcone while keeping the thienyl pyridine and the enone moieties intact.

Three main aspects were explored in the SAR study: the impact of α -conformational restriction (cyclic analogs), particularly with tetralone ring; the effect of varying the methoxylation pattern; and the effect of replacing methoxy with other electron-donating groups (EDG) or electron-withdrawing groups (EWG).

As shown in Figure 38, all the newly synthesized analogs (**17-26**) possessed excellent cytotoxicity, especially against PC3 cell line (>90% reduction in cell viability at 10 μ M concentration) except for compound **23**. To distinguish between the activity of different analogs, compounds were tested at lower concentrations (2.5 and 5 μ M).

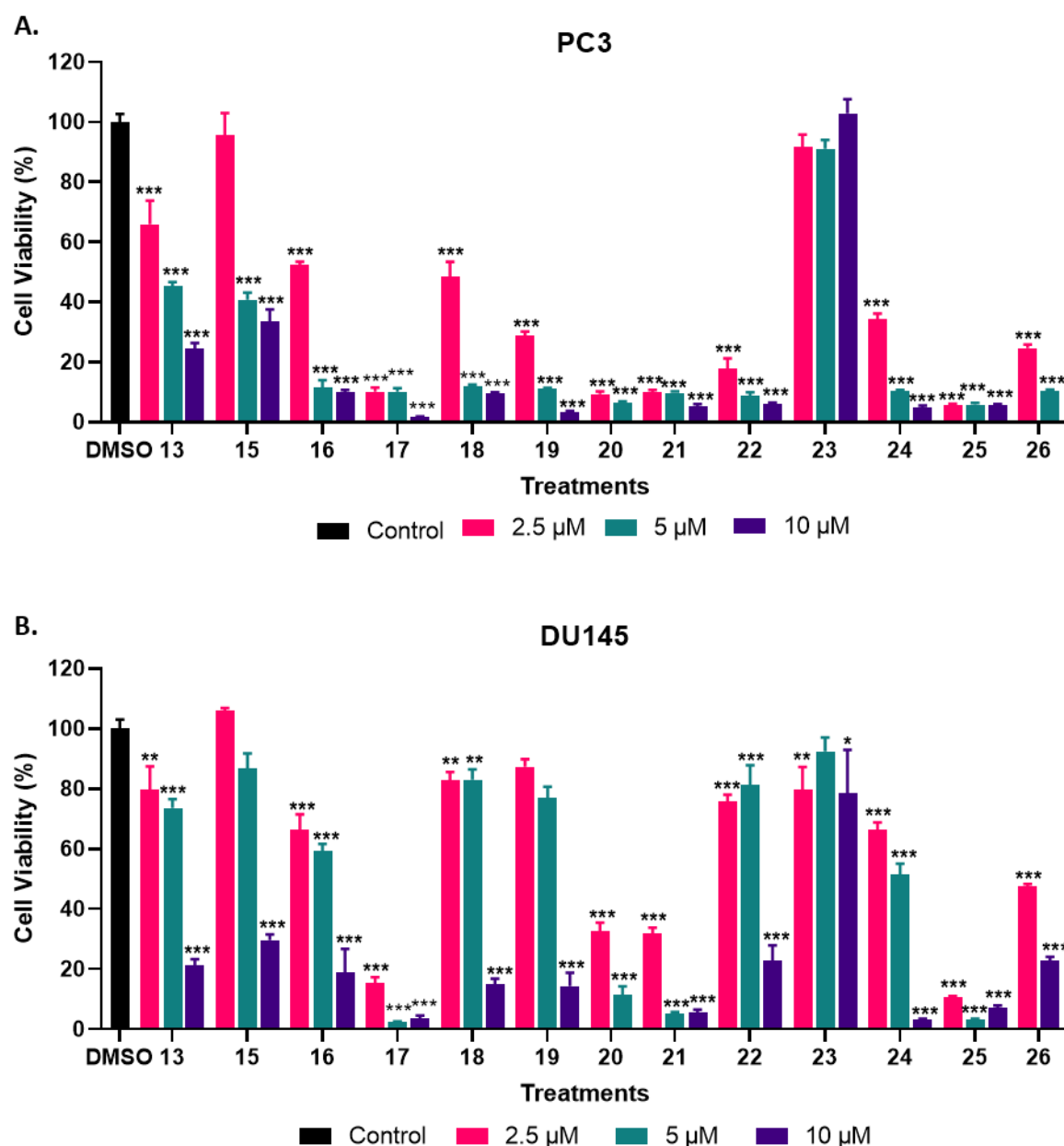


Figure 39. Effect of thienyl pyridine chalcone hybrids (**13-26**) on the cell viability of (A) PC3 and (B) DU145 cell lines. The cells were treated with 2.5, 5 and 10 μ M concentrations of compounds **13-26**. Cell viability relative to control (0.1% DMSO) was measured by AlamarBlue after 48 hours of treatment. Data are presented as Mean \pm SEM of three independent experiments. One-way ANOVA followed by Tukey's posthoc test was used to compare the treatment groups. Results were considered statistically significant when $p < 0.05$. * $p < 0.05$, ** $p < 0.01$, and *** $p < 0.001$.

First, we evaluated the cytotoxicity of tetralone-based chalcones (**13**, **14** and **15**) in comparison with their matched non-cyclic chalcones (**16**, **18** and **19**). The data clearly shows that the non-cyclic chalcones displayed higher cytotoxicity, suggesting that the tetralone ring lowered the antiproliferative activity of the thienyl pyridine chalcone hybrids.

Next, we examined various mono, di, and tri-methoxy substituted analogs. Interestingly, changing the position of the methoxy group from C3 to C2 resulted in a profound improvement in the cytotoxicity where the reduction in cell viability of PC3 induced by 2.5 μ M treatment increased from 47.5% to 84.7% for compound **16** and **17**, respectively. Investigation of various methoxy substituted analogs revealed that 2-methoxy induced the most favorable antiproliferative activity, followed by 2,3,4- and 2,4,6-tri-methoxy substituents. On the other hand, analogs with 4-methoxy substituents, including 3,4-dimethoxy and 3,4,5-trimethoxy, showed reduced activity, especially against DU145 cell line.

Then, we evaluated the effect of incorporating other EDG or EWG at position-2 and -4. Replacing 4-methoxy in (**18**) with 4-fluoro (**26**) improved the cytotoxic activity. In contrast, substituting it with methyl sulfonyl (**23**) was detrimental for the activity. For position 2, replacing the methoxy in (**17**) with trifluoromethyl group maintained relatively similar cytotoxicity, whereas replacing it with less bulky EDG (hydroxy) decreased the cytotoxicity.

Overall, it could be concluded that 2-methoxy and 2-trifluoromethyl substitutions on ring A are optimum for the antiproliferative potential of thienyl-pyridine chalcone hybrids (Figure 39). Taken together, these findings indicate that compounds **17** and **23** holds a highly promising potential of being lead anticancer molecule and thus further *in vitro* and *in vivo* studies on these analogs are warranted.

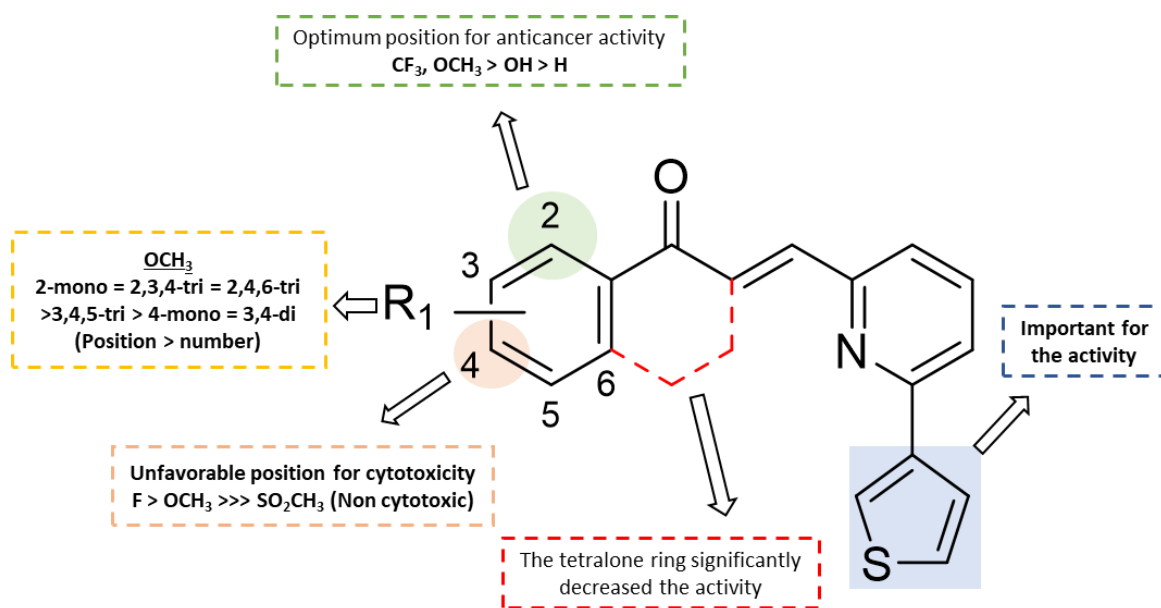


Figure 40. Key structure-activity relationship (SAR) findings.

CHAPTER 4: DISCUSSION

PCa is the second most frequently diagnosed malignancy and a leading cause of cancer-related mortality in men globally (1, 2). Despite the initial response to targeted hormonal therapy, the majority of patients ultimately progress to a lethal form of the disease, termed castration-resistant prostate cancer (CRPC) (78). Several new therapeutic options were approved for the treatment of CRPC over the past decade, yet treatment resistance remains inevitable. Besides, these therapies suffered from several limitations, including but not limited to unsatisfactory therapeutic benefits and serious toxicities. Moreover, the use of some drugs, such as androgen receptor targeting agents, was found to induce significant changes in cancer cell biology, leading accumulation of aggressive subpopulations and upregulations of pathways linked to cancer, complicating future treatment (106, 155). Therefore, there is an urgent need for new effective and safe therapeutic agents that could improve PCa patients' survival and quality of life.

One of the highly attractive scaffolds that are currently being investigated as potential multitargeted anticancer agents is chalcone. Due to their fascinating biological properties, chalcones-rich plants were historically used in traditional medicine. Besides, population-based studies in countries with a high dietary intake of chalcones were correlated with a lower incidence of cancer (160). Particularly in prostate cancer, chalcones have shown an attractive ability to target cancer-related pathways and processes. However, they have not been studied deeply enough to enter into subsequent developmental steps for the treatment of PCa. This could be partially attributed to the poor pharmacokinetic profile, lack of selectivity, and/ or modest potency. From our comprehensive review on the reported chalcones with activity against PCa, we noticed that the natural chalcones tend to have a better ADMET profile and selectivity but a

lower potency. On the other hand, many of the optimized synthetic chalcones exhibited high potency but a poor ADMET profile, hindering further development (Table S1 in Appendix A and Figure 40). Moreover, the chalcone scaffold has been known for a long time; therefore, many of the chalcones showing anticancer activity are not completely novel and patentable. Evaluating drugs in clinical trials is the most costly stage in the drug development process. Therefore, drug companies do not invest in compounds without ensuring their protection regardless of their efficacy *in vitro* or *in vivo* (179).

Therefore, we hypothesized that the design of novel chalcone analogs with improved potency, selectivity and ADMET profile might lead to overcoming current chalcones' limitations and increase the probability of moving along the drug development process. To achieve this goal, we sought to develop novel chalcones through hybridization with heteroaromatic rings that are known to possess anticancer activity such as pyridine, pyrrole and thiophene, aiming to improve their efficacy. Moreover, we incorporated *in silico* ADMET prediction to guide our design process towards prioritizing hits with favorable drug-likeness properties to reduce the risk of failing subsequent development steps. Additionally, we focused on aromatic rings that were not investigated before as anticancer nor in any other application. More specifically, for series B and C, we moved beyond ensuring the novelty of single analogs towards designing an entirely new series of chalcones with moieties that were hybridized with chalcone scaffold for the first time.

In this study, we designed three series of novel chalcone analogs comprising nitrogen mustard (series A), cyclopropyl pyrrole (series B) or thienyl pyridine (series C) in ring B. Within each series, we compared cyclic (tetralone-based) chalcones with the non-cyclic (basic) chalcone scaffold. Besides, the effect of incorporating different

electron-donating or withdrawing groups were investigated with a particular focus on methoxylation pattern. This is because methoxylation pattern was found to modulate the anticancer activity in many studies (280). Specifically, the SAR was thoroughly investigated in series C due to its promising anticancer potential. Next, ADMET *in silico* screening was implemented, and analogs with favorable drug-likeness properties were prioritized.

A total of 26 analogs were then synthesized, purified and their structures were elucidated by various characterization studies (FT-IR, ¹H-NMR, ¹³C-NMR, COSY NMR, ESI-MS and elemental analysis). Additional analyses were conducted for selected analogs (HMBC, HSQC, HMQC, NOESY, ¹⁹F-NMR) to fully assign protons and carbons. Of note, the synthetic yield of the non-cyclic chalcones was generally higher than their matched tetralone-based chalcone analogs. Besides, we were able to assign the configuration of open chain chalcones with high confidence based on the typical coupling constant of (*E*) configuration. On the other hand, we could not confirm tetralone-based chalcones' configuration in the same way due to the lack of α -proton. Nevertheless, the available NOESY NMR data suggest (*E*) configuration, consistent with previous studies (276, 277). To certainly assign the configuration for these analogs, we need to do additional analysis such as x-ray crystallography.

The Synthesis of the selected analogs was done side-by-side with the biological anticancer screening, where series showing promising anticancer activities were expanded and those showing weak cytotoxicity were terminated. For the biological evaluation, we focused on two AR-negative cell lines (PC3 and DU145). These cells were selected as they are among the most widely used *in vitro* models for CRPC, the deadly stage of prostate cancer (281). Besides, these cell lines are reported to exhibit neuroendocrine and cancer-stem cell markers, two of the most aggressive and lethal

subtypes of CRPC (282, 283).

As a start point, we first evaluated a series of tetralone-based chalcone analogs (series A) related to the nitrogen mustard-based chalcone (**DK14**) developed by our research team, which was recently patented and published (170, 272). This analog was able to significantly target TNBC cells *in vitro* (IC_{50} 6.3-9.22) and reduce tumor growth *in vivo*. In this series, we synthesized five analogs and tested them in comparison with **DK14**. In contrast to the findings from the TNBC study, the effect of both **DK14** and our newly synthesized analogs (**1-5**) against PCa cell lines (PC3 and DU145) was modest ($IC_{50} >10 \mu M$). Next, we developed another **DK14** related series by replacing the nitrogen mustard with a cyclopropyl pyrrole functional group as a potential bioisostere. In addition to its potential activity, this group leads to a dramatic improvement in the predicted ADMET profile. The predicted ADMET risk (number of possible ADMET problems the drug might face in development) for this series ranged from (1.6-2.5) compared to 5.77 for **DK14**. More specifically, series B analogs are expected to have better solubility and bioavailability profiles (Table 4). Similar to series A, these analogs did not result in highly potent cytotoxicity against PCa cell lines and their effect was comparable to **DK14**.

Due to unsatisfactory cytotoxic activity generated by the first two series, we designed a new line of chalcone derivatives. In this series, we adopted a molecular hybridization strategy as it was shown to be effective in improving the pharmacological activity of many reported molecules (186). Among the different potential heteroaromatic rings with reported anticancer activity, we focused on pyridine and thiophene rings. An analysis of the most privileged structures among the approved drugs showed that N-heterocyclic rings were the most commonly reported moieties (incorporated in 59% of the approved drugs) (284). Among them, pyridine was the most

commonly identified N-heteroaromatic ring. For instance, the second generation ARAT agent, abiraterone acetate, used for the treatment of CRPC is a pyridine-based androstane steroid. In this study, we developed different 3'-pyridine substituted chalcones, among which thienyl pyridine-containing analogs (**13**, **15**, and **16**) showed the most promising cytotoxicity against both DU145 and PC3 cell lines.

Therefore, these analogs were selected for further screening to evaluate their antitumor potential and explore their mechanism of action against CRPC. In the mechanistic study, we explored their selectivity and effect on the main carcinogenesis-related cellular processes, namely colony formation, cell cycle, apoptosis, and migration. Besides, their effect on major cancer-related molecular pathways was studied by western blot. Additionally, their impact on angiogenesis was evaluated *in ovo* using the CAM of the chicken embryo.

Compounds (**13**, **15** and **16**) significantly induced cytotoxicity in both PC3 and DU145 cell lines with relatively good potency. Notably, compound **16** showed the most potent cytotoxicity with an IC₅₀ of 4.32 and 5.2 μ M against PC3 and DU145, respectively. Interestingly, the three compounds have shown high selectivity toward PCa lines as compared to normal dental cells (selectivity index ranging from 5.7 to more than 8.9). However, the selectivity data need to be interpreted with caution since primary dental cells were used for safety assessment due to the lack of more relevant models (i.e., primary prostate epithelial cells).

Apoptosis is a fundamental process to target as it regulates the balance between cell survival and cell death, and prevent tumor growth. (285). Morphological examination of cells treated with compounds **13**, **15** and **16** showed cell detachment, wall deformation, and formation of apoptotic bodies. To confirm the potential effects of the tested compounds on apoptosis, we used flow cytometric analysis, which

revealed a significant induction of apoptosis by compounds **15** and **16**, mainly at 10 μ M and to increase the Bax/Bcl-2 ratio. These findings are impressive because apoptosis was reported to be significantly deregulated in PCa and to directly contribute to androgen-ablation and progression to CRPC (286). Interestingly, compound **16** induced a higher percentage of apoptotic cells than the positive control docetaxel when compared at the same concentration. Consistent with our findings, numerous chalcone derivatives were shown to promote apoptosis in PCa by modulating different apoptosis-related pathways. Similar to our findings, Deeb D. et al. reported significant upregulation of the pro-apoptotic protein Bax with a simultaneous down-regulation of the anti-apoptotic protein Bcl-2 in CRPC cell lines following treatment with a natural chalcone analog, Xanthohumol (207).

Given the high prevalence of cell cycle defects in PCa and their significant impact on tumorigenesis, we further explored whether these actions were linked to cell cycle alterations. Compound **13** was found to induce some G2/M phase arrest which was cell line-specific. These findings were consistent with reports from other chalcone derivatives in CRPC cells. For instance, licochalcone-A was shown to reduce cyclin B1 and its catalytic partner cdc2 in PC3 prostate cancer cell line leading to cell cycle arrest at the G2/M phase (225). Microtubule inhibition and subsequent G2/M arrest are among the most repeatedly proposed mechanism for chalcone's anticancer activity (232, 234, 287). However, no cell cycle arrest was recorded for compound **16** on both cell lines, which may designate that induction of apoptosis by this compound is mediated by a different mechanism of action that might not be linked to DNA damage.

While localized prostate cancer has a good prognosis, progression to metastatic PCa dramatically reduces the 5-year survival rate to 30.2% (7). The metastatic spread of cancer involves several steps, including cell invasion and migration. At the molecular

level, EMT is thought to be an important mechanism responsible for metastasis (236). Therefore, we examined the effect of our compounds on inhibiting cell migration and targeting EMT-related proteins. Our results showed that compound **16**, significantly inhibited cell migration of PC3 and DU145 cell lines in both trans-well and wound healing assay. Consistent with these findings, compound **16** was found to induce modest upregulation in the expression of epithelial marker (E-cadherin) and downregulation of (β -Catenin) in DU145 cell line, suggesting that it may act by reverting EMT. On the other hand, no significant changes were observed in PC3 cell line. Lack of effect in PC3 cells might be attributed to the high rate of apoptosis induced by the compound which is known to induce cleavage of adhesion and surface proteins (288, 289).

Uncontrolled angiogenesis is a key factor in cancer progression, invasion and metastasis (246). Compound **16** showed a significant reduction in blood vessel formation in the CAM of the chicken embryos. These findings indicate that the compound might have favorable activity when tested *in vivo* since cancer cells rely on blood vessel formation to maintain the supply of nutrients and oxygen (246, 248). The anticancer activity of chalcones in prostate cancer was only linked with the effect on angiogenesis in one study. Moon et al. showed that butein treated PC3 cells implanted in mice had significantly lower blood vessel formation as compared to control (243).

The activation of PI3K/AKT/mTOR signaling pathway was reported in PCa, which correlates with tumor growth, disease progression and resistance to therapy (264, 265). Several studies reported an elevated activity of PI3K-AKT-mTOR signaling in prostate cancer, which was more significant in CRPC (155, 266). Our results reveal that compounds **13**, **15** and **16** could significantly downregulate Akt expression in DU145 cell line, while only compound **15** was found to significantly downregulate Akt in PC3

cell line.

Another pathway that was significantly inhibited by our compounds is the JNK1/2/3 pathway. JNK protein was found to exhibit contradictory roles where it is involved in the regulation of cell proliferation, differentiation, cell survival as well as apoptosis (290, 291). Numerous chemotherapeutic agents were found to target prostate cancer cells via inhibiting or activating the JNK pathway (290).

Taken together, these findings indicate that thienyl pyridine-based chalcone (**16**) is a highly promising lead compound for the treatment of CRPC. Based on these findings and since our study is the first to report the incorporation of thienyl pyridine within the chalcone scaffold, we decided to expand further in this series and conduct structure-activity relationship (SAR) study to explore if we can further enhance the efficacy of these analogs. Therefore, ten additional analogs (**17-26**) were synthesized and evaluated against CRPC cell lines. The SAR study showed that non-cyclic chalcones were significantly more potent than their matched cyclic (tetralone-based) analogs. Interestingly, changing the methoxy group's position in compound **16** from C3 to C2 dramatically improved the cytotoxicity. Treatment of PC3 cells with compound **17** at 2.5 μM concentration reduced cell viability by 84.7% as compared to 47.5% reduction with compound **16**. These findings suggest that the IC_{50} for compound **17** is way less than 2.5 μM). Moreover, replacing the methoxy with trifluoromethyl functional group in compound **25** resulted in a similar improvement in cytotoxicity. While compounds **17** and **25** showed relatively similar efficacy, compound **17** showed a more favorable ADMET profile. Figure 40 summarizes the IC_{50} and ADMET risk for all heteroaromatic-based chalcones reported in literature with activity against prostate cancer. Taken both the efficacy and the pharmacokinetic profile into consideration, our lead molecule (**17**) can be considered among the most promising reported chalcone

hybrids privileged with both high potency and relatively favorable ADMET profile.

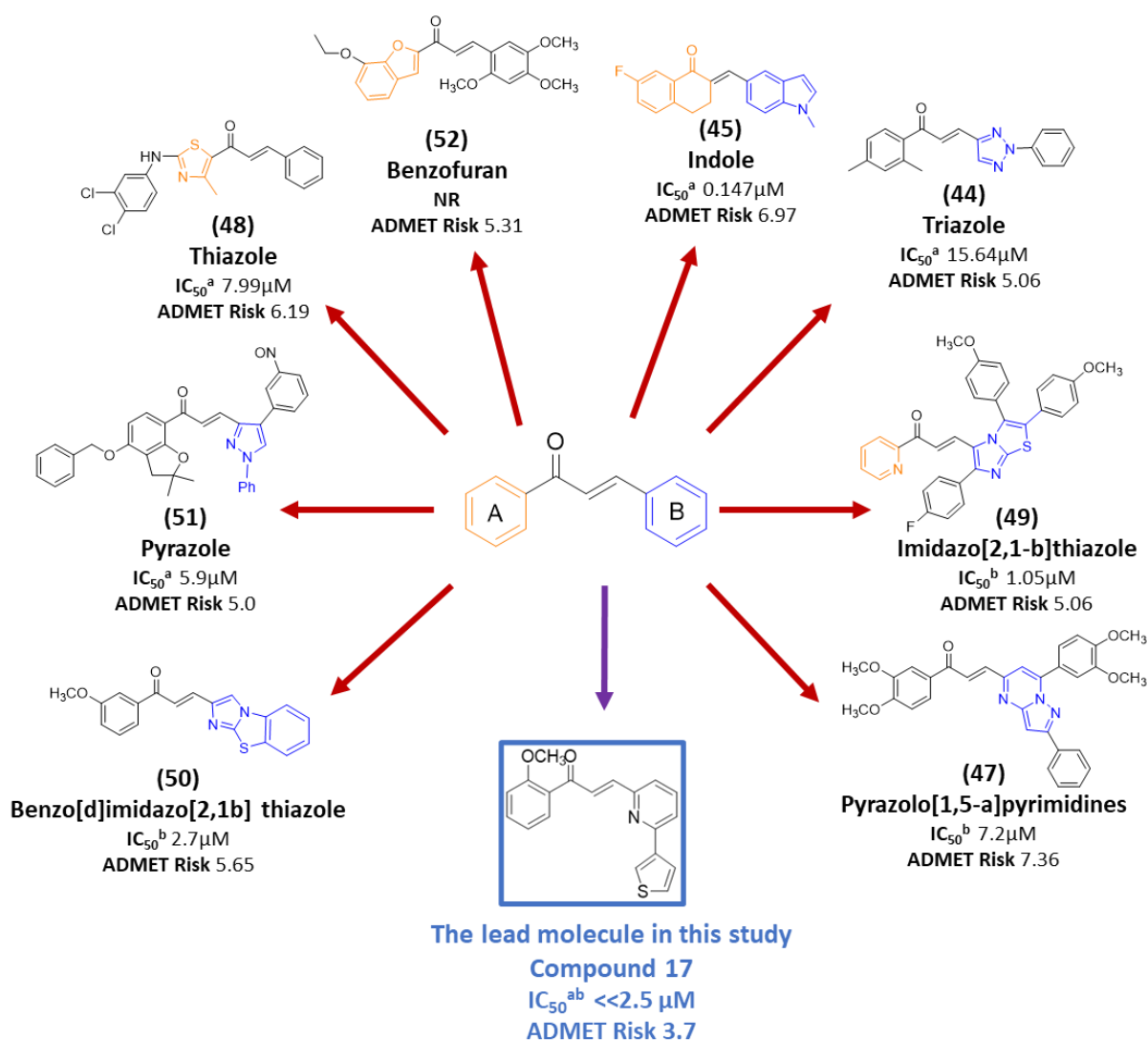


Figure 41. Summary of the known heteroaromatic-based chalcone derivatives with reported activity against PCa in comparison to our novel lead molecule (compound **17**). Analogs number and IC_{50} values were extracted from Table S1 in Appendix A, while the ADMET risks were computed using Simulations Plus' ADMET Predictor Version 8.5.1.1. The ADMET risk score indicates the number of potential ADMET issues that a compound may face.

CHAPTER 6: CONCLUSION AND FUTURE DIRECTIONS

Castration-resistant prostate cancer (CRPC) is a debilitating and deadly disease that lacks curative therapeutic options. Despite all the efforts to develop effective therapies for CRPC, the available treatments could not improve patient's survival beyond few months. In this study, we reported for the first time a series of thienyl pyridine chalcones that are highly effective against CRPC when tested *in vitro* against two of the most aggressive prostate cancer cell lines (PC3 and DU145) and *in ovo* for the effect on angiogenesis. Interestingly, the lead compound (**16**) in our study behaved better than the first-line chemotherapy used in the treatment of CRPC, docetaxel, in terms of apoptosis induction and reduction of colony formation. As compared to previously reported chalcones in literature, our compounds have the advantage of simultaneously having high potency and a relatively favorable ADMET profile. Therefore, these analogs have a high potential of succeeding *in vivo* as well as preclinical studies and further stages of drug development processes.

Based on the highly promising data generated by this project on the anticancer activity of the thienyl pyridine based chalcones, our research team started two new studies focusing on the development of gold nanoparticle formulation, as a targeted delivery system, for the most potent analogs and on exploring their effect on other aggressive types of human cancer, including breast and colorectal cancer. Taken together, we believe that thienyl pyridine chalcones could serve as potential promising lead molecules for the treatment of CRPC.

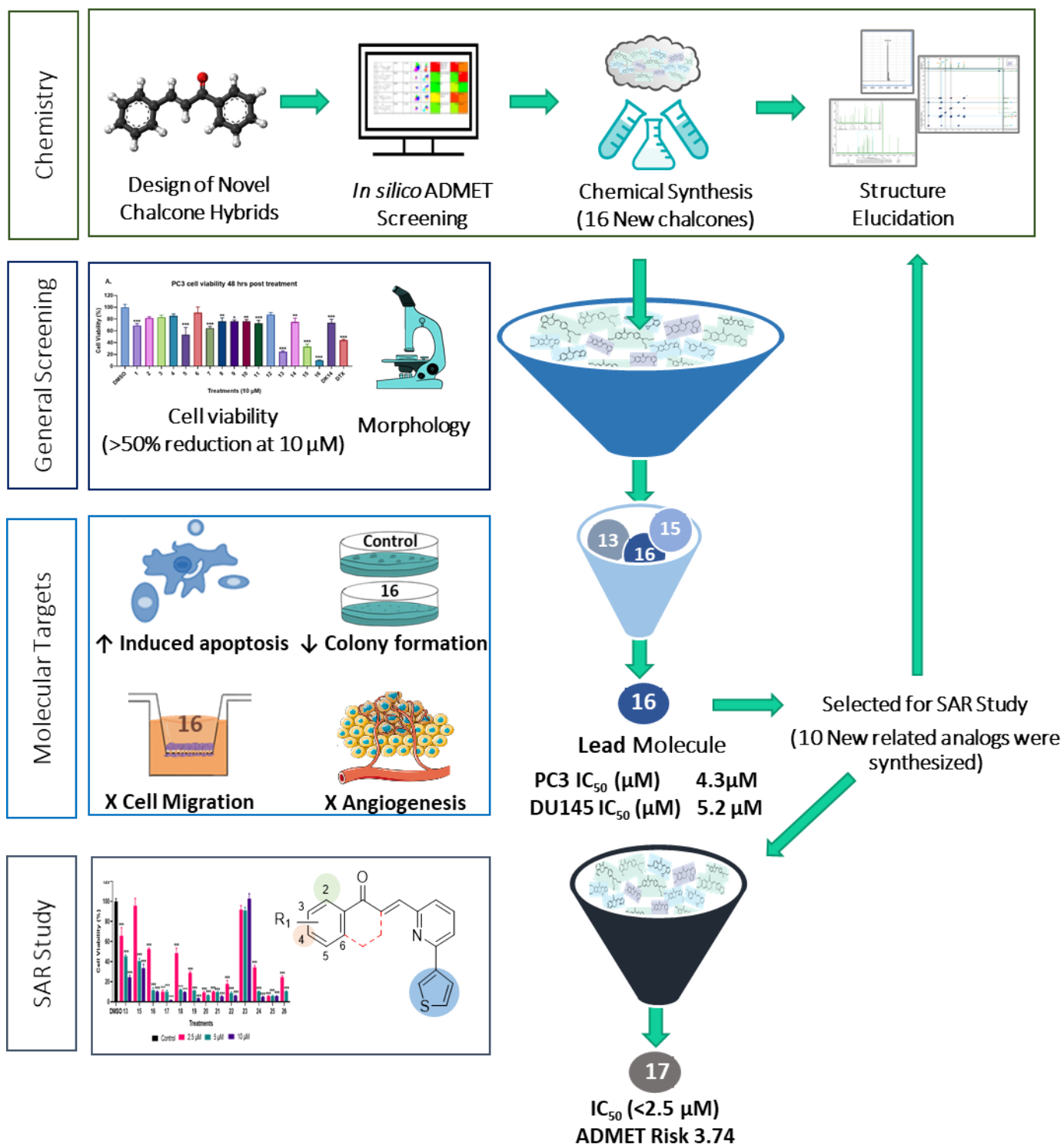


Figure 42. Summary of the main study findings.

REFERENCES

1. GLOBOCAN. Global Cancer Observatory (GCO): International Agency for Research on Cancer; 2020 [2020 August 15]. Available from: <https://gco.iarc.fr/>.
2. Dasgupta P, Baade PD, Aitken JF, Ralph N, Chambers SK, Dunn J. Geographical variations in prostate cancer outcomes: A systematic review of international evidence. *Front Oncol.* 2019;9:238-.
3. Center MM, Jemal A, Lortet-Tieulent J, Ward E, Ferlay J, Brawley O, et al. International variation in prostate cancer incidence and mortality rates. *Eur Urol.* 2012;61(6):1079-92.
4. Siegel RL, Miller KD, Jemal A. Cancer statistics, 2020. *CA Cancer J Clin.* 2020;70(1):7-30.
5. GLOBOCAN. Qatar Facts Sheet World Health Organization The Global Cancer Observatory; 2018 [2020 Aug 15]. Available from: <https://gco.iarc.fr/today/data/factsheets/populations/634-qatar-fact-sheets.pdf>.
6. SEER. Cancer Stat Facts: Prostate Cancer: National Cancer Institute; 2017 [2020 Aug 15]. Available from: <https://seer.cancer.gov/statfacts/html/prost.html>.
7. SEER. Cancer Stat Facts: Common Cancer Sites: National Cancer Institute; 2020 [Available from: <https://seer.cancer.gov/statfacts/html/common.html>].
8. Crona DJ, Whang YE. Androgen receptor-dependent and -independent mechanisms involved in prostate cancer therapy resistance. *Cancers.* 2017;9(6).
9. Sartor AO. Risk factors for prostate cancer UpToDate: Wolters Kluwer; 2020 [2020 Aug 15]. Available from: <https://0-www.uptodate.com.mylibrary.qu.edu.qa/contents/risk-factors-for-prostate->

cancer?search=prostate%20cancer%20risk%20factors&source=search_result&selectedTitle=1~150&usage_type=default&display_rank=1#H41.

10. Haiman CA, Chen GK, Blot WJ, Strom SS, Berndt SI, Kittles RA, et al. Characterizing genetic risk at known prostate cancer susceptibility loci in african americans. *PLOS Genet.* 2011;7(5):e1001387.
11. Barber L, Gerke T, Markt SC, Peisch SF, Wilson KM, Ahearn T, et al. Family history of breast or prostate cancer and prostate cancer risk. *Clin Cancer Res.* 2018;24(23):5910-7.
12. Kalish LA, McDougal WS, McKinlay JB. Family history and the risk of prostate cancer. *Urology.* 2000;56(5):803-6.
13. Attard G, Parker C, Eeles RA, Schröder F, Tomlins SA, Tannock I, et al. Prostate cancer. *Lancet.* 2016;387(10013):70-82.
14. Kote-Jarai Z, Leongamornlert D, Saunders E, Tymrakiewicz M, Castro E, Mahmud N, et al. BRCA2 is a moderate penetrance gene contributing to young-onset prostate cancer: implications for genetic testing in prostate cancer patients. *Br J Cancer.* 2011;105(8):1230-4.
15. Thompson D, Easton D. Variation in cancer risks, by mutation position, in BRCA2 mutation carriers. *Am J Hum Genet.* 2001;68(2):410-9.
16. Freedman ML, Monteiro AN, Gayther SA, Coetzee GA, Risch A, Plass C, et al. Principles for the post-GWAS functional characterization of cancer risk loci. *Nat Genet.* 2011;43(6):513-8.
17. Sinha R, Park Y, Graubard BI, Leitzmann MF, Hollenbeck A, Schatzkin A, et al. Meat and meat-related compounds and risk of prostate cancer in a large prospective cohort study in the United States. *Am J Epidemiol.* 2009;170(9):1165-77.

18. Allen NE, Key TJ, Appleby PN, Travis RC, Roddam AW, Tjønneland A, et al. Animal foods, protein, calcium and prostate cancer risk: the European Prospective Investigation into Cancer and Nutrition. *Br J Cancer*. 2008;98(9):1574-81.
19. Chamie K, De Vere White RW, Lee D, Ok JH, Ellison LM. Agent Orange exposure, Vietnam War veterans, and the risk of prostate cancer. *Cancer*. 2008;113(9):2464-70.
20. Ballon-Landa E, Parsons JK. Nutrition, physical activity, and lifestyle factors in prostate cancer prevention. *Curr Opin Urol*. 2018;28(1):55-61.
21. Shen MM, Abate-Shen C. Molecular genetics of prostate cancer: new prospects for old challenges. *Genes Dev*. 2010;24(18):1967-2000.
22. McNeal JE. Normal histology of the prostate. *Am J Surg Pathol*. 1988;12(8):619-33.
23. Toivanen R, Shen MM. Prostate organogenesis: tissue induction, hormonal regulation and cell type specification. *Development*. 2017;144(8):1382-98.
24. McNeal JE. Normal and pathologic anatomy of prostate. *Urology*. 1981;17(Suppl 3):11-6.
25. Timms BG, Hofkamp LE. Prostate development and growth in benign prostatic hyperplasia. *Differentiation*. 2011;82(4-5):173-83.
26. Cohen RJ, Shannon BA, Phillips M, Moorin RE, Wheeler TM, Garrett KL. Central zone carcinoma of the prostate gland: a distinct tumor type with poor prognostic features. *J Urol*. 2008;179(5):1762-7; discussion 7.
27. Khan H. Determinants of prostate cancer: the Birmingham prostatic neoplasms association study. University of Birmingham Research Archive: University of Birmingham; 2011.

28. Huang YH, Zhang YQ, Huang JT. Neuroendocrine cells of prostate cancer: biologic functions and molecular mechanisms. *Asian J Androl.* 2019;21(3):291-5.
29. Wang Y, Hayward S, Cao M, Thayer K, Cunha G. Cell differentiation lineage in the prostate. *Differentiation.* 2001;68(4-5):270-9.
30. Verhagen APM, Ramaekers FCS, Aalders TW, Schaafsma HE, Debruyne FMJ, Schalken JA. Colocalization of basal and luminal cell-type cytokeratins in human prostate cancer. *Cancer Res.* 1992;52(22):6182.
31. di Sant'Agnese PA. Neuroendocrine cells of the prostate and neuroendocrine differentiation in prostatic carcinoma: a review of morphologic aspects. *Urology.* 1998;51(5A Suppl):121-4.
32. El-Alfy M, Pelletier G, Hermo LS, Labrie F. Unique features of the basal cells of human prostate epithelium. *Microsc Res Tech.* 2000;51(5):436-46.
33. Grisanzio C, Signoretti S. P63 in prostate biology and pathology. *J Cell Biochem.* 2008;103(5):1354-68.
34. Humphrey PA. Diagnosis of adenocarcinoma in prostate needle biopsy tissue. *J Clin Pathol.* 2007;60(1):35-42.
35. Garber K. A tale of two cells: discovering the origin of prostate cancer. *J Natl Cancer Inst.* 2010;102(20):1528-9, 35.
36. Wang ZA, Toivanen R, Bergren SK, Chambon P, Shen MM. Luminal cells are favored as the cell of origin for prostate cancer. *Cell Rep.* 2014;8(5):1339-46.
37. Stoyanova T, Cooper AR, Drake JM, Liu X, Armstrong AJ, Pienta KJ, et al. Prostate cancer originating in basal cells progresses to adenocarcinoma propagated by luminal-like cells. *Proc Natl Acad Sci U S A.* 2013;110(50):20111-6.

38. Saranyutanon S, Srivastava SK, Pai S, Singh S, Singh AP. Therapies targeted to androgen receptor signaling axis in prostate cancer: progress, challenges, and hope. *Cancers*. 2019;12(1).
39. Choi W, Porten S, Kim S, Willis D, Plimack ER, Hoffman-Censits J, et al. Identification of distinct basal and luminal subtypes of muscle-invasive bladder cancer with different sensitivities to frontline chemotherapy. *Cancer Cell*. 2014;25(2):152-65.
40. Sakr WA, Haas GP, Cassin BF, Pontes JE, Crissman JD. The frequency of carcinoma and intraepithelial neoplasia of the prostate in young male patients. *The Journal of urology*. 1993;150(2 Pt 1):379-85.
41. Zynger DL, Yang X. High-grade prostatic intraepithelial neoplasia of the prostate: the precursor lesion of prostate cancer. *Int J Clin Exp Pathol*. 2009;2(4):327-38.
42. Ayala AG, Ro JY. Prostatic intraepithelial neoplasia: recent advances. *Arch Pathol Lab Med*. 2007;131(8):1257-66.
43. Montironi R, Mazzucchelli R, Lopez-Beltran A, Scarpelli M, Cheng L. Prostatic intraepithelial neoplasia: its morphological and molecular diagnosis and clinical significance. *BJU Int*. 2011;108(9):1394-401.
44. Bostwick DG, Brawer MK. Prostatic intra-epithelial neoplasia and early invasion in prostate cancer. *Cancer*. 1987;59(4):788-94.
45. Klink JC, Miocinovic R, Magi Galluzzi C, Klein EA. High-grade prostatic intraepithelial neoplasia. *Korean J Urol*. 2012;53(5):297-303.
46. Elo JP, Visakorpi T. Molecular genetics of prostate cancer. *Ann Med*. 2001;33(2):130-41.
47. Nelson WG, De Marzo AM, Isaacs WB. Prostate cancer. *N Engl J Med*. 2003;349(4):366-81.

48. Baltaci S, Orhan D, Ozer G, Tolunay O, Göğöüs O. Bcl-2 proto-oncogene expression in low- and high-grade prostatic intraepithelial neoplasia. *BJU Int.* 2000;85(1):155-9.
49. Bostwick DG, Qian J. High-grade prostatic intraepithelial neoplasia. *Mod Pathol.* 2004;17(3):360-79.
50. Erdamar S, Yang G, Harper JW, Lu X, Kattan MW, Thompson TC, et al. Levels of expression of p27KIP1 protein in human prostate and prostate cancer: an immunohistochemical analysis. *Mod Pathol.* 1999;12(8):751-5.
51. Bowen C, Bubendorf L, Voeller HJ, Slack R, Willi N, Sauter G, et al. Loss of NKX3.1 expression in human prostate cancers correlates with tumor progression. *Cancer Res.* 2000;60(21):6111-5.
52. Brooks JD, Weinstein M, Lin X, Sun Y, Pin SS, Bova GS, et al. CG island methylation changes near the GSTP1 gene in prostatic intraepithelial neoplasia. *Cancer Epidemiol Biomarkers Prev.* 1998;7(6):531-6.
53. Wu CL, Yang XJ, Tretiakova M, Patton KT, Halpern EF, Woda BA, et al. Analysis of alpha-methylacyl-CoA racemase (P504S) expression in high-grade prostatic intraepithelial neoplasia. *Hum Pathol.* 2004;35(8):1008-13.
54. Schoenborn JR, Nelson P, Fang M. Genomic profiling defines subtypes of prostate cancer with the potential for therapeutic stratification. *Clin Cancer Res.* 2013;19(15):4058-66.
55. Arora K, Barbieri CE. Molecular subtypes of prostate cancer. *Current Oncology Reports.* 2018;20(8):58.
56. Yang XJ. Precancerous lesions of the prostate: Pathology and clinical implications UpToDate: Wolters Kluwer; 2019 [Available from: <https://0->

www.uptodate.com.mylibrary.qu.edu.qa/contents/precancerous-lesions-of-the-prostate-pathology-and-clinical-implications/abstract/24.

57. Morais CL, Guedes LB, Hicks J, Baras AS, De Marzo AM, Lotan TL. ERG and PTEN status of isolated high-grade PIN occurring in cystoprostatectomy specimens without invasive prostatic adenocarcinoma. *Hum Pathol.* 2016;55:117-25.
58. Liu H, Shi J, Wilkerson M, Yang XJ, Lin F. Immunohistochemical evaluation of ERG expression in various benign and malignant tissues. *Ann Clin Lab Sci.* 2013;43(1):3-9.
59. McMenamin ME, Soung P, Perera S, Kaplan I, Loda M, Sellers WR. Loss of PTEN expression in paraffin-embedded primary prostate cancer correlates with high Gleason score and advanced stage. *Cancer Res.* 1999;59(17):4291-6.
60. Packer JR, Maitland NJ. The molecular and cellular origin of human prostate cancer. *Biochim Biophys Acta.* 2016;1863(6 Pt A):1238-60.
61. Tamburrino L, Salvianti F, Marchiani S, Pinzani P, Nesi G, Serni S, et al. Androgen receptor (AR) expression in prostate cancer and progression of the tumor: Lessons from cell lines, animal models and human specimens. *Steroids.* 2012;77(10):996-1001.
62. Huggins C, Hodges CV. Studies on prostatic cancer. I. The effect of castration, of estrogen and of androgen injection on serum phosphatases in metastatic carcinoma of the prostate. *Cancer Res.* 1941;1(4):293-7.
63. Elshan N, Rettig MB, Jung ME. Molecules targeting the androgen receptor (AR) signaling axis beyond the AR-ligand binding domain. *Med Res Rev.* 2019;39(3):910-60.

64. Shaffer PL, Jivan A, Dollins DE, Claessens F, Gewirth DT. Structural basis of androgen receptor binding to selective androgen response elements. *Proc Natl Acad Sci U S A*. 2004;101(14):4758-63.
65. Gelmann EP. Molecular biology of the androgen receptor. *J Clin Oncol*. 2002;20(13):3001-15.
66. Norris LB, Kolesar JM. Prostate cancer. In: DiPiro JT, Talbert RL, Yee GC, Matzke GR, Wells BG, Posey LM, editors. *Pharmacotherapy: A Pathophysiologic Approach*, 10e. New York, NY: McGraw-Hill Education; 2017.
67. Feng Q, He B. Androgen receptor signaling in the development of castration-resistant prostate cancer. *Front Oncol*. 2019;9(858).
68. Leung JK, Sadar MD. Non-genomic actions of the androgen receptor in prostate cancer. *Front Endocrinol*. 2017;8(2).
69. NCCN Clinical Practice Guidelines in Oncology (NCCN Guidelines®). Prostate Cancer: NCCN; 2019 [Available from: <https://www2.tri-kobe.org/nccn/guideline/urological/english/prostate.pdf>].
70. Bekelman JE, Rumble RB, Chen RC, Pisansky TM, Finelli A, Feifer A, et al. Clinically localized prostate cancer: ASCO clinical practice guideline endorsement of an american urological association/american society for radiation oncology/society of urologic oncology guideline. *J Clin Oncol*. 2018;36(32):3251-8.
71. Sanda MG, Cadeddu JA, Kirkby E, Chen RC, Crispino T, Fontanarosa J, et al. Clinically localized prostate cancer: AUA/ASTRO/SUO guideline. Part I: Risk stratification, shared decision making, and care options. *The Journal of urology*. 2018;199(3):683-90.

72. Climent M, León-Mateos L, González Del Alba A, Pérez-Valderrama B, Méndez-Vidal MJ, Mellado B, et al. Updated recommendations from the spanish oncology genitourinary group for the treatment of patients with metastatic castration-resistant prostate cancer. *Crit Rev Oncol Hematol*. 2015;96(2):308-18.
73. Loblaw DA, Virgo KS, Nam R, Somerfield MR, Ben-Josef E, Mendelson DS, et al. Initial hormonal management of androgen-sensitive metastatic, recurrent, or progressive prostate cancer: 2006 update of an American society of clinical oncology practice guideline. *J Clin Oncol*. 2007;25(12):1596-605.
74. Heidenreich A, Bastian PJ, Bellmunt J, Bolla M, Joniau S, van der Kwast T, et al. EAU guidelines on prostate cancer. Part II: Treatment of advanced, relapsing, and castration-resistant prostate cancer. *Eur Urol*. 2014;65(2):467-79.
75. Hoang DT, Iczkowski KA, Kilari D, See W, Nevalainen MT. Androgen receptor-dependent and -independent mechanisms driving prostate cancer progression: Opportunities for therapeutic targeting from multiple angles. *Oncotarget*. 2017;8(2):3724-45.
76. Oudard S. Progress in emerging therapies for advanced prostate cancer. *Cancer Treat Rev*. 2013;39(3):275-89.
77. Seruga B, Ocana A, Tannock IF. Drug resistance in metastatic castration-resistant prostate cancer. *Nat Rev Clin Oncol*. 2011;8(1):12-23.
78. Frieling JS, Basanta D, Lynch CC. Current and emerging therapies for bone metastatic castration-resistant prostate cancer. *Cancer Control*. 2015;22(1):109-20.
79. Hotte SJ, Saad F. Current management of castrate-resistant prostate cancer. *Curr Oncol*. 2010;17 Suppl 2(Suppl 2):S72-9.
80. Shaffer DR, Scher HI. Prostate cancer: a dynamic illness with shifting targets. *Lancet Oncol*. 2003;4(7):407-14.

81. Feldman BJ, Feldman D. The development of androgen-independent prostate cancer. *Nat Rev Cancer*. 2001;1(1):34-45.
82. Antonarakis ES, Lu C, Wang H, Luber B, Nakazawa M, Roeser JC, et al. AR-V7 and resistance to enzalutamide and abiraterone in prostate cancer. *N Engl J Med*. 2014;371(11):1028-38.
83. Zhao S, Yu EY. Castrate-resistant prostate cancer: postdocetaxel management. *Curr Opin Urol*. 2013;23(3):201-7.
84. Hussain A, Dawson MA. Chemotherapy in advanced castration-resistant prostate cancer UpToDate: Wolters Kluwer; 2020 [Available from: https://0-www.uptodate.com.mylibrary.qu.edu.qa/contents/chemotherapy-in-advanced-castration-resistant-prostate-cancer?sectionName=Chemotherapy-na%C3%AFve%20patients&search=castration%20resistant&topicRef=112896&anchor=H8&source=see_link#H8].
85. Tannock IF, de Wit R, Berry WR, Horti J, Pluzanska A, Chi KN, et al. Docetaxel plus prednisone or mitoxantrone plus prednisone for advanced prostate cancer. *N Engl J Med*. 2004;351(15):1502-12.
86. Petrylak DP, Tangen CM, Hussain MHA, Lara PN, Jones JA, Taplin ME, et al. Docetaxel and estramustine compared with mitoxantrone and prednisone for advanced refractory prostate cancer. *N Engl J Med*. 2004;351(15):1513-20.
87. Crombag MBS, de Vries Schultink AHM, van Doremalen JGC, Otten HM, Bergman AM, Schellens JHM, et al. Age-Associated Hematological Toxicity in Patients with Metastatic Castration-Resistant Prostate Cancer Treated with Docetaxel in Clinical Practice. *Drugs Aging*. 2019;36(4):379-85.
88. Ho MY, Mackey JR. Presentation and management of docetaxel-related adverse effects in patients with breast cancer. *Cancer Manag Res*. 2014;6:253-9.

89. Dawson NA, Leger P. Overview of the treatment of castration-resistant prostate cancer (CRPC) UpToDate: Wolters Kluwer; 2020 [Available from: https://0-www.uptodate.com.mylibrary.qu.edu.qa/contents/overview-of-the-treatment-of-castration-resistant-prostate-cancer-crpc?search=castration-resistant%20prostate%20cancer&source=search_result&selectedTitle=1~64&usage_type=default&display_rank=1].
90. de Bono JS, Oudard S, Ozguroglu M, Hansen S, Machiels JP, Kocak I, et al. Prednisone plus cabazitaxel or mitoxantrone for metastatic castration-resistant prostate cancer progressing after docetaxel treatment: a randomised open-label trial. *Lancet*. 2010;376(9747):1147-54.
91. (FDA) USFaDA. 2010 Notifications FDA 2010 [Available from: <https://www.fda.gov/drugs/resources-information-approved-drugs/2010-notifications>].
92. Oudard S, Fizazi K, Sengeløv L, Daugaard G, Saad F, Hansen S, et al. Cabazitaxel versus docetaxel as first-line therapy for patients with metastatic castration-resistant prostate cancer: A randomized phase III trial-FIRSTANA. *J Clin Oncol*. 2017;35(28):3189-97.
93. Lexicomp. Sipuleucel-T: Drug information: Wolters Kluwer; 2020 [2020 Aug 26]. Available from: https://0-www.uptodate.com.mylibrary.qu.edu.qa/contents/sipuleucel-t-drug-information?search=castration-resistant%20prostate%20cancer&topicRef=112896&source=see_link.
94. Goldstein NS. Immunophenotypic characterization of 225 prostate adenocarcinomas with intermediate or high Gleason scores. *Am J Clin Pathol*. 2002;117(3):471-7.

95. Kantoff PW, Higano CS, Shore ND, Berger ER, Small EJ, Penson DF, et al. Sipuleucel-T immunotherapy for castration-resistant prostate cancer. *N Engl J Med.* 2010;363(5):411-22.
96. Lexicomp. Radium-223: Drug information: Wolters Kluwer; 2020 [Available from:
<https://www.google.com/search?q=wolters+kluwer&oq=wolter&aqs=chrome.0.69i59j69i57j0l3j46j69i60j69i61.1928j0j7&sourceid=chrome&ie=UTF-8>.
97. Parker C, Nilsson S, Heinrich D, Helle SI, O'Sullivan JM, Fosså SD, et al. Alpha emitter radium-223 and survival in metastatic prostate cancer. *N Engl J Med.* 2013;369(3):213-23.
98. Montgomery RB, Mostaghel EA, Vessella R, Hess DL, Kalhorn TF, Higano CS, et al. Maintenance of intratumoral androgens in metastatic prostate cancer: a mechanism for castration-resistant tumor growth. *Cancer Res.* 2008;68(11):4447-54.
99. Labrie F. Mechanism of action and pure antiandrogenic properties of flutamide. *Cancer.* 1993;72(S12):3816-27.
100. Longo DL. New therapies for castration-resistant prostate cancer. *N Engl J Med.* 2010;363(5):479-81.
101. Potter GA, Barrie SE, Jarman M, Rowlands MG. Novel steroidal inhibitors of human cytochrome P45017 alpha (17 alpha-hydroxylase-C17,20-lyase): potential agents for the treatment of prostatic cancer. *J Med Chem.* 1995;38(13):2463-71.
102. Tran C, Ouk S, Clegg NJ, Chen Y, Watson PA, Arora V, et al. Development of a second-generation antiandrogen for treatment of advanced prostate cancer. *Science.* 2009;324(5928):787-90.

103. Scher HI, Beer TM, Higano CS, Anand A, Taplin ME, Efstathiou E, et al. Antitumour activity of MDV3100 in castration-resistant prostate cancer: a phase 1-2 study. *Lancet*. 2010;375(9724):1437-46.
104. Scher HI, Fizazi K, Saad F, Taplin M-E, Sternberg CN, Miller K, et al. Increased survival with enzalutamide in prostate cancer after chemotherapy. *N Engl J Med*. 2012;367(13):1187-97.
105. Fizazi K, Scher HI, Molina A, Logothetis CJ, Chi KN, Jones RJ, et al. Abiraterone acetate for treatment of metastatic castration-resistant prostate cancer: final overall survival analysis of the COU-AA-301 randomised, double-blind, placebo-controlled phase 3 study. *Lancet Oncol*. 2012;13(10):983-92.
106. Kita Y, Goto T, Akamatsu S, Yamasaki T, Inoue T, Ogawa O, et al. Castration-resistant prostate cancer refractory to second-generation androgen receptor axis-targeted agents: opportunities and challenges. *Cancers (Basel)*. 2018;10(10):345.
107. (FDA) USFaDA. FDA grants accelerated approval to rucaparib for BRCA-mutated metastatic castration-resistant prostate cancer 2020 [Available from: <https://www.fda.gov/drugs/fda-grants-accelerated-approval-rucaparib-brca-mutated-metastatic-castration-resistant-prostate>].
108. Pritchard CC, Mateo J, Walsh MF, De Sarkar N, Abida W, Beltran H, et al. Inherited DNA-repair gene mutations in men with metastatic prostate cancer. *N Engl J Med*. 2016;375(5):443-53.
109. (FDA) USFaDA. FDA approves olaparib for HRR gene-mutated metastatic castration-resistant prostate cancer 2020 [Available from: <https://www.fda.gov/drugs/drug-approvals-and-databases/fda-approves-olaparib-hrr-gene-mutated-metastatic-castration-resistant-prostate-cancer>].

110. (FDA) USFaDA. FDA approves first cancer treatment for any solid tumor with a specific genetic feature 2017 [Available from: <https://www.fda.gov/news-events/press-announcements/fda-approves-first-cancer-treatment-any-solid-tumor-specific-genetic-feature>].
111. Hu R, Dunn TA, Wei S, Isharwal S, Veltri RW, Humphreys E, et al. Ligand-independent androgen receptor variants derived from splicing of cryptic exons signify hormone-refractory prostate cancer. *Cancer Res.* 2009;69(1):16-22.
112. Dehm SM, Schmidt LJ, Heemers HV, Vessella RL, Tindall DJ. Splicing of a novel androgen receptor exon generates a constitutively active androgen receptor that mediates prostate cancer therapy resistance. *Cancer Res.* 2008;68(13):5469-77.
113. Liu C, Lou W, Zhu Y, Nadiminty N, Schwartz CT, Evans CP, et al. Niclosamide inhibits androgen receptor variants expression and overcomes enzalutamide resistance in castration-resistant prostate cancer. *Clin Cancer Res.* 2014;20(12):3198-210.
114. Schweizer MT, Haugk K, McKiernan JS, Gulati R, Cheng HH, Maes JL, et al. A phase I study of niclosamide in combination with enzalutamide in men with castration-resistant prostate cancer. *PLoS One.* 2018;13(6):e0198389.
115. Madan RA, Schmidt KT, Karzai F, Peer CJ, Cordes LM, Chau CH, et al. Phase 2 study of seviteronel (ino-464) in patients with metastatic castration-resistant prostate cancer after enzalutamide treatment. *Clin Genitourin Cancer.* 2020;18(4):258-67.e1.
116. Taplin ME, Antonarakis ES, Ferrante KJ, Horgan K, Blumenstein B, Saad F, et al. Androgen receptor modulation optimized for response-splice variant: a phase 3, randomized trial of galeterone versus enzalutamide in androgen receptor splice

- variant-7-expressing metastatic castration-resistant prostate cancer. *Eur Urol*. 2019;76(6):843-51.
117. Xie N, Cheng H, Lin D, Liu L, Yang O, Jia L, et al. The expression of glucocorticoid receptor is negatively regulated by active androgen receptor signaling in prostate tumors. *Int J Cancer*. 2015;136(4):E27-38.
118. Arora VK, Schenkein E, Murali R, Subudhi SK, Wongvipat J, Balbas MD, et al. Glucocorticoid receptor confers resistance to antiandrogens by bypassing androgen receptor blockade. *Cell*. 2013;155(6):1309-22.
119. Grindstad T, Andersen S, Al-Saad S, Donnem T, Kiselev Y, Nordahl Melbø-Jørgensen C, et al. High progesterone receptor expression in prostate cancer is associated with clinical failure. *PLoS One*. 2015;10(2):e0116691-e.
120. Grindstad T, Richardsen E, Andersen S, Skjefstad K, Rakaee Khanehkenari M, Donnem T, et al. Progesterone receptors in prostate cancer: Progesterone receptor B is the isoform associated with disease progression. *Sci Rep*. 2018;8(1):11358-.
121. Kim J, Jin H, Zhao JC, Yang YA, Li Y, Yang X, et al. FOXA1 inhibits prostate cancer neuroendocrine differentiation. *Oncogene*. 2017;36(28):4072-80.
122. Yuan T-C, Veeramani S, Lin F-F, Kondrikou D, Zelivianski S, Igawa T, et al. Androgen deprivation induces human prostate epithelial neuroendocrine differentiation of androgen-sensitive LNCaP cells. *Endocr Relat Cancer*. 2006;13(1):151.
123. Santoni M, Conti A, Burattini L, Berardi R, Scarpelli M, Cheng L, et al. Neuroendocrine differentiation in prostate cancer: novel morphological insights and future therapeutic perspectives. *Biochim Biophys Acta*. 2014;1846(2):630-7.
124. Gupta K, Gupta S. Neuroendocrine differentiation in prostate cancer: key epigenetic players. *Transl Cancer Res*. 2017;6(Suppl 1):S104-S8.

125. Komiya A, Yasuda K, Watanabe A, Fujiuchi Y, Tsuzuki T, Fuse H. The prognostic significance of loss of the androgen receptor and neuroendocrine differentiation in prostate biopsy specimens among castration-resistant prostate cancer patients. *Mol Clin Oncol*. 2013;1(2):257-62.
126. Lee JK, Phillips JW, Smith BA, Park JW, Stoyanova T, McCaffrey EF, et al. N-Myc Drives Neuroendocrine Prostate Cancer Initiated from Human Prostate Epithelial Cells. *Cancer Cell*. 2016;29(4):536-47.
127. Ku SY, Rosario S, Wang Y, Mu P, Seshadri M, Goodrich ZW, et al. Rb1 and Trp53 cooperate to suppress prostate cancer lineage plasticity, metastasis, and antiandrogen resistance. *Science*. 2017;355(6320):78-83.
128. Patel GK, Chugh N, Tripathi M. Neuroendocrine differentiation of prostate Cancer-an Intriguing example of tumor evolution at play. *Cancers (Basel)*. 2019;11(10):1405.
129. Deng X, Liu H, Huang J, Cheng L, Keller ET, Parsons SJ, et al. Ionizing radiation induces prostate cancer neuroendocrine differentiation through interplay of CREB and ATF2: implications for disease progression. *Cancer Res*. 2008;68(23):9663-70.
130. Parimi V, Goyal R, Poropatich K, Yang XJ. Neuroendocrine differentiation of prostate cancer: a review. *Am J Clin Exp Urol*. 2014;2(4):273-85.
131. Sun Y, Niu J, Huang J. Neuroendocrine differentiation in prostate cancer. *Am J Transl Res*. 2009;1(2):148-62.
132. Carver BS. Defining and Targeting the Oncogenic Drivers of Neuroendocrine Prostate Cancer. *Cancer Cell*. 2016;29(4):431-2.

133. Clermont P-L, Ci X, Pandha H, Wang Y, Crea F. Treatment-emergent neuroendocrine prostate cancer: molecularly driven clinical guidelines. *Int J Endocr Oncol.* 2019;6(2):IJE20.
134. Epstein JI, Amin MB, Beltran H, Lotan TL, Mosquera JM, Reuter VE, et al. Proposed morphologic classification of prostate cancer with neuroendocrine differentiation. *Am J Surg Pathol.* 2014;38(6):756-67.
135. Humphrey PA, Moch H, Cubilla AL, Ulbright TM, Reuter VE. The 2016 WHO classification of tumours of the urinary system and male genital organs-part b: prostate and bladder tumours. *Eur Urol.* 2016;70(1):106-19.
136. Conteduca V, Oromendia C, Eng KW, Bareja R, Sigouros M, Molina A, et al. Clinical features of neuroendocrine prostate cancer. *Eur J Cancer.* 2019;121:7-18.
137. Spetsieris N, Boukovala M, Patsakis G, Alafis I, Efstathiou E. Neuroendocrine and aggressive-variant prostate cancer. *Cancers (Basel).* 2020;12(12):3792.
138. Alane S, Moore A, Nutt M, Holland B, Dynda D, El-Zawahry A, et al. Contemporary Incidence and Mortality Rates of Neuroendocrine Prostate Cancer. *Anticancer Res.* 2015;35(7):4145-50.
139. Wang W, Epstein JI. Small Cell Carcinoma of the Prostate: A Morphologic and Immunohistochemical Study of 95 Cases. *Am J Surg Pathol.* 2008;32(1).
140. Beltran H, Oromendia C, Danila DC, Montgomery B, Hoimes C, Szmulewitz RZ, et al. A phase II trial of the aurora kinase A inhibitor alisertib for patients with castration-resistant and neuroendocrine prostate cancer: efficacy and biomarkers. *Clin Cancer Res.* 2019;25(1):43-51.
141. Reya T, Morrison SJ, Clarke MF, Weissman IL. Stem cells, cancer, and cancer stem cells. *Nature.* 2001;414(6859):105-11.

142. Moltzahn F, Thalmann GN. Cancer stem cells in prostate cancer. *Transl Androl Urol.* 2013;2(3):242-53.
143. Harris KS, Kerr BA. Prostate cancer stem cell markers drive progression, therapeutic resistance, and bone metastasis. *Stem Cells Int.* 2017;2017:8629234.
144. Visvader JE, Lindeman GJ. Cancer stem cells in solid tumours: accumulating evidence and unresolved questions. *Nat Rev Cancer.* 2008;8(10):755-68.
145. Ojo D, Lin X, Wong N, Gu Y, Tang D. Prostate cancer stem-like cells contribute to the development of castration-resistant prostate cancer. *Cancers (Basel).* 2015;7(4):2290-308.
146. Gao W, Wu D, Wang Y, Wang Z, Zou C, Dai Y, et al. Development of a novel and economical agar-based non-adherent three-dimensional culture method for enrichment of cancer stem-like cells. *Stem Cell Res Ther.* 2018;9(1):243.
147. Wang Z, Li Y, Wang Y, Wu D, Lau AHY, Zhao P, et al. Targeting prostate cancer stem-like cells by an immunotherapeutic platform based on immunogenic peptide-sensitized dendritic cells-cytokine-induced killer cells. *Stem Cell Res Ther.* 2020;11(1):123.
148. Qin J, Liu X, Laffin B, Chen X, Choy G, Jeter CR, et al. The PSA(-/lo) prostate cancer cell population harbors self-renewing long-term tumor-propagating cells that resist castration. *Cell Stem Cell.* 2012;10(5):556-69.
149. Eramo A, Ricci-Vitiani L, Zeuner A, Pallini R, Lotti F, Sette G, et al. Chemotherapy resistance of glioblastoma stem cells. *Cell Death Differ.* 2006;13(7):1238-41.
150. Phillips TM, McBride WH, Pajonk F. The response of CD24(-/low)/CD44+ breast cancer-initiating cells to radiation. *J Natl Cancer Inst.* 2006;98(24):1777-85.

151. Bao S, Wu Q, McLendon RE, Hao Y, Shi Q, Hjelmeland AB, et al. Glioma stem cells promote radioresistance by preferential activation of the DNA damage response. *Nature*. 2006;444(7120):756-60.
152. Foley C, Mitsiades N. Moving Beyond the Androgen Receptor (AR): Targeting AR-Interacting Proteins to Treat Prostate Cancer. *Horm Cancer*. 2016;7(2):84-103.
153. Nelson PS. Beyond the androgen receptor: Targeting actionable drivers of prostate cancer. *JCO Precis Oncol*. 2017(1):1-3.
154. Chandrasekar T, Yang JC, Gao AC, Evans CP. Targeting molecular resistance in castration-resistant prostate cancer. *BMC Med*. 2015;13(1):206.
155. Carver BS, Chapinski C, Wongvipat J, Hieronymus H, Chen Y, Chandarlapaty S, et al. Reciprocal feedback regulation of PI3K and androgen receptor signaling in PTEN-deficient prostate cancer. *Cancer Cell*. 2011;19(5):575-86.
156. Sweeney CJ, Chen YH, Carducci M, Liu G, Jarrard DF, Eisenberger M, et al. Chemohormonal therapy in metastatic hormone-sensitive prostate cancer. *N Engl J Med*. 2015;373(8):737-46.
157. Schweizer MT, Zhou XC, Wang H, Bassi S, Carducci MA, Eisenberger MA, et al. The influence of prior abiraterone treatment on the clinical activity of docetaxel in men with metastatic castration-resistant prostate cancer. *Eur Urol*. 2014;66(4):646-52.
158. Cheng HH, Gulati R, Azad A, Nadal R, Twardowski P, Vaishampayan UN, et al. Activity of enzalutamide in men with metastatic castration-resistant prostate cancer is affected by prior treatment with abiraterone and/or docetaxel. *Prostate Cancer Prostatic Dis*. 2015;18(2):122-7.

159. Mezynski J, Pezaro C, Bianchini D, Zivi A, Sandhu S, Thompson E, et al. Antitumour activity of docetaxel following treatment with the CYP17A1 inhibitor abiraterone: clinical evidence for cross-resistance? *Ann Oncol.* 2012;23(11):2943-7.
160. Orlikova B, Tasdemir D, Golais F, Dicato M, Diederich M. Dietary chalcones with chemopreventive and chemotherapeutic potential. *Genes Nutr.* 2011;6(2):125-47.
161. Zhuang C, Zhang W, Sheng C, Zhang W, Xing C, Miao Z. Chalcone: a privileged structure in medicinal chemistry. *Chem Rev.* 2017;117(12):7762-810.
162. Mahapatra DK, Bharti SK, Asati V. Anti-cancer chalcones: Structural and molecular target perspectives. *Eur J Med Chem.* 2015;98:69-114.
163. Aksöz BE, Ertan R, editors. *Chemical and Structural Properties of Chalcones* I2014.
164. Batovska DI, Todorova IT. Trends in utilization of the pharmacological potential of chalcones. *Curr Clin Pharmacol.* 2010;5(1):1-29.
165. Isaac AT, Du L, Chowdhury A, Xiaoke G, Lu Q, Yin X. Signaling pathways and proteins targeted by antidiabetic chalcones. *Life Sci.* 2020:118982.
166. Emam SH, Sonousi A, Osman EO, Hwang D, Kim GD, Hassan RA. Design and synthesis of methoxyphenyl- and coumarin-based chalcone derivatives as anti-inflammatory agents by inhibition of NO production and down-regulation of NF- κ B in LPS-induced RAW264.7 macrophage cells. *Bioorg Chem.* 2021;107:104630.
167. Yadav P, Lal K, Kumar A. Antimicrobial screening, in silico studies and QSAR of chalcone-based 1,4-disubstituted 1,2,3-triazole Hybrids. *Drug Res (Stuttg).* 2020.

168. Guazelli CFS, Fattori V, Ferraz CR, Borghi SM, Casagrande R, Baracat MM, et al. Antioxidant and anti-inflammatory effects of hesperidin methyl chalcone in experimental ulcerative colitis. *Chem Biol Interact.* 2021;333:109315.
169. Bukhari SN, Butt AM, Amjad MW, Ahmad W, Shah VH, Trivedi AR. Synthesis and evaluation of chalcone analogues based pyrimidines as angiotensin converting enzyme inhibitors. *Pak J Biol Sci.* 2013;16(21):1368-72.
170. Elkhalfifa D, Siddique AB, Qusa M, Cyprian FS, El Sayed K, Alali F, et al. Design, synthesis, and validation of novel nitrogen-based chalcone analogs against triple negative breast cancer. *Eur J Med Chem.* 2020;187:111954.
171. Srinivasan B, Johnson TE, Lad R, Xing C. Structure-activity relationship studies of chalcone leading to 3-hydroxy-4,3',4',5'-tetramethoxychalcone and its analogues as potent nuclear factor kappaB inhibitors and their anticancer activities. *J Med Chem.* 2009;52(22):7228-35.
172. Das M, Manna K. Chalcone scaffold in anticancer armamentarium: A molecular insight. *J Toxicol.* 2016;2016:7651047.
173. Sharma V, Kumar V, Kumar P. Heterocyclic chalcone analogues as potential anticancer agents. *Anticancer Agents Med Chem.* 2013;13(3):422-32.
174. Mah SH. Chalcones in Diets. In: Xiao J, Sarker SD, Asakawa Y, editors. *Handbook of Dietary Phytochemicals.* Singapore: Springer Singapore; 2019. p. 1-52.
175. Cazarolli LH, Kappel VD, Zanatta AP, Suzuki DOH, Yunes RA, Nunes RJ, et al. Chapter 2 - Natural and synthetic chalcones: tools for the study of targets of action—insulin secretagogue or insulin mimetic? In: Atta ur R, editor. *Studies in Natural Products Chemistry.* 39: Elsevier; 2013. p. 47-89.
176. Dao TTH, Linthorst HJM, Verpoorte R. Chalcone synthase and its functions in plant resistance. *Phytochemistry Rev.* 2011;10(3):397.

177. Hahlbrock K, Scheel D. Physiology and Molecular Biology of Phenylpropanoid Metabolism. *Annu Rev Plant Physiol.* 1989;40(1):347-69.
178. Banoth R, Thatikonda A. A review on natural chalcones as update. *Int J Pharm Sci Res.* 2020;11(3):546-55.
179. Ni L, Meng CQ, Sikorski JA. Recent advances in therapeutic chalcones. *Expert Opin Ther Pat.* 2004;14(12):1669-91.
180. Higuchi K, Watanabe T, Tanigawa T, Tominaga K, Fujiwara Y, Arakawa T. Sofalcone, a gastroprotective drug, promotes gastric ulcer healing following eradication therapy for *Helicobacter pylori*: a randomized controlled comparative trial with cimetidine, an H₂-receptor antagonist. *J Gastroenterol Hepatol.* 2010;25 Suppl 1:S155-60.
181. Gomes MN, Muratov EN, Pereira M, Peixoto JC, Rosseto LP, Cravo PVL, et al. Chalcone derivatives: Promising starting points for drug design. *Molecules.* 2017;22(8).
182. Guex JJ, Avril L, Enrici E, Enriquez E, Lis C, Taïeb C. Quality of life improvement in latin american patients suffering from chronic venous disorder using a combination of *Ruscus aculeatus* and hesperidin methyl-chalcone and ascorbic acid (quality study). *Int Angiol.* 2010;29(6):525-32.
183. Allaert FA. Combination of *Ruscus aculeatus* extract, hesperidin methyl chalcone and ascorbic acid: a comprehensive review of their pharmacological and clinical effects and of the pathophysiology of chronic venous disease. *Int Angiol.* 2016;35(2):111-6.
184. Kar Mahapatra D, Asati V, Bharti SK. An updated patent review of therapeutic applications of chalcone derivatives (2014-present). *Expert Opin Ther Pat.* 2019;29(5):385-406.

185. Jandial DD, Blair CA, Zhang S, Krill LS, Zhang YB, Zi X. Molecular targeted approaches to cancer therapy and prevention using chalcones. *Curr Cancer Drug Targets*. 2014;14(2):181-200.
186. Karthikeyan C, Moorthy NS, Ramasamy S, Vanam U, Manivannan E, Karunakaran D, et al. Advances in chalcones with anticancer activities. *Recent Pat Anticancer Drug Discov*. 2015;10(1):97-115.
187. Viegas-Junior C, Danuello A, da Silva Bolzani V, Barreiro EJ, Fraga CA. Molecular hybridization: a useful tool in the design of new drug prototypes. *Curr Med Chem*. 2007;14(17):1829-52.
188. Gao F, Huang G, Xiao J. Chalcone hybrids as potential anticancer agents: Current development, mechanism of action, and structure-activity relationship. *Med Res Rev*. 2020;40(5):2049-84.
189. Wei H, Ruan J, Zhang X. Coumarin–chalcone hybrids: promising agents with diverse pharmacological properties. *RSC Adv*. 2016;6(13):10846-60.
190. Steiner GG. The correlation between cancer incidence and kava consumption. *Hawaii Med J*. 2000;59(11):420-2.
191. Kerr JF, Wyllie AH, Currie AR. Apoptosis: a basic biological phenomenon with wide-ranging implications in tissue kinetics. *Br J Cancer*. 1972;26(4):239-57.
192. Hanahan D, Weinberg RA. The hallmarks of cancer. *Cell*. 2000;100(1):57-70.
193. Plati J, Bucur O, Khosravi-Far R. Dysregulation of apoptotic signaling in cancer: molecular mechanisms and therapeutic opportunities. *J Cell Biochem*. 2008;104(4):1124-49.
194. Mita MM, Mita AC, Tolcher AW. Apoptosis: mechanisms and implications for cancer therapeutics. *Target Oncol*. 2006;1(4):197-214.

195. Mohammad RM, Muqbil I, Lowe L, Yedjou C, Hsu HY, Lin LT, et al. Broad targeting of resistance to apoptosis in cancer. *Semin Cancer Biol.* 2015;35 Suppl(0):S78-s103.
196. DiPaola RS, Patel J, Rafi MM. Targeting apoptosis in prostate cancer. *Hematol Oncol Clin North Am.* 2001;15(3):509-24.
197. Cryns V, Yuan J. Proteases to die for. *Genes & development.* 1998;12(11):1551-70.
198. Uzzo RG, Haas NB, Crispen PL, Kolenko VM. Mechanisms of apoptosis resistance and treatment strategies to overcome them in hormone-refractory prostate cancer. *Cancer.* 2008;112(8):1660-71.
199. McKenzie S, Kyprianou N. Apoptosis evasion: the role of survival pathways in prostate cancer progression and therapeutic resistance. *J Cell Biochem.* 2006;97(1):18-32.
200. Kajiwara T, Takeuchi T, Ueki T, Moriyama N, Ueki K, Kakizoe T, et al. Effect of Bcl-2 overexpression in human prostate cancer cells in vitro and in vivo. *Int J Urol.* 1999;6(10):520-5.
201. Winter RN, Kramer A, Borkowski A, Kyprianou N. Loss of caspase-1 and caspase-3 protein expression in human prostate cancer. *Cancer Res.* 2001;61(3):1227-32.
202. Kagan J, Stein J, Babaian RJ, Joe YS, Pisters LL, Glassman AB, et al. Homozygous deletions at 8p22 and 8p21 in prostate cancer implicate these regions as the sites for candidate tumor suppressor genes. *Oncogene.* 1995;11(10):2121-6.
203. Hernandez-Cueto A, Hernandez-Cueto D, Antonio-Andres G, Mendoza-Marin M, Jimenez-Gutierrez C, Sandoval-Mejia AL, et al. Death receptor 5 expression is

- inversely correlated with prostate cancer progression. *Mol Med Rep.* 2014;10(5):2279-86.
204. Wong RSY. Apoptosis in cancer: from pathogenesis to treatment. *J Exp Clin Cancer Res.* 2011;30(1):87.
205. Jung JI, Lim SS, Choi HJ, Cho HJ, Shin HK, Kim EJ, et al. Isoliquiritigenin induces apoptosis by depolarizing mitochondrial membranes in prostate cancer cells. *J Nutr Biochem.* 2006;17(10):689-96.
206. Marquina S, Maldonado-Santiago M, Sánchez-Carranza JN, Antúnez-Mojica M, González-Maya L, Razo-Hernández RS, et al. Design, synthesis and QSAR study of 2'-hydroxy-4'-alkoxy chalcone derivatives that exert cytotoxic activity by the mitochondrial apoptotic pathway. *Bioorg Med Chem.* 2019;27(1):43-54.
207. Deeb D, Gao X, Jiang H, Arbab AS, Dulchavsky SA, Gautam SC. Growth inhibitory and apoptosis-inducing effects of xanthohumol, a prenylated chalone present in hops, in human prostate cancer cells. *Anticancer Res.* 2010;30(9):3333-9.
208. Li X, Pham V, Tippin M, Fu D, Rendon R, Song L, et al. Flavokawain B targets protein neddylation for enhancing the anti-prostate cancer effect of Bortezomib via Skp2 degradation. *Cell Commun Signal.* 2019;17(1):25.
209. Kłósek M, Mertas A, Król W, Jaworska D, Szymuszal J, Szliszka E. Tumor necrosis factor-related apoptosis-inducing ligand-induced apoptosis in prostate cancer cells after treatment with Xanthohumol-A natural compound present in *Humulus lupulus L.* *Int J Mol Sci.* 2016;17(6).
210. Lee YH, Yun J, Jung JC, Oh S, Jung YS. Anti-tumor activity of benzylideneacetophenone derivatives via proteasomal inhibition in prostate cancer cells. *Pharmazie.* 2016;71(5):274-9.

211. Szliszka E, Czuba ZP, Mazur B, Paradysz A, Krol W. Chalcones and dihydrochalcones augment TRAIL-mediated apoptosis in prostate cancer cells. *Molecules*. 2010;15(8):5336-53.
212. Szliszka E, Czuba ZP, Mazur B, Sedek L, Paradysz A, Krol W. Chalcones enhance TRAIL-induced apoptosis in prostate cancer cells. *Int J Mol Sci*. 2009;11(1):1-13.
213. Ismail B, Fagnere C, Limami Y, Ghezali L, Pouget C, Fidanzi C, et al. 2'-Hydroxy-4-methylsulfonylchalcone enhances TRAIL-induced apoptosis in prostate cancer cells. *Anticancer Drugs*. 2015;26(1):74-84.
214. Yu B, Liu H, Kong X, Chen X, Wu C. Synthesis of new chalcone-based homoserine lactones and their antiproliferative activity evaluation. *Eur J Med Chem*. 2019;163:500-11.
215. Thorburn A, Behbakht K, Ford H. TRAIL receptor-targeted therapeutics: resistance mechanisms and strategies to avoid them. *Drug Resist Updat*. 2008;11(1-2):17-24.
216. Otto T, Sicinski P. Cell cycle proteins as promising targets in cancer therapy. *Nat Rev Cancer*. 2017;17(2):93-115.
217. Ding L, Cao J, Lin W, Chen H, Xiong X, Ao H, et al. The roles of cyclin-dependent kinases in cell-cycle progression and therapeutic strategies in human breast cancer. *Int J Mol Sci*. 2020;21(6):1960.
218. Asghar U, Witkiewicz AK, Turner NC, Knudsen ES. The history and future of targeting cyclin-dependent kinases in cancer therapy. *Nat Rev Drug Discov*. 2015;14(2):130-46.
219. Diaz-Moralli S, Tarrado-Castellarnau M, Miranda A, Cascante M. Targeting cell cycle regulation in cancer therapy. *Pharmacol Ther*. 2013;138(2):255-71.

220. Carnero A. Targeting the cell cycle for cancer therapy. *Br J Cancer*. 2002;87(2):129-33.
221. Aaltomaa S, Eskelinen M, Lipponen P. Expression of cyclin A and D proteins in prostate cancer and their relation to clinopathological variables and patient survival. *Prostate*. 1999;38(3):175-82.
222. Comstock CES, Revelo MP, Buncher CR, Knudsen KE. Impact of differential cyclin D1 expression and localisation in prostate cancer. *Br J Cancer*. 2007;96(6):970-9.
223. Cao Z, Chen X, Xu Y, Guo F, Ji J, Xu H, et al. Differential Expression and Prognostic Value of Cytoplasmic and Nuclear Cyclin D1 in Prostate Cancer. *Biomed Res Int*. 2020;2020:1692658.
224. Halvorsen OJ, Haukaas SA, Akslen LA. Combined loss of pten and p27 expression is associated with tumor cell proliferation by ki-67 and increased risk of recurrent disease in localized prostate cancer. *Clin Cancer Res*. 2003;9(4):1474-9.
225. Fu Y, Hsieh TC, Guo J, Kunicki J, Lee MY, Darzynkiewicz Z, et al. Licochalcone-A, a novel flavonoid isolated from licorice root (*Glycyrrhiza glabra*), causes G2 and late-G1 arrests in androgen-independent PC-3 prostate cancer cells. *Biochem Biophys Res Commun*. 2004;322(1):263-70.
226. Fu DJ, Li JH, Yang JJ, Li P, Zhang YB, Liu S, et al. Discovery of novel chalcone-dithiocarbamates as ROS-mediated apoptosis inducers by inhibiting catalase. *Bioorg Chem*. 2019;86:375-85.
227. Sun YW, Huang WJ, Hsiao CJ, Chen YC, Lu PH, Guh JH. Methoxychalcone induces cell-cycle arrest and apoptosis in human hormone-resistant prostate cancer cells through PI 3-kinase-independent inhibition of mTOR pathways. *Prostate*. 2010;70(12):1295-306.

228. Lee YM, Lim DY, Choi HJ, Jung JI, Chung WY, Park JH. Induction of cell cycle arrest in prostate cancer cells by the dietary compound isoliquiritigenin. *J Med Food*. 2009;12(1):8-14.
229. Zhang Y, Srinivasan B, Xing C, Lü J. A new chalcone derivative (E)-3-(4-methoxyphenyl)-2-methyl-1-(3,4,5-trimethoxyphenyl)prop-2-en-1-one suppresses prostate cancer involving p53-mediated cell cycle arrests and apoptosis. *Anticancer Res*. 2012;32(9):3689-98.
230. Peyrot V, Leynadier D, Sarrazin M, Briand C, Rodriguez A, Nieto JM, et al. Interaction of tubulin and cellular microtubules with the new antitumor drug MDL 27048. A powerful and reversible microtubule inhibitor. *J Biol Chem*. 1989;264(35):21296-301.
231. Wang K, Zhang W, Wang Z, Gao M, Wang X, Han W, et al. Flavokawain A inhibits prostate cancer cells by inducing cell cycle arrest and cell apoptosis and regulating the glutamine metabolism pathway. *J Pharm Biomed Anal*. 2020;186:113288.
232. Saito Y, Mizokami A, Tsurimoto H, Izumi K, Goto M, Nakagawa-Goto K. 5'-Chloro-2,2'-dihydroxychalcone and related flavanoids as treatments for prostate cancer. *Eur J Med Chem*. 2018;157:1143-52.
233. Hussaini SM, Yedla P, Babu KS, Shaik TB, Chityal GK, Kamal A. Synthesis and Biological Evaluation of 1,2,3-triazole tethered Pyrazoline and Chalcone Derivatives. *Chem Biol Drug Des*. 2016;88(1):97-109.
234. Shaffer CV, Cai S, Peng J, Robles AJ, Hartley RM, Powell DR, et al. Texas native plants yield compounds with cytotoxic activities against prostate cancer cells. *J Nat Prod*. 2016;79(3):531-40.

235. Steeg PS. Tumor metastasis: mechanistic insights and clinical challenges. *Nat Med.* 2006;12(8):895-904.
236. Yao D, Dai C, Peng S. Mechanism of the mesenchymal-epithelial transition and its relationship with metastatic tumor formation. *Mol Cancer Res.* 2011;9(12):1608-20.
237. Odero-Marah V, Hawsawi O, Henderson V, Sweeney J. Epithelial-mesenchymal transition (emt) and prostate cancer. In: Schatten H, editor. *Cell & Molecular Biology of Prostate Cancer: Updates, Insights and New Frontiers.* Cham: Springer International Publishing; 2018. p. 101-10.
238. Montanari M, Rossetti S, Cavaliere C, D'Aniello C, Malzone MG, Vanacore D, et al. Epithelial-mesenchymal transition in prostate cancer: an overview. *Oncotarget.* 2017;8(21):35376-89.
239. Khan T, Scott KF, Becker TM, Lock J, Nimir M, Ma Y, et al. The prospect of identifying resistance mechanisms for castrate-resistant prostate cancer using circulating tumor cells: Is epithelial-to-mesenchymal transition a key player? *Prostate cancer.* 2020;2020:7938280-.
240. Chen C, Huang S, Chen CL, Su SB, Fang DD. Isoliquiritigenin Inhibits Ovarian cancer metastasis by reversing epithelial-to-mesenchymal transition. *Molecules.* 2019;24(20).
241. Jeong JH, Jang HJ, Kwak S, Sung GJ, Park SH, Song JH, et al. Novel TGF- β 1 inhibitor antagonizes TGF- β 1-induced epithelial-mesenchymal transition in human A549 lung cancer cells. *J Cell Biochem.* 2019;120(1):977-87.
242. Chua AW, Hay HS, Rajendran P, Shanmugam MK, Li F, Bist P, et al. Butein downregulates chemokine receptor CXCR4 expression and function through

- suppression of NF- κ B activation in breast and pancreatic tumor cells. *Biochem Pharmacol.* 2010;80(10):1553-62.
243. Moon DO, Choi YH, Moon SK, Kim WJ, Kim GY. Butein suppresses the expression of nuclear factor-kappa B-mediated matrix metalloproteinase-9 and vascular endothelial growth factor in prostate cancer cells. *Toxicol In Vitro.* 2010;24(7):1927-34.
244. Ma Y, Xu B, Yu J, Huang L, Zeng X, Shen X, et al. Fli-1 activation through targeted promoter activity regulation using a novel 3', 5'-diprenylated chalcone inhibits growth and metastasis of prostate cancer cells. *Int J Mol Sci.* 2020;21(6).
245. Kwon GT, Cho HJ, Chung WY, Park KK, Moon A, Park JH. Isoliquiritigenin inhibits migration and invasion of prostate cancer cells: possible mediation by decreased JNK/AP-1 signaling. *J Nutr Biochem.* 2009;20(9):663-76.
246. Folkman J. Role of angiogenesis in tumor growth and metastasis. *Semin Oncol.* 2002;29(6 Suppl 16):15-8.
247. Hanahan D, Weinberg Robert A. Hallmarks of cancer: The next generation. *Cell.* 2011;144(5):646-74.
248. Meleghe Z, Oltean S. Targeting angiogenesis in prostate cancer. *Int J Mol Sci.* 2019;20(11):2676.
249. Pang RWC, Poon RTP. Clinical implications of angiogenesis in cancers. *Vasc Health Risk Manag.* 2006;2(2):97-108.
250. Shibuya M. Vascular endothelial growth factor (VEGF) and its receptor (VEGFR) signaling in angiogenesis: A crucial target for anti- and pro-angiogenic therapies. *Genes Cancer.* 2011;2(12):1097-105.
251. Green MML, Hiley CT, Shanks JH, Bottomley IC, West CML, Cowan RA, et al. Expression of vascular endothelial growth factor (VEGF) in locally invasive

- prostate cancer is prognostic for radiotherapy outcome. *Int J Radiat Oncol Biol Phys.* 2007;67(1):84-90.
252. Woollard DJ, Opeskin K, Coso S, Wu D, Baldwin ME, Williams ED. Differential expression of VEGF ligands and receptors in prostate cancer. *Prostate.* 2013;73(6):563-72.
253. Bender RJ, Mac Gabhann F. Dysregulation of the vascular endothelial growth factor and semaphorin ligand-receptor families in prostate cancer metastasis. *BMC Syst Biol.* 2015;9(1):55.
254. McKay RR, Zurita AJ, Werner L, Bruce JY, Carducci MA, Stein MN, et al. A randomized phase II trial of short-course androgen deprivation therapy with or without Bevacizumab for patients with recurrent prostate cancer after definitive local therapy. *J Clin Oncol.* 2016;34(16):1913-20.
255. Kelly WK, Halabi S, Carducci M, George D, Mahoney JF, Stadler WM, et al. Randomized, double-blind, placebo-controlled phase III trial comparing docetaxel and prednisone with or without bevacizumab in men with metastatic castration-resistant prostate cancer: CALGB 90401. *J Clin Oncol.* 2012;30(13):1534-40.
256. Tannock IF, Fizazi K, Ivanov S, Karlsson CT, Fléchon A, Skoneczna I, et al. Aflibercept versus placebo in combination with docetaxel and prednisone for treatment of men with metastatic castration-resistant prostate cancer (VENICE): a phase 3, double-blind randomised trial. *Lancet Oncol.* 2013;14(8):760-8.
257. Michaelson MD, Oudard S, Ou YC, Sengeløv L, Saad F, Houede N, et al. Randomized, placebo-controlled, phase III trial of sunitinib plus prednisone versus prednisone alone in progressive, metastatic, castration-resistant prostate cancer. *J Clin Oncol.* 2014;32(2):76-82.

258. Keizman D, Zahurak M, Sinibaldi V, Carducci M, Denmeade S, Drake C, et al. Lenalidomide in nonmetastatic biochemically relapsed prostate cancer: results of a phase I/II double-blinded, randomized study. *Clin Cancer Res.* 2010;16(21):5269-76.
259. Mahmoud A, Elkhalfa D, Alali F, Al Moustafa AE, Khalil A. Novel polymethoxylated chalcones as potential compounds against KRAS-mutant colorectal cancers. *Curr Pharm Des.* 2020;26(14):1622-33.
260. Zhang Y, Yang J, Wen Z, Chen X, Yu J, Yuan D, et al. A novel 3',5'-diprenylated chalcone induces concurrent apoptosis and GSDME-dependent pyroptosis through activating PKC δ /JNK signal in prostate cancer. *Aging (Albany NY).* 2020;12(10):9103-24.
261. Jackson KM, Frazier MC, Harris WB. Suppression of androgen receptor expression by dibenzoylmethane as a therapeutic objective in advanced prostate cancer. *Anticancer Res.* 2007;27(3b):1483-8.
262. Chen S, Gao J, Halicka HD, Traganos F, Darzynkiewicz Z. Down-regulation of androgen-receptor and PSA by phytochemicals. *Int J Oncol.* 2008;32(2):405-11.
263. Zhou J, Geng G, Batist G, Wu JH. Syntheses and potential anti-prostate cancer activities of ionone-based chalcones. *Bioorg Med Chem Lett.* 2009;19(4):1183-6.
264. Porta C, Paglino C, Mosca A. Targeting PI3K/Akt/mTOR signaling in cancer. *Front Oncol.* 2014;4:64-.
265. Shorning BY, Dass MS, Smalley MJ, Pearson HB. The PI3K-AKT-mTOR pathway and prostate cancer: At the crossroads of AR, MAPK, and WNT signaling. *Int J Mol Sci.* 2020;21(12):4507.
266. Pearson HB, Li J, Meniel VS, Fennell CM, Waring P, Montgomery KG, et al. Identification of Pik3ca Mutation as a Genetic Driver of Prostate Cancer That

- Cooperates with Pten Loss to Accelerate Progression and Castration-Resistant Growth. *Cancer Discov.* 2018;8(6):764-79.
267. Grasso CS, Wu Y-M, Robinson DR, Cao X, Dhanasekaran SM, Khan AP, et al. The mutational landscape of lethal castration-resistant prostate cancer. *Nature.* 2012;487(7406):239-43.
268. Taylor BS, Schultz N, Hieronymus H, Gopalan A, Xiao Y, Carver BS, et al. Integrative genomic profiling of human prostate cancer. *Cancer Cell.* 2010;18(1):11-22.
269. Jung JI, Chung E, Seon MR, Shin HK, Kim EJ, Lim SS, et al. Isoliquiritigenin (ISL) inhibits ErbB3 signaling in prostate cancer cells. *Biofactors.* 2006;28(3-4):159-68.
270. Khor TO, Yu S, Barve A, Hao X, Hong JL, Lin W, et al. Dietary feeding of dibenzoylmethane inhibits prostate cancer in transgenic adenocarcinoma of the mouse prostate model. *Cancer Res.* 2009;69(17):7096-102.
271. Yo YT, Shieh GS, Hsu KF, Wu CL, Shiau AL. Licorice and licochalcone-A induce autophagy in LNCaP prostate cancer cells by suppression of Bcl-2 expression and the mTOR pathway. *J Agric Food Chem.* 2009;57(18):8266-73.
272. Khalil A AMA, Alali F, Elkhailifa D, inventor Novel chalcone-based chemotherapeutic compound for triple negative breast cancer. . US2020 December 17, 2020.
273. Zhu X-P, Lin G-S, Duan W-G, Li Q-M, Li F-Y, Lu S-Z. Synthesis and antiproliferative evaluation of novel longifolene-derived tetralone derivatives bearing 1,2,4-triazole moiety. *Molecules.* 2020;25(4):986.

274. V PK, J R, C TF, K TA, R SK, Varughese S, et al. Antibacterial and antitubercular evaluation of dihydronaphthalenone-indole hybrid analogs. *Chem Biol Drug Des.* 2017;90(5):703-8.
275. Beteck RM, Legoabe LJ, Isaacs M, Khanye SD, Laming D, Hoppe HC. Anti-trypanosomal and antimalarial properties of tetralone derivatives and structurally related benzocycloalkanones. *Medicina (Kaunas, Lithuania).* 2019;55(5):206.
276. Dimmock JR, Kandepu NM, Nazarali AJ, Kowalchuk TP, Motaganahalli N, Quail JW, et al. Conformational and quantitative structure–activity relationship study of cytotoxic 2-arylidenebenzocycloalkanones. *J Med Chem.* 1999;42(8):1358-66.
277. Dimmock JR, Zello GA, Oloo EO, Quail JW, Kraatz H-B, Perjési P, et al. Correlations between cytotoxicity and topography of some 2-arylidenebenzocycloalkanones determined by X-ray crystallography. *J Med Chem.* 2002;45(14):3103-11.
278. ADME in drug discovery: Cyprotex; [Available from: <http://www.cyprotex.com/admguide/introduction/adme-in-drug-discovery>.
279. Lyons SM, Alizadeh E, Mannheimer J, Schuamberg K, Castle J, Schroder B, et al. Changes in cell shape are correlated with metastatic potential in murine and human osteosarcomas. *Biol Open.* 2016;5(3):289-99.
280. Valdameri G, Gauthier C, Terreux R, Kachadourian R, Day BJ, Winnischofer SM, et al. Investigation of chalcones as selective inhibitors of the breast cancer resistance protein: critical role of methoxylation in both inhibition potency and cytotoxicity. *J Med Chem.* 2012;55(7):3193-200.
281. Cunningham D, You Z. In vitro and in vivo model systems used in prostate cancer research. *J Biol Methods.* 2015;2(1).

282. Tai S, Sun Y, Squires JM, Zhang H, Oh WK, Liang CZ, et al. PC3 is a cell line characteristic of prostatic small cell carcinoma. *Prostate*. 2011;71(15):1668-79.
283. Yuan TC, Veeramani S, Lin MF. Neuroendocrine-like prostate cancer cells: neuroendocrine transdifferentiation of prostate adenocarcinoma cells. *Endocr Relat Cancer*. 2007;14(3):531-47.
284. Vitaku E, Smith DT, Njardarson JT. Analysis of the structural diversity, substitution patterns, and frequency of nitrogen heterocycles among U.S. FDA approved pharmaceuticals. *J Med Chem*. 2014;57(24):10257-74.
285. Pfeffer CM, Singh ATK. Apoptosis: A target for anticancer therapy. *Int J Mol Sci*. 2018;19(2):448.
286. Ali A, Kulik G. Signaling pathways that control apoptosis in prostate cancer. *Cancers (Basel)*. 2021;13(5):937.
287. Shankaraiah N, Nekkanti S, Brahma UR, Praveen Kumar N, Deshpande N, Prasanna D, et al. Synthesis of different heterocycles-linked chalcone conjugates as cytotoxic agents and tubulin polymerization inhibitors. *Bioorg Med Chem*. 2017;25(17):4805-16.
288. Saraste A, Pulkki K. Morphologic and biochemical hallmarks of apoptosis. *Cardiovasc Res*. 2000;45(3):528-37.
289. Steinhilber U, Weiske J, Badock V, Tauber R, Bommert K, Huber O. Cleavage and shedding of E-cadherin after induction of apoptosis *. *Journal of Biological Chemistry*. 2001;276(7):4972-80.
290. Xu R, Hu J. The role of JNK in prostate cancer progression and therapeutic strategies. *Biomedicine & Pharmacotherapy*. 2020;121:109679.
291. Bubici C, Papa S. JNK signalling in cancer: in need of new, smarter therapeutic targets. *British Journal of Pharmacology*. 2014;171(1):24-37.

292. Sung B, Cho SG, Liu M, Aggarwal BB. Butein, a tetrahydroxychalcone, suppresses cancer-induced osteoclastogenesis through inhibition of receptor activator of nuclear factor-kappaB ligand signaling. *Int J Cancer*. 2011;129(9):2062-72.
293. Khan N, Adhami VM, Afaq F, Mukhtar H. Butein induces apoptosis and inhibits prostate tumor growth in vitro and in vivo. *Antioxid Redox Signal*. 2012;16(11):1195-204.
294. Kanazawa M, Satomi Y, Mizutani Y, Ukimura O, Kawauchi A, Sakai T, et al. Isoliquiritigenin inhibits the growth of prostate cancer. *Eur Urol*. 2003;43(5):580-6.
295. Zhang B, Lai Y, Li Y, Shu N, Wang Z, Wang Y, et al. Antineoplastic activity of isoliquiritigenin, a chalcone compound, in androgen-independent human prostate cancer cells linked to G2/M cell cycle arrest and cell apoptosis. *Eur J Pharmacol*. 2018;821:57-67.
296. Zhang X, Yeung ED, Wang J, Panzhinskiy EE, Tong C, Li W, et al. Isoliquiritigenin, a natural anti-oxidant, selectively inhibits the proliferation of prostate cancer cells. *Clin Exp Pharmacol Physiol*. 2010;37(8):841-7.
297. Lackova Z, Buchtelova H, Buchtova Z, Klejdus B, Heger Z, Brtnicky M, et al. Anticarcinogenic effect of spices due to phenolic and flavonoid compounds-In vitro evaluation on prostate cells. *Molecules*. 2017;22(10).
298. Gul HI, Yerdelen KO, Das U, Gul M, Pandit B, Li PK, et al. Synthesis and cytotoxicity of novel 3-aryl-1-(3'-dibenzylaminomethyl-4'-hydroxyphenyl)-propenones and related compounds. *Chem Pharm Bull*. 2008;56(12):1675-81.

299. Li X, Xu X, Ji T, Liu Z, Gu M, Hoang BH, et al. Dietary feeding of Flavokawain A, a Kava chalcone, exhibits a satisfactory safety profile and its association with enhancement of phase II enzymes in mice. *Toxicol Rep.* 2014;1:2-11.
300. Li X, Yokoyama NN, Zhang S, Ding L, Liu HM, Lilly MB, et al. Flavokawain-A induces deNEDDylation and Skp2 degradation leading to inhibition of tumorigenesis and cancer progression in the TRAMP transgenic mouse model. *Oncotarget.* 2015;6(39):41809-24.
301. Tang Y, Li X, Liu Z, Simoneau AR, Xie J, Zi X. Flavokawain B, a kava chalcone, induces apoptosis via up-regulation of death-receptor 5 and Bim expression in androgen receptor negative, hormonal refractory prostate cancer cell lines and reduces tumor growth. *Int J Cancer.* 2010;127(8):1758-68.
302. Wen D, Peng Y, Lin F, Singh RK, Mahato RI. Micellar Delivery of miR-34a Modulator Rubone and Paclitaxel in Resistant Prostate Cancer. *Cancer Res.* 2017;77(12):3244-54.
303. El-Naga RN. Pre-treatment with cardamonin protects against cisplatin-induced nephrotoxicity in rats: impact on NOX-1, inflammation and apoptosis. *Toxicol Appl Pharmacol.* 2014;274(1):87-95.
304. Pascoal AC, Ehrenfried CA, Lopez BG, de Araujo TM, Pascoal VD, Gilioli R, et al. Antiproliferative activity and induction of apoptosis in PC-3 cells by the chalcone cardamonin from *Campomanesia adamantium* (Myrtaceae) in a bioactivity-guided study. *Molecules.* 2014;19(2):1843-55.
305. Zhang J, Sikka S, Siveen KS, Lee JH, Um JY, Kumar AP, et al. Cardamonin represses proliferation, invasion, and causes apoptosis through the modulation of signal transducer and activator of transcription 3 pathway in prostate cancer. *Apoptosis.* 2017;22(1):158-68.

306. Syam S, Abdelwahab SI, Al-Mamary MA, Mohan S. Synthesis of chalcones with anticancer activities. *Molecules*. 2012;17(6):6179-95.
307. Kim YS, Kumar V, Lee S, Iwai A, Neckers L, Malhotra SV, et al. Methoxychalcone inhibitors of androgen receptor translocation and function. *Bioorg Med Chem Lett*. 2012;22(5):2105-9.
308. Moses MA, Kim YS, Rivera-Marquez GM, Oshima N, Watson MJ, Beebe KE, et al. Targeting the Hsp40/Hsp70 Chaperone Axis as a Novel Strategy to Treat Castration-Resistant Prostate Cancer. *Cancer Res*. 2018;78(14):4022-35.
309. Delmulle L, Bellahcène A, Dhooge W, Comhaire F, Roelens F, Huvaere K, et al. Anti-proliferative properties of prenylated flavonoids from hops (*Humulus lupulus* L.) in human prostate cancer cell lines. *Phytomedicine*. 2006;13(9-10):732-4.
310. Bartmańska A, Tronina T, Popłoński J, Milczarek M, Filip-Psurska B, Wietrzyk J. Highly cancer selective antiproliferative activity of natural prenylated flavonoids. *Molecules*. 2018;23(11).
311. Li K, Zheng Q, Chen X, Wang Y, Wang D, Wang J. Isobavachalcone induces ROS-mediated apoptosis via targeting thioredoxin reductase 1 in human prostate cancer PC-3 cells. *Oxid Med Cell Longev*. 2018;2018:1915828.
312. Borges-Argáez R, Balnburry L, Flowers A, Giménez-Turba A, Ruiz G, Waterman PG, et al. Cytotoxic and antiprotozoal activity of flavonoids from *Lonchocarpus* spp. *Phytomedicine*. 2007;14(7-8):530-3.
313. Liu Y, Zhang J, Wen R, Tu GZ, Chen HB, Liang H, et al. Anti-inflammatory and antiproliferative prenylated chalcones from *Hedysarum gmelinii*. *J Asian Nat Prod Res*. 2018;20(11):1009-18.

314. Wen Z, Zhang Y, Wang X, Zeng X, Hu Z, Liu Y, et al. Novel 3',5'-diprenylated chalcones inhibited the proliferation of cancer cells in vitro by inducing cell apoptosis and arresting cell cycle phase. *Eur J Med Chem.* 2017;133:227-39.
315. Su SY, Xue JJ, Yang GY, Lei C, Hou AJ. New cytotoxic alkylated chalcones from *fatoua villosa*. *Chem Biodivers.* 2017;14(6).
316. Fu H, Zhang Y, Wang X, Han Y, Peng X, Efferth T, et al. Synthesis and anti-tumor activity of novel aminomethylated derivatives of isoliquiritigenin. *Molecules.* 2014;19(11):17715-26.
317. Liu G, Ge Z, Zhao M, Zhou Y. Design, synthesis and cytotoxic activities of novel aliphatic amino-substituted flavonoids. *Molecules.* 2013;18(11):14070-84.
318. Lorenzo P, Alvarez R, Ortiz MA, Alvarez S, Piedrafita FJ, de Lera AR. Inhibition of I κ B kinase-beta and anticancer activities of novel chalcone adamantyl arotinoids. *J Med Chem.* 2008;51(17):5431-40.
319. Lorenzo P, Ortiz MA, Alvarez R, Piedrafita FJ, de Lera AR. Adamantyl arotinoids that inhibit I κ B kinase α and I κ B kinase β . *ChemMedChem.* 2013;8(7):1184-98.
320. Ismail B, Ghezali L, Gueye R, Limami Y, Pouget C, Leger DY, et al. Novel methylsulfonyl chalcones as potential antiproliferative drugs for human prostate cancer: involvement of the intrinsic pathway of apoptosis. *Int J Oncol.* 2013;43(4):1160-8.
321. Rodrigues J, Abramjuk C, Vásquez L, Gamboa N, Domínguez J, Nitzsche B, et al. New 4-maleamic acid and 4-maleamide peptidyl chalcones as potential multitarget drugs for human prostate cancer. *Pharm Res.* 2011;28(4):907-19.
322. Rioux B, Pouget C, Fidanzi-Dugas C, Gamond A, Laurent A, Semaan J, et al. Design and multi-step synthesis of chalcone-polyamine conjugates as potent antiproliferative agents. *Bioorg Med Chem Lett.* 2017;27(18):4354-7.

323. Gul HI, Yerdelen KO, Gul M, Das U, Pandit B, Li PK, et al. Synthesis of 4'-hydroxy-3'-piperidinomethylchalcone derivatives and their cytotoxicity against PC-3 cell lines. *Arch Pharm (Weinheim)*. 2007;340(4):195-201.
324. Reddy MV, Su CR, Chiou WF, Liu YN, Chen RY, Bastow KF, et al. Design, synthesis, and biological evaluation of Mannich bases of heterocyclic chalcone analogs as cytotoxic agents. *Bioorg Med Chem*. 2008;16(15):7358-70.
325. Tu HY, Huang AM, Hour TC, Yang SC, Pu YS, Lin CN. Synthesis and biological evaluation of 2',5'-dimethoxychalcone derivatives as microtubule-targeted anticancer agents. *Bioorg Med Chem*. 2010;18(6):2089-98.
326. Lei Q, Zhang S, Liu M, Li J, Zhang X, Long Y. Synthesis and biological evaluation of glycosides containing triazene-chalcones. *Mol Divers*. 2017;21(4):957-66.
327. Burcu Gürdere M, Aydın A, Yencilek B, Ertürk F, Özbek O, Erkan S, et al. Synthesis, Antiproliferative and Cytotoxic Activities, DNA Binding Features and Molecular Docking Study of Novel Enamine Derivatives. *Chem Biodivers*. 2020.
328. Wang M, Xu S, Wu C, Liu X, Tao H, Huang Y, et al. Design, synthesis and activity of novel sorafenib analogues bearing chalcone unit. *Bioorg Med Chem Lett*. 2016;26(22):5450-4.
329. Wani ZA, Guru SK, Rao AV, Sharma S, Mahajan G, Behl A, et al. A novel quinazolinone chalcone derivative induces mitochondrial dependent apoptosis and inhibits PI3K/Akt/mTOR signaling pathway in human colon cancer HCT-116 cells. *Food Chem Toxicol*. 2016;87:1-11.
330. Kamal A, Ramakrishna G, Raju P, Viswanath A, Ramaiah MJ, Balakishan G, et al. Synthesis and anti-cancer activity of chalcone linked imidazolones. *Bioorg Med Chem Lett*. 2010;20(16):4865-9.

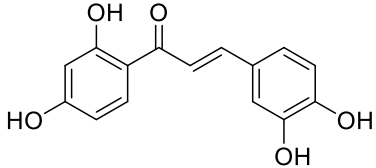
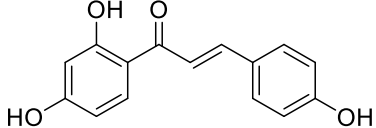
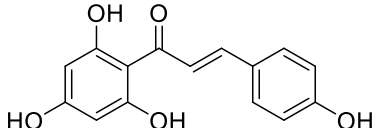
331. Singh P, Raj R, Kumar V, Mahajan MP, Bedi PM, Kaur T, et al. 1,2,3-Triazole tethered β -lactam-chalcone bifunctional hybrids: synthesis and anticancer evaluation. *Eur J Med Chem.* 2012;47(1):594-600.
332. Pinheiro S, Pessôa JC, Pinheiro EMC, Muri EMF, Filho EV, Loureiro LB, et al. 2H-1,2,3-Triazole-chalcones as novel cytotoxic agents against prostate cancer. *Bioorg Med Chem Lett.* 2020;30(19):127454.
333. Wegiel B, Wang Y, Li M, Jernigan F, Sun L. Novel indolyl-chalcones target stathmin to induce cancer cell death. *Cell Cycle.* 2016;15(9):1288-94.
334. Wang Y, Hedblom A, Koerner SK, Li M, Jernigan FE, Wegiel B, et al. Novel synthetic chalcones induce apoptosis in the A549 non-small cell lung cancer cells harboring a KRAS mutation. *Bioorg Med Chem Lett.* 2016;26(23):5703-6.
335. Bagul C, Rao GK, Makani VKK, Tamboli JR, Pal-Bhadra M, Kamal A. Synthesis and biological evaluation of chalcone-linked pyrazolo[1,5-a]pyrimidines as potential anticancer agents. *Medchemcomm.* 2017;8(9):1810-6.
336. Shi HB, Zhang SJ, Ge QF, Guo DW, Cai CM, Hu WX. Synthesis and anticancer evaluation of thiazolyl-chalcones. *Bioorg Med Chem Lett.* 2010;20(22):6555-9.
337. Kamal A, Balakrishna M, Nayak VL, Shaik TB, Faazil S, Nimbarte VD. Design and synthesis of imidazo[2,1-b]thiazole-chalcone conjugates: microtubule-destabilizing agents. *ChemMedChem.* 2014;9(12):2766-80.
338. Wang Q, Arnst KE, Wang Y, Kumar G, Ma D, Chen H, et al. Structural modification of the 3,4,5-trimethoxyphenyl moiety in the tubulin inhibitor VERU-111 leads to improved antiproliferative activities. *J Med Chem.* 2018;61(17):7877-91.
339. Nagaraju M, Gnana Deepthi E, Ashwini C, Vishnuvardhan MV, Lakshma Nayak V, Chandra R, et al. Synthesis and selective cytotoxic activity of novel hybrid

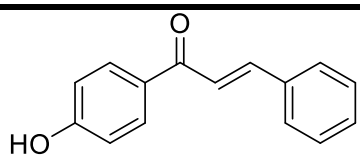
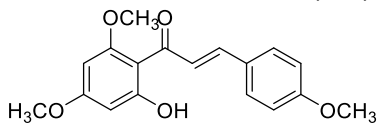
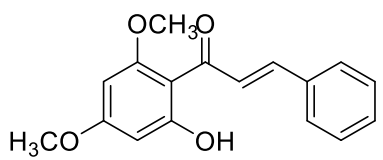
- chalcones against prostate cancer cells. *Bioorg Med Chem Lett.* 2012;22(13):4314-7.
340. Coskun D, Erkisa M, Ulukaya E, Coskun MF, Ari F. Novel 1-(7-ethoxy-1-benzofuran-2-yl) substituted chalcone derivatives: Synthesis, characterization and anticancer activity. *Eur J Med Chem.* 2017;136:212-22.
341. Isa NM, Abdelwahab SI, Mohan S, Abdul AB, Sukari MA, Taha MM, et al. In vitro anti-inflammatory, cytotoxic and antioxidant activities of boesenbergin A, a chalcone isolated from *Boesenbergia rotunda* (L.) (fingerroot). *Braz J Med Biol Res.* 2012;45(6):524-30.
342. Chinthala Y, Thakur S, Tirunagari S, Chinde S, Domatti AK, Arigari NK, et al. Synthesis, docking and ADMET studies of novel chalcone triazoles for anti-cancer and anti-diabetic activity. *Eur J Med Chem.* 2015;93:564-73.
343. Popłoński J, Turlej E, Sordon S, Tronina T, Bartmańska A, Wietrzyk J, et al. Synthesis and antiproliferative activity of minor hops prenylflavonoids and new insights on prenyl group cyclization. *Molecules.* 2018;23(4).
344. Vijaya Bhaskar Reddy M, Shen YC, Ohkoshi E, Bastow KF, Qian K, Lee KH, et al. Bis-chalcone analogues as potent NO production inhibitors and as cytotoxic agents. *Eur J Med Chem.* 2012;47(1):97-103.
345. Ocasio-Malavé C, Donate MJ, Sánchez MM, Sosa-Rivera JM, Mooney JW, Pereles-De León TA, et al. Synthesis of novel 4-Boc-piperidone chalcones and evaluation of their cytotoxic activity against highly-metastatic cancer cells. *Bioorg Med Chem Lett.* 2020;30(1):126760.
346. Liu Y, Zhang X, Kelsang N, Tu G, Kong D, Lu J, et al. Structurally diverse cytotoxic dimeric chalcones from *Oxytropis chiliophylla*. *J Nat Prod.* 2018;81(2):307-15.

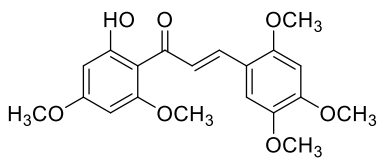
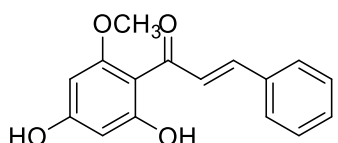
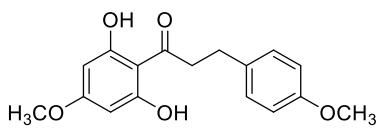
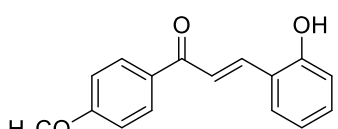
347. El Sayed Aly MR, Abd El Razek Fodah HH, Saleh SY. Antiobesity, antioxidant and cytotoxicity activities of newly synthesized chalcone derivatives and their metal complexes. *Eur J Med Chem.* 2014;76:517-30.
348. Gaur R, Pathania AS, Malik FA, Bhakuni RS, Verma RK. Synthesis of a series of novel dihydroartemisinin monomers and dimers containing chalcone as a linker and their anticancer activity. *Eur J Med Chem.* 2016;122:232-46.
349. Gibson MZ, Nguyen MA, Zingales SK. Design, synthesis, and evaluation of (2-(pyridinyl)methylene)-1-tetralone chalcones for anticancer and antimicrobial activity. *Med Chem.* 2018;14(4):333-43.
350. Maguire CJ, Carlson GJ, Ford JW, Strecker TE, Hamel E, Trawick ML, et al. Synthesis and biological evaluation of structurally diverse α -conformationally restricted chalcones and related analogues. *Medchemcomm.* 2019;10(8):1445-56.
351. Eachkoti R, Reddy MV, Lieu YK, Cosenza SC, Reddy EP. Identification and characterisation of a novel heat shock protein 90 inhibitor ONO4140. *Eur J Cancer.* 2014;50(11):1982-92.
352. Lokesh BVS, Prasad YR, Shaik AB. Synthesis, Biological Evaluation and Molecular Docking Studies of New Pyrazolines as an Antitubercular and Cytotoxic Agents. *Infect Disord Drug Targets.* 2019;19(3):310-21.

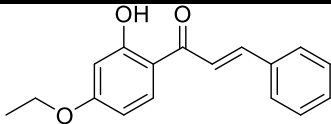
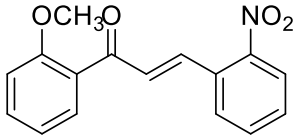
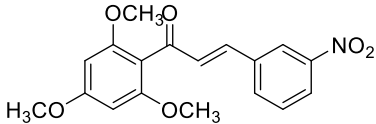
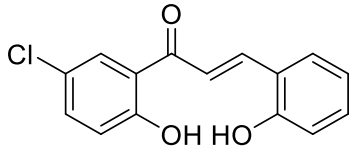
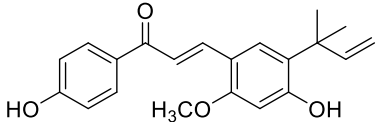
APPENDIX A. REPORTED CHALCONES' ACTIVITY AGAINST PCA

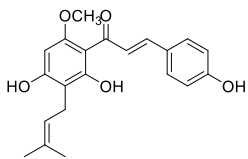
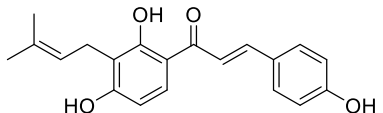
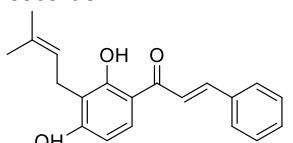
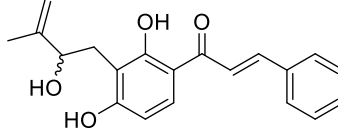
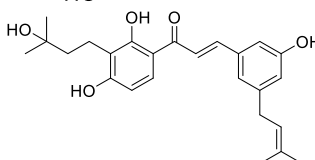
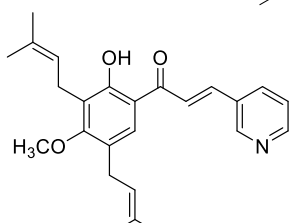
Table S1. Natural and Synthetic Chalcone derivatives tested on different PCa cell lines

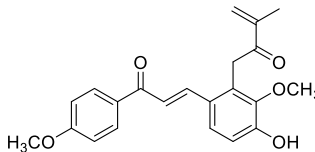
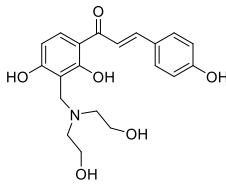
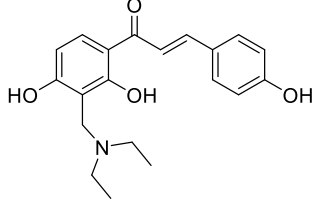
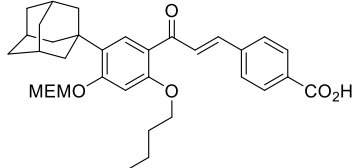
Structure	Source	Experimental Model	IC ₅₀	Effect	Molecular Target	Ref
<p>1</p> <p>Butein</p> 	Nat	<i>In vitro</i> : PC3, DU145 LNCaP and CWR22Rv1 <i>In vivo</i> : athymic nude mice	NR	<ul style="list-style-type: none"> • Inhibited cancer cells proliferation • Induced apoptosis • Induced G2/M phase arrest • Inhibited tumor growth in nude mice • Inhibited cell migration, invasion and angiogenesis 	↓VEGF, MMP-9 ↓NF-κB ↓RANKL X IκBα kinase, ↓p-IκBα ↓PSA levels	(242, 243, 292, 293)
<p>2</p> <p>Isoliquiritigenin</p> 	Nat	<i>In vitro</i> : DU145 LNCaP PC-3 22RV1 <i>In vivo</i> : PC-3 xenograft tumor	23.3 μM 15.7 μM, 19.6 μM 36.6 μM	<ul style="list-style-type: none"> • Inhibited cell growth/proliferation • Induced S and G2/M phase arrest • Induced apoptosis • Disrupted mitochondrial membrane potential • Suppressed epidermal growth factor (EGF)-induced cell invasion and migration • Decreased ROS levels • Repressed the growth of PC-3 xenograft tumor 	↑GADD153 X ErbB3 signaling: ↓ErbB3, p-ErbB3 X PI3K/Akt: ↓p85, ↓p-Akt ↓PSA ↓Cox-1, COX-2 X JNK-Ap-1 X EGF: ↓MMP-9, uPA, VEGF, TIMP-1, ↑TIMP-2 ↓ROS ↑AMPK	(205, 228, 245, 262, 269, 294- 296)
<p>3</p> <p>Naringenin chalcone</p> 	Nat	<i>In vitro</i> : PNT1A PC3 22RV1	~1 μM ~1 μM >1 μM	<ul style="list-style-type: none"> • Inhibited cell growth 	-	(297)

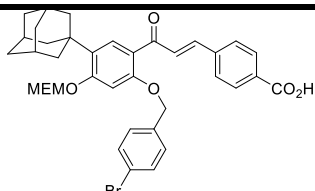
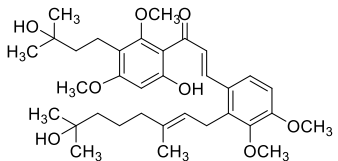
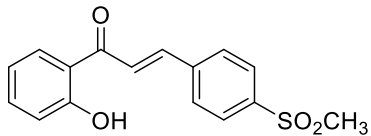
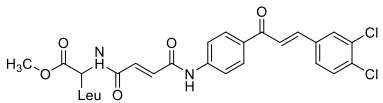
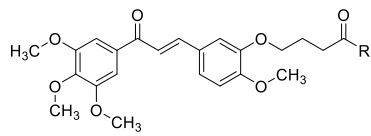
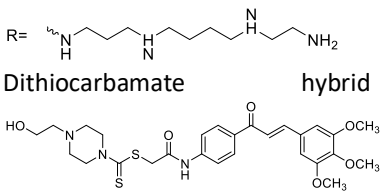
Structure	Source	Experimental Model	IC ₅₀	Effect	Molecular Target	Ref
<p>4</p> 	Syn	<i>In vitro</i> : PC3	6.19 μM	<ul style="list-style-type: none"> Inhibited cell proliferation 		(298)
<p>5</p> <p>Flavokawain A (FKA)</p> 	Nat	<i>In vitro</i> : PC3 DU145 22Rv1 PrECs & PrSCs	22.86 μM NR NR NS (80 μM)	<ul style="list-style-type: none"> Selectivity inhibited growth of Prostate cancer cells especially pRb deficient cell lines with no effect on the growth of normal prostate epithelial nor stromal cells (PrECs & PrSCs) Induced apoptosis and cell cycle arrest at G2/M phase Inhibited formation of HG-PIN, prostate adenocarcinomas and metastasis in TRAMP mice Dietary feeding of FKA showed no adverse effects on major organ function and homeostasis in FVB/N mice 	<ul style="list-style-type: none"> ↓ Tubulin polymerization ↑ glutamine metabolism ↓ intracellular glutamine, glutamic acid and proline ↓ GSS, ↑ GSTP1 → ↓ GSH → ↑ ROS → ↑ Apoptosis Proteasome-dependent and ubiquitination mediated Skp2 degradation ↓ Skp2 → ↑ p27/Kip1, ↓ Nedd8-Cullin1, ↓ Nedd8-UBC12 	(231, 299, 300)
<p>6</p> <p>Flavokavain B</p> 	Nat	<i>In vitro</i> : DU145, PC-3, LAPC4 & LNCaP	3.9, 6.2, 32 & 48.3 μM, respectively (48 h)	<ul style="list-style-type: none"> Inhibited cancer cells growth Induced Apoptosis Inhibited tumor growth in mice 	<ul style="list-style-type: none"> ↑ DR5, Bim, Puma ↓ XIAP, surviving ↓ Nedd8-Cullin1 ↓ Nedd8-UBC12 ↓ Skp2 (↑ Skp2 degradation in an ubiquitin and proteasome dependent manner) ↑ p21, p27 	(208, 301)
		<i>In vivo</i> : mice bearing DU145 xenograft tumors				

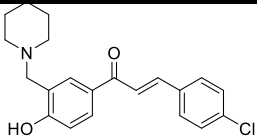
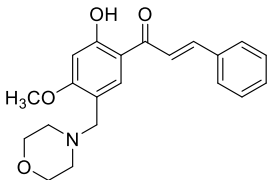
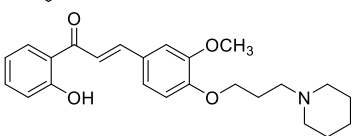
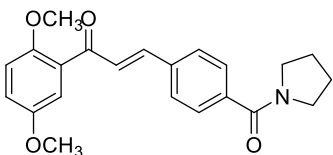
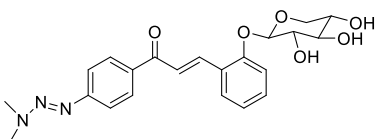
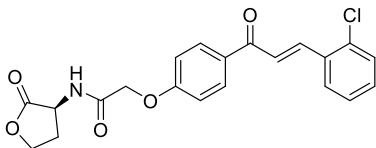
Structure	Source	Experimental Model	IC ₅₀	Effect	Molecular Target	Ref
7 Rubone 	Nat	<i>In vitro</i> : LNCaP C4-2 PC3 DU145 RWPE-1 PC3-PTX DU145-PTX	>50 μM in all cell lines (MTT, NR)	Combined treatment Rubone+ Paclitaxel: <ul style="list-style-type: none"> Reversed PTX chemoresistance in DU145-TXR and PC3-TXR cell resistant cell lines (reduced IC₅₀ from 2.58 μM to 0.0932 nM against PC3-TXR) with no effect on the proliferation of normal prostate cells Inhibited PC3-TXR cell growth, sphere formation in 3D model, migration and invasion Suppressed growth of cancer stem cells Prevented tumor growth in prostate cancer bearing nude mice 	Rubone single treatment: Increased miRNA-34a expression in androgen refractory cells especially Taxol resistant cell lines and reversed its downstream signals ↑miRNA-34a → ↑E-Cadherin, ↓SIRT1, ↓CyclinD1, and ↑Bax ↑Tap73, Elk-1	(302)
8 Cardamonin 	Nat	<i>In vitro</i> PC3 DU145 LNCaP	41.9 μM NR NR (SRB, 48h)	<ul style="list-style-type: none"> Inhibited Cell proliferation Induced apoptosis through DNA fragmentation Repressed invasion and migration Enhanced cisplatin cytotoxicity (reduced IC₅₀ from 2.7 to 0.62 μg/ml) when used as combination at subtoxic concentration IC5 (25 μM) Reduced Cisplatin induced nephrotoxicity 	↓ NF-κB ↓p-JAK2 → ↓ p-STAT3 (Tyr705), translocation & DNA binding ↓VEGF, MMP-9, COX-2, XIAP	(303-305)
9 	Nat	<i>In vitro</i> : LNCaP	NR	<ul style="list-style-type: none"> Augmented TRAIL-induced cytotoxicity and apoptosis suggesting a role in PCa chemoprevention 		(211)
10 	Syn	<i>In vitro</i> : PC3	23.14 μM (MTT, 24 h)	<ul style="list-style-type: none"> Inhibited cell growth/proliferation 		(306)

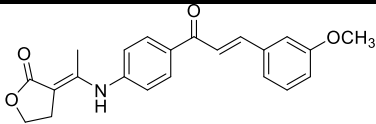
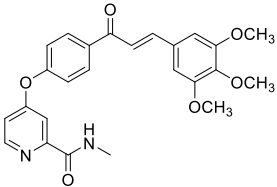
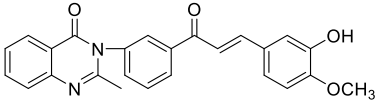
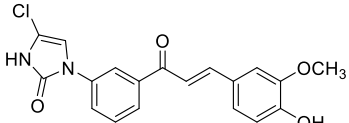
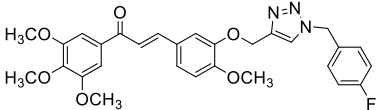
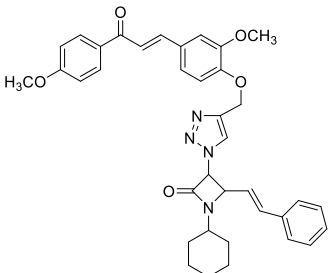
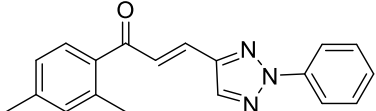
Structure	Source	Experimental Model	IC ₅₀	Effect	Molecular Target	Ref
11 	Syn	<i>In vitro</i> : PC3	8.2 μM (Cell titer, 48h)	<ul style="list-style-type: none"> • Selectively Inhibited cancer cells proliferation without affecting normal fibroblast cells (BJ cells IC₅₀ 207.87) • Induced cell cycle arrest at G2/M phase • Induced mitochondrial dependent apoptosis • Inhibited cell growth 	<ul style="list-style-type: none"> • ↑Bax and ↓ Bcl-2 • ↑Caspase-3/7 activation 	(206)
12 	Syn	<i>In vitro</i> : LNCaP	3.4 μM (72 h)	<ul style="list-style-type: none"> • Inhibited cancer cells proliferation • Inhibited tumor growth in ADT-resistant CRPC model with no overt signs of toxicity 	<ul style="list-style-type: none"> • Lock the HSP90-AR complex in an androgen non-responsive state, thus inhibit AR translocation and transcription of AR target genes 	(307)
13 	Syn	<i>In vitro</i> : 22Rv1 <i>In vivo</i> : CRPC (22Rv1) mice xenograft model	NR	<ul style="list-style-type: none"> • Inhibited proliferation of AR-dependent and AR-independent PCa cells • Induced SubG1 accumulation • Inhibited tumor growth in <i>in vivo</i> xenograft model 	<ul style="list-style-type: none"> • Inhibit Hsp40/Hsp70 chaperone axis → destabilize full length AR, ARv and GR → reduce the transcription of AR target genes. 	(308)
14 	Syn	<i>In vitro</i> : LNCaP PC3 DU145 <i>In vivo</i> : PC-3 xenograft model	3.74 μM 1.52 μM 4.5 μM (SRB, 72h)	<ul style="list-style-type: none"> • Induced caspase dependent apoptosis • Arrested cell cycle at G2/M phase • Induced autophagy 	<ul style="list-style-type: none"> • Suppressed AR dependent transcription • Blocked DHT-dependent growth stimulation • Disturbed microtubule network 	(232)
15 Licochalcone-A 	Nat	<i>In vitro</i> : PC3 LNCaP	NR	<ul style="list-style-type: none"> • Induced caspase dependent apoptosis • Arrested cell cycle at G2/M phase • Induced autophagy 	<ul style="list-style-type: none"> • ↓p-Rb (S780) • ↓transcription factor E2F • ↑formation of acidic vesicular organelles (AVOs) • ↓m-TOR 	(225, 271)

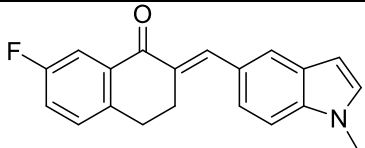
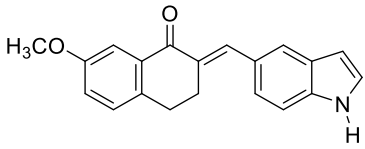
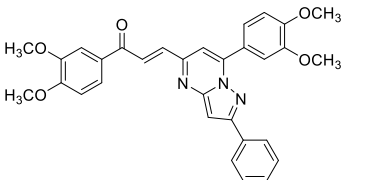
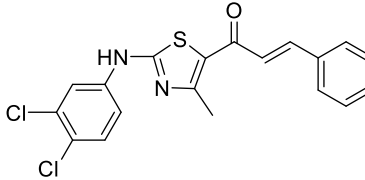
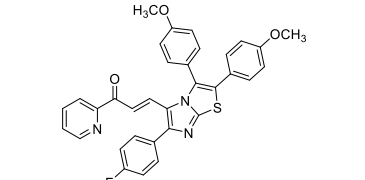
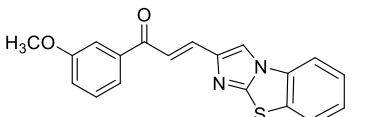
Structure	Source	Experimental Model	IC ₅₀	Effect	Molecular Target	Ref
16  Xanthohumol	Nat	<i>In vitro</i> : DU145 PC3 LNCaP C4-2	12.3 μM 13.2 μM NR NR (48 h)	<ul style="list-style-type: none"> • Preferentially inhibited PCa & proliferation cells as compared to MCF-10 (SI 6.5-8.5) but not endothelial cells HLMEC (SI 1.1-1.5) • Induced apoptosis • Sensitized TRAIL-resistant cancer cells to TRAIL induced apoptosis and cytotoxicity 	Induced mitochondrial depolarization ↑release of cyt-c ↓NF-κB, Akt, mTOR, Bcl-2, and survivin	(207, 209, 309, 310)
17  Isobavachalcone	Nat	<i>In vitro</i> : PC3 LNCaP	19.25 μM NR (MTT, 48h)	<ul style="list-style-type: none"> • Inhibited cancer cells proliferation • Induced ROS-mediated apoptosis • Augmented TRAIL mediated apoptosis and cytotoxicity 	↓TrxR1 activity → ↑ROS → ↑ ER stress markers (↑GRP-78, ATF-4, XBP-1, CHOP, P-EIF2α), ↑cleaved caspase3	(212, 311)
18  Isocordoin	Nat	<i>In vitro</i> : PC3	NR	<ul style="list-style-type: none"> • Induced G2/M cell cycle arrest 		(312)
19  Sanjuanolid	Nat	<i>In vitro</i> : PC3 DU145	11 μM 7 μM (SRB 48h)	<ul style="list-style-type: none"> • Inhibited cell proliferation and induced cytotoxicity • Reduced colony formation • Induced cell cycle arrest at G2/M phase 	<ul style="list-style-type: none"> • Promote formation of abnormal mitotic spindles and increase rate of tubulin polymerization but not total tubulin 	(234)
20 	Nat	<i>In vitro</i> DU145	>10 μM (MTT, 24h)	<ul style="list-style-type: none"> • Inhibited cell proliferation 		(313)
21 	Syn	<i>In vitro</i> PC3 DU145 RWPE-1 <i>In vivo</i> :	4.67 μM 6.56 μM 5.00 μM (MTT, 48h)	<ul style="list-style-type: none"> • Non preferentially inhibited cell proliferation (SI 0.76-1.07) • Inhibited cancer cells proliferation • Induced apoptosis, GSDME-dependent pyroptosis • Arrested cell cycle at sub-G1 	<ul style="list-style-type: none"> • Apoptosis markers ↓caspase-3, -8, -9; ↑active- Caspase-3, -8, -9, ↑PARP-cleavage, ↑Bax/Bcl-2 ratio, ↑cyt-c, ↓survivin, ↓p-P38/MAPK, ↓p-ERK1/2, ↓MDM2, ↓Bcl-2, ↓P-ERK) • Proliferation markers (↑SHIP-1, ↓p110, ↓Gata-1) 	(244, 260, 314)

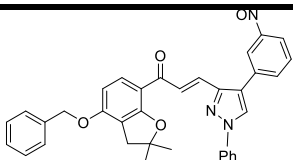
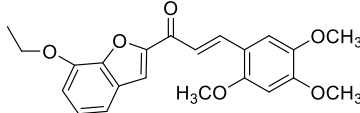
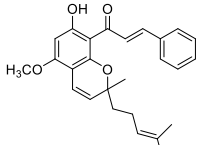
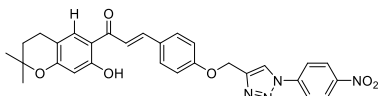
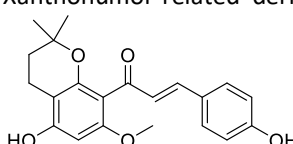
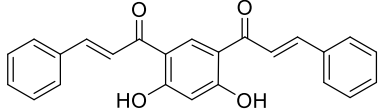
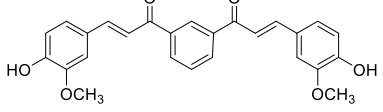
Structure	Source	Experimental Model	IC ₅₀	Effect	Molecular Target	Ref
		PC3 xenograft mice mode		<ul style="list-style-type: none"> • Reduced metastasis, migration and invasion • Reduced colony formation • Inhibited <i>in vivo</i> tumor growth 	<ul style="list-style-type: none"> • Cell cycle regulators ↓ Cyclins D1 and D2, ↓ CDKs 2 and 6, and c-Myc, ↑ P21^{cip1} & P27^{kip1}, ↓ PCNA • Metastasis markers (↓ VEGF-1, ↓ ICAM-1, ↓ TGF-β2, ↓ MMP-1) • ↑ Fli-1 expression and Fli-1 target genes • ↑ PKCδ, ↑ p-SAPK/JNK, ↑ IL-6 • GSDME cleavage → ↑ GSDME-N 	
22	Villosin	A Nat	<i>In vitro</i> PC3	1.9 μM (MTT, 48h)	<ul style="list-style-type: none"> • Induced cytotoxicity 	(315)
						
23	Aminomethylated derivative of Isoliquiritigenin	Syn	<i>In vitro</i> : PC3	35.14 μM (MTT, 72h)	<ul style="list-style-type: none"> • Inhibited cell proliferation 	(316)
						
24		Syn	<i>In vitro</i> : PC3	3.9 μM (MTT, 72h)	<ul style="list-style-type: none"> • Induced cytotoxicity 	(317)
						
25		Syn	<i>In vitro</i> : PC3	0.74 μM (MTT, 48 h)	<ul style="list-style-type: none"> • Inhibited cell growth/proliferation 	Inhibited IkappaB kinase-beta (IKKβ) (318)
						

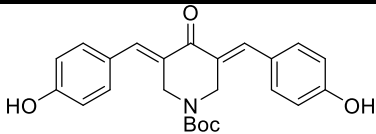
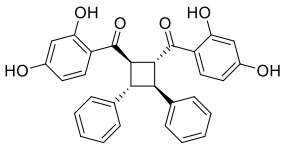
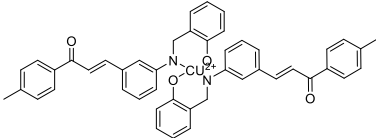
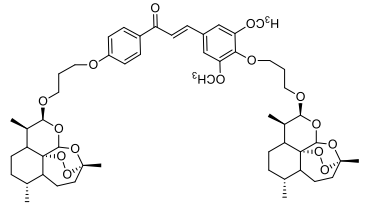
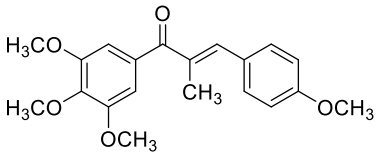
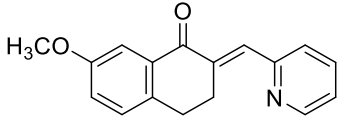
Structure	Source	Experimental Model	IC ₅₀	Effect	Molecular Target	Ref
	Syn	<i>In vitro</i> : PC3	NR	<ul style="list-style-type: none"> Reduced cell viability Induced of apoptosis 	↓ IκBα kinase α (IKKα) and IκBα kinase β (IKKβ)	(319)
	Syn	<i>In vitro</i> : PC3 DU-145 LNCaP	5.8 9.2 2.2 μM (SRB, 48h)	<ul style="list-style-type: none"> Inhibited cell growth/proliferation Induced G1 arrest 	↓ p-RB, E2F-1, cyclin D1, cyclin E, CDKs 2 & 4, Cdc25A ↓ mTOR and survivin	(227)
	Syn	<i>In vitro</i> : PC3 DU145 LNCaP	~15μM ~20μM ~15μM (MTT, 48h)	<ul style="list-style-type: none"> Reduced cell proliferation Induced of apoptosis Sensitized PCa cells to TRAIL-induced apoptosis Induced DNA fragmentation 	↓ Δψ _m ↓ Bcl-2/NF-κB and COX-2 ↑ DNA fragmentation ↓ p-Akt	(213, 320)
	Syn	<i>In vitro</i> : PC-3 LNCaP <i>In vivo</i> : nude-mice xenografts	29.5 & 21.4 μg/ml, respectively (72 h)	<ul style="list-style-type: none"> Inhibited cell cycle progression, cell adhesion, invasion, migration and colony formation Reduced neovascularization in chick embryos and MMP-9 activity Strongly inhibited tumor development in nude mice 	↓ MMP-p activity	(321)
	Syn	<i>In vitro</i> : PC3 DU145	31.8 μM 28.5 μM (MTT, 48h)	<ul style="list-style-type: none"> Inhibited cancer cells proliferation 		(322)
	hybrid	Syn <i>In vitro</i> : PC3	1.05μM (MTT, 72)	<ul style="list-style-type: none"> Inhibited cancer cells proliferation Reduced colony formation Induced cell cycle arrest at G2/M phase, DNA damage and mitochondrial apoptosis 	Apoptosis ↑ caspase activation, ↓ Δψ _m , ↑ ROS production, ↓ catalase activity X EMT (↑ E-Cadherin, ↓ N-Cadherin, ↓ Vimentin, ↓ activated-MMP2, ↓ activated-MMP9)	(226)

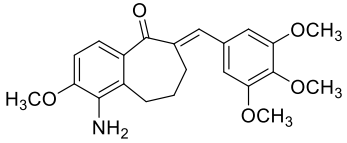
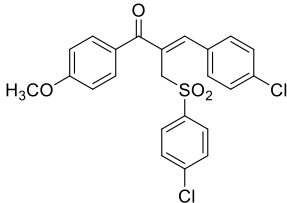
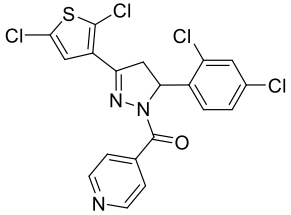
Structure	Source	Experimental Model	IC ₅₀	Effect	Molecular Target	Ref
	Syn	<i>In vitro</i> : PC3	3.7 μM (Cell Titer, 72 h)	<ul style="list-style-type: none"> Inhibited cell growth/proliferation 		(323)
	Syn	<i>In vitro</i> : PC3	0.78 μg/mL (72 h)	<ul style="list-style-type: none"> Inhibited cell growth/proliferation 		(324)
	Syn	<i>In vitro</i> : PC3 DU145	1.95 μM 2.73 μM (MTT, 48h)	<ul style="list-style-type: none"> Inhibited cancer cells proliferation Induced apoptosis 	X tubulin polymerization and formation of microtubule	(287)
	syn	<i>In vitro</i> : PC3	0.53 μM	<ul style="list-style-type: none"> Induced G1, S and G2/M phase arrests Increased apoptotic cell death 		(325)
	Syn	<i>In vitro</i> : PC3	28.2 μM (MTT, 48h)	<ul style="list-style-type: none"> Inhibited cancer cells proliferation 		(326)
	Syn	<i>In vitro</i> : PC3 DU145 Normal GES-1	4.61 3.24 μM 13.37 (MTT, 72h)	<ul style="list-style-type: none"> Selectively Inhibited cancer cells proliferation (SI 2.9-4.1) Reduced colony formation and cell migration Induced apoptosis Sensitized the PCa cells to TRAIL induced apoptosis and growth inhibition (synergistic effect) 	↑DR5 → sensitized cells to TRAIL induced apoptosis and growth inhibition ↑Caspase3/7 activity	(214)

Structure	Source	Experimental Model	IC ₅₀	Effect	Molecular Target	Ref
	Syn	<i>In vitro</i> PC3 FL normal cells	69.92 μM 86.45 μM (MTT, NR)	<ul style="list-style-type: none"> Inhibited cancer cells proliferation and induced cytotoxicity (SI 1.23) 	Forms adduct with DNA	(327)
	Syn	<i>In vitro</i> PC3	3.15 μM (MTT, 72h)	<ul style="list-style-type: none"> Induced cytotoxicity 	X VEGFR-2 and B-Raf Kinase activites	(328)
	Quinazolinone chalcone	Syn <i>In vitro</i> : PC3 <i>In vivo</i> : Non PCa	54 μM (MTT, 48h)	<ul style="list-style-type: none"> Inhibited cancer cells proliferation Induced apoptosis Inhibited tumor growth in vivo with no observed toxicity 		(329)
	syn	<i>In vitro</i> : PC3	1.95 μM (NR)	<ul style="list-style-type: none"> Inhibited cancer cells growth/proliferation 		(330)
	Syn	<i>In vitro</i> : DU145	1.3 μM (SRB, 48h)	<ul style="list-style-type: none"> Inhibited cancer cells proliferation Induced apoptosis and cell cycle arrest at G2/M phase 	X Inhibit tubulin polymerization ↓ Δψ _m ↑ caspase-3 & 9 activation	(233)
	Syn	<i>In vitro</i> : PC-3	67.1 μM (SRB, 48 h)	<ul style="list-style-type: none"> Inhibited cell growth/proliferation 		(331)
	Syn	PC3	15.64 μM (MTT, 24h)	<ul style="list-style-type: none"> Reduced cancer cells viability 		(332)

Structure	Source	Experimental Model	IC ₅₀	Effect	Molecular Target	Ref
	Syn	<i>In vitro</i> : PC3	0.147 μM (Crystal 72h)	violet, <ul style="list-style-type: none"> Inhibited cancer cells proliferation Induced apoptosis Increased cancer cells death Reduced cancer cells invasion 	<ul style="list-style-type: none"> Microtubule destabilization ↓p-STMN1 → ↑STMN1 knockdown of STMN1 restored cancer cell viability 	(333)
	Syn	<i>In vitro</i> : PC3 Normal lung bronchial epithelial	~3 μM >>10μM (Crystal 72h)	violet, <ul style="list-style-type: none"> Inhibited cancer cells proliferation Selectively induced apoptosis in cancer cells 		(334)
	Syn	<i>In vitro</i> : DU145	7.2μM (MTT, 48h)	<ul style="list-style-type: none"> Inhibited cancer cells proliferation 		(335)
	Syn	<i>In vitro</i> : PC-3 <i>In vivo</i> : ICR mice bearing sarcoma 180	7.99 μM (NR)	<ul style="list-style-type: none"> Inhibited cell growth/proliferation Moderate tumor inhibition <i>in vivo</i> Precipitated partially in body and caused obstruction in mouse intestine 		(336)
	Syn	<i>In vitro</i> : DU145	1.05 μM (MTT, 48h)	<ul style="list-style-type: none"> Inhibited cancer cells proliferation Induced apoptosis and cell cycle arrest at G2/M phase 	X Tubulin polymerization through competing on colchicine binding site	(337)
	Syn	<i>In vitro</i> : DU145	2.7μM (MTT, 48h)	<ul style="list-style-type: none"> Inhibited cancer cells proliferation 	X Microtubule assembly	(338)

Structure	Source	Experimental Model	IC ₅₀	Effect	Molecular Target	Ref
	Syn	<i>In vitro</i> : PC3	5.9 μM (time specified)	<ul style="list-style-type: none"> Inhibited cell growth/proliferation not		(339)
	Syn	<i>In vitro</i> : PC3	NR	<ul style="list-style-type: none"> Inhibited cancer cells growth and reduced cell viability by ~85% at 20 μM Induced apoptosis 	↑Caspase3/7 activation ↓Δψ _m	(340)
Boesenbergin A 	Nat	<i>In vitro</i> : PC3	27.95 μM (MTT, 24 h)	<ul style="list-style-type: none"> Inhibited cell growth/proliferation 		(341)
	Syn	<i>In vitro</i> : DU145	29.9 μM (MTT, NR)	<ul style="list-style-type: none"> Inhibited cancer cells growth 		(342)
Xanthohumol related derivatives 	Nat	<i>In vitro</i> : PC3	10.7 μM (SRB, 24h)	<ul style="list-style-type: none"> Inhibited cancer cells proliferation 		(343)
	Syn	<i>In vitro</i> : DU145	1.70 μM (SRB, 72 h)	<ul style="list-style-type: none"> Inhibited cell growth/proliferation 		(344)
	Syn	<i>In vitro</i> : PC3 LNCaP	5.04 μM 4.15 μM (MTT, 24h)	<ul style="list-style-type: none"> Induced cancer cells death and apoptosis 	X proteasomal activity ↑ubiquitinated proteins ↑Bax, aCaspase-3, cleaved PARP	→ (210)

Structure	Source	Experimental Model	IC ₅₀	Effect	Molecular Target	Ref
	Syn	<i>In vitro</i> : PC3 22RV1	22.9µg/ml 17.1µg/ml (=56.1 & 41.1 µM)	<ul style="list-style-type: none"> Suppressed cellular proliferation Induced apoptosis Non selectively induced cytotoxicity, showed higher toxicity to normal colorectal cell line (CCD180Co) than prostate cancer cells (SI<1) 	↓NF- κB ↓KI67 ↑Caspase3/7 activation	(345)
(+)-oxyfadichalcone 	C Nat	<i>In vitro</i> : PC3	3.5µM (MTT, 48h)	<ul style="list-style-type: none"> Induced cytotoxicity 	-	(346)
	Syn	<i>In vitro</i> : PC3	5.95 µM (SRB, 48h)	<ul style="list-style-type: none"> Induced cytotoxicity Exerted Antioxidant effect 		(347)
	syn	<i>In vitro</i> : PC3	MTT (48h) 10µM	<ul style="list-style-type: none"> Selectivity Inhibited cancer cell proliferation as compared to normal VERO cell line (SI 210) 		(348)
	Syn	<i>In vitro</i> : DU-145, LNCaP, 22Rv1, PC3, C4-2 <i>In vivo</i> : 22Rv1 xenograft Male Nu/Nu nude mice	14-40 nM (Crystal violet, 48h)	<ul style="list-style-type: none"> Inhibited cancer cell growth Induced Caspase dependent apoptosis Induced cell cycle arrest at G2/M phase in 22Rv1 and at G0/G1 in LNCaP and C4-2 cells Suppressed growth of 22Rv1 xenograft tumor 	↑ P53, ↑ p21 ^{Cip1} ↑cPARP Xenograft tumor IHC: ↓Ki67 ↑TUNEL, ↑P53, ↑21	(229)
	Syn	<i>In vitro</i> : PC3 DU145	>10 µM <10 µM	<ul style="list-style-type: none"> Inhibited cancer cells proliferation 		(349)

Structure	Source	Experimental Model	IC ₅₀	Effect	Molecular Target	Ref
	Syn	<i>In vitro</i> : DU145 HUVEC	(48h) 0.237 μM 24.7 (SRB, 48h)	<ul style="list-style-type: none"> • Selectivity Inhibited cancer cells (SI against HUVEC >100) 		(350)
	Syn	<i>In vitro</i> : DU145	5.0 μM (Cell Titer-Blue, 72h)	<ul style="list-style-type: none"> • Inhibited cancer cells proliferation • Induced apoptosis 	X Hsp90	(351)
	Syn	<i>In vitro</i> : DU145	4.95 μM (MTT, NR)	<ul style="list-style-type: none"> • Inhibited cancer cells proliferation 		(352)

APPENDIX B. SPECTROSCOPIC ANALYSIS

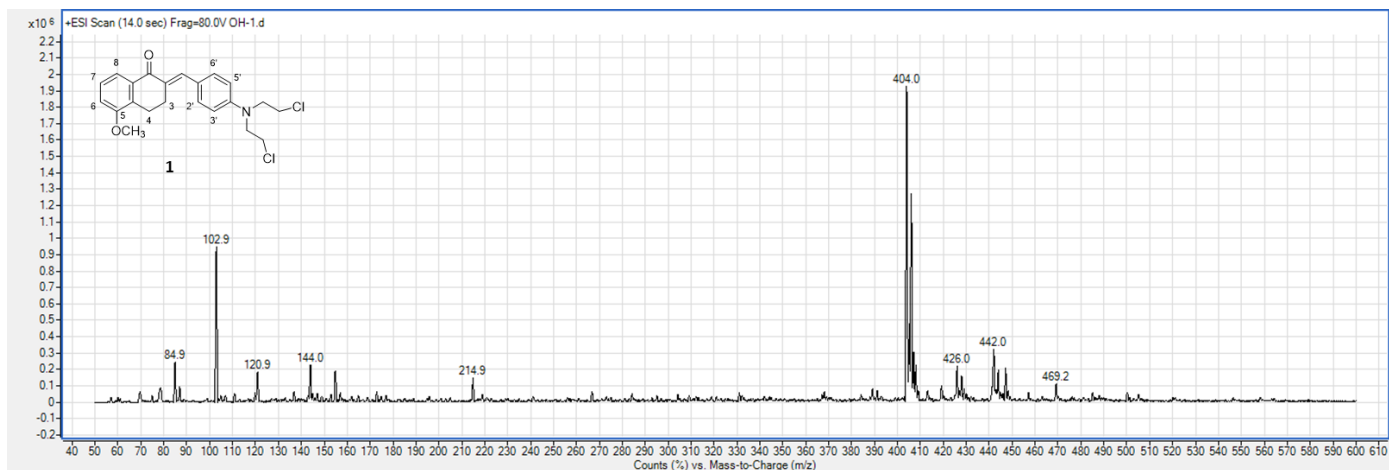


Figure 43. (+)-ESI mass spectrum of compound 1.

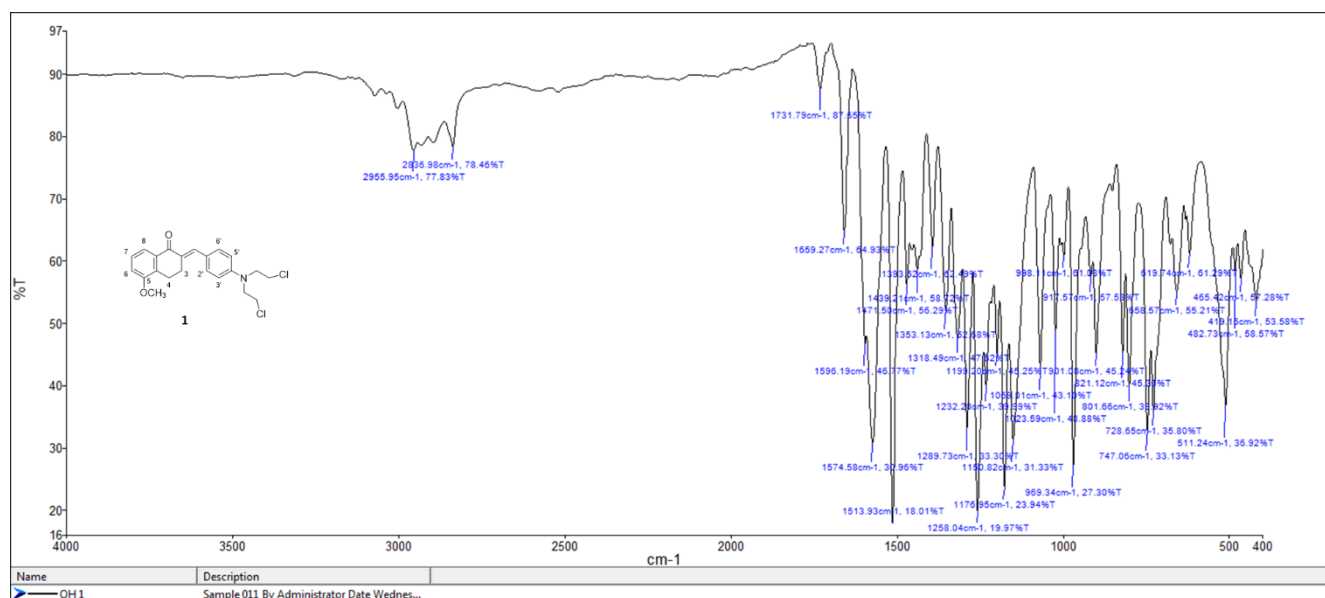


Figure 44. FT-IR spectrum of compound 1.

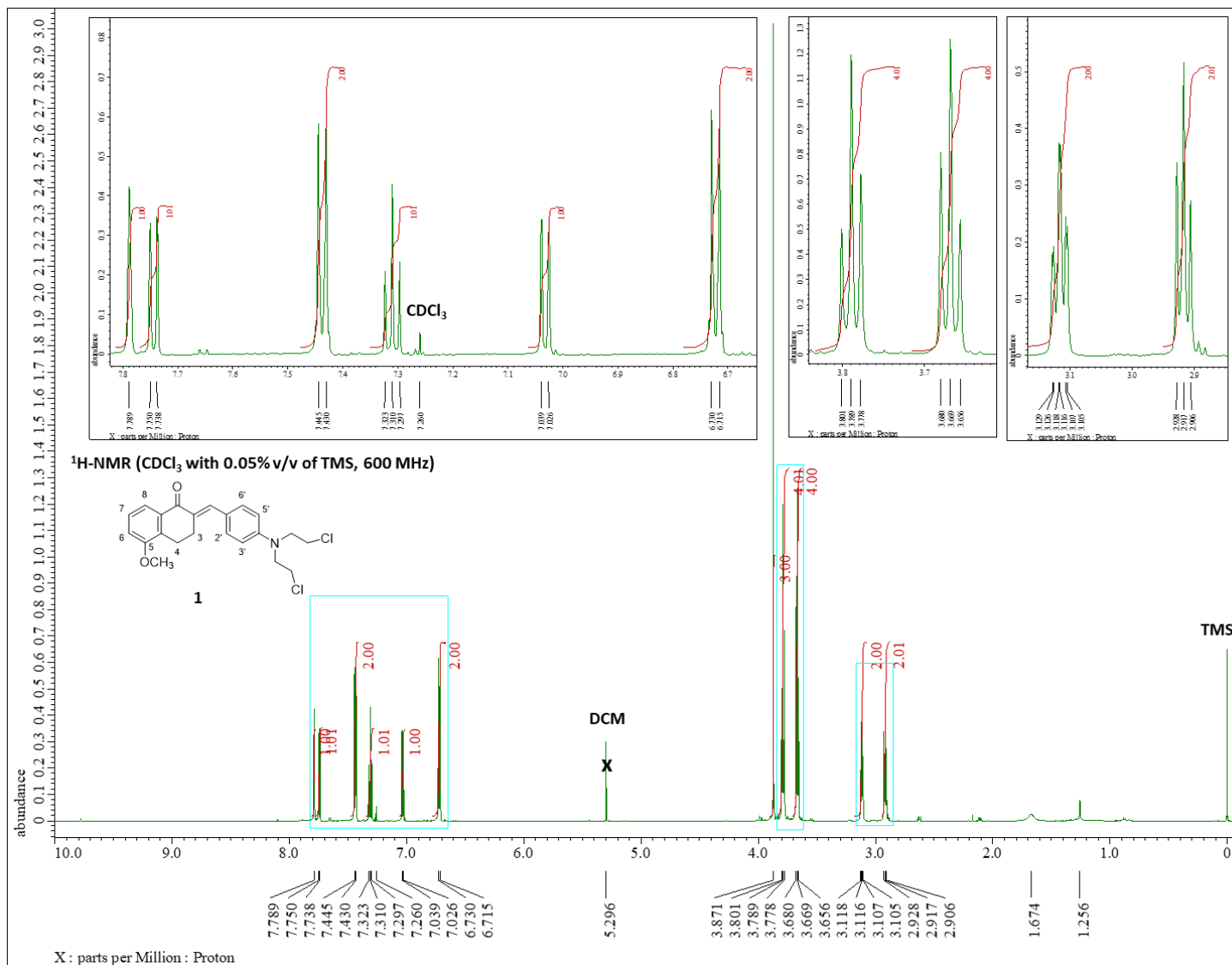


Figure 45. ¹H-NMR spectrum (CDCl₃ with 0.05% v/v of TMS, 600 MHz) of compound **1**.

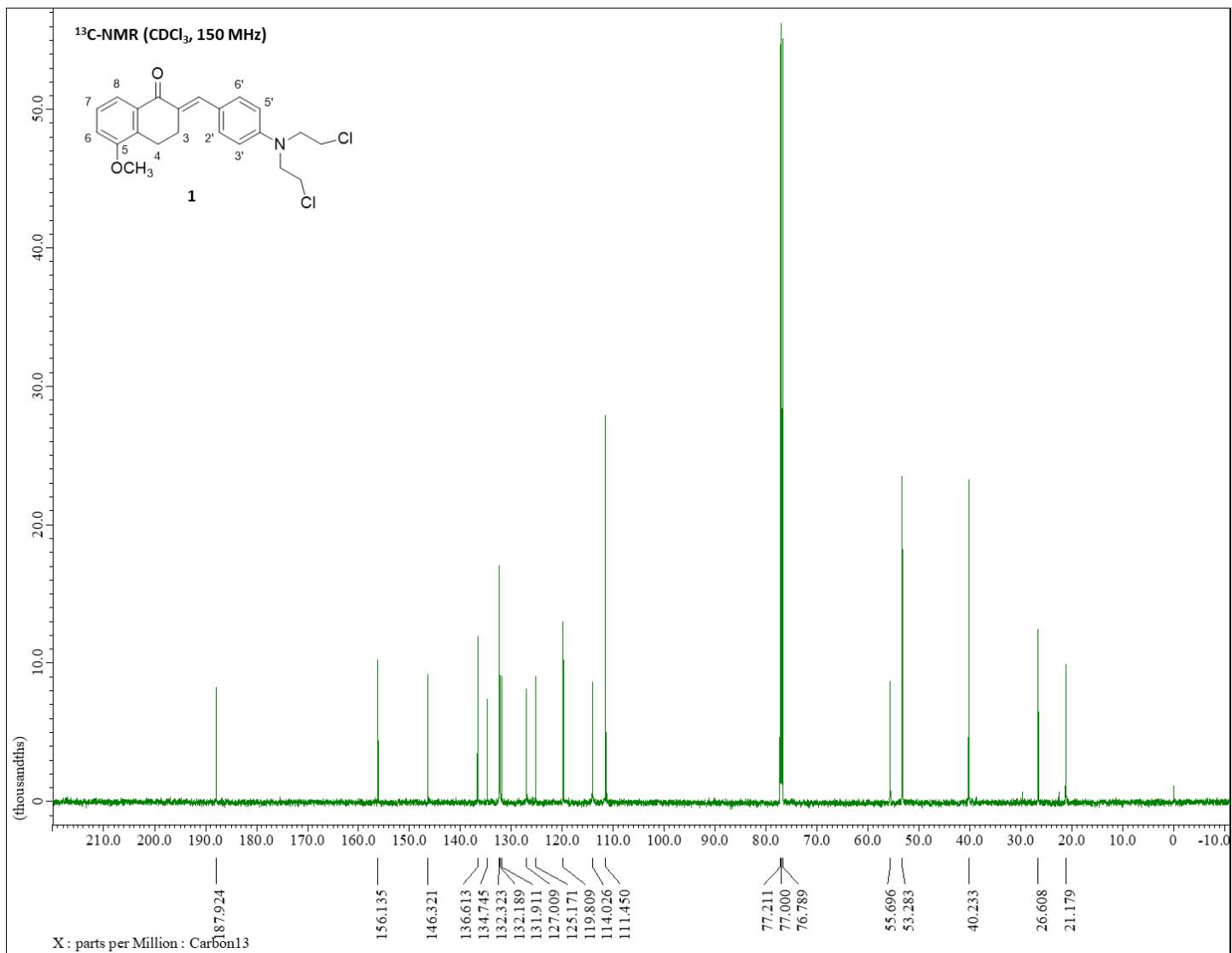


Figure 46. ¹³C-NMR spectrum (CDCl₃, 150 MHz) of compound **1**.

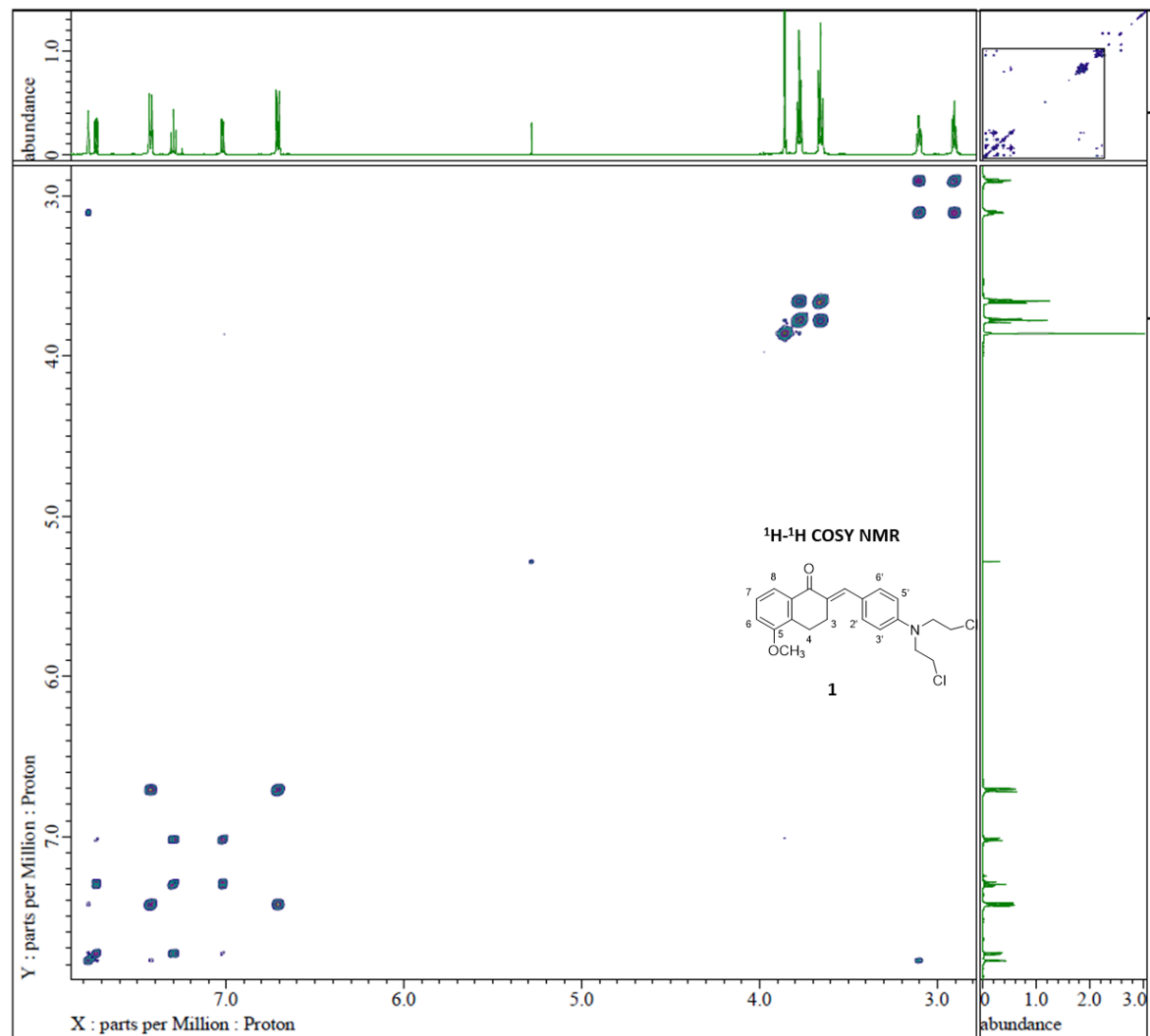


Figure 47. ^1H - ^1H COSY NMR of compound **1**.

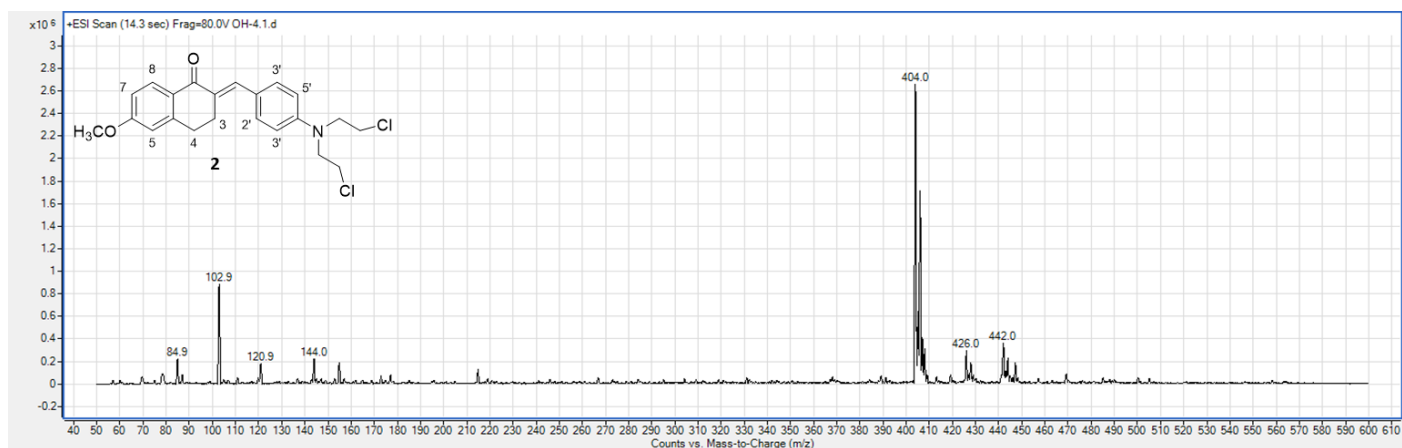


Figure 48. (+)-ESI Mass spectrum of compound **2**.

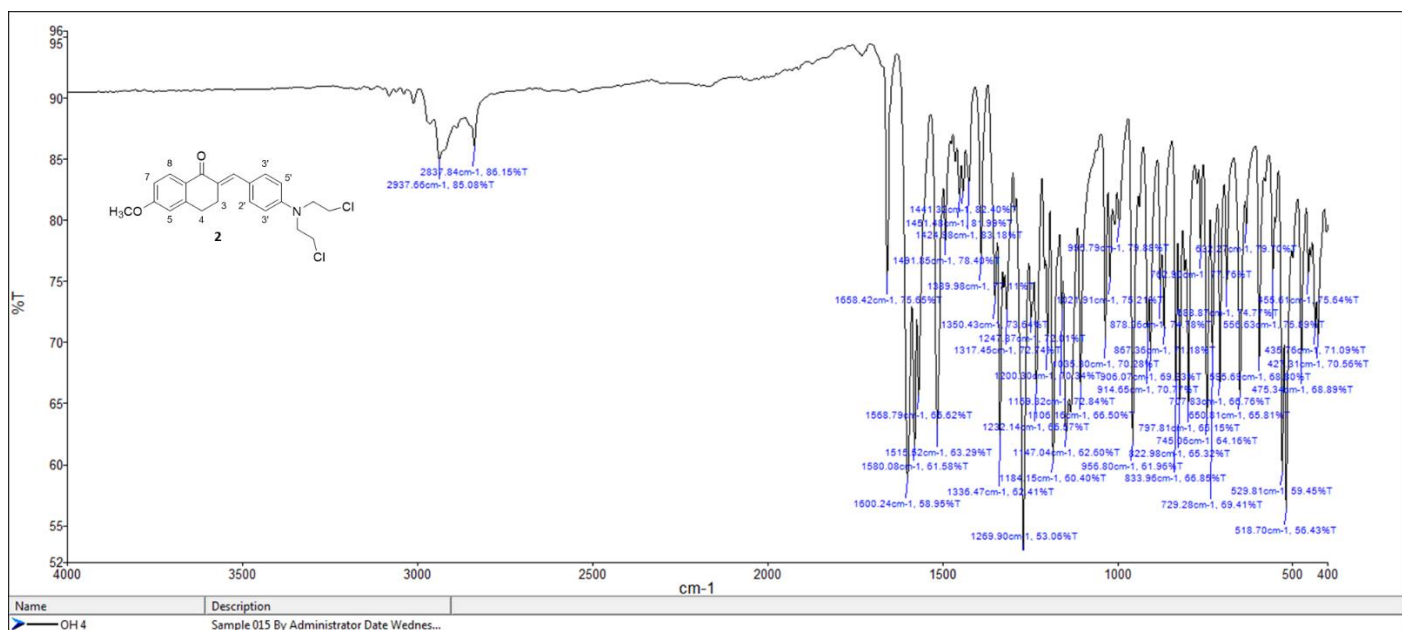


Figure 49. FT-IR spectrum of compound **2**.

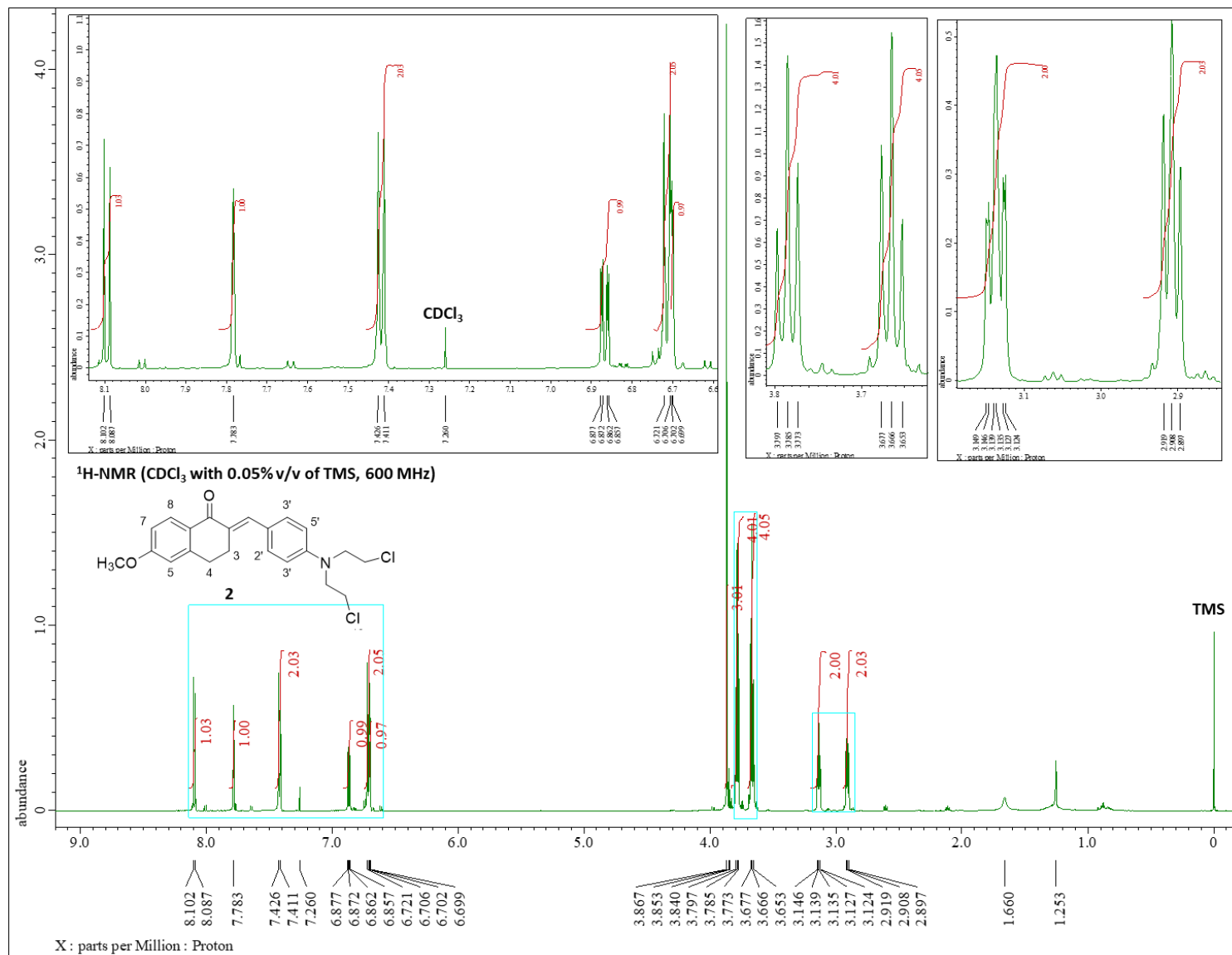


Figure 50. ¹H-NMR spectrum (CDCl₃ with 0.05% v/v of TMS, 600 MHz) of compound **2**.

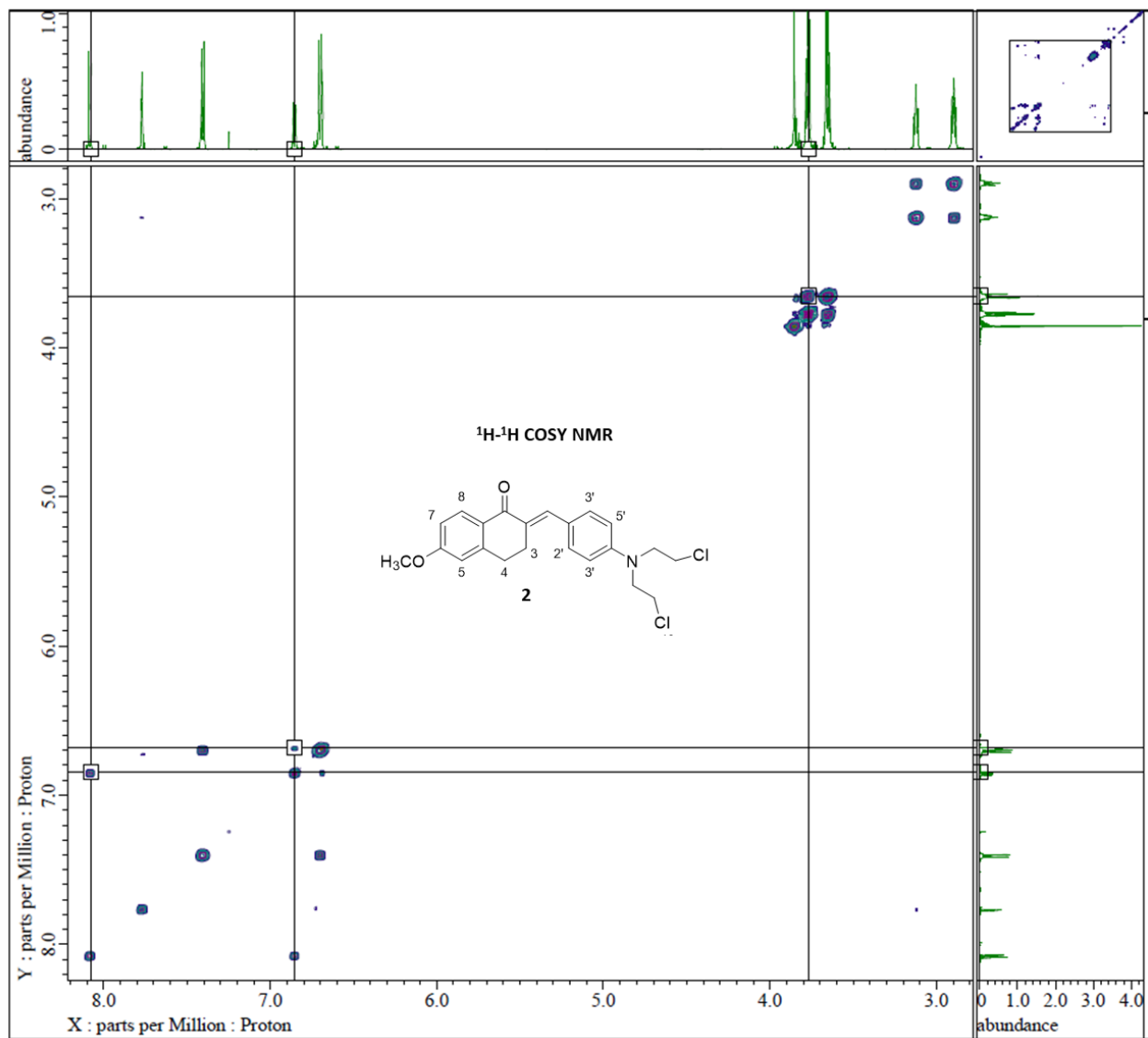


Figure 51. ^1H - ^1H COSY NMR of compound **2**.

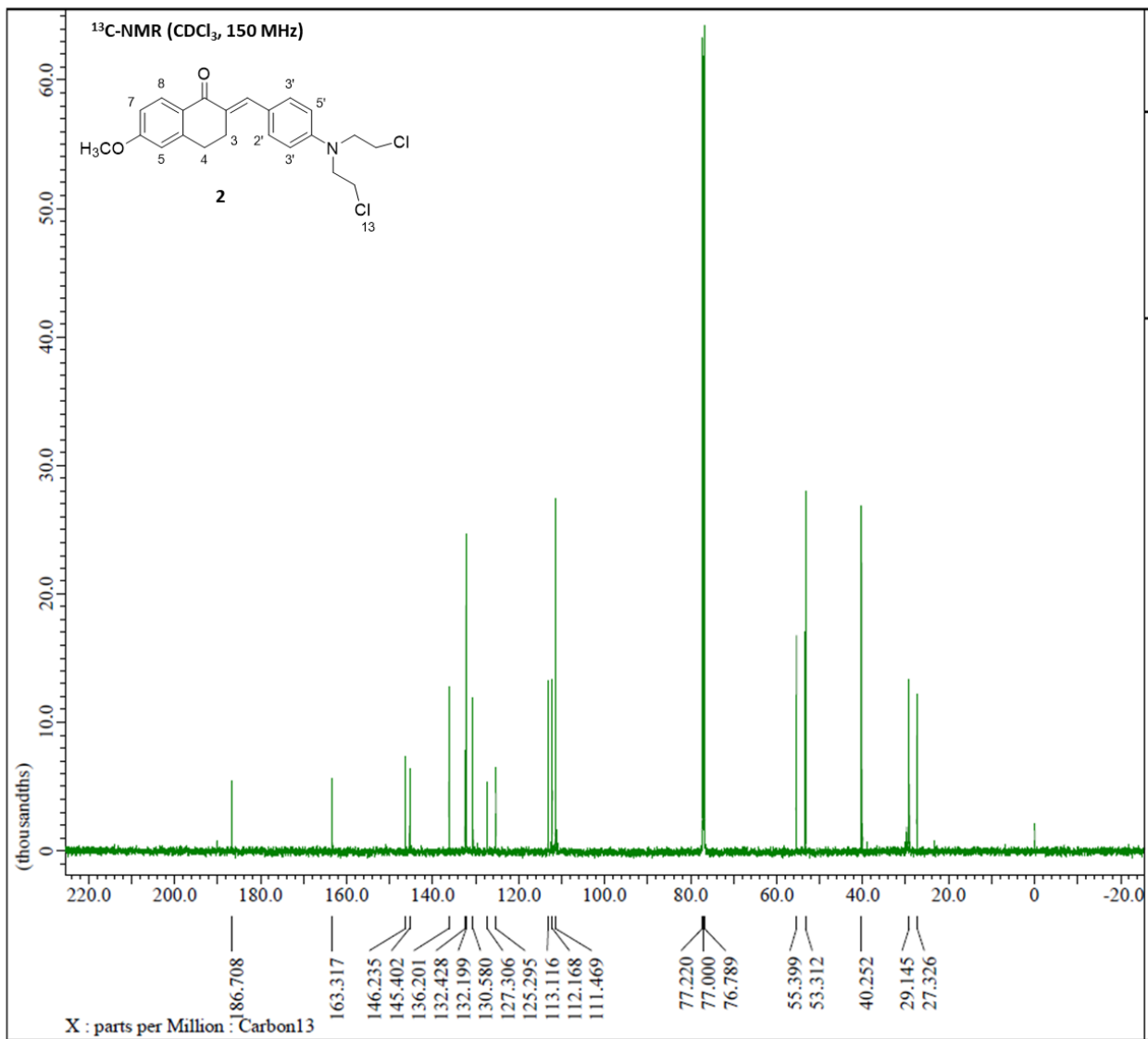


Figure 52. ¹³C-NMR spectrum (CDCl₃, 150 MHz) of compound **2**.

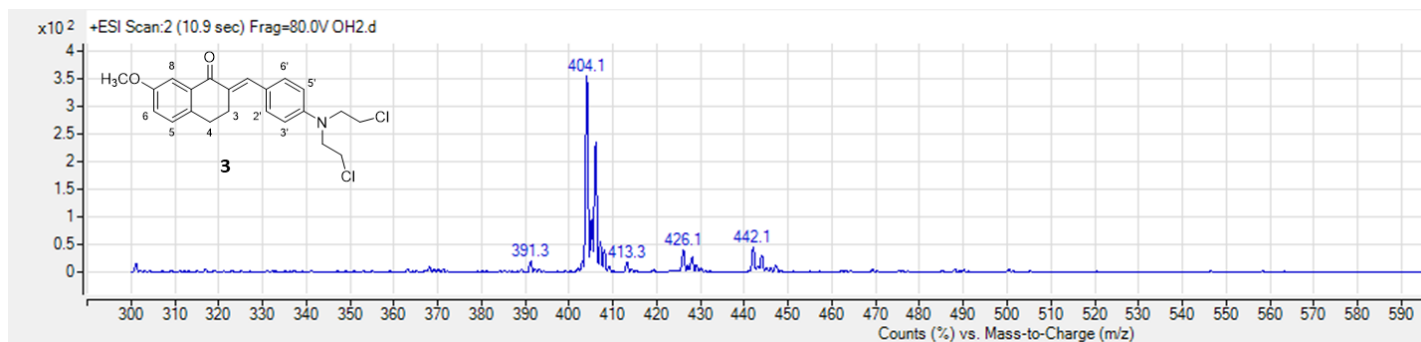


Figure 53. (+)-ESI Mass spectrum of compound **3**.

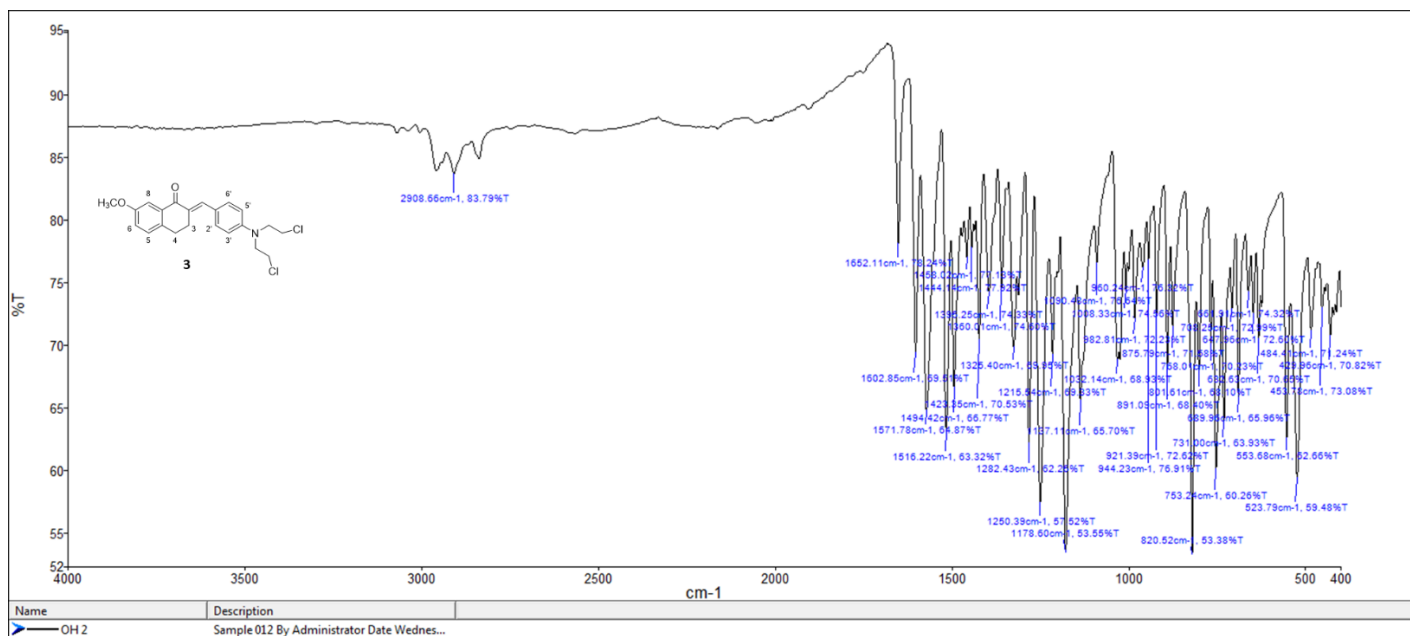


Figure 54. FT-IR spectrum of compound **3**.

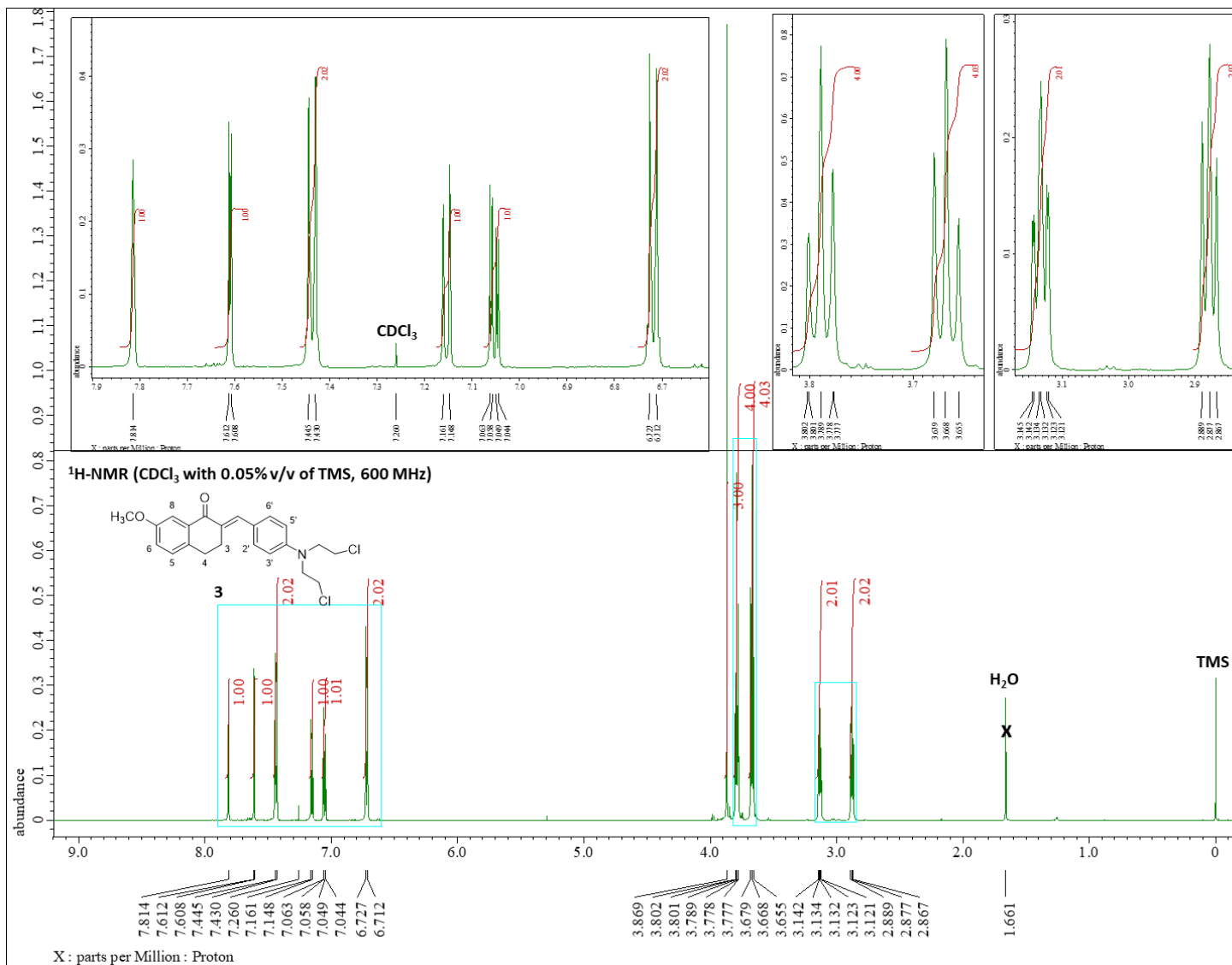


Figure 55. ¹H-NMR spectrum (CDCl₃ with 0.05% v/v of TMS, 600 MHz) of compound **3**.

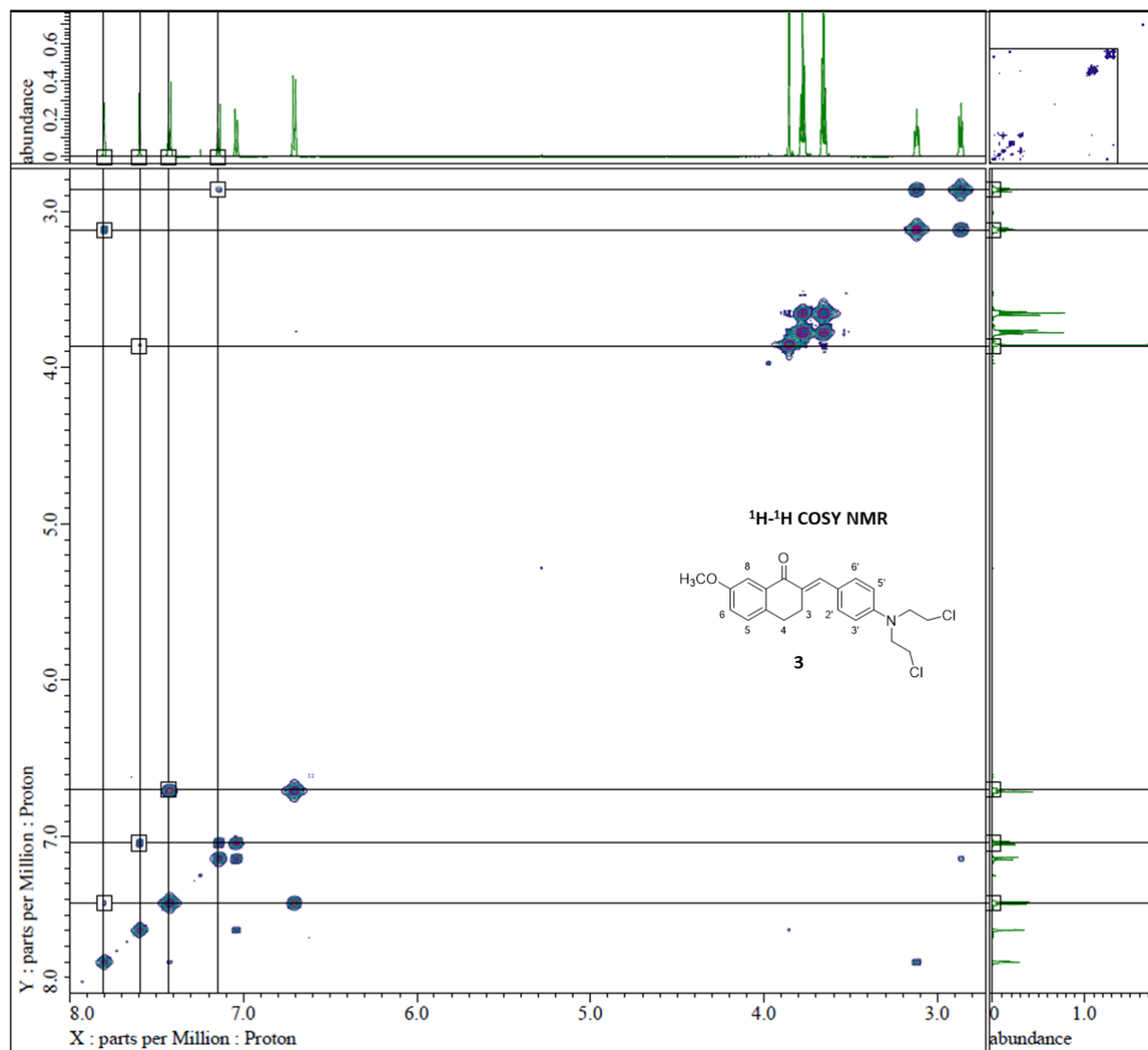


Figure 56. ^1H - ^1H COSY NMR of compound **3**.

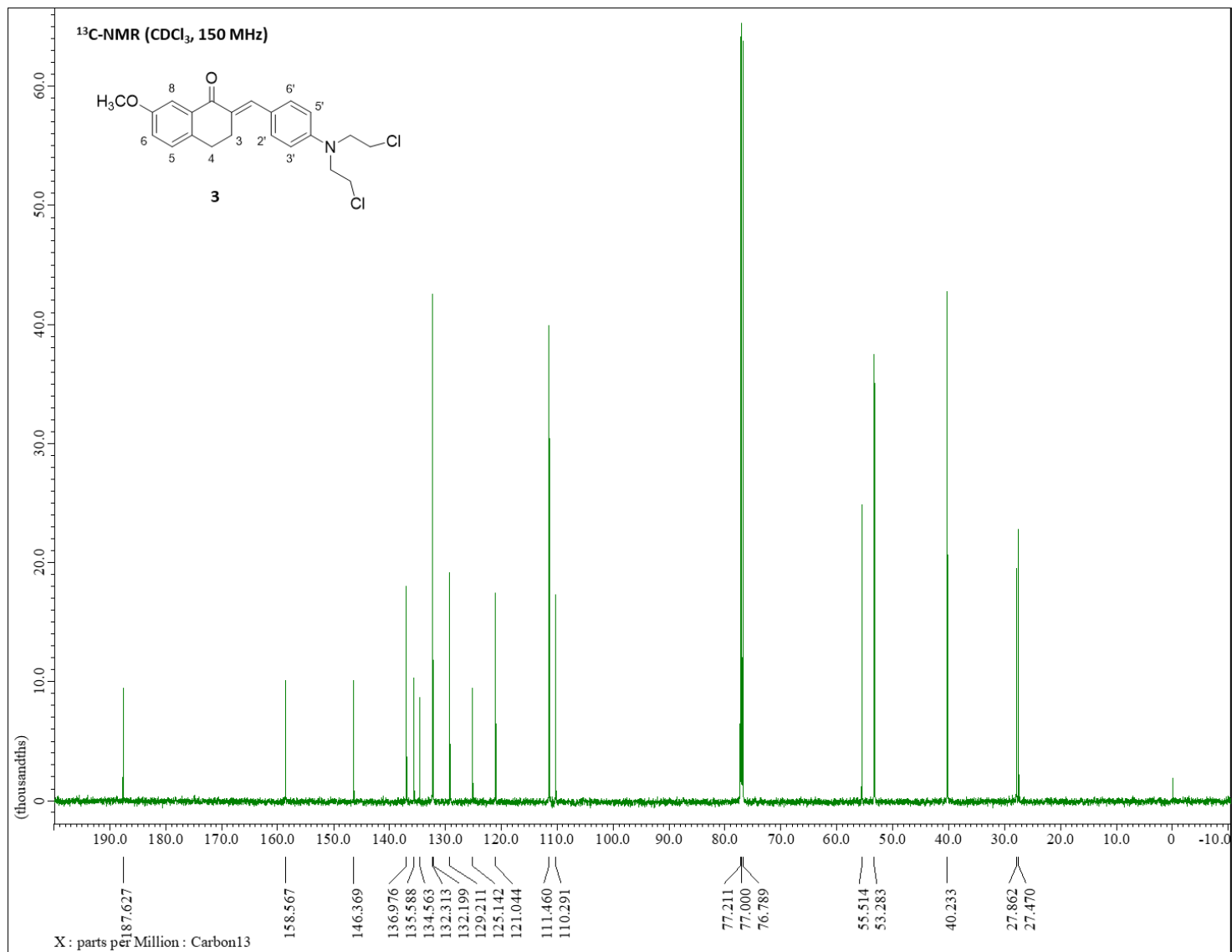


Figure 57. ¹³C-NMR spectrum (CDCl₃, 150 MHz) of compound **3**.

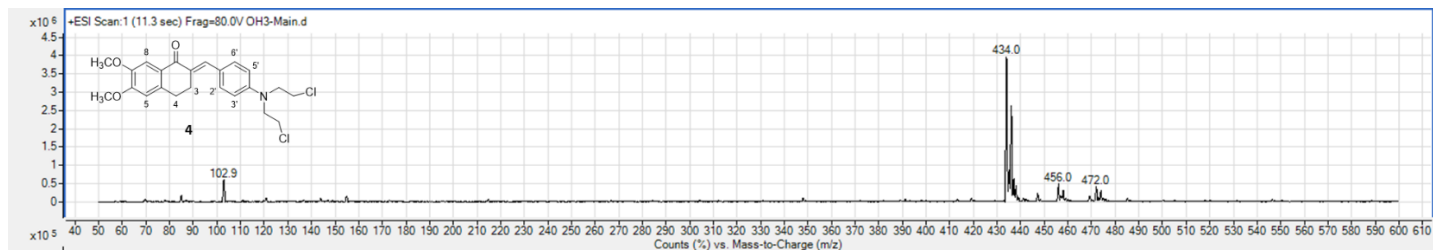


Figure 58. (+)-ESI Mass spectrum of compound **4**.

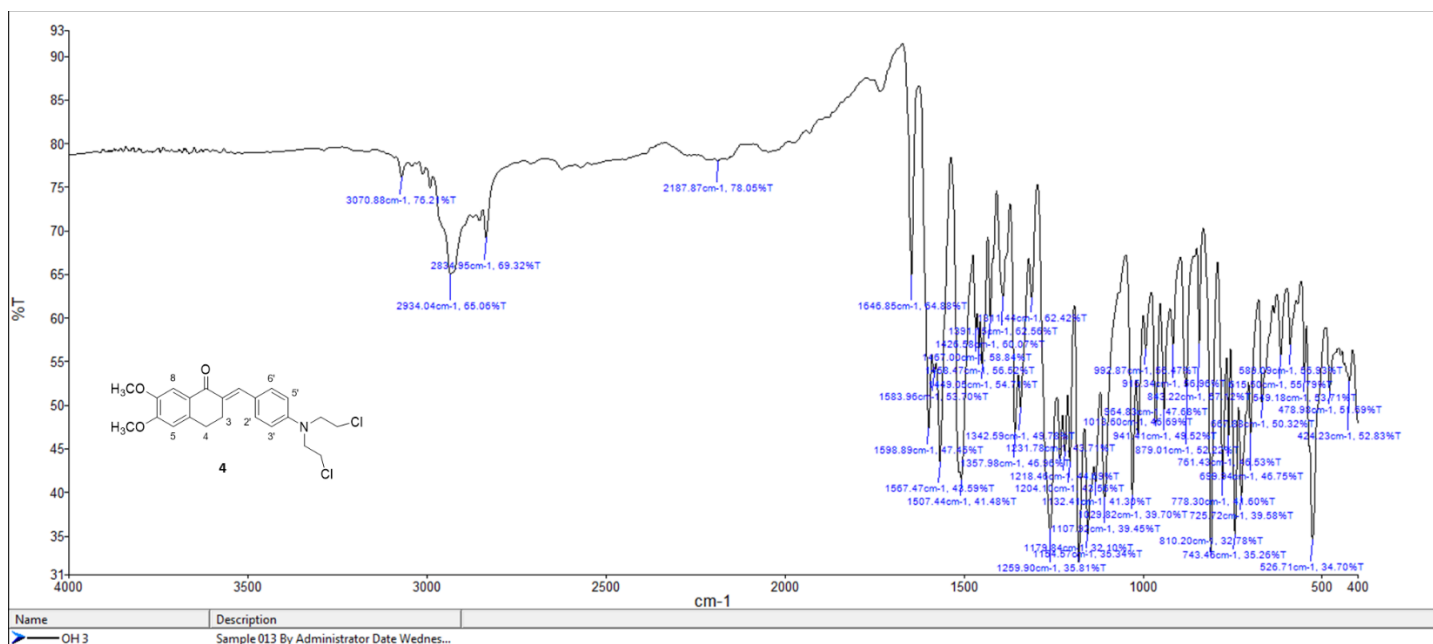


Figure 59. FT-IR spectrum of compound **4**.

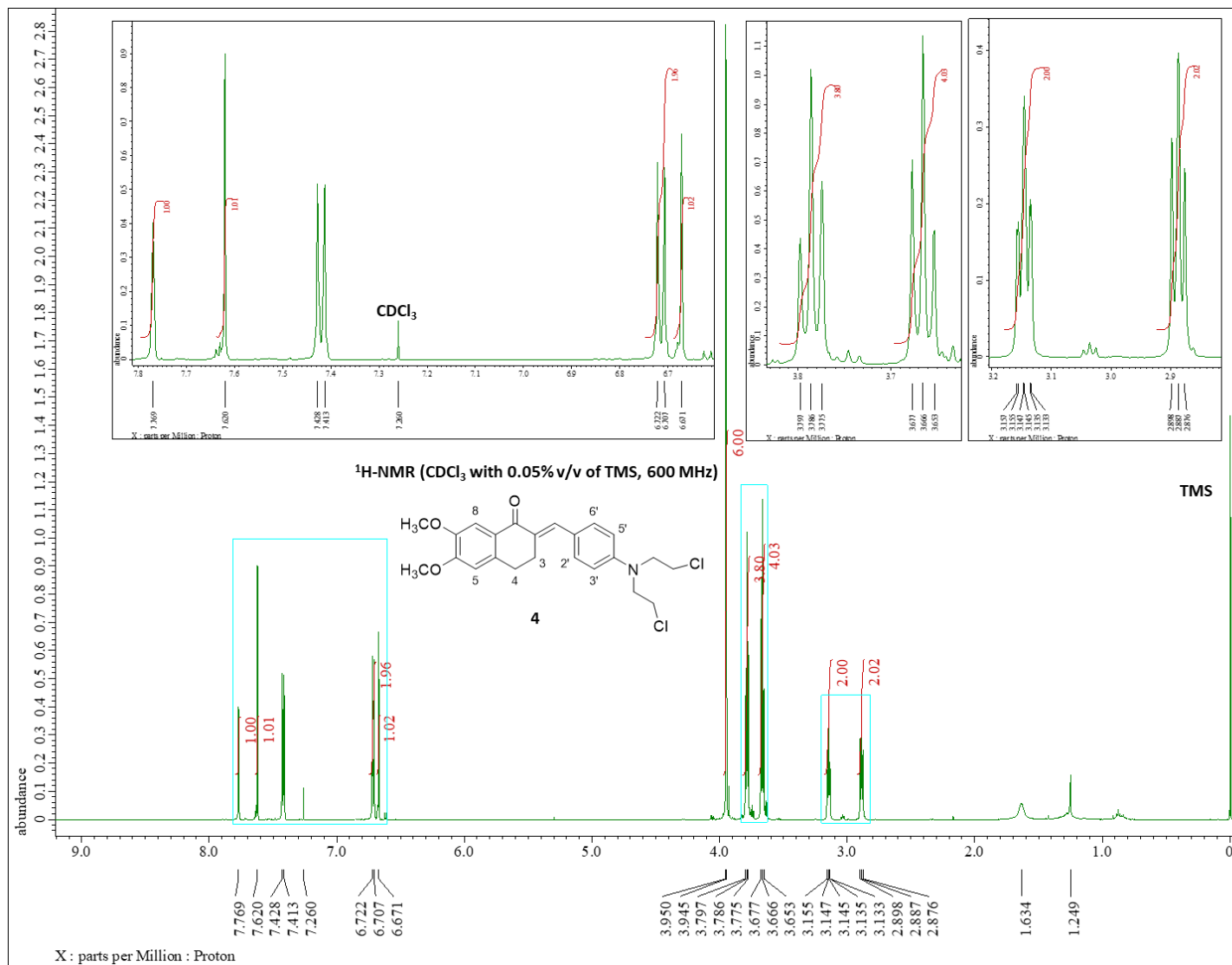


Figure 60. ¹H-NMR spectrum (CDCl₃ with 0.05% v/v of TMS, 600 MHz) of compound **4**.

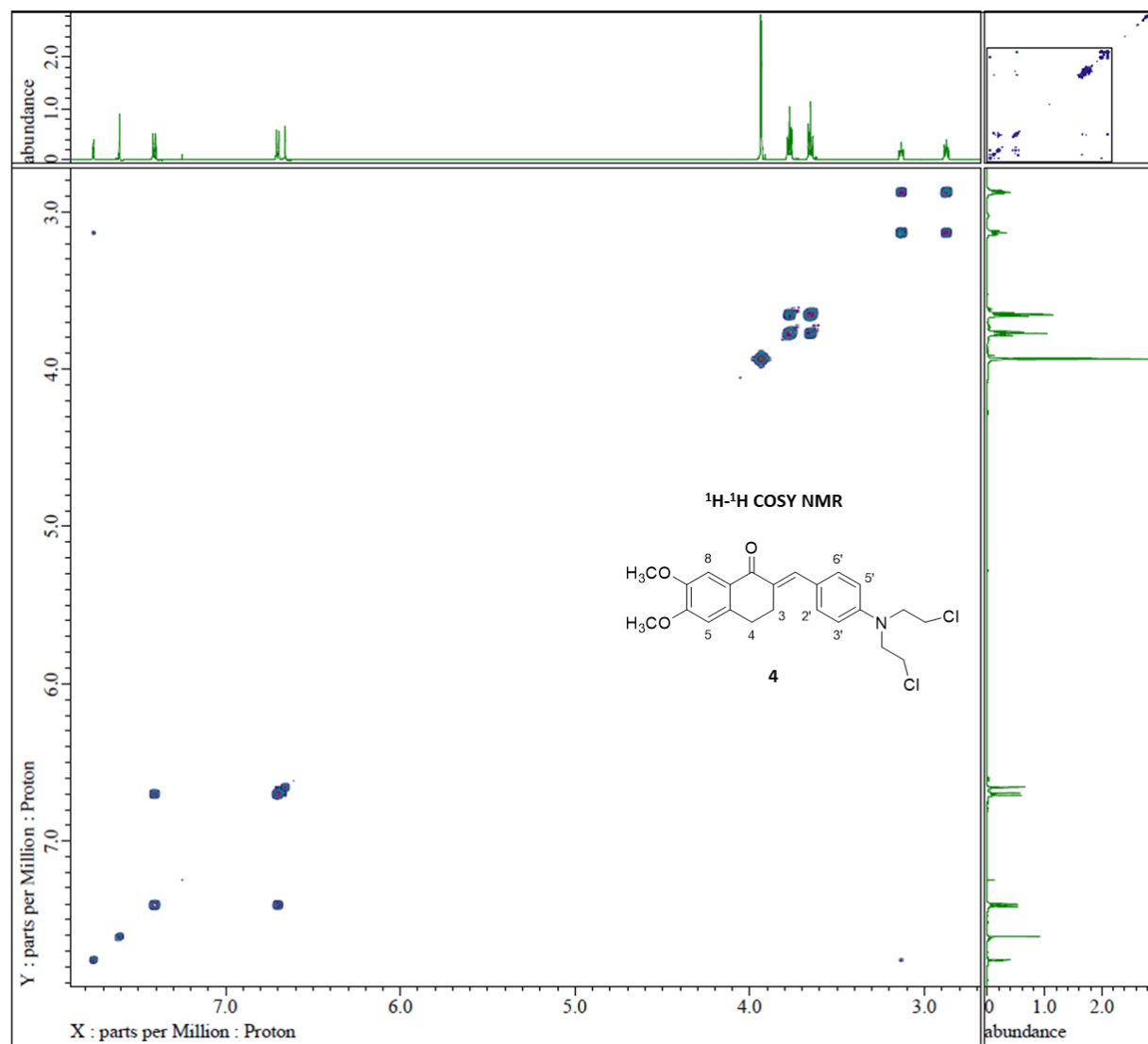


Figure 61. ^1H - ^1H COSY NMR of compound **4**.

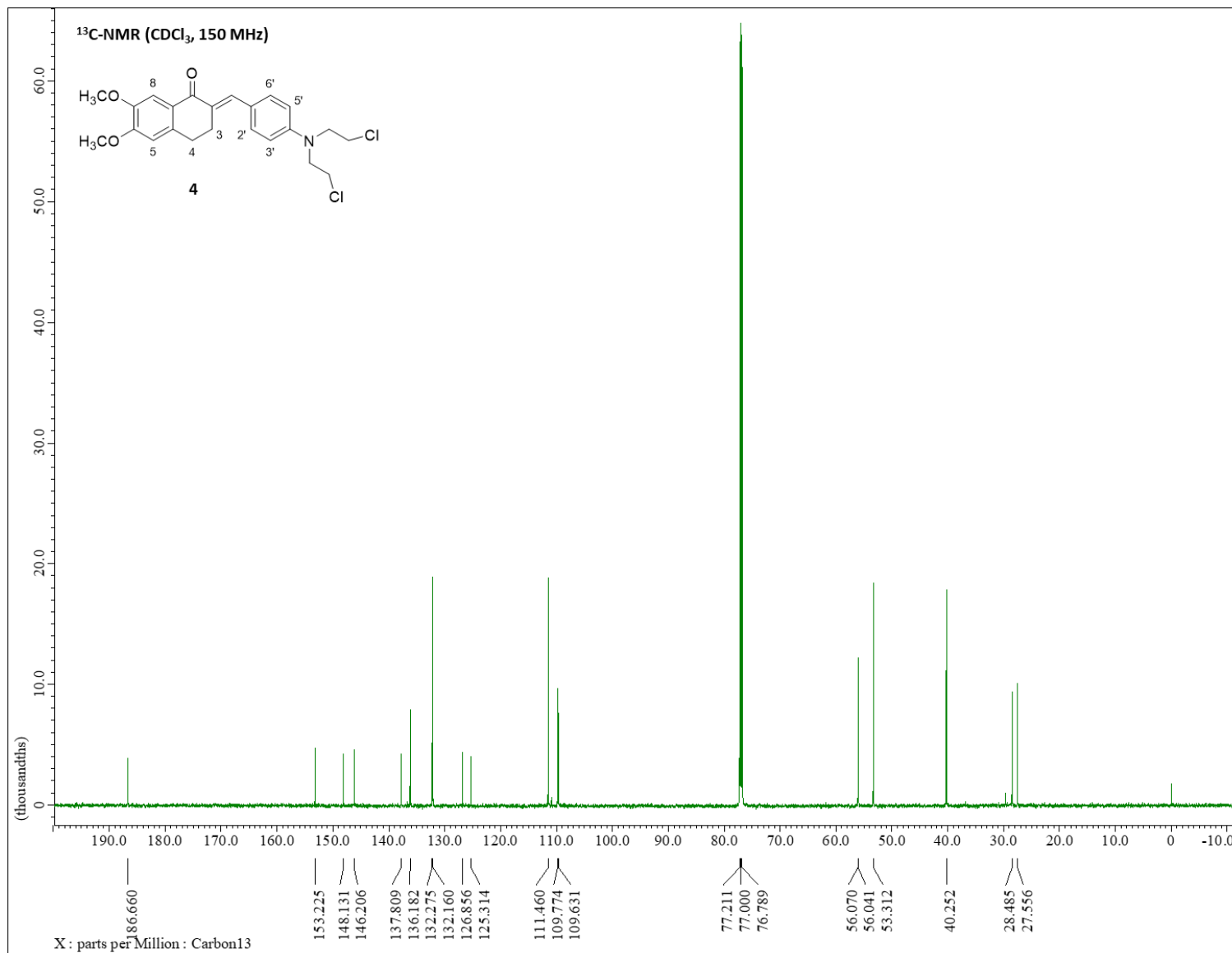


Figure 62. ¹³C-NMR spectrum (CDCl₃, 150 MHz) of compound **4**.

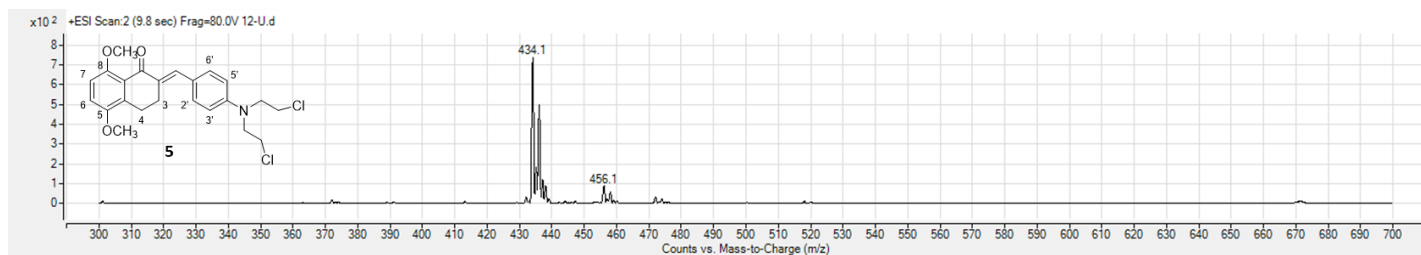


Figure 63. (+)-ESI Mass spectrum of compound **5**.

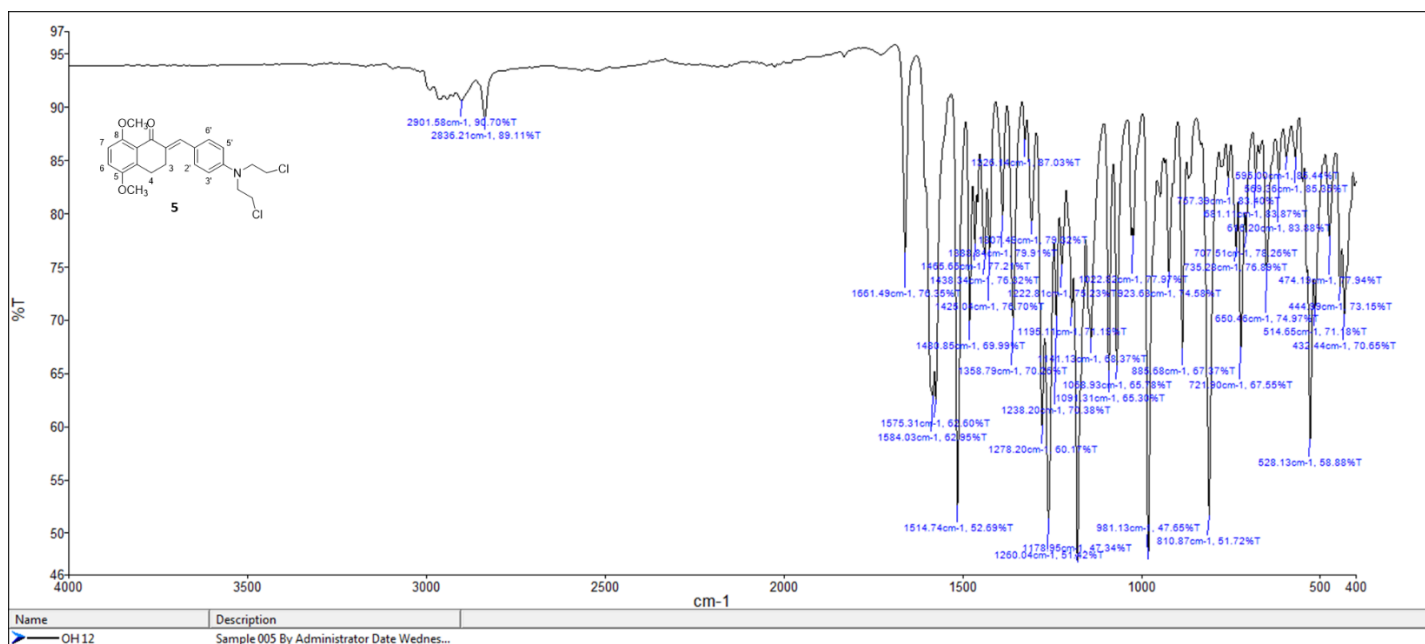


Figure 64. FT-IR spectrum of compound **5**.

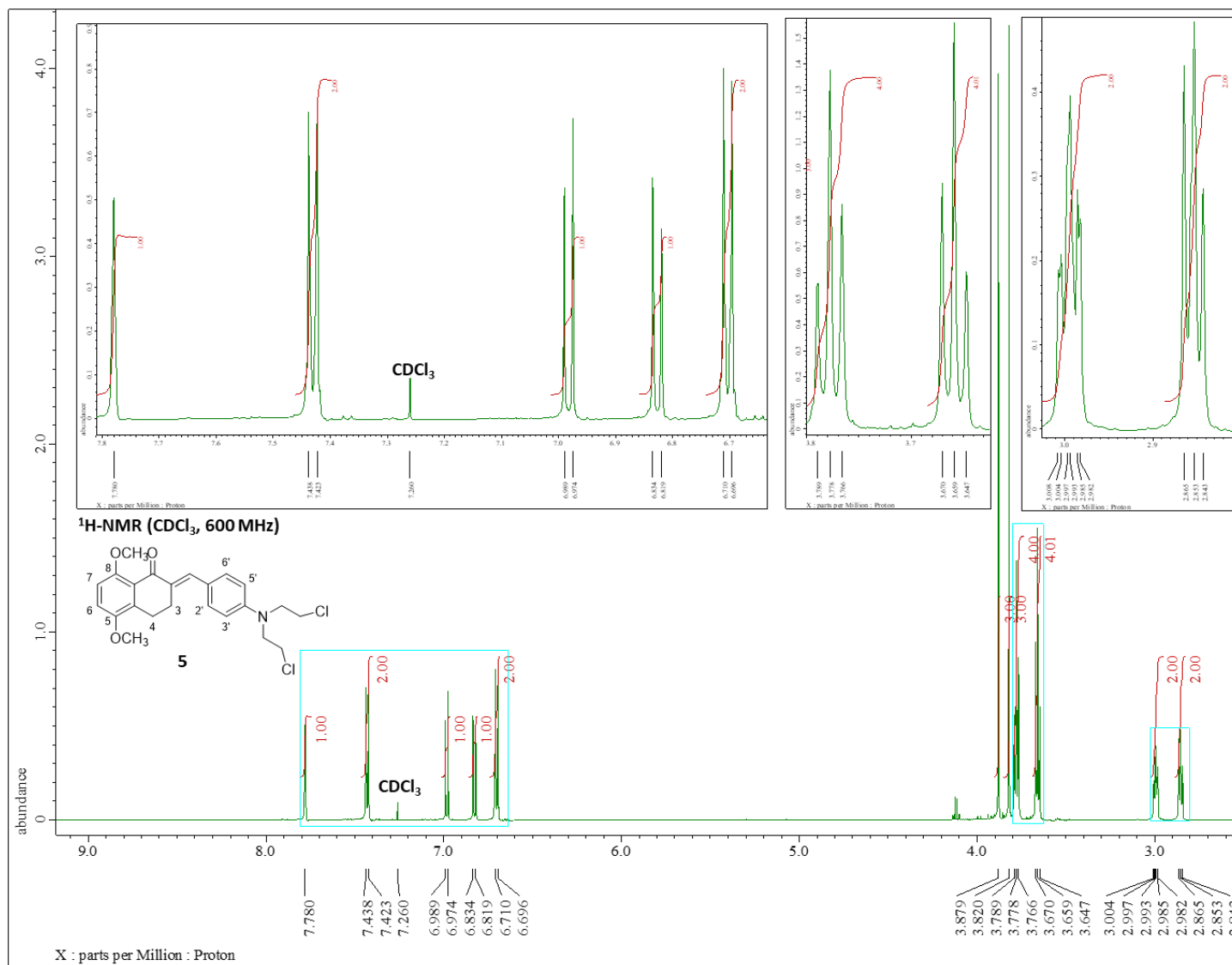


Figure 65. ¹H-NMR spectrum (CDCl₃ with 0.05% v/v of TMS, 600 MHz) of compound **5**.

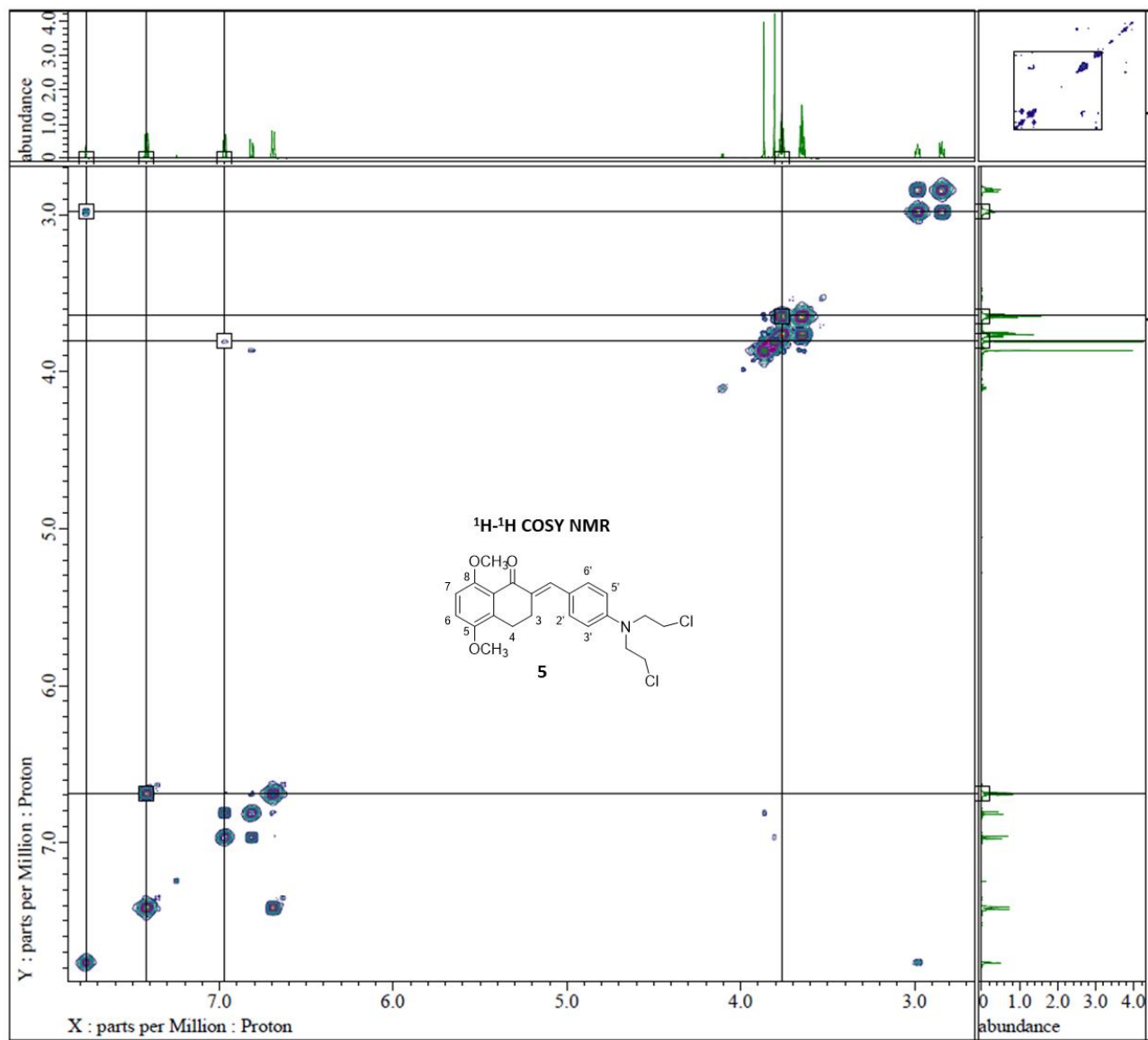


Figure 66. ^1H - ^1H COSY NMR of compound **5**.

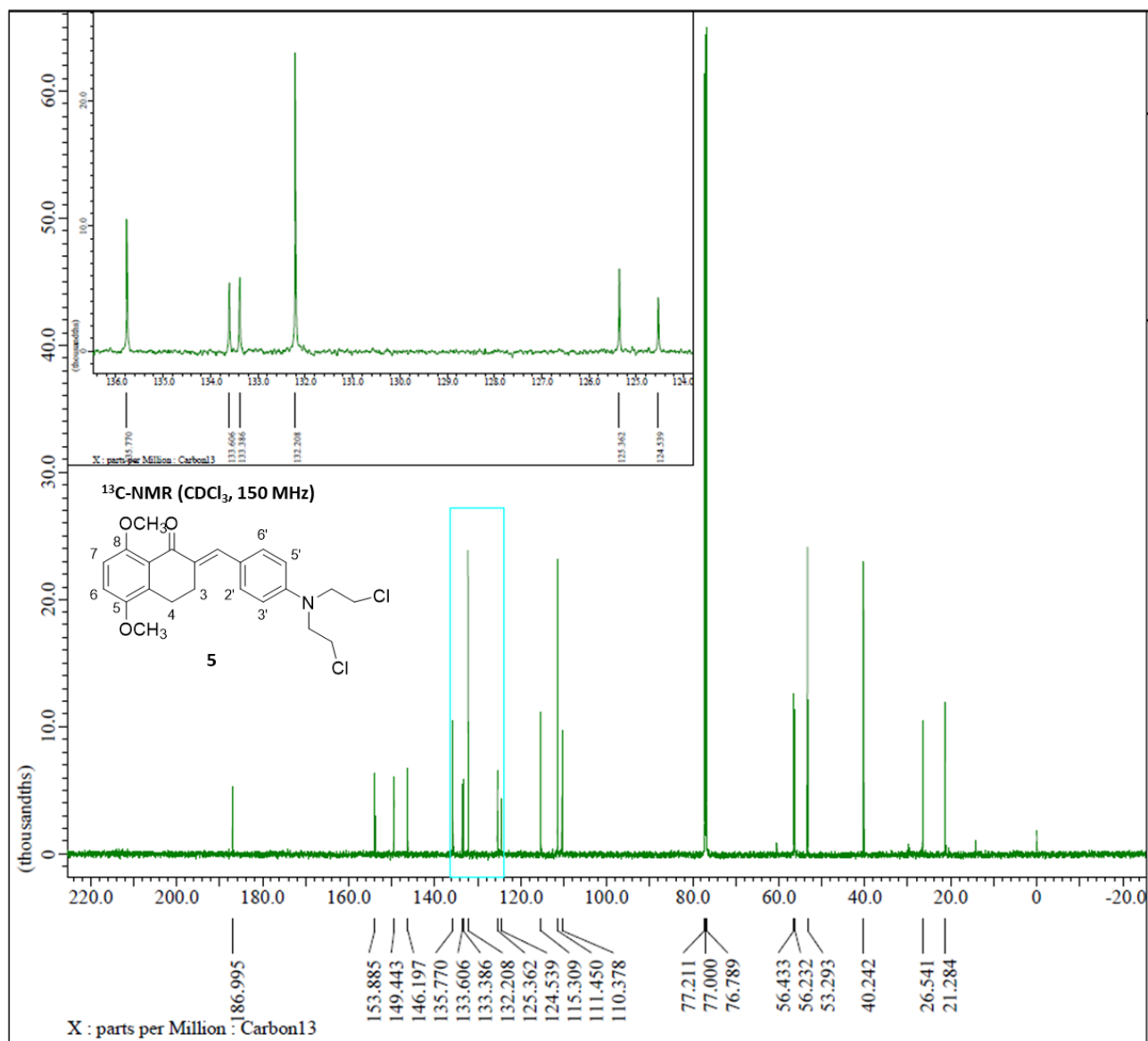


Figure 67. ¹³C-NMR spectrum (CDCl₃, 150 MHz) of compound **5**.

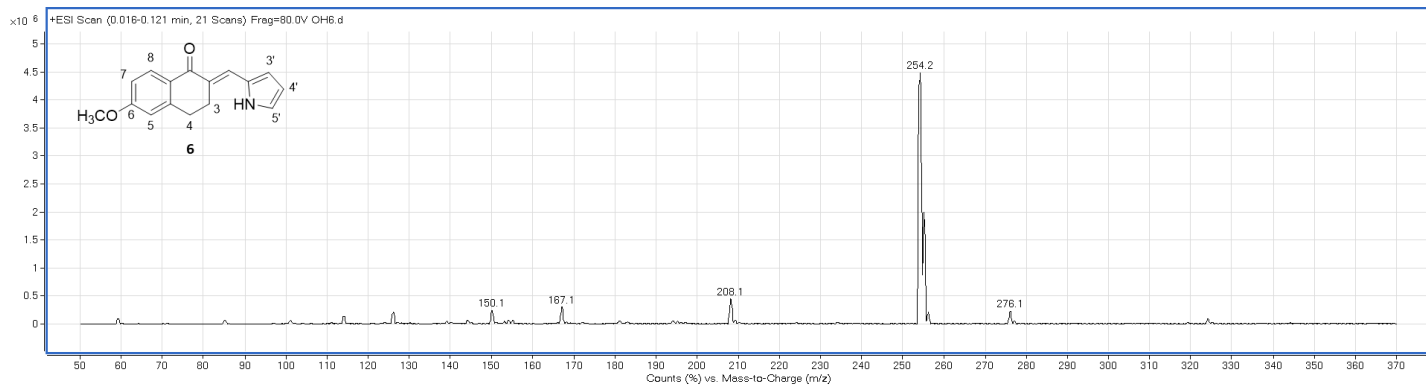


Figure 68. (+)-ESI Mass spectrum of compound **6**.

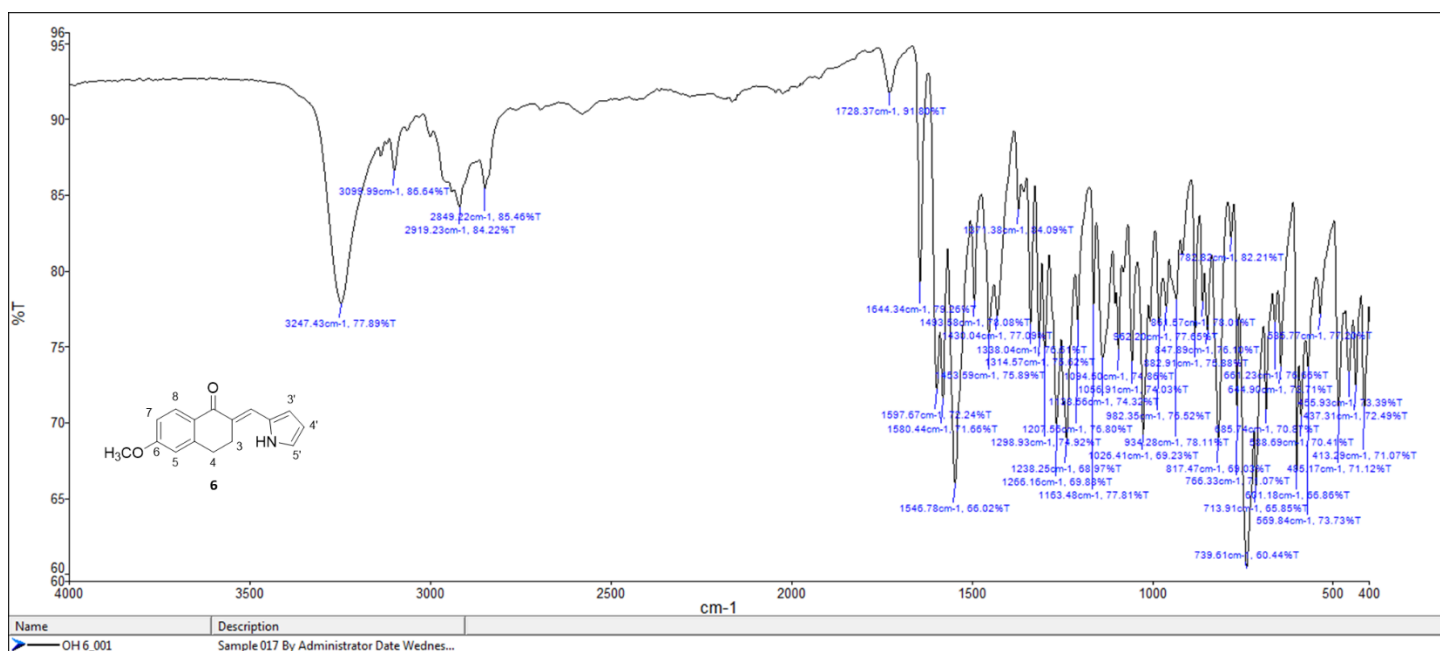


Figure 69. FT-IR spectrum of compound **6**.

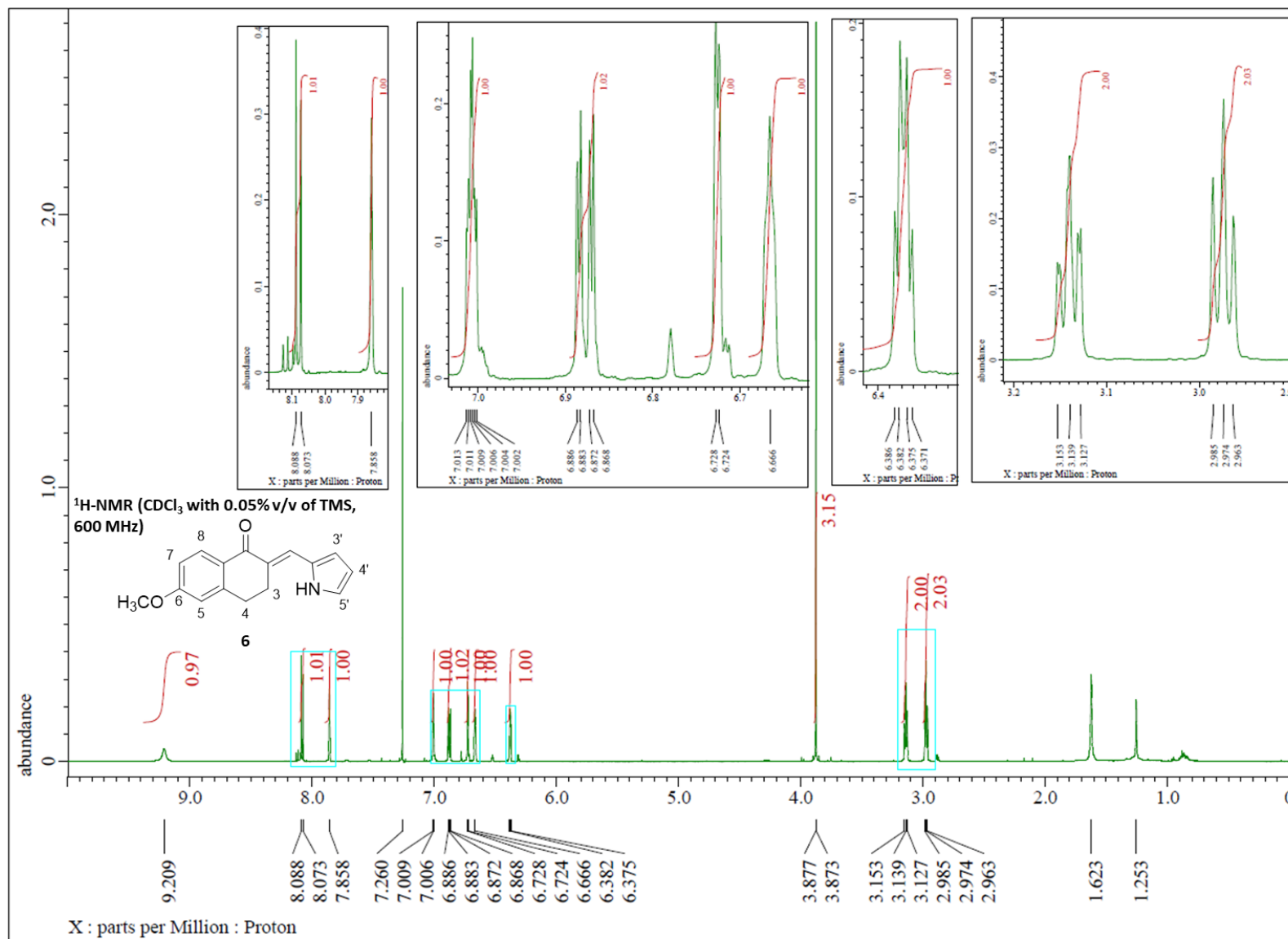


Figure 70. ¹H-NMR spectrum (CDCl₃ with 0.05% v/v of TMS, 600 MHz) of compound **6**.

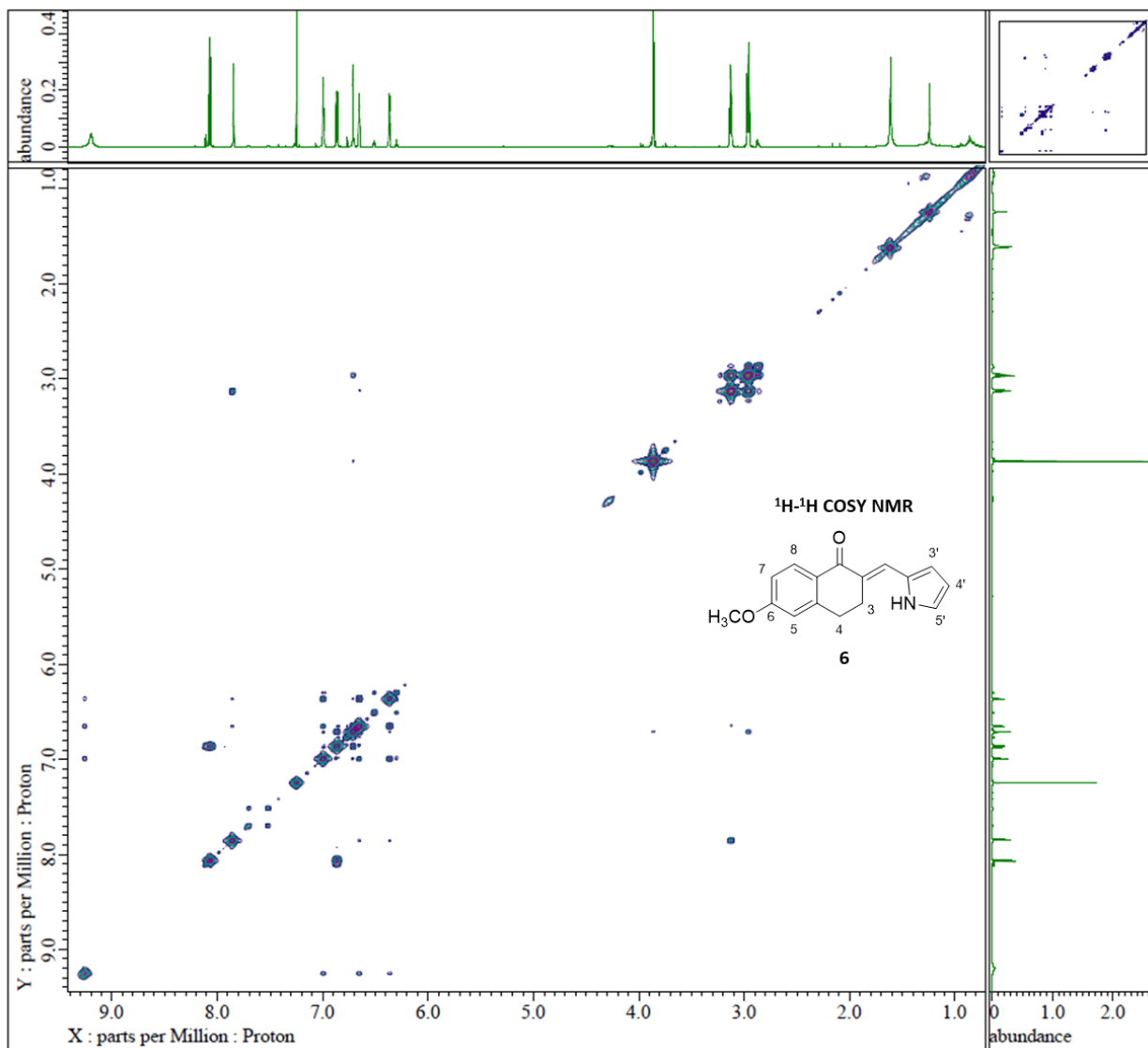


Figure 71. ¹H-¹H COSY NMR of compound **6**.

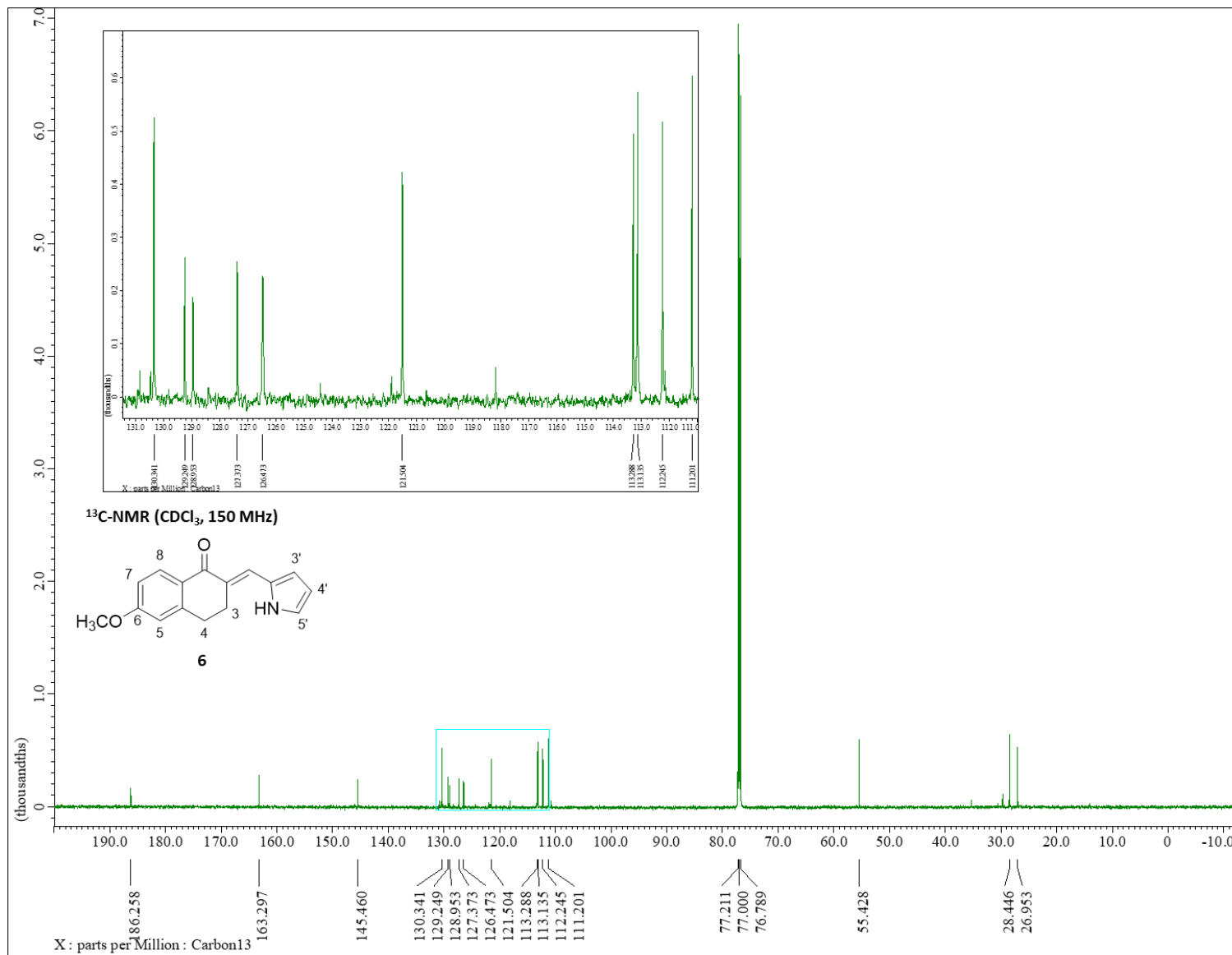


Figure 72. ¹³C-NMR spectrum (CDCl₃, 150 MHz) of compound **6**.

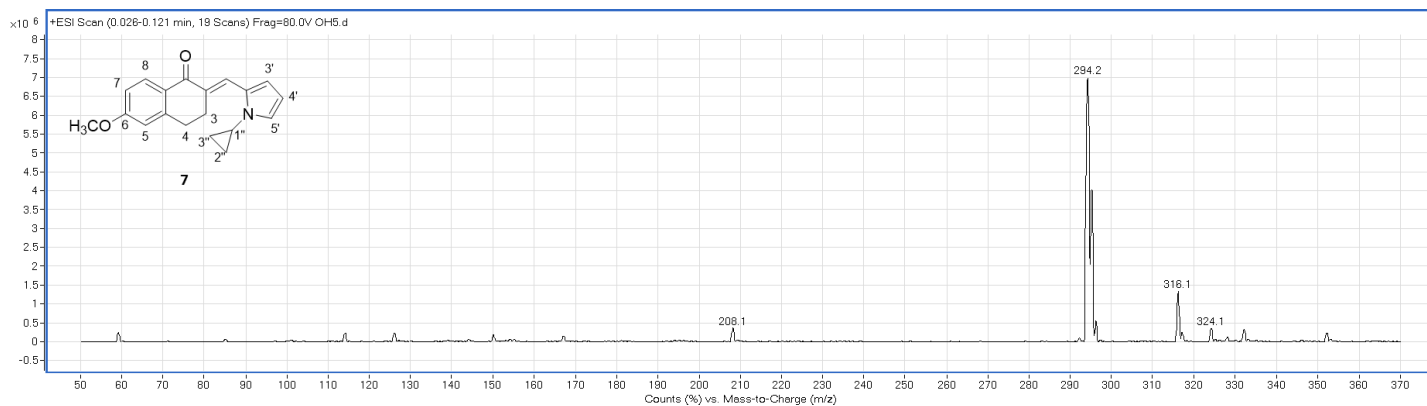


Figure 73. (+)-ESI Mass spectrum of compound 7.

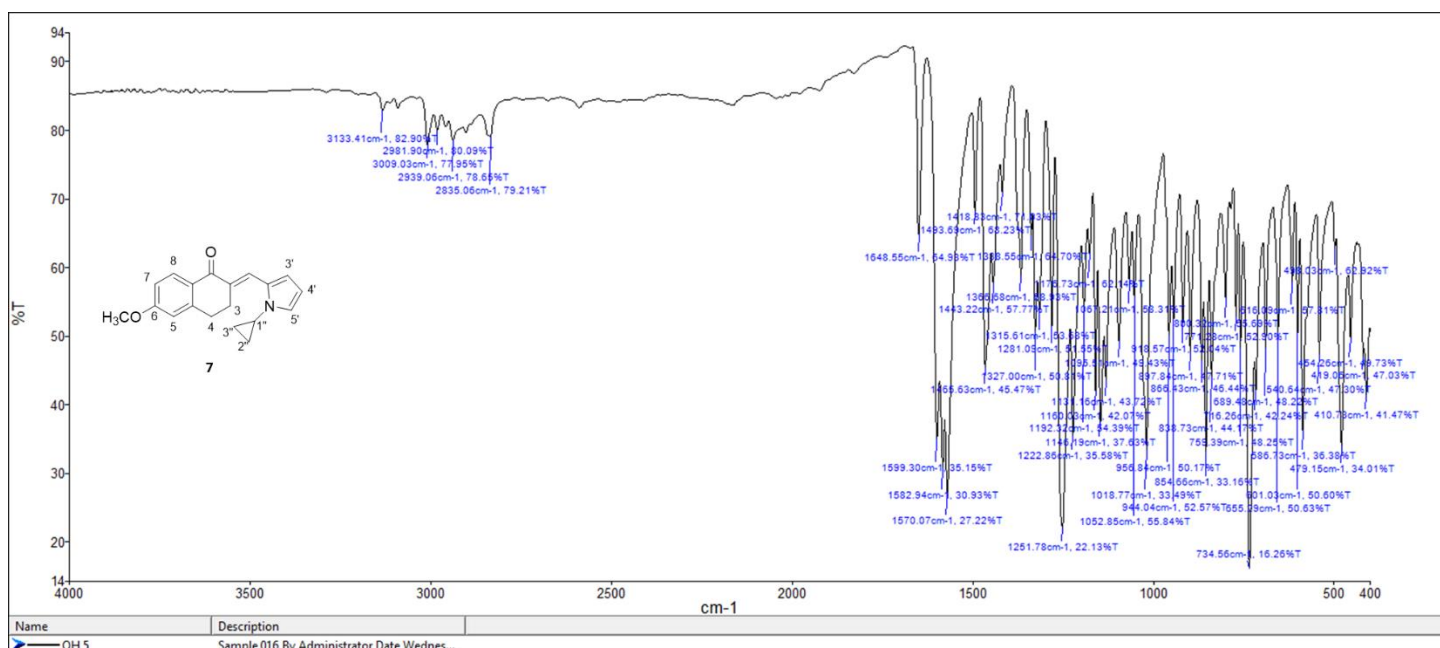


Figure 74. FT-IR spectrum of compound 7.

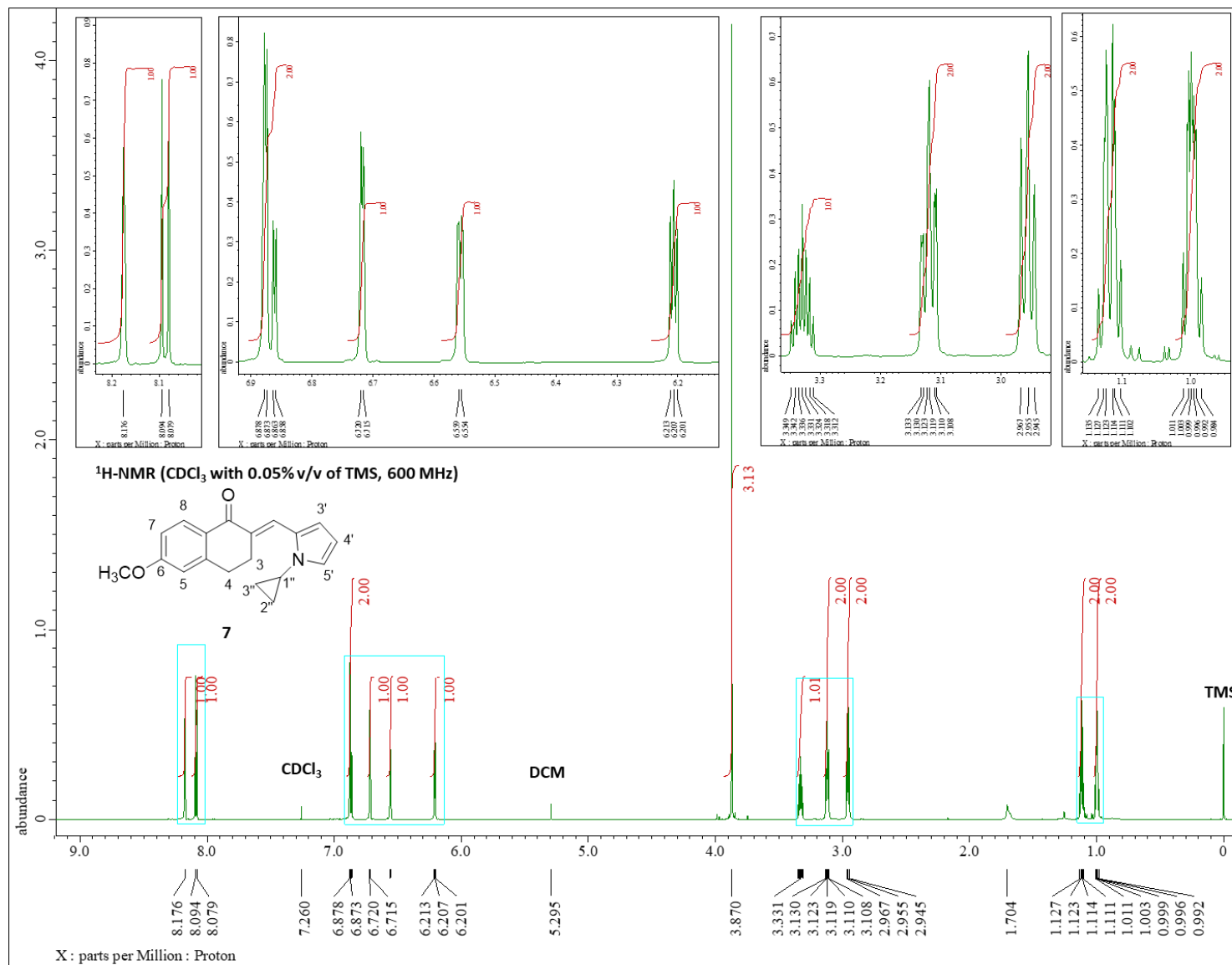


Figure 75. ¹H-NMR spectrum (CDCl₃ with 0.05% v/v of TMS, 600 MHz) of compound **7**.

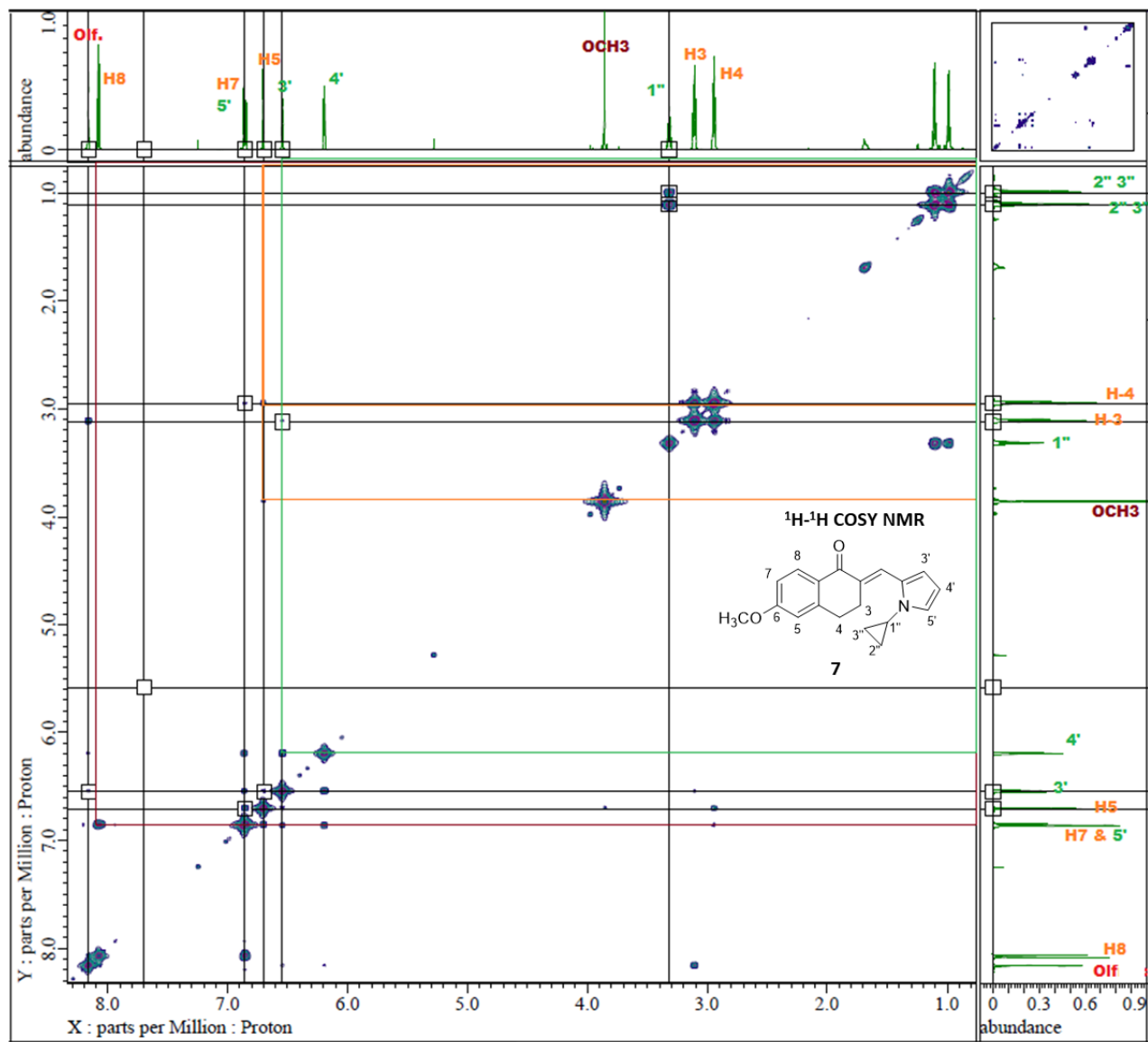


Figure 76. ^1H - ^1H COSY NMR of compound **7**.

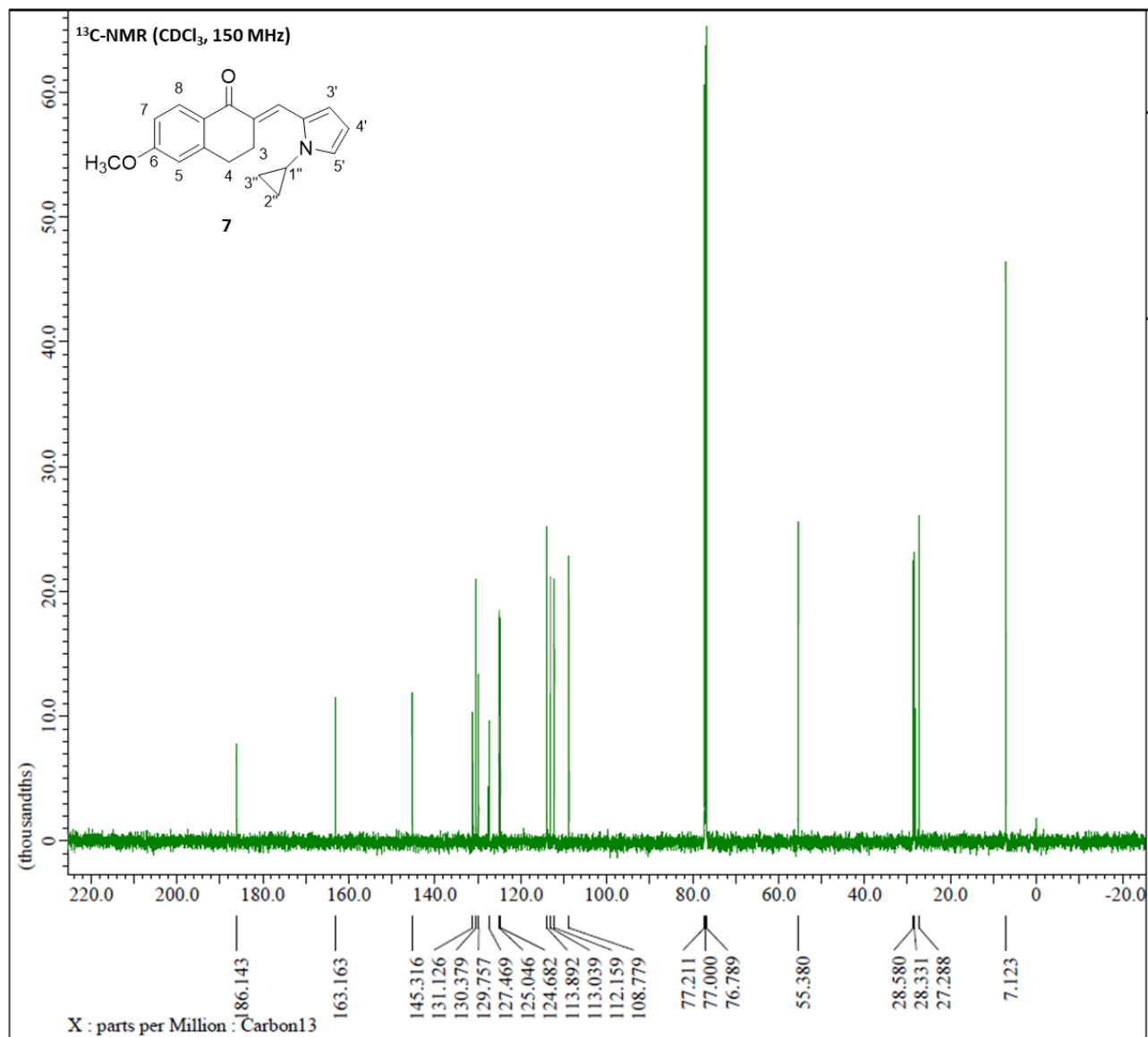


Figure 77. ¹³C-NMR spectrum (CDCl₃, 150 MHz) of compound **7**.

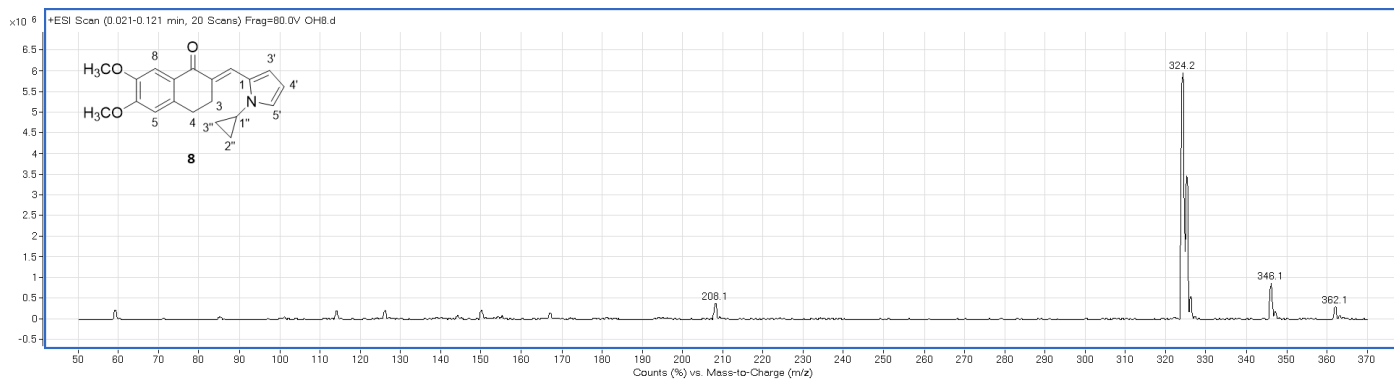


Figure 78. (+)-ESI Mass spectrum of compound **8**.

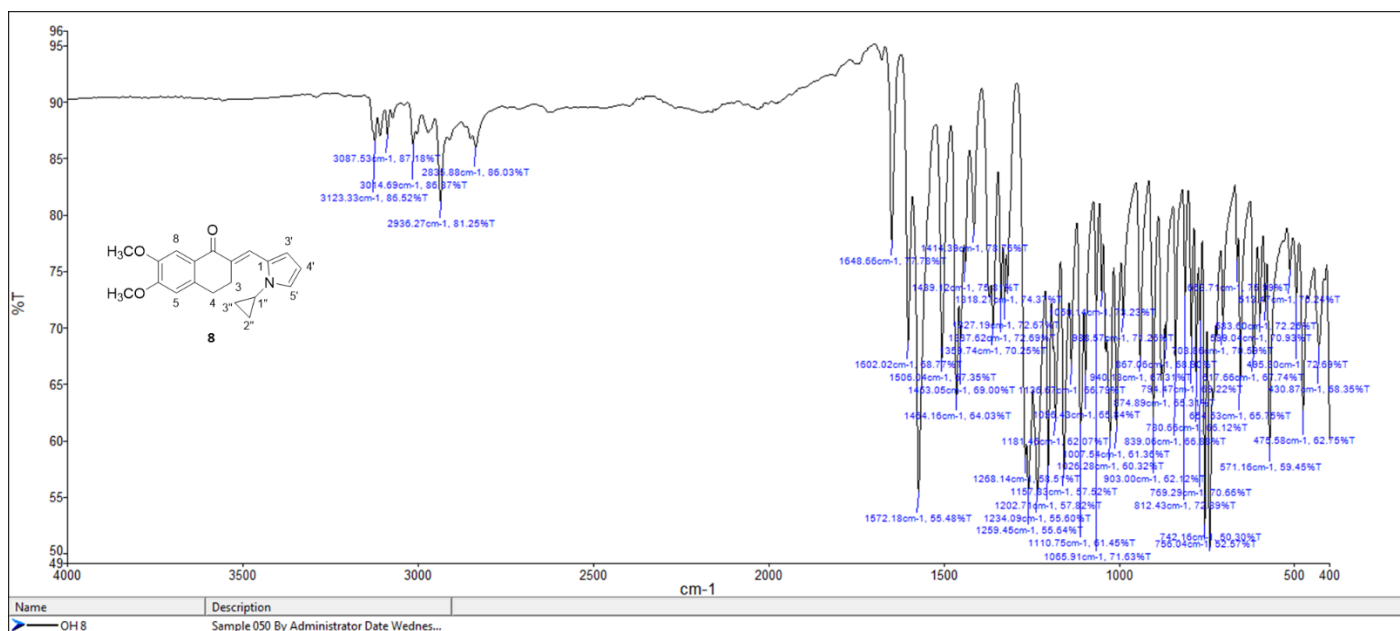


Figure 79. FT-IR spectrum of compound **8**.

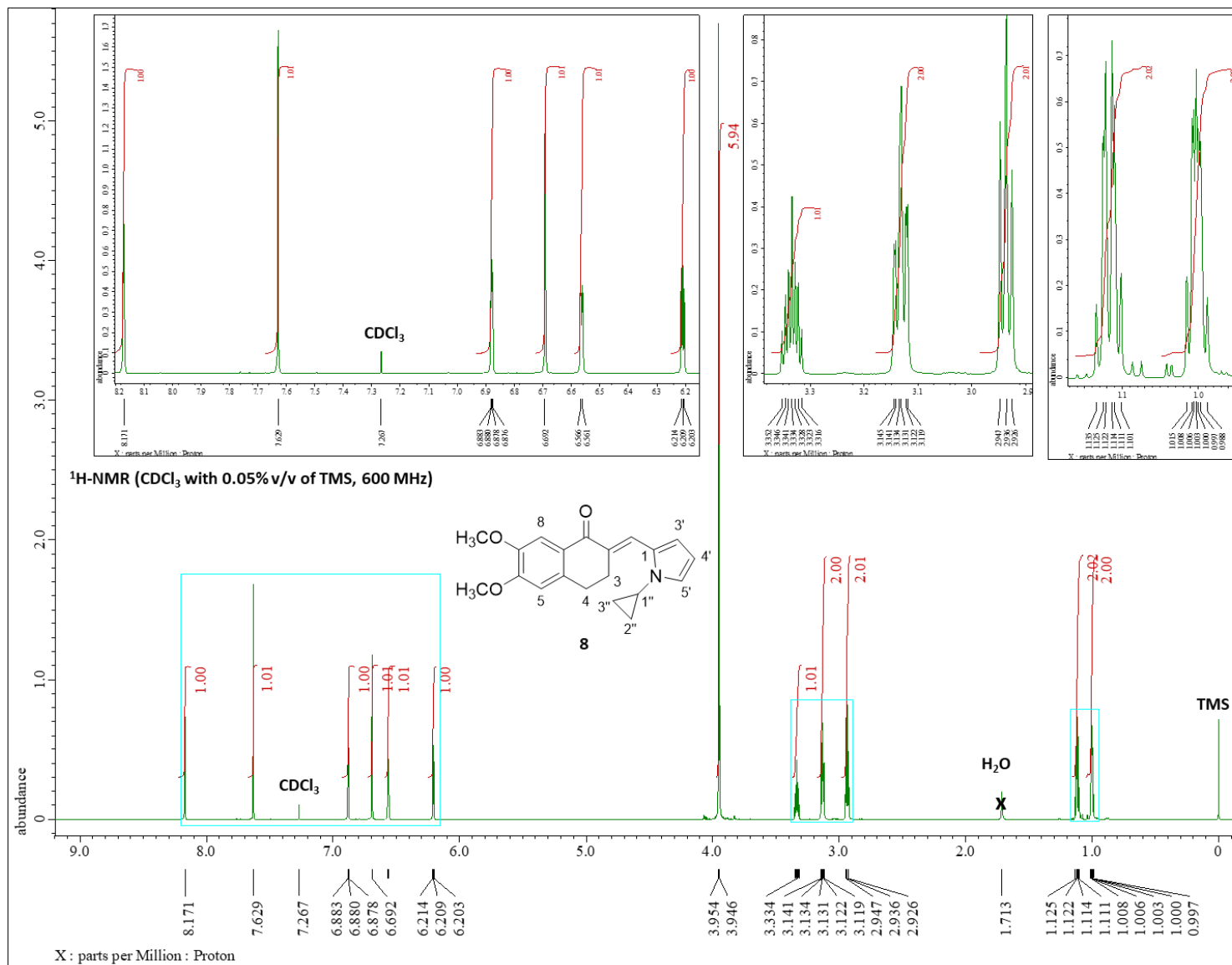


Figure 80. ¹H-NMR spectrum (CDCl₃ with 0.05% v/v of TMS, 600 MHz) of compound **8**.

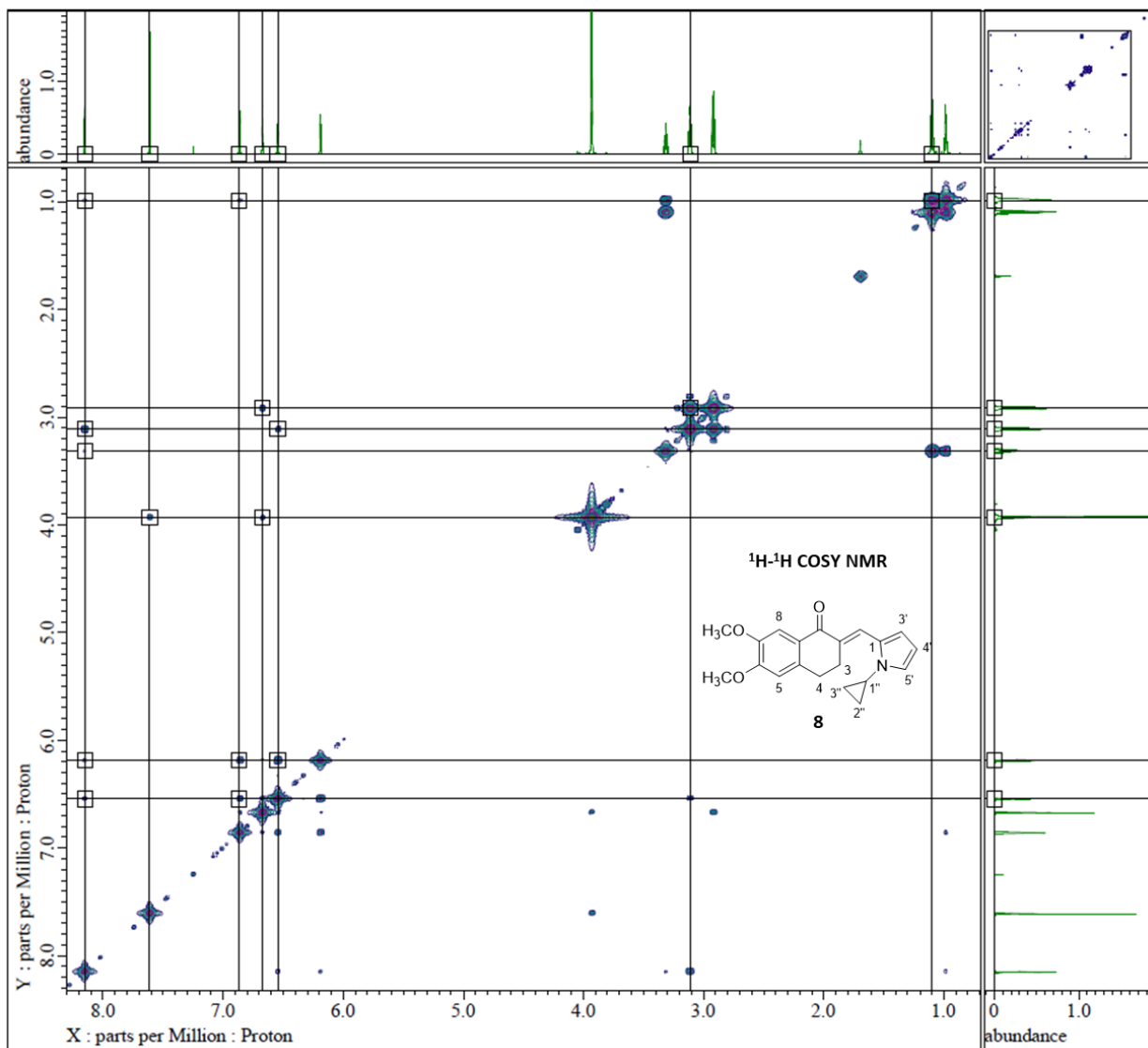


Figure 81. ^1H - ^1H COSY NMR of compound **8**.

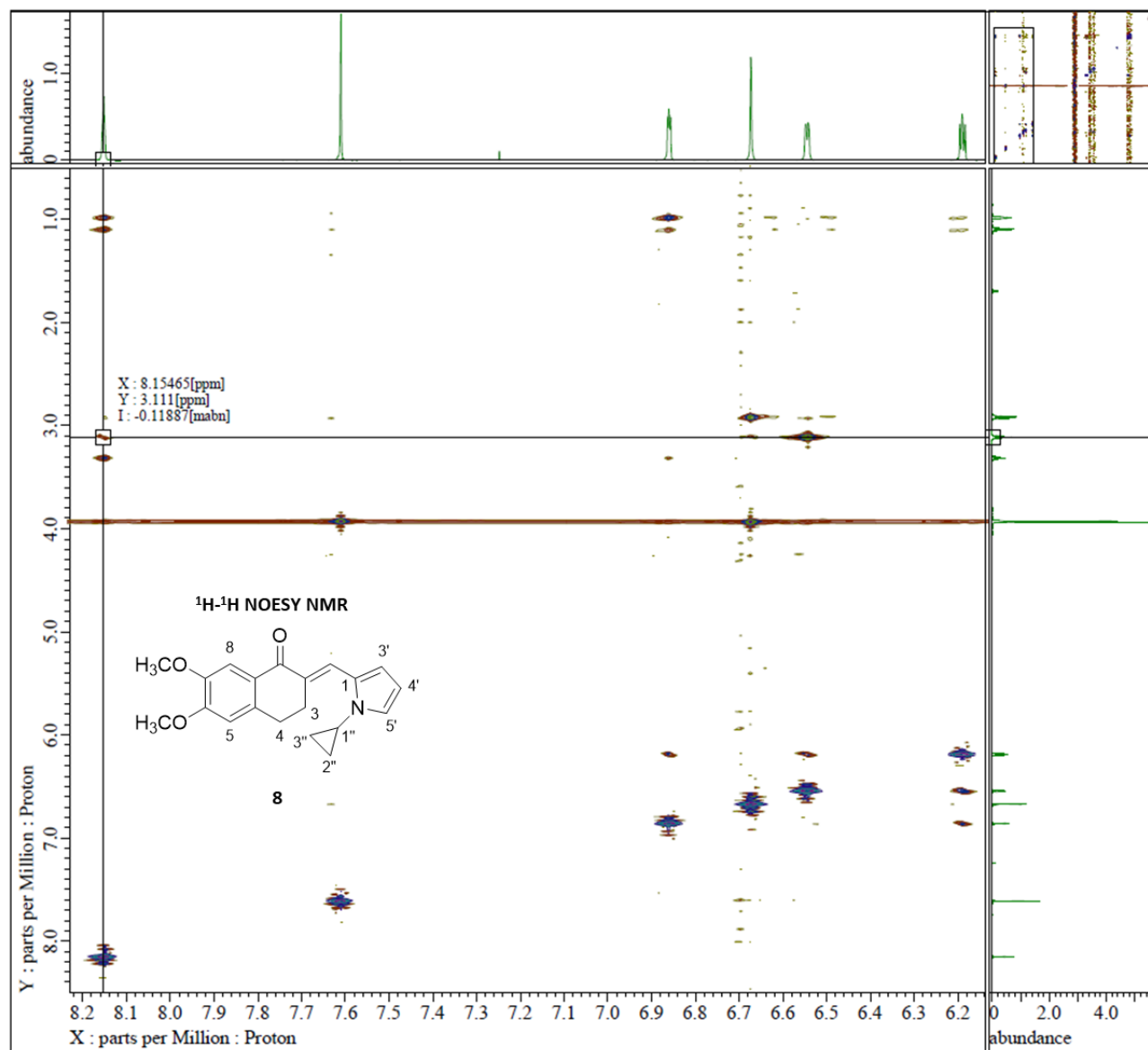


Figure 82. ¹H-¹H NOESY NMR of compound **8**.

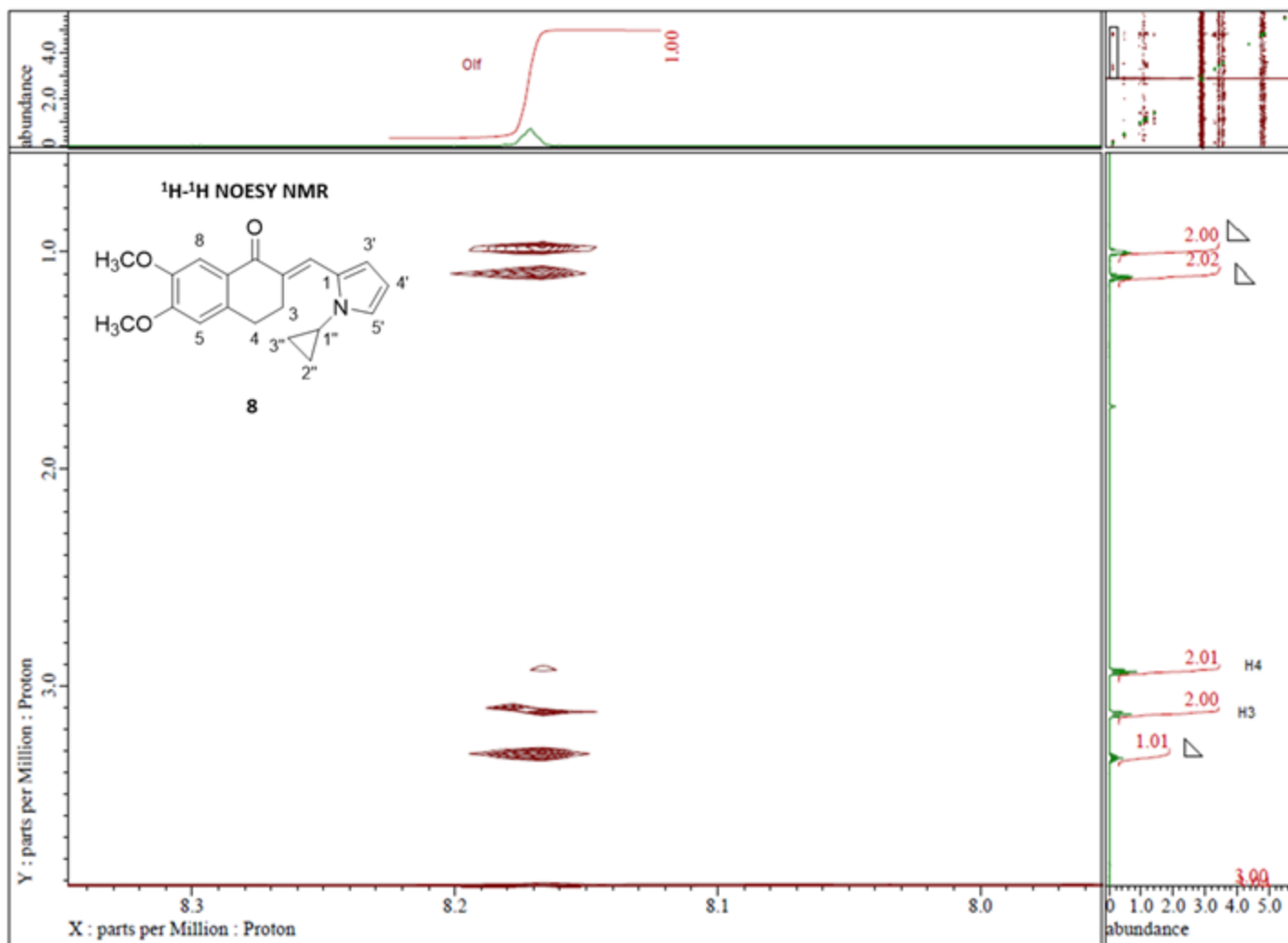


Figure 83. Expanded region of ¹H-¹H NOESY NMR of compound **8** showing the correlation between H3 and the Olefinic proton.

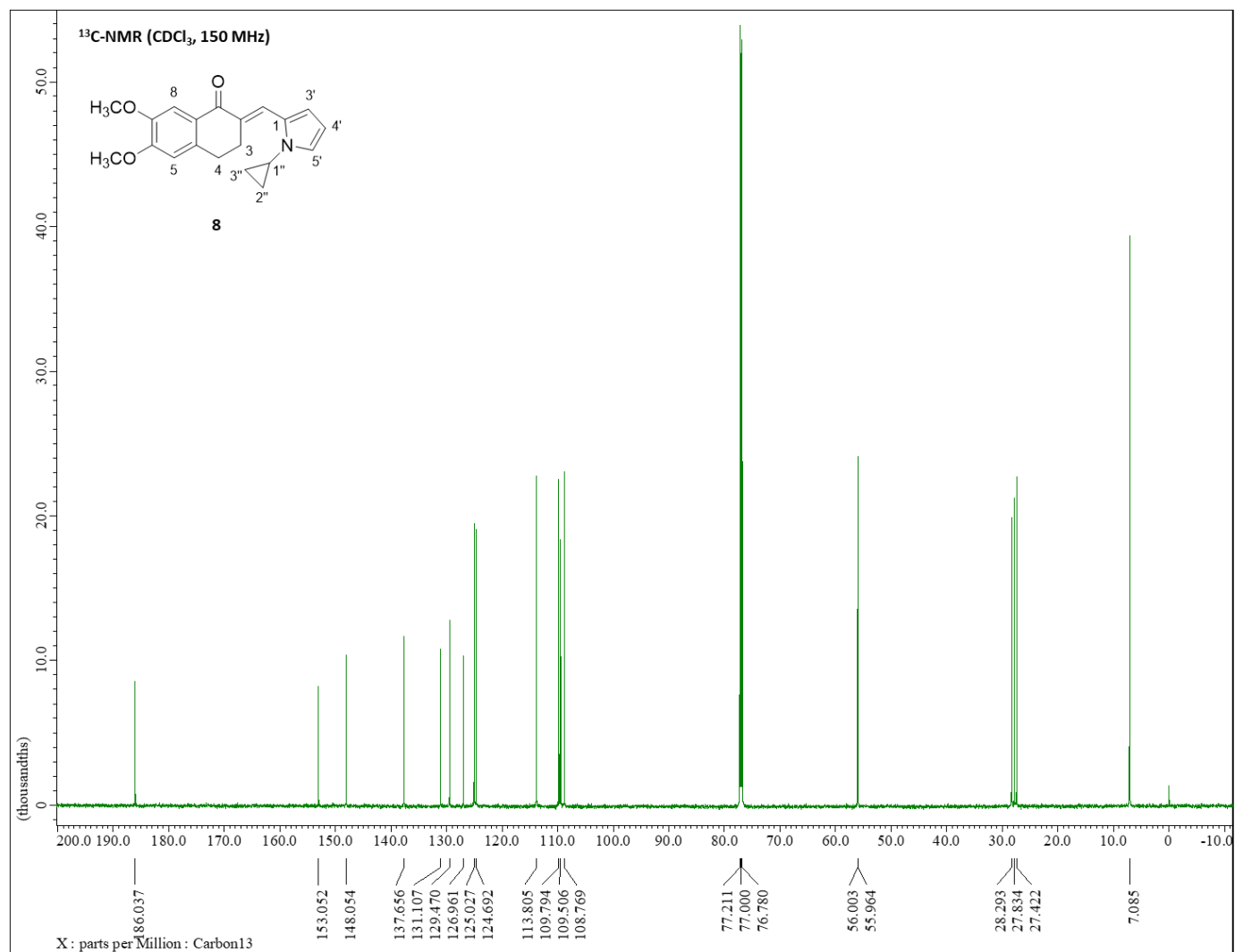


Figure 84. ¹³C-NMR spectrum (CDCl₃, 150 MHz) of compound **8**.

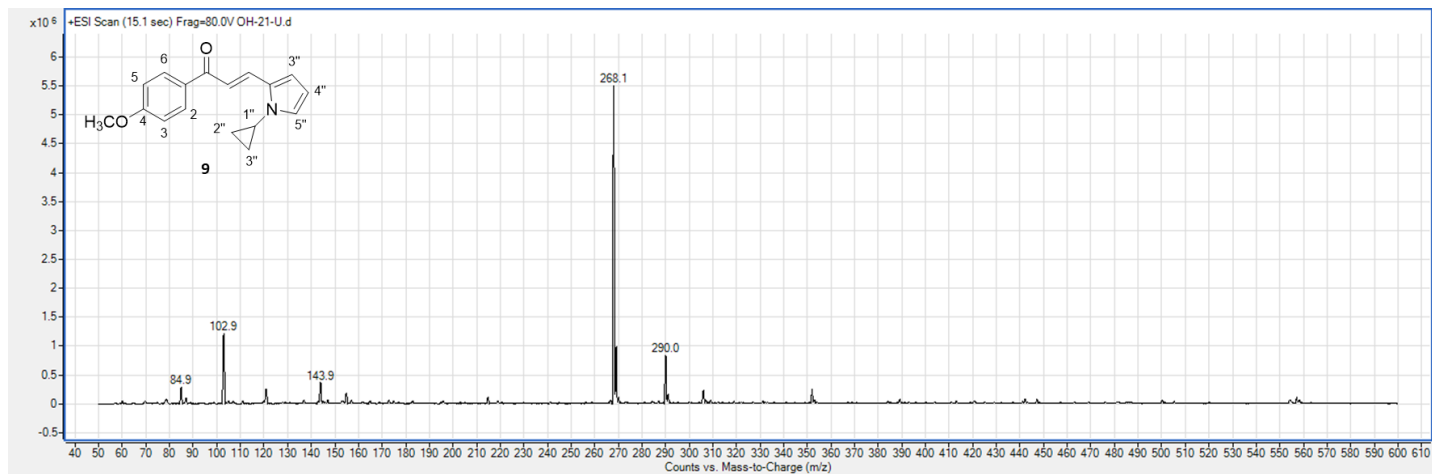


Figure 85. (+)-ESI Mass spectrum of compound **9**.

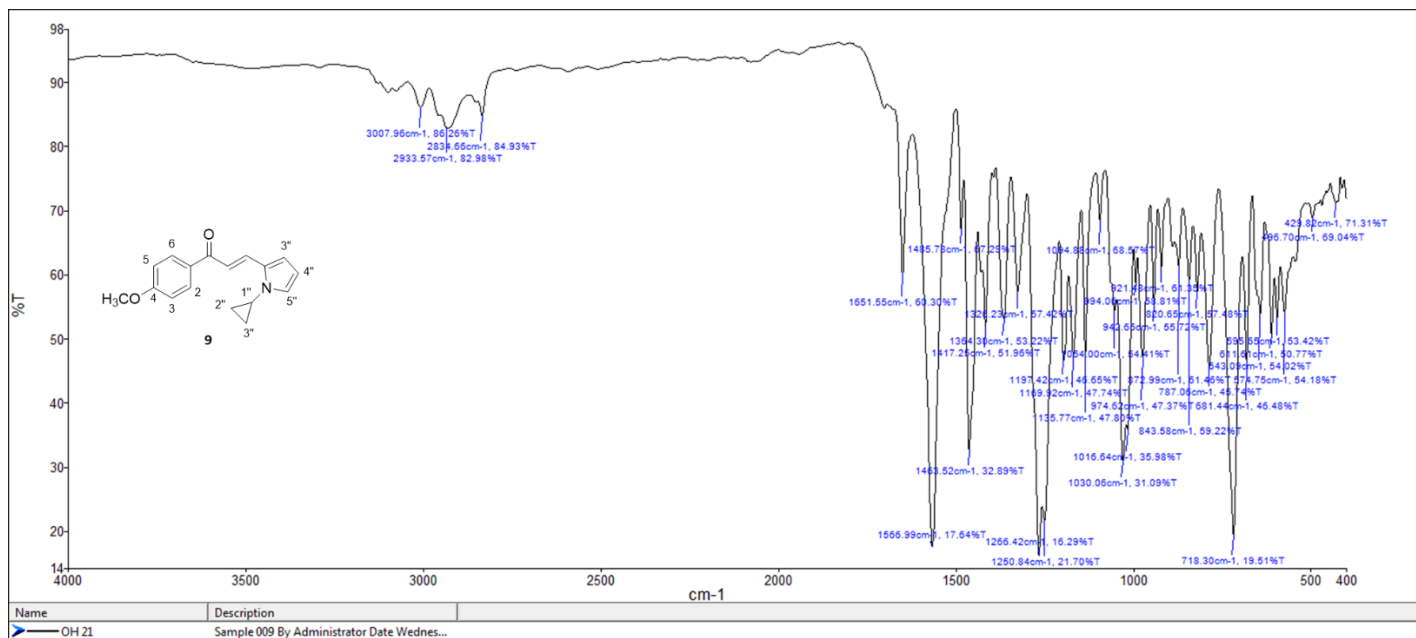


Figure 86. FT-IR spectrum of compound **9**.

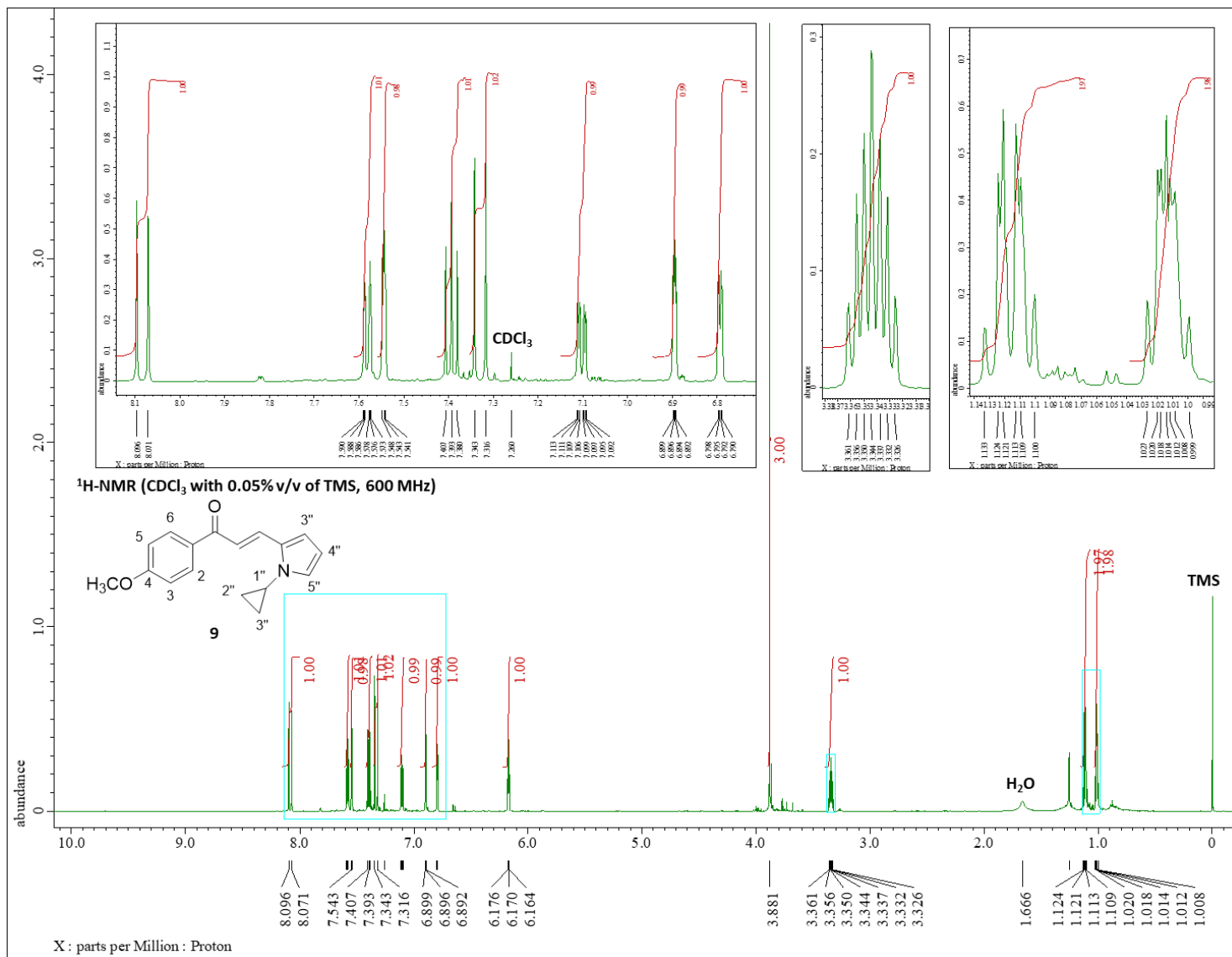


Figure 87. ¹H-NMR spectrum (CDCl₃ with 0.05% v/v of TMS, 600 MHz) of compound **9**.

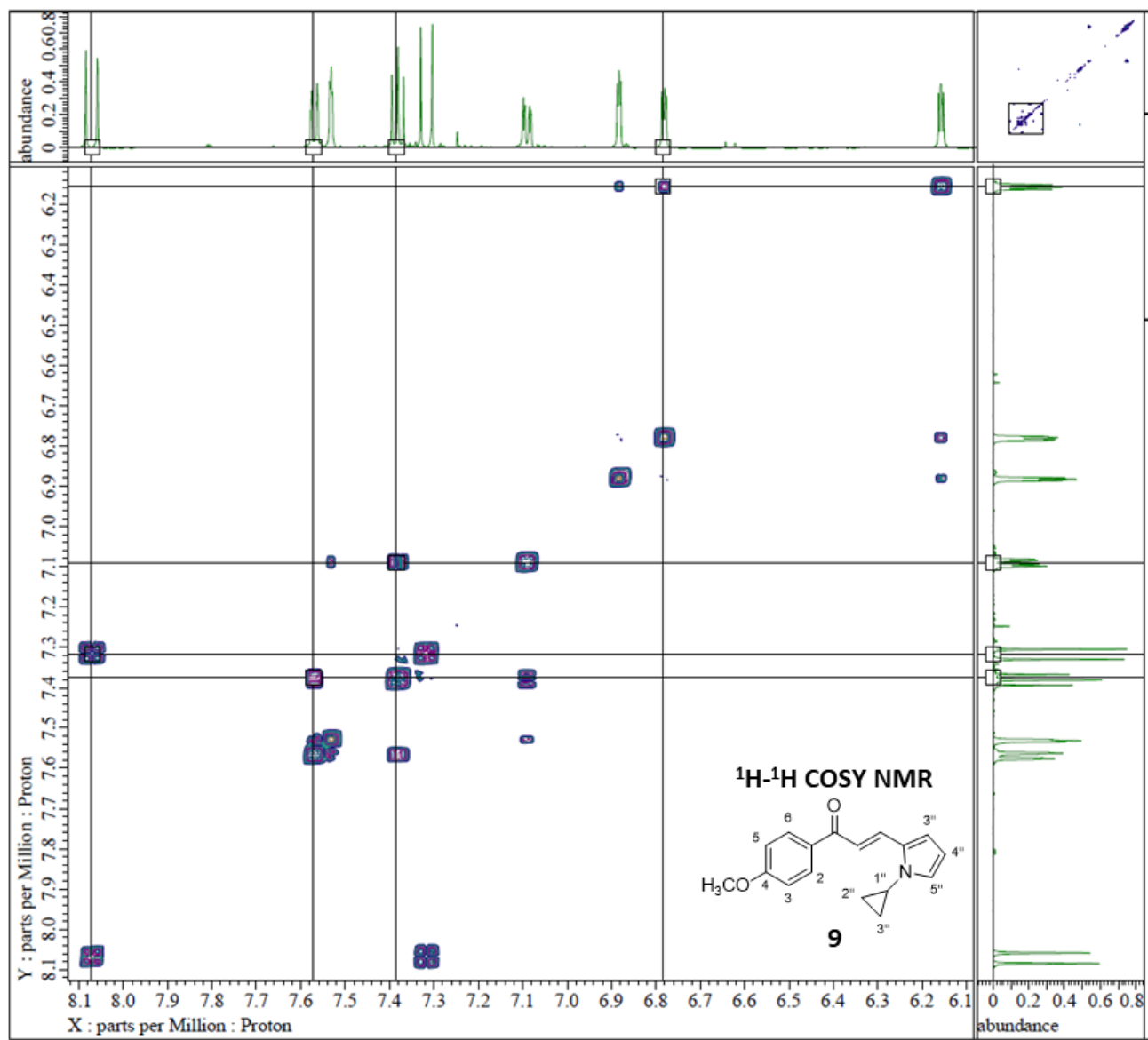


Figure 88. ^1H - ^1H COSY NMR of compound **9**.

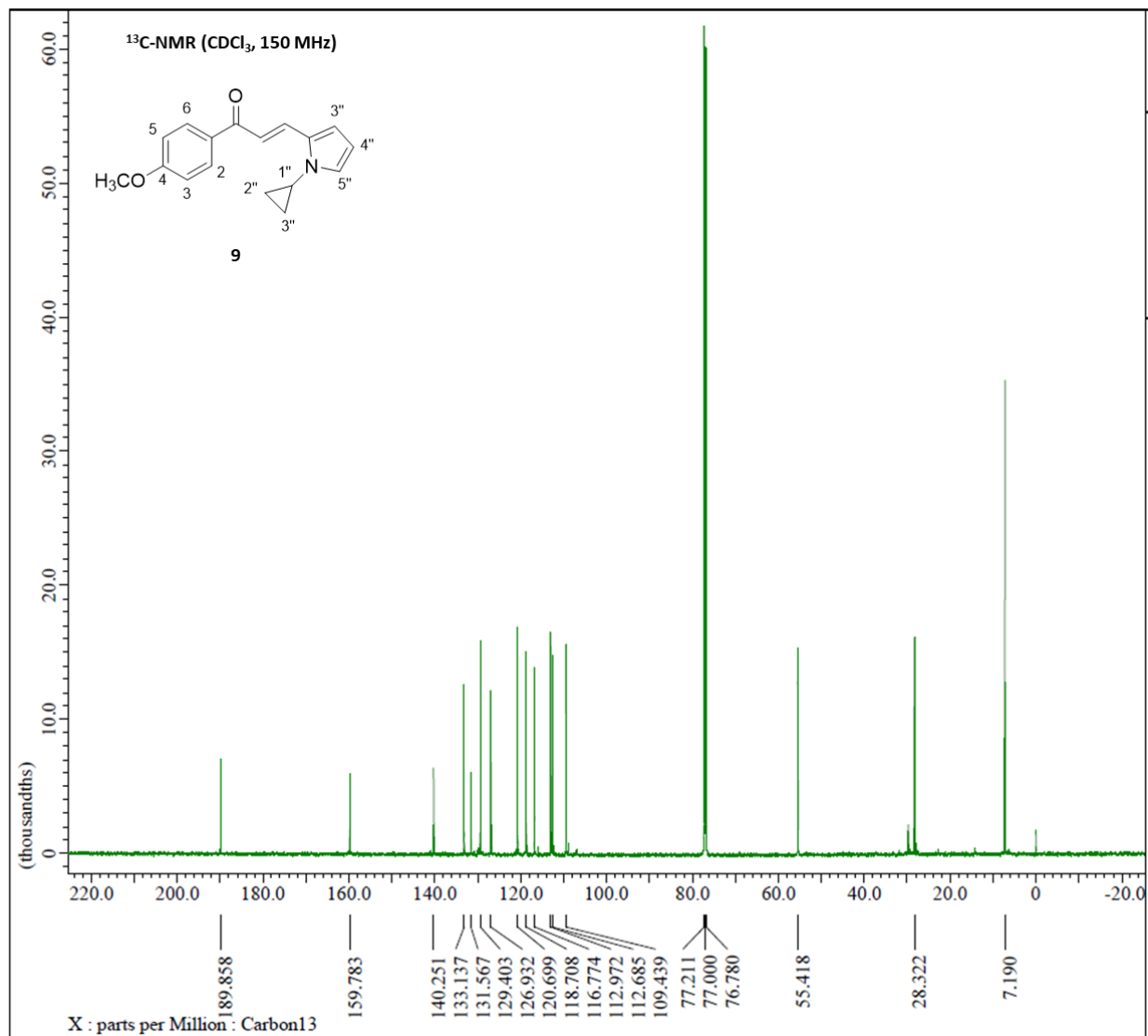


Figure 89. ¹³C-NMR spectrum (CDCl₃, 150 MHz) of compound **9**.

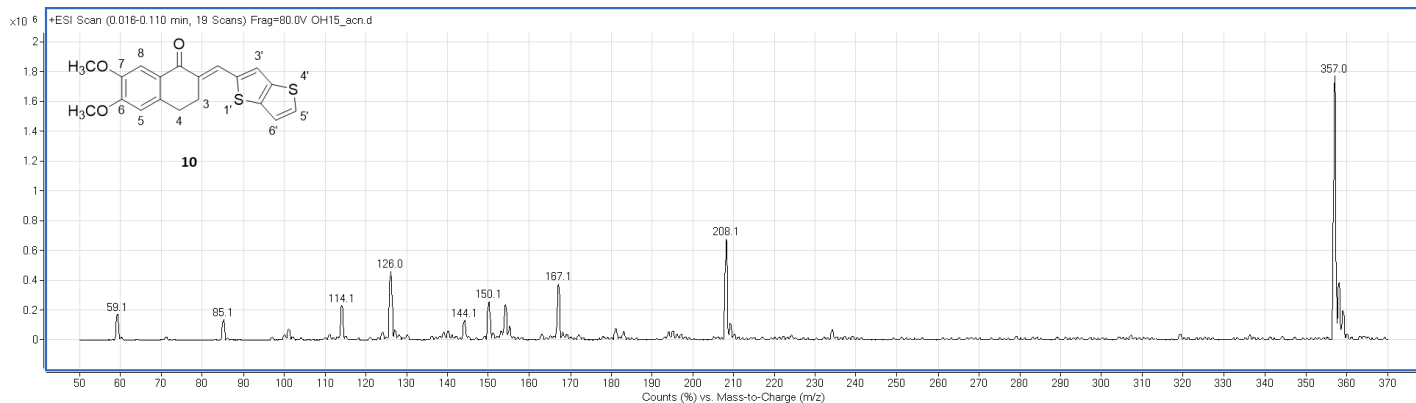


Figure 90. (+)-ESI Mass spectrum of compound **10**.

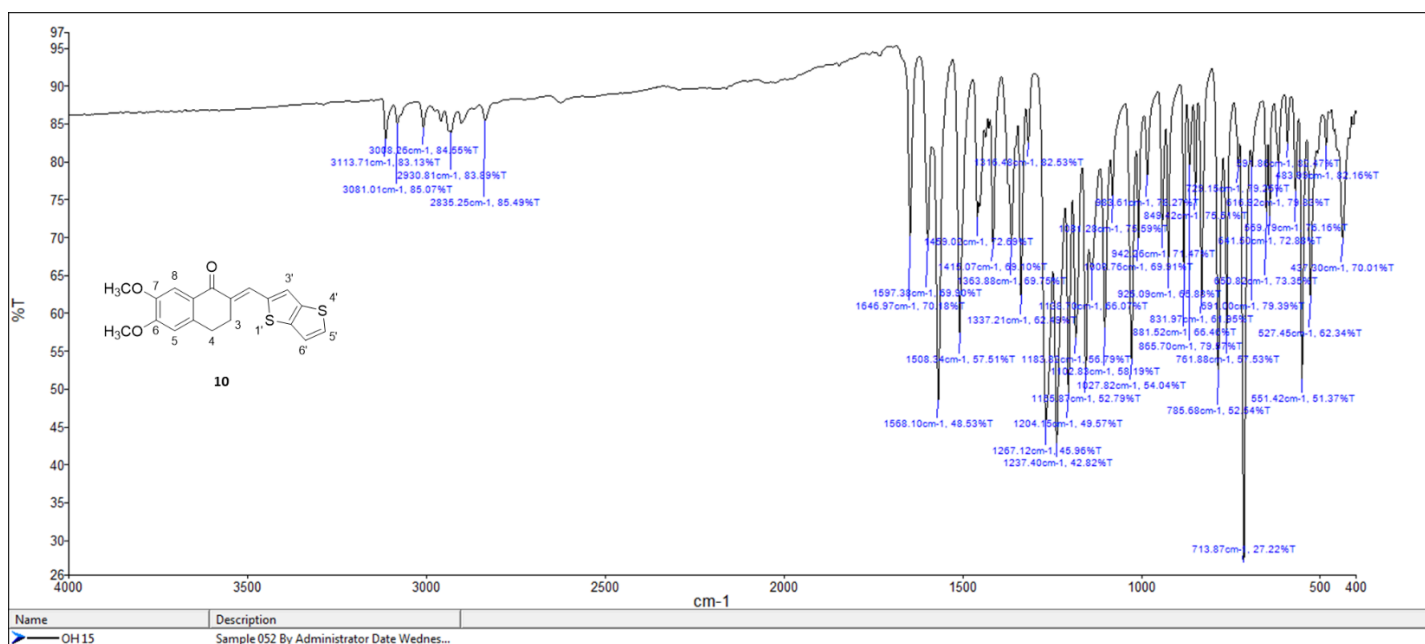


Figure 91. FT-IR spectrum of compound **10**.

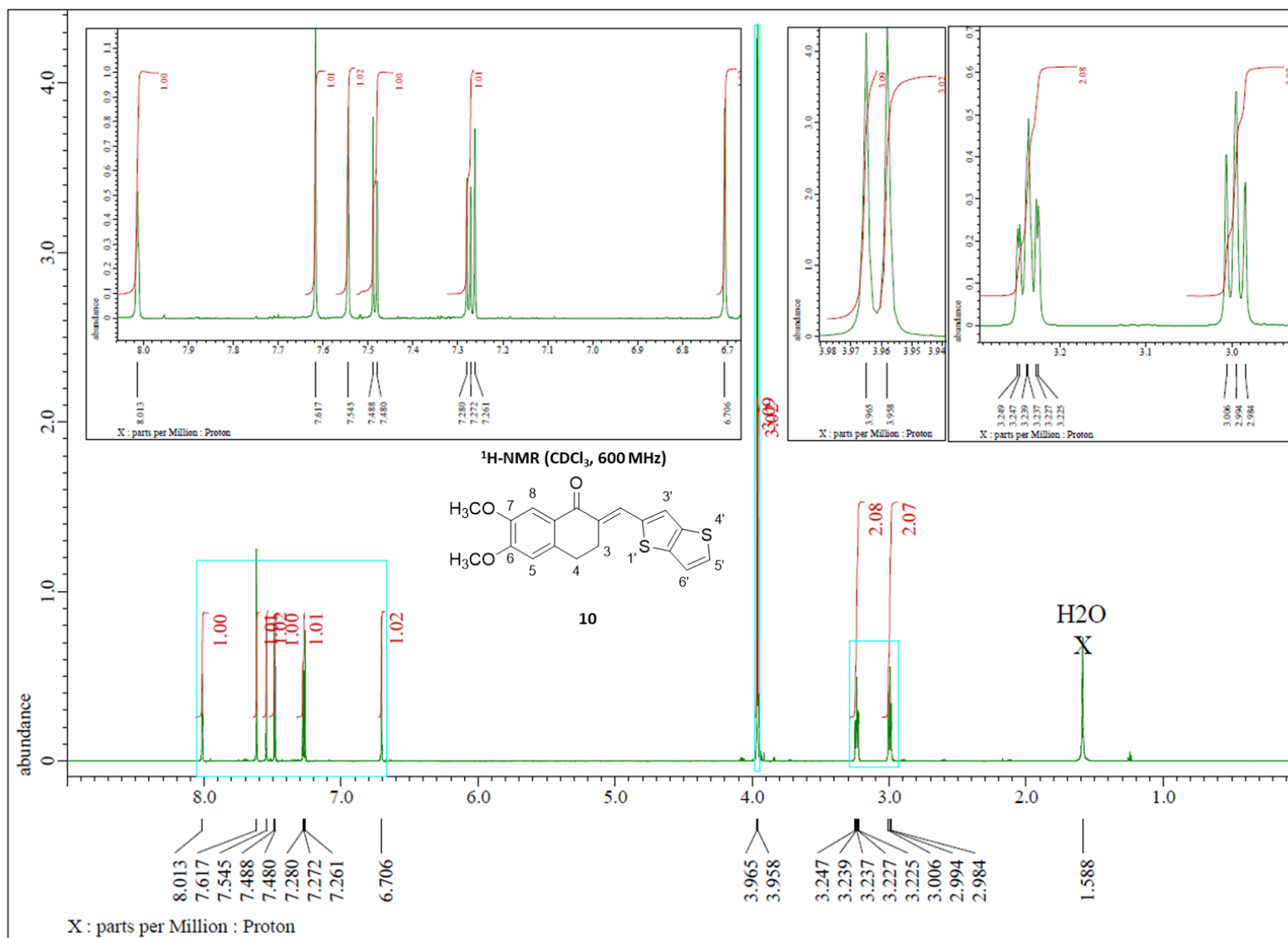


Figure 92. ¹H-NMR spectrum (CDCl₃ with 0.05% v/v of TMS, 600 MHz) of compound **10**.

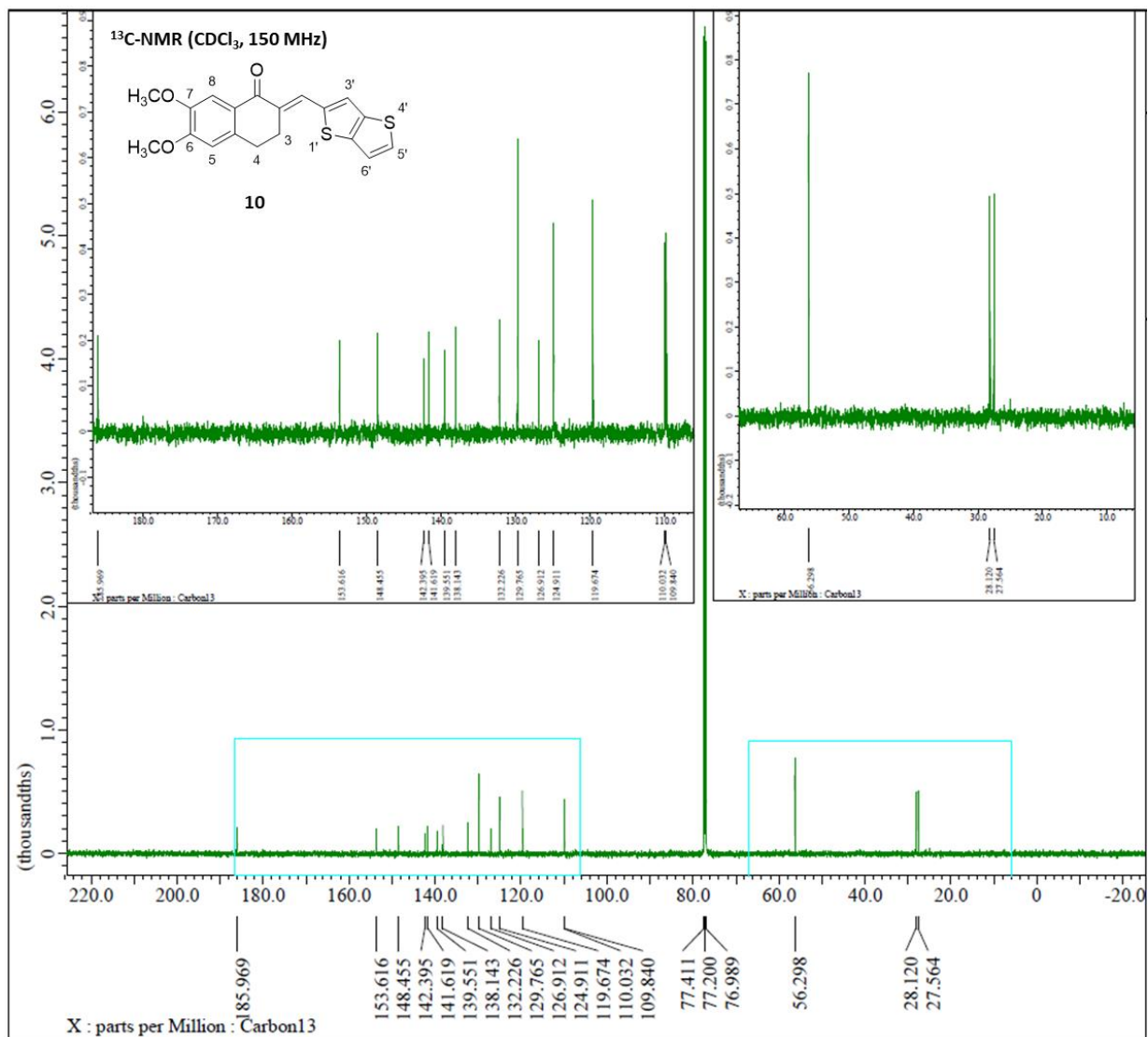


Figure 93. ¹³C-NMR spectrum (CDCl₃, 150 MHz) of compound **10**.

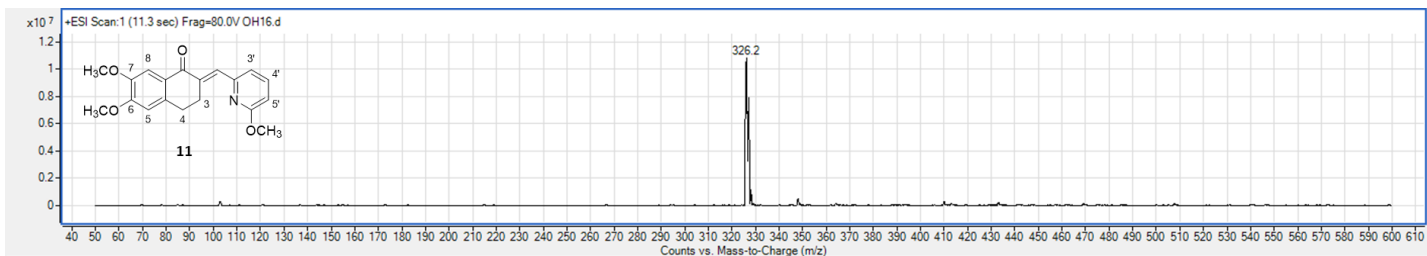


Figure 94. (+)-ESI Mass spectrum of compound **11**.

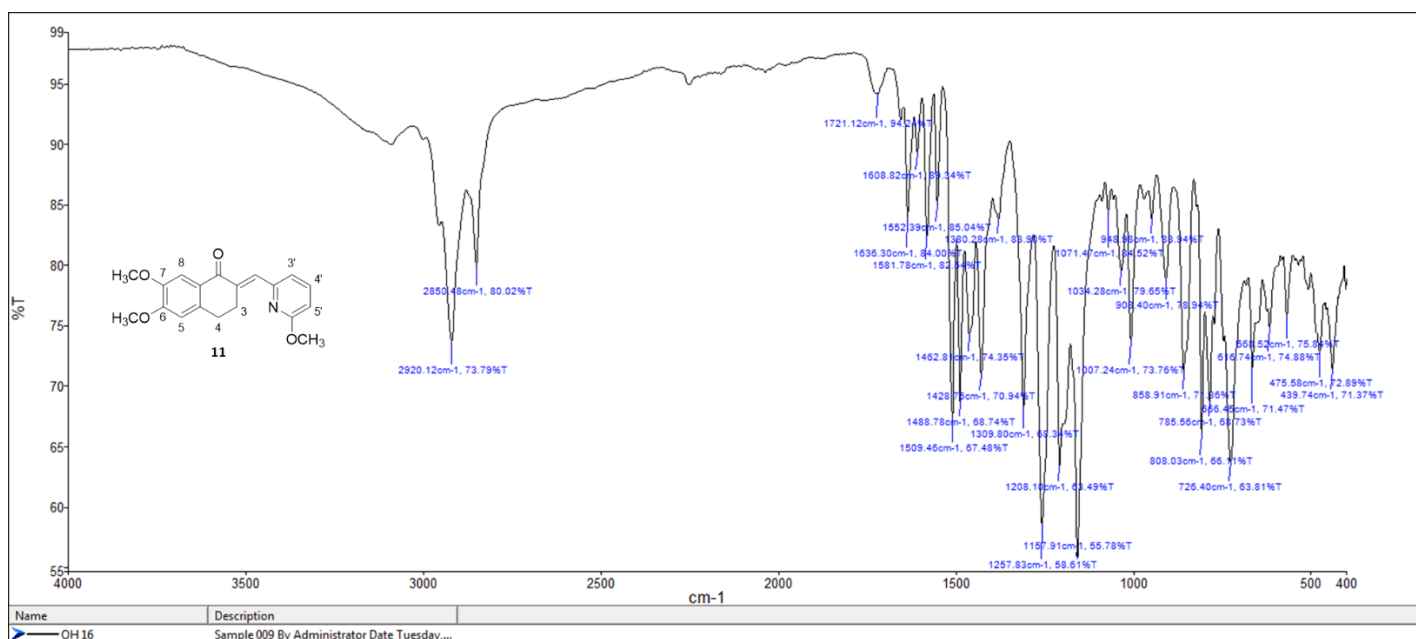


Figure 95. FT-IR spectrum of compound **11**.

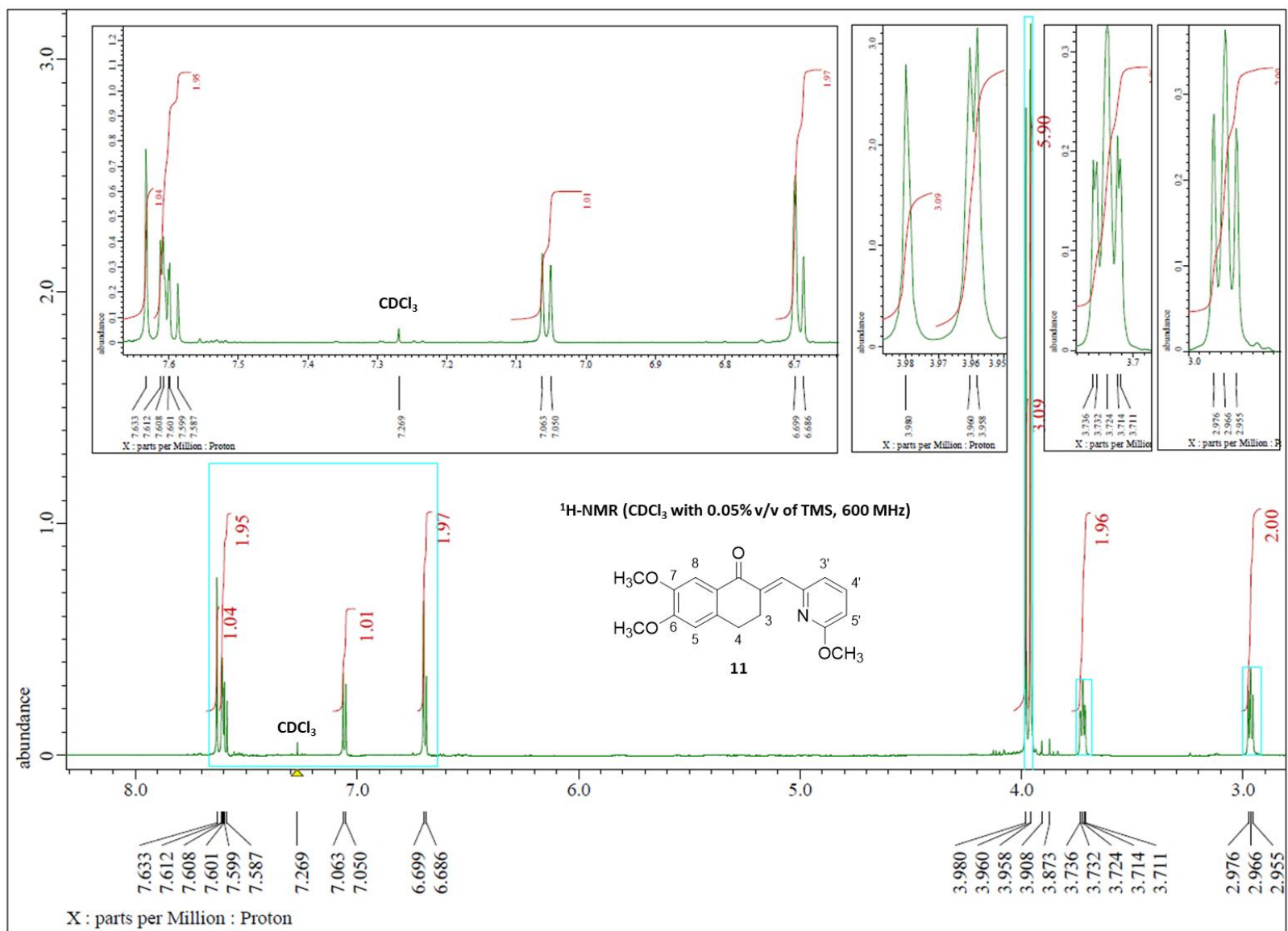


Figure 96. ¹H-NMR spectrum (CDCl₃ with 0.05% v/v of TMS, 600 MHz) of compound **11**.

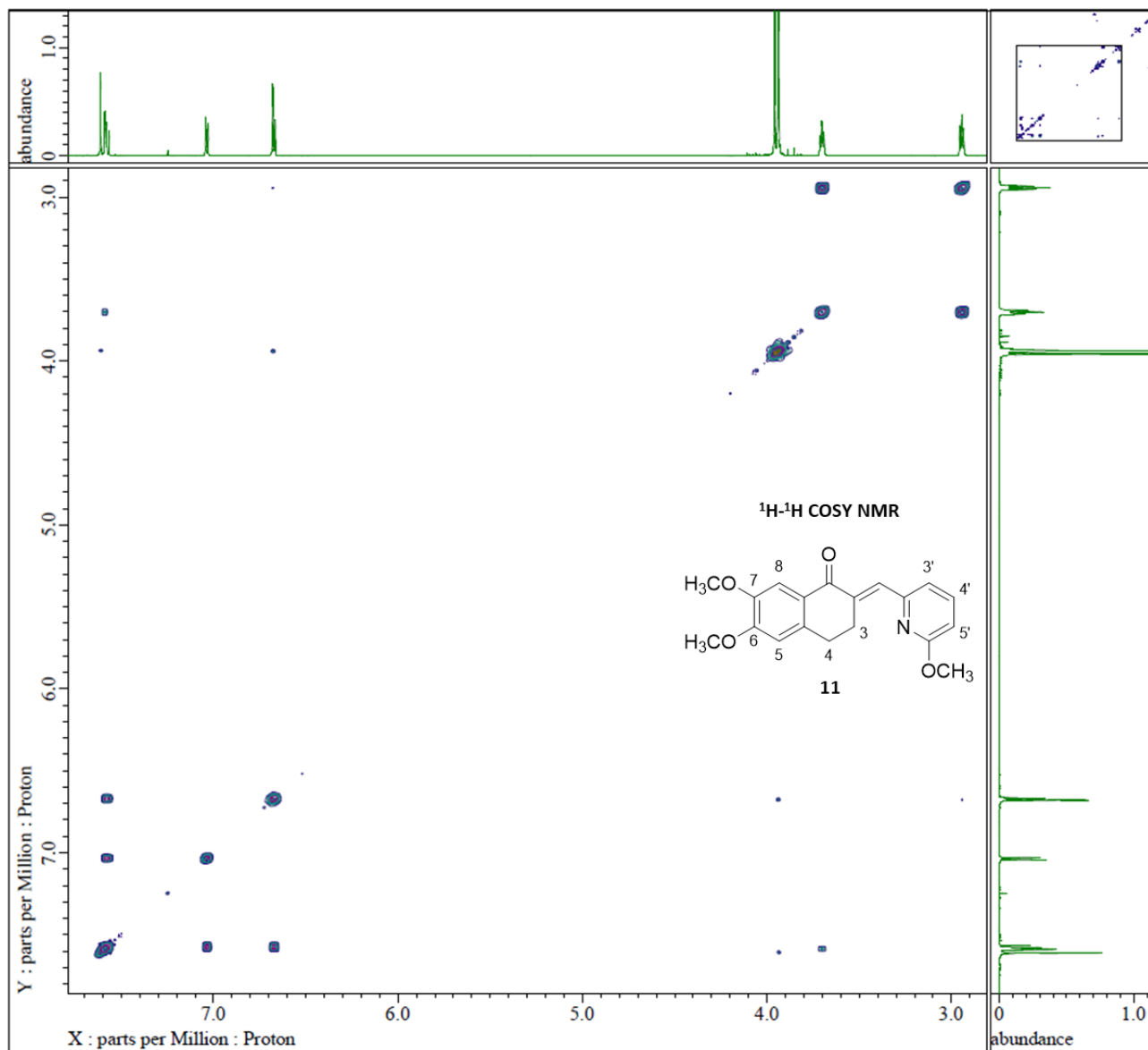


Figure 97. ¹H-¹H COSY NMR of compound **11**.

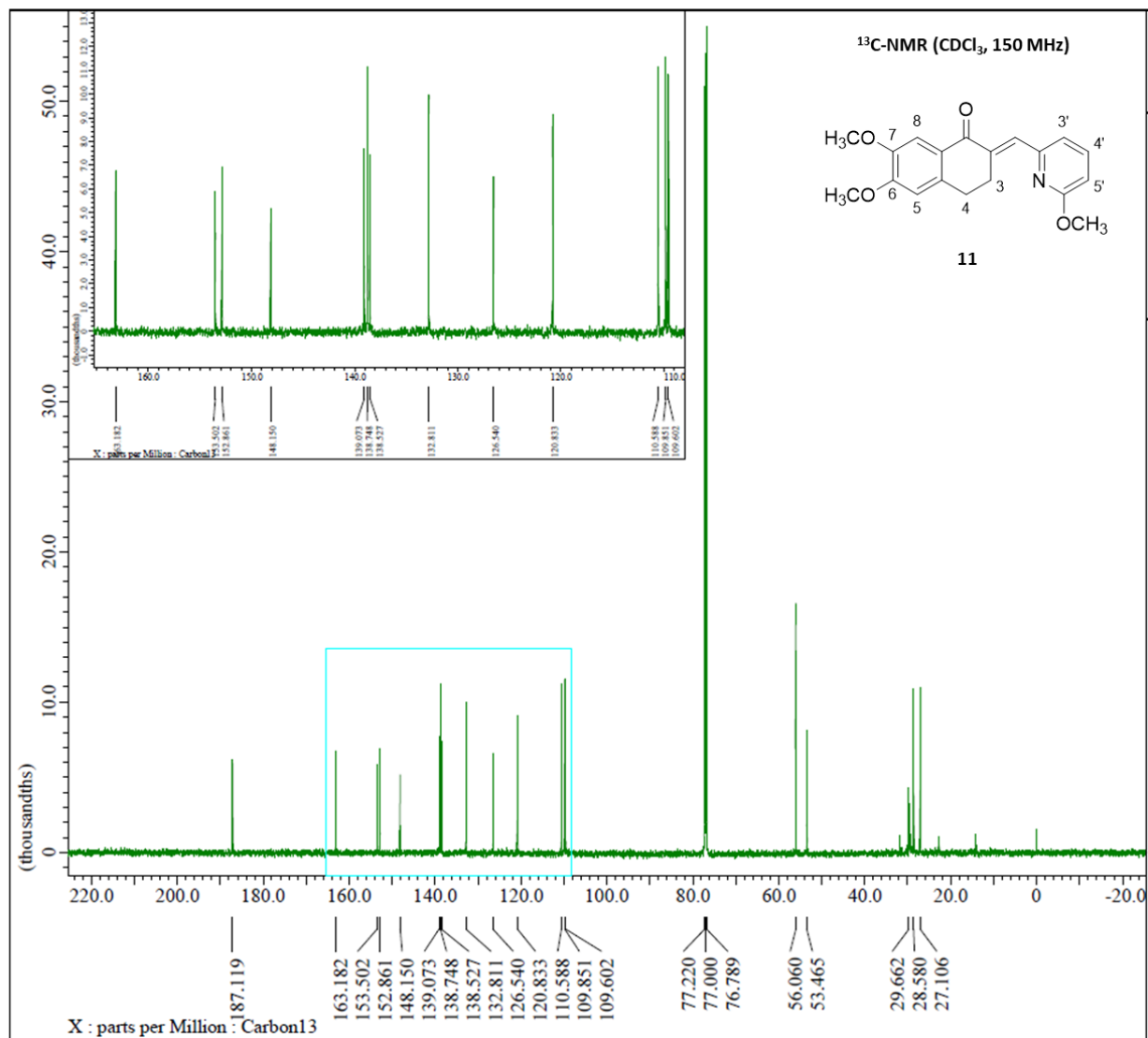


Figure 98. ¹³C-NMR spectrum (CDCl₃, 150 MHz) of compound **11**.

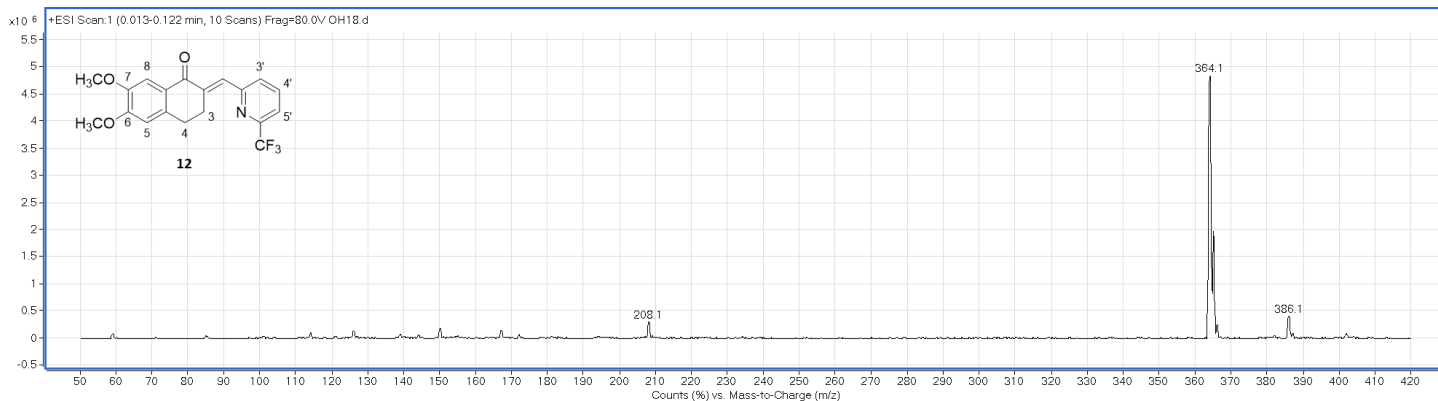


Figure 99. (+)-ESI Mass spectrum of compound **12**.

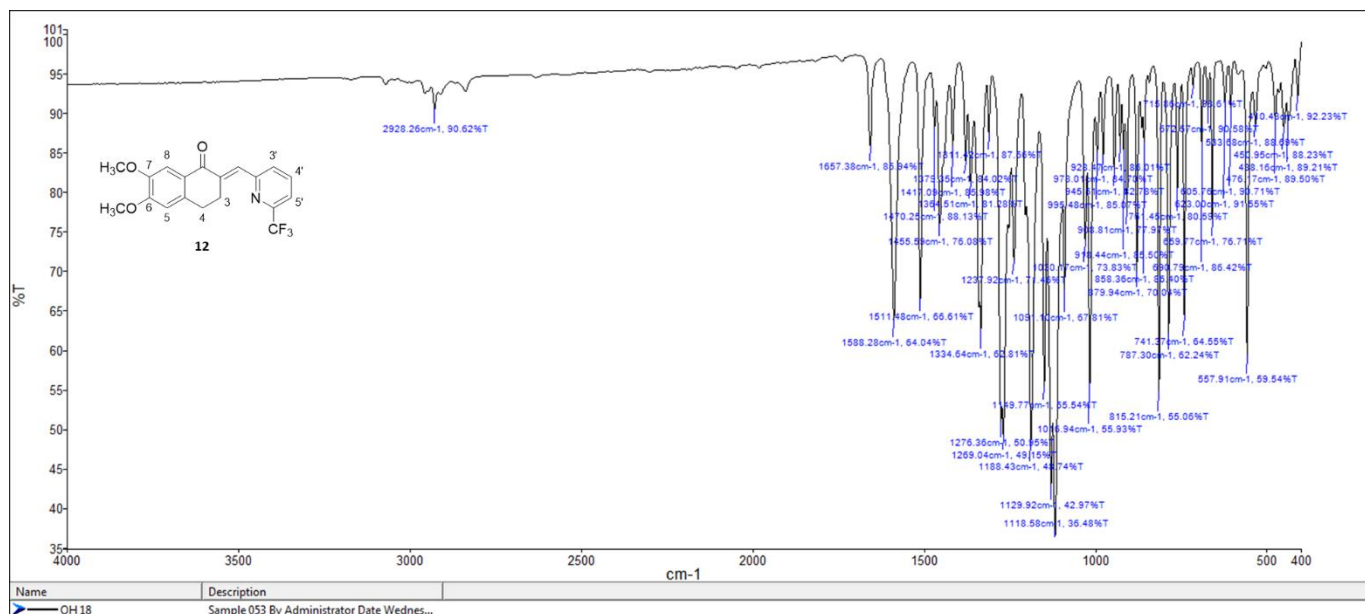


Figure 100. FT-IR spectrum of compound **12**.

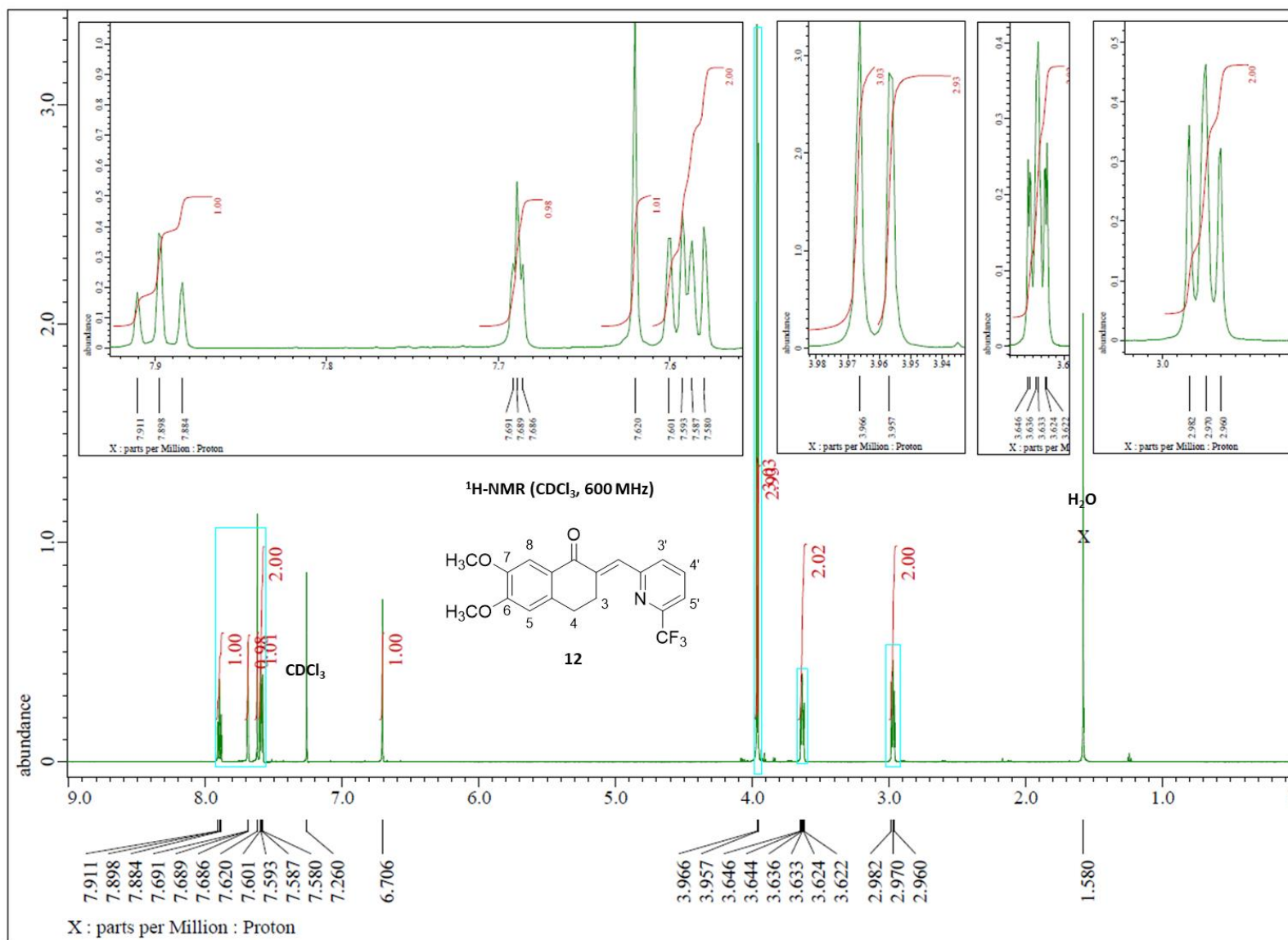


Figure 101. ¹H-NMR spectrum (CDCl₃, 600 MHz) of compound **12**.

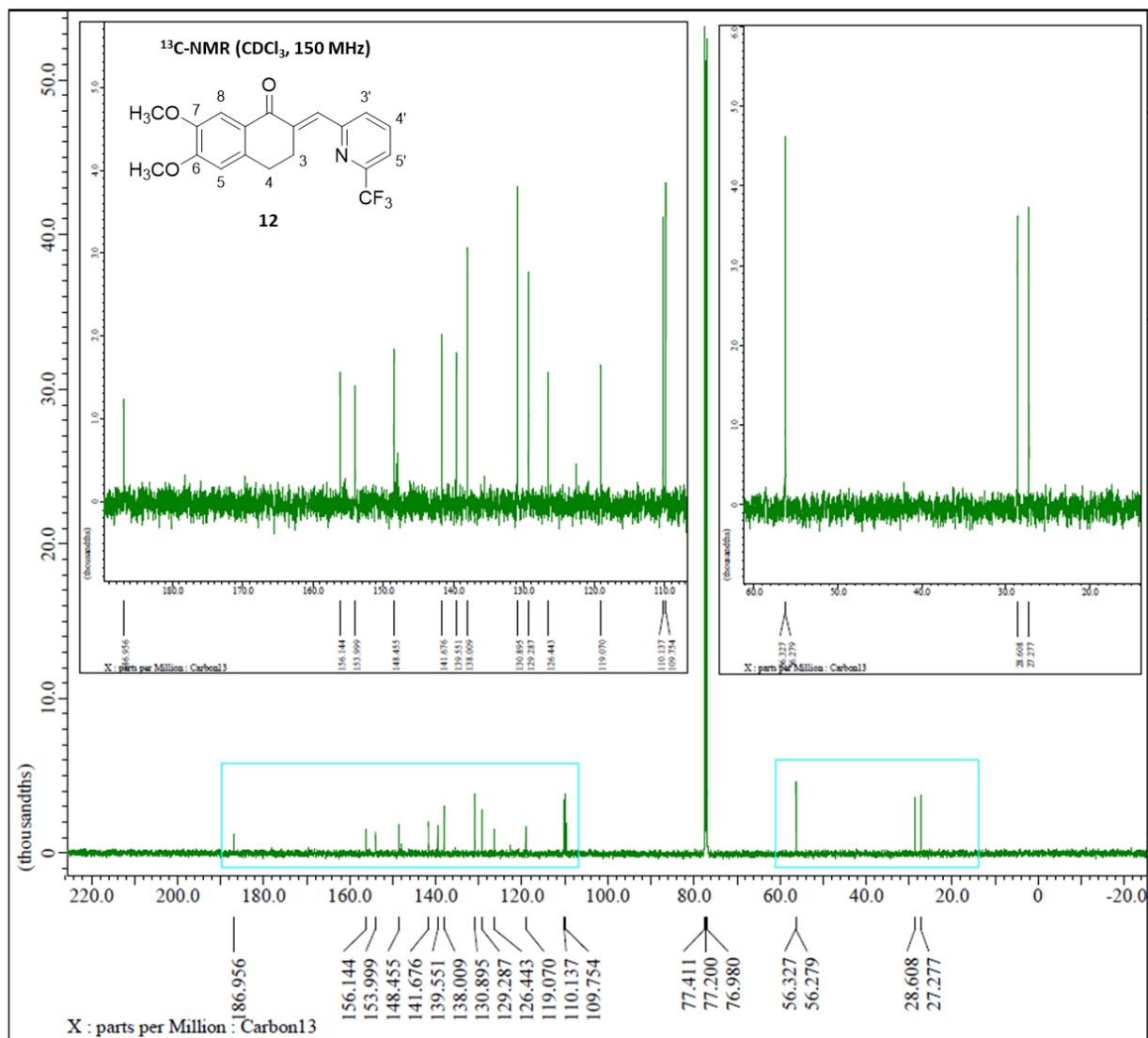


Figure 102. ¹³C-NMR spectrum (CDCl₃, 150 MHz) of compound **12**.

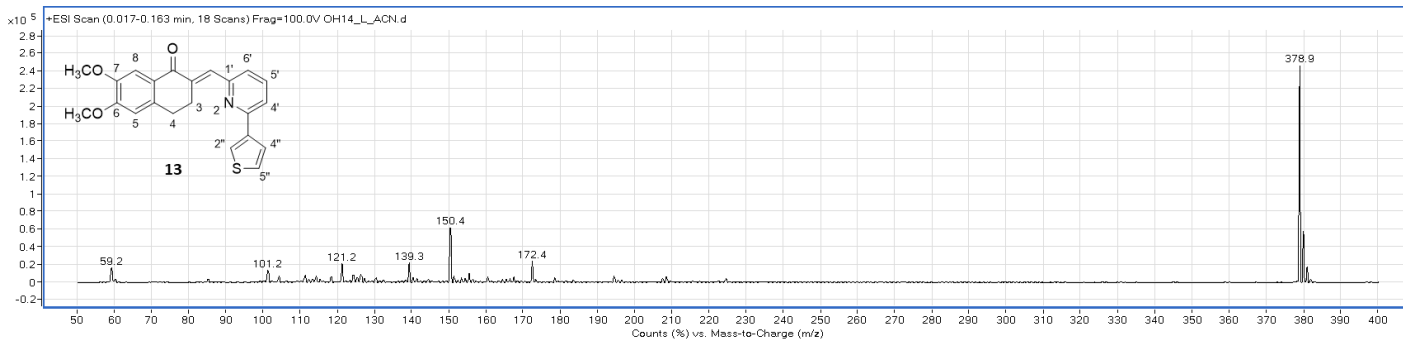


Figure 103. (+)-ESI Mass spectrum of compound 13.

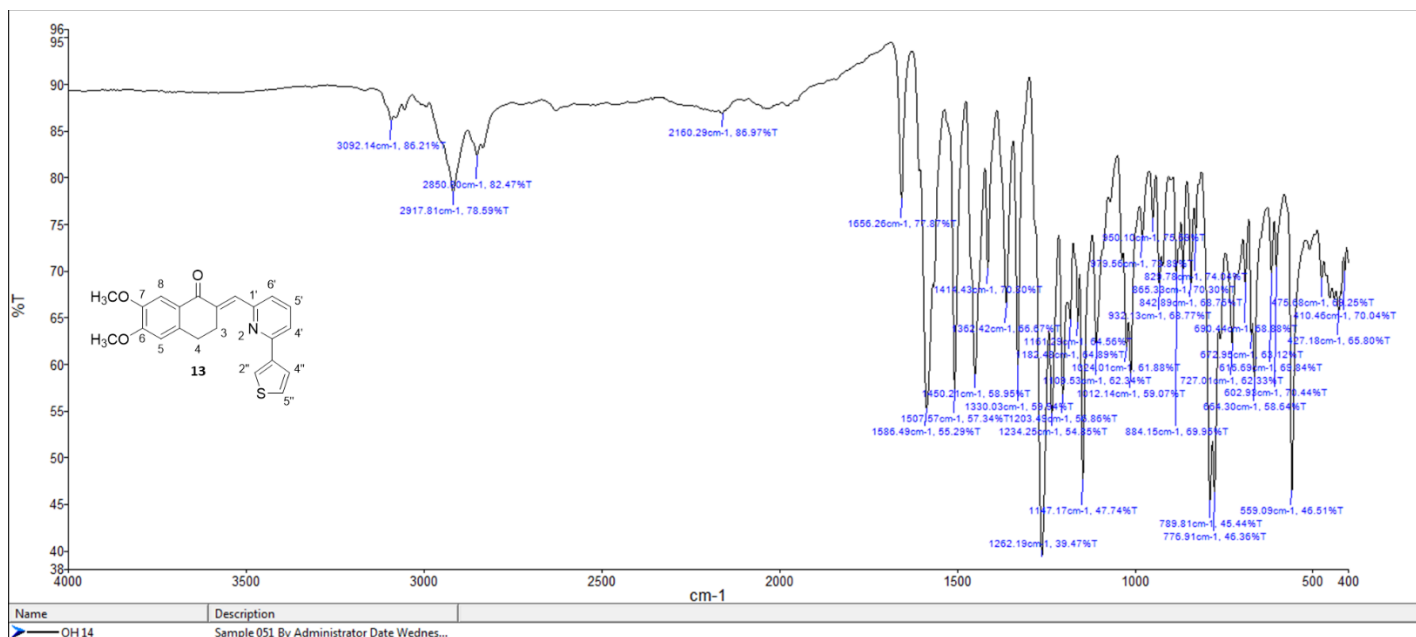


Figure 104. FT-IR spectrum of compound 13.

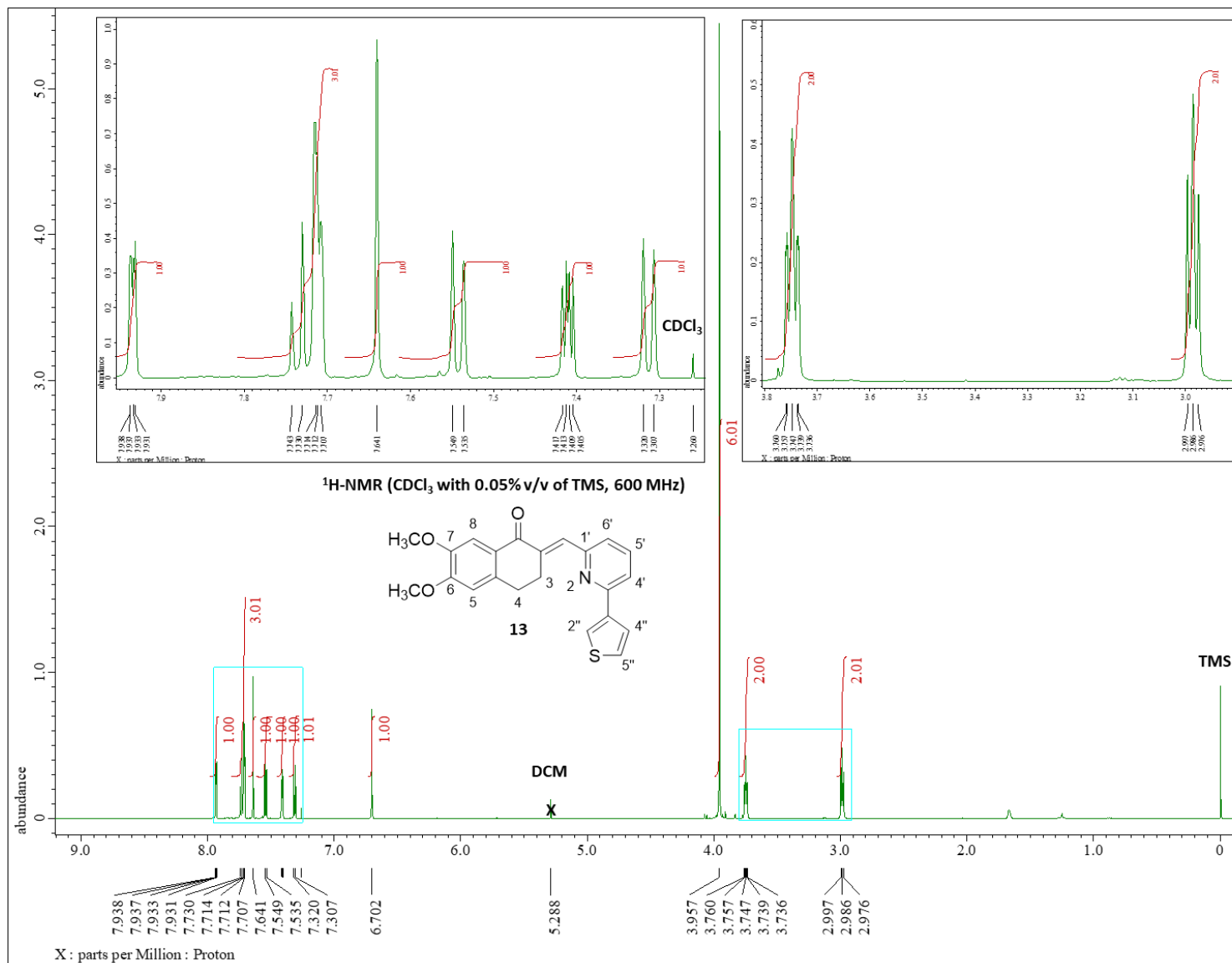


Figure 105. ¹H-NMR spectrum (CDCl₃ with 0.05% v/v of TMS, 600 MHz) of compound **13**.

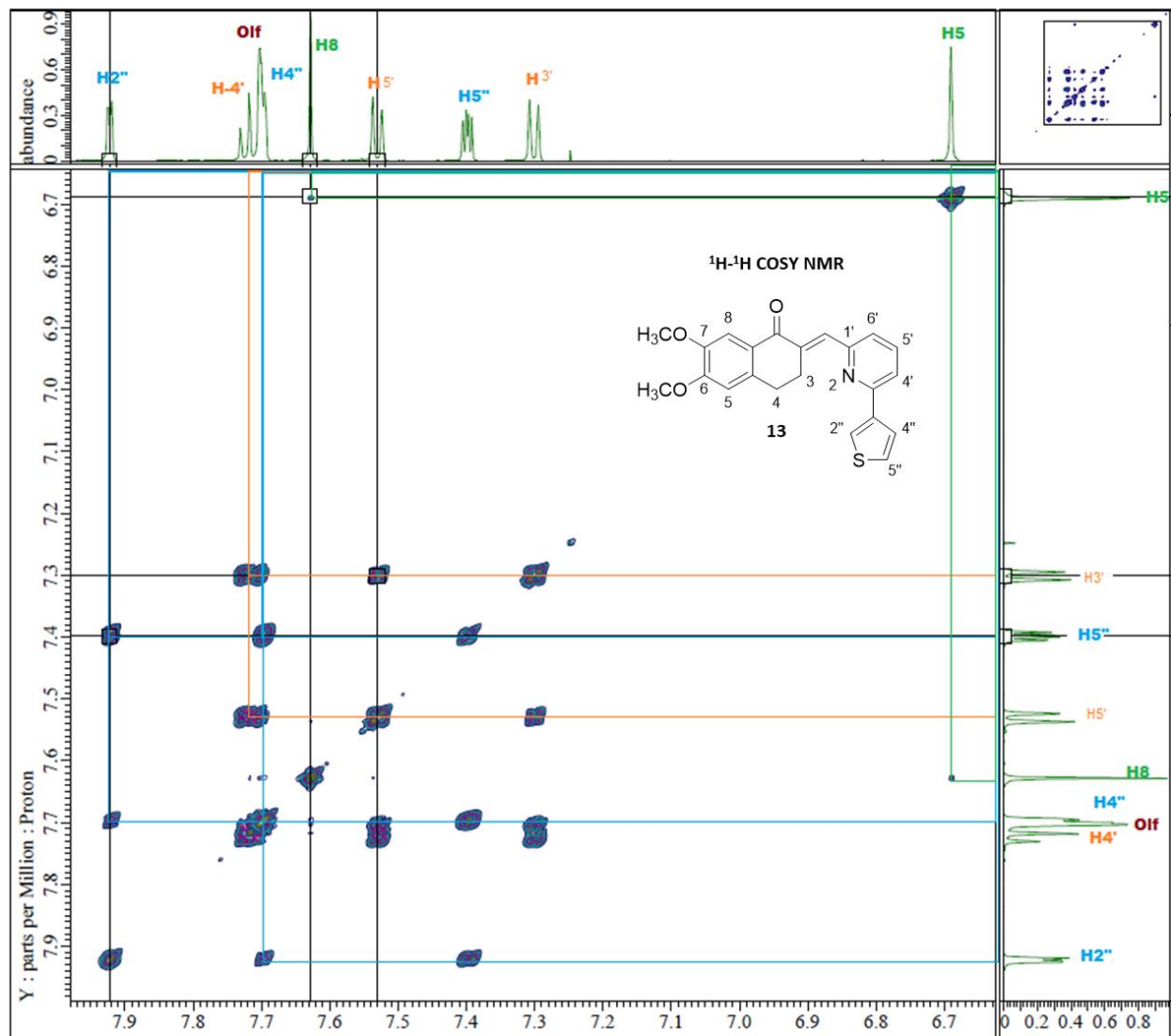


Figure 106. ¹H-¹H COSY NMR of compound **13**.

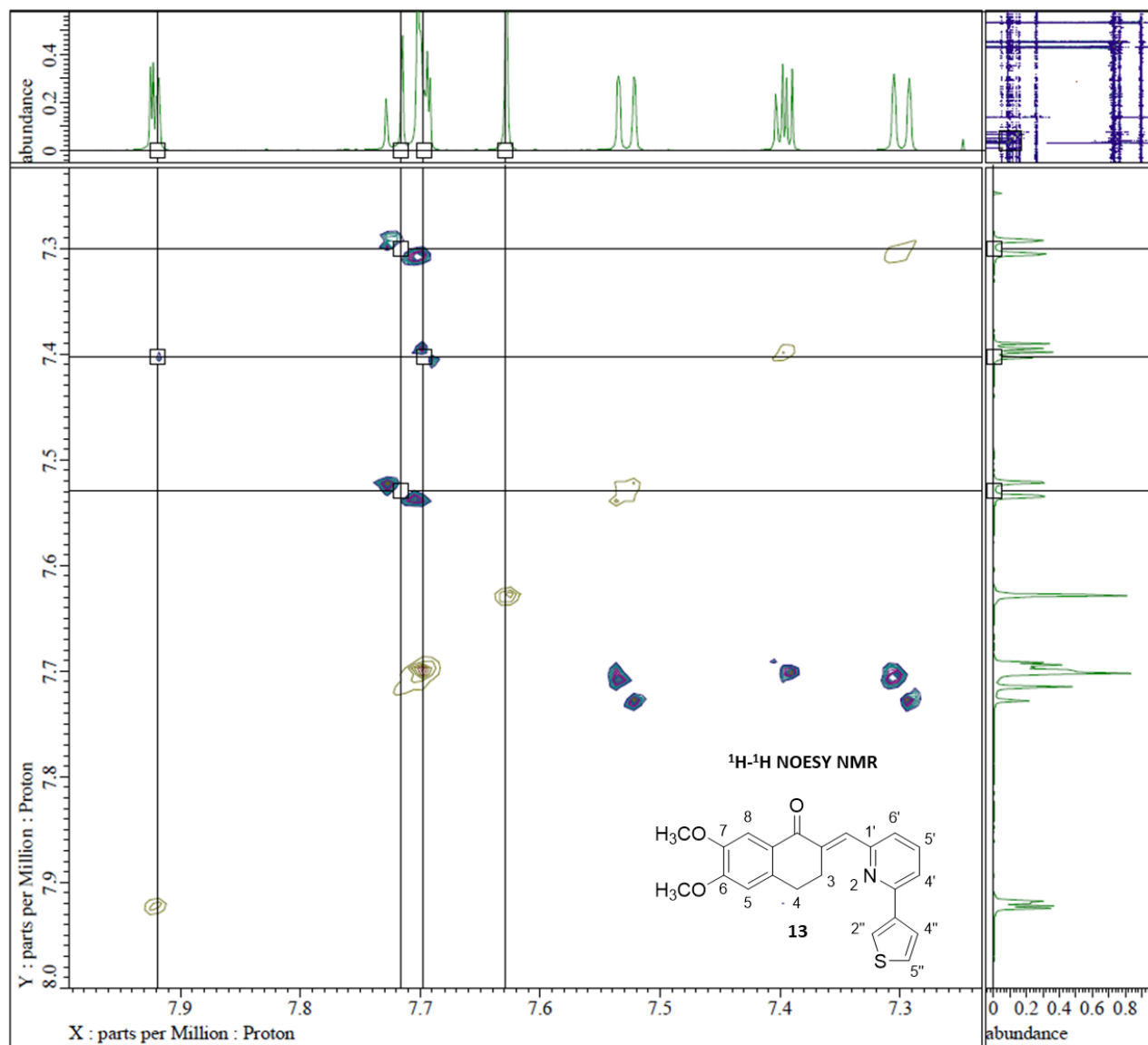


Figure 107. ¹H-¹H NOESY NMR of compound **13**.

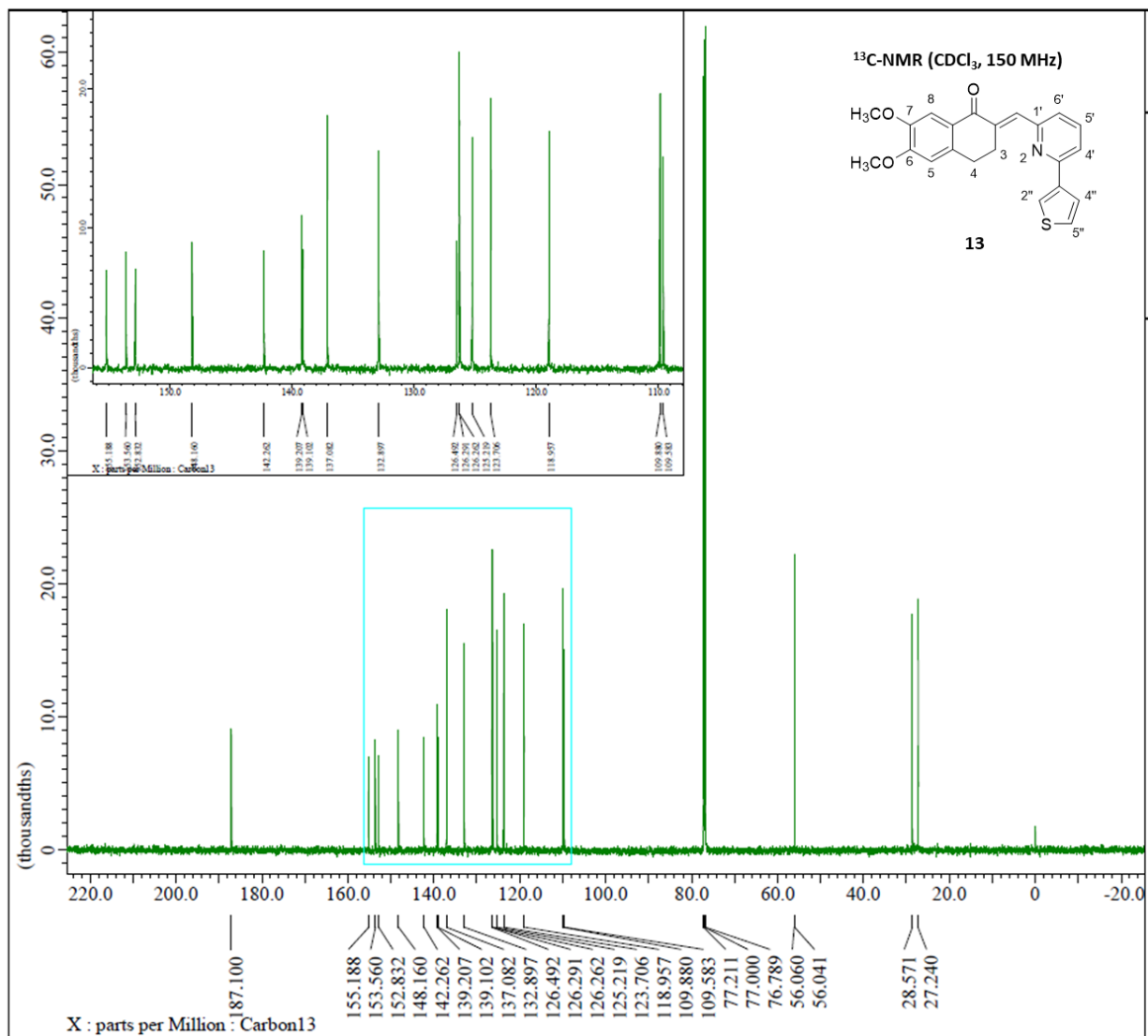


Figure 108. ¹³C-NMR spectrum (CDCl₃, 150 MHz) of compound **13**.

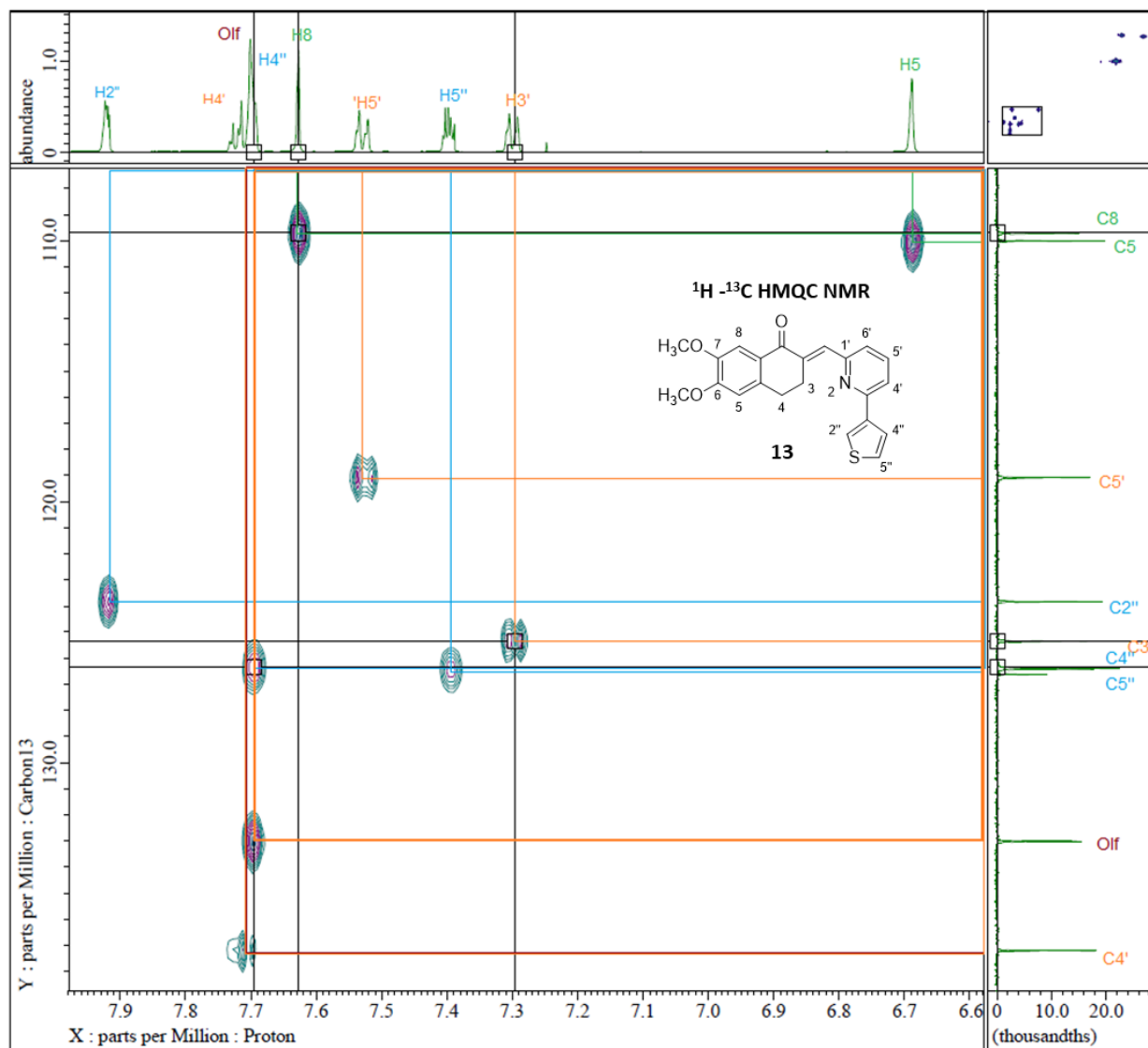


Figure 109. ^1H - ^{13}C HMQC NMR of compound **13**.

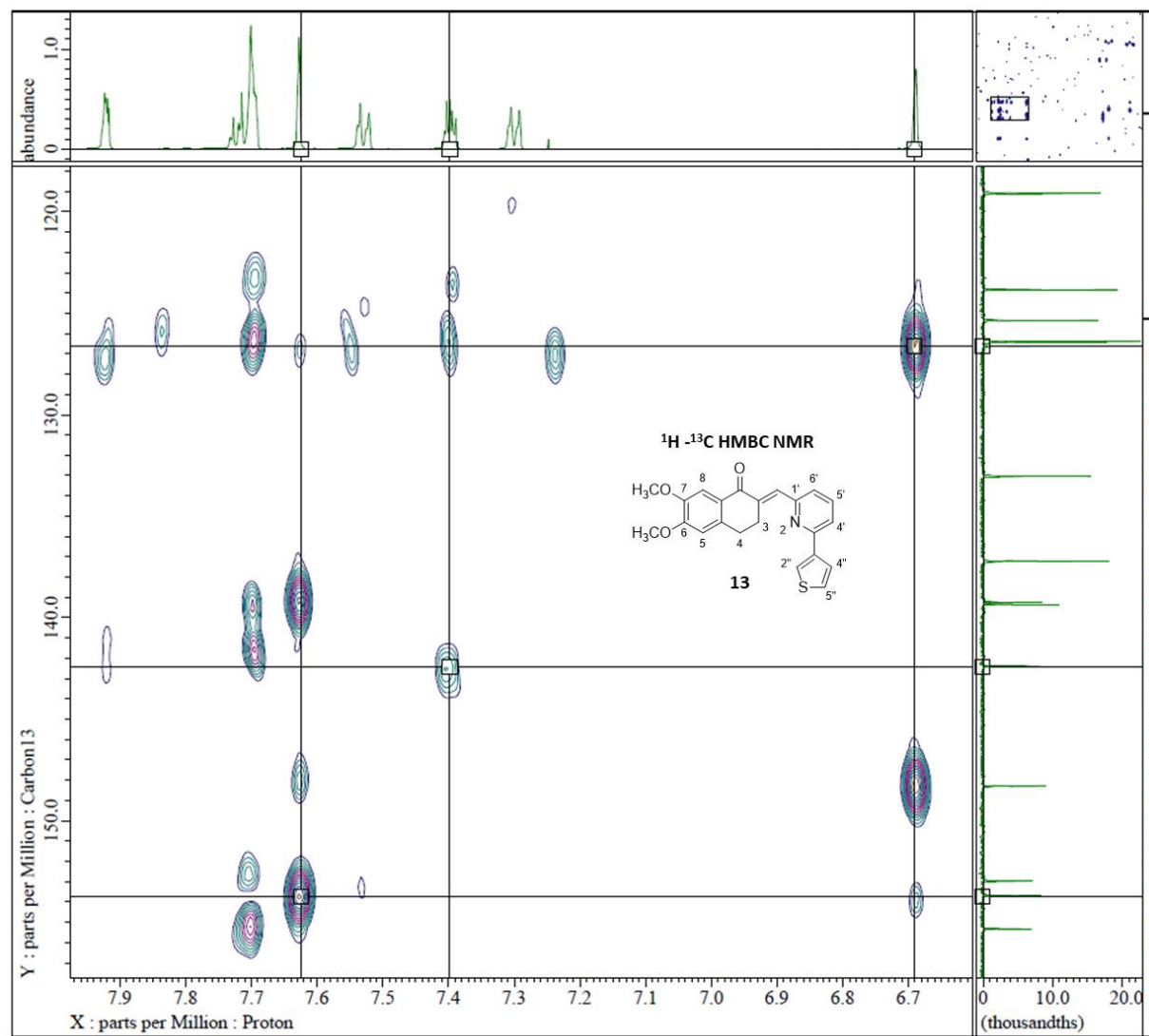


Figure 110. ^1H - ^{13}C HMBC NMR of compound **13**.

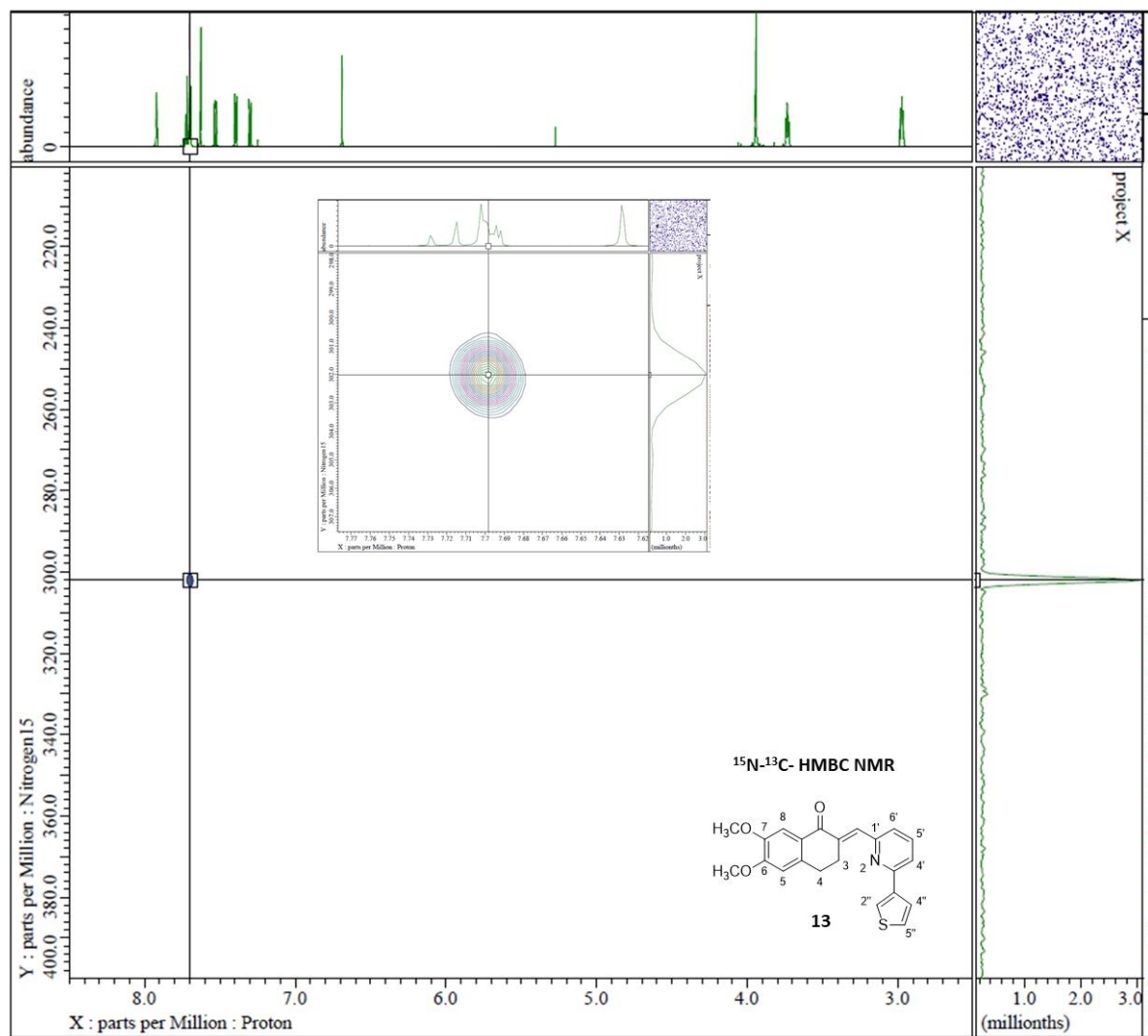


Figure 111. ^1H - ^{15}N HMBC NMR of compound **13**.

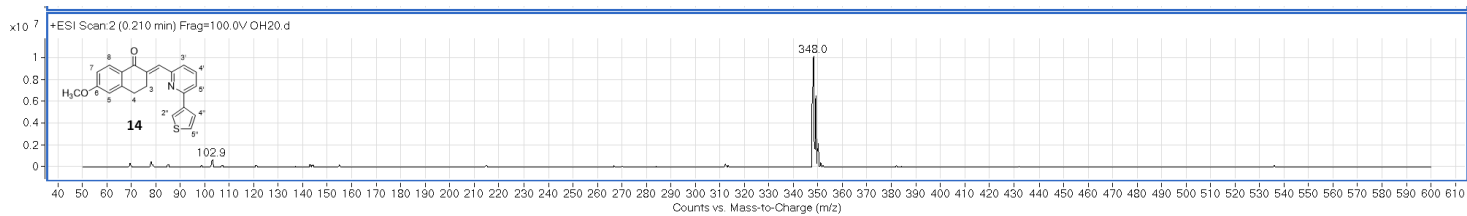


Figure 112. (+)-ESI Mass spectrum of compound 14.

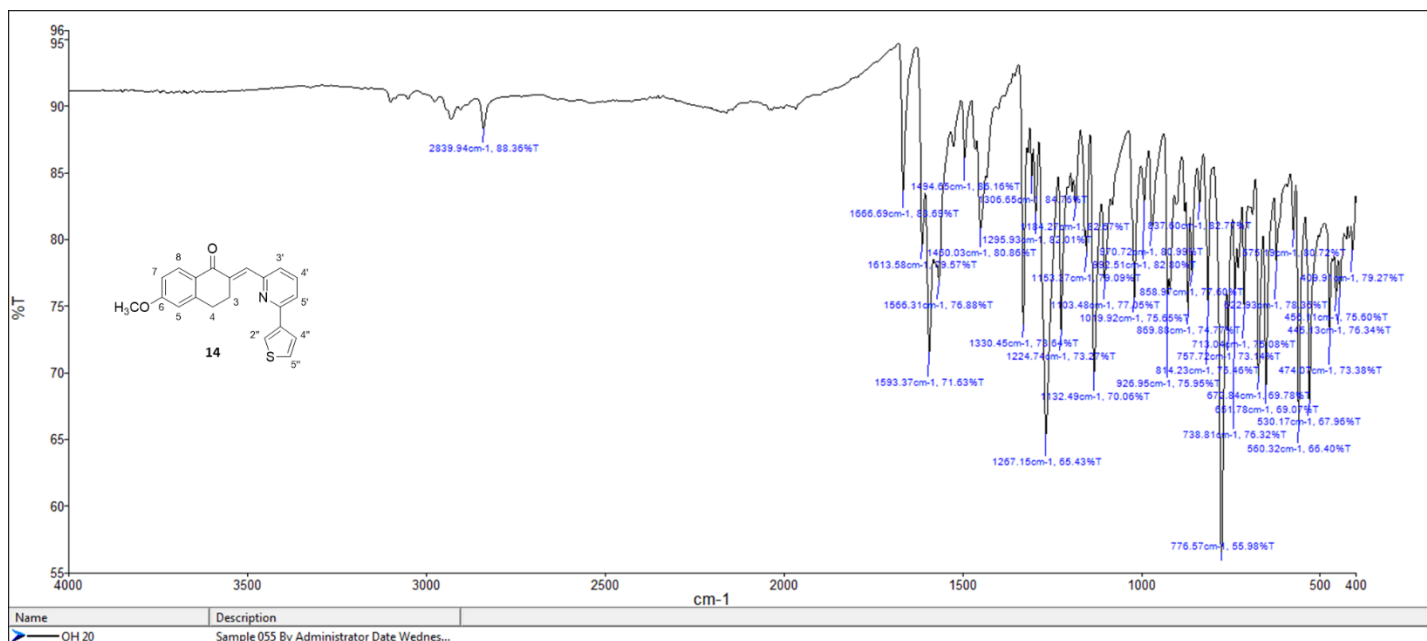


Figure 113. FT-IR spectrum of compound 14.

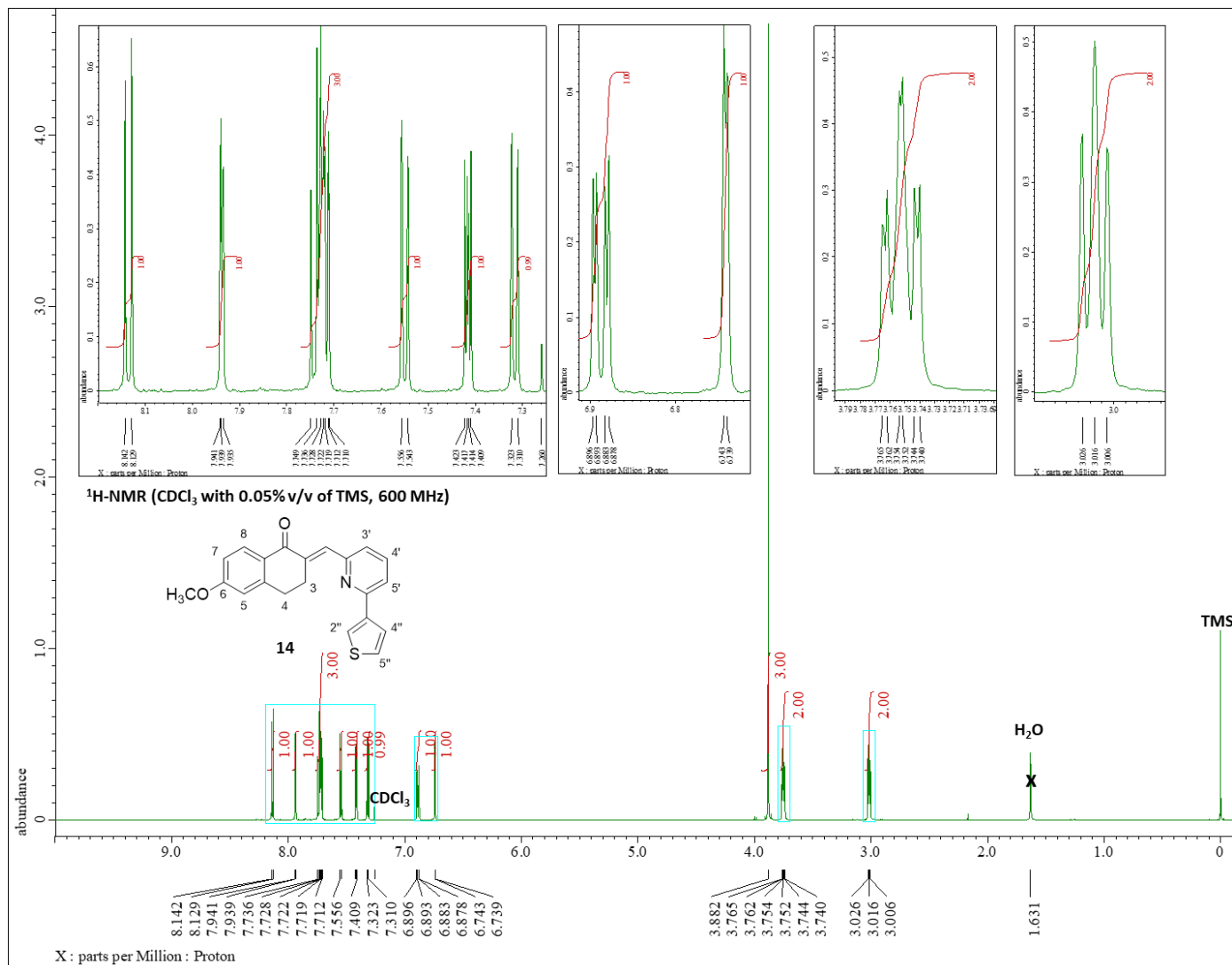


Figure 114. ¹H-NMR spectrum (CDCl₃ with 0.05% v/v of TMS, 600 MHz) of compound **14**.

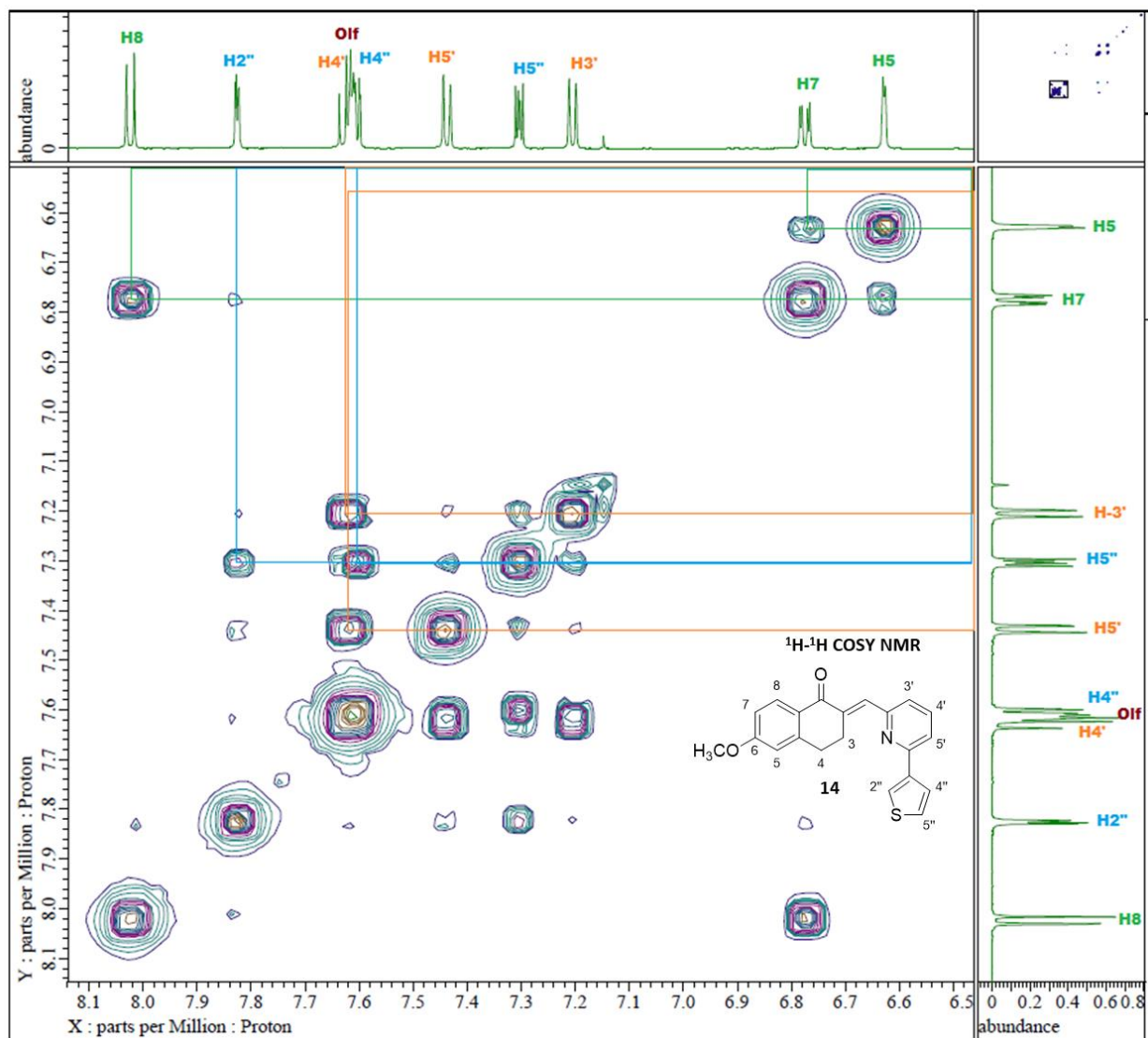


Figure 115. ^1H - ^1H COSY NMR of compound **14**.

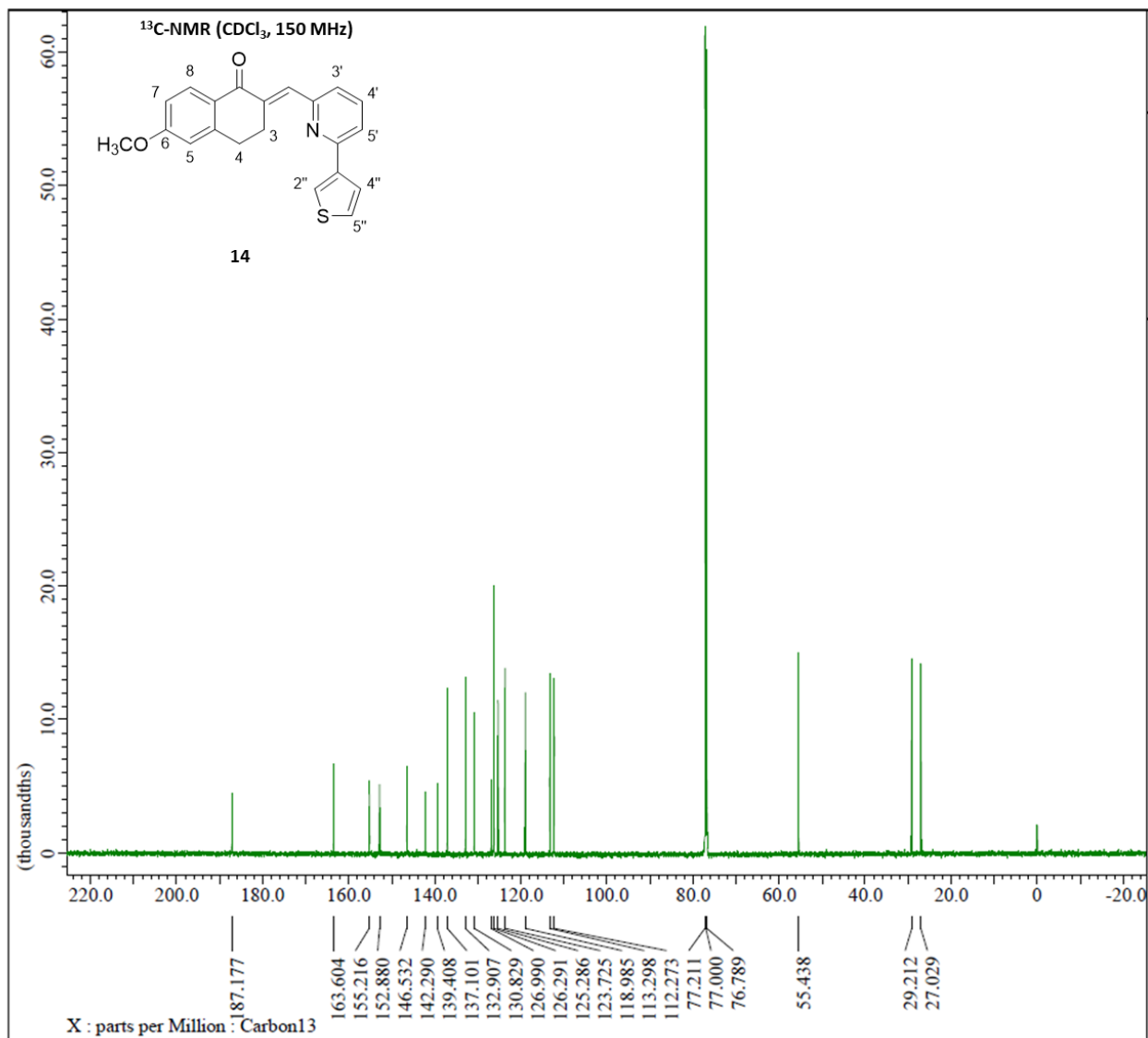


Figure 116. ¹³C-NMR spectrum (CDCl₃, 150 MHz) of compound **14**.

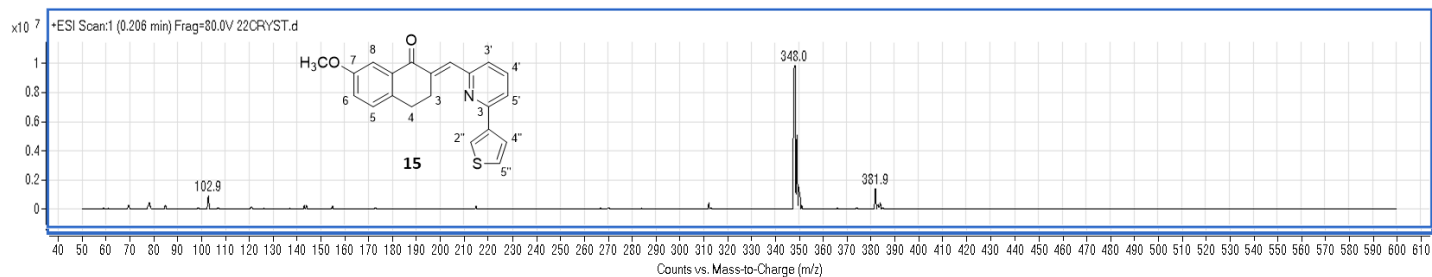


Figure 117. (+)-ESI Mass spectrum of compound 15.

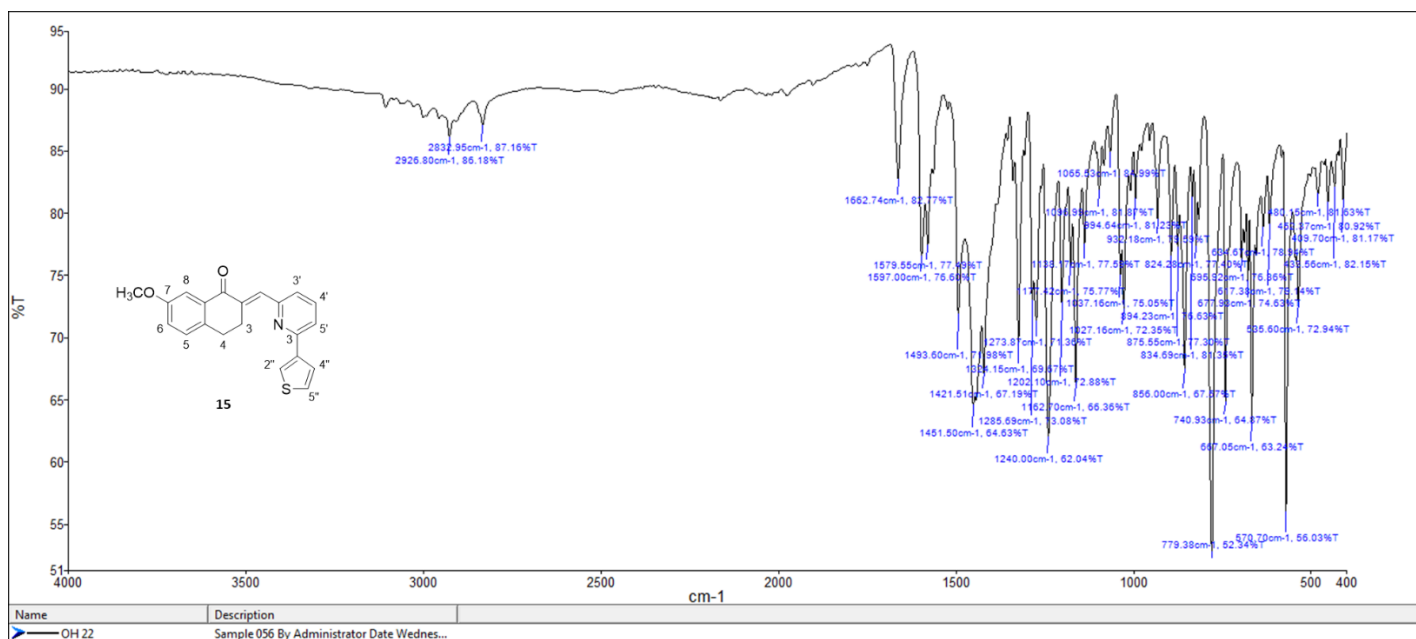


Figure 118. FT-IR spectrum of compound 15.

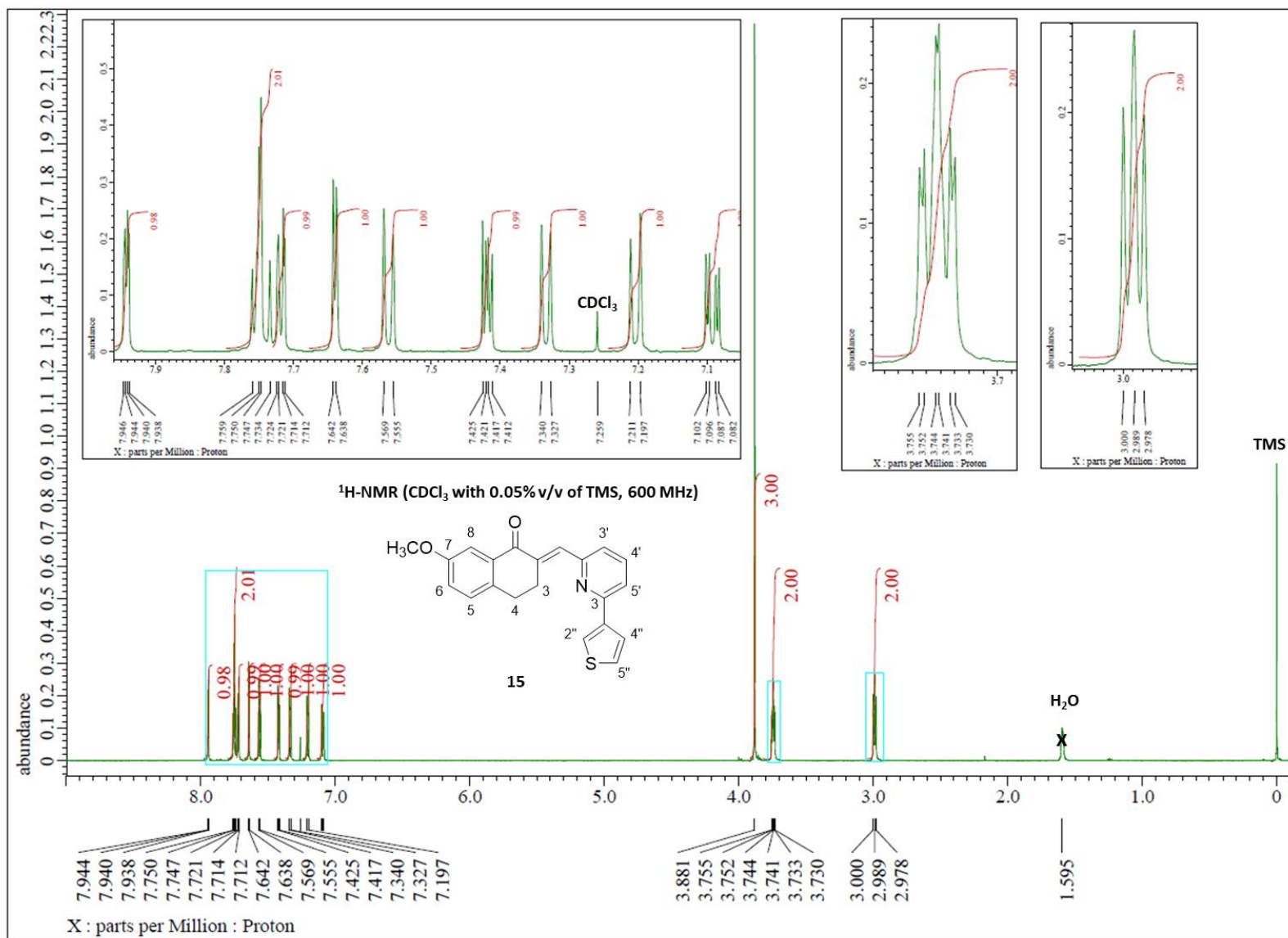


Figure 119. ¹H-NMR spectrum (CDCl₃ with 0.05% v/v of TMS, 600 MHz) of compound **15**.

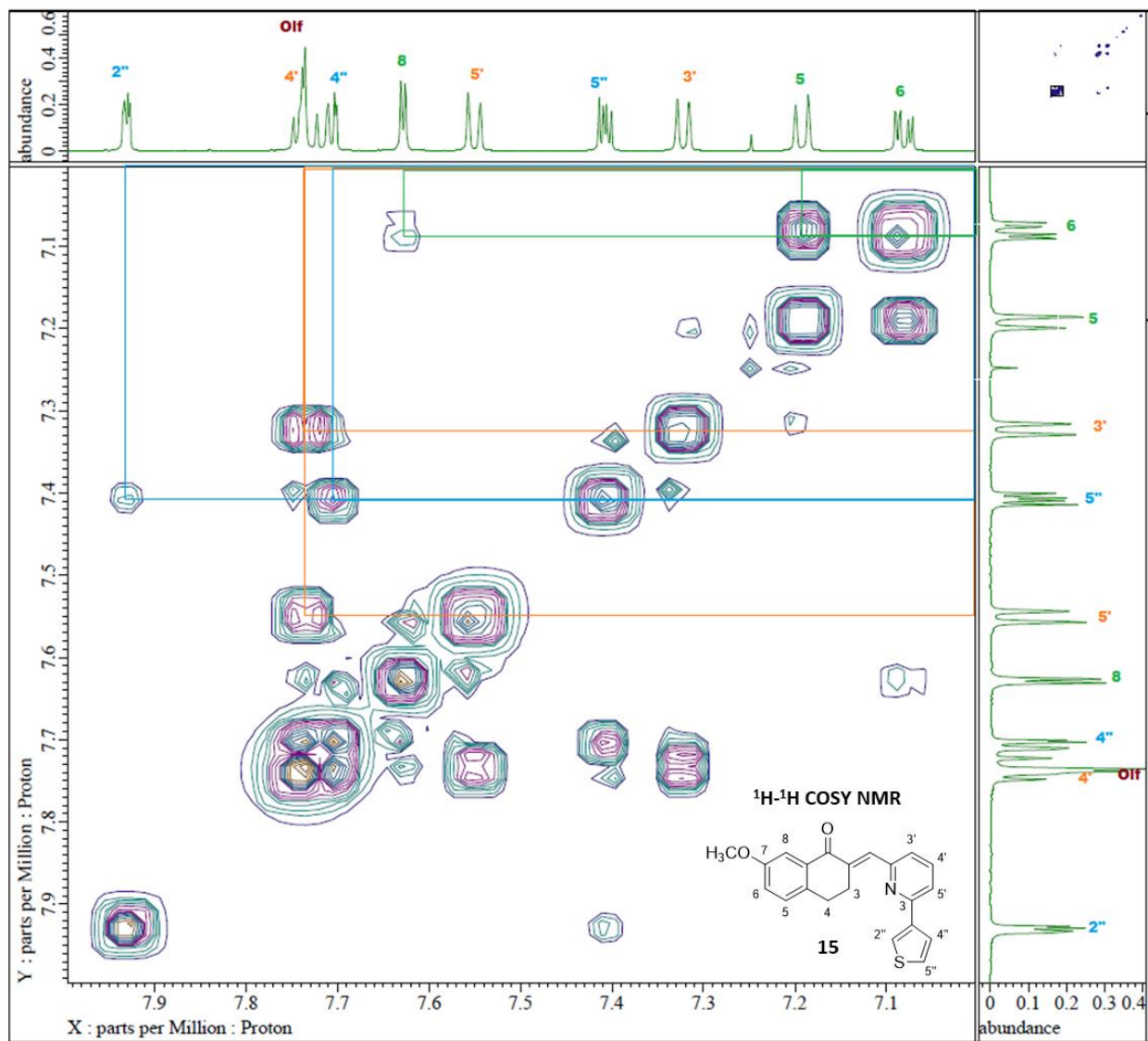


Figure 120. ¹H-¹H COSY NMR of compound **15**.

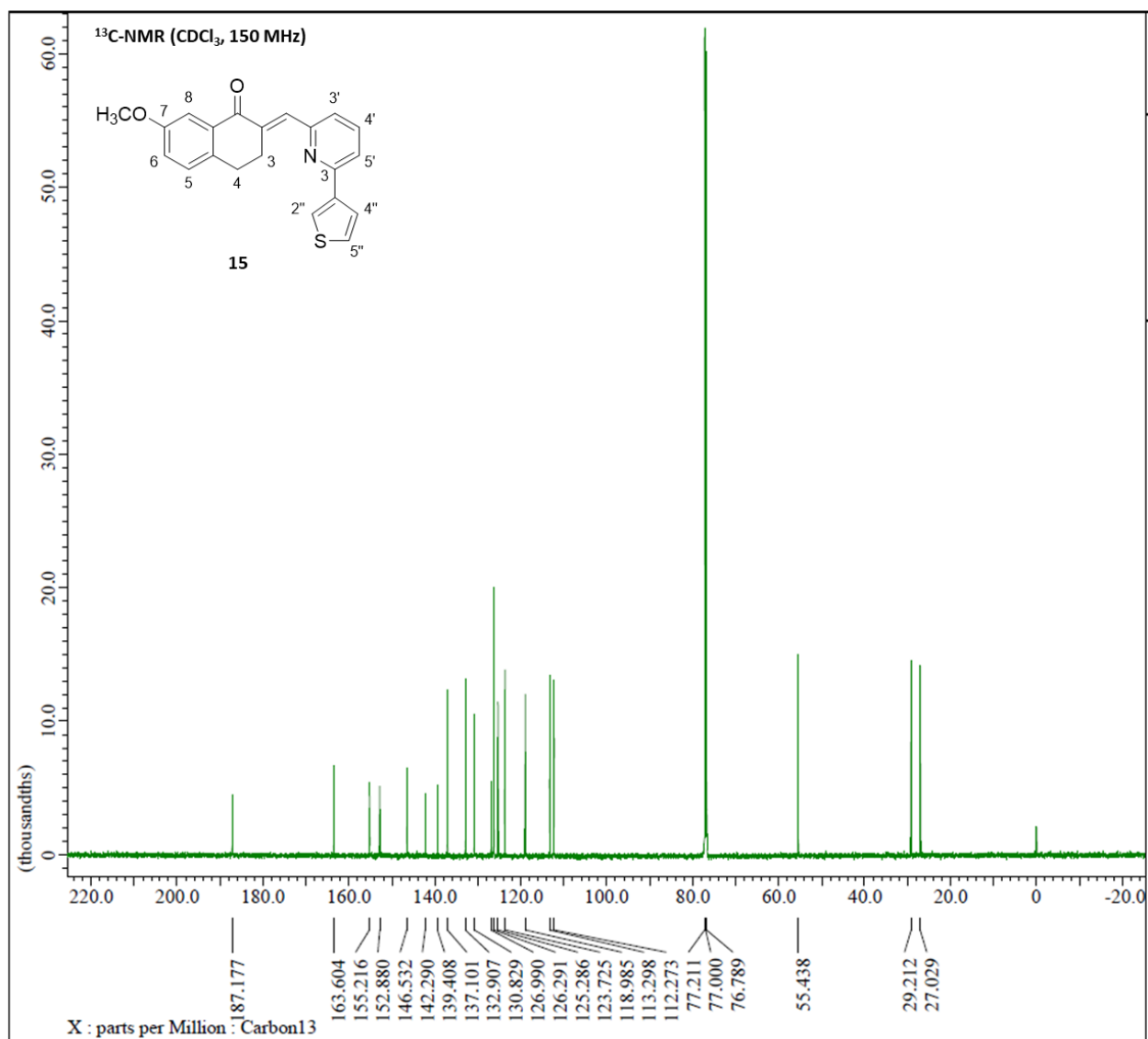


Figure 121. ¹³C-NMR spectrum (CDCl₃, 150 MHz) of compound **15**.

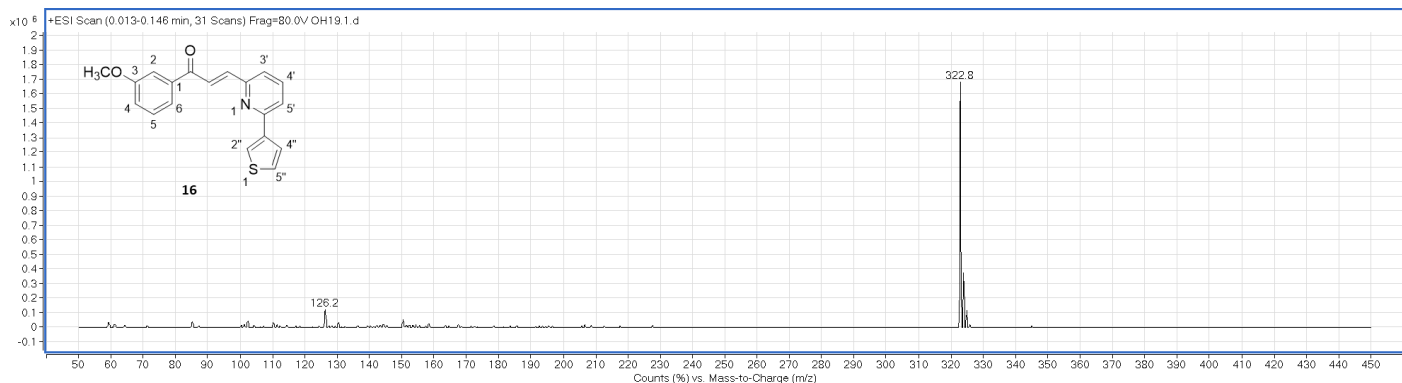


Figure 122. (+)-ESI Mass spectrum of compound 16.

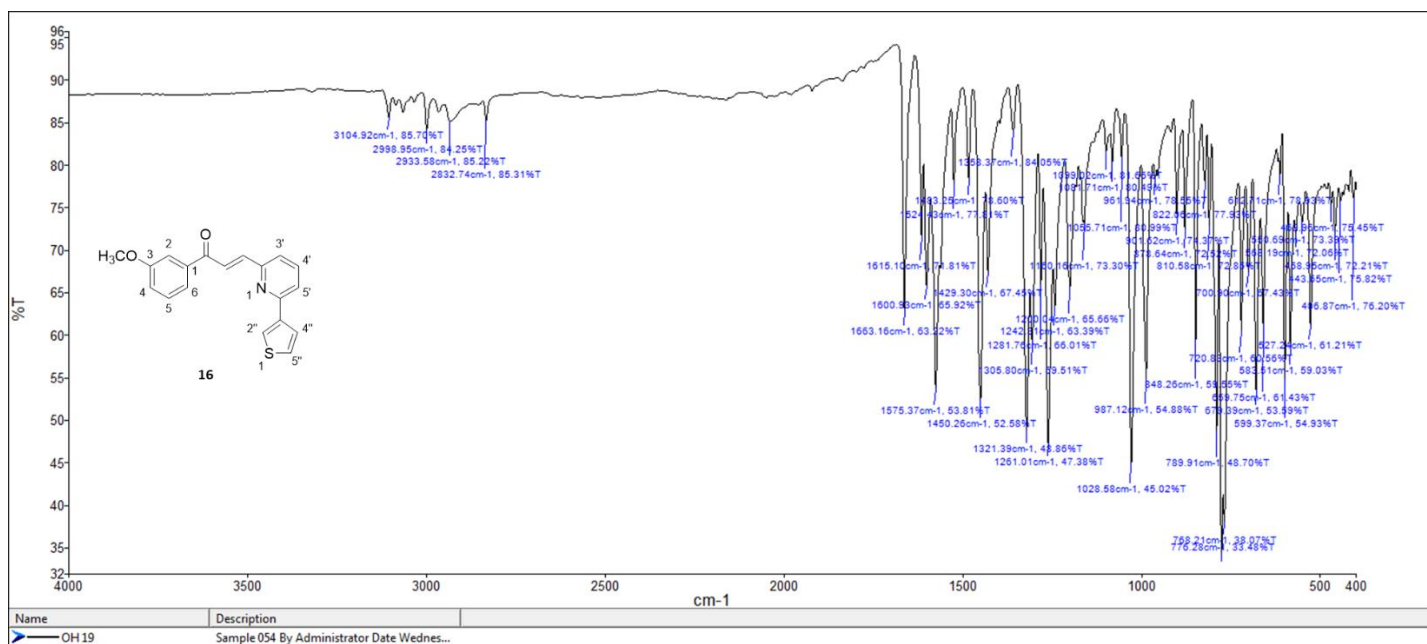


Figure 123. FT-IR spectrum of compound 16.

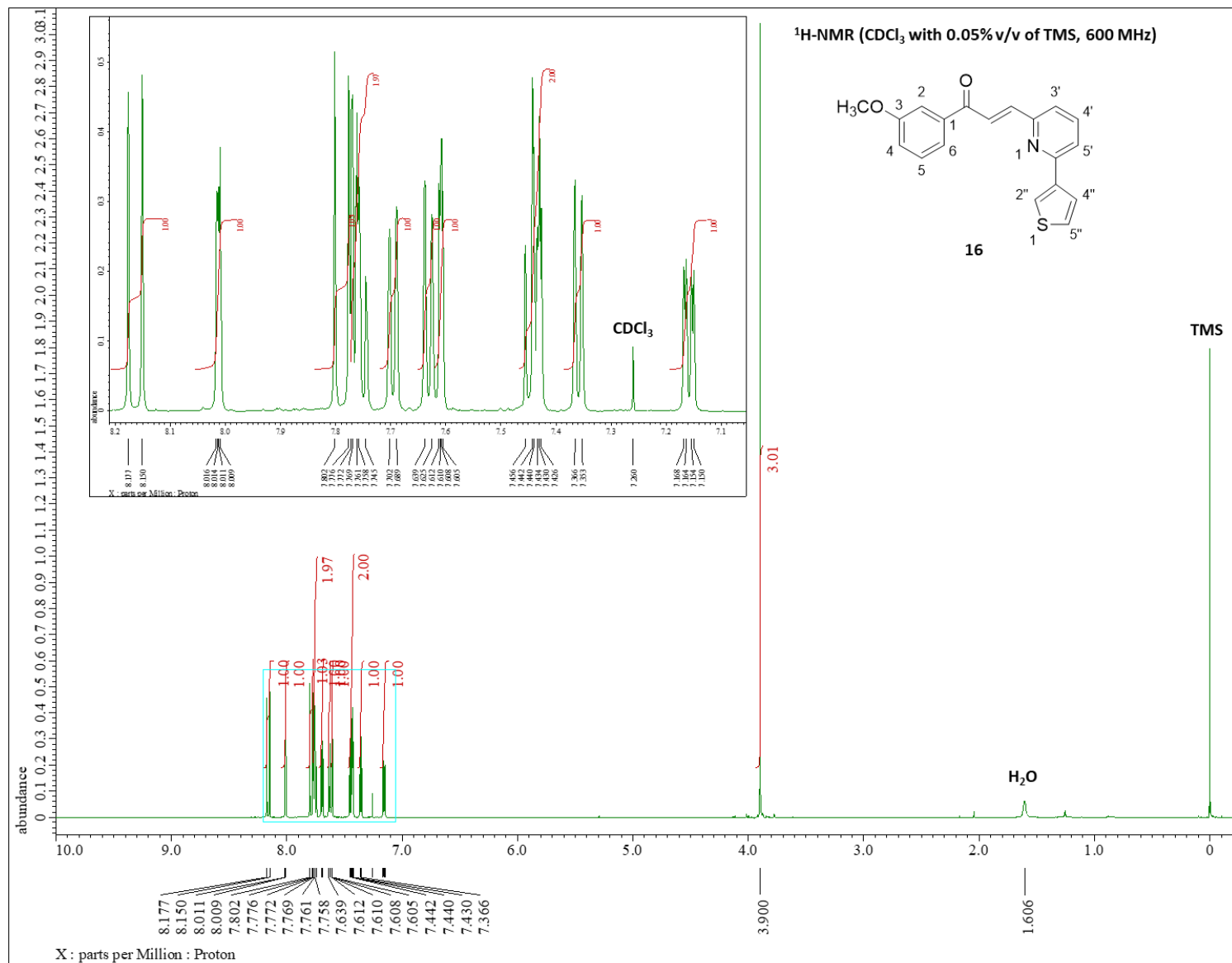


Figure 124. ¹H-NMR spectrum (CDCl₃ with 0.05% v/v of TMS, 600 MHz) of compound **16**.

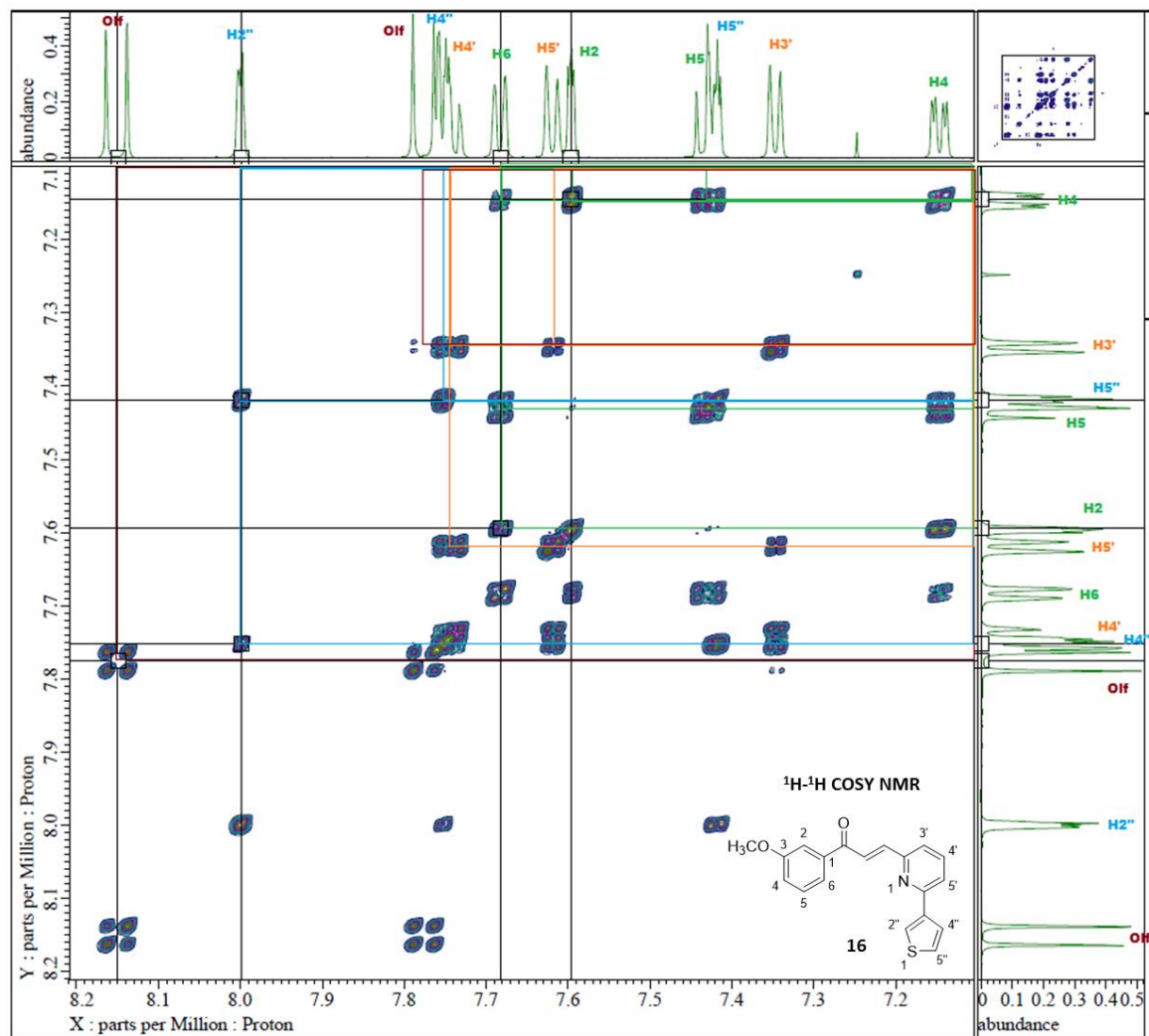


Figure 125. $^1\text{H}-^1\text{H}$ COSY NMR of compound **16**.

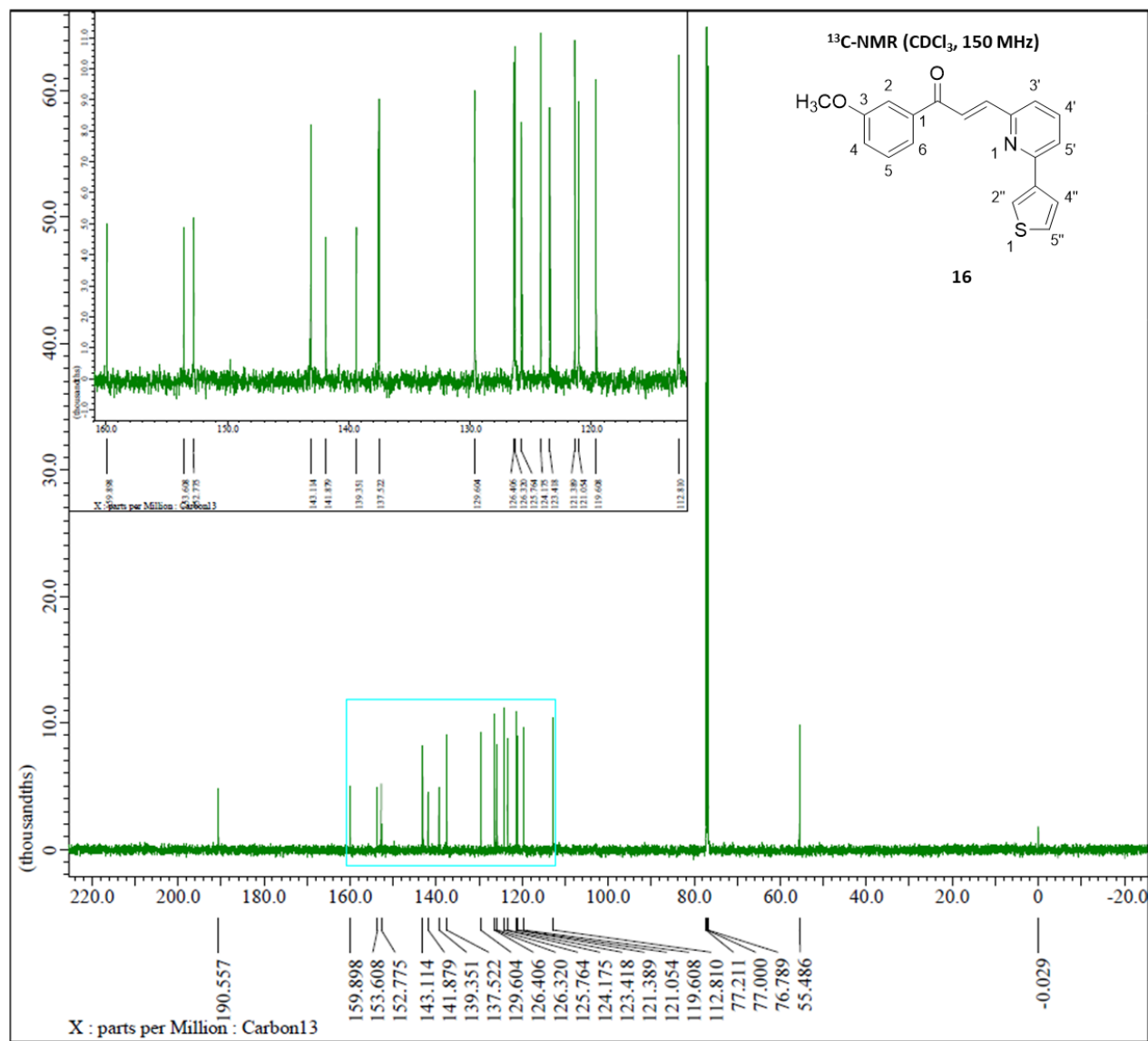


Figure 126. ¹³C-NMR spectrum (CDCl₃, 150 MHz) of compound **16**.

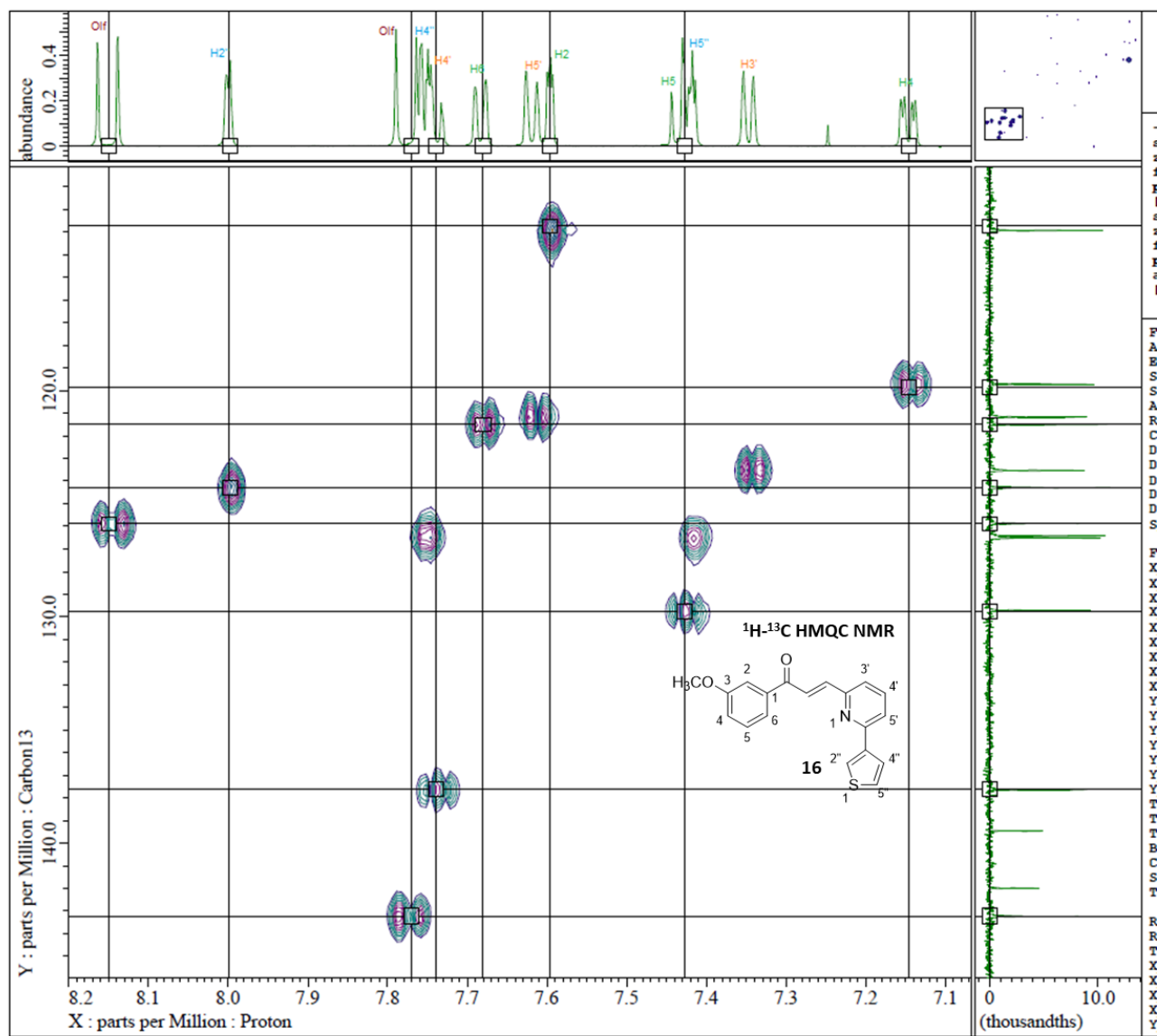


Figure 127. ¹H-¹³C HMQC NMR of compound **16**.

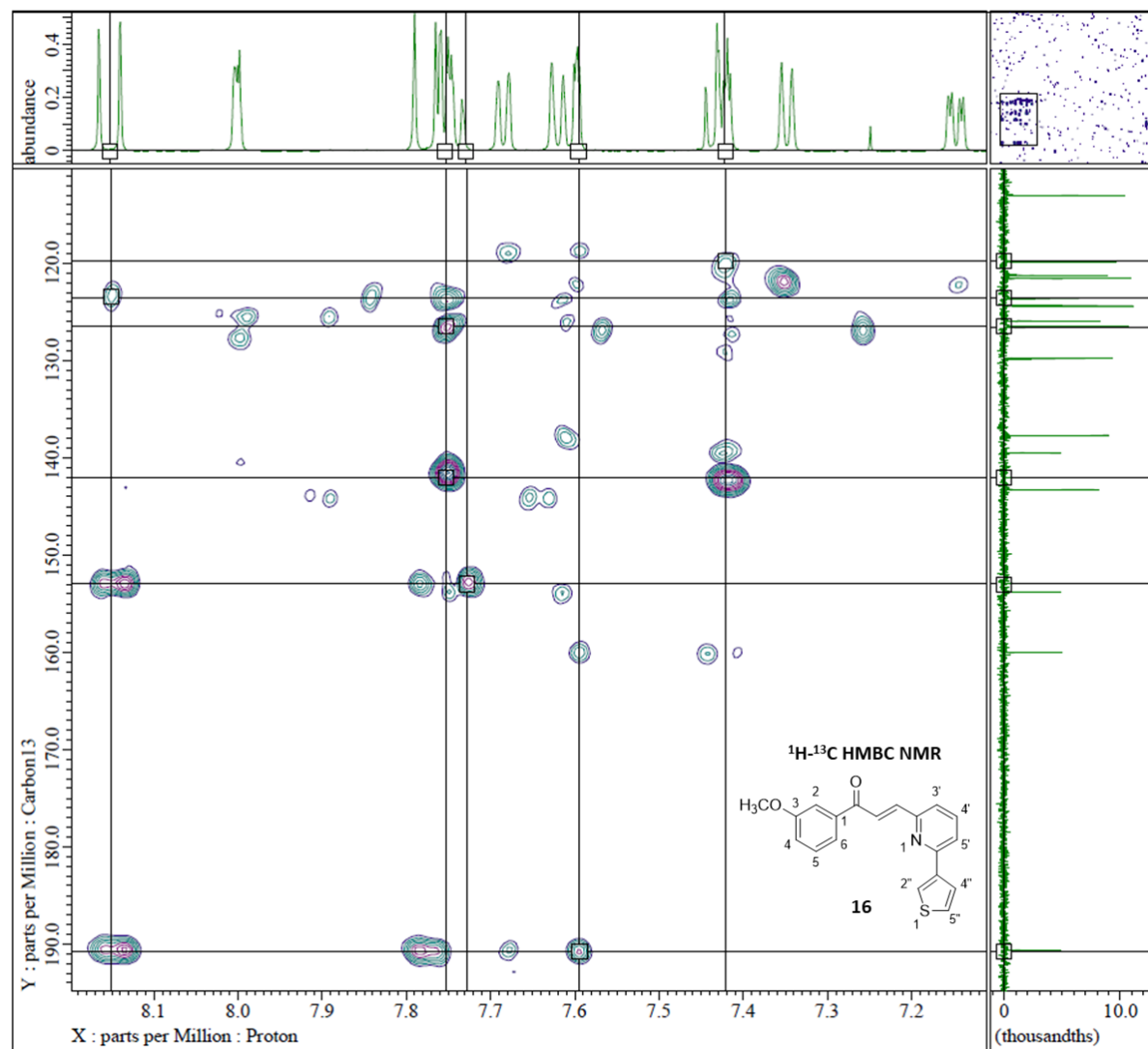


Figure 128. ^1H - ^{13}C HMBC NMR of compound **16**

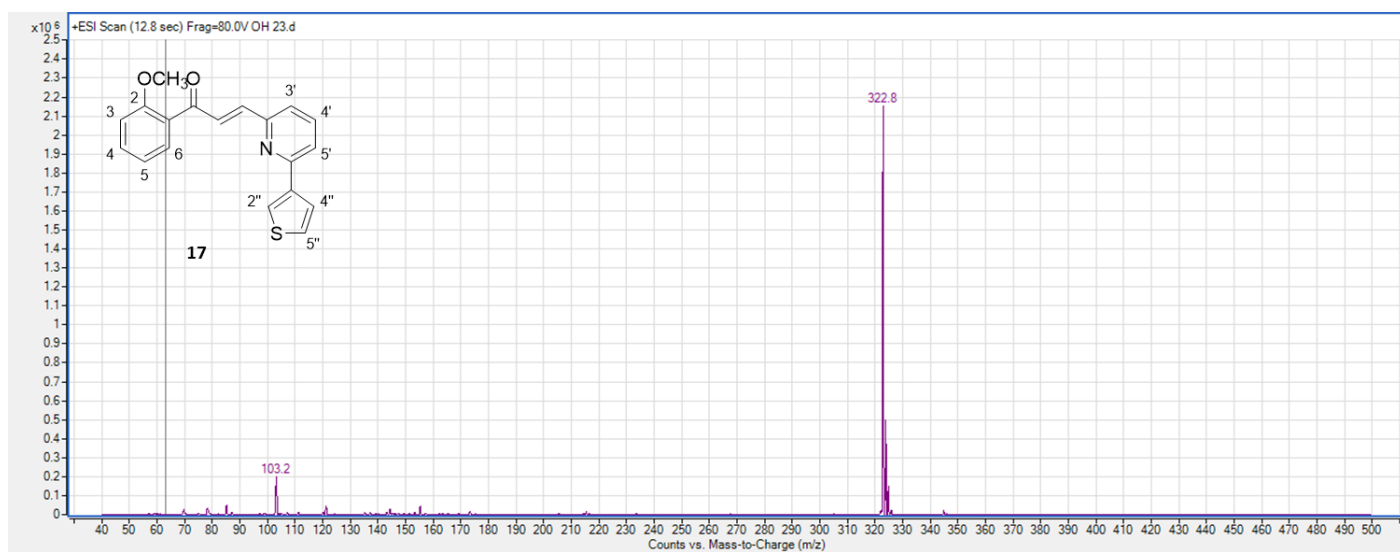


Figure 129. (+)-ESI Mass spectrum of compound **17**.

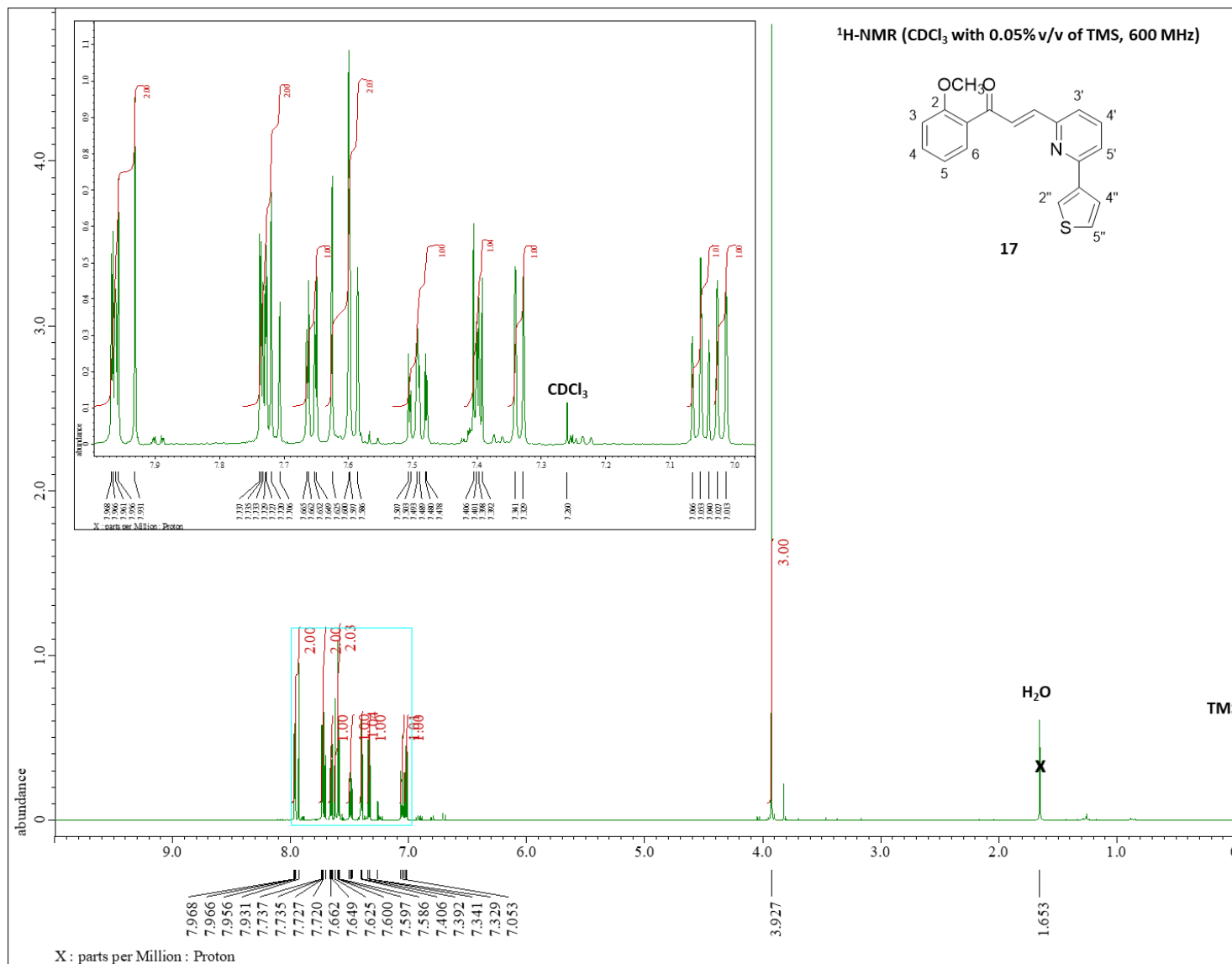


Figure 130. ¹H-NMR spectrum (CDCl₃ with 0.05% v/v of TMS, 600 MHz) of compound **17**.

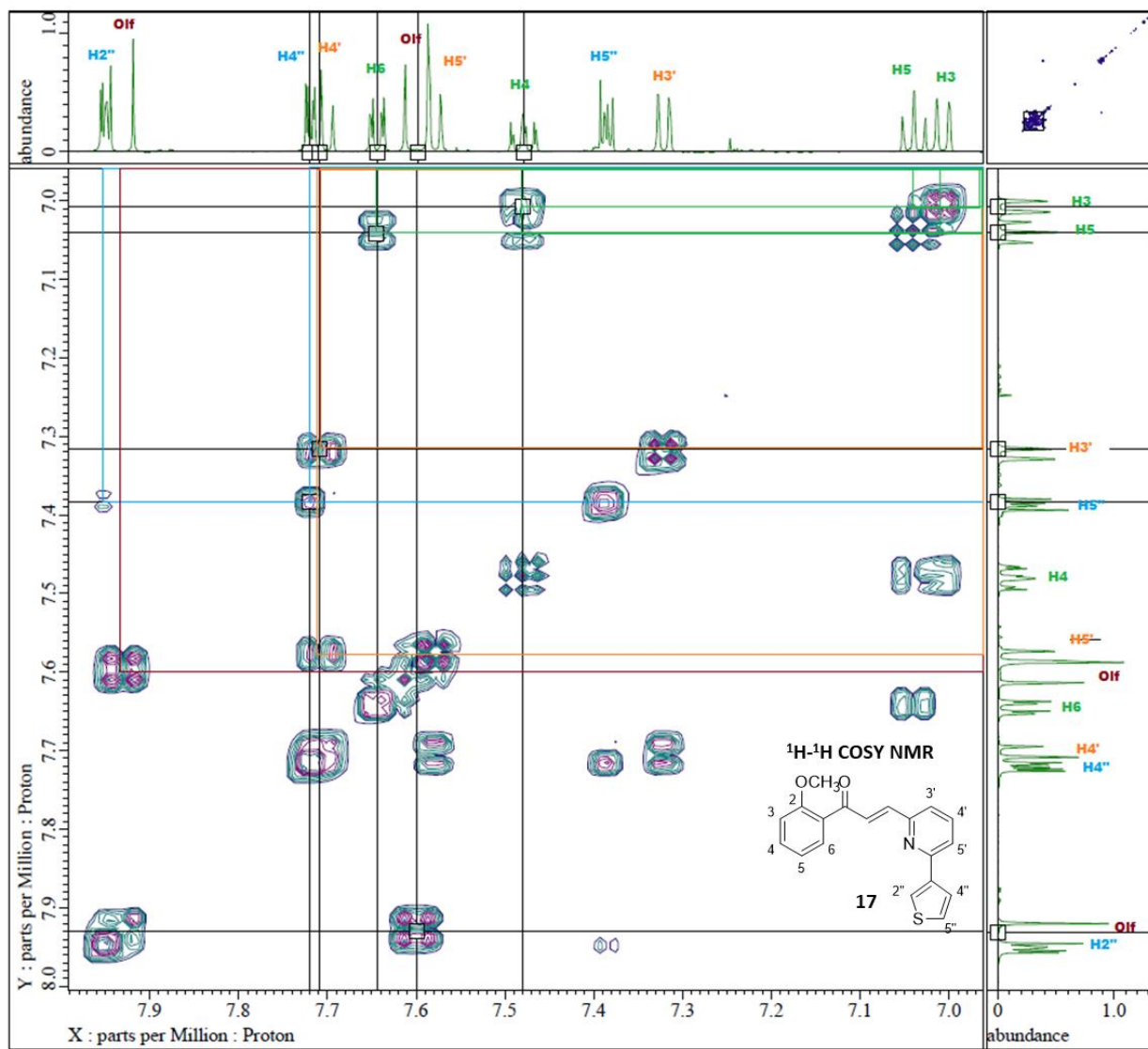


Figure 131. ¹H-¹H COSY NMR of compound **17**.

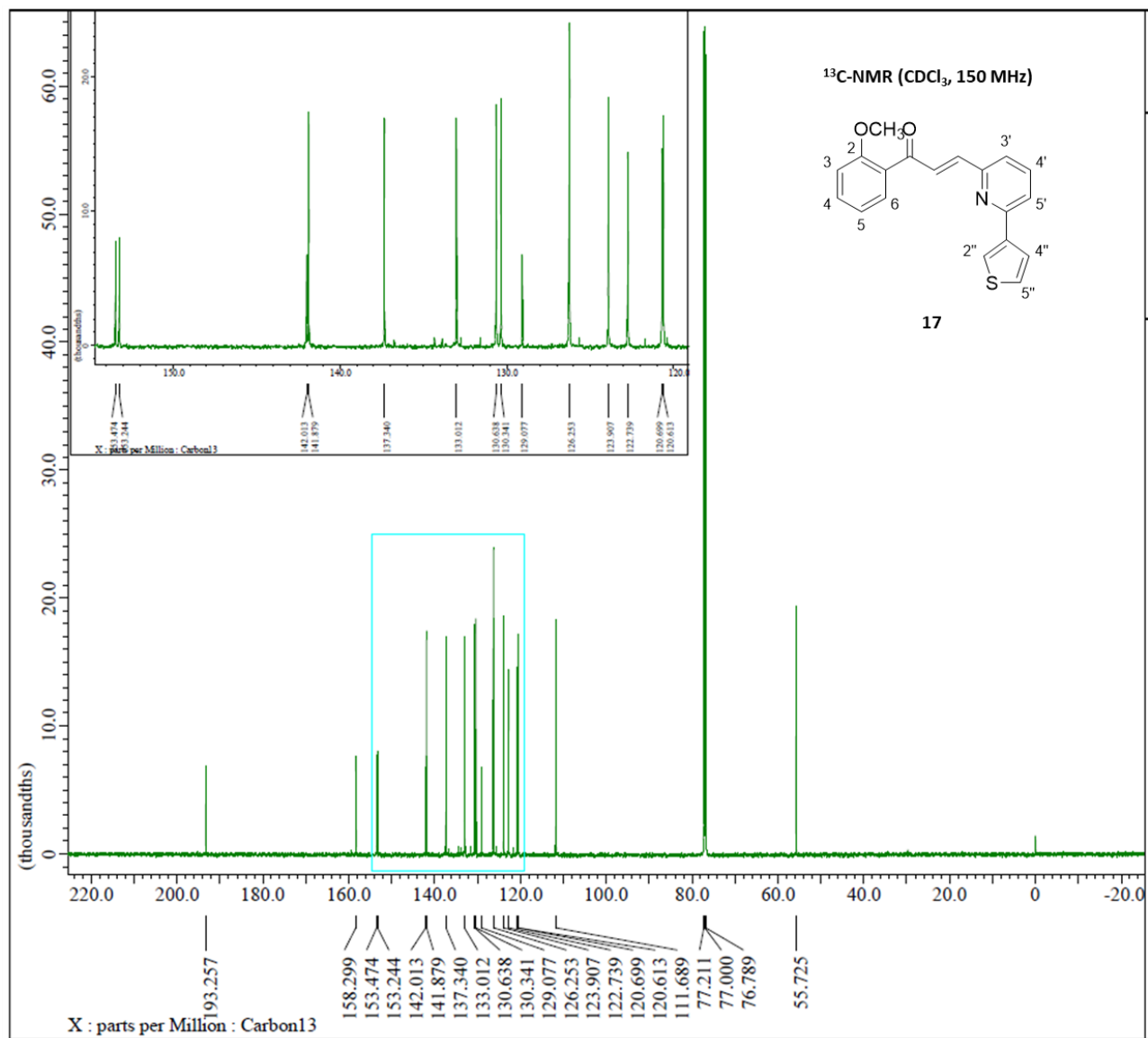


Figure 132. ¹³C-NMR spectrum (CDCl₃, 150 MHz) of compound **17**.

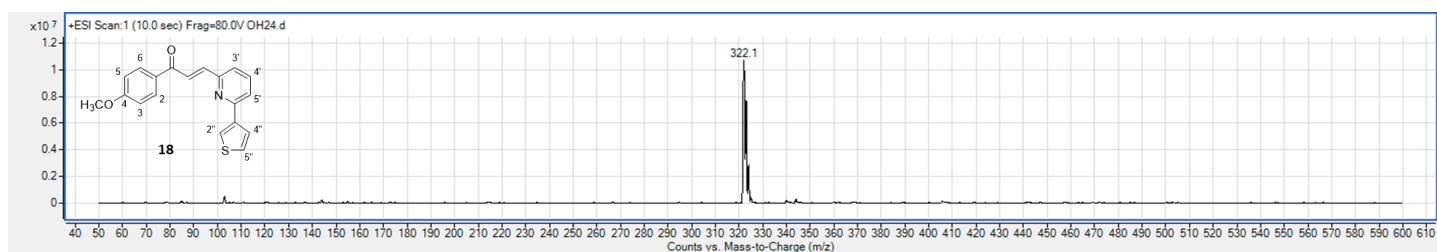


Figure 133. (+)-ESI Mass spectrum of compound 18.

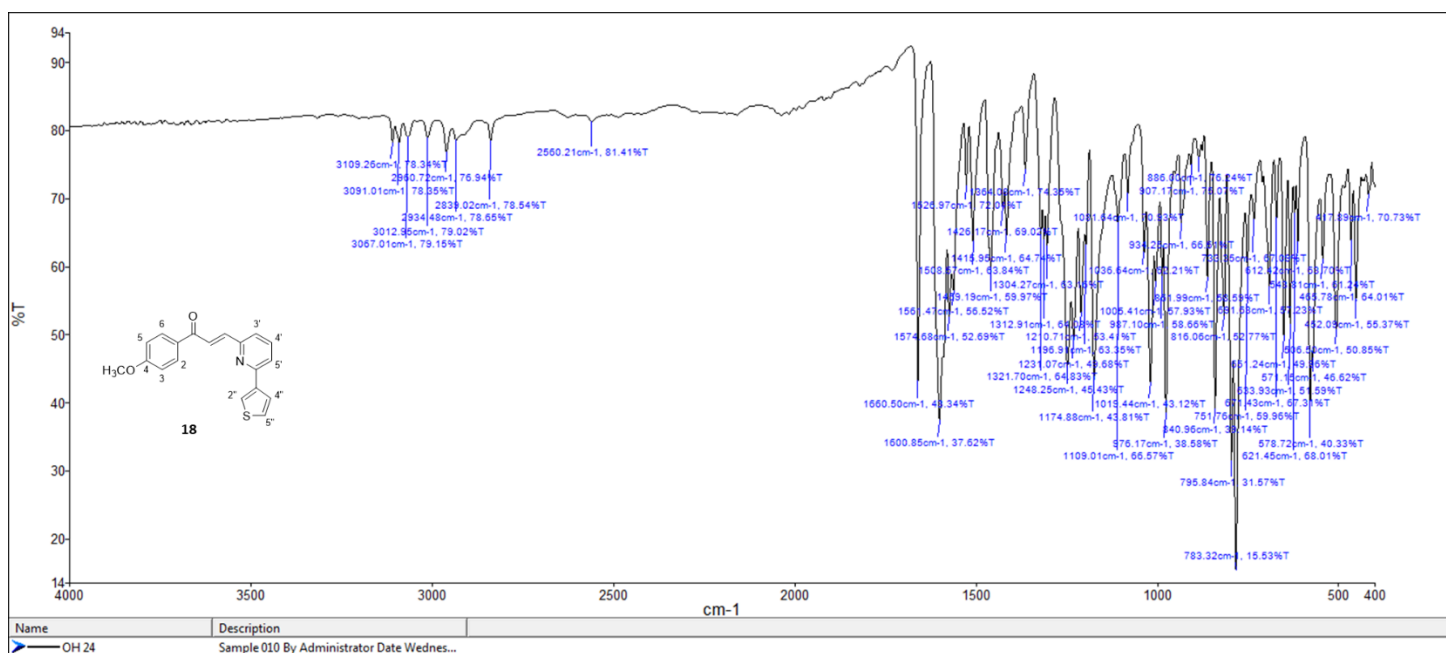


Figure 134. FT-IR spectrum of compound 18.

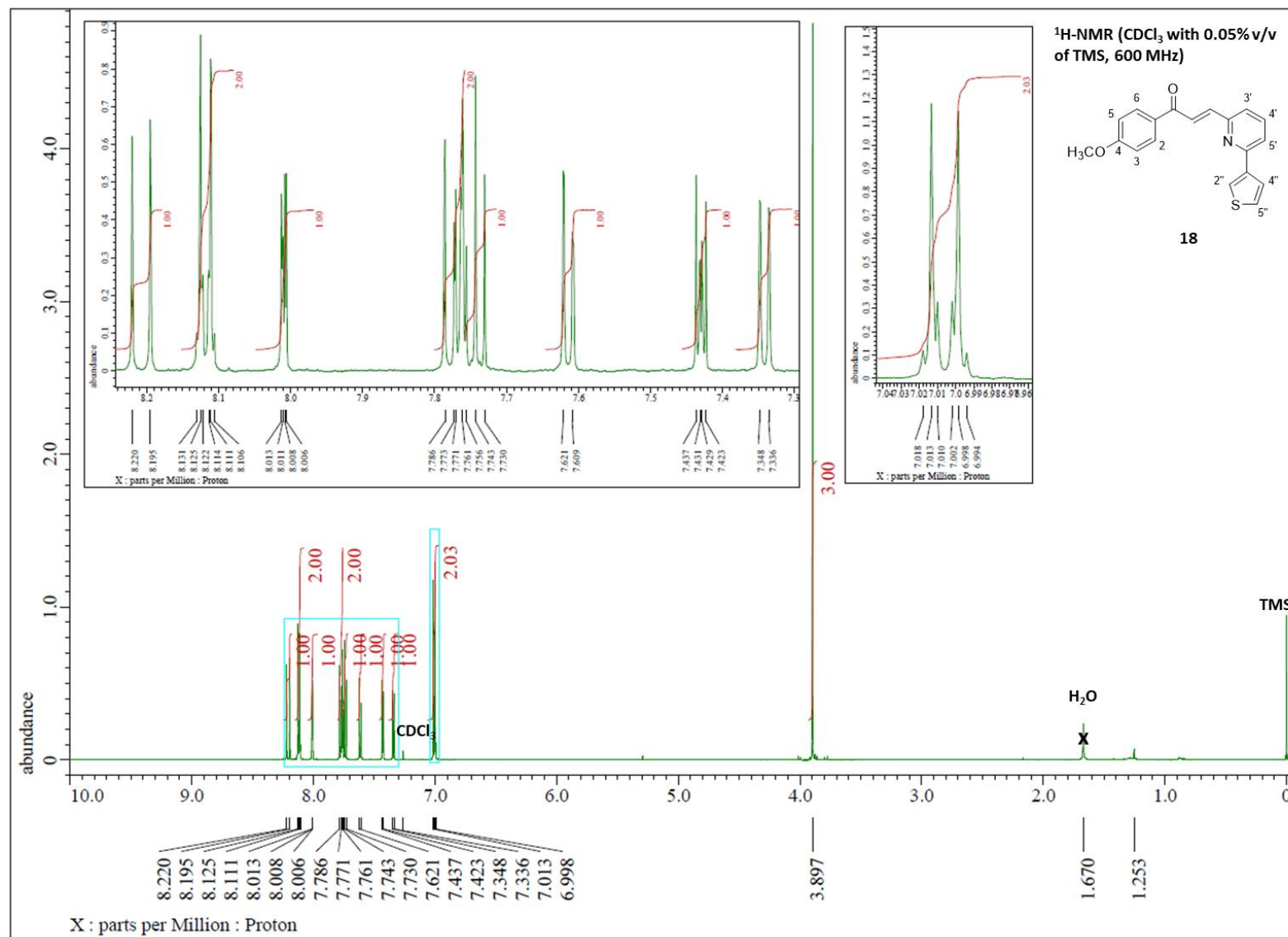


Figure 135. ¹H-NMR spectrum (CDCl₃ with 0.05% v/v of TMS, 600 MHz) of compound **18**.

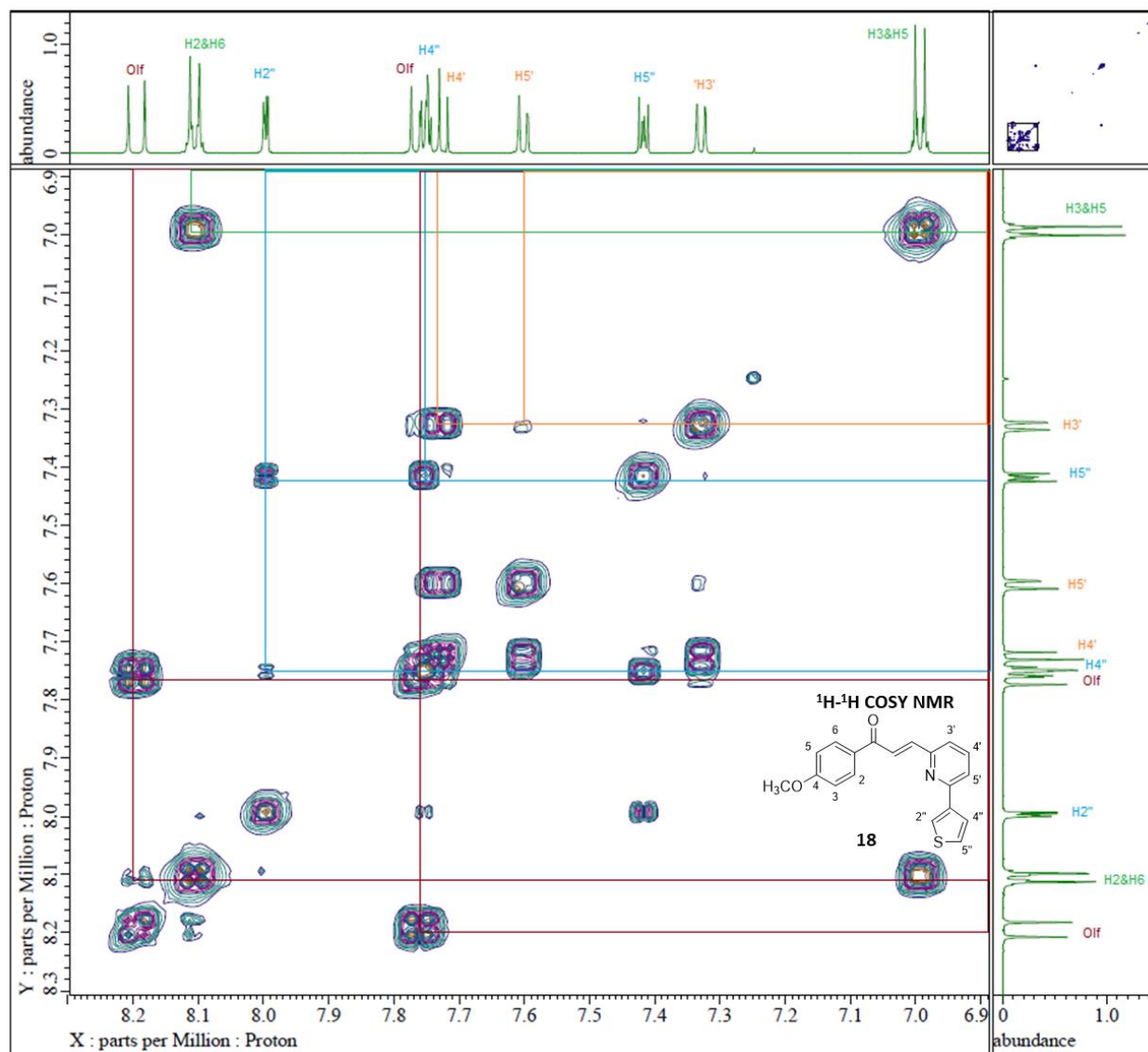


Figure 136. ¹H-¹H COSY NMR of compound **18**.

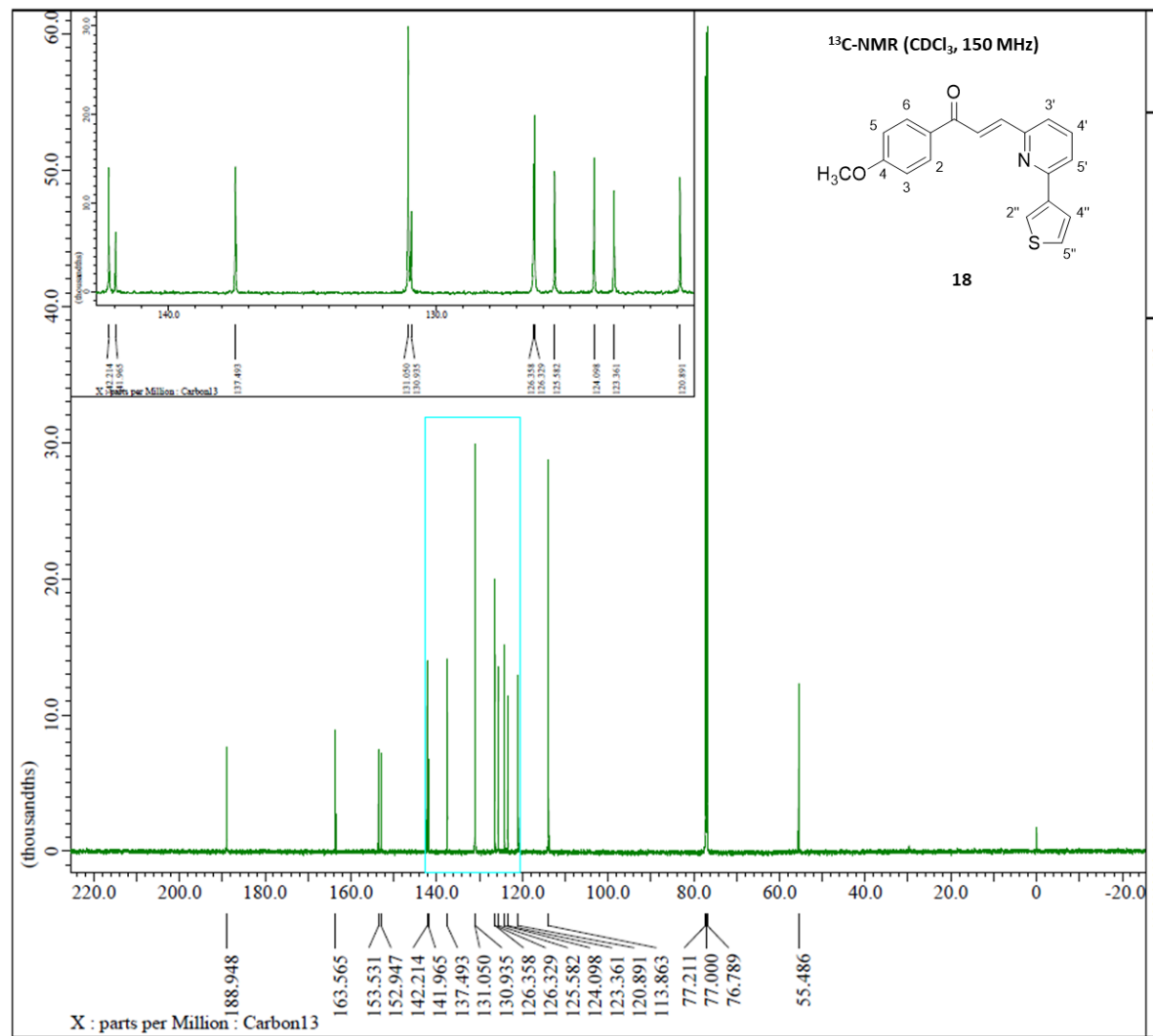


Figure 137. ¹³C-NMR spectrum (CDCl₃, 150 MHz) of compound **18**.

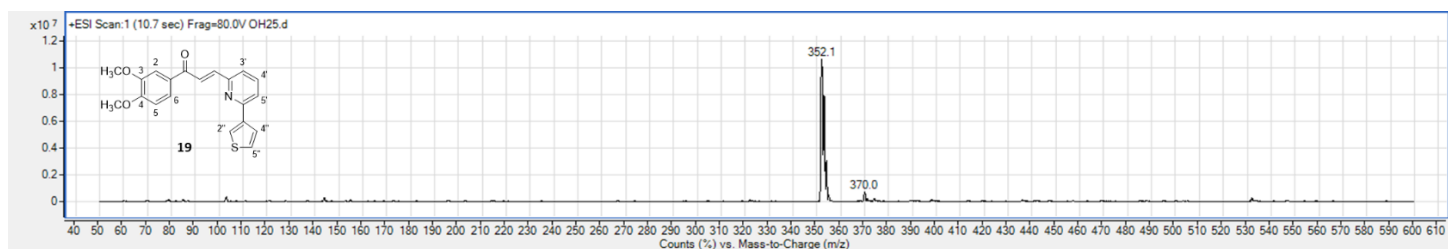


Figure 138. (+)-ESI Mass spectrum of compound 19.

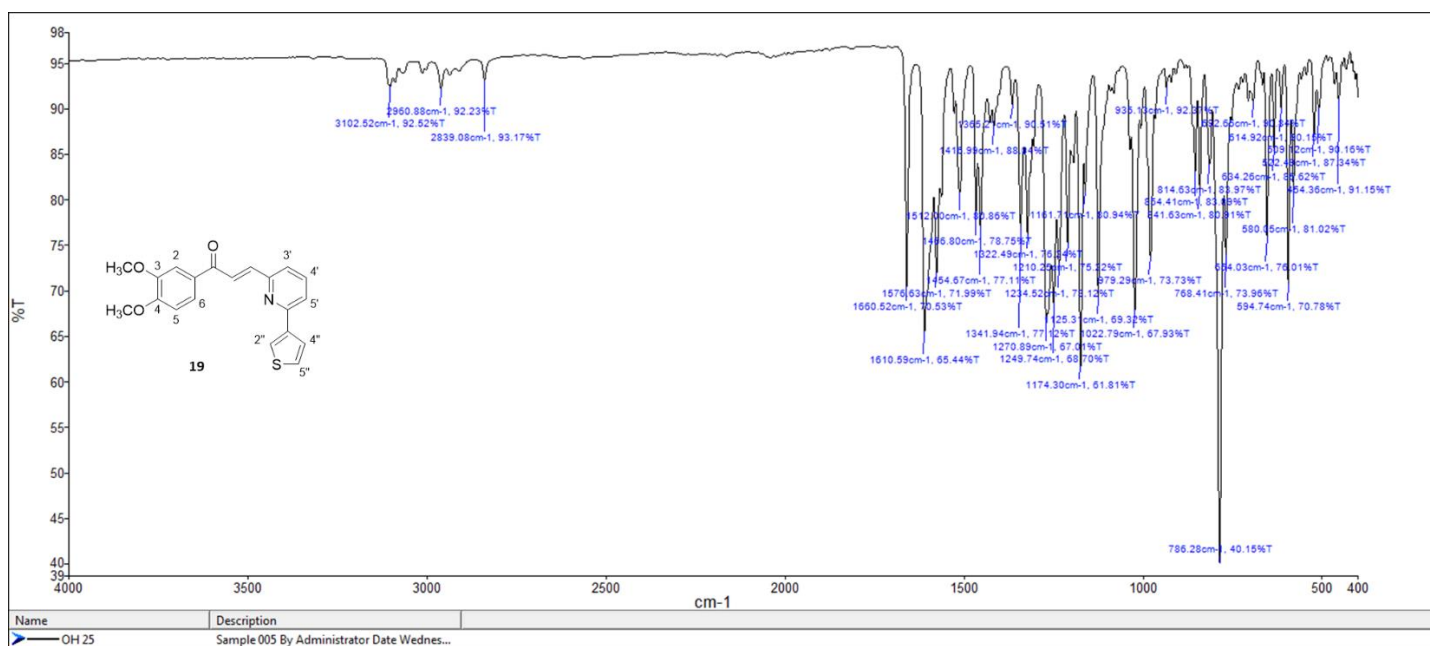


Figure 139. FT-IR spectrum of compound 19.

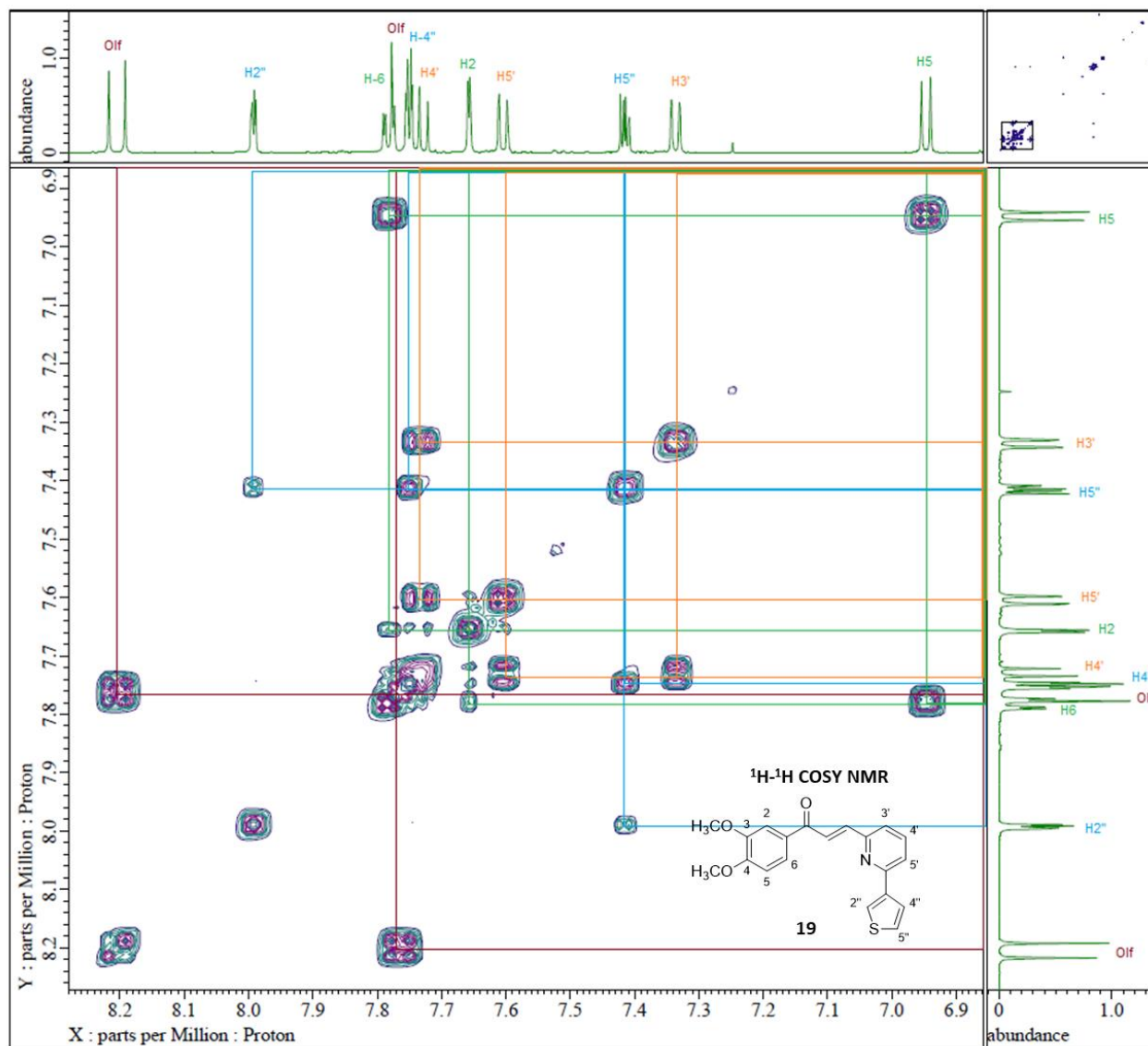


Figure 141. ¹H-¹H COSY NMR of compound **19**.

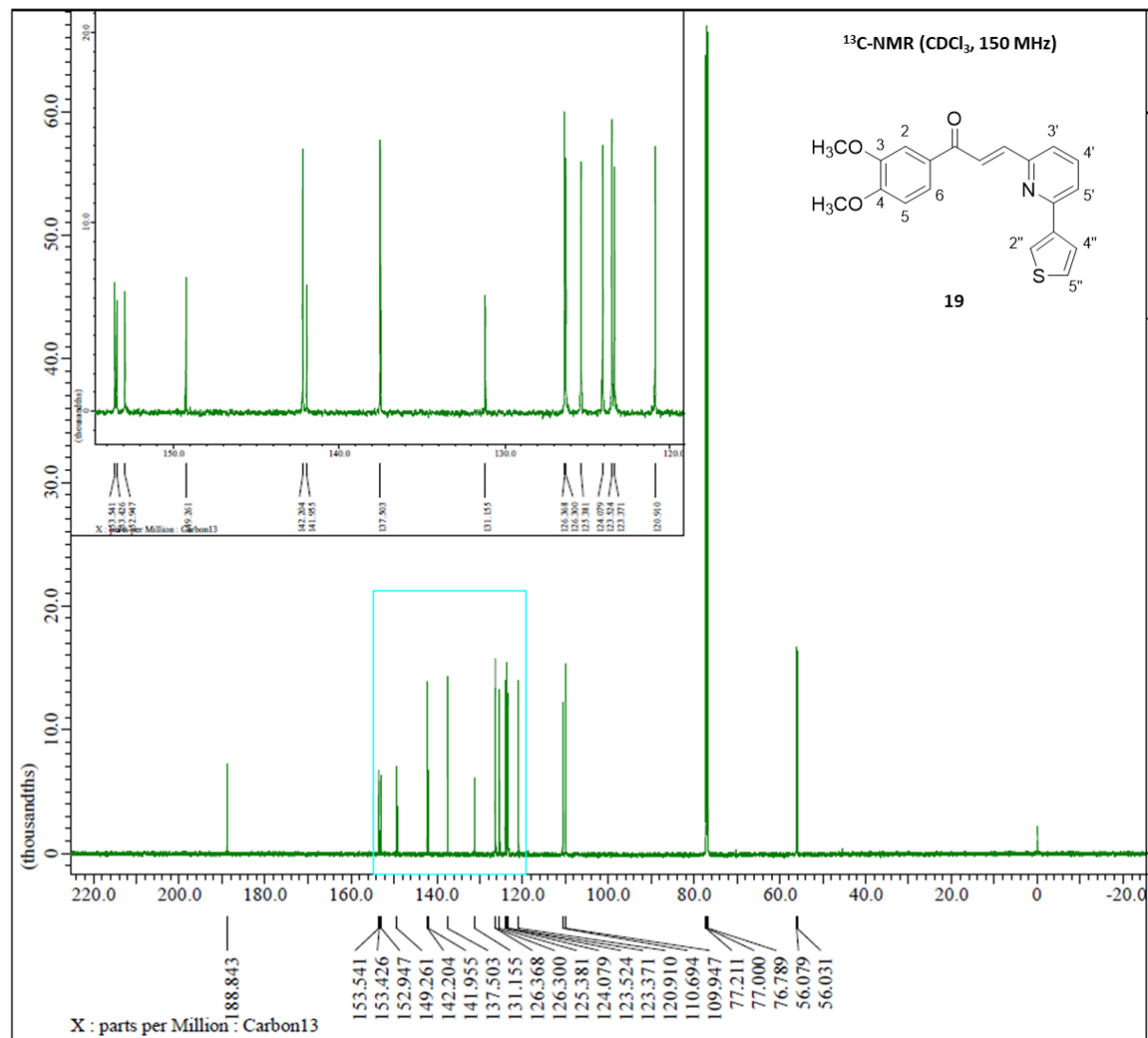


Figure 142. ¹³C-NMR spectrum (CDCl₃, 150 MHz) of compound **19**.

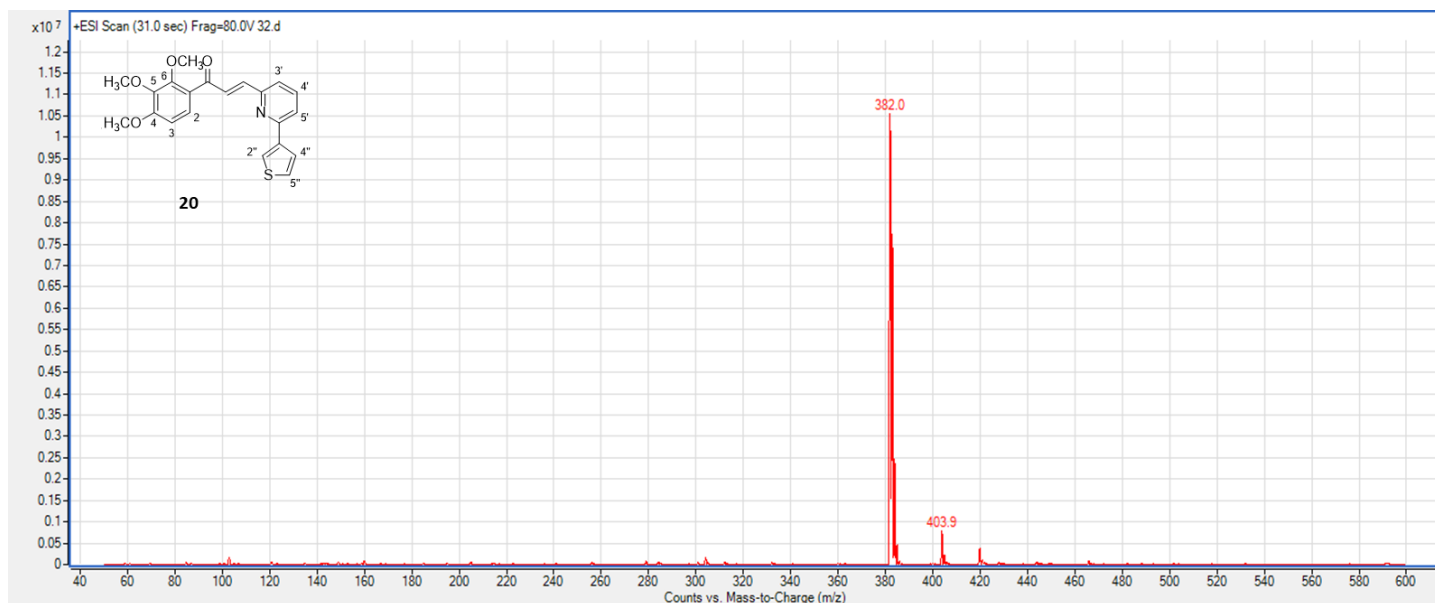


Figure 143. (+)-ESI Mass spectrum of compound 20.

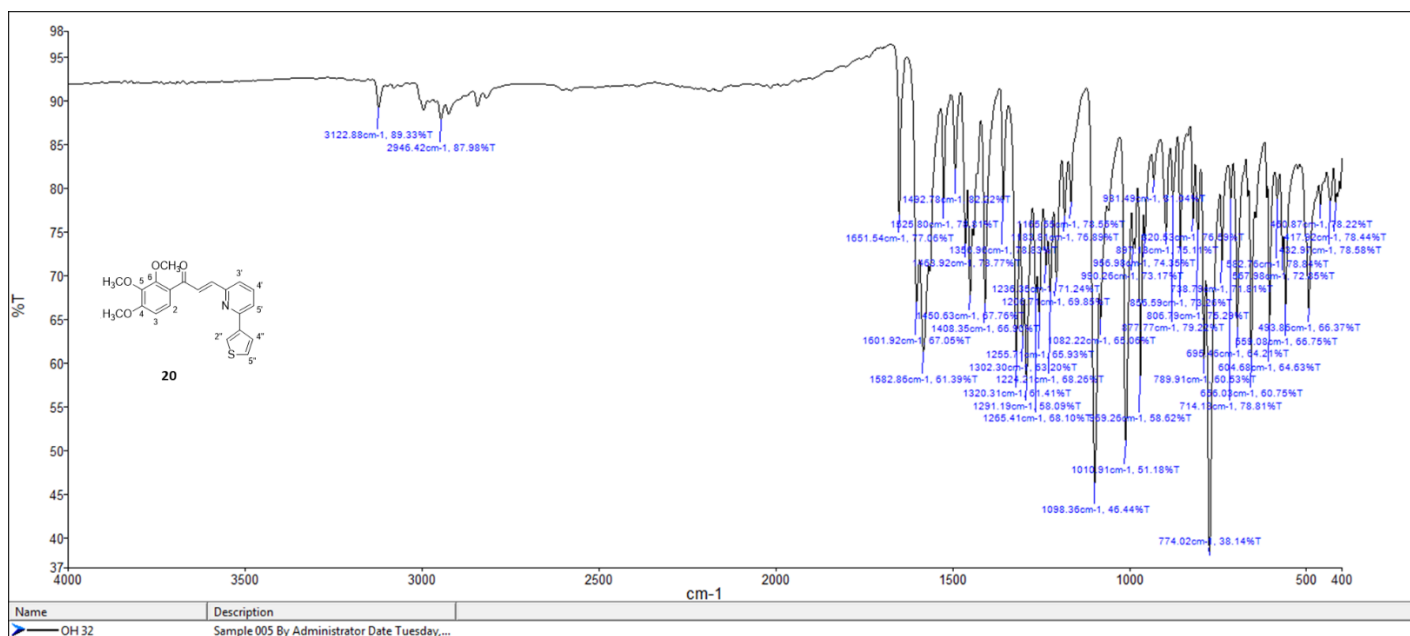


Figure 144. FT-IR spectrum of compound 20.

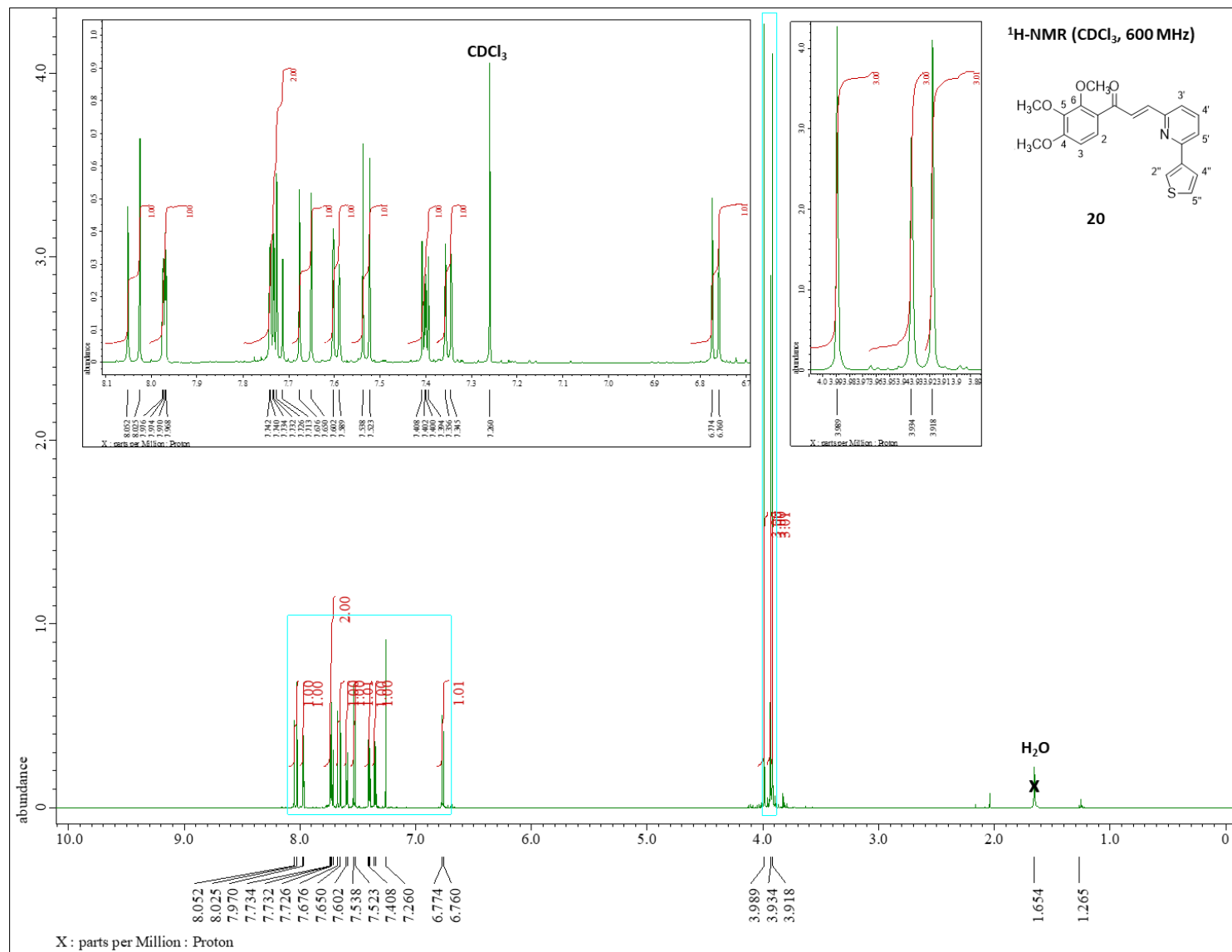


Figure 145. ¹H-NMR spectrum (CDCl₃ with 0.05% v/v of TMS, 600 MHz) of compound **20**.

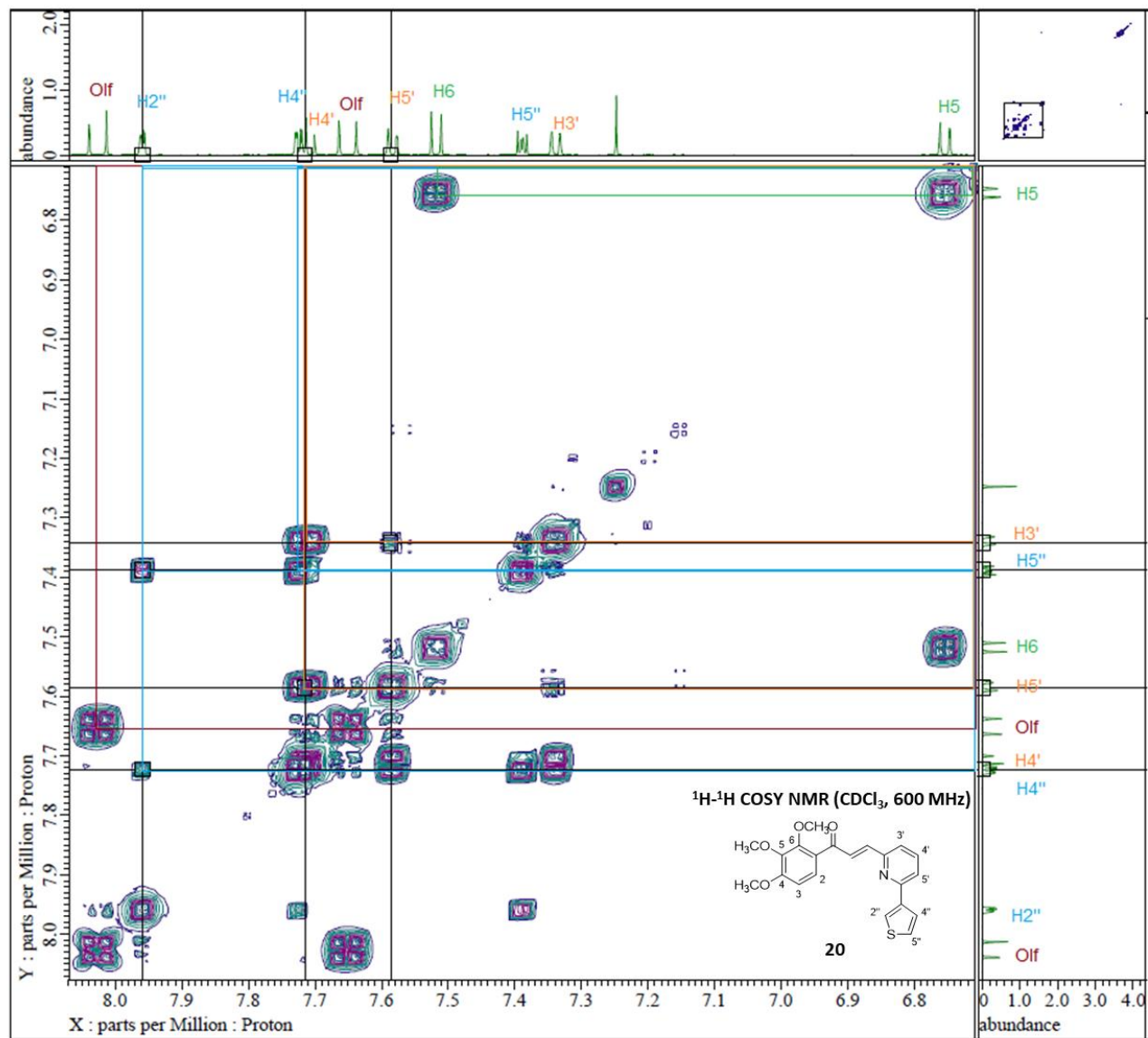


Figure 146. ¹H-¹H COSY NMR of compound **20**.

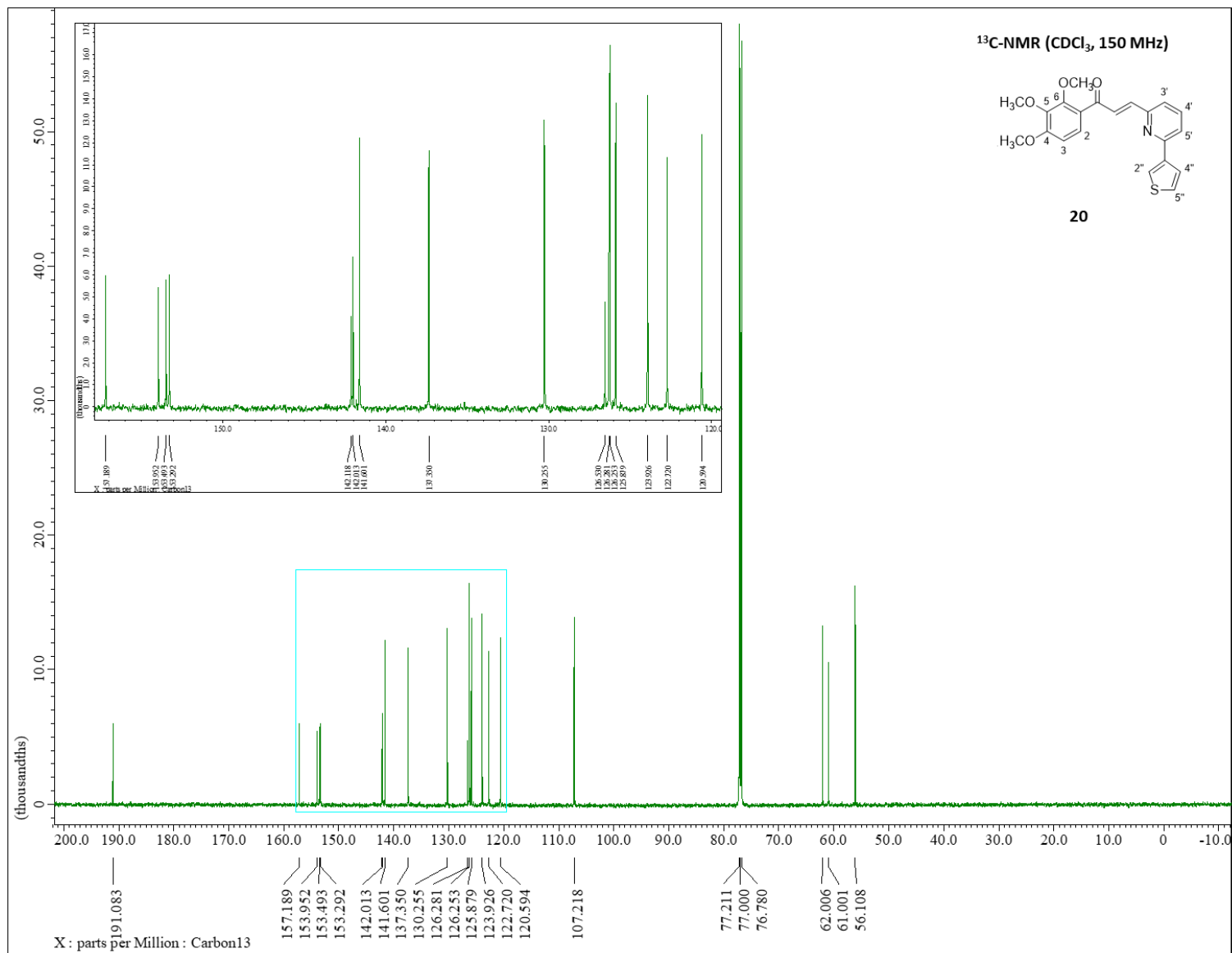


Figure 147. ¹³C-NMR spectrum (CDCl₃, 150 MHz) of compound **20**.

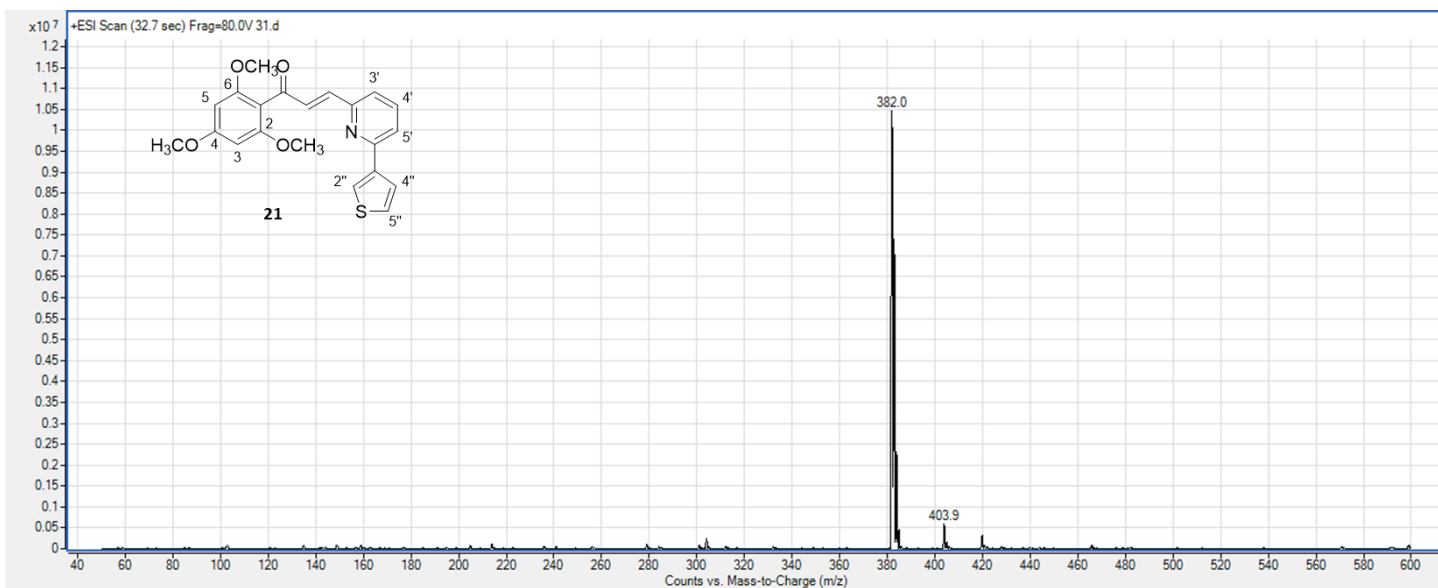


Figure 148. (+)-ESI Mass spectrum of compound 21.

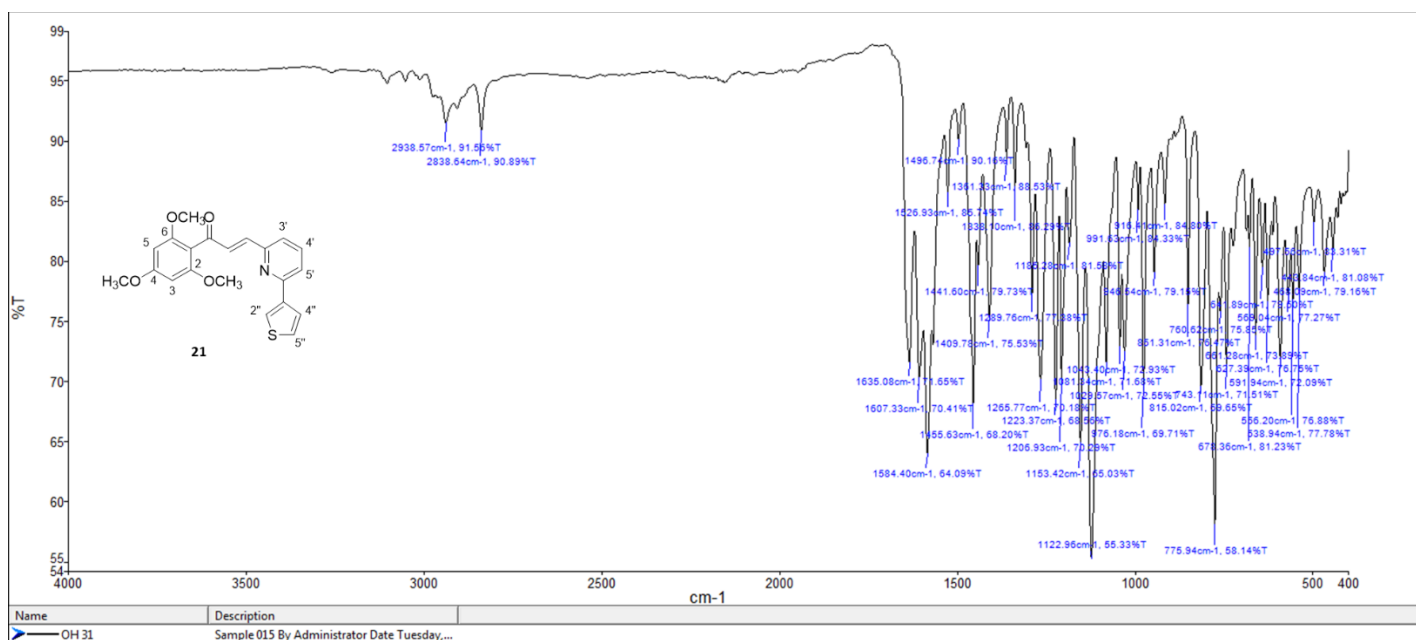


Figure 149. FT-IR spectrum of compound 21.

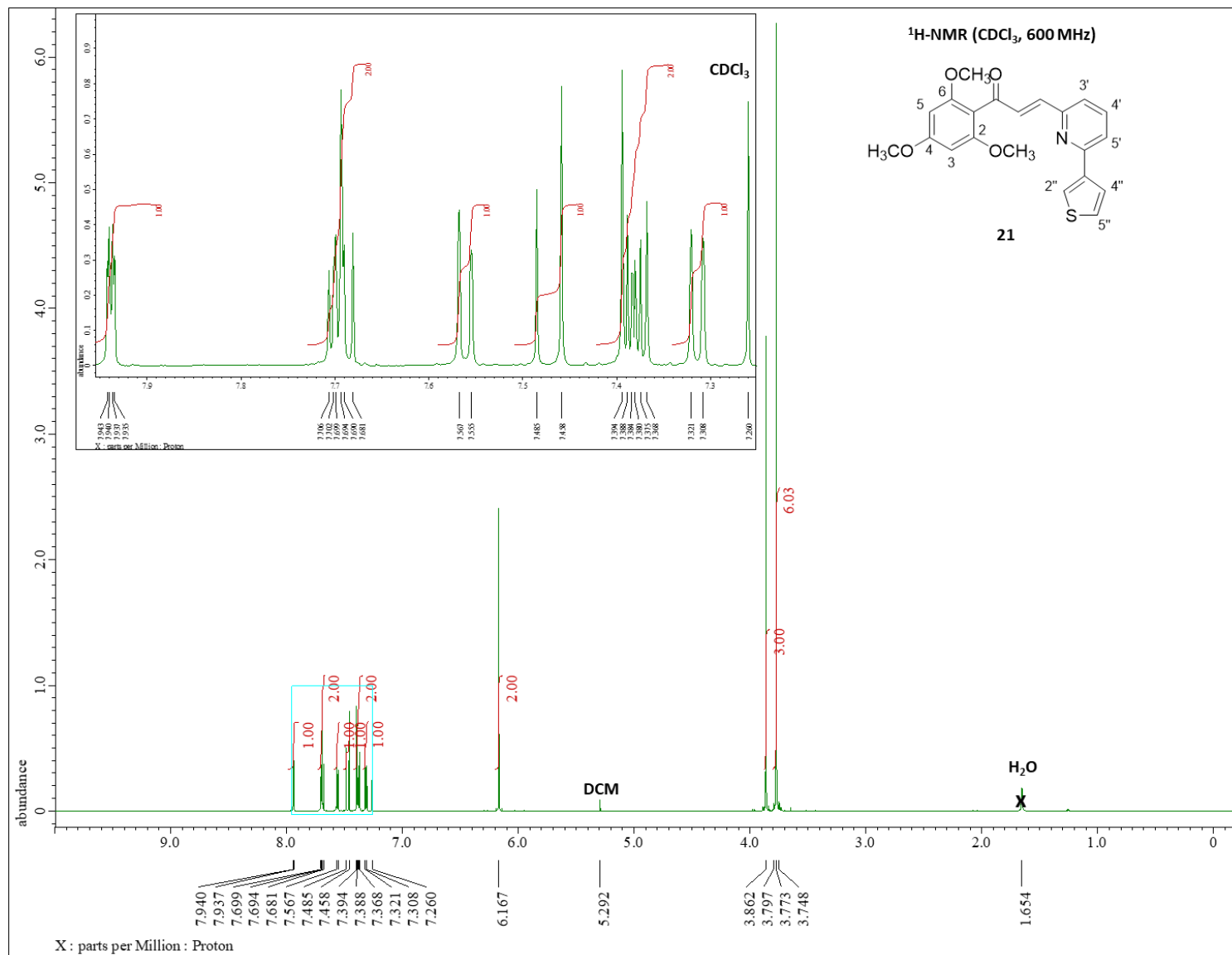


Figure 150. ¹H-NMR spectrum (CDCl₃, 600 MHz) of compound **21**.

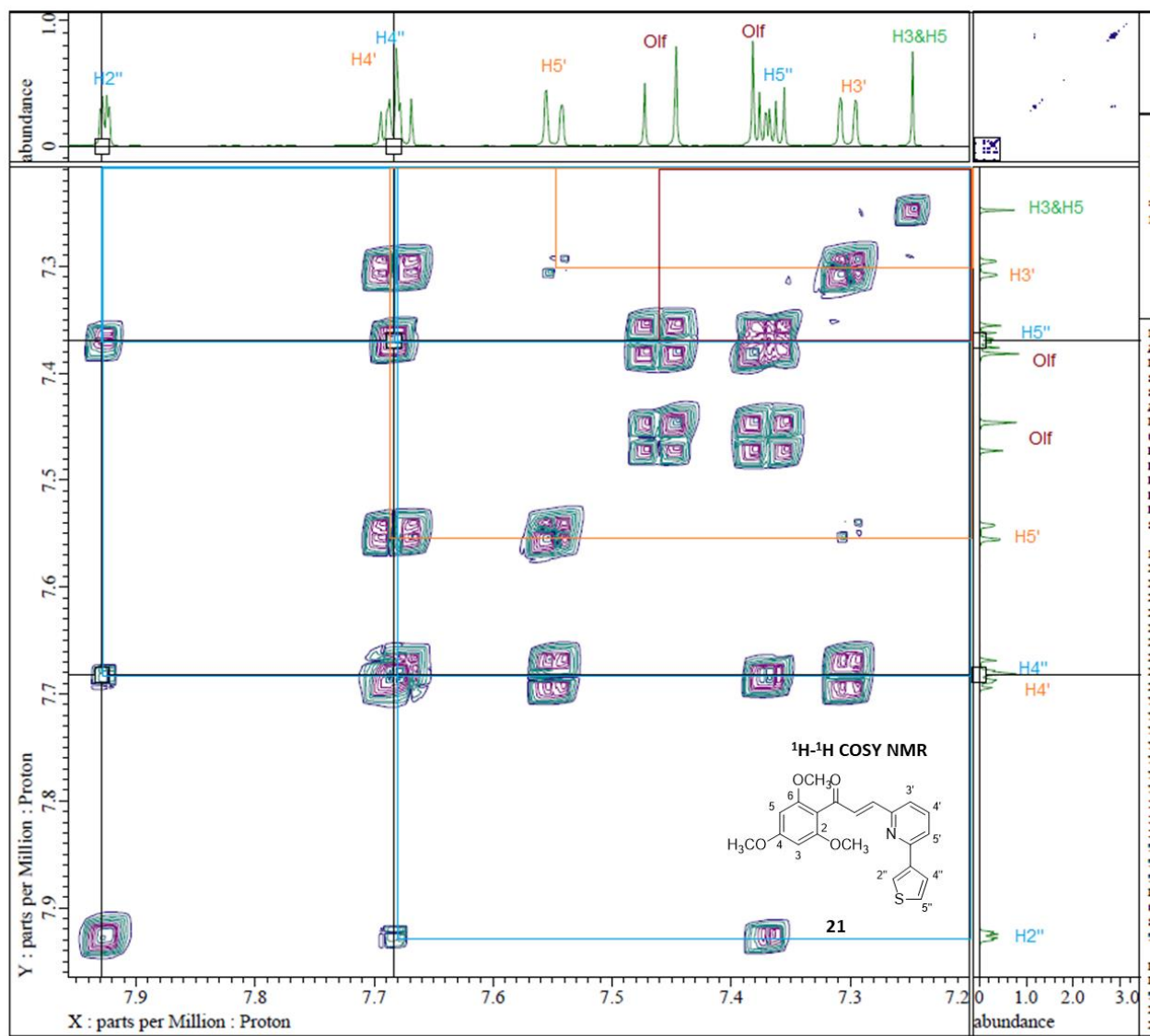


Figure 151. ¹H-¹H COSY NMR of compound **21**.

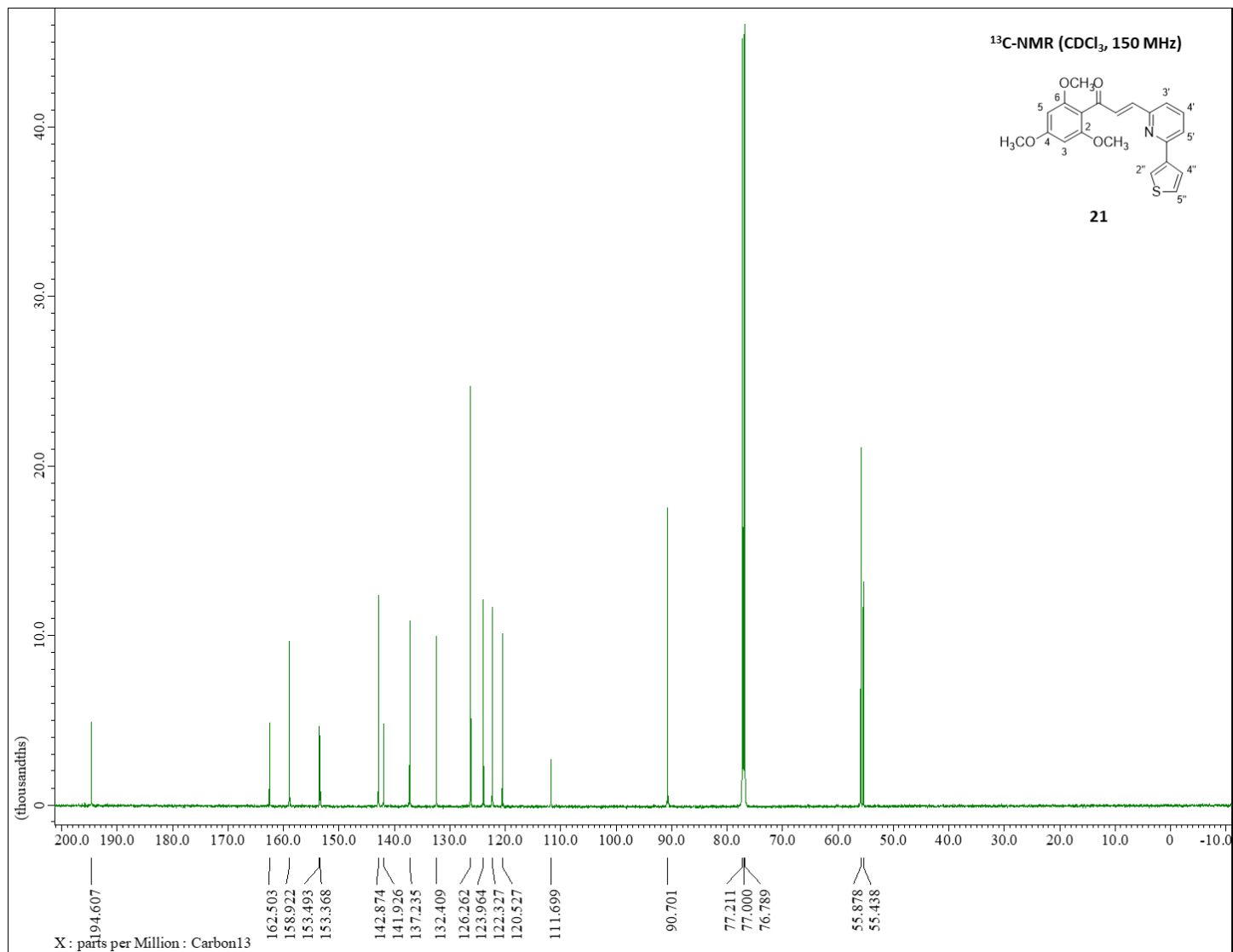


Figure 152. ¹³C-NMR spectrum (CDCl₃, 150 MHz) of compound **21**.

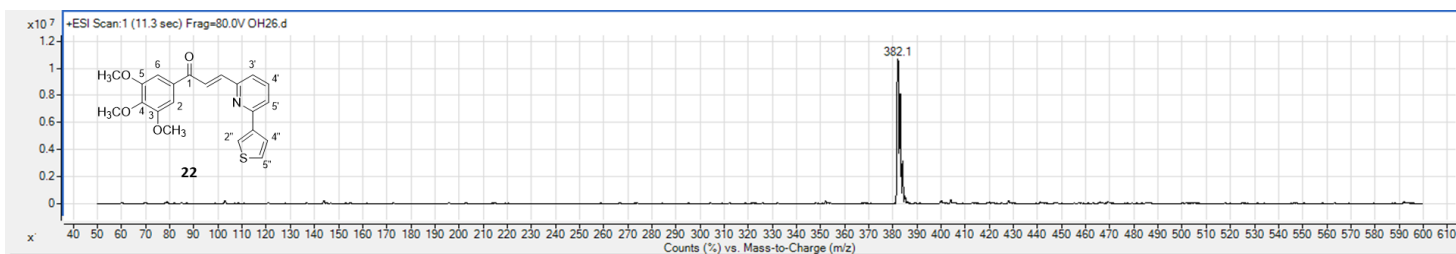


Figure 153. (+)-ESI Mass spectrum of compound **22**.

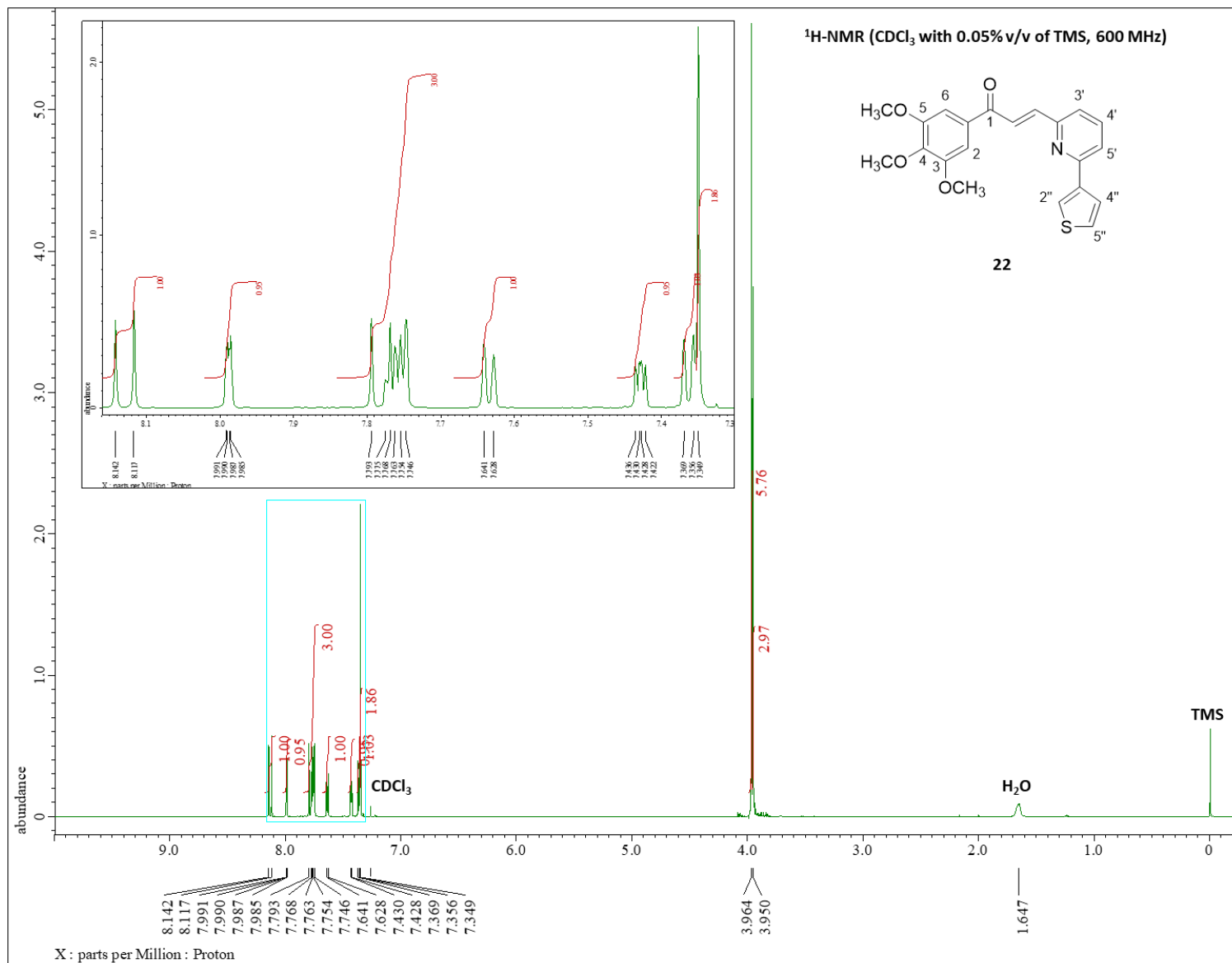


Figure 154. ¹H-NMR spectrum (CDCl₃ with 0.05% v/v of TMS, 600 MHz) of compound **22**.

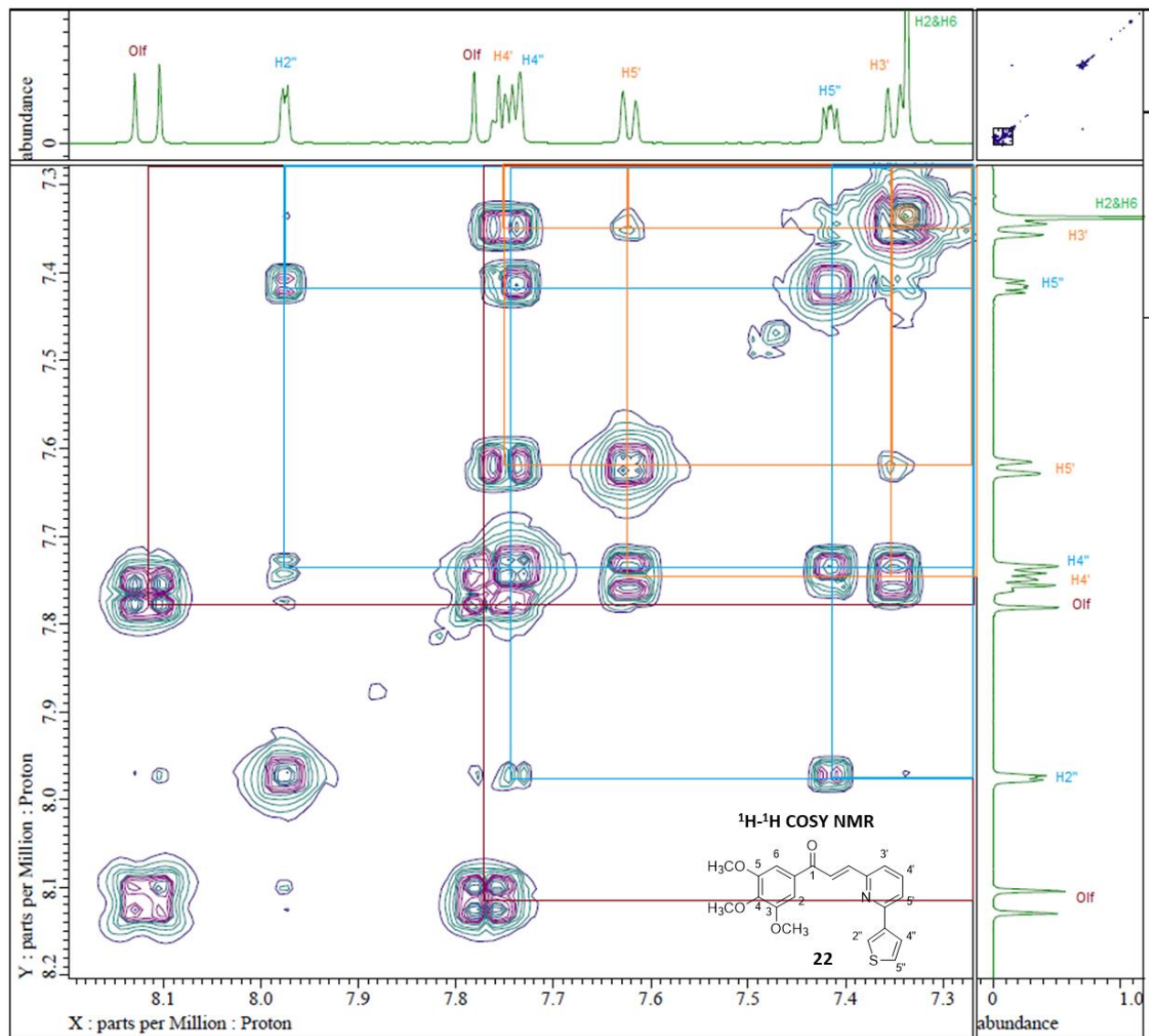


Figure 155. ¹H-¹H COSY NMR of compound **22**.

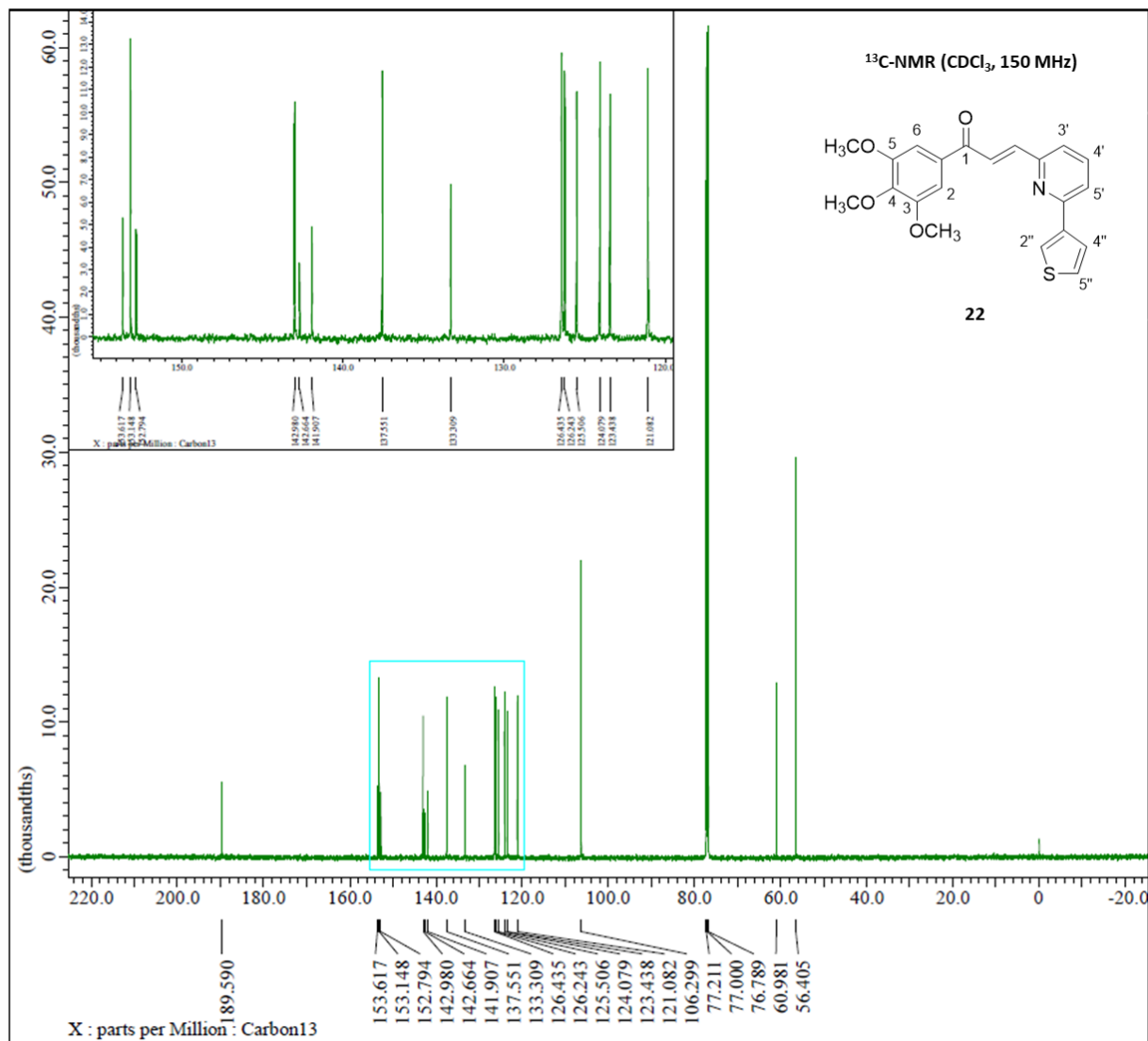


Figure 156. ¹³C-NMR spectrum (CDCl₃, 150 MHz) of compound **22**.

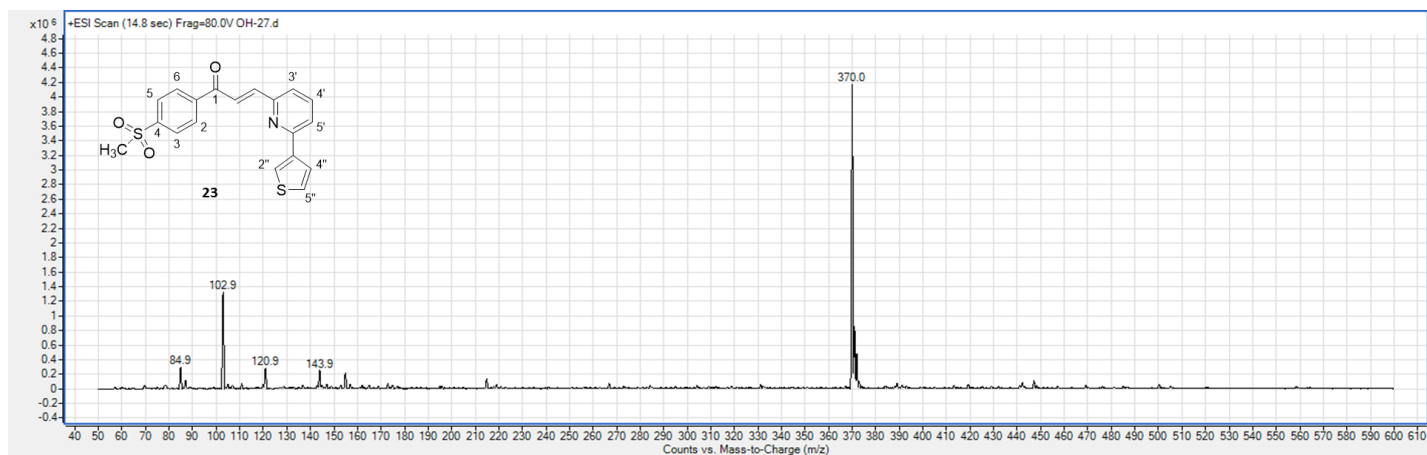


Figure 157. (+)-ESI Mass spectrum of compound **23**.

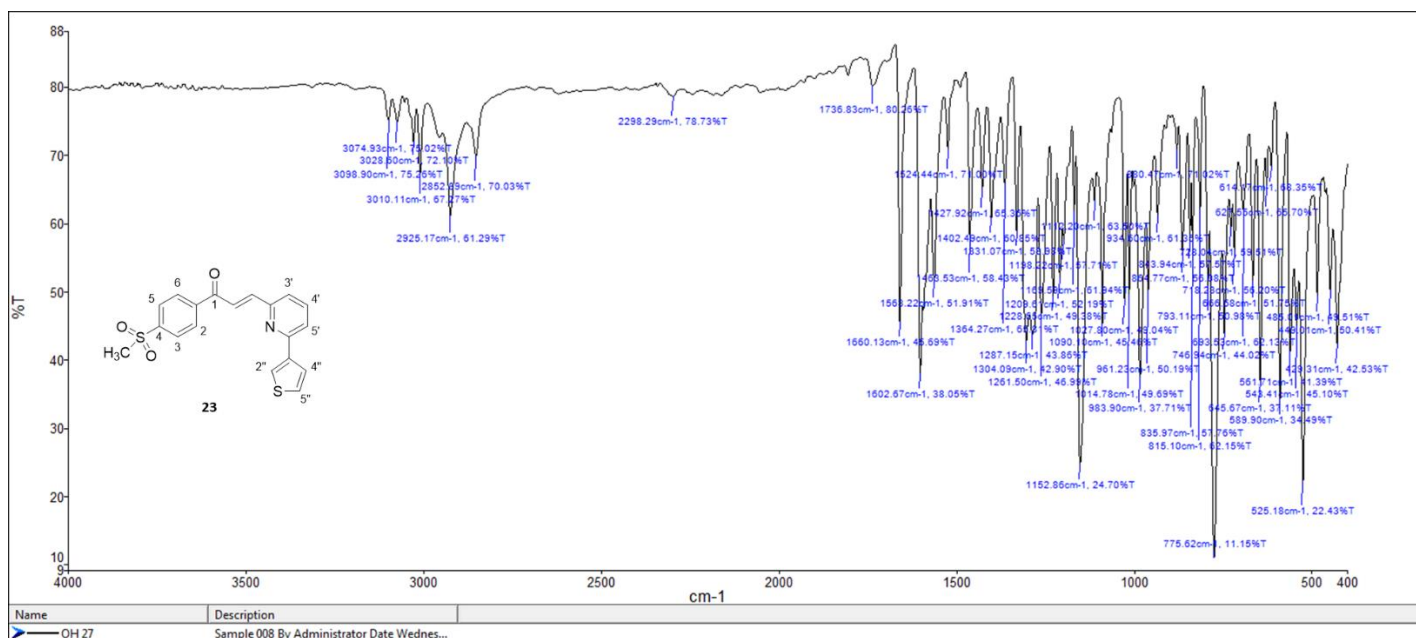


Figure 158. FT-IR spectrum of compound **23**.

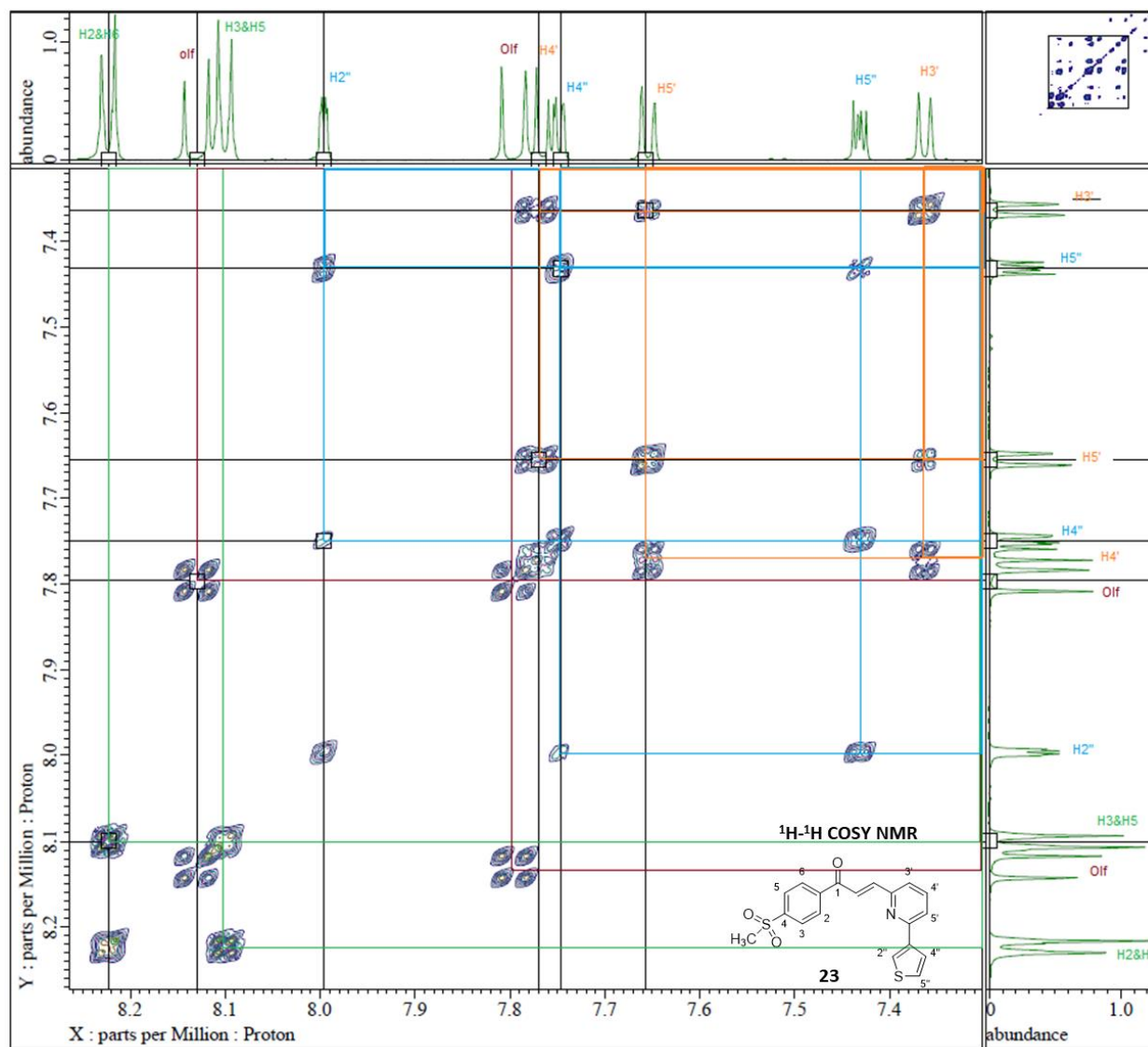


Figure 160. ¹H-¹H COSY NMR of compound **23**.

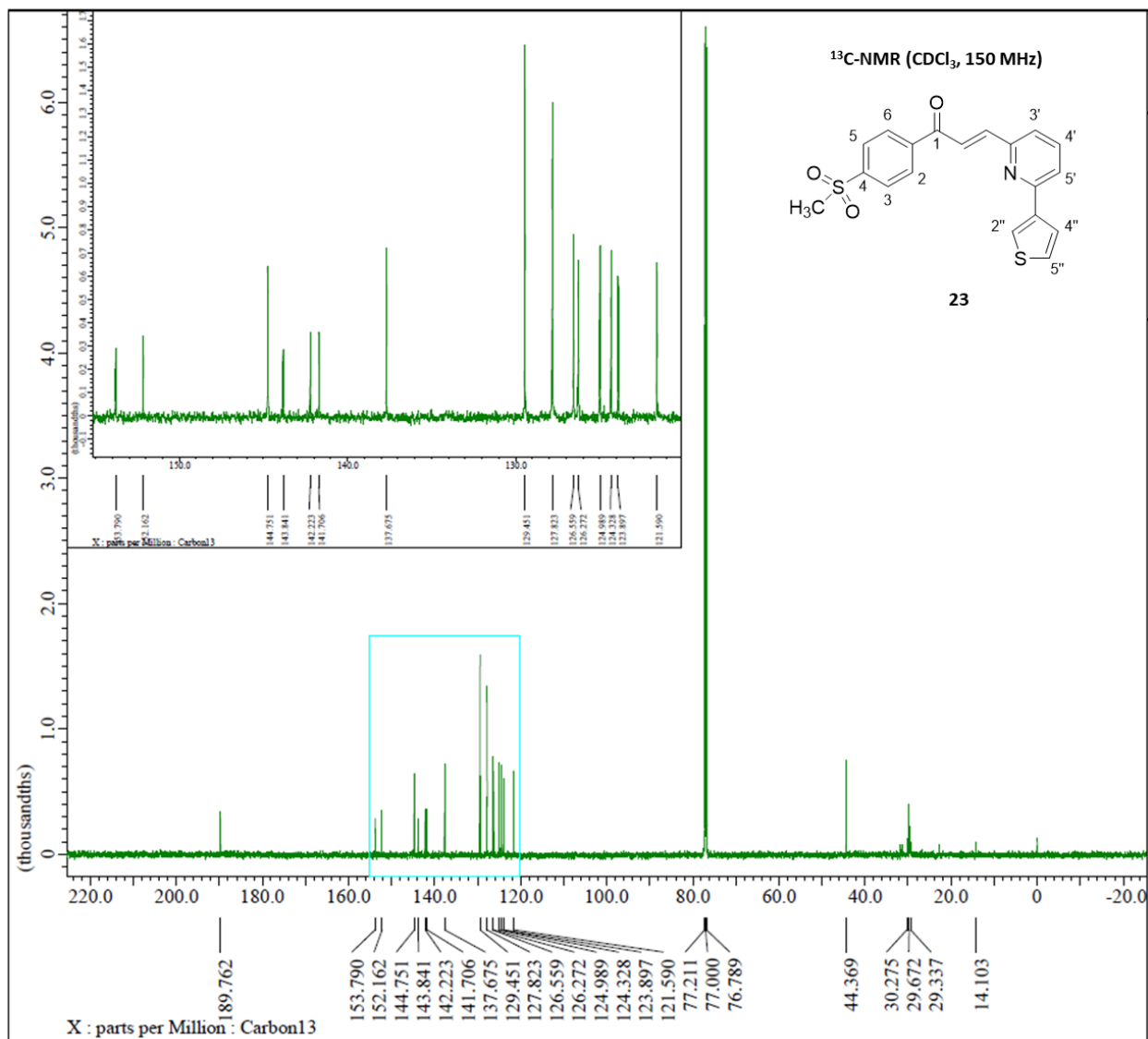


Figure 161. ¹³C-NMR spectrum (CDCl₃, 150 MHz) of compound **23**.

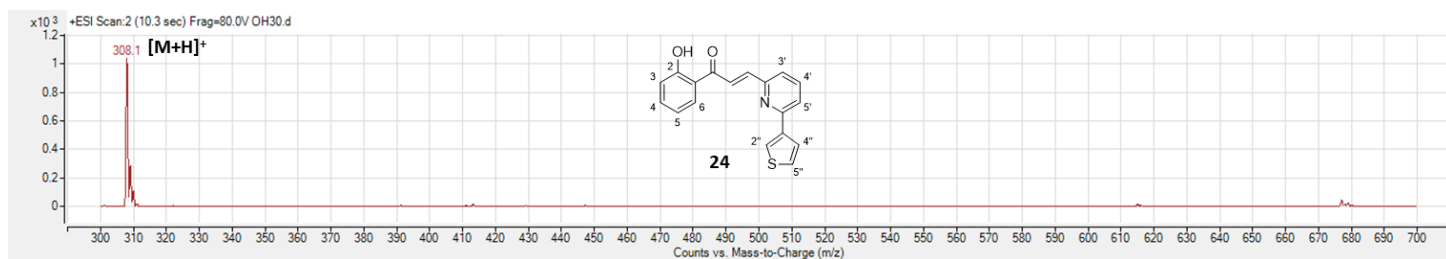


Figure 162. (+)-ESI Mass spectrum of compound **24**.

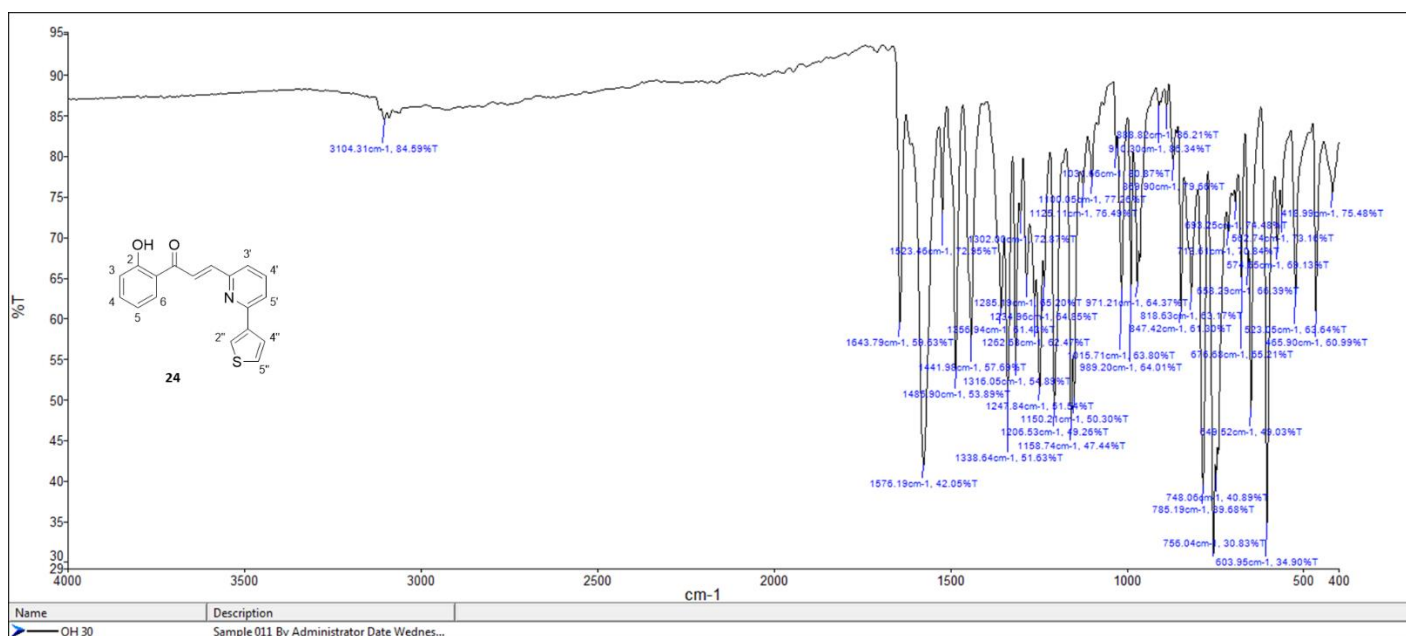


Figure 163. FT-IR spectrum of compound **24**.

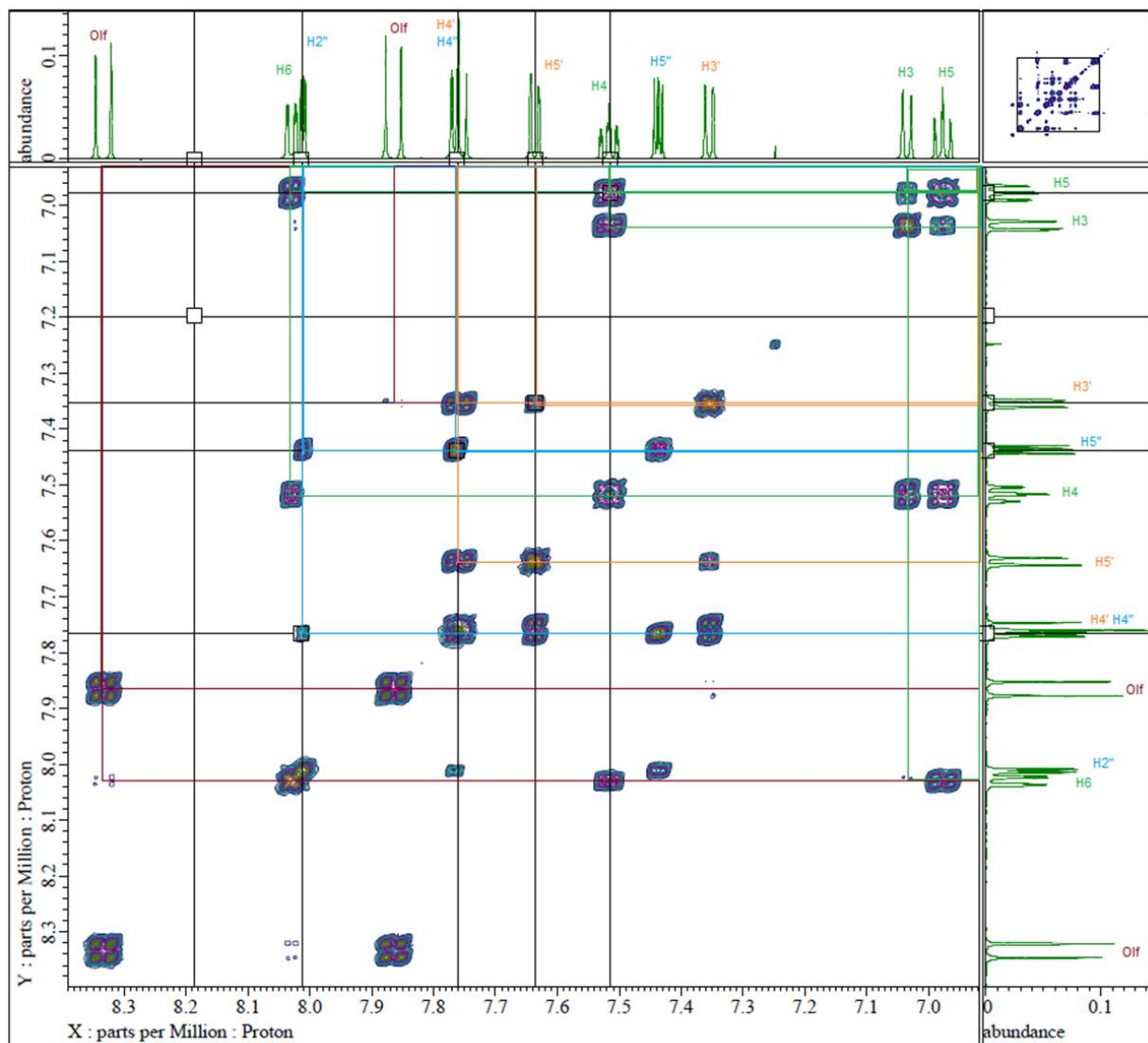


Figure 165. ^1H - ^1H COSY NMR of compound **24**.

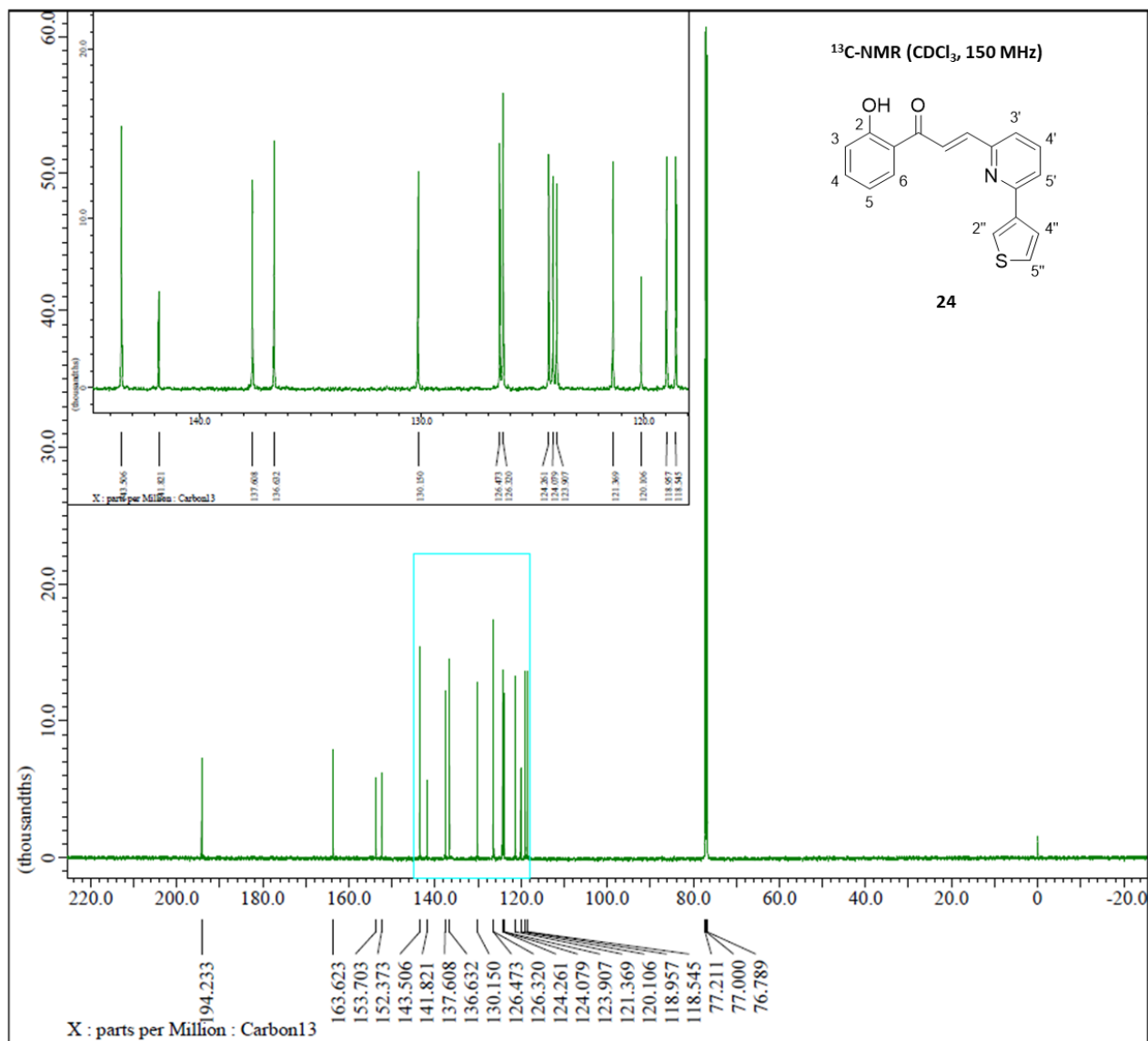


Figure 166. ¹³C-NMR spectrum (CDCl₃, 150 MHz) of compound **24**.

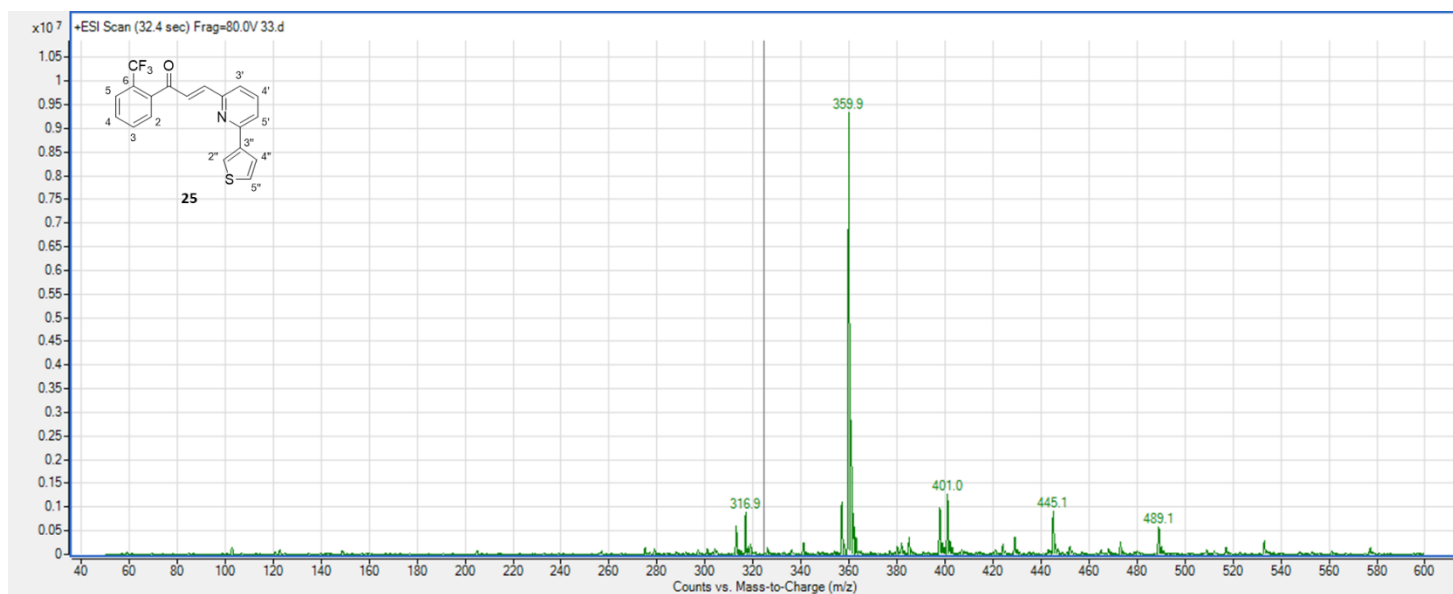


Figure 167. (+)-ESI Mass spectrum of compound **25**.

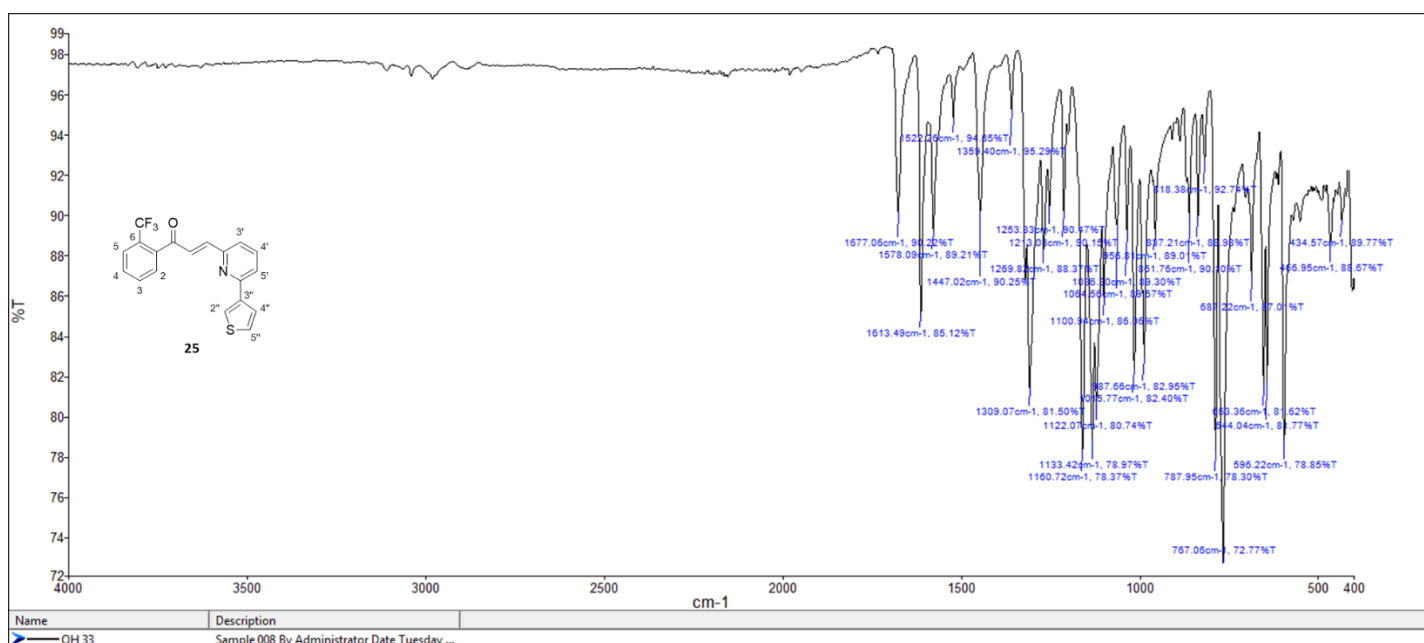


Figure 168. FT-IR spectrum of compound **25**.

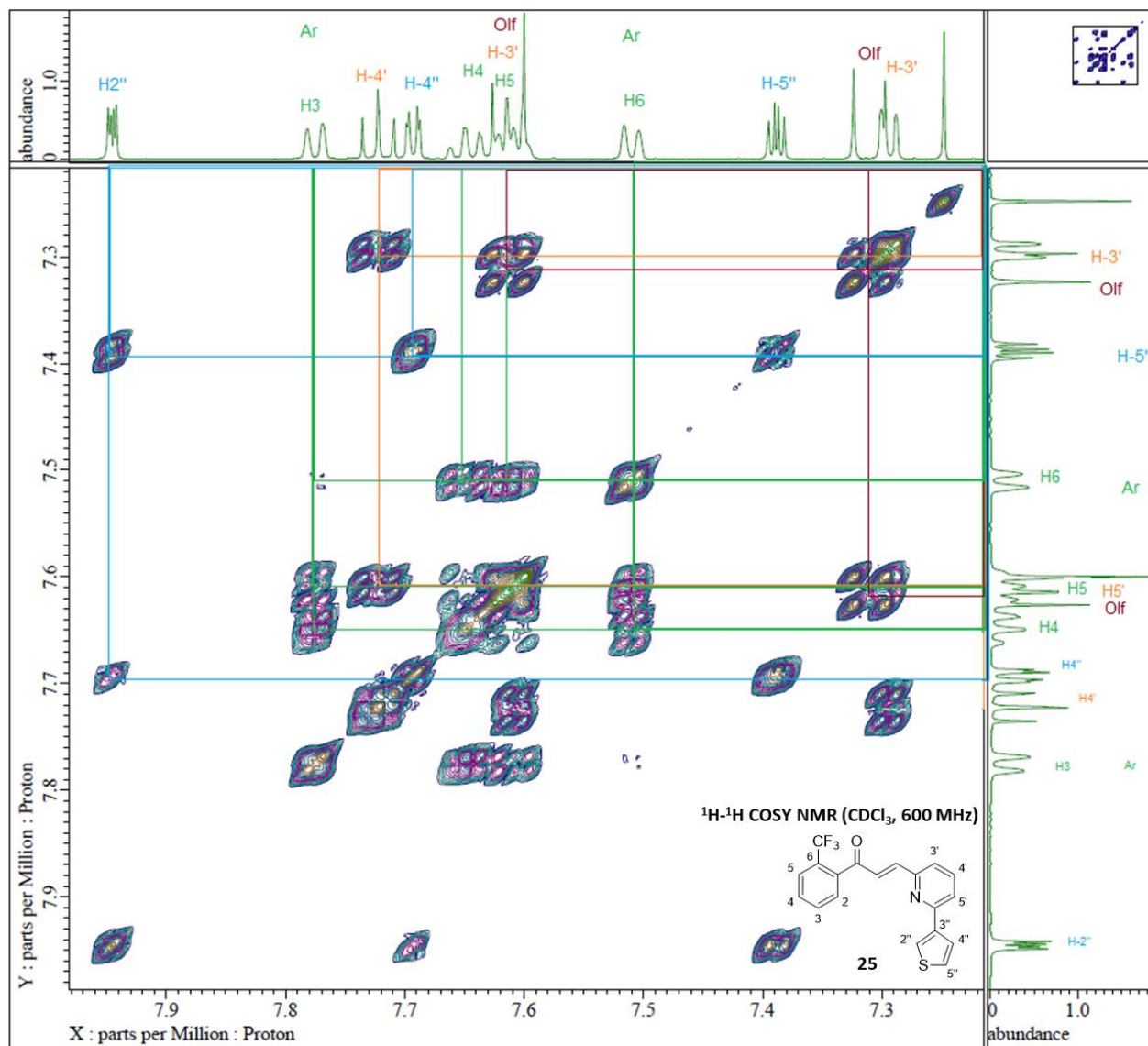


Figure 170. ^1H - ^1H COSY NMR of compound **25**.

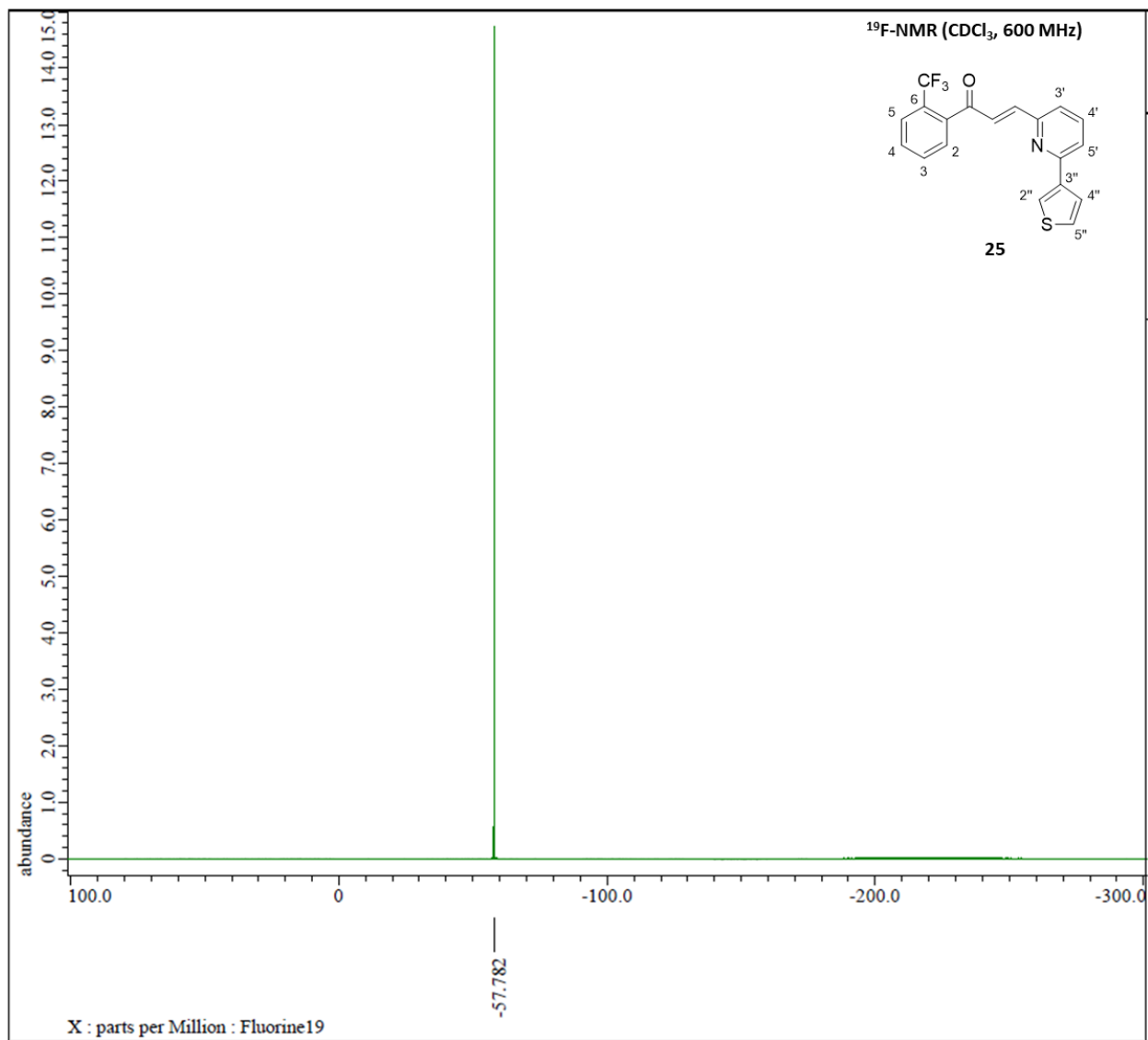


Figure 171. ¹⁹F-NMR spectrum (CDCl₃, 600 MHz) of compound **25**.

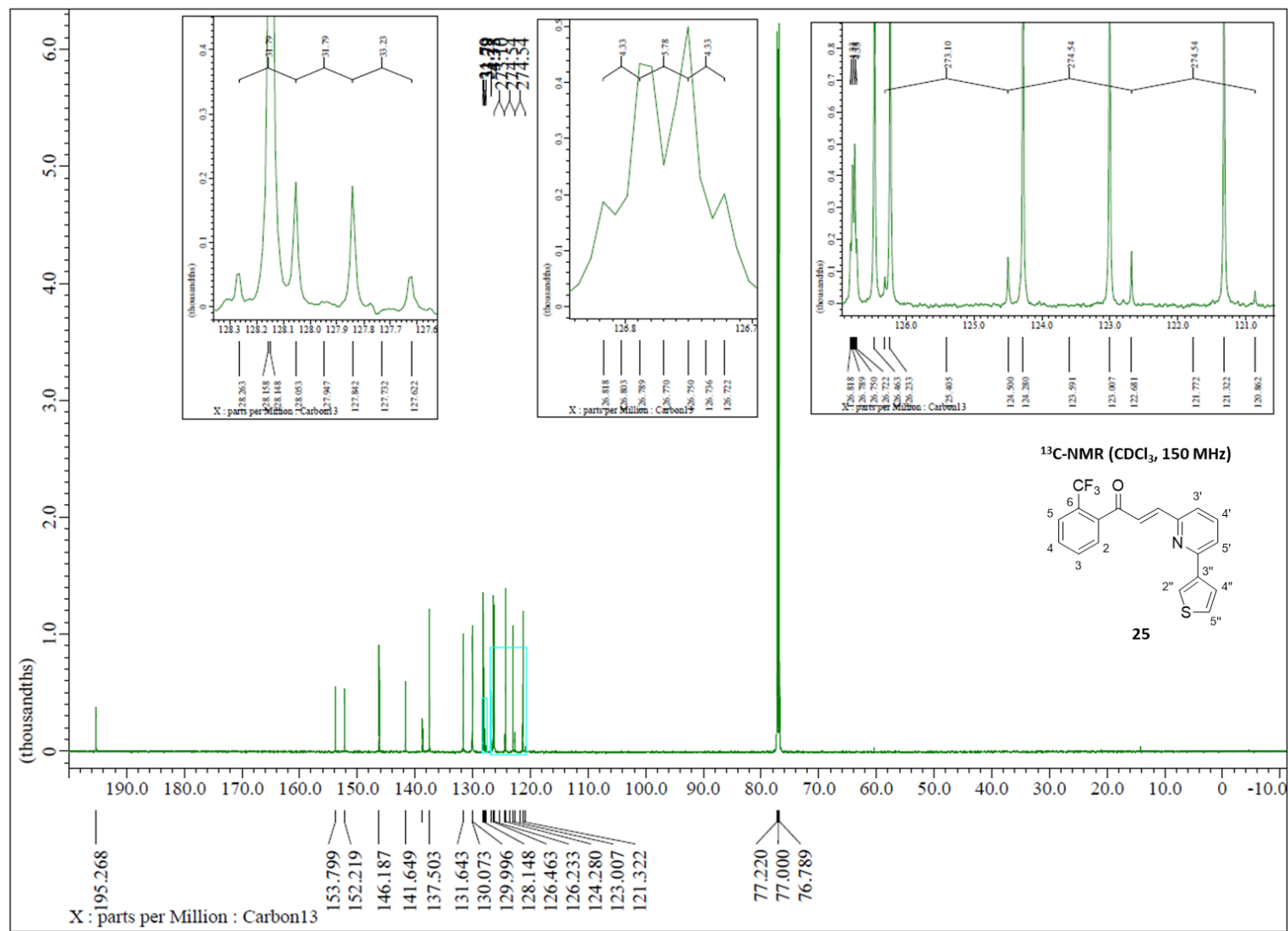


Figure 172. ¹³C-NMR spectrum (CDCl₃, 150 MHz) of compound **25**.

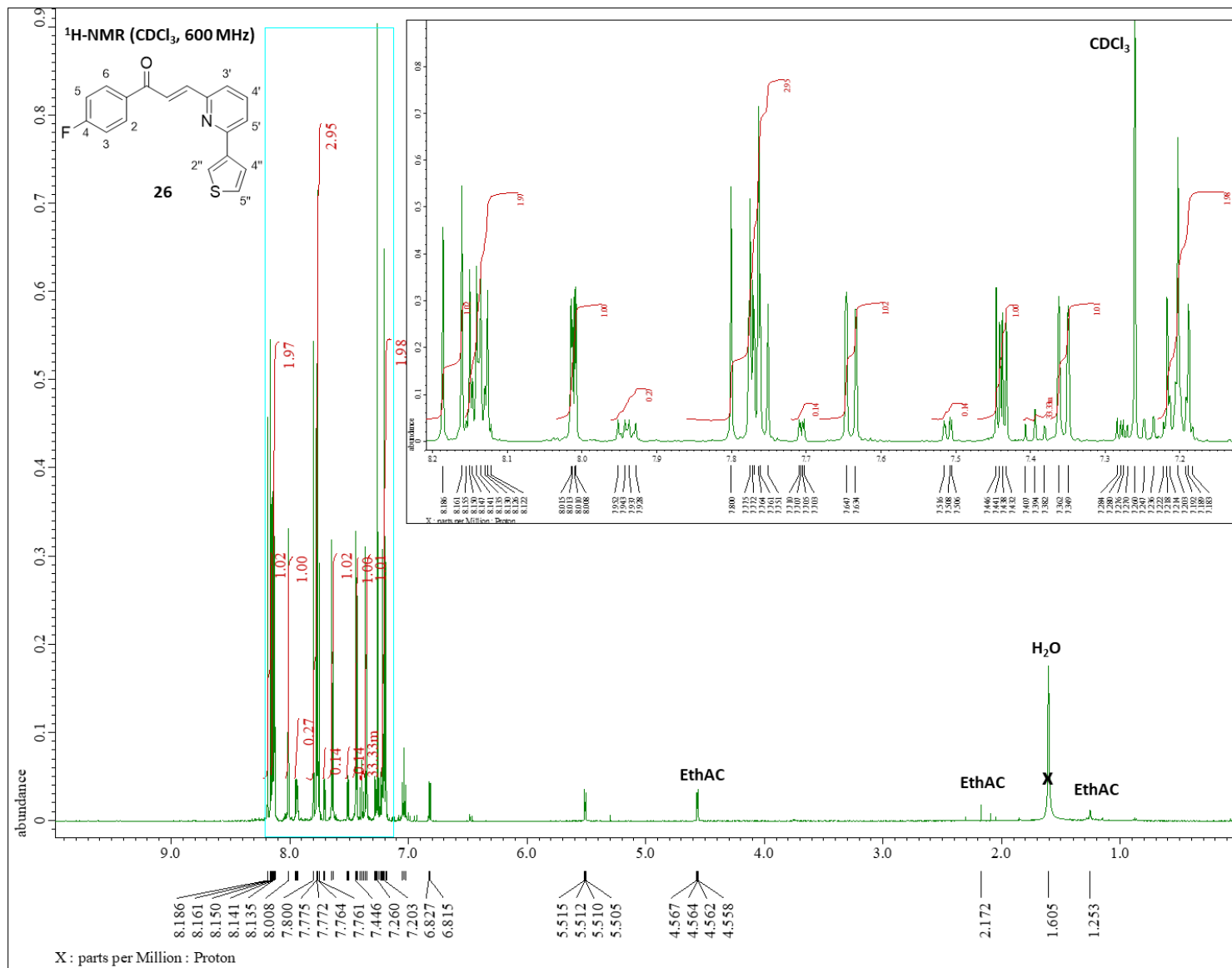


Figure 173. ¹H-NMR spectrum (CDCl₃ with 0.05% v/v of TMS, 600 MHz) of compound

